frontiers | Research Topics

Pharmacology of infectious diseases: World tuberculosis day 2022

Edited by
Johannes Alffenaar, Sebastian G. Wicha and Shashikant Srivastava

Published in
Frontiers in Pharmacology

ISSN 1664-8714
ISBN 978-2-8325-2830-3
DOI 10.3389/978-2-8325-2830-3

About Frontiers

Frontiers is more than just an open access publisher of scholarly articles: it is a pioneering approach to the world of academia, radically improving the way scholarly research is managed. The grand vision of Frontiers is a world where all people have an equal opportunity to seek, share and generate knowledge. Frontiers provides immediate and permanent online open access to all its publications, but this alone is not enough to realize our grand goals.

Frontiers journal series

The Frontiers journal series is a multi-tier and interdisciplinary set of open-access, online journals, promising a paradigm shift from the current review, selection and dissemination processes in academic publishing. All Frontiers journals are driven by researchers for researchers; therefore, they constitute a service to the scholarly community. At the same time, the *Frontiers journal series* operates on a revolutionary invention, the tiered publishing system, initially addressing specific communities of scholars, and gradually climbing up to broader public understanding, thus serving the interests of the lay society, too.

Dedication to quality

Each Frontiers article is a landmark of the highest quality, thanks to genuinely collaborative interactions between authors and review editors, who include some of the world's best academicians. Research must be certified by peers before entering a stream of knowledge that may eventually reach the public - and shape society; therefore, Frontiers only applies the most rigorous and unbiased reviews. Frontiers revolutionizes research publishing by freely delivering the most outstanding research, evaluated with no bias from both the academic and social point of view. By applying the most advanced information technologies, Frontiers is catapulting scholarly publishing into a new generation.

What are Frontiers Research Topics?

Frontiers Research Topics are very popular trademarks of the *Frontiers journals series*: they are collections of at least ten articles, all centered on a particular subject. With their unique mix of varied contributions from Original Research to Review Articles, Frontiers Research Topics unify the most influential researchers, the latest key findings and historical advances in a hot research area.

Find out more on how to host your own Frontiers Research Topic or contribute to one as an author by contacting the Frontiers editorial office: frontiersin.org/about/contact

Pharmacology of infectious diseases: World tuberculosis day 2022

Topic editors

Johannes Alffenaar — The University of Sydney, Australia

Sebastian G. Wicha — University of Hamburg, Germany

Shashikant Srivastava — University of Texas at Tyler, United States

Citation

Alffenaar, J., Wicha, S. G., Srivastava, S., eds. (2023). *Pharmacology of infectious diseases: World tuberculosis day 2022*. Lausanne: Frontiers Media SA.

doi: 10.3389/978-2-8325-2830-3

Table of contents

frontiers | Frontiers in Pharmacology

TYPE Editorial
PUBLISHED 13 June 2023
DOI 10.3389/fphar.2023.1233347

OPEN ACCESS

EDITED AND REVIEWED BY
Hendrik W. Van Veen,
University of Cambridge, United Kingdom

*CORRESPONDENCE
Shashikant Srivastava,
Shashi.kant@uthct.edu

RECEIVED 02 June 2023
ACCEPTED 07 June 2023
PUBLISHED 13 June 2023

CITATION
Srivastava S, Alffenaar JW and Wicha SG (2023), Editorial: Pharmacology of infectious diseases: world tuberculosis day 2022.
Front. Pharmacol. 14:1233347.
doi: 10.3389/fphar.2023.1233347

Editorial: Pharmacology of infectious diseases: world tuberculosis day 2022

Shashikant Srivastava[1,2,3]*, Johannes W. Alffenaar[4,5,6] and Sebastian G. Wicha[7]

[1]Department of Medicine, School of Medicine, University of Texas at Tyler, Tyler, TX, United States, [2]Department of Cellular and Molecular Biology, University of Texas Health Science Center at Tyler, Tyler, TX, United States, [3]Center for Biomedical Research, University of Texas Health Science Centre at Tyler, Tyler, TX, United States, [4]Sydney Institute for Infectious Diseases, The University of Sydney, Sydney, NSW, Australia, [5]Faculty of Medicine and Health, School of Pharmacy, The University of Sydney, Sydney, NSW, Australia, [6]Westmead Hospital, Sydney, NSW, Australia, [7]Department of Clinical Pharmacy, Institute of Pharmacy, University of Hamburg, Hamburg, Germany

KEYWORDS

pharmacology, infectious diseases, tuberculosis, drug discovery, modeling

Editorial on the Research Topic
Pharmacology of infectious diseases: world tuberculosis day 2022

Robert Koch discovered *Mycobacterium tuberculosis* (*Mtb*), the causative agent of tuberculosis (TB), in 1882 (Koch, 1882). Significant progress has been made since then to treat TB and now we have treatment regimens with a four-month duration for drug-susceptible TB (Gillespie et al., 2014) and the possibility that the therapy duration can further be shortened (Gumbo et al., 2022). However, the emergence of drug resistance during therapy remains a major challenge and continuous efforts are needed to develop new drugs, regimens, and biomarkers for therapy outcomes. The series of articles in this Research Topic of "Frontiers in Pharmacology" provides an insight into the pharmacokinetics/pharmacodynamics (PK/PD) of anti-tuberculosis drugs, various mathematical and computer-aided simulation models on the PK/PD as well methods to use Mycobacteria Growth Indicator Tube (MGIT) derived time-to-positive (TTP) as a biomarker for therapeutic outcome.

The first review article, by Alffenaar et al. discusses *in vitro*, *in vivo,* and human studies, the factors to consider in a study design, the importance of uniform reporting including microbiological and clinical outcome assessments, and modeling approaches to link the PK/PD and other output from these studies. Regarding the *in vitro* studies examining the efficacy of drugs against *Mtb*, the authors discussed the importance of determining the MIC using various methods, time-kill kinetic studies at static concentrations, and how a dynamic hollow fiber system of tuberculosis (HFS-TB) can be used not only to determine the drug exposure for *Mtb* kill and resistance suppression but also to investigate different metabolic populations of *Mtb*. Regarding the animal studies, Alffenaar et al. discussed the effect of routes of infection, PK in blood versus at the site of infection, PD read-outs (CFU and TTP), biomarkers and use of the *in vivo* systems to evaluate the differences in treatment in terms of sterilization on infection, relapse, and death. The review also discusses the human PKPD with a focus on early bactericidal activity (EBA) studies and proposed the inclusion of PK and therapeutic drug monitoring (TDM) in clinical trials. An overview of the *in silico* modeling and computer-aided clinical trial simulation to link *in vitro*, *in vivo,* and human

studies were also included to discuss how the modeling approach can bridge the translation of pre-clinical findings to clinical settings.

The second review article in the series, by Stadler et al. is on clofazimine that was introduced in the clinics due to the reported *in vitro* anti-TB activity but without the PK and safety evaluation. Interestingly, while clofazimine lacks the EBA, is synergistic with many first- and second-line drugs. This review summarizes the clinical studies on the safety and efficacy outcomes of clofazimine-containing regimens as well as a comprehensive list of recently completed and ongoing clinical trials to investigate the efficacy of clofazimine against both drug-susceptible and drug-resistant forms of TB. Stadler et al. literature review also provides a rationale for developing novel clofazimine analogs with improved antimycobacterial activity as well as better PK and tolerability profile, to add to the armament of anti-TB drugs.

Linezolid is one of the core drugs now included in the multidrug-resistant (MDR)-TB treatment regimen, including the BPaLM regimen recommended by the World_Health Organizaton (2022). Zhang et al. performed a prospective multi-center cohort study including 168 participants with MDR-TB for clinical validation of the linezolid exposure target identified in the HFS-TB (Srivastava et al., 2017). The authors used a population PK model for linezolid and used classification and regression tree analyses (CART) to identify the ratio of 0–24 h area under the concentration-time curve ($AUC_{0\text{-}24}$) to the minimal inhibitory concentration (MIC) associated with successful treatment outcome. The authors analyzed a total of 1,008 linezolid plasma concentrations using a two-compartment model with first-order absorption and elimination to identify $AUC_{0\text{–}24}$/MIC of >125 as the threshold for successful treatment outcome, close to the threshold identified in the HFS-TB as an $AUC_{0\text{–}24}$/MIC of 119 (Srivastava et al., 2017). The time to culture conversion in patients with $AUC_{0\text{-}24}$/MIC >125 was also similar to the HFS-TB predicted 2-month threshold. The authors concluded that with the standard 600 mg once daily dose of linezolid, the probability of target attainment was 100% up to the MIC ≤0.25 mg/L. Thus, Zhang et al. study provides crucial clinical evidence that preclinical models, such as HFS-TB, combined with mathematical modeling and clinical trial simulations can accurately predict clinical outcomes.

The second study on linezolid by Resendiz-Galvan et al. compared the therapeutic outcomes and adverse events between linezolid 600 mg versus 300 mg daily dose in patients with MDR-TB treated at a tertiary care hospital in Mumbai, India. Intensive or sparse blood sampling was performed for the PK analysis in 183 study participants. The authors concluded that the likelihood of failing to achieve the optimal exposure target with linezolid 300 mg once daily dose was 21%, whereas the probability of target attainment (PTA) of 600 mg daily dose was >90%. However, there was a higher likelihood of exceeding toxicity thresholds with a 600 mg dose (31%) versus the 300 mg daily dose (9.6%). The findings of Resendiz-Galvan et al. also highlight another aspect of personalized medicine, i.e., therapeutic drug monitoring (TDM) to individualize linezolid dosing to improve the treatment efficacy while balancing the risk of drug-induced toxicity for the treatment of MDR-TB (Nahid et al., 2019; Alffenaar et al., 2022).

Bedaquiline is included in the treatment regimen for MDR-TB. However, measurement of bedaquiline plasma concentrations could be tricky, thus information on drug exposure to associate with treatment outcome is limited. The study by Shao et al. performed population PK modeling, using a three-compartment model, to evaluate the WHO-recommended 400 mg once daily dose for 14 days followed by 200 mg three times a week after 2–4 weeks of treatment. The model was developed using 1,205 bedaquiline plasma concentrations from 55 patients and showed a wide concentration range between 0.04 mg/L to 5.96 mg/L. The model validation cohort included 159 patients. Patients on bedaquiline treatment achieving an $AUC_{0\text{-}24}$/MIC >175.5 were predicted to have a higher probability of culture conversion after two-months of therapy. The study also reported that in 13 patients bedaquiline was either discontinued or a dose reduction was required due to moderate and serious QT prolongation.

To exert the antimicrobial effect, penetration of the drugs at the site of infection is an important factor when selecting the drugs in a combination regimen (Dheda et al., 2018). TB meningitis is difficult to treat as many of the drugs do not penetrate the central nervous system. Maranchick et al. evaluated the cerebrospinal fluid (CSF) concentrations of fluoroquinolones and carbapenems in patients with TB meningitis. The authors evaluated levofloxacin, moxifloxacin, ofloxacin, imipenem, and meropenem concentrations in 22 patients treated for TB meningitis, among them only eight were confirmed cases, highlighting the difficulty of establishing a diagnosis in central nervous system TB. The levofloxacin CSF/serum ratio at 2–6 h sampling time points was 0.41–0.63, respectively. For moxifloxacin, the adjusted CSF/serum ratios at 2–6 h sampling time points were 0.44–0.62, respectively. While Maranchick et al. study evaluated only two time points, a previous study with intensive PK sampling reported that moxifloxacin C_{max} in the CSF was observed after 4hrs of drug administration, and the mean plasma to CSF AUC ratio for total concentrations was 0.82 (range 0.70–0.94). Therefore, the observed difference between the two studies could be the timepoint of sampling. This also highlights the importance of performing full PK instead of sparse sampling for drugs, where toxicity could be a concern, to calculate the actual drug exposure and dose adjustments as needed. Regarding the carbapenems, among the 76 CSF samples, the authors reported that drug concentration was below the limit of detection in 79% of samples. In summary, the findings of Maranchick et al. reinforce the use of fluoroquinolones in TB meningitis, but questions carbapenem's utility in the treatment of TB meningitis.

Continuing the search for drugs with penetration at disease-specific anatomic sites, the study by Deshpande et al. used the HFS-TB to determine the potential role of minocycline in the treatment of TB. The same study also tested several combinations of minocycline with tedizolid, moxifloxacin, and rifampin mimicking intrapulmonary PK of each drug. In addition, Deshpande et al. explored the possibility of an intermittent regimen by combining minocycline with tedizolid. Notably, the authors determined the intra-bacterial minocycline PK as a potential explanation for the effectiveness of the proposed once-a-week regimen. The authors proposed a hypothesis of "system hysteresis" as the basic mechanism of minocycline's extended efficacy against intracellular *Mtb* and termed it as "pharmacologic memory" allowing intermittent dosing of minocycline. The authors found that in the HFS-TB, the minocycline-containing once-a-week combination regimen was as

effective as daily therapy. Clinical validation of these findings is warranted.

While the development of new drugs and combination regimens is needed to further shorten both drug-susceptible and MDR-TB, identifying new methods to determine the drug efficacy is equally important to expedite the process. The study by Mockeliunas et al. describes a pharmacometric model-based approach that could be used in the clinical trials designed to determine the early bactericidal activity of the drugs. The authors used an estimate of MGIT-generated TTP slope, variability in TTP slope, impact of covariates, and drug PKs to link all these covariates with efficacy. The seven-step approach of this paper that employed the expertise of microbiologists, clinicians, and pharmacometricians could potentially be used to evaluate the EBA of monotherapies as well as combination regimens.

The culture of *Mtb* takes many weeks to grow. Therefore, alternative methods and biomarkers that can be used to measure the changes in the bacterial burden upon drug treatment are needed. The study by Alsoud et al. describes the role of TTP and CFU to develop a biomarker for TB drug development and to establish the efficacy of drugs in EBA studies. To develop a quantitative biomarker model for TTP and CFU to inform future EBA studies, paired TTP and CFU data from 83 patients with uncomplicated pulmonary TB receiving rifampicin monotherapy (dose range 10–40 mg/kg) was included. These patients were from the HIGHRIF1 study (Boeree et al., 2015). While the proposed PK-CFU-TTP model was able to identify the relationship between CFU and TTP, the data on the bacterial growth phase, and the difference in the growth rate of different *Mtb* metabolic subpopulations including nonreplicating persisters was not estimated. Further, the authors caution against extrapolation of their findings outside the range (10–40 mg/kg) as well as consideration of bacterial susceptibly and treatment duration when using such a modeling approach.

Finally, the study by Wasmann et al. addresses the treatment approach in special populations. This study describes the methods to develop a new dosing strategy to facilitate short-course regimens for TB meningitis in children, based on globally available new drug formulations. The authors simulated several dosing options in a virtual population of children using population PK modeling. We agree with the authors that the development of dosing strategies should be informed by efficacy, safety, and PK data. Similarly, the availability of age-appropriate drug formulations is important for program implementation considerations. Given the age and size, with a given mg/kg dose, the drug exposure predictions in children are more complex compared to adults. Therefore, it is important to consider developmental PK that can otherwise result in toxic or subtherapeutic concentrations. The authors also provided a simple MS Excel dosing tool to allow clinicians to develop the dosing strategy for TB meningitis in situations where a recommended formulation is not available.

Author contributions

All authors listed have made a substantial, direct, and intellectual contribution to the work and approved it for publication.

Conflict of interest

The authors declare that the research was conducted in the absence of any commercial or financial relationships that could be construed as a potential conflict of interest.

Publisher's note

References

Alffenaar, J. W. C., Stocker, S. L., Forsman, L. D., Garcia-Prats, A., Heysell, S. K., Aarnoutse, R. E., et al. (2022). Clinical standards for the dosing and management of TB drugs. *Int. J. Tuberc. Lung Dis.* 26, 483–499. doi:10.5588/ijtld.22.0188

Boeree, M. J., Diacon, A. H., Dawson, R., Narunsky, K., Du Bois, J., Venter, A., et al. (2015). A dose-ranging trial to optimize the dose of rifampin in the treatment of tuberculosis. *Am. J. Respir. Crit. Care Med.* 191, 1058–1065. doi:10.1164/rccm.201407-1264OC

Dheda, K., Lenders, L., Magombedze, G., Srivastava, S., Raj, P., Arning, E., et al. (2018). Drug-penetration gradients associated with acquired drug resistance in patients with tuberculosis. *Am. J. Respir. Crit. Care Med.* 198, 1208–1219. doi:10.1164/rccm.201711-2333OC

Gillespie, S. H., Crook, A. M., Mchugh, T. D., Mendel, C. M., Meredith, S. K., Murray, S. R., et al. (2014). Four-month moxifloxacin-based regimens for drug-sensitive tuberculosis. *N. Engl. J. Med.* 371, 1577–1587. doi:10.1056/NEJMoa1407426

Gumbo, T., Chapagain, M., Magombedze, G., Srivastava, S., Deshpande, D., Pasipanodya, J. G., et al. (2022). Novel tuberculosis combination regimens of two and three-months therapy duration. *bioRxiv* 2022, 484155.

Koch, R. (1882). Die atiologie der tuberkulose. *Berl. Klin. Wocheschrift* 15, 221–230.

Nahid, P., Mase, S. R., Migliori, G. B., Sotgiu, G., Bothamley, G. H., Brozek, J. L., et al. (2019). Treatment of drug-resistant tuberculosis. An official ATS/CDC/ERS/IDSA clinical practice guideline. *Am. J. Respir. Crit. Care Med.* 200, e93–e142. doi:10.1164/rccm.201909-1874ST

Srivastava, S., Magombedze, G., Koeuth, T., Sherman, C., Pasipanodya, J. G., Raj, P., et al. (2017). Linezolid dose that maximizes sterilizing effect while minimizing toxicity and resistance emergence for tuberculosis. *Antimicrob. Agents Chemother.* 61, e00751–e00717. doi:10.1128/AAC.00751-17

World Health Organizaton (2022). Rapid communication: Key changes to the treatment of drug-resistant tuberculosis. Switzerland: World Health Organizaton.

frontiers | Frontiers in Pharmacology

TYPE Original Research
PUBLISHED 14 October 2022
DOI 10.3389/fphar.2022.1023704

OPEN ACCESS

EDITED BY
Shashikant Srivastava,
University of Texas at Tyler,
United States

REVIEWED BY
Lisa Armitige,
The University of Texas Health Science Center at Tyler, United States
Amita Jain,
King George's Medical University, India
Yong-Soo Kwon,
Chonnam National University Medical School, South Korea

*CORRESPONDENCE
Dinh Hoa Vu,
vudinhhoa@gmail.com

SPECIALTY SECTION
This article was submitted to Pharmacology of Infectious Diseases, a section of the journal Frontiers in Pharmacology

RECEIVED 20 August 2022
ACCEPTED 26 September 2022
PUBLISHED 14 October 2022

CITATION
Nguyen TMP, Nguyen BH, Hoang TTT, Nguyen HA, Vu DH, Nguyen MH, Nguyen BN, Decroo T and Nguyen VN (2022), Safety and effectiveness of all-oral and injectable-containing, bedaquiline-based long treatment regimen for pre-XDR tuberculosis in Vietnam.
Front. Pharmacol. 13:1023704.
doi: 10.3389/fphar.2022.1023704

Safety and effectiveness of all-oral and injectable-containing, bedaquiline-based long treatment regimen for pre-XDR tuberculosis in Vietnam

Thi Mai Phuong Nguyen[1], Binh Hoa Nguyen[1], Thi Thanh Thuy Hoang[1], Hoang Anh Nguyen[2], Dinh Hoa Vu[2]*, Mai Hoa Nguyen[2], Bao Ngoc Nguyen[3], Tom Decroo[4] and Viet Nhung Nguyen[1]

[1]Vietnam National Lung Hospital, Hanoi, Vietnam, [2]National Drug Information and Adverse Drug Reaction Monitoring Centre, Hanoi University of Pharmacy, Hanoi, Vietnam, [3]School of Pharmacy, Memorial University of Newfoundland, John's, NL, Canada, [4]Institute of Tropical Medicine Antwerp, Antwerp, Belgium

Background: The World health organization (WHO) recently recommended standardized all-oral shorter regimens for rifampicin resistant Tuberculosis (RR-TB). For highly resistant Tuberculosis patients such as pre-XDR-TB: RR-TB plus additional resistance to fluoroquinolones (FQ), the 6–9-months bedaquiline (bedaquiline)-based regimens or BDQ-based long regimens are recommended. The role of second-line injectable (SLI) drugs in the treatment of drug resistant TB is restricted because of safety concerns. Nevertheless, it is not well-known how all-oral long regimens (BDQ-long) perform compared to SLI-containing long regimens (BDQ/SLI-long) in terms of safety and effectiveness among patients with highly resistant TB.

Method: A prospective observational cohort of patients with RR-TB additionally resistant to fluoroquinolones and/or second-line injectable, treated with either BDQ-long or BDQ/SLI-long regimens according to the guidance of the National Tuberculosis Program of Vietnam, enrolled between December 2015 and June 2017.

Results: Of 99 patients enrolled, 42 (42%) patients were treated with BDQ-long and 57 (57%) with BDQ/SLI-long. More than 85% of patients were previously exposed to both FQ and SLI. FQ and SLI resistance were confirmed in 28 (67%) and 41 (98%) in the BDQ-long cohort and 48 (84%) and 17 (30%) in the BDQ/SLI-long cohort, respectively. Treatment success was achieved among 29 (69%) and 46 (81%) patients on the BDQ-long and BDQ/SLI-long regimen, respectively (p = 0.2). For both regimens, median time to first smear/culture sputum conversion was 2 months. All patients experienced at least one adverse event (AE) and 85% of them had at least one severe Adverse events. The median time to a first severe adverse event was

2 months. Among patients treated with BDQ-long a higher proportion of patients had three QT-prolonging drugs in the regimen (26.2% versus 7.0%; p = 0.009). The severe prolonged QTcF was observed in 22 (52.4%) and 22 (38.6%) patients on BDQ-long and BDQ/SLI-long, respectively. Overall, 30 (30%) patients had to either temporary or permanently discontinued or more TB drugs due to AEs.

Conclusion: Treatment success was similar for both all-oral and SLI-containing BDQ-based long regimens in highly resistant TB patients. Both regimens had a similar high frequency of AEs. For both BDQ-long and BDQ/SLI-long regimens active AEs monitoring is essential.

KEYWORDS

pre-XDR TB treatment, all oral regimen, injectable secondline drug, QT prolongation, bedaquline

Introduction

Tuberculosis (TB) remains one of the most frequent, transmissible, life-threatening diseases globally, with high mortality and morbidity. Furthermore, the emergence of rifampicin resistant TB (RR-TB) has threatened global efforts in ending the disease. Treatment of RR-TB, especially in patients with more advanced resistance patterns such as pre-extensively drug-resistant tuberculosis (pre-XDR-TB) had poor outcomes until the recent introduction of bedaquiline (Abubakar et al., 2021). According to 2020 World Health Organization (WHO)'s global TB report, about 57% of patients with RR-TB were successfully treated and, compared to 47% of patients with pre-XDR-TB (World Health Organization, 2020). Vietnam is one of 30 high TB burden countries in the world, with high rates of RR-TB. In 2019, there were an estimated 170,000 new TB and 8,400 new RR-TB cases (World Health Organization, 2020). The prevalence of FQ resistance among patients with RR-TB was 16,7% (Nhung et al., 2015).

Over the last decade, WHO has issued a number of new guidelines for the management of RR-TB in order to improve the outcome and tolerability of RR-TB treatment regimens (World Health Organization, 2013; World Health Organization, 2014; World Health Organization, 2015; World Health Organization, 2016a; World Health Organization, 2016b; World Health Organization, 2020; Mirzayev et al., 2021; World Health Organization, 2022). RR-TB treatment regimens recommended by WHO have evolved from long (more than 18 months) injectable-containing regimens to shorter all-oral regimens (using bedaquiline [BDQ] instead of the injectable drugs). The most recent guidelines recommend the use of either 9–11-months all-oral BDQ-based regimen or a novel 6–9-months treatment regimen, which includes BDQ and a new drug, pretomanid (World Health Organization, 2022). For pre-XDR-TB patients, the novel 6–9 -month BPaL (BDQ, pretomanid and linezolid) regimen showed to be effective in a one-arm trial (Conradie et al., 2020) and has been recommended by WHO in the updated guidelines (World Health Organization, 2022). However, patients who were previously exposed to any component of BPaL are not eligible for this regimen. Additionally, given that pretomanid is not yet available in most settings, BDQ-based long regimens are recommended for these highly resistant patients (World Health Organization, 2020).

Since BDQ was introduced as a new and highly potential anti-TB drug (World Health Organization, 2013) a number of studies have been conducted to assess the outcomes of BDQ-based regimens for the treatment of drug-resistant TB. The majority of these studies were about RR-TB treatment while some focused-on smaller cohorts of pre-XDR-TB patients (Hatami et al., 2022). Overall, BDQ-containing regimens showed high culture conversion and treatment success rate among drug-resistant TB patients (Hatami et al., 2022). In its 2020 consolidated guidelines, WHO recommended the use of BDQ as a core drug in all-oral regimens to optimize treatment outcomes and minimize the toxicity of injectable agents (World Health Organization, 2020). However, in patients with more advanced resistance patterns (pre-XDR-TB), the choice of effective drugs is limited. Second-line injectables (SLIs) might still be an option as companion drugs to support and protect BDQ in the regimen (van Deun et al., 2018). Moreover, in drug-resistant TB patients with limited treatment options, the exclusion of injectable drugs may lead to a combination of drugs with a similar toxicity profile, for example when multiple QT prolonging drugs, such as fluoroquinolones, clofazimine, and bedaquiline, are used in the same regimen (Brust et al., 2021; Hughes et al., 2022). A number of previous studies described the effectiveness of BDQ-based regimens, with or without SLIs, but only treatment outcomes were assessed (Hatami et al., 2022). How all-oral long regimens (BDQ-long) perform compared to SLI-containing long regimens (BDQ/SLI-long) in terms of safety was less well described. To our best knowledge, no comparison has been made between all-oral

BDQ-based and injectable-containing BDQ-based regimens in terms of both safety and effectiveness.

In Vietnam, in addition to standardized regimens for RR-TB patients, individualized long regimens were indicated for patients with pre-XDR-TB and patients who did not tolerate one ore more components of the standardized RR-TB regimen. This study aimed to describe the effectiveness and safety of individualized BDQ based long regimens with and without SLI drug on pre-XDR-TB patients.

Methods

Study design

This prospective observational cohort study invovled pre-XDR-TB patients treated with BDQ-based long regimen in three sites including Ha Noi, Ho Chi Minh city and Can Tho between December 2015 and June 2017 under the treatment guidance of National Tuberculosis Program of Vietnam (NTP).

Setting and study population

Vietnam is a high TB and RR-TB burden country. In 2016, there were an estimated 126,000 new TB and 5,500 new RR-TB cases nationally, of which, only 2,450 RR-TB cases were enrolled on treatment. This study included RR-TB patients over 18 years of age, who had TB additionally resistant to either FQ (pre-XDR-TB) or SLI or both. Exclusion criteria included being at risk of cardiovascular complications (QTcF >500 ms), having end-stage of liver or renal diseases, being pregnant, or being a nursing mother.

RR-TB and pre-XDR-TB management

Xpert MTB/RIF (Cepheid Inc, Sunnyvale, CA, United States) was used for the diagnosis of RR-TB. Once diagnosed, RR-TB patients were screened for resistance to FQ by either genotypic (GenoType Hain MTBDRsl (Nehren, Germany); second-line line probe assay) or phenotypic drug susceptibility testing (DST). In addition, other drugs resistance including firstline drugs such as isoniazid, ethambutol, streptomycin, and SLIs including amikacin, capreomycin and kanamycin, were also assessed at baseline. After assessing eligibility, patients were registered and started on either the BDQ-long or BDQ/SLI-long treatment regimen, following WHO and national Programmatic Management of Drug resistant TB guidelines. In Vietnam, when this study was conducted, there were no short, standardized treatment options for pre-XDR-TB and/or SLI-resistant RR-TB. Such patients were put on individualized long regimens without new drugs (BDQ, delamanid or pretomanid). Only at our three study sites, BDQ-based long regimens were available. Based on the patients' treatment history and DST profile, the National Clinical Committee decided whether to put patients on the BDQ-long or BDQ/SLI-long regimen. In most cases, the patients were put on the BDQ-long regimen if their DST results showed resistance to secondline injectables. Nevertheless, 17/57 patients with initial resistance to one SLI but susceptible to another SLIs on phenotypic DST, were treated with the SLI (kanamycin or capreomycin) for which susceptibility had been shown (BDQ/SLI-long). For both groups, the total treatment duration was 20 months. SLI were provided during 8 months in injectable-containing regimen group. BDQ was used in 24 weeks. In case bacteriological and clinical response to treatment was poor, the use of BDQ was prolonged with an additional 4–8 weeks, following the decision of the National Clinical Committee. Patients were followed up monthly during treatment (clinical examination, smear, liquid culture BACTEC MGIT 960, chest Xray and other tests). ECG monitoring was three times per week during the first 2 weeks, once per week in the following 2 weeks and then monthly until the end of treatment (see Supplementary Table S1 for a detailed monitoring schedule). Patients were hospitalized during the first 1–2 months, then discharged for ambulatory management at district or commune levels. Adverse events (AEs) were managed and reported monthly following the cohort event monitoring (CEM) protocol as part of a prospective, observational, cohort study of AEs (Bao Ngoc et al., 2021; World Health Organization, 2012).

Study variables and definition

Exposure variables included patient age, sex, body mass index, resistance profile, previous TB drugs exposure, HIV and other co-morbidity status, and treatment regimen. Monthly sputum smear and culture results were used to determine the month of conversion. Based on WHO and national guidelines, treatment outcomes were grouped as favorable (cured or treatment completed) and unfavorable (treatment failure, died, or lost-to-follow-up [LTFU]). For the safety analysis, all abnormal clinical symptoms and test results were recorded and reported during treatment using CEM reports. Grading of AEs was based on the "Table of Grading the Severity of Adult and Pediatric Adverse Events, version 2.0" (November 2014) of the U.S National Institute of Allergy and Infectious disease (US Department of Health and Human Services et al., 2014). Grade 3 and 4 adverse events were reported as severe AEs. Serious AEs (SAEs) included any death, hospitalization, life-threatening AE, permanently disability or any grade 4 AEs. Severe prolonged QTcF was defined as QTcF >500 ms or an increase of 60 ms compared to the baseline QTcF value. To assess potential drug-drug

TABLE 1 Patient characteristics by regimen.

Patient characteristics	Total (N = 99)		BDQ-long (n = 42)		BDQ/SLI-long (n = 57)		p value
	Mean	SD	Mean	SD	Mean	SD	
Age (year)	43.5	(13.9)	42.8	(10.7)	44.0	(15.9)	0.673
Body mass index (kg/m^2)	18.4	(3.3)	18.3	(3.0)	18.4	(3.6)	0.828
Follow-up time (months)	17.4	(4.9)	16.7	(5.3)	17.8	(4.7)	0.292
	n	(%)	*n*	(%)	*n*	(%)	
Male	71	(71,7)	29	(69.0)	42	(73.7)	0.613
Resistance to any SLID	58	(58.6)	41	(97.6)	17	(29.8)*	<0.001
Resistance to FQ	76	(76.8)	28	(66.7)	48	(84.2)	0.041
Previous SLID treatment	86	(86.7)	37	(88.1)	49	(86.0)	0.756
Previous FQ treatment	85	(86.9)	36	(85.7)	49	(86.6)	0.972
Asthenia	23	(23,2)	12	(28.6)	11	(19.3)	0.280
Smoking	12	(12.1)	5	(11.9)	7	(12.3)	0.955
Alcohol dependence	5	(5.1)	2	(4.8)	3	(5.3)	1.000
Co-morbidities							
At least one co-morbidity	43	(43.4)	17	40.5	26	45.6	0.610
Diabetes	22	(22.2)	10	(23.8)	12	(21.1)	0.744
Peptic ulcer	9	(9.1)	2	(4.8)	7	(13.5)	0.294
Hepatitis	7	(7.1)	4	(9.5)	3	(5.3)	0.453
Osteoarthritis	5	(5.1)	1	(2.4)	4	(7.0)	0.392
Anemia	5	(5.1)	2	(4.8)	3	(5.3)	1.000
COPD	5	(5.1)	1	(2.4)	4	(7.0)	0.392
HIV infection	3	(3.0)	2	(4.8)	1	(1.8)	0.573
Renal failure	2	(2.0)	1	(2.4)	1	(1.8)	1.000
Initial Treatment Regimens							
Secondline injectables	57	(57.6)	0	(0.0)	57	(100.0)	NA
Kanamycin	34	(34.3)	0	(0.0)	34	(59.6)	NA
Capreomycin	23	(23.2)	0	(0.0)	23	(40.4)	NA
Bedaquiline	99	(100.0)	42	(100.0)	57	(100.0)	NA
Levofloxacin	16	(16.2)	10	(23.8)	6	(10.5)	0.076
Linezolid	58	(58.6)	36	(85.7)	22	(38.6)	<0.001
Clofazimine	86	(86.9)	41	(97.6)	45	(78.9)	0.007
Cycloserin	24	(24.2)	8	(19.0)	16	(28.1)	0.301
Pyrazinamide	90	(90.9)	40	(95.2)	50	(87.7)	0.294
Prothionamide	51	(51.5)	21	(50.0)	30	(52.6)	0.796
P-aminosalicyclic acid	34	(34.3)	20	(47.6)	14	(24.6)	0.017
Ethambutol	14	(14.1)	6	(14.3)	8	(14.0)	0.972
High dose Isoniazid	5	(5,1)	0	(0.0)	5	(8.8)	0.070
Potential QT prolongation drug—drug interactions							
LFX_CFZ_BDQ	15	(15.2)	11	(26.2)	4	(7.0)	0.009
LFX_BDQ	19	(19.2)	12	(28.6)	7	(12.3)	0.042
CFZ_BDQ	88	(88.9)	41	(97.6)	47	(82.5)	0.022
Microbiology							
Positive AFB	60	(60.6)	25	(59.5)	35	(61.4)	0.850
Positive culture	76	(76.8)	30	(71.4)	46	(80.7)	0.280

SD, standard deviation; SLI, second-line injectable; FQ, fluoroquinolone; COPD, chronic obstructive pulmonary disease; HIV, human immunodeficiency virus; WHO, world health organization; BDQ, bedaquiline; LFX, levofloxacin; CFZ, clofazimine; AFB, Acid-fast bacillus.

*17/57 patients with initial resistance to one SLI, but susceptible to another SLI, were treated with the SLI, for which susceptibility had been shown.

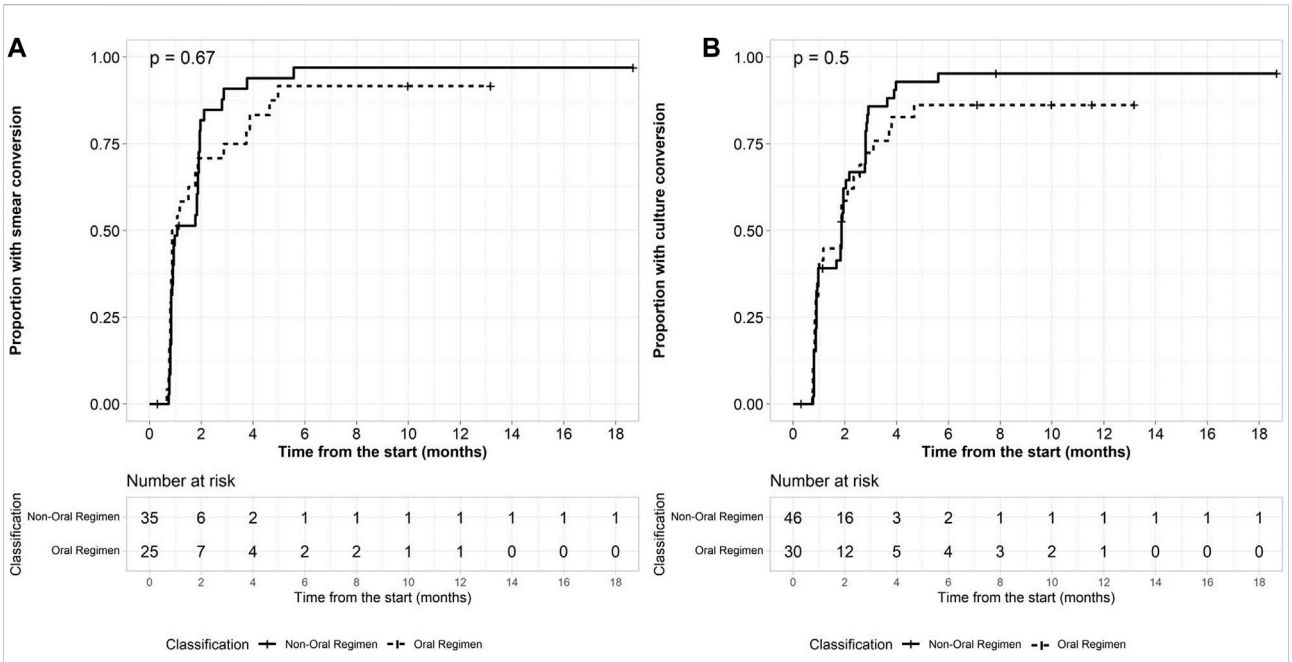

FIGURE 1
Baseline load predicts conversion. **(A)** Time to smear conversion in patients with positive microbiology **(B)** Time to culture conversion in patients with positive microbiology.

TABLE 2 Treatment outcome of BDQ-based regimens in the treatment of pre-XDR-TB.

	BDQ-long (*N* = 42)		BDQ/SLI—long (*N* = 57)		Total (*N* = 99)	
	n	(%)	*n*	(%)	*n*	(%)
Favorable outcome	29	(69.0)	46	(80.7)	75	(75.8)
Cured	24	(57.1)	38	(66.7)	62	(62.6)
Completed	5	(11.9)	8	(14.0)	13	(13.1)
Unfavorable outcome	13	(31.0)	11	(19.3)	24	(24.2)
Failure	1	(2.4)	1	(1.8)	2	(2.0)
Lost to follow up	8	(19.0)	7	(12.3)	15	(15.2)
Death	4	(9.5)	3	(5.3)	7	(7.1)

interactions that can cause QT prolongation we counted the number of drugs included in each of the regimens that were also listed on the CredibleMeds' QT drugs list (Woosley et al., 2022).

Data collection and analyses

Pre-designed paper forms were developed to collect data from the patient's medical records, including baseline patient information form; monthly clinical and bacteriological follow-up forms; and CEM forms. Then, the data collected was entered in the Microsoft Access 2013 database for further analysis. Frequencies and proportions were used to summarise categorical variables; medians and interquartile ranges were used to summarise continuous variables. The chi-square test was used to assess associations between exposure and outcome variables, a multivariable regression model was used to find predictors of having an unfavorable outcome. We used Kaplan Meier curves to visualize the probability of events (time to the first severe adverse event, time to drug discontinuation and time to sputum smear/culture conversion) during treatment. The Log-rank test was conducted to compare the time-to-event between different groups. A *p*-value less than 0.05 was considered statistically significant. Data analyses were performed using software R 3.4.4.

TABLE 3 Number of patients with severe AE by regimen.

	Total (N = 99)		BDQ-long (N = 42)		BDQ/SLI-long (N = 57)		p value
	n	(%)	n	(%)	n	(%)	
At least one severe AE	84	(84.8)	36	(85.7)	48	(84.2)	0.841
At least two severe AE	51	(51.5)	18	(42.9)	33	(57.9)	0.139
At least three severe AE	22	(22.2)	10	(23.8)	12	(21.1)	0.740
Heart rate disorders (prolonged QTcF)	44	(44.4)	22	(52.4)	22	(38.6)	0.172
Metabolic disorders	32	(32.3)	12	(28.6)	20	(35.1)	0.493
Hyperglycemia	18	(18.2)	8	(19)	10	(17.5)	0.842
Hypoglycemia	4	(4)	2	(4.8)	2	(3.5)	1.000
Hyperuricemia	15	(15.2)	5	(11.9)	10	(17.5)	0.238
Liver and biliary disorders	27	(27.3)	13	(31.0)	14	(24.6)	0.480
Increased direct bilirubin	23	(23.2)	10	(23.8)	13	(22.8)	0.920
Hepatitis	11	(11.1)	6	(14.3)	5	(8.8)	0.520
Electrolyte disturbances	18	(18.2)	8	(19.0)	10	(17.5)	0.841
Hypocalcemia	6	(6.1)	2	(4.8)	4	(7)	0.700
Hypomagnesemia	4	(4)	2	(4.8)	2	(3.5)	1.000
Hyperkalemia	2	(2)	1	(2.4)	1	(1.8)	1.000
Hypokalemia	8	(8.1)	4	(9.5)	4	(7)	1.000
Hematologic disorders	10	(10.1)	6	(14.3)	4	(7)	0.315
Gastrointestinal disorders	6	(6.1)	3	(7.1)	3	(5.3)	1.000
Vision disorders	6	(6.1)	3	(7.1)	3	(5.3)	1.000
Renal disorders (increased creatinine)	4	(4)	0	(0.0)	4	(7)	0.135
Hearing disorders	3	(3)	0	(0.0)	3	(5.3)	0.260
Psychiatric disorders	2	(2)	0	(0.0)	2	(3.5)	0.506
Any neurological disorders	2	(2.0)	0	(0.0)	2	(3.5)	0.506
Central nervous system disorders	1	(1)	0	(0.0)	1	(1.8)	1.000
Peripheral neuropathy	1	(1)	0	(0.0)	1	(1.8)	1.000
Muscoloskeletal disorders (arthralgia)	1	(1)	0	(0.0)	1	(1.8)	1.000
Anaphylactic reactions	1	(1)	0	(0.0)	1	(1.8)	1.000

AE, adverse event; AST, aspartate aminotransferase; ALT, alanine aminotransferase; QTcF, QT, interval corrected for heart rate using Fridericia's formula.

Ethics approval

Ethical approval of this study was obtained from the Independent Ethic Committee of the Ministry of Health and National Lung hospital in Vietnam. Written informed consent was obtained from all studied patients.

Results

Patient characteristics

Baseline characteristics of 99 eligible patients are shown in Table 1. Of those, 42 (42.4%) were on the BDQ-long and 57 (57.6%) were on the BDQ/SLI-long regimens, respectively. The mean age of patients was 43.5 years. More than two thirds were male. In both groups, the initial treatment regimen contained a median of 5 (interquartile range [IQR] = 5–6) anti TB drugs. Overall, 76 (76.8%) patients had confirmed resistance to FQ (pre-XDR-TB), with 66.7% in the BDQ-long and 84.2% in the BDQ/SLI-long regimen group, respectively. The majority of patients were exposed previously to FQ (86.9%) and SLI (86.7%). A baseline positive culture was recorded in 71.4% of patients (n = 30) treated with BDQ-long and 80.7% of patients (n = 47) treated with the BDQ/SLI-long regimen.

Eleven (26.2%) patients in all-oral regimen group had the combination of BDQ with both levofloxacin (LFX) and clofazimine (CFZ) in the regimen while only 4 (7.0%) of patients in the other group had BDQ plus both drugs (p = 0.009).

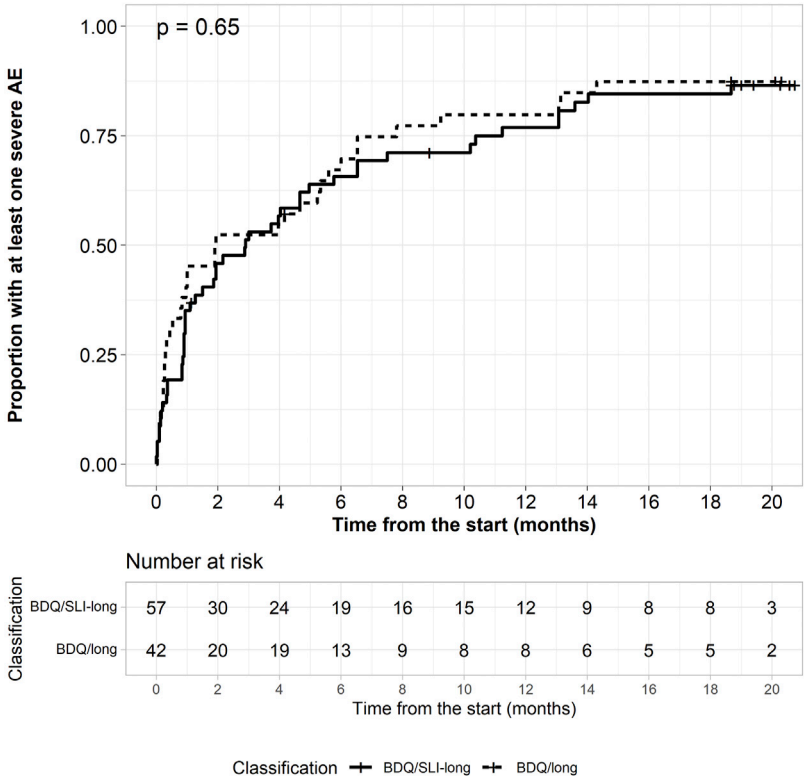

FIGURE 2
Kaplan-Meier plot for time to the first severe adverse event.

Treatment outcome

Bacteriological response was assessed in 76 patients with a positive culture sputum at baseline. Culture conversion at 2 months was achieved in 18 of 30 (60.0%) patients on BDQ-long and 30 of 46 (65.2%) patients on BDQ/SLI-long (p = 0.5). After 6 months of treatment, 86.7% (n = 26) and 95.7% (n = 44) patients culture converted in the BDQ-long and BDQ/SLI-long cohort (Figure 1). Treatment success was achieved among 29 (69.0%) and 46 (80.7%) patients of the BDQ-long and BDQ/SLI-long cohort (Table 2). The proportion with a favorable outcome was not significantly different between the 2 treatment groups (p = 0.2). No predictors having significant association with the favorable/unfavorable outcomes were found.

Adverse events

All 99 (100%) patients experienced at least one AE (grade 1–4) during their treatment, with a median of 7 (IQR: 5–10) AEs per patients. The proportion of patients having at least one severe AE (grade 3–4) was 85.7% (36/42) in the BDQ-long and 84.2% (48/57) in the BDQ/SLI-long cohort (Table 3). QT prolongation, metabolic disorders (hyper/hypoglycemia, hyperuricemia), liver function disorder, and electrolyte abnormalities were the most common severe AEs. There was no significant difference between the 2 regimens in relation to these abnormalities. Severe prolonged QTcF (defined as QTcF >500 ms or an increase of 60 ms compared to baseline) appeared in 44 (44.4%) patients. It occured in 22 (52.4%) patients treated with BDQ-long and 22 (38.6%) patients treated with the BDQ/SLI-long regimen. About half of patients with a first severe AE experienced it during the first 2 months of treatment (Figure 2). Serious AEs (SAE) were observed in 16 (38%) and 28 (49%) of those on BDQ-long and BDQ/SLI-long, respectively (p = 0.28) (Supplementary Table S2).

Overall, 30 (30.3%) patients had to either temporary or permanently discontinue one or more TB drugs due to AE. Of group A drugs, linezolid (LZD) was discontinued most often: in 14.5% (11/76) patients having this drug in their regimen, compared to 7.1% (7/99) for bedaquiline and 3% (3/99) for fluroquinolone. Other drugs which were temporarily or permanently stopped in more than 13% of patients included ethambutol (14.3%, 2/14), SLI (14%, 8/57), cycloserine (13.5%, 5/37), p-aminosalysilic acid (13.3%, 6/45), and prothionamide (13.2%, 7/53) (Table 4). Regarding dose adjustment, 7 patients needed to reduce the dose of SLI because of electrolyte

TABLE 4 Consequences of adverse events.

	Temporary or permanent		Permanent		Reasons for permanent discontinuation
	n	(%)	*n*	(%)	
Group A					
BDQ (*n* = 99)	7	(7.1)	3	(3.0)	Prolonged QTcF (*n* = 1), Gastrointestinal disorders (*n* = 1), Hepatitis (*n* = 1)
FQ (*n* = 21)	1	(4.8)	0	(0.0)	No
LZD (*n* = 76)	11	(14.5)	4	(5.3)	Prolonged QTcF (*n* = 1), Visual impairment (*n* = 2), Hepatitis (*n* = 1)
Group B					
CFZ (*n* = 94)	10	(10.6)	2	(2.1)	Prolonged QTcF (*n* = 1), Visual impairment (*n* = 2)
CS (*n* = 37)	5	(13.5)	2	(5.4)	Central nervous system disorders (*n* = 1), Psychiatric disorders (*n* = 1), Anaphylactic reactions (*n* = 1)
Group C					
PZA (n = 92)	6	(6.5)	4	(4.3)	Increased AST (*n* = 1), Gastrointestinal disorders (*n* = 1), Arthralgia (*n* = 1), Hepatitis (*n* = 2), Increased ALT (*n* = 1)
PTO (*n* = 53)	7	(13.2)	4	(7.5)	Increased AST (*n* = 1), Gastrointestinal disorders (*n* = 2), Psychiatric disorders (*n* = 1), Hepatitis (*n* = 1), Increased ALT (*n* = 1)
PAS (*n* = 45)	6	(13.3)	3	(6.7)	Gastrointestinal disorders (*n* = 2), Arthralgia (*n* = 1), Hepatitis (*n* = 1)
EMB (*n* = 14)	2	(14.3)	1	(7.1)	Gastrointestinal disorders (*n* = 1)
hINH (*n* = 12)	0	(0.0)	0	(0.0)	No
SLI (*n* = 57)	8	(14.0)	3	(5.3)	Hypokalemia (*n* = 1), Increased creatinine (*n* = 2), Peripheral neuropathy (*n* = 1), Hypomagnesemia (*n* = 1)

BDQ, bedaquiline; FQ, fluoroquinolone; LZD, linezolid; CFZ, clofazimine; CS, cycloserin; PZA, pyrazinamide; PTO, prothionamide; PAS, acid para-aminosalicylic; EMB, ethambutol; hINH, high dose isoniazid; SLI, second line injectable; AST, aspartate aminotransferase; ALT, alanine aminotransferase; QTcF, QT, interval corrected for heart rate using Fridericia's formula.

disturbances, increased creatinine and amylase, while the dose of LZD was reduced in 2 patients with hematologic disorders.

No difference in terms of time to severe AE was observed between the two cohorts. Figure 3 shows the time to drug interruption (either temporarily or permanently) of both regimens, in the first 6 months of treatment: 6 (14.3%) patients in the BDQ-long group had to stop drugs due to AE compared to 15 (26.3%) on BDQ/SLI-long ($p = 0.76$). Median time to drug interruption in BDQ-long group was 6.4 months (IQR: 0.2–10.5) while it was 1 month (IQR: 0.2–5.5) in the other group ($p = 0.09$).

Discussion

This cohort study of BDQ-based long regimens did not only assess the overall safety and effectiveness of BDQ-based long regimens among pre-XDR-TB patients but also determined the effect of regimen choice (BDQ-long or BDQ/SLI-long) on the QT prolongation effect, timing of having a severe AEs, drug discontinuation and time to conversion. To our best knowledge, this was the first comparison which has been made between all-oral and injectable-containing BDQ-based regimens in terms of both effectiveness and safety.

Regarding effectiveness assessment, compared to the globally reported 47% treatment success among patients treated for pre-XDR-TB (World Health Organization, 2020), BDQ-based long treatment regimens in this study showed high effectiveness among patients with highly resistant TB. Treatment success was similar for both BDQ-long and BDQ/SLI-long regimens. Overall, 76% success rate for BDQ-based long regimens among highly resistant TB was comparable with findings different settings (Barvaliya et al., 2020; Hatami et al., 2022; Ndjeka et al., 2018). In comparison with the reported treatment success rate of 47% among pre-XDR-TB patients in the program in Vietnam at the same period (Annual NTP report, 2019), the outcomes for BDQ-based long regimens reported in this study were superior. BDQ-based treatment should be used in all patients with highly resistant TB. The proportion with a favorable outcome was not significantly different between the BDQ-long and BDQ/SLI-long groups. Our sample size was not big enough to detect relatively small differences.

The reason that WHO recommends to restrict the use of SLI drugs in drug resistant TB was the concern about its high risk of ototoxicity and nephrotoxicity (Buziashvili et al., 2019; Shibeshi et al., 2019). Nevertheless, with an active drug safety monitoring system (aDSM), the early detection and management of AEs could

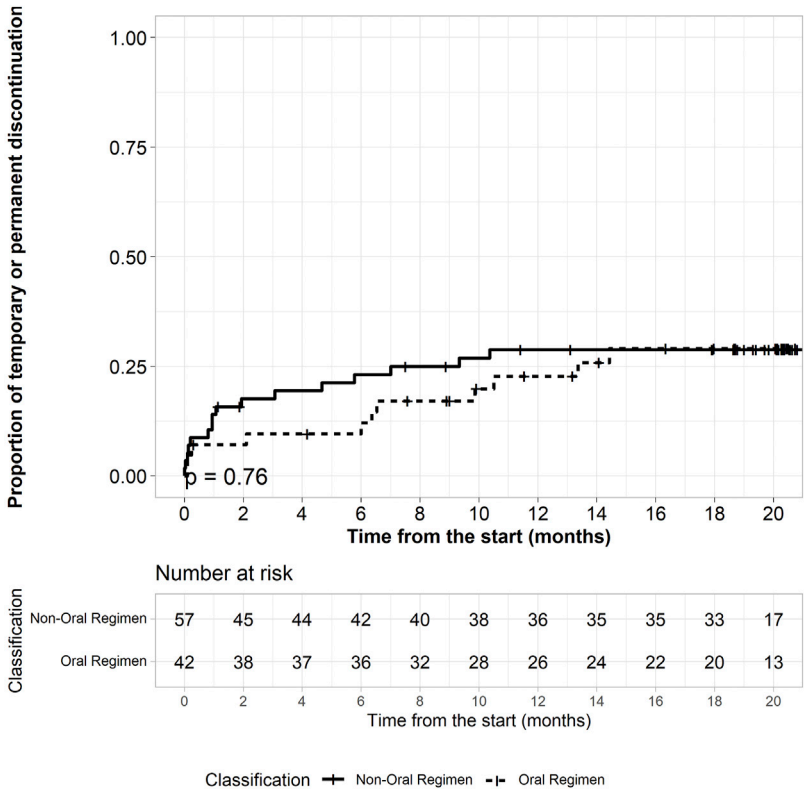

FIGURE 3
Time to temporary or permanent drug discontinuation by regimen.

mitigate eventual grave long-term consequences (World Health Organization, 2012; WHO, 2015). Taking into account the modest number of effective drugs left for pre-XDR-TB patients, SLI may still have a role to play, as long as its toxicity were adequately monitored. SLI can protect effective core drugs (such as BDQ, FQ) during the initial treatment period (van Deun et al., 2018), and prevent acquired resistance. Our sample was too small to assess this rare but important treatment outcome.

Both all-oral and SLI-containing BDQ-based long regimens had a similar high frequency of AEs as the proportion of patients having at least one severe AEs (grade 3–4) were 85.7% in BDQ-long and 84.2% in BDQ/SLI-long regimen. There was no significant difference between the two groups in terms of severe and serious QT prolongation. However, this AE tended to be more frequent in the BDQ-long group (52.4% with severe QT prolongation) in comparison with 38.6% in the BDQ/SLI-long group. This might be due to the difference in number of drugs with QT prolonging effect, as a significantly higher proportion of patients on BDQ-long had 3 QT prolonging drugs in the regimen, as the result of not using SLI in all-oral regimen. The combination of 3 anti-TB drugs with risk of QT prolongation (LFX_CFZ_BDQ) (Woosley et al., 2022) appeared in 26.2% (n = 11) of patients in the BDQ-long group, but only in 7.0% (n = 4) of patients in the BDQ/SLI-long group (p = 0.009). When constructing pre-XDR-TB regimens, it is essential to consider the effectiveness and safety of not only a single drug but also the combination of drugs. Other drugs than SLI can also cause severe AE (Borisov et al., 2019; Khan et al., 2022). Of WHO's group A drugs, LZD was discontinued in 14.5% of patients having this drug in their regimen more often than other group A drugs (BDQ, LFX). The use of LZD increased significantly, as a substitute for SLI, and also as component of recently recommended RR-TB and pre-XDR-TB treatment regimens (BPaLM and BPaL) (World Health Organization, 2022). Subsequently, AEs and SAEs known to be caused by this drug, more specifically hematological and neurological AE, will also increase (Borisov et al., 2019; Sotgiu et al., 2012). Hence, even though all-oral BDQ-based long regimens can prevent toxicity due to injectable agents, active AE monitoring is still essential for these regimens.

There was no significant difference between BDQ-long and BDQ/SLI-long regimens groups in terms of time to severe AEs/SAEs and time to drug discontinuation. However, the BDQ/SLI-long regimen tended to have earlier drug interruption than BDQ-long regimen group. Median time to drug interruption in BDQ/SLI-long group was 1 month (IQR: 0.2–5.5) while it was 6.4 months (IQR: 0.2–10.5) in the other group (p = 0.09). Active drug safety

monitoring using the CEM protocol resulted in an early detectionand informed the management of adverse effects that occured during treatment. Our previous study revealed that the risk of SLI related nephrotoxicity was associated with SLI dosing (Bao Ngoc et al., 2021). Therefore, the optimization of the dose of SLI should be considered to minimize the risk of toxicity. For LZD, neurological toxicity (peripheral and optic neuropathy) was usually seen after several months of use, median 5 months in the study by (Narita et al., 2007), thus, this drug could be considered for a limited time only, during the early treatment phase when high bactericidal activity is mostly required (van Deun et al., 2018).

We acknowledge that this study has its own strengths and limitations. One of the strengths was the use of the CEM protocol to prospectively record and report the AEs of patients during their entire treatment course, s (World Health Organization, 2012). Therefore, the safety information of all treatment regimens was well-captured, even for mild to moderate AEs, which were often under-reported by other studied reporting AEs (Borisov et al., 2019). The prospective design also led to comprehensive monitoring and rigorous data collection and cleaning. The limitation of our study was the relatively small sample size. Differences between the two regimens may have remained undetected. Moreover, multivariate analysis was not appropriate, and confounders could not be controlled for.

Conclusion

Treatment success was similar for both all-oral and SLI-containing BDQ-based long regimens in patients with highly resistant TB. Both regimens had a similar high frequency of AEs. For both BDQ-long and BDQ/SLI-long regimens, active AEs monitoring is essential.

Data availability statement

The raw data supporting the conclusion of this article will be made available by the authors, without undue reservation.

Ethics statement

The studies involving human participants were reviewed and approved by Independent Ethic Committee (IEC), Ministry of Health, Vietnam. The patients/participants provided their written informed consent to participate in this study.

Author contributions

TN, BN, TH, HN, DV, MN, TD, and VN contributed to conception and design of the study. TN, MN, and BN conducted the investigation, data collection and organized the database. BN performed the statistical analysis. TN wrote the first draft of the manuscript. All authors contributed to manuscript revision, read, and approved the submitted version.

Funding

The Global Fund and Clinton Health Access Initiative (CHAI) Vietnam.

Acknowledgments

We would like to acknowledge the great contribution of the Global Fund for their financial support through the NTP to provide diagnosis and treatment service to all RR-TB patients in Vietnam; CHAI Vietnam for their technical support in the study.

Conflict of interest

The authors declare that the research was conducted in the absence of any commercial or financial relationships that could be construed as a potential conflict of interest.

Publisher's note

Supplementary material

The Supplementary Material for this article can be found online at: https://www.frontiersin.org/articles/10.3389/fphar.2022.1023704/full#supplementary-material

References

Abubakar, M., Ahmad, N., Ghafoor, A., Latif, A., Ahmad, I., Atif, M., et al. (2021). Treatment outcomes of extensively drug-resistant tuberculosis in Pakistan: A countrywide retrospective record review. *Front. Pharmacol.* 12, 640555. doi:10.3389/fphar.2021.640555

Bao Ngoc, N., Vu Dinh, H., Thi Thuy, N., van Quang, D., Thi Thu Huyen, C., Mai Hoa, N., et al. (2021). Active surveillance for adverse events in patients on longer treatment regimens for multidrug-resistant tuberculosis in Viet Nam. *PLoS One* 16, e0255357. doi:10.1371/journal.pone.0255357

Barvaliya, S. v., Desai, M. K., Panchal, J. R., and Solanki, R. N. (2020). Early treatment outcome of bedaquiline plus optimised background regimen in drug resistant tuberculosis patients. *Indian J. Tuberc.* 67 (2), 222–230. doi:10.1016/j.ijtb.2020.03.002

Borisov, S., Danila, E., Maryandyshev, A., Dalcolmo, M., Miliauskas, S., Kuksa, L., et al. (2019). Surveillance of adverse events in the treatment of drug-resistant tuberculosis: First global report. *Eur. Respir. J.* 54, 1901522. doi:10.1183/13993003.01522-2019

Brust, J. C., Gandhi, N. R., Wasserman, S., Maartens, G., v Omar, S., Ismail, N. A., et al. (2021). Effectiveness and cardiac safety of bedaquiline-based therapy for drug-resistant tuberculosis: A prospective cohort study. *Clin. Infect. Dis.* 73 (11), 2083–2092. doi:10.1093/cid/ciab335

Buziashvili, M., Mirtskhulava, V., Kipiani, M., Blumberg, H. M., Baliashvili, D., Magee, M. J., et al. (2019). Rates and risk factors for nephrotoxicity and ototoxicity among tuberculosis patients in Tbilisi, Georgia. *Int. J. Tuberc. Lung Dis.* 23 (9), 1005–1011. doi:10.5588/ijtld.18.0626

Conradie, F., Diacon, A. H., Ngubane, N., Howell, P., Everitt, D., Crook, A. M., et al. (2020). Treatment of highly drug-resistant pulmonary tuberculosis. *N. Engl. J. Med.* 382 (10), 893–902. doi:10.1056/nejmoa1901814

Hatami, H., Sotgiu, G., Bostanghadiri, N., Abadi, S. S. D., Mesgarpour, B., Goudarzi, H., et al. (2022). Bedaquiline-containing regimens and multidrug-resistant tuberculosis: A systematic review and meta-analysis. *J. Bras. Pneumol.* 48 (2), e20210384. doi:10.36416/1806-3756/e20210384

Hughes, G., Bern, H., Chiang, C.-Y., Goodall, R. L., Nunn, A. J., Rusen, I. D., et al. (2022). QT prolongation in the STREAM stage 1 trial. *Int. J. Tuberc. Lung Dis.* 26 (4), 334–340. doi:10.5588/ijtld.21.0403

Khan, F. U., Khan, A., Khan, F. U., Hayat, K., Rehman, A. ur., Chang, J., et al. (2022). Assessment of adverse drug events, their risk factors, and management among patients treated for multidrug-resistant TB: A prospective cohort study from Pakistan. *Front. Pharmacol.* 13, 876955. doi:10.3389/fphar.2022.876955

Mirzayev, F., Viney, K., Linh, N. N., Gonzalez-Angulo, L., Gegia, M., Jaramillo, E., et al. (2021). World health organization recommendations on the treatment of drug-resistant tuberculosis, 2020 update. *Eur. Respir. J.* 57, 2003300. doi:10.1183/13993003.03300-2020

Narita, M., Tsuji, B. T., and Yu, V. L. (2007). Linezolid-associated peripheral and optic neuropathy, lactic acidosis, and serotonin syndrome. *Pharmacotherapy* 27 (8), 1189–1197. doi:10.1592/phco.27.8.1189

Ndjeka, N., Schnippel, K., Master, I., Meintjes, G., Maartens, G., Romero, R., et al. (2018). High treatment success rate for multidrug-resistant and extensively drug-resistant tuberculosis using a bedaquiline-containing treatment regimen. *Eur. Respir. J.* 52, 1801528. doi:10.1183/13993003.01528-2018

Nhung, N. v., Hoa, N. B., Hennig, C. M., and Dean, A. S. (2015). The fourth national anti-tuberculosis drug resistance survey in Viet Nam. *Int. J. Tuberc. Lung Dis.* 19, 670–675. doi:10.5588/ijtld.14.0785

Shibeshi, W., Sheth, A. N., Admasu, A., Berha, A. B., Negash, Z., and Yimer, G. (2019). Nephrotoxicity and ototoxic symptoms of injectable second-line anti-tubercular drugs among patients treated for MDR-TB in Ethiopia: A retrospective cohort study. *BMC Pharmacol. Toxicol.* 20, 31. doi:10.1186/s40360-019-0313-y

Sotgiu, G., Centis, R., D'Ambrosio, L., Alffenaar, J. W. C., Anger, H. A., Caminero, J. A., et al. (2012). Efficacy, safety and tolerability of linezolid containing regimens in treating MDR-TB and XDR-TB: Systematic review and meta-analysis. *Eur. Respir. J.* 40 (6), 1430–1442. doi:10.1183/09031936.00022912

US Department of Health and Human Services, ; National Institutes of Health, ; National Institute of Allergy and Infectious Diseases (2014), Division of AIDS table for grading the severity of adult and pediatric adverse events Version 2.0. November 2014. Available at: https://rsc.niaid.nih.gov/sites/default/files/daids-ae-grading-table-v2-nov2014.pdf

van Deun, A., Decroo, T., Piubello, A., de Jong, B. C., Lynen, L., Rieder, H. L., et al. (2018). Principles for constructing a tuberculosis treatment regimen: The role and definition of core and companion drugs. *Int. J. Tuberc. Lung Dis.* 22 (3), 239–245. doi:10.5588/ijtld.17.0660

WHO (2015). Companion handbook to the WHO guidelines for the programmatic management of drug-resistant tuberculosis. Geneva, Switzerland. Available at: http://apps.who.int/iris/bitstream/10665/130918/1/9789241548809_eng.pdf?ua=1&ua=1.

Woosley, R., Heise, C., Gallo, T., Tate, J., Woosley, D., Romero, K., et al. (2022). QTdrugs list. Available at: www.CredibleMeds.org (accessed August 17, 2022).

World Health Organization (2012). A practical handbook on the pharmacovigilance of medicines used in the treatment of tuberculosis enhancing the safety of the TB patient. Available at: https://apps.who.int/iris/handle/10665/336226.

World Health Organization (2015). Framework for implementation active tuberculosis drug-safety monitoring and management (ADSM). Available at: https://www.who.int/publications/i/item/WHO-HTM-TB-2015.28 (accessed August 17, 2022).

World Health Organization (2020a). *Global tuberculosis report 2020*. Geneva, Switzerland: World Health Organization.

World Health Organization (2016a). Interim policy - the use of delamanid in the treatment of multidrug-resistant tuberculosis in children and adolescents. Available at: https://apps.who.int/iris/handle/10665/250614.

World Health Organization (2022). Rapid communication: Key changes to the treatment of drug-resistant tuberculosis. Available at: https://www.who.int/about/licensing.

World Health Organization (2013). *The use of bedaquiline in the treatment of multidrug-resistant tuberculosis, interim policy guidance*. Geneva, Switzerland: World Health Organization.

World Health Organization (2014). The use of delamanid in the treatment of multidrug-resistant tuberculosis: Interim policy guidance. 1–65. Available at: http://apps.who.int/iris/bitstream/10665/137334/1/WHO_HTM_TB_2014.23_eng.pdf.

World Health Organization (2020b). Geneva, Switzerland: World Health Organization.WHO consolidated guidelines on tuberculosis. Module 4: Drug-resistant tuberculosis treatment.

World Health Organization (2016b). WHO treatment guidelines for drug-resistant tuberculosis 2016 update. Available at: https://www.who.int/publications/i/item/9789241549639 (accessed June 17, 2022).

frontiers | Frontiers in Pharmacology

TYPE Original Research
PUBLISHED 18 October 2022
DOI 10.3389/fphar.2022.1024608

OPEN ACCESS

EDITED BY
Emmanuel Abraham Mpolya,
Nelson Mandela African Institution of Science and Technology, Tanzania

REVIEWED BY
Damian Kajunguri,
Kabale University, Uganda
Peter Mbelele,
Kibong'oto Infectious Diseases Hospital (KIDH), Tanzania

*CORRESPONDENCE
Tawanda Gumbo,
rozvi1@praedicareinc.com

SPECIALTY SECTION
This article was submitted to Pharmacology of Infectious Diseases, a section of the journal Frontiers in Pharmacology

RECEIVED 22 August 2022
ACCEPTED 30 September 2022
PUBLISHED 18 October 2022

CITATION
Deshpande D, Srivastava S, Pasipanodya JG and Gumbo T (2022), Minocycline intra-bacterial pharmacokinetic hysteresis as a basis for pharmacologic memory and a backbone for once-a-week pan-tuberculosis therapy.
Front. Pharmacol. 13:1024608.
doi: 10.3389/fphar.2022.1024608

Minocycline intra-bacterial pharmacokinetic hysteresis as a basis for pharmacologic memory and a backbone for once-a-week pan-tuberculosis therapy

Devyani Deshpande[1], Shashikant Srivastava[2], Jotam Garaimunashe Pasipanodya[3] and Tawanda Gumbo[3,4]*

[1]Baylor University Medical Center, Dallas, TX, United States, [2]Department of Pulmonary Immunology, University of Texas Health Science Center at Tyler, Tyler, TX, United States, [3]Quantitative Preclinical and Clinical Sciences Department, Praedicare Inc, Dallas, TX, United States, [4]Hollow Fiber System and Experimental Therapeutics Laboratories, Praedicare Inc., Dallas, TX, United States

Background: There is need for shorter duration regimens for the treatment of *tuberculosis*, that can treat patients regardless of multidrug resistance status (pan-tuberculosis).

Methods: We combined minocycline with tedizolid, moxifloxacin, and rifampin, in the hollow fiber system model of *tuberculosis* and mimicked each drugs' intrapulmonary pharmacokinetics for 28 days. Minocycline-tedizolid was administered either as a once-a-week or a daily regimen. In order to explore a possible explanation for effectiveness of the once-a-week regimen, we measured systemic and intra-bacterial minocycline pharmacokinetics. Standard daily therapy (rifampin, isoniazid, pyrazinamide) was the comparator. We then calculated γ_f or kill slopes for each regimen and ranked the regimens by time-to-extinction predicted in patients.

Results: The steepest γ_f and shortest time-to-extinction of entire bacterial population was with daily minocycline-rifampin combination. There was no difference in γ_f between the minocycline-tedizolid once-a-week *versus* the daily therapy (p = 0.85). Standard therapy was predicted to cure 88% of patients, while minocycline-rifampin would cure 98% of patients. Minocycline concentrations fell below minimum inhibitory concentration after 2 days of once-weekly dosing schedule. The shape of minocycline intra-bacterial concentration-time curve differed from the extracellular pharmacokinetic system and lagged by several days, consistent with system hysteresis. Hysteresis explained the persistent microbial killing after hollow fiber system model of *tuberculosis* concentrations dropped below the minimum inhibitory concentration.

Conclusion: Minocycline could form a backbone of a shorter duration once-a-week pan-tuberculosis regimen. We propose a new concept of post-antibiotic microbial killing, distinct from post-antibiotic effect. We propose system hysteresis as the basis for the novel concept of pharmacologic memory, which allows intermittent dosing.

KEYWORDS

post antibiotic microbial killing, gama slope, hollow fiber model system, post-antibiotic effect, shannon entropy

Introduction

The scourge of *tuberculosis* (TB) has been exacerbated by the emergence of multidrug-resistant TB (MDR-TB) and extensively drug-resistant TB (XDR-TB) (Dheda et al., 2017). Therapy for MDR-TB has a success rate of about 50%, while that for XDR-TB is about 20%, and patients with XDR-TB often die within 10-month (Dheda et al., 2017). The recently approved regimen of bedaquiline, pretomanid and linezolid cures greater than 85% of patients with drug-resistant TB when therapy is administered over 6-month (WHO, 2022). However, the adverse side-effect profile is high such that this combination regimen is recommended for highly resistant TB with no other treatment option (Conradie et al., 2020). Therefore, there is an urgent need to find drugs that could be immediately used to treat these unfortunate patients safely and effectively.

There are several possible approaches to improve the therapeutic outcomes of the treatment regimens, including 1) repurposing old drugs used for other indications and found to be effective against *Mycobacterium tuberculosis* (*Mtb*), and 2) develop new specific anti-TB drugs that are safe and effective, among others. While both strategies are commonly used; the latter strategy requires several years to decades before a drug and resultant combination regimen(s) can be used in the clinic. With the repurposing strategy, β-lactam/β-lactamase inhibitors, minocycline and its congener tigecycline, and new oxazolidinones such as tedizolid, have been found to be highly effective anti-TB drugs (Ramon-Garcia et al., 2016; Deshpande et al., 2017; Deshpande et al., 2018b; Srivastava et al., 2018b; Deshpande et al., 2019a; Deshpande et al., 2019b; Srivastava et al., 2020b; Srivastava et al., 2021a; Srivastava et al., 2021b). Minocycline kills both extracellular and intracellular bacilli directly, and the optimal dose for MDR-TB was identified as 7 mg/kg (Deshpande et al., 2019b). In addition, minocycline demonstrated dose-dependent anti-inflammatory activity, including inhibition of sonic hedgehog-patched-gli signaling, which has implications for improving lung remodeling (Deshpande et al., 2019b). Here, we performed pharmacokinetics-pharmacodynamics (PK/PD) studies using the hollow fiber system model of TB (HFS-TB) to determine if minocycline can be used as the backbone of the once-a-week combination regimen (Alffenaar et al., 2020). Microbial kill rates with different experimental regimens were calculated using γ_f slopes (Gumbo et al., 2004; Magombedze et al., 2018; Srivastava et al., 2019; Magombedze et al., 2021; Gumbo et al., 2022).

Methods

Materials and bacterial strains

Mtb reference laboratory strains, the virulent strain and attenuated virulence strain that were cultured from the *Mtb* H37 parent strain isolated from a patient in 1905, and designated Mtb H37Ra (ATCC#25177) and H37Rv (ATCC# 27294), were used in the studies (Steenken and Gardner, 1946). *Mtb* were grown to logarithmic phase (log-phase) growth in Middlebrook 7H9 broth plus 10% oleic acid, albumin, dextrose, and catalase (OADC) (herein called "broth") under 5% CO_2 at 37°C for 4 days before each experiment. All study drugs were purchased from Sigma-Aldrich except moxifloxacin, which was purchased from the hospital pharmacy. Hollow fiber cartridges were obtained from FiberCell systems. Mycobacterial Growth Indicator Tube (MGIT) liquid culture systems and supplies were purchased from Becton Dickinson.

Comparison of combination regimens in the hollow fiber system model of *tuberculosis*

The HFS-TB has been described in detail in the past in a number of our previous publications (Deshpande et al., 2017; Deshpande et al., 2018b; Srivastava et al., 2018b; Deshpande et al., 2019a; Deshpande et al., 2019b; Srivastava et al., 2020b; Srivastava et al., 2021a; Srivastava et al., 2021b). We utilized log-phase growth extracellular bacilli in the HFS-TB studies instead of intracellular bacilli to eliminate the prolonged persistence of drugs inside infected macrophages and to eliminate the pro-apoptotic effect of minocycline which we have shown elsewhere as a mechanism of *Mtb* kill (Deshpande et al., 2019b). There were two HFS-TB studies performed.

The first HFS-TB study was performed to determine if the different combinations of minocycline could be used as a backbone of a once-a-week regimen. We inoculated 20 ml log-phase growth *Mtb* H37Ra cultures into the peripheral compartment of the HFS-TB units, after which the systems were treated once daily with one of several experimental regimens over a 28-day study period. There were two HFS-TB replicates per regimen as follows: 1) isoniazid (300 mg/day) plus rifampin (600 mg/day), 2) isoniazid plus rifampin plus pyrazinamide (1.5 g/day) [standard regimen], 3) minocycline (7 mg/kg/day) plus rifampin, 4), minocycline plus moxifloxacin (800 mg/day), 5) minocycline plus tedizolid (200 mg/day), 6) minocycline plus tedizolid once-a-week, 7) non-treated controls. We utilized intrapulmonary pharmacokinetics (PKs) of minocycline and tedizolid at a half-life of 13 h, and a pulmonary-to-serum free drug AUC ratio of 3.8 for minocycline and 4.0 for tedizolid (Naline et al., 1991; Housman et al., 2012; Flanagan S. D. et al., 2014). Minocycline was administered at a weekly (168 h) AUC/MIC

ratio of 440 and tedizolid at 1,800. Isoniazid and rifampin doses were at a 3 h half-life, pyrazinamide half-life was set to 12 h, and moxifloxacin half-life at 6 h (Gumbo et al., 2004; Srivastava et al., 2011). The central compartment of each HFS-TB unit was sampled at pre-determined timepoints for drug concentration measurements, whereas the peripheral compartment was sampled for enumeration of the bacterial burden either using the solid agar (Middlebrook 7H10 supplemented with 10% OADC) culture method or by inoculating the MGIT tubes to record the time-to-positive (TTP) as the second pharmacodynamic measure.

The second HFS-TB study was performed to identify intra-bacterial concentrations (henceforth shortened to "bacterial PKs") of minocycline *versus* microbial kill using *Mtb* H37Rv to explain prolonged bacterial kill with minocycline. After inoculation of 20 ml of bacterial cultures, minocycline and tedizolid were administered as a single bolus at t = 0. Simultaneous central compartment and peripheral compartment sampling were performed at 0 h (pre-dose) followed by 1, 6, 24, 48, 72, 96, 120, 144 and 168 h post-dosing for measurement of extracellular drug concentration as well as bacterial PKs. For the intra-bacterial drug concentration measurement, 1 mL sample from the peripheral compartment was added to dolphin tubes pre-filled with silicone oil mixture, as we have described elsewhere, at a ratio of 1:1 (Gumbo et al., 2007). Centrifugation was performed at 13,000 rpm for 5 min following which the bacterial pellet was collected in 70% acetone. Additionally, to ensure there was no degradation of drugs from acetone, we spiked three sets of samples with a known amount of three different minocycline concentrations and added either 70% acetone or broth, to which we blinded the team of researchers responsible to measure the drug concentrations. Acetone was allowed to evaporate prior to measurement of intra-bacillary drug concentrations using the assay described in our previous publications (Srivastava et al., 2011; Srivastava et al., 2018b; Deshpande et al., 2019b). The samples from the peripheral compartment of each HFS-TB unit were also inoculated into MGIT tubes to record the TTP as the second pharmacodynamic measure.

Pharmacokinetic analyses

Compartmental PK analyses of drug concentrations were performed using ADAPT software from Biomedical Simulations Resource (BMSR) at the University of Southern California (D'Argenio et al., 2009). For the concentration of minocycline inside *Mtb*, we assumed an *Mtb bacillus* volume of 8.4 μm^3 based on the bionumbers details - (http://bionumbers.hms.harvard.edu/bionumber.aspx?id=101691). The bacterial burden of *Mtb* at each sampling point was factored in while calculating the total bacterial volume at each time point.

Pharmacodynamic analyses using γ-slopes

Previously we have published a system of ordinary differential Eqs. 1,2, that were applied to both patients sputa and the HFS-TB readouts, allowing us to map back-and-forth between HFS-TB and patients using morphisms and extinction mathematics (Gumbo et al., 2004; Magombedze et al., 2018; Srivastava et al., 2019; Magombedze et al., 2021). The equations are:

$$\frac{dB_f}{dt} = \left(1-\epsilon_f\right) r_f B_f \left(1 - \frac{B_s + B_f}{K_{max}}\right) - \gamma_f B_f, \quad (1)$$

$$\frac{dB_s}{dt} = (1-\epsilon_s) r_s B_s \left(1 - \frac{B_s + B_f}{K_{max}}\right) - \gamma_s B_s. \quad (2)$$

where, B_f is CFU/mL of *fast* replicating bacteria, B_s is semidormant/non-replicating [*slow*] bacteria CFU/mL, t is time, r_f and r_s model the rate of replication of the fast and slow replicating bacteria, K_{max} is bacteria-carrying capacity, γ_s and γ_f are the antibiotic regimen kill slopes for slow and fast replicating bacteria respectively. Here, we used fast replicating bacteria in the HFS-TB, and thus applied Eq. 1 for comparisons of regimens. All model parameter estimates were calculated directly from HFS-TB CFU/mL and TTP *versus* time data; none were fixed based on prior work. We then mapped these to patients, using the translation factor derived and described elsewhere (Magombedze et al., 2018).

Monte-Carlo experiments (MCE) for dose selection to use in once-a-week regimen

Since PK variability and resultant drug concentrations, drug penetration into lung lesions, PK/PD parameters, and MICs explain most of the variance in therapy outcomes in TB patients, modeling for dose selection should take into account PK and MIC variability (Pasipanodya et al., 2013; Gumbo et al., 2014a; Gumbo et al., 2014b; Chigutsa et al., 2015; Deshpande et al., 2018a; Dheda et al., 2018). We performed MCE using ADAPT 5 software, with steps detailed in the past, to identify the once-a-week minocycline and tedizolid dose that would achieve the PK/PD exposures achieved by each of these drugs in the dual therapy regimen (Gumbo et al., 2004; Pasipanodya and Gumbo, 2011). For the domain of input, we utilized the minocycline PK parameter estimates from the MINOS study in which patients received a dose of 10 mg/kg daily, and from two other separate studies that also identified similar PK parameters but at lower doses (Welling et al., 1975; Yamamoto et al., 1999; Fagan et al., 2010). For minocycline, we assumed an oral absorption of 100%, and a lung-to-serum penetration ratio of 3.8 based on prior studies (Naline et al., 1991). The MIC distribution used was that we identified with clinical strains in the past (Deshpande et al., 2019b). For tedizolid, we used PK parameter estimates from the

TABLE 1 Drug exposures of antibiotics achieved in the HFS-TB units.

	Cumulative weekly $AUC_{0\text{-}168}$ [mg*h/L]	$AUC_{0\text{-}24}$ [mg*h/L]	$AUC_{0\text{-}24}$/MIC
Minocycline daily	204.2	29.14	58.28
Minocycline once weekly	219	31.29	62.58
Tedizolid daily	1,353	193.3	386.6
Tedizolid once weekly	904.4	129.2	258.4
Isoniazid daily	-	32.43	518.88
Rifampin daily	-	10.04	160.64
Moxifloxacin daily	-	108.3	1,442.4
Pyrazinamide daily	-	1,371	54.84

study of Flanagan et al., and a free drug lung-serum AUC ratio of 4 (Housman et al., 2012; Flanagan S. et al., 2014; Srivastava et al., 2018b). We used the tedizolid MIC distribution identified by Vera-Cabrera *et al* (Vera-Cabrera et al., 2006). We examined the tedizolid doses of 350, 700 mg, 1,000 mg, and 1,400 mg administered as a single dose once a week. Target exposures were those achieved in the HFS-TB shown in Table 1.

Results

Minimum inhibitory concentration

The MIC of drugs against H37Rv were as following: isoniazid 0.06 mg/L, rifampin 0.125 mg/L, pyrazinamide 12.5 mg/L, minocycline 2 mg/L, moxifloxacin 0.25 mg/L, and tedizolid 0.25 mg/L, similar to those reported in prior publications (Srivastava et al., 2011; Srivastava et al., 2020a). The MICs against H37Ra were as following: isoniazid 0.06 mg/L, rifampin 0.06 mg/L, pyrazinamide 25 mg/L, minocycline 0.5 mg/L, moxifloxacin 0.125 mg/L, and tedizolid 0.25 mg/L, as has been reported in our prior publications (Srivastava et al., 2018a; Deshpande et al., 2018c; Deshpande et al., 2019b).

Hollow fiber system model of *tuberculosis* results

Figure 1A and Supplementary Figure S1 show the concentration-time profile of drugs achieved in the HFS-TB, with Table 1 listing the AUCs achieved by each of the drug based on concentration measurements in the HFS-TB units. Table 2 compares the intended *versus* achieved peak concentrations (C_{max}) in the HFS-TB and demonstrates the accuracy of HFS-TB in achieving the intended drug concentrations. The C_{max} and AUCs were in the range achieved by standard dose rifampin and isoniazid, and high dose pyrazinamide and moxifloxacin, inside TB lesions (Pasipanodya et al., 2013; Dheda et al., 2018; Ordonez et al., 2020). Minocycline concentrations in the HFS-TB fell below MIC after 48 h of drug administration when given as a once-a-week regimen. To reiterate, the minocycline concentrations in the HFS-TB treated with the once-a-week schedule were below the MIC between day 3–7 (with once-a-week dosing schedule).

Figure 2A shows the time-kill curves for log_{10} cfu/mL, which is the traditional method of bacterial burden quantification that allowed us to compare results presented here with our previous HFS-TB studies. Minocycline-rifampin and rifampin-isoniazid regimen treated HFS-TB units had negative cultures by day 7, whereas all other regimens showed negative cultures by the study day 14. Figure 2B shows the time-kill curves by each regimen in the HFS-TB, using MGIT derived TTP readouts; the lower the bacterial burden the higher the TTP. In our MGIT assay, the time-in protocol was set to 56 days (compared to 42-day used in the clinical microbiology laboratories) after which the samples were recorded as negative for bacterial growth. Based on TTP readout, therapy duration (time) to negative cultures was 21 days for minocycline-rifampin, isoniazid-rifampin, and standard therapy, while remaining regimens took one more week to achieve negative culture.

Regimen ranking using γ-slopes

The use of γ-slopes offers the advantage of integrating both cfu/mL values and TTP readouts into one equation, and the approach is agnostic of kill pattern, and thus can be used to rank regimens by γ_f (speed of kill), or time-to-extinction (shortest duration of therapy), or proportion of patients expected to be cured for all time points (Gumbo et al., 2022). The γ_f slopes of each regimen in the HFS-TB are shown in Figure 3 and Table 3. We utilize standard therapy outcomes for model validation and quality control and Table 2 shows that the γ_f and time-to-extinction was similar to that observed in the HFS-TB in the past (Magombedze et al., 2018), and the prediction that 88% (95% credible intervals: 80%–94%) of patients would be cured at all time points is virtually identical to clinical observations. This means that both the HFS-TB experiments and the modeling performed according to specifications and standard operating procedures.

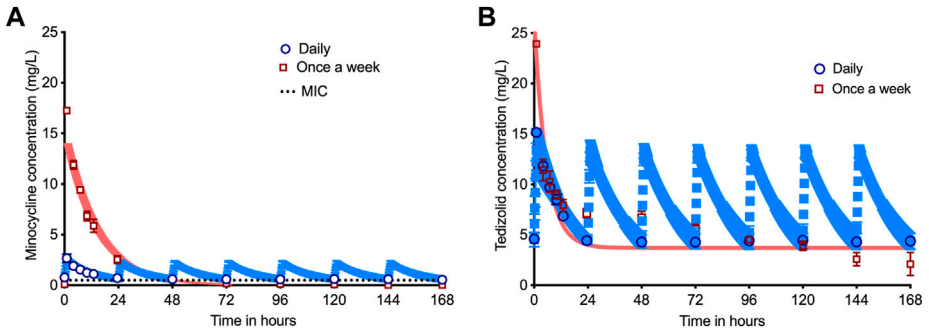

FIGURE 1
Pharmacokinetics of minocycline and tedizolid in dual therapy. The symbols are mean concentrations, error bars are standard deviation, and shaded areas are pharmacokinetic (PK) model predicted concentrations. The blue line is PK-model predicted for daily therapy, while the salmon colored line is PK-model predicted for once a week therapy. **(A)** Concentration-time profile for the once-a-week minocycline doses compared to daily doses demonstrated that minocycline concentration declined below the MIC by 48 h (28.57% of the once-a-week dosing interval) for the once-a-week dosing schedule but stayed above the MIC for 100% of 168 h with daily dose. **(B)** Concentration-time profile for the companion once-a-week tedizolid doses *versus* daily dose demonstrates that the tedizolid peak concentration could not reach 7 times that of the daily dose due to solubility issues, which means that the once-a-week regimen was prejudiced compared to daily therapy since the daily therapy schedule achieved a 49.6% higher cumulative AUC per week than once-a-week regimen.

TABLE 2 Intended *versus* HFS-TB measured peak concentration of each drug in the regimen.

Drug	Intended C_{max} (mg/L)	Measured C_{max} (mg/L)
Isoniazid	6.8	4.75 ± 0.29
Rifampin	3	1.88 ± 0.45
Pyrazinamide	54	83.31 ± 6.07
Moxifloxacin	8.4	7.28 ± 0.79
Minocycline	2.6	2.67 ± 0.41
Tedizolid	2.6	2.37 ± 0.64

Figure 3 and Table 3 show that the minocycline-rifampin combination regimen was ranked top by γ_f, time-to-extinction, and the predicted proportion of patients cured at all time points. Moreover, the γ_f of the daily and once-a-week minocycline-tedizolid combination overlapped (p = 0.85), as did time-to-extinction and proportion of patients cured. In other words, the pharmacodynamic effects of daily therapy and once a week therapy with minocycline-tedizolid were similar. Since the minocycline-tedizolid combination had the lowest γ_f of all (slowest kill speed), but the once-a-week regimen was as good as the daily, it meant that the once-a-week regimen must continue to kill *Mtb* long after the drug concentrations fell below the MIC.

Minocycline intra-bacterial PKs and pharmacologic memory

To understand why minocycline continues to kill 4 days after drug concentrations declined below the MIC in the HFS-TB, we investigated the possibility of longer persistence of drug inside bacteria as a possible explanation. We treated log-phase growth *Mtb* H37Rv with a single bolus of minocycline and tedizolid, in triplicate HFS-TB, at deliberately shorter half-life for minocycline, and measured HFS-TB external compartment concentrations daily over 7 days. Figure 4A shows the results of the model derived *versus* measured extracellular minocycline concentrations in the HFS-TB. The minocycline clearance rate in the HFS-TB was 0.035 ± 0 L/h with a volume of 0.320 ± 0.004 L and a half-life of 6.34 ± 0.852 h. The minocycline bacterial PKs were those shown in Figure 4B. Figure 4B shows that while there was a bolus given to the HFS-TB the time to peak concentration inside *Mtb* was 96 h, followed by a decline, such that the shape of the minocycline concentration-versus-time decline inside *Mtb* was different from that in the extracellular HFS-TB. This is consistent with system hysteresis (Ewing, 1882; Mayergoyz, 2003), which led to minocycline concentrations persisting inside *Mtb* for at least 4-day after the drug concentration declined below limits of detection in extracellular fluid in the HFS-TB. The mass-charge ratio, by the LC-MS/MS assay, on each day demonstrated that it was the intact minocycline molecule that persisted inside the *Mtb* and not its metabolites. Figure 4C shows the corresponding TTPs during the 7-day HFS-TB study. The TTP in non-treated controls stayed relatively constant in the 7 days Figure 4C demonstrated continued microbial kill beyond day 2 (i.e, progressively increasing TTPs), during the time period of 2–7 days when minocycline concentration persisted inside the bacteria but had fallen below detection in the HFS-TB extracellular fluid.

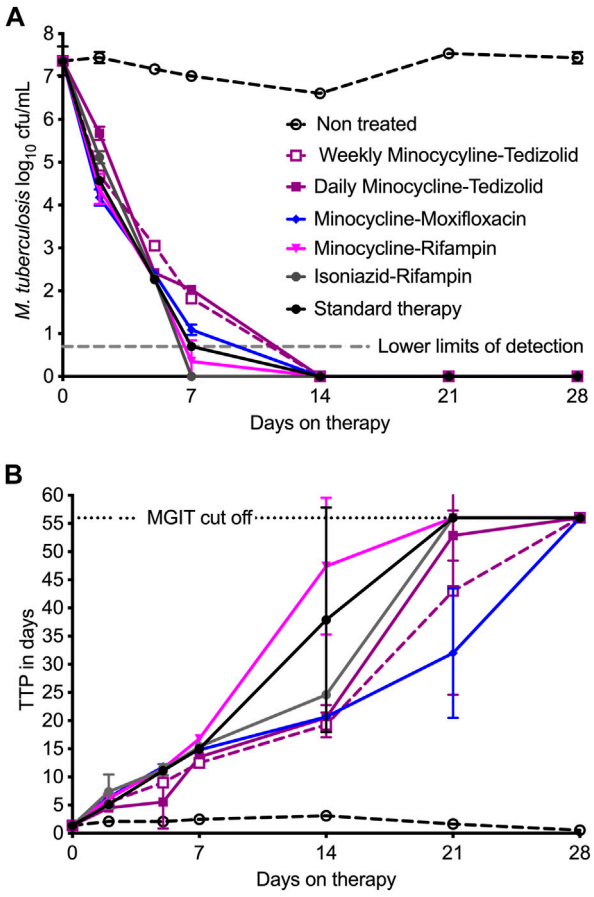

FIGURE 2
Comparisons of dual therapy regimens to standard triple therapy. Symbols are mean and error bars are standard deviation. **(A)** Using cfu/mL readouts, minocycline-rifampin and isoniazid-rifampin fell below the lower limits of detection by day 7, and by this metric would be the highest ranked. The kill pattern was not necessarily exponential decline and differed between the regimens. **(B)** TTP, with negative culture call at 56 days, had a wider dynamic range and shows that cultures only became negative on day 21 for all regimens, except for minocycline-tedizolid daily and once-a-week regimens which achieved that on day 28.

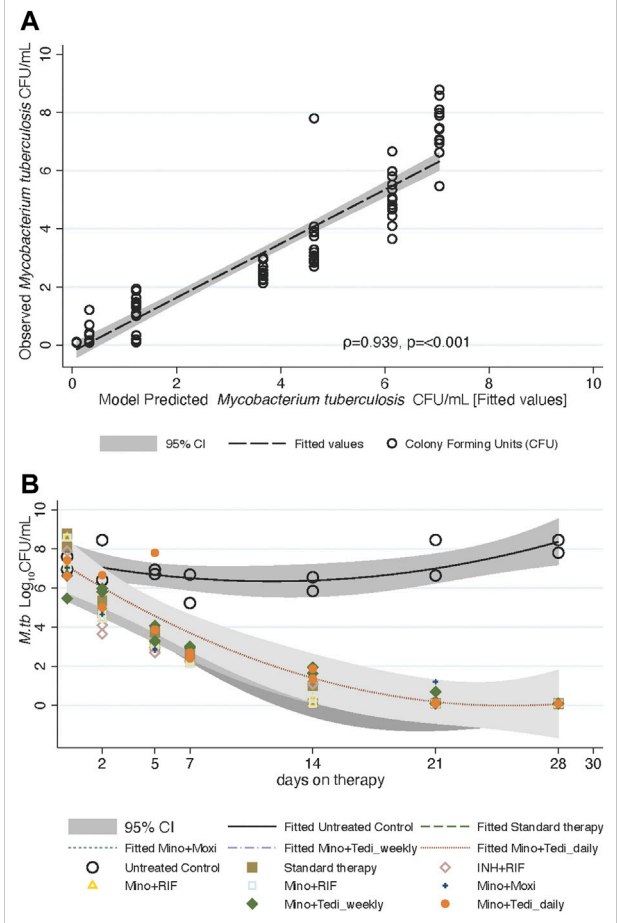

FIGURE 3
Mycobacterium tuberculosis trajectories and γ_f in HFS-TB treated. **(A)** The modeled cfu/mL *versus* observed cfu/mL using ordinary differential equation #1 for all data points are shown, as a diagnostic. The model was a very good fit. **(B)** Shaded areas are 95% credible intervals. Many of the γ_f overlapped, but the most steep (deepest gray) was the minocycline-rifampin combination regimen. In the non-treated HFS-TB, bacteria grew.

Target attainment probability with clinical doses

Next, we performed a 10,000 virtual patient MCE to identify the once-a-week doses of minocycline and tedizolid that would achieve a minocycline $AUC_{0\text{-}168}$/MIC of 438 and a tedizolid $AUC_{0\text{-}168}$/MIC of 1808.4, for use in patients with TB. We implemented the MCE in ADAPT 5 software: for the domain of input, we utilized the PK parameter estimates and variability of minocycline and tedizolid shown in Table 4 based on several PK studies from the literature and the lung penetration ratios of each drug published elsewhere (Naline et al., 1991; Yamamoto et al., 1999; Gumbo et al., 2004; Fagan et al., 2010; Pasipanodya and Gumbo, 2011). The PK parameter outputs of the 10,000-patient MCE (Table 4) for each drug demonstrate that our simulation experiment accurately recapitulated parameters encountered in the clinic. Figure 5A shows the performance of different once-a-week minocycline doses, starting with 5 mg/kg of minocycline, across a range of minocycline MIC in clinical isolates (Deshpande et al., 2019b). Figure 5B shows that after summation over the MIC distribution, the optimal minocycline dose would be 30 mg/kg once-a-week, which will achieve the target exposure in ~90% of the patients. For tedizolid, Table 4 also summarizes the PK parameters in the 10,000 simulated TB patients. Figure 5C shows the performance of each once-a-week tedizolid dose over the MIC distribution range reported by Vera-Cabrera et al. Vera-Cabrera et al. (2006). The summation based on that MIC distribution

TABLE 3 ODE derived parameters of γ_f and time-to-extinction in the HFS-TB, and proportion of patients expected to be cured.

Rank	Regimen	Data points	Mean negative γ_f $\log_{10}$ cfu/ml/day (95% CI)	Median time-to-extinction in days (95% CrI)	Mean proportion cured all time points (95%CI)
1	Minocycline-rifampin*/**	14	0.34 (0.25–0.43)	20.24 (10.68–70.76)	0.98 (0.93–1.00)
2	Standard Therapy*	14	0.34 (0.25–0.44)	19 (4.36–105)	0.88 (0.80–0.94)
3	Minocycline-moxifloxacin	14	0.26 (0.17–0.34)	62.94 (22.33–483.07)	0.53 (0.43–0.63)
4	Isoniazid-rifampin	14	0.25 (0.15–0.35)	29.18 (12.78–148.99)	0.92 (0.84–0.96)
5	Minocycline-tedizolid daily	14	0.20 (0.10–0.30)	29.96 (13.59–156.89)	0.82 (0.73–0.89)
5	Minocycline-tedizolid weekly	14	0.19 (0.13–0.21)	43.39 (25.44–129.81)	100

*p = 0.038 compared to minocycline-tedizolid daily and **p = 0.003 compared to minocycline-tedizolid weekly.

represents the proportion of patients who would achieve the tedizolid exposure in the lung, that was achieved with the once-a-week tedizolid regimen in the HFS-TB (Figure 5D). The tedizolid optimal once-a-week dose was identified as 1,050 mg, which is less than the cumulative amount of 200 mg/day standard dose (i.e, 1,400 mg/week) of that drug for the week.

Discussion

The present study reports several important findings with regards to the different drug combinations of two- and three-drug regimens for TB. First, we found that daily minocycline dual-drug combinations with rifampin was highly effective and equaled the three-drug regimen of isoniazid-rifampin-pyrazinamide. The combination of minocycline and rifampin is already being employed in the treatment of leprosy and has been shown to be synergistic for the treatment of *Staphylococcus* infections (Zinner et al., 1981; Segreti et al., 1989). In addition, the minocycline derivative omadacycline when combined with rifapentine also demonstrated excellent synergy against *Mycobacterium kansasii* (Singh et al., 2022). Our HFS-TB findings suggest that the minocycline-rifampin combination could also be useful in TB patients, although it will not work with MDR-TB. Moxifloxacin dual therapy was also effective and could be useful in MDR-TB patients, especially if a third drug is added. A potential combination of minocycline-moxifloxacin with the delamanid- OPC-167832 combination which we have noted to be synergistic elsewhere could be explored to shorten therapy duration (Gumbo et al., 2022).

On the other hand, while tedizolid-minocycline had the lowest γ_f, minocycline, tedizolid, and moxifloxacin, and rifapentine share certain properties that make pairing them with minocycline advantageous. Replacement of rifampin with rifapentine could also take advantage of the remarkable minocycline-rifapentine effect (Singh et al., 2022). First, these anti-microbials agents achieve high *free* drug concentrations in lungs, lung lesions, bone, and cerebrospinal fluid, which are the most common sites of TB (Housman et al., 2012; Dheda et al., 2018; Rifat et al., 2018). Second, their long half-lifes could allow for intermittent dosing for the treatment of TB. Third, the PK/PD driver for these pharmacophores in the treatment of TB is AUC/MIC (Gumbo et al., 2007; Pasipanodya et al., 2013; Chigutsa et al., 2015; Swaminathan et al., 2016; Srivastava et al., 2017; Srivastava et al., 2018b; Deshpande et al., 2018c; Deshpande et al., 2019a; Deshpande et al., 2019b). While the current studies were performed with log-phase growth *Mtb*, elsewhere we have shown that some of these drugs also have excellent sterilizing effect even as intermittent therapy (Srivastava et al., 2018b). Based on the foregoing considerations, if cumulative weekly doses of each drug could be tolerated, combinations would be as effective as once-daily therapy (Srivastava et al., 2018b; Deshpande et al., 2019a; Deshpande et al., 2019b). Indeed, in the case of tedizolid and for all oxazolidinones, the more intermittent the administration the safer it could be, since trough concentrations and time-above certain threshold concentrations have been associated with mitochondrial toxicity (Pea et al., 2012; Flanagan et al., 2015; Song et al., 2015). Addition of a third drug with a long half-life, say OPC-167832 (Hariguchi et al., 2020), could make minocycline-tedizolid-OPC-167832 a highly effective once-a-week regimen with potential to shorten therapy duration. This has major implications for TB programs in the treatment of drug-susceptible, MDR-TB, and XDR-TB. A once-a-week triple drug regimen could dramatically reduce the use of resources by healthcare programs (CDC, 2020).

The possibility of a once-a-week dosing concept led us to ask two related fundamental pharmacology questions. First, can antibiotics continue killing after they are gone from the system? If so, why do such antibiotics continue working after they are gone? Post antibiotic exposure effects are defined as the period of suppression or delay of growth after a short exposure of micro-organisms to antibiotic (Mouton et al., 2005). Common parameters include post antibiotic effect (PAE), sub-MIC effect, post antibiotic sub-MIC effects (PAE SME), which are all are

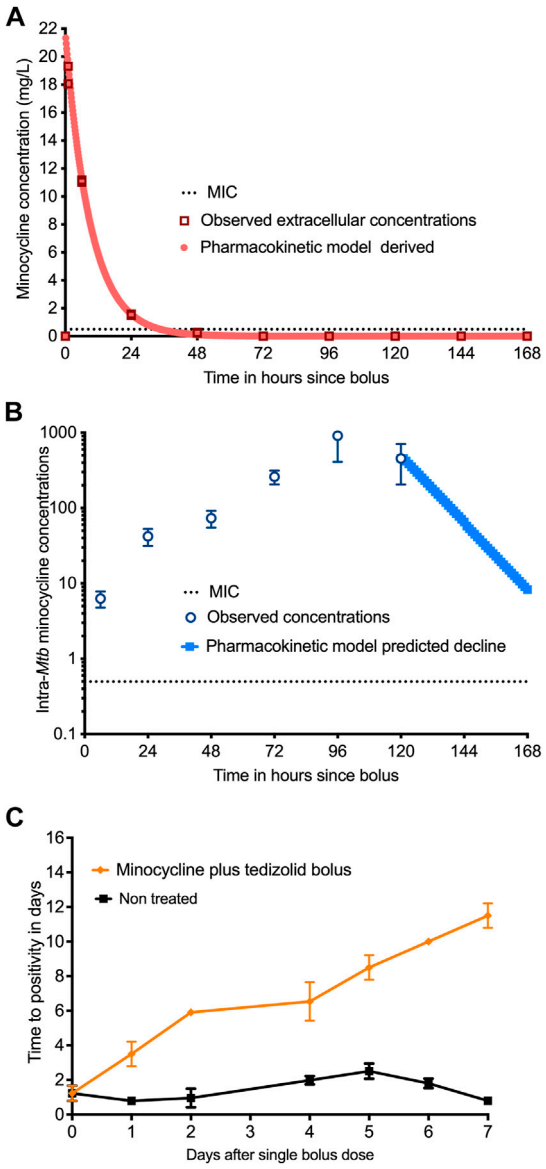

FIGURE 4
Measurement of intra-bacterial minocycline concentrations. **(A)** Extracellular minocycline concentrations following once-a-week dosing against *Mtb* fell below MIC after 48 h similar to the first HFS-TB experiment. **(B)** Intra-bacterial (inside *Mtb*) minocycline concentrations persisted above MIC well beyond 48 h, and the concentration-time curve lagged by 4 days behind extra-bacterial pharmacokinetics. **(C)** There were three replicate HFS-TB units treated with a single bolus dose of tedizolid and minocycline, at a half-life of 12 h. In parallel with measuring the intra-bacterial concentrations, we also quantified the bacterial burden using TTP in days. The figure shows continued microbial kill even after the minocycline extracellular concentrations dropped below the MIC in extracellular HFS-TB compartment by 48 h, which was however, parallel to the intra-*Mtb* concentrations.

measured as the time (hours or days) it takes to grow 1.0 $\log_{10}$ CFU/mL (Mouton et al., 2005). The concept of a PAE is actually as old as the beginning of the antibiotic chemotherapy, though the idea received more systematic impetus when Bill Craig was setting the basis of PK/PD, some 40 years ago (Eagle and Musselman, 1949; McDonald et al., 1977; Vogelman et al., 1988; Craig et al., 1991). Here, we found that long after a bolus of minocycline and the drug was eliminated from the HFS-TB PK system, the drug persisted inside *Mtb* for many days and *continued killing* the bacteria for an additional 5-day, in two separate experiments. Thus, we documented continued *microbial kill* after falling below MIC and detection limits. We propose this as a separate PK/PD parameter from PAEs, post antibiotic microbial killing (PAMK). PAMK is defined as the time (in hours) of continued microbial kill (here quantitively measured as persistently negative γ) after drug falls below the MIC.

The second fundamental question follows from the definition of PAMK: why would such antibiotics continue microbial kill after they are gone? In the case of PAE, the standard explanation has been that antibiotics have a good PAE because of the time it takes for an organism to recover from the effects of an antibiotic and resume normal growth after the brief exposure. Since the most profound PAE was encountered with bacterial protein and nucleic acid synthesis inhibitors, one popular mechanistic explanation has been that inhibition of DNA and protein synthesis upon antibiotic exposure continue for several hours following antibiotic removal, delaying growth, until DNA synthesis resumes at a much later time, also called a "hit-and-run" scenario (Guan et al., 1992; Odenholt et al., 2001; Svensson et al., 2002). However for PAMK, there is persistent microbial kill as if antibiotic is still around. For minocycline the bacterial PKs were consistent with system hysteresis. The concept of hysteresis was first described in electromagnetism by Ewing in 1882 (Ewing, 1882), but mathematical formalism was achieved only recently by Mayergoyz (2003). Hysteresis is when a system (bacterial PKs in this case) lags the input (HFS-TB PK system) but is dependent on that history of input. Here, we found that the PAMK paralleled the system hysteresis. Therefore, we would like to propose the concept of "pharmacologic memory" arising from system hysteresis. By definition, a memory system requires that the dependent variable should retain information at a later time after the input is gone. In basic information theory, Claude Shannon assumed that memory is finite, and that the output would depend on both the history and present state of the system (Shannon, 1997). In our case, the dependent variable is bacterial PK, while the finite input is the extracellular HFS-TB PK system or even the bolus. The minocycline bacterial PK differed from the HFS-TB PK profile, consistent with a dynamic lag and thus system in hysteresis or memory. To our knowledge, this is the first time that bacterial concentrations have been measured when exposed to an external dynamic concentration profile instead of static concentrations: the HFS-TB PKs. On the

TABLE 4 Pharmacokinetic parameter input and output in Monte Carlo experiments.

	Subroutine PRIOR (clinical studies)		10,000 simulated TB patients	
	Mean	Standard deviation	Mean	Standard deviation
Minocycline				
Clearance (L/hr/kg)	0.03	0.009	0.03	0.01
Volume (L/kg)	0.57	0.26	0.57	0.39
Absorption constant (hr^{-1})	3.00	0.40	3.01	1.14
Tedizolid				
Total clearance (L/hr)	6.69	2.0	6.71	3.71
Central Volume (L)	69	12.42	68.9	29.4
Intercompartmental clearance (L/hr)	0.96	0.29	0.97	0.54
Peripheral volume (L)	13.6	2.44	13.5	5.57
Absorption constant (hr^{-1})	1.99	3.86	1.98	2.85

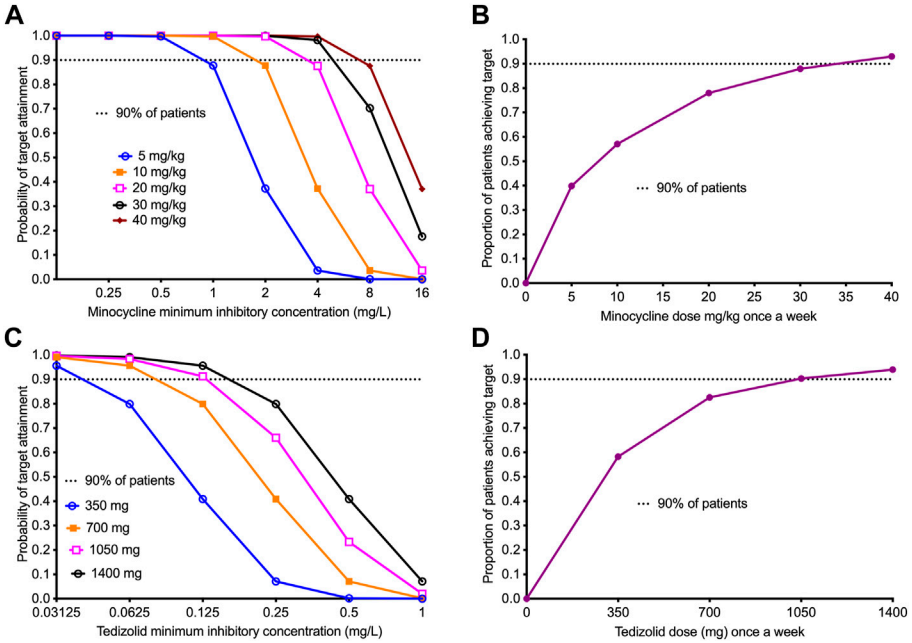

FIGURE 5
Performance of once-a-week minocycline and tedizolid doses in 10,000 virtual patients with *tuberculosis*. All data points show the proportion of 10,000 patients treated with a dose and dosing schedule who would achieve or exceed the target AUC/MIC exposure associated with optimal effect. 95% confidence intervals were very tight and virtually overlapped with prediction (not shown in the figure). **(A)** The target attainment probability (TAP) for minocycline doses administered once-a-week with the increasing MIC. The TAP of 90% was achieved at doses ≥30 mg/kg up to MIC of 8 mg/L, beyond which the TAP declines indicating that 8 mg/L would be the susceptibility breakpoint for once-a-week dosing. **(B)** The figure shows proportion of 10,000 TB patients achieving the weekly target minocycline cumulative exposure with the different weekly doses. The dose of 30 mg/kg, just shy of the 90% target, was determined as the optimal dose for clinical use. **(C)** The target attainment probability (TAP) for different doses of tedizolid administered weekly with increasing MICs. The TAP with the lowest dose falls below 90% at MIC >0.03125 mg/L, however, for larger doses than 700 mg, the TAP of 90% was achieved up to MIC of 0.125 mg/L. **(D)** The figure shows proportion of 10,000 TB patients achieving the weekly target tedizolid cumulative exposure with the different weekly doses. The dose of 1,050 mg achieved the 90% target and was proposed as the optimal dose.

flip side, it is unclear is PK system hysteresis could have a deleterious effect on the patient. Regarding minocycline adverse events in patients, and the fact that the minocycline concentrations in patient's circulatory system will decrease below detection for 60% of dosing interval with once-a-week dosing, while persistent in the bacteria, suggests there would be fewer side effects to the patient. However, the effect of bacterial PK system hysteresis on emergence of antimicrobial resistance are unclear, and this will require further urgent study.

There are some limitations to our HFS-TB studies. First, we examined only two laboratory strains in our study. The findings could differ in clinical isolates with varying MICs. Elsewhere we have shown widespread susceptibility of MDR-TB and XDR-TB clinical strains to minocycline and tedizolid (Srivastava et al., 2018b; Deshpande et al., 2019b). Therefore, the effect is not likely limited to laboratory strains only. Second, the tolerability of 30 mg/kg/week of minocycline and 1,050 mg tedizolid that we found to be effective as once-a-week therapy is yet unclear. In the MINOS study with 41 stroke patients who received the highest minocycline dose of 10 mg/kg/day for 3 days (30 mg/kg/week) was well-tolerated and achieved a serum half-life of 24 h (Fagan et al., 2010). Additionally, a recent study demonstrated that there was rapid reversal of tedizolid toxic effects upon discontinuous administration and that an intermittent dosing schedule led to lower tedizolid toxicity (Milosevic et al., 2018). Therefore, a once-a-week regimen is expected to have lower or no toxicity. Nevertheless, these higher doses need to have their safety examined and compared to daily therapy in the clinical setting.

In summary, we found that the best drugs to combine with minocycline for TB were rifampin and moxifloxacin. Second, once-a-week minocycline plus tedizolid regimen was as effective as a daily regimen in the HFS-TB. Third, we measured bacterial PKs in the face of extracellular dynamic PKs and identified system hysteresis. We propose this drug persistence inside *Mtb* and system hysteresis as a basis for a concept of pharmacologic memory. Fourth, we propose the PK/PD concept of PAMK, which could be explained by bacterial PK system hysteresis.

Data availability statement

The original contributions presented in the study are included in the article/Supplementary Material, further inquiries can be directed to the corresponding author.

Author contributions

Conceptualization and methodology: TG Hollow fiber experiments: DD and SS PK/PD modeling and simulations: TG γ-slope and time-to-extinction work: JP All authors read, edited, and approved the final version for publication.

Funding

TG was supported by R01AI079497, and R56 AI111985, from the National Institute of Allergy and Infectious Diseases (NIAID). SS is supported by 1R01HD099756 grant from Eunice Kennedy Shriver National Institute of Child Health and Human Development (NICHD), University of Texas System STARS award (250439/39411) and funding from the department of Pulmonary Immunology (423500/14000), UT Health Science Center at Tyler, Texas.

Conflict of interest

Author TG was the company CEO of Praedicare Inc, and founded Praedicare Africa. Author JGP was employed by the company Praedicare Inc.

The remaining authors declare that the research was conducted in the absence of any commercial or financial relationships that could be construed as a potential conflict of interest.

Publisher's note

Supplementary material

The Supplementary Material for this article can be found online at: https://www.frontiersin.org/articles/10.3389/fphar.2022.1024608/full#supplementary-material

References

Alffenaar, J. C., Gumbo, T., Dooley, K. E., Peloquin, C. A., McIlleron, H., Zagorski, A., et al. (2020). Integrating pharmacokinetics and pharmacodynamics in operational research to end tuberculosis. *Clin. Infect. Dis.* 70, 1774–1780. doi:10.1093/cid/ciz942

CDC (2020). "The costly burden of drug-resistant TB disease in the U.S," in *CDC facf sheet* (Atlanta, Georgia, United States: Center ofr Disease Control and Prevention).

Chigutsa, E., Pasipanodya, J. G., Visser, M. E., van Helden, P. D., Smith, P. J., Sirgel, F. A., et al. (2015). Impact of nonlinear interactions of pharmacokinetics and MICs on sputum bacillary kill rates as a marker of sterilizing effect in tuberculosis. *Antimicrob. Agents Chemother.* 59, 38–45. doi:10.1128/AAC.03931-14

Conradie, F., Everitt, D., and Crook, A. M. (2020). Treatment of highly drug-resistant pulmonary tuberculosis. Reply. *N. Engl. J. Med.* 382, 2377. doi:10.1056/NEJMc2009939

Craig, W. A., Redington, J., and Ebert, S. C. (1991). Pharmacodynamics of amikacin *in vitro* and in mouse thigh and lung infections. *J. Antimicrob. Chemother.* 27, 29–40. doi:10.1093/jac/27.suppl_c.29

D'Argenio, D. Z., Schumitzky, A., and Wang, X. (2009). *ADAPT 5 user's guide: Pharmacokinetic/pharmacodynamic systems analysis software*. Los Angeles: Biomedical Simulations Resource, University of Southern California.

Deshpande, D., Magombedze, G., Srivastava, S., Bendet, P., Lee, P. S., Cirrincione, K. N., et al. (2019a). Once-a-week tigecycline for the treatment of drug-resistant TB. *J. Antimicrob. Chemother.* 74, 1607–1617. doi:10.1093/jac/dkz061

Deshpande, D., Pasipanodya, J. G., Mpagama, S. G., Srivastava, S., Bendet, P., Koeuth, T., et al. (2018a). Ethionamide Pharmacokinetics/pharmacodynamics-derived dose, the role of MICs in clinical outcome, and the resistance arrow of time in multidrug-resistant tuberculosis. *Clin. Infect. Dis.* 67, S317–S326. doi:10.1093/cid/ciy609

Deshpande, D., Pasipanodya, J. G., Srivastava, S., Martin, K. R., Athale, S., van Zyl, J., et al. (2019b). Minocycline immunomodulates via sonic hedgehog signaling and apoptosis and has direct potency against drug-resistant tuberculosis. *J. Infect. Dis.* 219, 975–985. doi:10.1093/infdis/jiy587

Deshpande, D., Srivastava, S., Bendet, P., Martin, K. R., Cirrincione, K. N., Lee, P. S., et al. (2018b). Antibacterial and sterilizing effect of benzylpenicillin in tuberculosis. *Antimicrob. Agents Chemother.* 62, 022322–e2317. doi:10.1128/AAC.02232-17

Deshpande, D., Srivastava, S., Chapagain, M., Magombedze, G., Martin, K. R., Cirrincione, K. N., et al. (2017). Ceftazidime-avibactam has potent sterilizing activity against highly drug-resistant tuberculosis. *Sci. Adv.* 3, e1701102. doi:10.1126/sciadv.1701102

Deshpande, D., Srivastava, S., Nuermberger, E., Koeuth, T., Martin, K. R., Cirrincione, K. N., et al. (2018c). Multiparameter responses to tedizolid monotherapy and moxifloxacin combination therapy models of children with intracellular tuberculosis. *Clin. Infect. Dis.* 67, S342–S348. doi:10.1093/cid/ciy612

Dheda, K., Gumbo, T., Maartens, G., Dooley, K. E., McNerney, R., Murray, M., et al. (2017). The epidemiology, pathogenesis, transmission, diagnosis, and management of multidrug-resistant, extensively drug-resistant, and incurable tuberculosis. *Lancet Respir. Med.* S2213-2600, 291–360. doi:10.1016/S2213-2600(17)30079-6

Dheda, K., Lenders, L., Magombedze, G., Srivastava, S., Raj, P., Arning, E., et al. (2018). Drug-penetration gradients associated with acquired drug resistance in patients with tuberculosis. *Am. J. Respir. Crit. Care Med.* 198, 1208–1219. doi:10.1164/rccm.201711-2333OC

Eagle, H., and Musselman, A. D. (1949). The slow recovery of bacteria from the toxic effects of penicillin. *J. Bacteriol.* 58, 475–490. doi:10.1128/JB.58.4.475-490.1949

Ewing, J. A. (1882). VII. On the production of transient electric currents in iron and steel conductors by twisting them when magnetised or by magnetising them when twisted. *Proc. R. Soc. Lond.* 33, 21–23.

Fagan, S. C., Waller, J. L., Nichols, F. T., Edwards, D. J., Pettigrew, L. C., Clark, W. M., et al. (2010). Minocycline to improve neurologic outcome in stroke (MINOS): A dose-finding study. *Stroke* 41, 2283–2287. doi:10.1161/STROKEAHA.110.582601

Flanagan, S. D., Bien, P. A., Munoz, K. A., Minassian, S. L., and Prokocimer, P. G. (2014b). Pharmacokinetics of tedizolid following oral administration: Single and multiple dose, effect of food, and comparison of two solid forms of the prodrug. *Pharmacotherapy* 34, 240–250. doi:10.1002/phar.1337

Flanagan, S., Fang, E., Munoz, K. A., Minassian, S. L., and Prokocimer, P. G. (2014a). Single- and multiple-dose pharmacokinetics and absolute bioavailability of tedizolid. *Pharmacotherapy* 34, 891–900. doi:10.1002/phar.1458

Flanagan, S., McKee, E. E., Das, D., Tulkens, P. M., Hosako, H., Fiedler-Kelly, J., et al. (2015). Nonclinical and pharmacokinetic assessments to evaluate the potential of tedizolid and linezolid to affect mitochondrial function. *Antimicrob. Agents Chemother.* 59, 178–185. doi:10.1128/AAC.03684-14

Guan, L., Blumenthal, R. M., and Burnham, J. C. (1992). Analysis of macromolecular biosynthesis to define the quinolone-induced postantibiotic effect in *Escherichia coli*. *Antimicrob. Agents Chemother.* 36, 2118–2124. doi:10.1128/aac.36.10.2118

Gumbo, T., Chapagain, M., Magombedze, G., Srivastava, S., Deshpande, D., Pasipanodya, J. G., et al. (2022). *Novel tuberculosis combination regimens of two and three-months therapy duration*. bioRxiv. doi:10.1101/2022.03.13.484155

Gumbo, T., Chigutsa, E., Pasipanodya, J., Visser, M., van Helden, P. D., Sirgel, F. A., et al. (2014a). The pyrazinamide susceptibility breakpoint above which combination therapy fails. *J. Antimicrob. Chemother.* 69, 2420–2425. doi:10.1093/jac/dku136

Gumbo, T., Louie, A., Deziel, M. R., Liu, W., Parsons, L. M., Salfinger, M., et al. (2007). Concentration-dependent *Mycobacterium tuberculosis* killing and prevention of resistance by rifampin. *Antimicrob. Agents Chemother.* 51, 3781–3788. doi:10.1128/AAC.01533-06

Gumbo, T., Louie, A., Deziel, M. R., Parsons, L. M., Salfinger, M., and Drusano, G. L. (2004). Selection of a moxifloxacin dose that suppresses drug resistance in *Mycobacterium tuberculosis*, by use of an *in vitro* pharmacodynamic infection model and mathematical modeling. *J. Infect. Dis.* 190, 1642–1651. doi:10.1086/424849

Gumbo, T., Pasipanodya, J. G., Wash, P., Burger, A., and McIlleron, H. (2014b). Redefining multidrug-resistant tuberculosis based on clinical response to combination therapy. *Antimicrob. Agents Chemother.* 58, 6111–6115. doi:10.1128/AAC.03549-14

Hariguchi, N., Chen, X., Hayashi, Y., Kawano, Y., Fujiwara, M., Matsuba, M., et al. (2020). OPC-167832, a novel carbostyril derivative with potent antituberculosis activity as a DprE1 inhibitor. *Antimicrob. Agents Chemother.* 64, 020200–e2119. doi:10.1128/AAC.02020-19

Housman, S. T., Pope, J. S., Russomanno, J., Salerno, E., Shore, E., Kuti, J. L., et al. (2012). Pulmonary disposition of tedizolid following administration of once-daily oral 200-milligram tedizolid phosphate in healthy adult volunteers. *Antimicrob. Agents Chemother.* 56, 2627–2634. doi:10.1128/AAC.05354-11

Magombedze, G., Pasipanodya, J. G., and Gumbo, T. (2021). Bacterial load slopes represent biomarkers of tuberculosis therapy success, failure, and relapse. *Commun. Biol.* 4, 664. doi:10.1038/s42003-021-02184-0

Magombedze, G., Pasipanodya, J. G., Srivastava, S., Deshpande, D., Visser, M. E., Chigutsa, E., et al. (2018). Transformation morphisms and time-to-extinction analysis that map therapy duration from preclinical models to patients with tuberculosis: Translating from apples to oranges. *Clin. Infect. Dis.* 67, S349–S358. doi:10.1093/cid/ciy623

Mayergoyz, I. D. (2003). "Mathematical models of hysteresis and their applications," in *Electromagnetism.* Second Edition (New York, NY: Academic Press).

McDonald, P. J., Craig, W. A., and Kunin, C. M. (1977). Persistent effect of antibiotics on *Staphylococcus aureus* after exposure for limited periods of time. *J. Infect. Dis.* 135, 217–223. doi:10.1093/infdis/135.2.217

Milosevic, T. V., Payen, V. L., Sonveaux, P., Muccioli, G. G., Tulkens, P. M., and Van Bambeke, F. (2018). Mitochondrial alterations (inhibition of mitochondrial protein expression, oxidative metabolism, and ultrastructure) induced by linezolid and tedizolid at clinically relevant concentrations in cultured human HL-60 promyelocytes and THP-1 monocytes. *Antimicrob. Agents Chemother.* 62, 015999–e1617. doi:10.1128/AAC.01599-17

Mouton, J. W., Dudley, M. N., Cars, O., Derendorf, H., and Drusano, G. L. (2005). Standardization of pharmacokinetic/pharmacodynamic (PK/PD) terminology for anti-infective drugs: An update. *J. Antimicrob. Chemother.* 55, 601–607. doi:10.1093/jac/dki079

Naline, E., Sanceaume, M., Toty, L., Bakdach, H., Pays, M., and Advenier, C. (1991). Penetration of minocycline into lung tissues. *Br. J. Clin. Pharmacol.* 32, 402–404. doi:10.1111/j.1365-2125.1991.tb03920.x

Odenholt, I., Lowdin, E., and Cars, O. (2001). Pharmacodynamics of telithromycin *in vitro* against respiratory tract pathogens. *Antimicrob. Agents Chemother.* 45, 23–29. doi:10.1128/AAC.45.1.23-29.2001

Ordonez, A. A., Wang, H., Magombedze, G., Ruiz-Bedoya, C. A., Srivastava, S., Chen, A., et al. (2020). Dynamic imaging in patients with tuberculosis reveals heterogeneous drug exposures in pulmonary lesions. *Nat. Med.* 26, 529–534. doi:10.1038/s41591-020-0770-2

Pasipanodya, J. G., McIlleron, H., Burger, A., Wash, P. A., Smith, P., and Gumbo, T. (2013). Serum drug concentrations predictive of pulmonary tuberculosis outcomes. *J. Infect. Dis.* 208, 1464–1473. doi:10.1093/infdis/jit352

Pasipanodya, J., and Gumbo, T. (2011). An oracle: Antituberculosis pharmacokinetics-pharmacodynamics, clinical correlation, and clinical trial simulations to predict the future. *Antimicrob. Agents Chemother.* 55, 24–34. doi:10.1128/AAC.00749-10

Pea, F., Viale, P., Cojutti, P., Del, P. B., Zamparini, E., and Furlanut, M. (2012). Therapeutic drug monitoring may improve safety outcomes of long-term treatment with linezolid in adult patients. *J. Antimicrob. Chemother.* 67, 2034–2042. doi:10.1093/jac/dks153

Ramon-Garcia, S., Gonzalez Del Rio, R., Villarejo, A. S., Sweet, G. D., Cunningham, F., Barros, D., et al. (2016). Repurposing clinically approved cephalosporins for tuberculosis therapy. *Sci. Rep.* 6, 34293. doi:10.1038/srep34293

Rifat, D., Prideaux, B., Savic, R. M., Urbanowski, M. E., Parsons, T. L., Luna, B., et al. (2018). Pharmacokinetics of rifapentine and rifampin in a rabbit model of

tuberculosis and correlation with clinical trial data. *Sci. Transl. Med.* 10, eaai7786. doi:10.1126/scitranslmed.aai7786

Segreti, J., Gvazdinskas, L. C., and Trenholme, G. M. (1989). *In vitro* activity of minocycline and rifampin against staphylococci. *Diagn. Microbiol. Infect. Dis.* 12, 253–255. doi:10.1016/0732-8893(89)90022-9

Shannon, C. E. (1997). The mathematical theory of communication 1963. *Md. Comput.* 14, 306–317.

Singh, S., Gumbo, T., Boorgula, G. D., Shankar, P., Heysell, S. K., and Srivastava, S. (2022). Omadacycline pharmacokinetics/pharmacodynamics in the hollow fiber system model and potential combination regimen for short course treatment of Mycobacterium kansasii pulmonary disease. *Antimicrob. Agents Chemother.* 66, e0068722. doi:10.1128/aac.00687-22

Song, T., Lee, M., Jeon, H. S., Park, Y., Dodd, L. E., Dartois, V., et al. (2015). Linezolid trough concentrations correlate with mitochondrial toxicity-related adverse events in the treatment of chronic extensively drug-resistant tuberculosis. *EBioMedicine* 2, 1627–1633. doi:10.1016/j.ebiom.2015.09.051

Srivastava, S., Cirrincione, K. N., Deshpande, D., and Gumbo, T. (2020a). Tedizolid, faropenem, and moxifloxacin combination with potential activity against nonreplicating *Mycobacterium tuberculosis*. *Front. Pharmacol.* 11, 616294. doi:10.3389/fphar.2020.616294

Srivastava, S., Deshpande, D., Magombedze, G., and Gumbo, T. (2018a). Efficacy versus hepatotoxicity of high-dose rifampin, pyrazinamide, and moxifloxacin to shorten tuberculosis therapy duration: There is still fight in the old warriors yet. *Clin. Infect. Dis.* 67, S359–S364. doi:10.1093/cid/ciy627

Srivastava, S., Deshpande, D., Magombedze, G., van Zyl, J., Cirrincione, K., Martin, K., et al. (2019). Duration of pretomanid/moxifloxacin/pyrazinamide therapy compared with standard therapy based on time-to-extinction mathematics. *J. Antimicrob. Chemother.* 75, 392–399. doi:10.1093/jac/dkz460

Srivastava, S., Deshpande, D., Nuermberger, E., Lee, P. S., Cirrincione, K., Dheda, K., et al. (2018b). The sterilizing effect of intermittent tedizolid for pulmonary tuberculosis. *Clin. Infect. Dis.* 67, S336–S341. doi:10.1093/cid/ciy626

Srivastava, S., Gumbo, T., and Thomas, T. (2021a). Repurposing cefazolin-avibactam for the treatment of drug resistant *Mycobacterium tuberculosis*. *Front. Pharmacol.* 12, 776969. doi:10.3389/fphar.2021.776969

Srivastava, S., Magombedze, G., Koeuth, T., Sherman, C., Pasipanodya, J. G., Raj, P., et al. (2017). Linezolid dose that maximizes sterilizing effect while minimizing toxicity and resistance emergence for tuberculosis. *Antimicrob. Agents Chemother.* 61, 007511–e817. doi:10.1128/AAC.00751-17

Srivastava, S., Pasipanodya, J. G., Meek, C., Leff, R., and Gumbo, T. (2011). Multidrug-resistant tuberculosis not due to noncompliance but to between-patient pharmacokinetic variability. *J. Infect. Dis.* 204, 1951–1959. doi:10.1093/infdis/jir658

Srivastava, S., Thomas, T., Howe, D., Malinga, L., Raj, P., Alffenaar, J. W., et al. (2021b). Cefdinir and beta-lactamase inhibitor independent efficacy against *Mycobacterium tuberculosis*. *Front. Pharmacol.* 12, 677005. doi:10.3389/fphar.2021.677005

Srivastava, S., van Zyl, J., Cirrincione, K., Martin, K., Thomas, T., Deshpande, D., et al. (2020b). Evaluation of ceftriaxone plus avibactam in an intracellular hollow fiber model of tuberculosis: Implications for the treatment of disseminated and meningeal tuberculosis in children. *Pediatr. Infect. Dis. J.* 39, 1092–1100. doi:10.1097/INF.0000000000002857

Steenken, W., Jr., and Gardner, L. U. (1946). History of H37 strain of tubercle bacillus. *Am. Rev. Tuberc.* 54, 62–66. doi:10.1164/art.1946.54.1.62

Svensson, M., Nilsson, L. E., Strom, M., Nilsson, M., and Sorberg, M. (2002). Pharmacodynamic effects of nitroimidazoles alone and in combination with clarithromycin on *Helicobacter pylori*. *Antimicrob. Agents Chemother.* 46, 2244–2248. doi:10.1128/aac.46.7.2244-2248.2002

Swaminathan, S., Pasipanodya, J. G., Ramachandran, G., Hemanth Kumar, A. K., Srivastava, S., Deshpande, D., et al. (2016). Drug concentration thresholds predictive of therapy failure and death in children with tuberculosis: Bread crumb trails in random forests. *Clin. Infect. Dis.* 63, S63–S74. doi:10.1093/cid/ciw471

Vera-Cabrera, L., Gonzalez, E., Rendon, A., Ocampo-Candiani, J., Welsh, O., Velazquez-Moreno, V. M., et al. (2006). *In vitro* activities of DA-7157 and DA-7218 against *Mycobacterium tuberculosis* and Nocardia brasiliensis. *Antimicrob. Agents Chemother.* 50, 3170–3172. doi:10.1128/AAC.00571-06

Vogelman, B., Gudmundsson, S., Leggett, J., Turnidge, J., Ebert, S., and Craig, W. A. (1988). Correlation of antimicrobial pharmacokinetic parameters with therapeutic efficacy in an animal model. *J. Infect. Dis.* 158, 831–847. doi:10.1093/infdis/158.4.831

Welling, P. G., Shaw, W. R., Uman, S. J., Tse, F. L., and Craig, W. A. (1975). Pharmacokinetics of minocycline in renal failure. *Antimicrob. Agents Chemother.* 8, 532–537. doi:10.1128/aac.8.5.532

WHO (2022). *Rapid communication: Key changes to the treatment of drug-resistant tuberculosis*. Geneva, Switzerland: World Health Organizaton.

Yamamoto, T., Takano, K., Matsuyama, N., Koike, Y., Minshita, S., Sanaka, M., et al. (1999). Pharmacokinetic characteristics of minocycline in debilitated elderly patients. *Am. J. Ther.* 6, 157–160. doi:10.1097/00045391-199905000-00006

Zinner, S. H., Lagast, H., and Klastersky, J. (1981). Antistaphylococcal activity of rifampin with other antibiotics. *J. Infect. Dis.* 144, 365–371. doi:10.1093/infdis/144.4.365

frontiers | Frontiers in Pharmacology

TYPE Review
PUBLISHED 31 October 2022
DOI 10.3389/fphar.2022.1021216

OPEN ACCESS

EDITED BY
Johannes Alffenaar,
The University of Sydney, Australia

REVIEWED BY
Ruo Wang,
Shanghai Jiao Tong University, China
Penke Vijaya Babu,
Curia India Pvt Ltd, India
Vipan Kumar,
Guru Nanak Dev University, India

*CORRESPONDENCE
Kaushik Chanda,
chandakaushik1@gmail.com

SPECIALTY SECTION
This article was submitted to Pharmacology of Infectious Diseases, a section of the journal Frontiers in Pharmacology

RECEIVED 17 August 2022
ACCEPTED 03 October 2022
PUBLISHED 31 October 2022

CITATION
Dasmahapatra U and Chanda K (2022), Synthetic approaches to potent heterocyclic inhibitors of tuberculosis: A decade review.
Front. Pharmacol. 13:1021216.
doi: 10.3389/fphar.2022.1021216

Synthetic approaches to potent heterocyclic inhibitors of tuberculosis: A decade review

Upala Dasmahapatra and Kaushik Chanda*

Department of Chemistry, School of Advanced Sciences, Vellore Institute of Technology, Vellore, India

Tuberculosis (TB) continues to be a significant global health concern with about 1.5 million deaths annually. Despite efforts to develop more efficient vaccines, reliable diagnostics, and chemotherapeutics, tuberculosis has become a concern to world health due to HIV, the rapid growth of bacteria that are resistant to treatment, and the recently introduced COVID-19 pandemic. As is well known, advances in synthetic organic chemistry have historically enabled the production of important life-saving medications that have had a tremendous impact on patients' lives and health all over the world. Small-molecule research as a novel chemical entity for a specific disease target offers in-depth knowledge and potential therapeutic targets. In this viewpoint, we concentrated on the synthesis of a number of heterocycles reported in the previous decade and the screening of their inhibitory action against diverse strains of *Mycobacterium tuberculosis*. These findings offer specific details on the structure-based activity of several heterocyclic scaffolds backed by their *in vitro* tests as a promising class of antitubercular medicines, which will be further useful to build effective treatments to prevent this terrible illness.

KEYWORDS

tuberculosis, heterocycles, synthesis, *in vitro*, *Mycobacterium tuberculosis*, docking

Introduction

The year 2020 gave us glimpses of what happens in reality when untreatable neglected infectious diseases spread freely. There are several issues such as healthcare, hospital saturation, mammoth lethality, economic burden, and political mistrust that accompanied this huge global pandemic (Yamey et al., 2017; Global Preparedness Monitoring Board, 2019). But to our knowledge, COVID-19 is not the only infectious disease with an epidemic potential. Tuberculosis (TB) is one of the most lethal infectious diseases that man has ever encountered. Since ancient times, tuberculosis has plagued the world, and a tuberculosis diagnosis was regarded as a death sentence. Tuberculosis (TB)

Abbreviations: WHO, World Health Organization; HIV, human immunodeficiency virus; FDA, Food and Drug Administration; INH, isoniazid; MIC, minimum inhibitory concentration; SAR, structure–activity relationship; *M.tb*, *Mycobacterium tuberculosis*; RIF, rifampicin; IC_{50}, inhibitory concentration; LD_{50}, lethal dose; CC_{50}, cytotoxic concentration; DNA, deoxyribonucleic acid; and ATP, adenosine triphosphate.

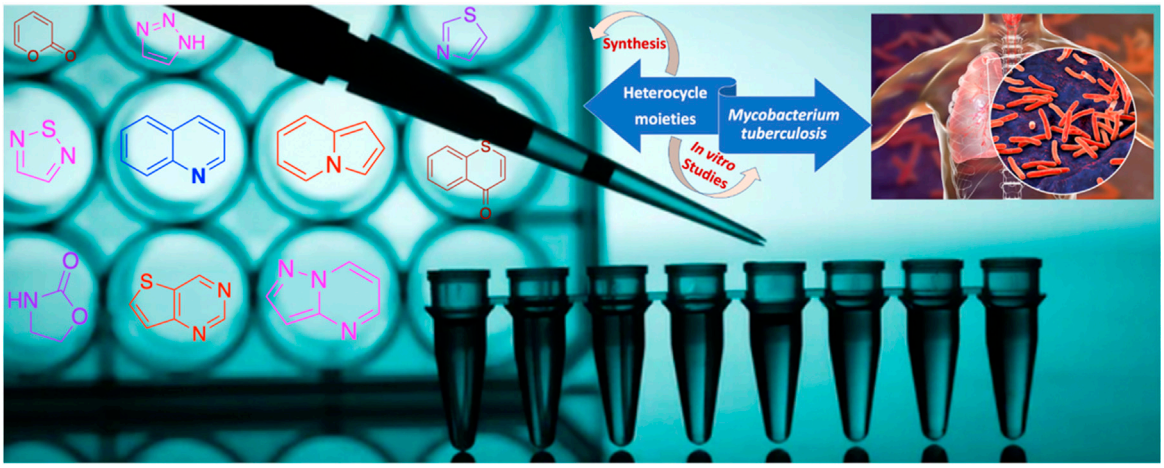

GRAPHICAL ABSTRACT

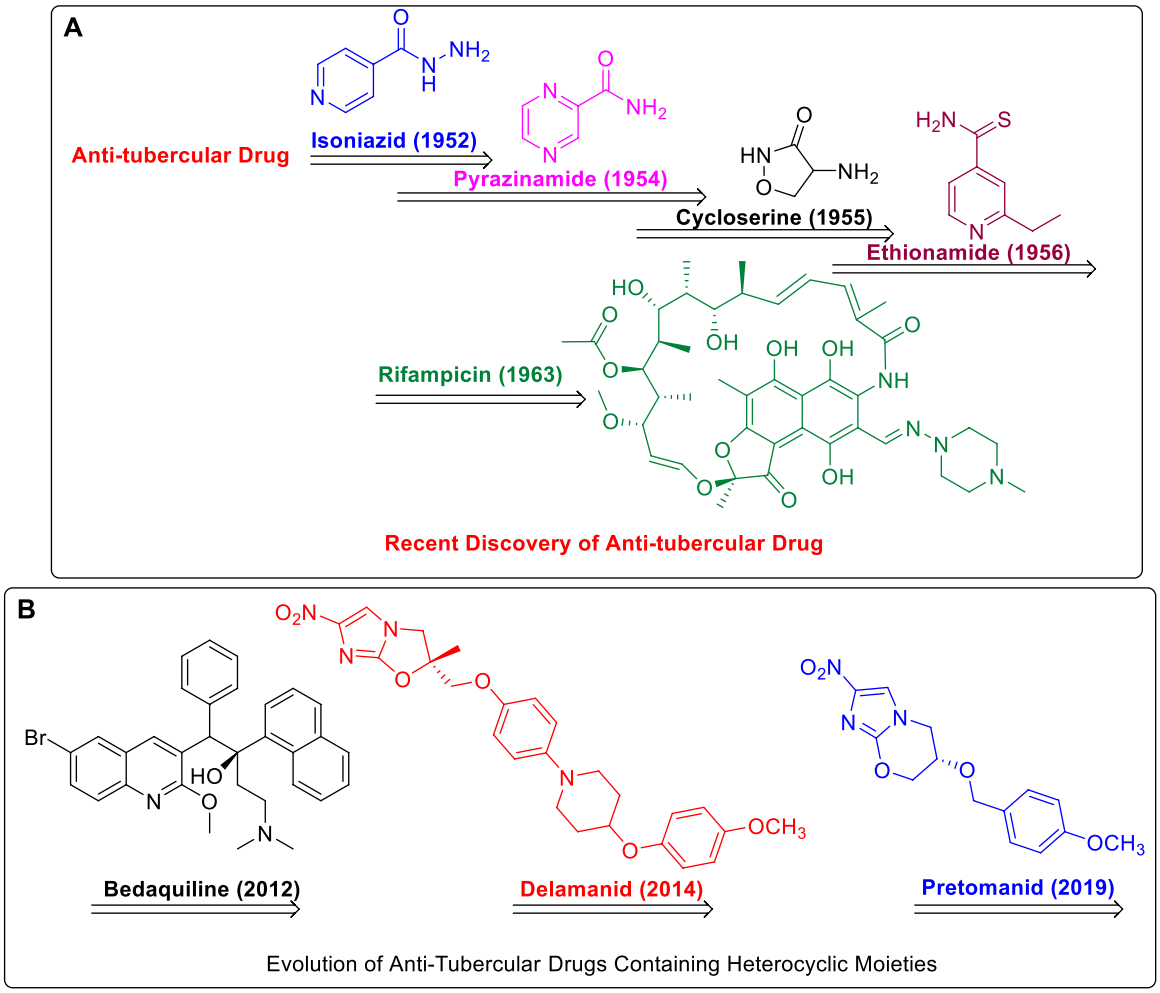

FIGURE 1
(A) Recent Discovery of Anti-Tubercular Drugs. **(B)** Evolution of Anti-Tubercular Drugs Containing Heterocyclic Moieties.

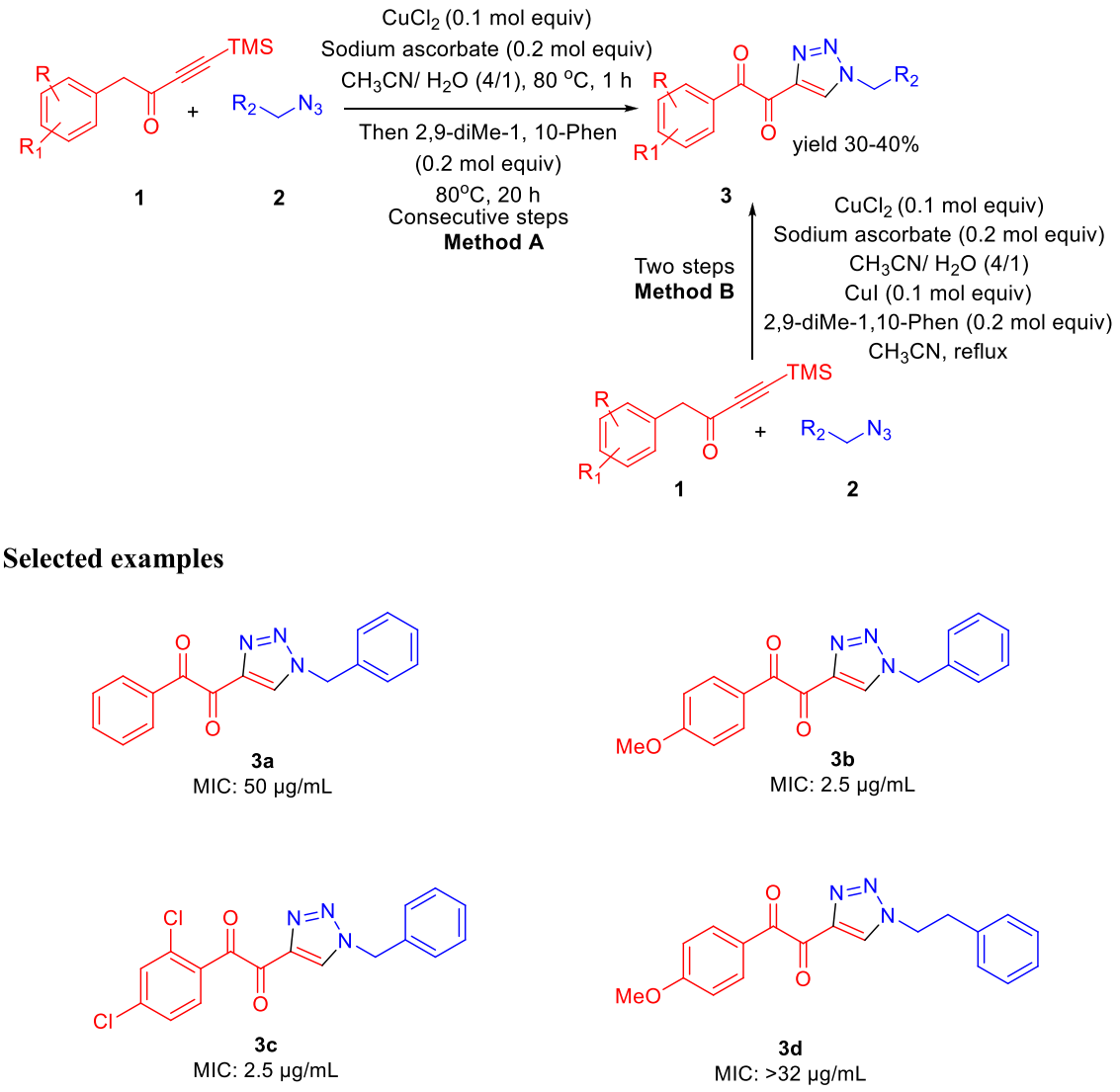

SCHEME 1
Synthesis of α,β-diketotriazoles from both TMS-ynones and azides *via* the click pathway.

can be caused by multiple *Mycobacterium tuberculosis* (*M.tb*) complexes such as *Mycobacterium pinnipedii*, *Mycobacterium microti*, *Mycobacterium canettii*, *Mycobacterium bovis*, *Mycobacterium africanum*, and *Mycobacterium caprae* (Furin et al., 2019; Torres Ortiz et al., 2021). The occurrence of multidrug and a wide range of drug-resistant strains of *Mycobacterium tuberculosis* (*M.tb*) is a growing concern that needs to be addressed (Zumla et al., 2013). Unlike other microorganisms, *Mycobacterium tuberculosis* has infected approximately 1.7 billion people around the world, accounting for more than 20% of the global population. This infectious disease, which is classified as a pandemic, sickens nearly 10 million people each year. According to WHO findings, tuberculosis (TB) nearly claimed the lives of 1.5 million people in 2020 (World Health Organization, 2021a). Due to the COVID-19 pandemic, there was a reduced access to its diagnosis, treatment, and the providing of essential services. Due to this, it has caused the mortality of already affected people and, simultaneously, it was spread among other healthy individuals. Tuberculosis mostly affects the lungs, which can spread from person to person through air, and active pulmonary TB patients are the main source of infection. Despite the fact that a large proportion of infected people may clear the latent infection with time, tuberculosis is one of the World Health Organization's top 10 causes of death (Holzheimer et al., 2021; World Health Organization, 2020; Fu

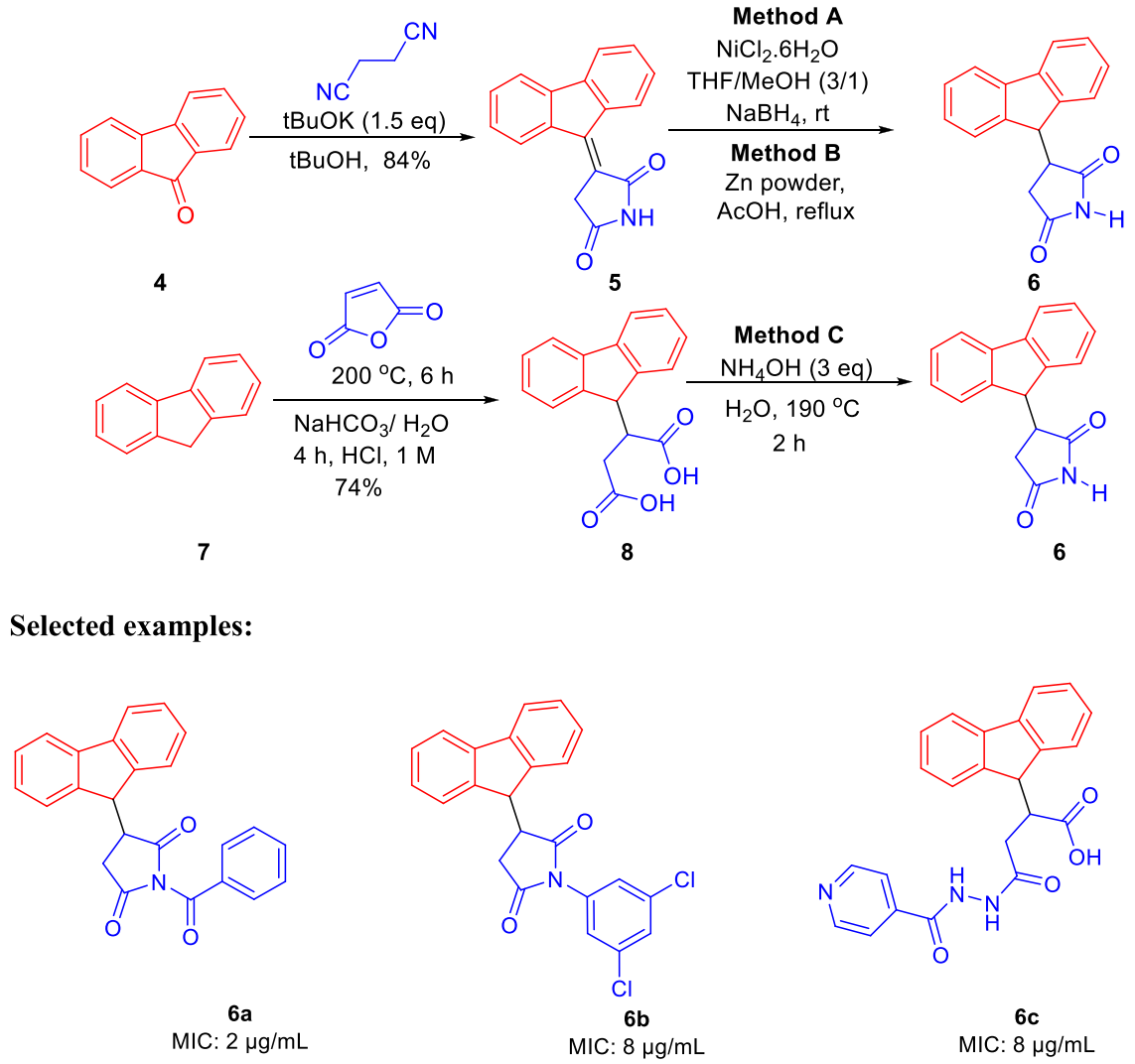

SCHEME 2
Synthesis of succinimides by multiple methods.

et al., 2021). One year is the typical treatment time for antitubercular drugs against drug-susceptible tuberculosis, whereas treatment for drug-resistant tuberculosis can take years. In both cases, a lengthy course of antibiotics is required, and adherence is essential for success (Gandhi et al., 2010). The bacterium is mostly shielded from other immune reactions while gaining access to host resources, and after antibiotic treatment, it frequently enters a dormant state inside the human host (Kiran et al., 2016). With the advent of HIV, the situation indirectly increased the severity of the disease; 1.3 million deaths were reported in 2020 among HIV-negative cases with additional deaths of 2.1 million in HIV-positive people. A total of 9.9 million cases were reported in 2020. South-East Asia and Africa are mostly prone to this disease with an account for 85% of total TB deaths in 2020. This trend was observed at all levels: global, regional, and country. The pandemic has inverted years of improvement and research on TB due to the feebleness of governing authorities in its diagnosis. It is estimated that TB would have caused an enormous number of deaths worldwide after the COVID-19 pandemic in 2020 (Ryckman et al., 2022). It affects people of all ages. However, men are more affected than women and children. Tuberculosis co-infected with HIV is more reported in the African region (World Health Organization, 2021b; Moyo et al., 2022).

Globally, the brighter part in tuberculosis elimination is that countries like the United States and European region have low incidence, whereas countries like India, China, and Indonesia constitute a major part of affected cases. For its treatment, the

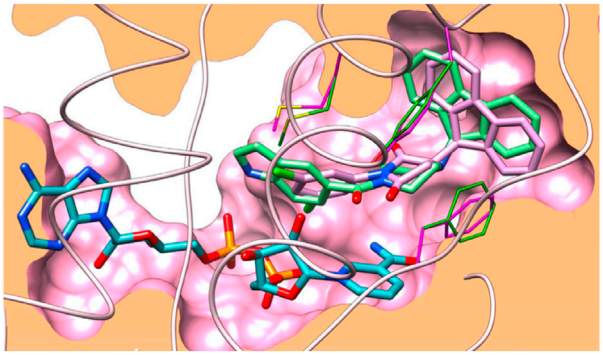

FIGURE 2
Docking binding of **6b** with InhA. Reproduced from Baltas et al., 2013, with permission from Elsevier, Copyright 2013.

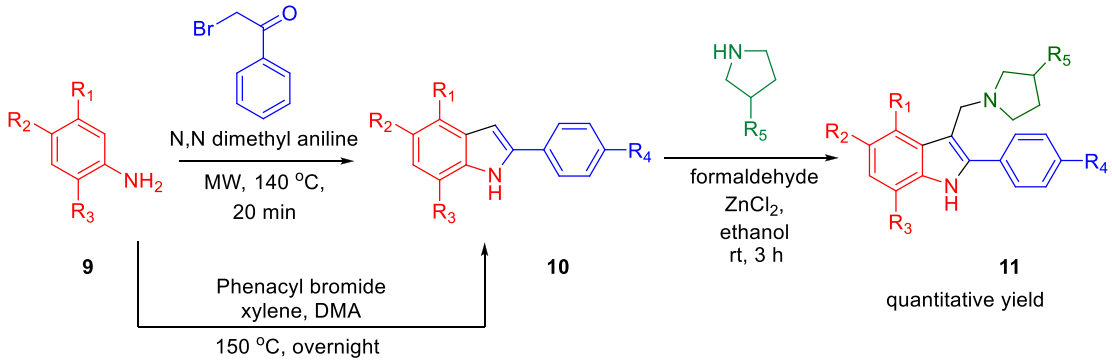

Selected examples:

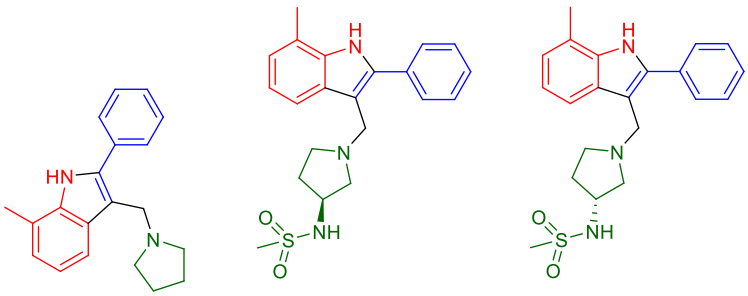

SCHEME 3
Microwave-assisted synthesis of phenylindoles.

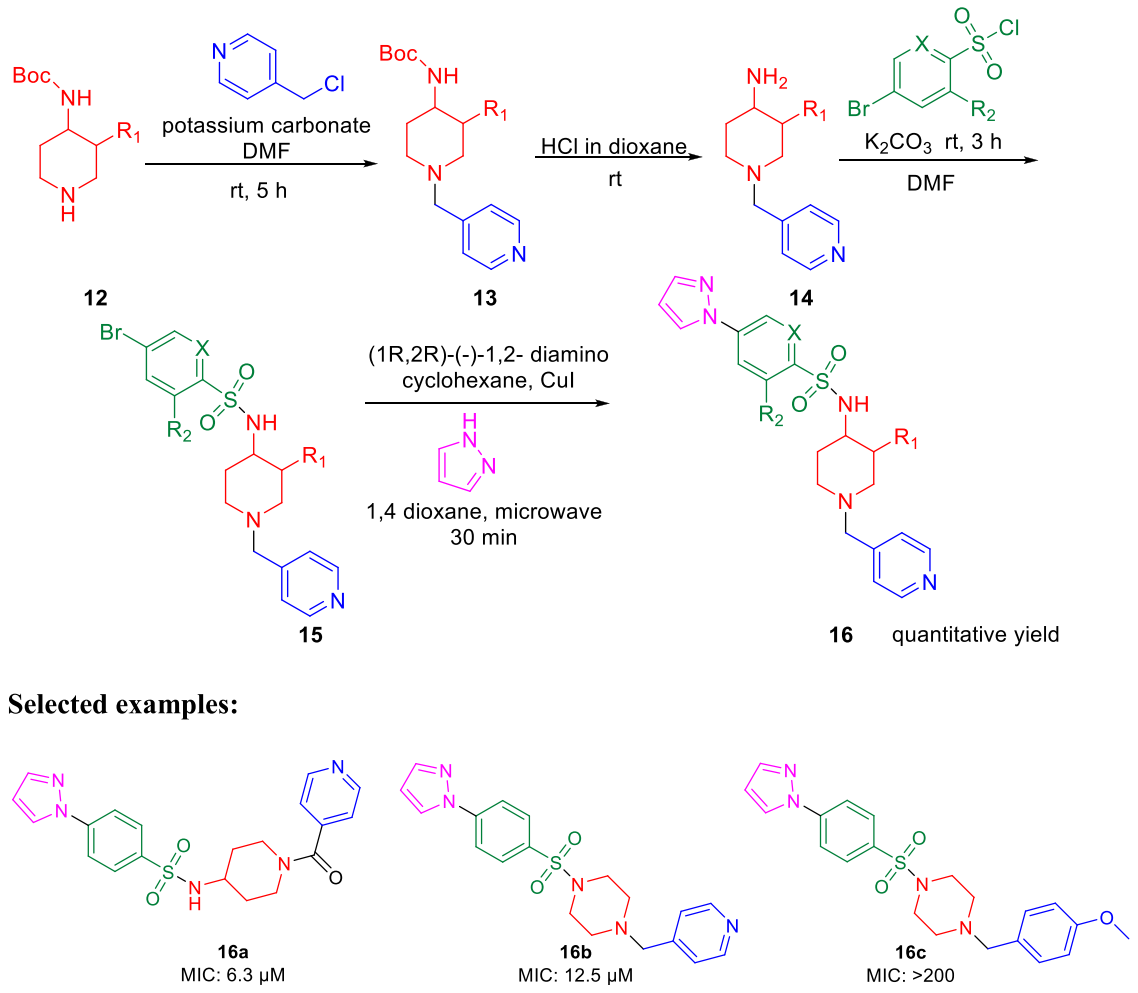

SCHEME 4
Microwave-assisted synthesis of arysulfonamide derivatives.

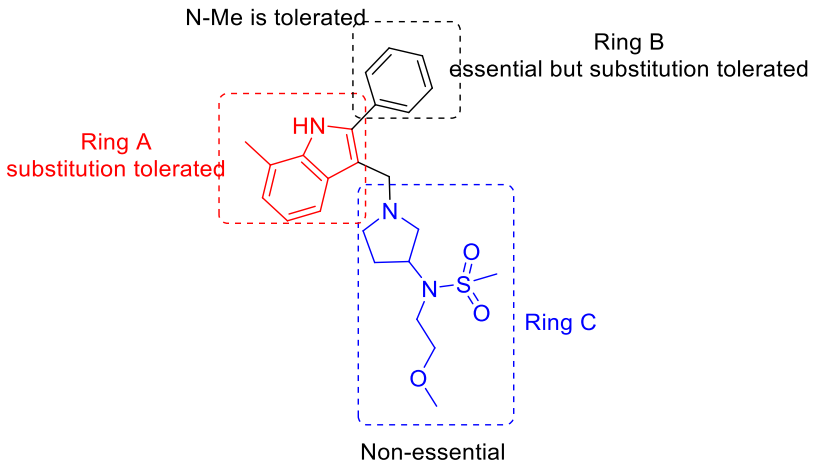

FIGURE 3
SAR for 2-phenylindoles.

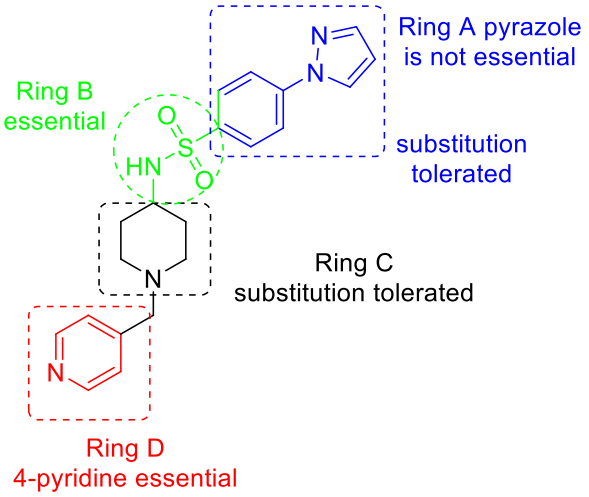

FIGURE 4
SAR for arylsulfonamides.

WHO divided drug-resistant TB into five categories. While many people have latent TB infections that are asymptomatic, active pulmonary TB patients are the main source of infection since it primarily affects the lungs and can spread from person to person through air.

Extensive research on tuberculosis involved many routes to find a potent molecule for its treatment. Many efforts have been made in recent years to develop an effective TB drug pipeline with currently positive results (Evans and Mizrahi, 2018; Libardo et al., 2018; Conradie et al., 2020). Several heterocyclic molecules (Yan and Ma, 2012), peptides (Usmani et al., 2018), and natural products (Igarashi et al., 2017) are also evaluated in drug discovery programs as antitubercular agents. Both medicinal chemistry targets and pharmaceuticals that are now on the market typically use heterocyclic scaffolds as their chemical building blocks. The extreme predominance of oxygen, sulfur, and particularly nitrogen-containing rings in pharmacological compounds is clear. Considering that heterocycles are the fundamental components of a variety of natural compounds, medicinal chemistry studies frequently center on mimicking similar structural patterns. Heterocyclic molecules are both biologically active and toxic, depending on various reasons such as concentration, metabolites formed, and half-life of the moiety. The major reason that controls all of the factors is molecular weight. Although the concentration of the lead molecule during biological studies can be tuned, a number of

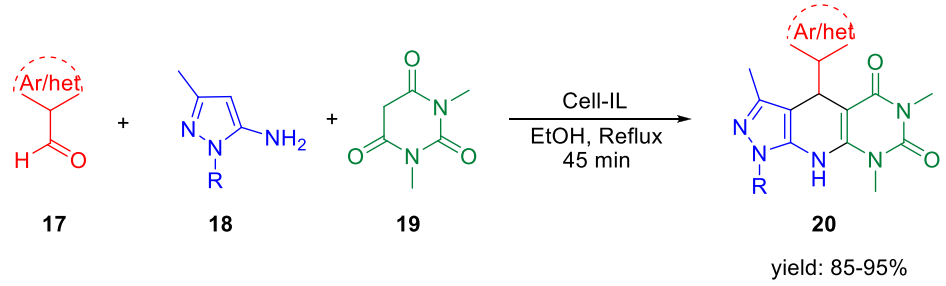

Selected examples:

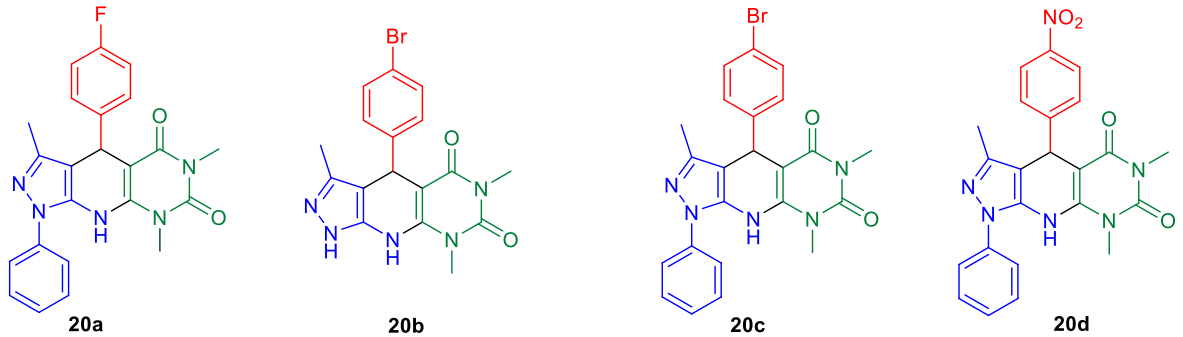

SCHEME 5
Cellulose-supported ionic liquid-catalyzed synthesis of pyrazole-based pyrido[2,3-d]pyrimidine-diones.

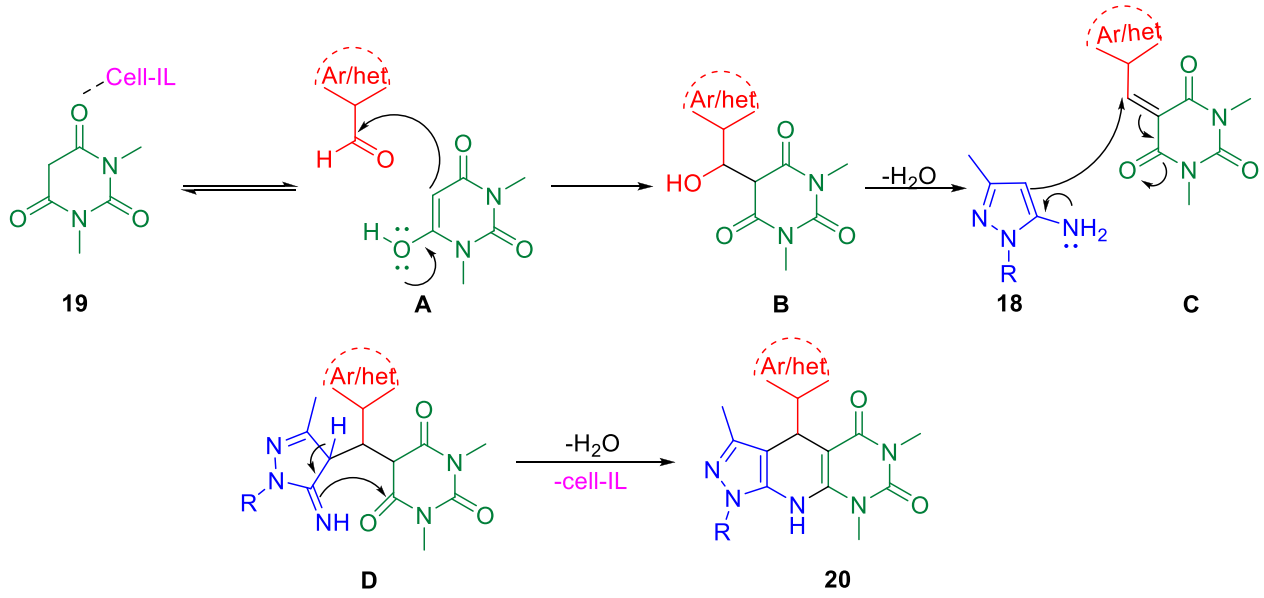

SCHEME 6
Plausible mechanistic pathway for the synthesis of pyrido[2,3-*d*]pyrimidine-diones.

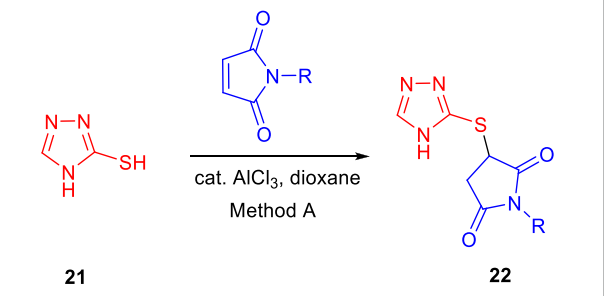

SCHEME 7
Synthesis of compound **22** from 4*H* to 1,2,4-triazole-3thiole by catalytic conjugate addition.

metabolites formed after phase-I and phase-II need to be checked at the desk (Bramhankar and Jaiswal, 1995).

The latest advancements in organic chemistry and strategic route reconnaissance, which are strongly supported by novel synthetic techniques, catalysis, machine learning, and high-throughput experimental technologies, are also thought to be significant for drug development. Within the framework of the research carried out by our group for the development of novel heterocyclic scaffolds (Rao and Chanda, 2022; Panchangam et al., 2021; Padmaja et al., 2019; Panchangam et al., 2019), we discuss various available heterocyclic moieties and drug candidates identified by a target-based approach against tuberculosis diseases. We go in depth on many synthetic techniques that start with distinct synthetic sequences and the ensuing antitubercular activity in this article. Last but not least, combining all synthetic modifications and antitubercular activity will provide essential solutions to the current difficulties in discovering novel antitubercular drugs and will also support knowledge about the current status of antitubercular drug discovery. This review study will also help medicinal and synthetic chemists work together to speed up the development of new antitubercular drugs.

Synthesis and antitubercular activity of heterocyclic moieties

Streptomycin, the first anti-TB drug found after penicillin, was developed in 1943 using *Streptomyces griseus*. Isoniazid, pyrazinamide, cycloserine, ethionamide, and rifampin are the most popular heterocyclic molecules developed until early 1960 as anti-TB drugs (Figure 1) (Chauhan et al., 2010). The treatment for TB has not changed much since then, and long-term use of these drugs is associated with substantial toxic side effects and treatment resistance. On 28th December 2012, the FDA approval of bedaquiline, that is, the first antituberculosis drug to be licensed in more than 40 years, was an important step in this direction. Subsequently, in 2014, delamanid was approved by the European Medicines Agency (EMA), and recently, pretomanid was approved by FDA strictly for use in combination with bedaquiline and linezolid to treat severe drug-resistant tuberculosis (Ryan and Lo, 2014; Keam, 2019; Lubanyana et al., 2020; Guo et al., 2021; Aono et al., 2022).

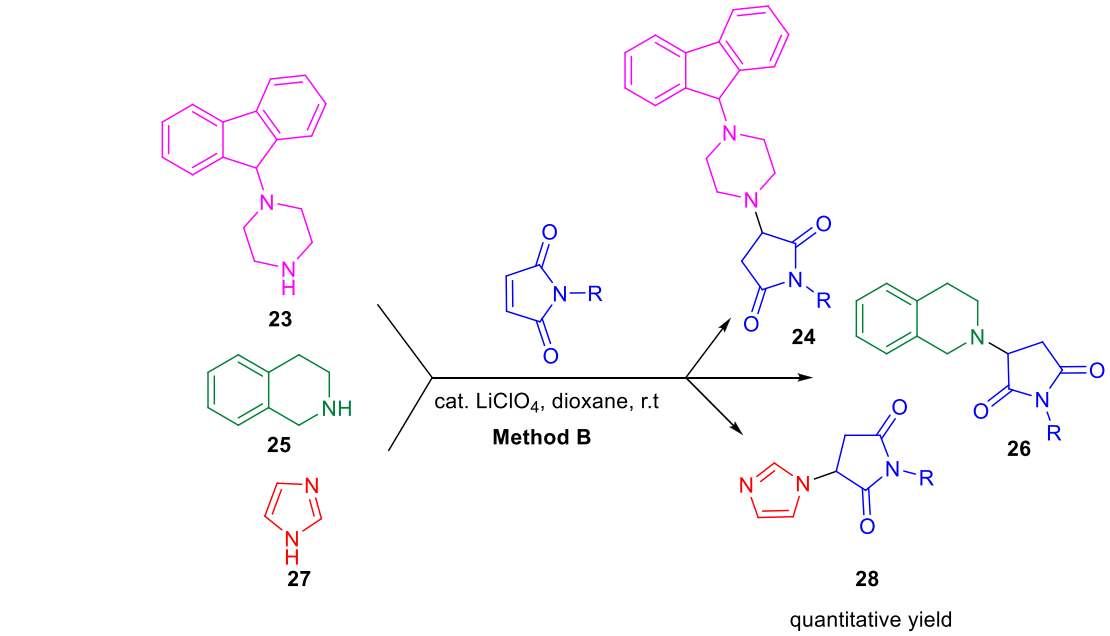

Selected examples:

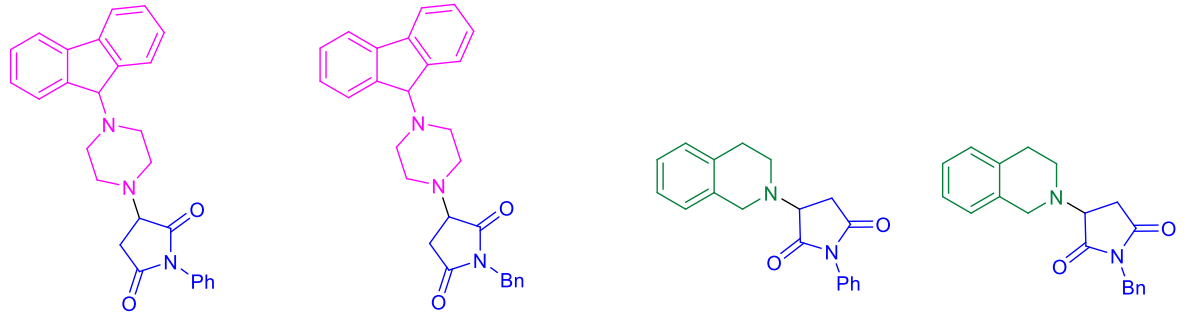

SCHEME 8
Lithium perchlorate catalyzed synthetic route to C–N Michael adducts.

This year, Fernandes et al. have extensively reviewed the *in vivo* efficacy of antitubercular drug candidates against *Mycobacterium tuberculosis*. The report covered only those molecules that entered into clinical trials in the last 6 years (Fernandes et al., 2022). Compared to the recent report in 2022 (Fernandes et al., 2022), where there were no synthetic methodologies described, we have made an effort to highlight the most noteworthy examples of heterocyclic moieties reported in the last decade, highlighting various strategies to develop potential novel compounds with antitubercular properties. The potential antitubercular action of hybrid compounds incorporating isoniazid with various heterocyclic scaffolds, on the other hand, was an intriguing finding in recent studies (Reis et al., 2019; Johansen et al., 2021; Alcaraz et al., 2022).

In 2013, Baltas *et al.* reported the synthesis of α,β-diketotriazoles and investigated the potential biological activity against *Mycobacterium tuberculosis* (Menendez et al., 2013). According to Scheme 1, TMS-ynones 1 and azide derivatives 2 were reacted together to produce α,β-ketotriazoles in the presence of $CuCl_2$ and sodium ascorbate using a CH_3CN-H_2O mixture as solvent. Subsequently, α,β-diketotriazole derivatives 3 were synthesized by two slightly different protocols. α,β-

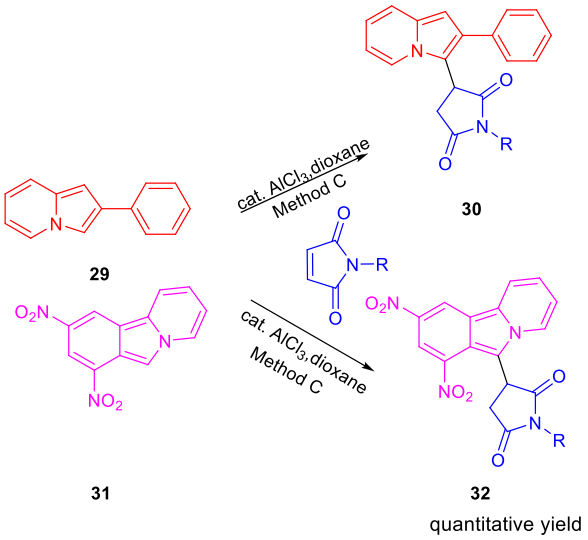

SCHEME 9
Synthesis of compound **30** and compound **32** by catalytic conjugate addition using N-substituted maleimides.

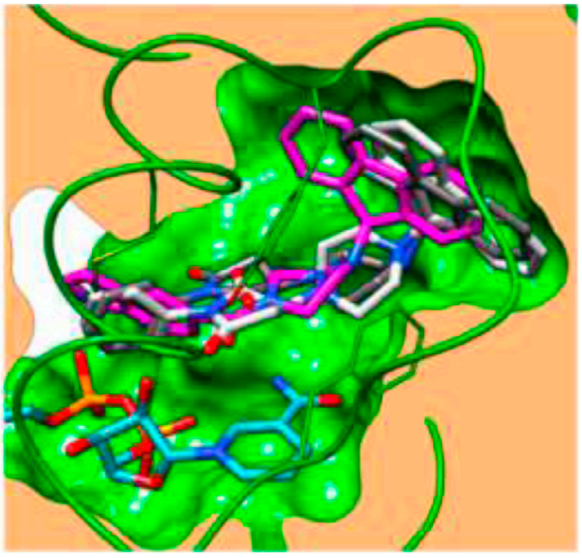

FIGURE 5
Predicted binding pattern of **24a.** Dark gray represents *R*-enantiomer and light gray represents *S*-enantiomer. Reproduced from Matviiuk et al., 2014a, with permission from Elsevier, Copyright 2014.

diketotriazole derivatives 3 were synthesized from the α-ketotriazoles using CuI or $CuCl_2$ under reflux conditions and $CH_3CN–H_2O$ mixture as solvent at 80°C for 1 h followed by the addition of 2,9-dimethyl-1,10-phenanthroline at the same temperature for 20 h (method A). The one-pot method B (two-step processes) was performed by TMS deprotection, followed by a 1,3-dipolar cycloaddition reaction between azide **2** and deprotected ynone **1** at 80°C using the CH_3CN-H_2O mixture as solvent. Finally, the α,β-diketotriazole derivatives 3 were obtained in moderate to excellent yields by the addition of CuI and 2,9-diMe-1,10-Phen under reflux conditions (Menendez et al., 2011; Menendez et al., 2012). On the most researched H37Rv strains of *M. tuberculosis* with a smooth colony shape, all produced α-ketotriazoles, and the corresponding α,β-diketotriazoles have been examined by their minimum inhibitory concentration (MIC). The attenuated tubercle *bacillus M. tb* H37Ra is closely linked to the virulent kind strain *M. tb* H37Rv. The differences between *Mycobacterium tuberculosis* H37Ra and H37Rv's membranes and carrier proteins may have an impact on how effective an antibiotic treatment is. Predominantly, among the synthesized library, compounds **3b** and **3c** have shown 2.5 μg/ml MIC value with no cytotoxicity toward the HCT116 and GM637 human cells.

The same group further developed 3-(9H-fluoren-9-yl) pyrrolidine-2,5-dione derivatives by three different pathways (**methods A, B,** and **C**) and evaluated their efficacies against *M. tuberculosis* in the same year (Matviiuk et al., 2013). In **method A**, the fluorenone 4 was condensed with succinonitrile under basic conditions resulting in 3-(9H-fluoren-9-ylidene)pyrrolidine-2,5-dione followed by the reduction of the double bond using $NiCl_2$ and $NaBH_4$, which led to the formation of compound **6** with 40% yield, whereas in **method B**, zinc powder and acetic acid were used under reflux conditions to gave a yield of 97% of compound **6** (López-Rodríguez et al., 1999; Ballini et al., 2003; Cheng et al., 2008). Compound **8** was prepared by reacting maleic anhydride and fluorene at 200°C followed by basification with ammonium hydroxide at 190°C resulting in the formation of compound **6** with a 73% yield in **method C** (Scheme 2) (Bergmann and Orchin, 1949). Compound **6a** strongly inhibited the growth of *M. tuberculosis* with an MIC value of 2 μg/ml toward H37Rv strain of *M. tb*. On other hand, compound **6b** having a 3,5-dichloromethyl substituent on nitrogen atom exhibited good inhibition with 8 μg/ml and was further chosen for molecular docking studies for being the best InhA inhibitor among the synthesized derivatives (Figure 2).

Like the GEQ inhibitor, compound **6b** binds to InhA's binding pocket following the same pattern. Hydrogen bonding with the residue of Tyr158 is predominantly conserved, while other binding site residues (Met161 and Phe149) showed minor deviations.

In 2014, Chatterji and co-workers demonstrated the synthetic route to 2-phenylindole along with arylsulfonamide and studied their potency against *M. tuberculosis* (Naik et al., 2014). Aniline derivative 9 was reacted with phenacyl bromide in the presence of *N,N′*-dimethyl aniline under microwave

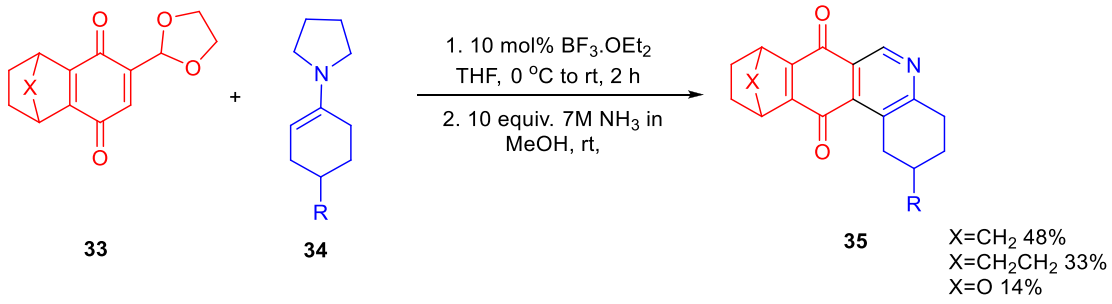

33 **34** **35**

Selected examples

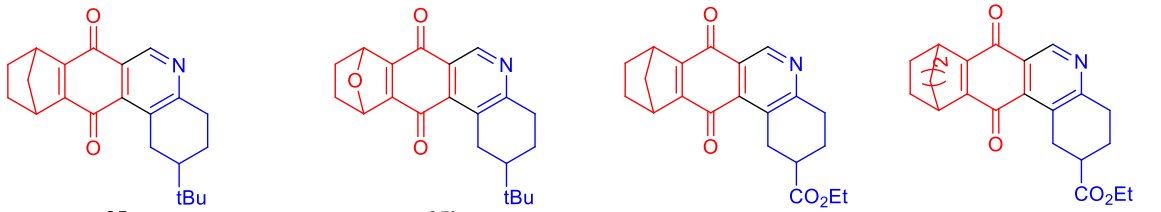

35a
MIC: 0.59 μM
IC_{50}: 51.35 μM
SI (IC_{50}/ MIC): 87.03

35b
MIC: 7.21 μM
IC_{50}: 53.23 μM
SI (IC_{50}/ MIC): 7.38

35c
MIC: 0.22 μM
IC_{50}: 8.49 μM
SI (IC_{50}/ MIC): 38.59

35d
MIC: 0.26 μM
IC_{50}: 49.76 μM
SI (IC_{50}/ MIC): 191.38

SCHEME 10
Synthesis of octahydrobenzo[*j*]phenanthridinediones *via* epoxy bridge ring opening.

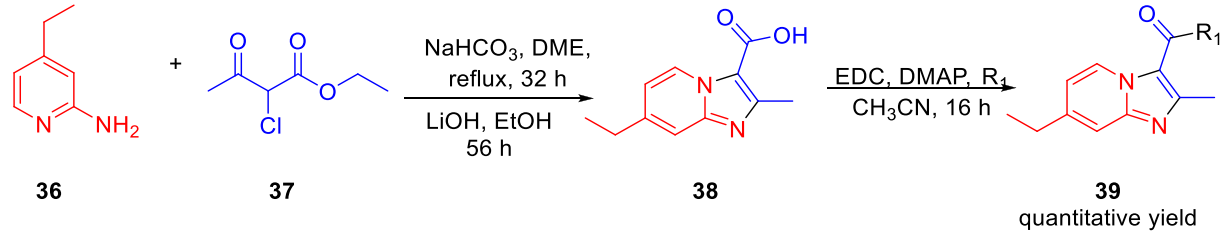

36 **37** **38** **39**
quantitative yield

Selected examples:

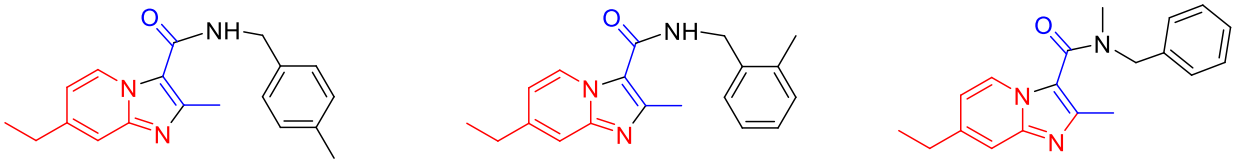

39a
MIC: 0.004 μM

39b
MIC: 2.5 μM

39c
MIC: >20 μM

SCHEME 11
Synthetic route to zolpidem analogs *via* saponification.

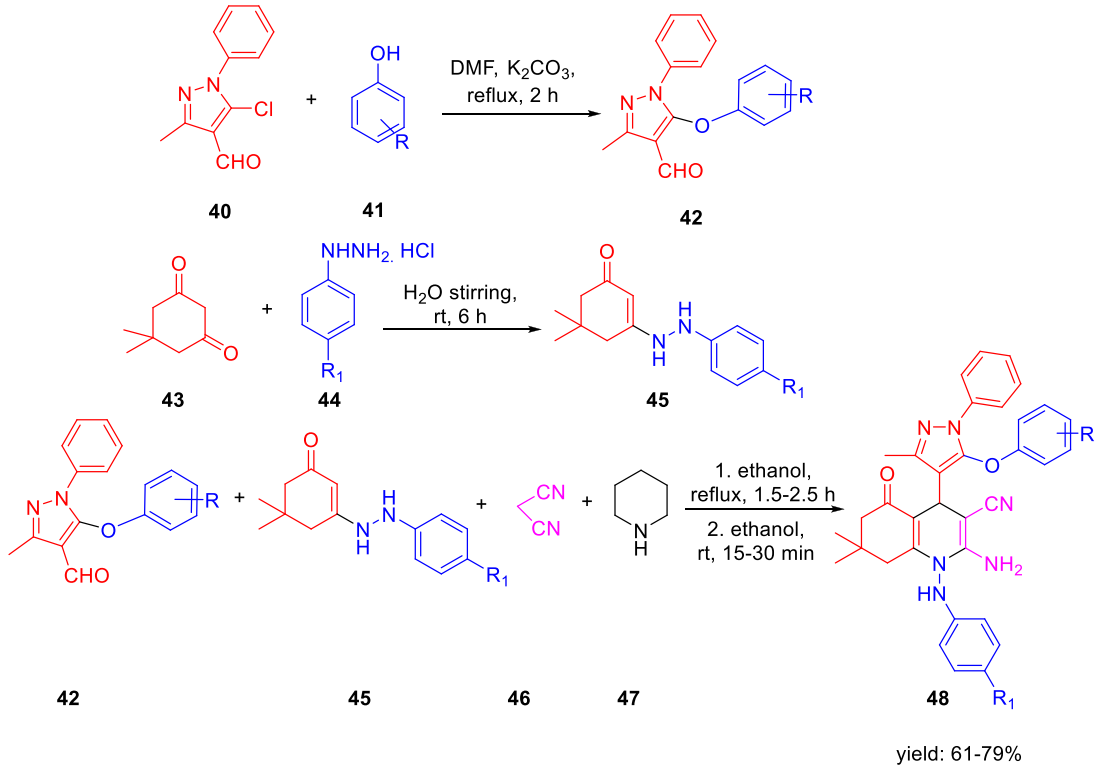

Selected examples:

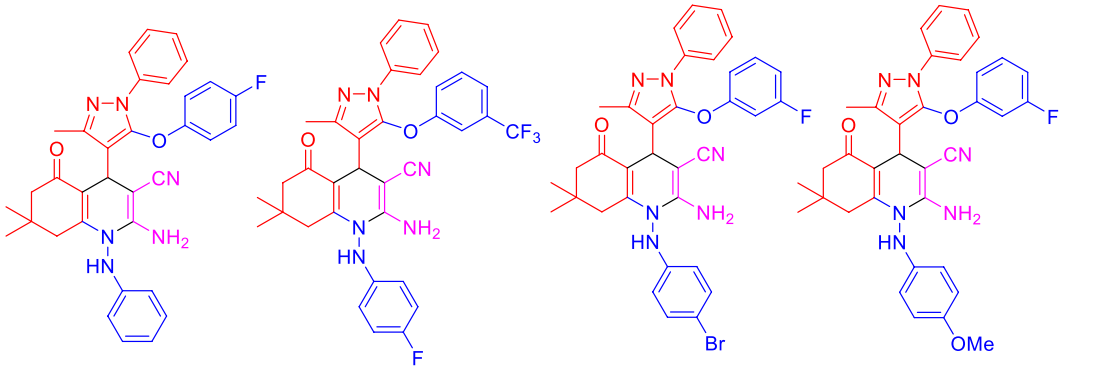

SCHEME 12
Multistep synthesis of polyhydroquinoline derivatives.

conditions for 20 min at 140°C, resulting in compound **10** (phenylindole), as depicted in Scheme 3. Compound **10** was also synthesized using another protocol, in which aniline derivative 9 was reacted with phenacyl bromide in the presence of xylene, DMA at 150°C for 12 h (Mahboobi et al., 2008; Amblard et al., 2013). Subsequently, 3-alkyl pyrrolidine reacted with compound **10** in the presence of $ZnCl_2$ and ethanol at ambient temperature for 3 h to produce the corresponding phenylindole derivative **11** with excellent yield.

Furthermore, arylsufonamides were synthesized from the NHBOC protected 4-aminopiperidine **12** using microwave irradiation. The NHBOC-protected 4-aminopiperidine **12** was reacted with pyridine methyl halide using K_2CO_3 as base in DMF solvent at ambient temperature for 5 h. Next,

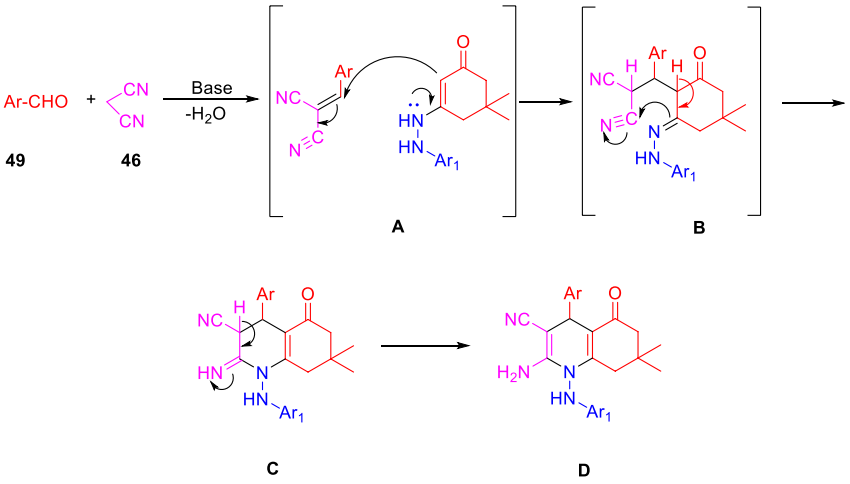

SCHEME 13
Plausible mechanism for the synthesis of polyhydroquinoline derivatives.

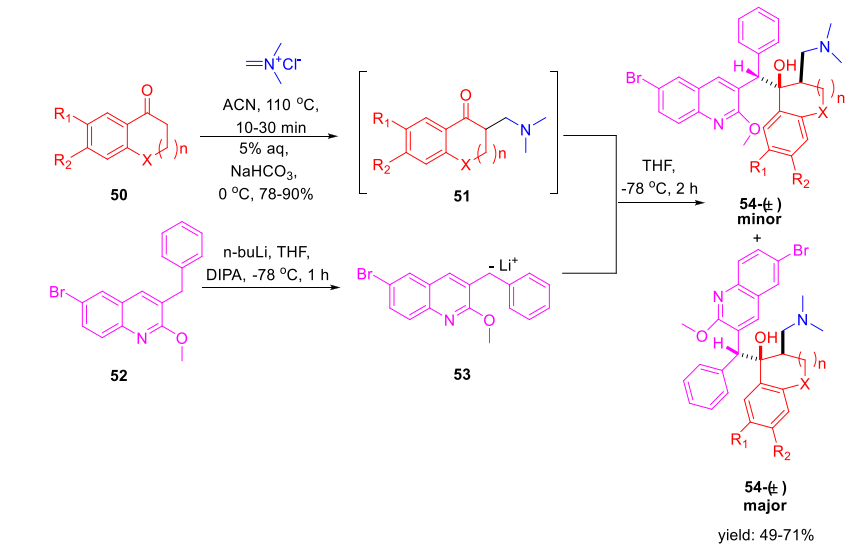

Selected examples:

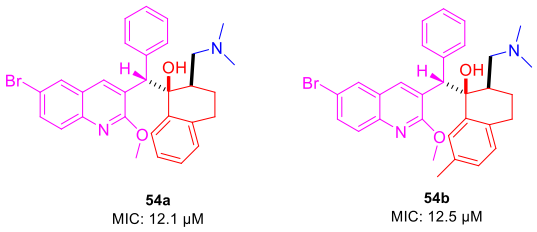

SCHEME 14
Synthetic route to TMC207 analogs using the Mannich base.

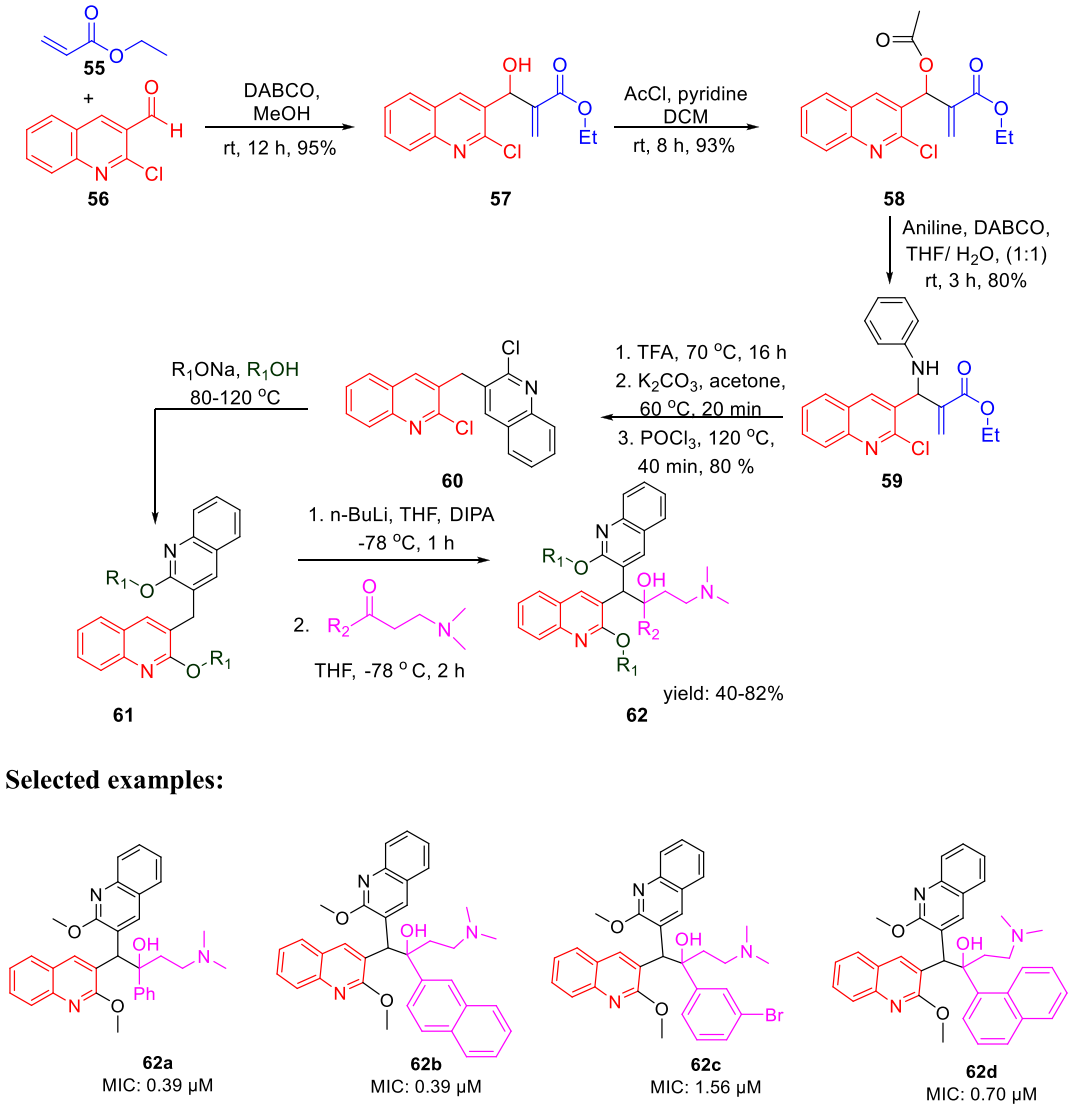

SCHEME 15
Synthetic route to bisquinoline derivatives using the Mannich base.

the BOC deprotection was performed in dioxane containing HCl solution at room temperature to obtain compound **14**. Subsequently, the NH-sulfonylation of compound **14** was executed in DMF solution using bromo-substituted sulfonyl chloride at room temperature for 3 h. Compound **15** was then reacted with pyrazoles using (1*R*,2*R*)-(−)-1,2-diaminocyclohexane and CuI as catalyst in dioxane solution under microwave conditions for 30 min to obtain the final compound **16** (Scheme 4).

For the 2-phenylindole scaffold, a robust SAR was constructed, which resulted in lead-like structures with good physicochemical attributes. The chemical optimization of 2-phenylindoles has been illustrated; 2-phenylindole was broadly divided into ring A, ring B, and ring C, as depicted in Figure 3. The impact of various groups on ring A also showed that electron-donating substituents such as methyl, methoxy, and isopropyl were allowed at the C-7 position, and ring C is a nonessential part.

Similarly, SAR of arylsulfonamide also suggested (Figure 4) that the presence of ring B is essential, whereas the presence of pyrazole ring A is not essential. The investigation showed that the alteration of the pyrazole moiety (ring A) to oxazole did not change the potency of the compounds as antitubercular agents. It was also found that ring C's substitution was tolerated, with the indication of necessity of ring D, that is, 4-pyridine. Testing of the

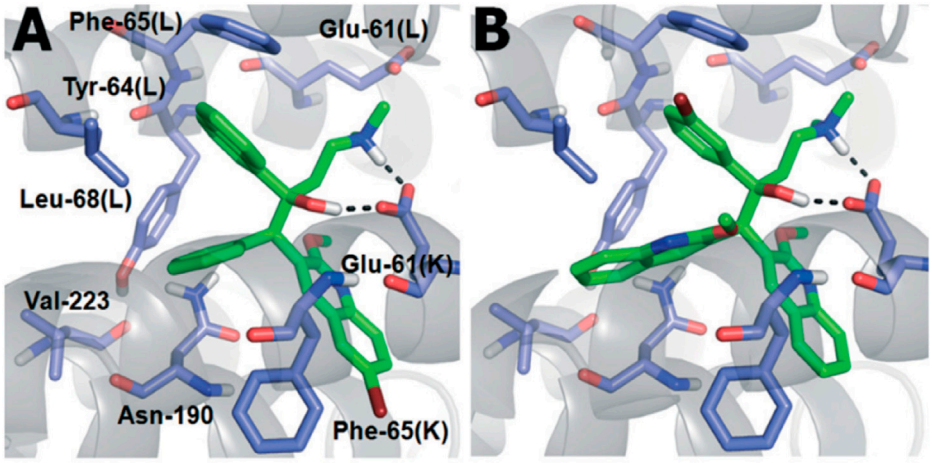

FIGURE 6
(A) Binding mode of TMC207; **(B)** Binding mode of **62C**. Reproduced from Kalia et al., 2015, with permission from Royal Society of Chemistry, Copyright 2015.

synthesized 2-phenylindoles showed the antimicrobial property to H37Rv strain with ~5–10 ratios of MBC to MIC, whereas the arylsulfonamides displayed ~1–2 ratios for the same. Among the synthesized phenylindoles, compounds **11b** and **11c** showed strong potency with an MIC value of 3.1 μM. The MIC values for synthesized arylsulfonamides **16a** and **16b** on the other hand were 6.3 and 12.5 μM, respectively.

Further, in the same year, Raval *et al.* accomplished the synthesis of pyrazole-fused pyrido[2,3-d]pyrimidine-dione derivatives and evaluated their biological properties (Satasia et al., 2014). Pyrazole-fused pyrido[2,3-d]pyrimidine-dione derivatives **20** were synthesized by the reaction of aldehyde **17**, aminopyrazoles **18**, and 1,3-dimethylbarbituric acid **19** in the presence of cell-IL as catalyst in ethanol solvent under reflux conditions and resulted in excellent yields (Scheme 5). The synthesis of cellulose-based ionic liquids (cell-ILs) was reported by the same group (Satasia et al., 2013). The solvents were found to have a significant influence on the synthesis of this particular series of compounds. Among the solvents such as acetonitrile, DMSO, methanol, ethanol, water, DMF, and THF, the best results were obtained in ethanol solvent in terms of influencing the reaction and isolating the targeted compound. A plausible mechanism for the synthesis of pyrido[2,3-d]pyrimidine-diones is depicted in Scheme 6. An attempt to perform the reaction without catalyst resulted in a very poor yield of the product. To evaluate the biological activities of this compound against the H37Rv strain of *M. tuberculosis*, *in vitro* antitubercular tests were performed using isoniazid and rifampicin drugs as the standard drugs. Primary screening was executed using the conventional method, that is, Lowenstein–Jensen medium, at 250 and 100 μg/ml, in which compound **20a** unveiled 91% inhibition at a concentration of 250 μg/ml and 88% inhibition at a concentration of 100 μg/ml.

Subsequently, Baltas and co-workers reported different methods of synthesizing 3-heteroaryl-substituted pyrrolidine-2,5-diones by catalytic Michael reaction and estimated their inhibition against *Mycobacterium tuberculosis* (Matviiuk et al., 2014a). Conjugated Michael addition is a well-studied tool to prepare peptide analogs, antibiotics, and pharmaceutical intermediates along with drugs (Kumagai et al., 2003; Bartoli et al., 2006; Shrestha et al., 2012). Compound **21** with encompassing ambident nucleophile was reacted with maleimide by conjugated Michael addition using a catalytic amount of aluminum chloride to generate compound **22** with high yields by **method A**, as depicted in Scheme 7. In another process (**method B**), Michael addition was performed using a catalytic amount of lithium perchlorate and dioxane at room temperature with good yield, as shown in Scheme 8. With **method C**, to carry out Michael addition between bulky heterocycles and nitrogen-substituted maleimides, various catalysts were used including zinc chloride, titanium tetrachloride, tin chloride, and bismuth trichloride. The screening results indicated that C–C conjugated addition was produced in better yields with anhydrous $AlCl_3$ as catalyst, whereas C–N conjugated addition was performed in a better way with a catalytic amount of $LiClO_4$ (Scheme 9). The synthesized moieties were tested for *in vitro* efficacies as an inhibitor of InhA at 50 μM and the MIC values toward *M. Tuberculosis* H37Rv strain. GEQ, triclosan, and isoniazid were used as standards for the comparative study toward the H37Rv inhibitor. Among all tested derivatives, compounds **24a** and **24b** demonstrated the finest activity on InhA protein with 52% and

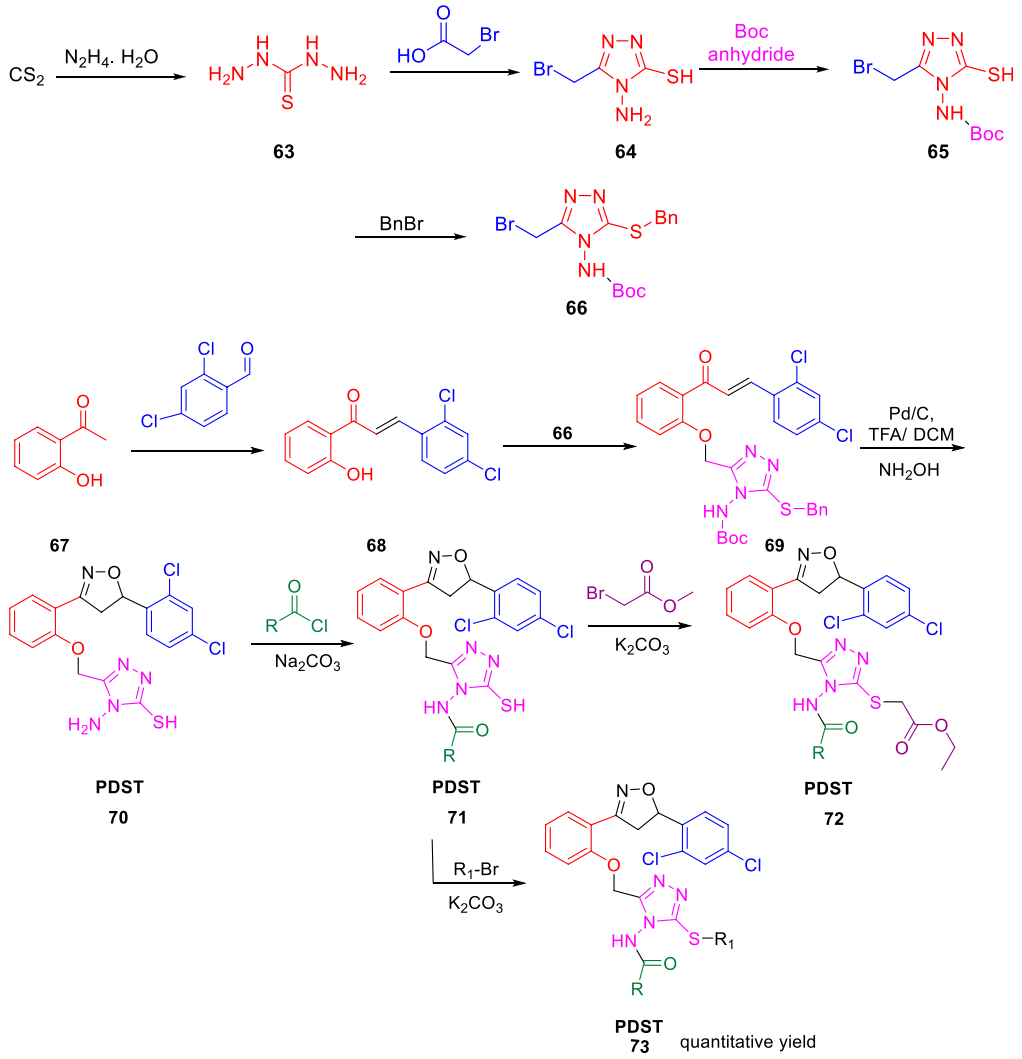

Selected examples:

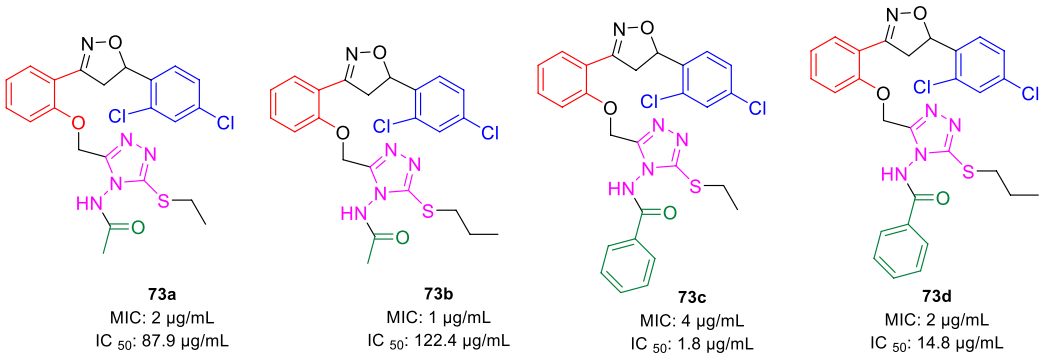

73a
MIC: 2 μg/mL
IC_{50}: 87.9 μg/mL

73b
MIC: 1 μg/mL
IC_{50}: 122.4 μg/mL

73c
MIC: 4 μg/mL
IC_{50}: 1.8 μg/mL

73d
MIC: 2 μg/mL
IC_{50}: 14.8 μg/mL

SCHEME 16
Multistep synthetic route to PDST.

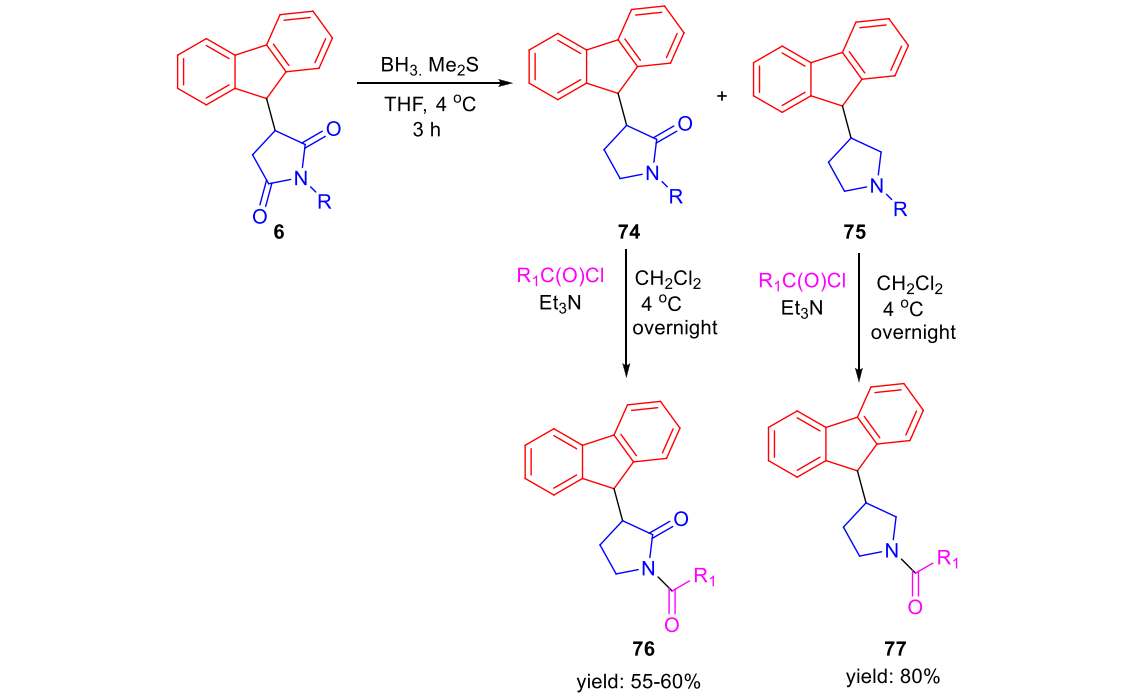

Selected examples:

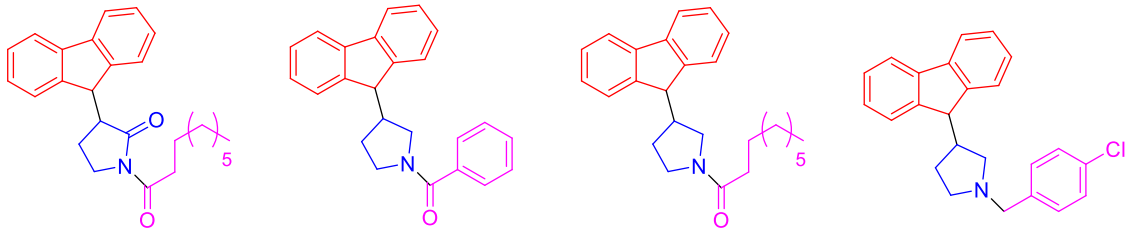

76a
MIC: 10.3 μM
% Inhibition (50 μM): 17%

77a
MIC: >16 μM
% Inhibition (50 μM): 87%

77b
MIC: 21.3 μM
% Inhibition (50 μM): 28%

77c
MIC: 1.4 μM
% Inhibition (50 μM): 15%

SCHEME 17
Synthetic route to pyrrolidinone and pyrrolidine derivatives *via* reduction followed by acylation.

56% inhibition, respectively, at 50 μM. To understand the binding pattern of pyrrolidine-2,5-dione-substituted analogs compared to known nanomolar inhibitors, molecular docking was carried out. *R* and *S* enantiomers of compound **24a** along with GEQ were docked inside the InhA binding site with the help of the calculated algorithm and procedure.

Docking (Figure 5) was accomplished with consideration of 11 amino acid residues from the lateral chain, along with a number of cofactor NAD^+-like traits inside the binding pocket of protein; 0.6 A° was the value of RMSD between crystallographic conformation and the best mode of GEQ docking. From the docking studies and the data of crystallography, it was seen that compound **24a** can be put into the active site by a different geometry. Surprisingly, compound **26a** produced high inhibition while another derivative **26b** showed a reduced activity. Among all of the isoquinoline derivatives, compounds **26a** and **26b** with phenyl and benzyl substituents showed higher inhibition, that is, 20% and 16%, respectively.

In the same year, Huygen and group reported 1,2,3,4,8,9,10,11-octahydrobenzo[j]phenanthridine-7,12-diones as an inhibitor against *Mycobacterium tuberculosis* (Cappoen et al., 2014). Condensation of compound **33** with compound **34** using 10 mol% of boron trifluoride and diethyl ether at 0°C and room temperature for 2 h followed by the addition of ammonia in methanol at room temperature

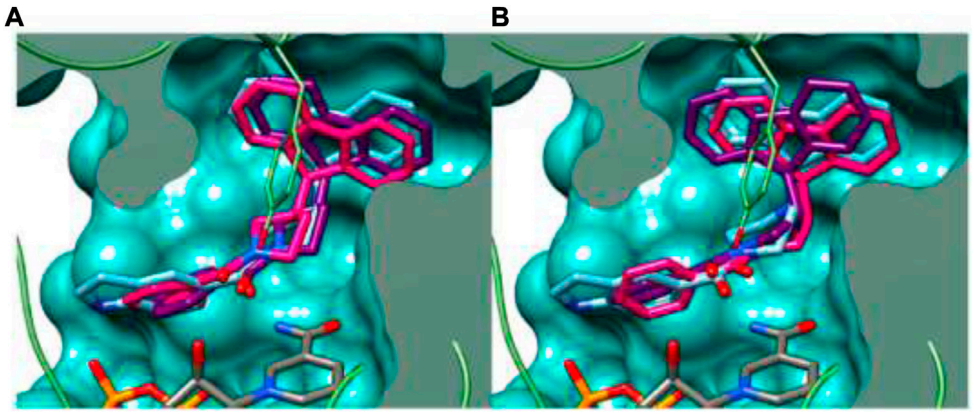

FIGURE 7
Binding mode of **77a** with InhA; **(A)** (R)-enantiomer and **(B)** (S)-enantiomer. Reproduced from Matviiuk et al., 2016, with permission from Elsevier, Copyright 2016.

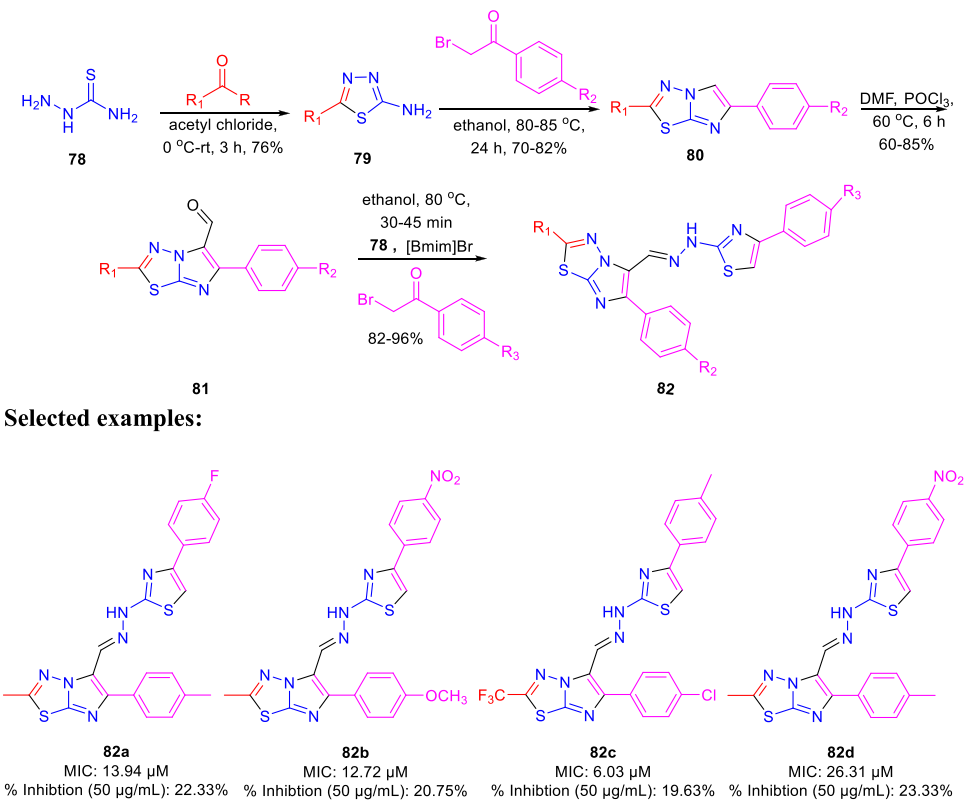

SCHEME 18
One-pot synthesis of 1-((6-phenylimidazo [2,1-b][1,3,4]thiadiazol-5-yl)methylene)-2-(4-phenylthiazol-2-yl)hydrazine derivatives.

obtained resulted in compound **35**, as shown in Scheme 10. Several derivatives of compound **35** were produced with good yield, and antimicrobial activities were tested against luminescent H37Rv strain of *M. tuberculosis* (Forge et al., 2012; Cappoen et al., 2013; Claes et al., 2013). Antitubercular property of these compounds were studied via the depletion of

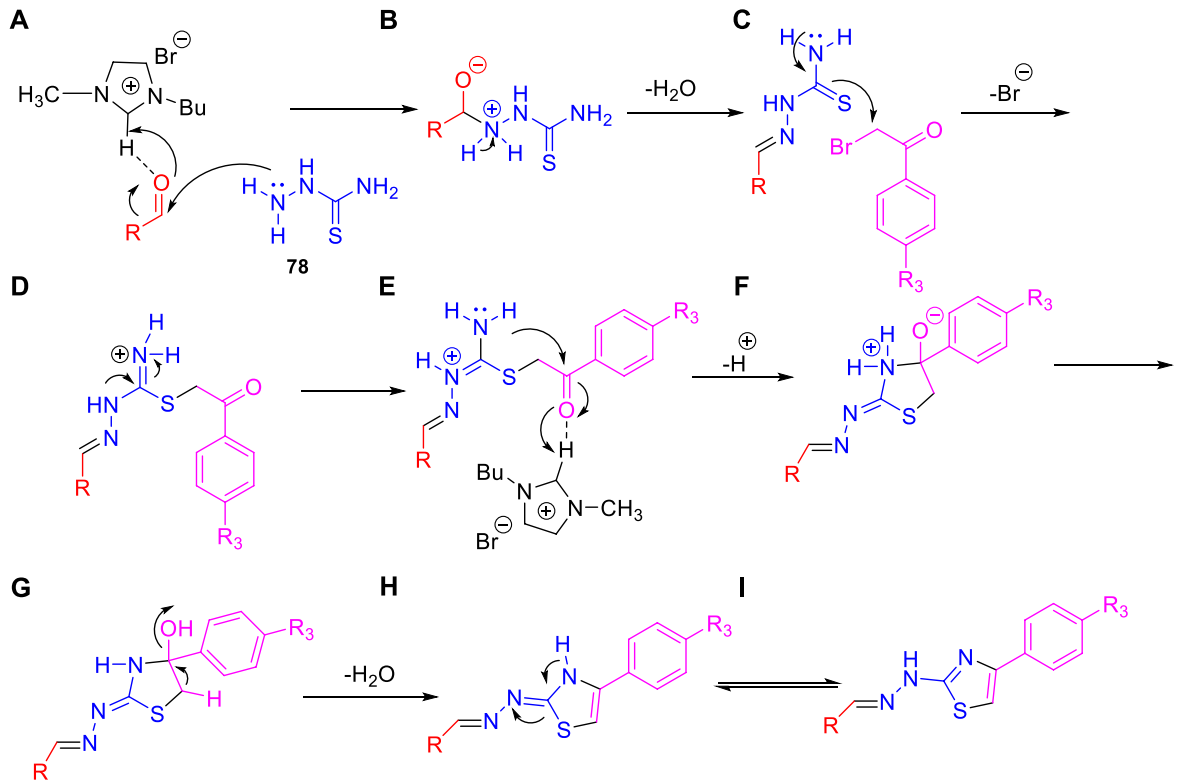

SCHEME 19
Plausible mechanism for the formation of 1-((6-phenylimidazo [2,1-b][1,3,4]thiadiazol-5-yl)methylene)-2-(4-phenylthiazol-2-yl)hydrazine derivatives.

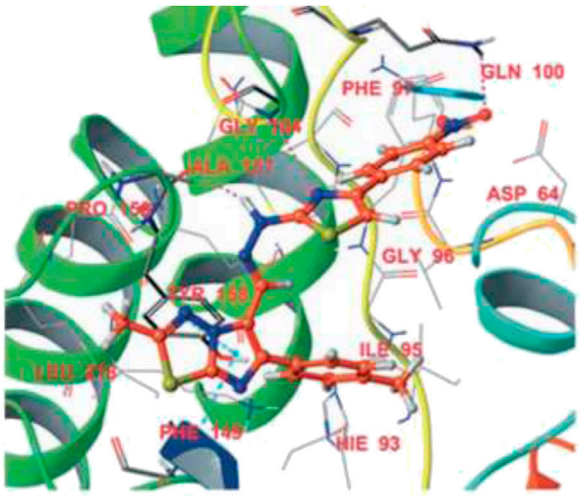

FIGURE 8
Binding mode of **82d** with InhA. Reproduced from Ramprasad et al., 2016, with permission from Royal Society of Chemistry, Copyright 2016.

emitted luminescence by an exposure to compound culture. Additionally, the toxicity of these analogs was checked toward the macrophage model of eukaryotic J774 A.1 cells, as these are the main host for tuberculosis infection. Acute toxic concentration (IC_{50}) of these compounds was divided by corresponding MIC values to achieve the selectivity index. Compound **35a** demonstrated higher activity (MIC = 0.59 μM) and significantly low toxicity (IC_{50} = 51.35 μg/ml), developing a suitable SI of 87.03. For epoxy-bridged molecule **35b**, the MIC value was reported at 7.21 μM along with a IC_{50} value of 53.23 μg/ml, resulting in 7.38 SI value. Both **35c** and **35d** showed extraordinary MIC values of 0.22 and 0.26 μM, respectively. But due to better IC_{50} values, **35d** resulted in the most favorable SI value, that is, 191.38.

Miller *et al.* in 2015 reported the potency of different antitubercular agents toward *M. tb* $H_{37}Rv$ strain and substantial drug-resistant *M. tb* strains (Moraski et al., 2016). As depicted in Scheme 11, the group synthesized 4-zolpidem analogs to discover the patterns that impact the biological function. All analogs were converted to form amide

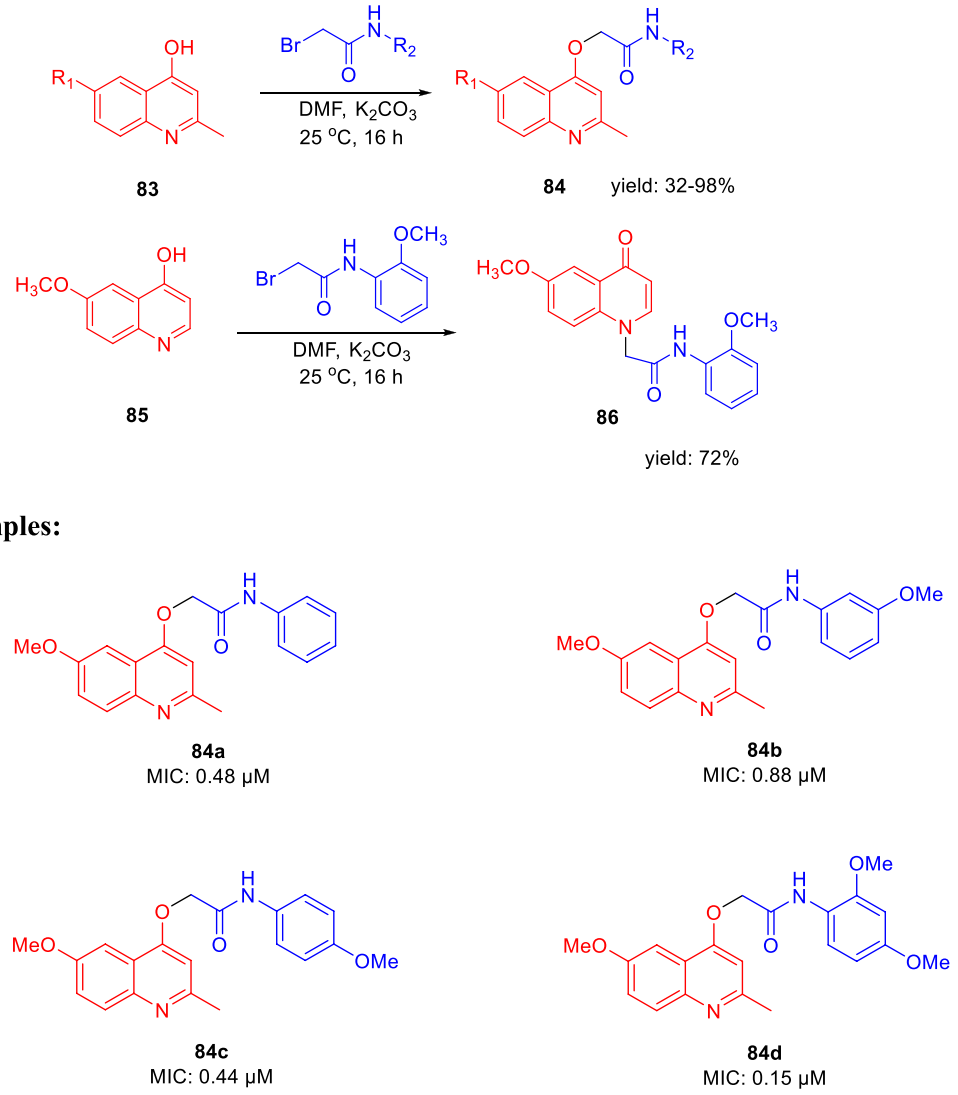

SCHEME 20
Synthesis of 2-(quinolin-4-yloxy)acetamide derivatives *via* O-alkylation reactions.

bond between the analogous carboxylic acid and amines. As per the anticipation, these rationally designed isomers indicated enhancement contrasted to zolpidem. With an MIC value of 0.004 μM, compound **39a** appeared to be the most potent one. It showed almost similar activity as rifampicin, which is a well-known first-line drug for tuberculosis treatment with an MIC value of 0.1 μM (Cohn et al., 1990). All compounds with insufficient hydrogen bond donors demonstrated weak activity. Considering the effect of stereochemistry, it was found that (*R*)-enantiomer had three times better activity than (*S*)-enantiomer. As a control, PA-824 was used to screen all molecules for *M. tb*-resistant strains (Tover et al., 2000). Surprisingly, compound **39a** showed significant activity with MIC value ˂ 0.03 μM against the most common clinical strains. *In vitro* toxicity testing indicated no significant toxicity to Vero cells (Lilienkampf et al., 2009) or PC-3. However, some of the compounds showed moderate toxicity in the HeLa cell line.

In the subsequent year, Karad and his group established a multistep protocol for the synthesis of a fluorinated 5-aryloxypyrazole nucleus through the cyclocondensation reaction, followed by the investigation of its antitubercular property (Karad et al., 2015). As depicted in Scheme 12, compound **40** and aromatic phenol **41** were refluxed in DMF using K_2CO_3 as a base to afford the desired product **42**. Hydrazinoketone **45** was synthesized under aqueous conditions by the reaction of compounds **43** and **44** at room temperature for 6 h. Finally, targeted moiety **48** was

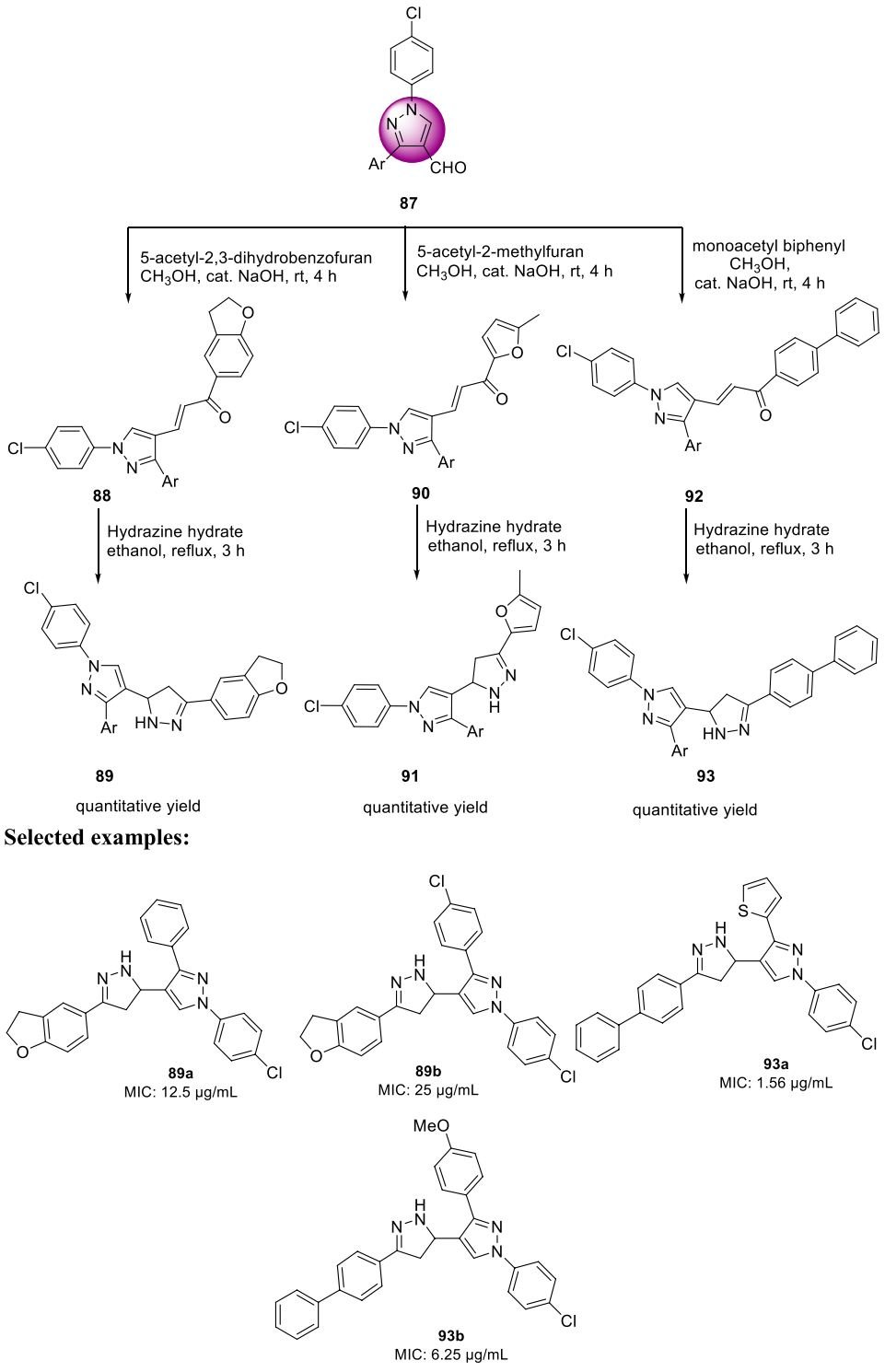

SCHEME 21
Multistep synthesis of pyrazole-containing pyrazoline derivatives.

obtained by refluxing compounds **42** and **45** *via* cyclocondensation reaction in the presence of malonitrile **46** and piperdine **47**. A plausible mechanism for the synthesis of polyhydroquinoline derivatives is depicted in Scheme 13. *In vitro* studies of antitubercular activity of the synthesized compounds were performed toward the H37Rv

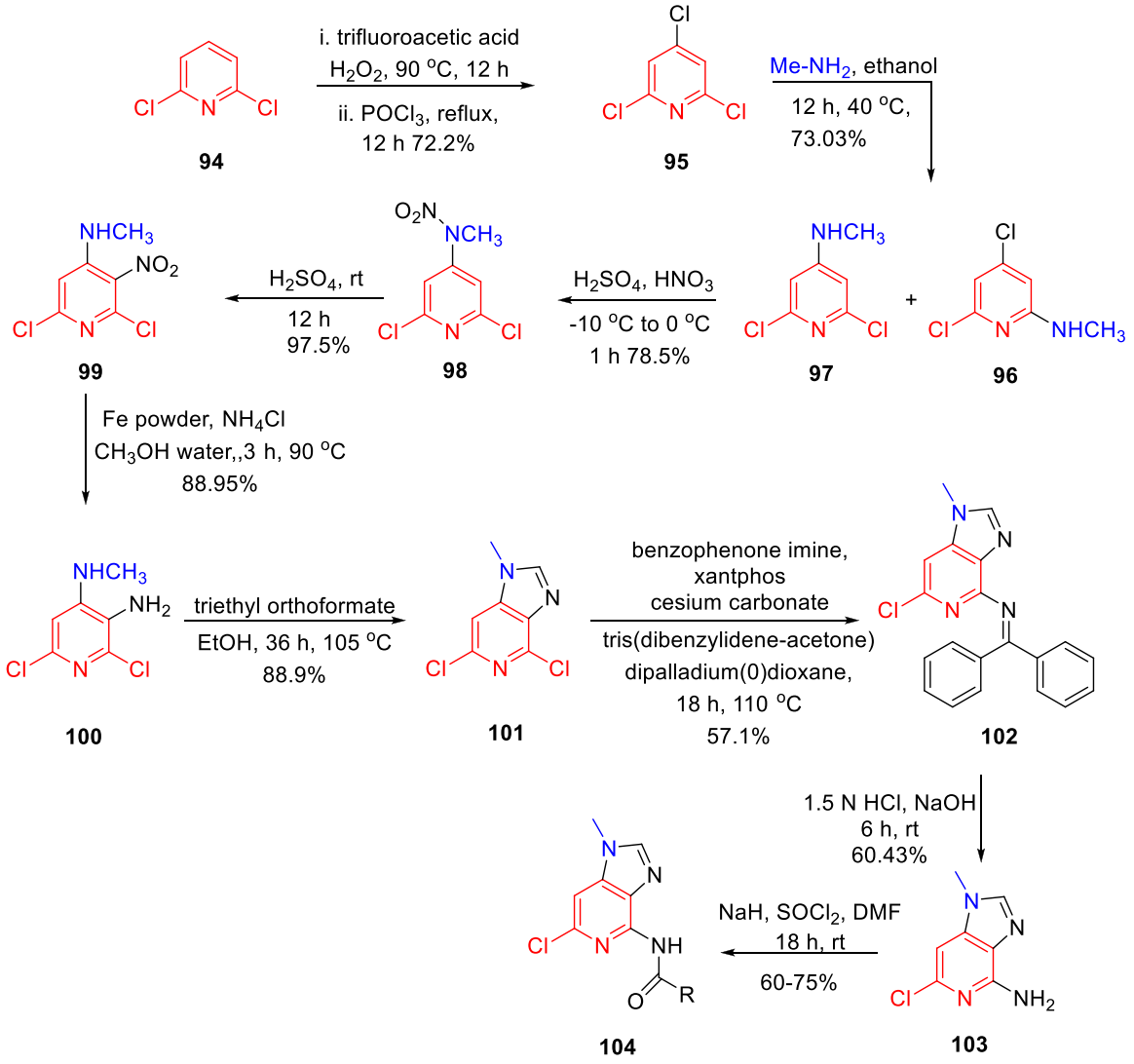

Selected examples:

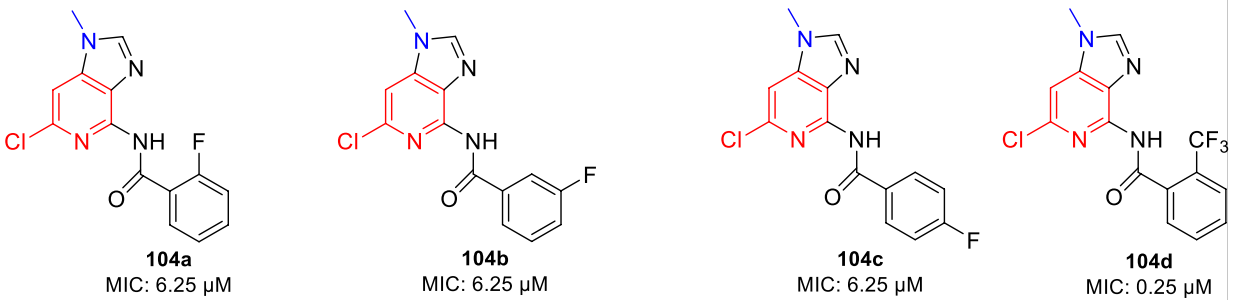

SCHEME 22
Multistep synthesis of imidazo[4,5-c-]pyridine derivatives.

strain using Lowenstein–Jensen medium, where rifampicin and isoniazid were taken as standard drugs. Compounds **48a**, **48b**, and **48c** possessed intense activity with 94%, 95%, and 91% inhibition, respectively, at 250 μg/ml. Further interesting facts were obtained when the cytotoxicity was checked for these molecules in the cellular level by the

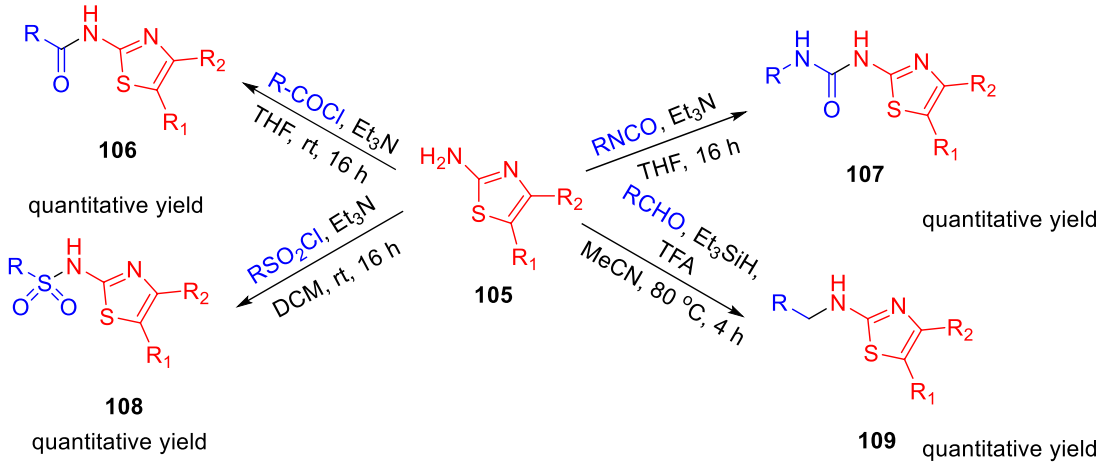

Selected examples:

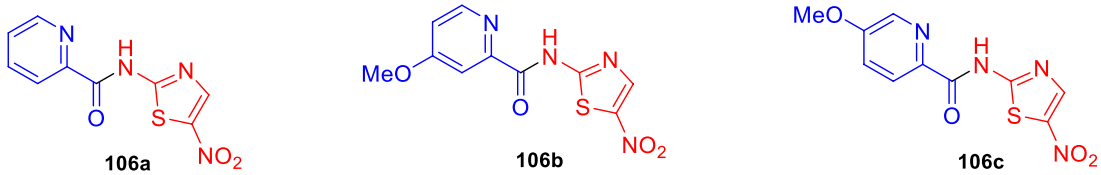

106a
MIC: 2.4 μM
TC_{50}: 20 μM

106b
MIC: 5.6 μM
TC_{50}: 11 μM

106c
MIC: 5.5 μM
TC_{50}: 4.3 μM

SCHEME 23
Synthetic route to nitazoxanide derivatives *via* amide bond formation.

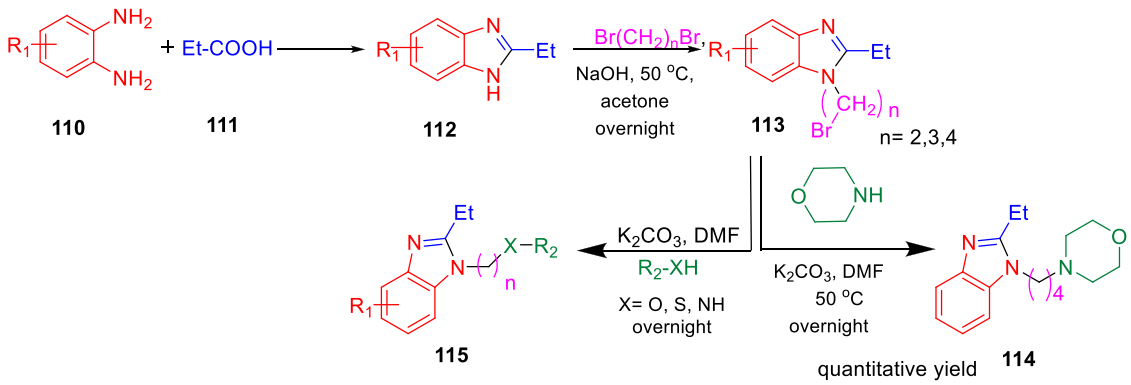

Selected examples:

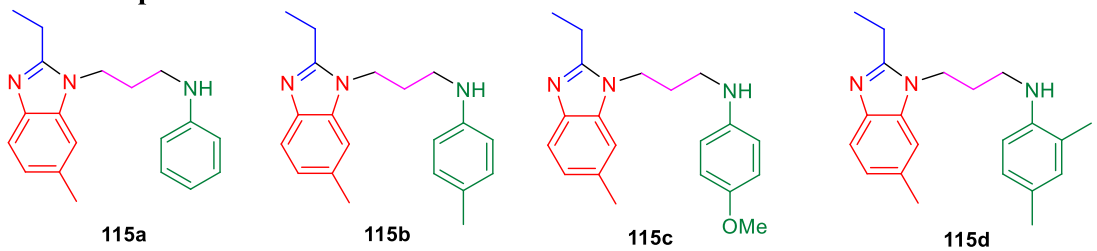

115a
MIC: 0.61 μM
TC_{50}: >50 μM
SI (TC_{50}/MIC): >893

115b
MIC: 0.67 μM
TC_{50}: 31 μM
SI (TC_{50}/MIC): 470

115c
MIC: 0.35 μM
TC_{50}: 91 μM
SI (TC_{50}/MIC): 260

115d
MIC: 0.07 μM
TC_{50}: 14 μM
SI (TC_{50}/MIC): 200

SCHEME 24
Synthesis of cycloalkyl benzimidazoles *via* a condensation reaction.

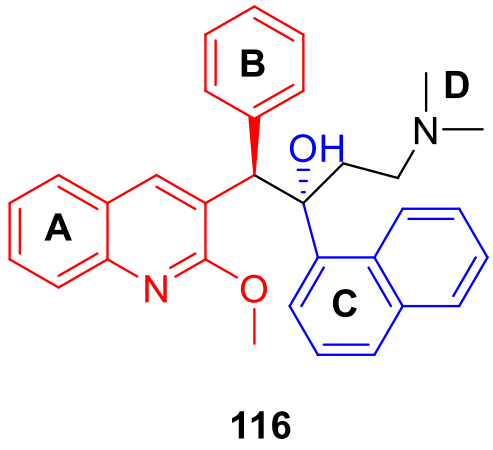

FIGURE 9
SAR study of bedaquinoline.

bioassay test of *S. pombe* cells. Variation in the concentration of different types of substituent has a significant effect on the toxicity level. Compound **48b** appeared to be most toxic, whereas compounds **48a** and **48c** are comparatively less toxic.

In the same year, Kalia *et al.* reported the synthesis of conformationally constrained and bisquinoline analogs of TMC207 and investigated their antitubercular activity (Kalia et al., 2015). Constricted analogs of TMC207 were prepared using benzyl quinoline anion with proper cyclic ketone analogs of the Mannich base as reported earlier (Guillemont et al., 2011). A diastereomeric combination of two conformationally restricted diarylquinolines **54** with five-, six-, and seven-membered rings were synthesized by treating the freshly produced Mannich base **51** with anion **53** (Scheme 14). Subsequently, the bisquinoline analogs of TMC207 were achieved by the reaction of the relevant Mannich bases with the dialkoxybisquinoline anions, which were produced by the treatment of several alkoxides with

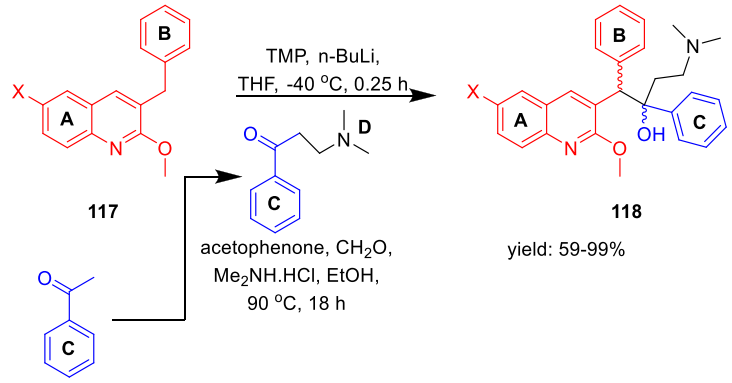

Selected examples:

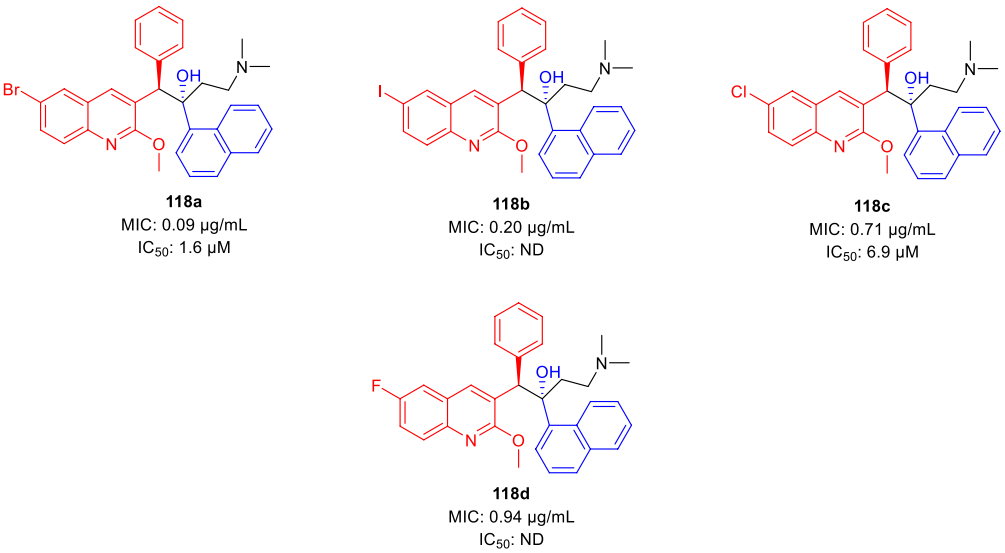

SCHEME 25
Synthetic route to diarylquinoline derivatives *via* a condensation reaction.

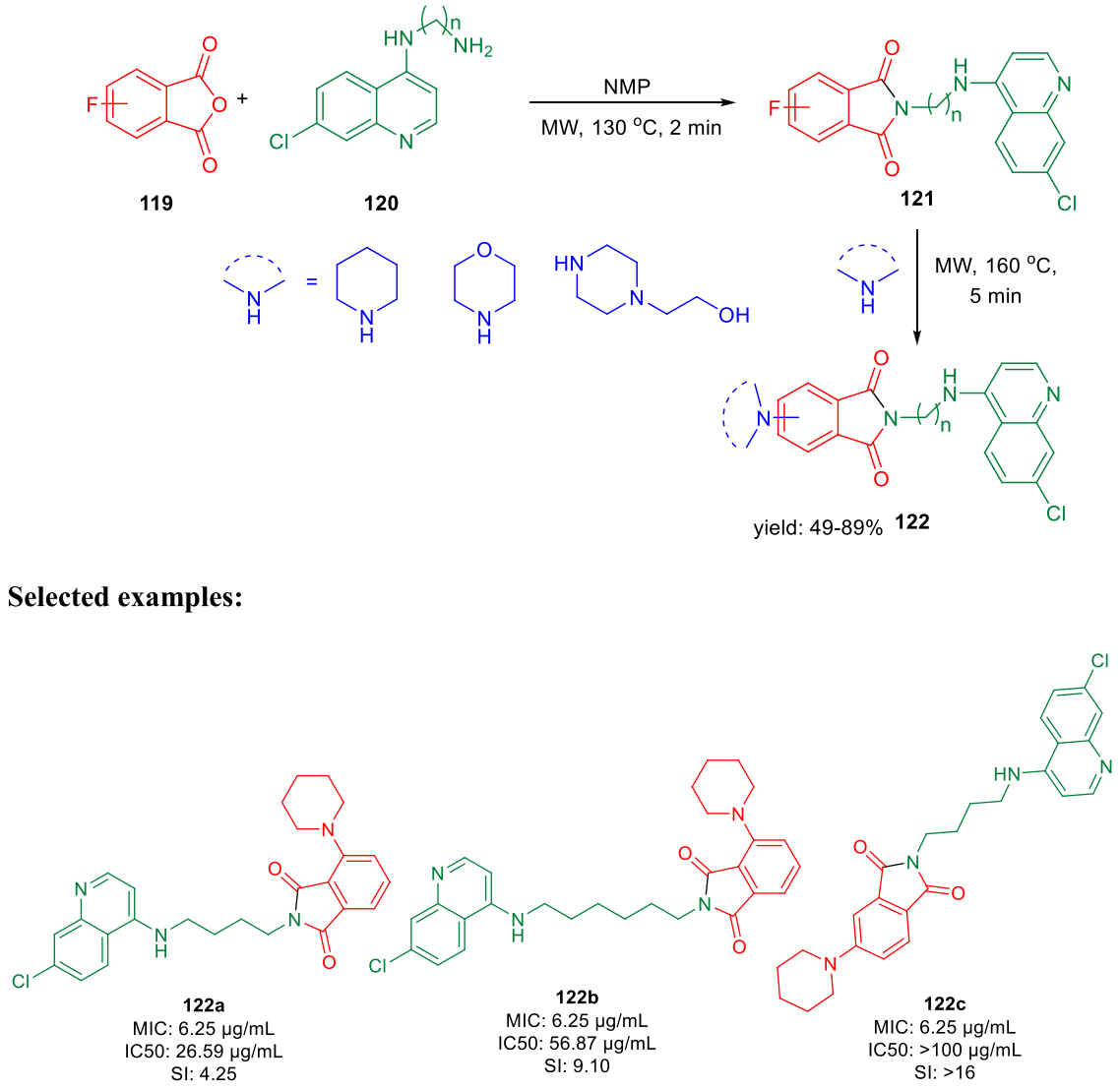

SCHEME 26
Microwave-assisted synthesis of isoindoline-1,3-dione-4-aminoquinolines (substitution of C-4/C-5 secondary amine).

dichlorobisquinolines. An earlier work that used the Baylis–Hillman adducts to produce quinoline derivatives served as the model to obtain compound **60**, which further reacted with sodium alkoxide under reflux conditions to produce bisalkoxyquinolines **61** (Pathak et al., 2007). In the last step, deprotonation of compound **61** at −78°C, followed by the addition of the Mannich base, led to the formation of compound **62** (Scheme 15). For evaluation of TMC207 analogs as antitubercular agents, BACTEC assay was used on H37Rv *M. tb* strain. It has been found that compound **54a** has the lowest MIC value of 12.1 µM, whereas compound **54b** demonstrated a value of 12.5 µM. A comparison study indicated that bisquinoline analogs of TMC207 have much higher activity than the conformationally constrained molecules.

There were six compounds with MIC values under 2 µM among the bisquinoline analogs, including compounds **62a** and **62b** (MIC: 0.39 µM). The methoxy group on the second quinoline ring of these molecules appears to be an important factor in their activity. Later on, the cytotoxicity of these compounds was determined toward the macrophages derived from the mouse bone marrow and also toward the Vero cells. Docking studies highlighted the crucial role of both hydrophobic and electrostatic interactions for the stabilization of these moieties to bind into the active site of ATP synthase enzyme, resulting in potent enzyme inhibition (Figure 6).

In 2016, Thore *et al.* reported the synthesis of hybrid triazoles and evaluated their potency as dual inhibitors of growth and efflux inhibition in *M. tuberculosis* (Dixit et al., 2016). Over the

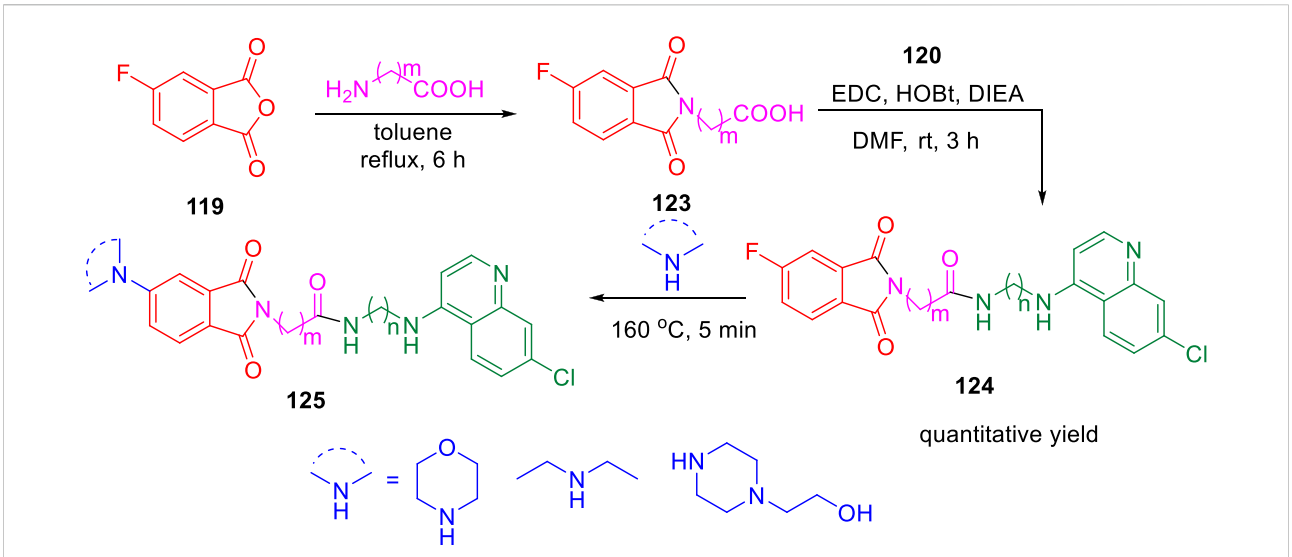

SCHEME 27
Synthetic route of C-5-substituted isoindoline-1,3-dione connected with 4-aminoquinolines *via* an amide spacer.

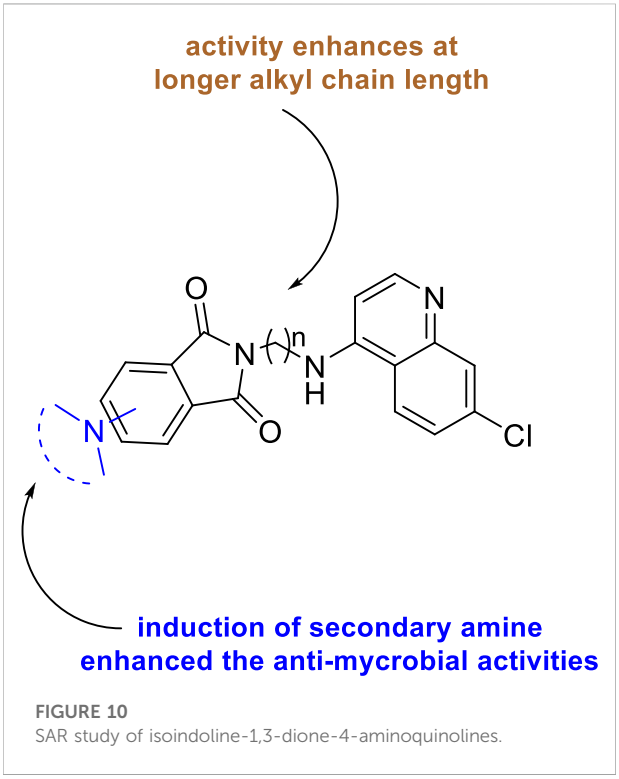

FIGURE 10
SAR study of isoindoline-1,3-dione-4-aminoquinolines.

years, fused and linked triazoles have emerged as a popular antitubercular agent (Shiradkar et al., 2007a; Shiradkar et al., 2007b; Gill et al., 2008; Jadhav et al., 2009). As presented in Scheme 16, hydrazine compound **63** reacted with bromoacetic acid followed by the Boc protection led to the formation of compound **65**. In the next step, the addition of benzyl bromide to compound **65** afforded the protected triazole **66**. Subsequently, compound **67** was treated with 2,4- dichlorobenzaldehyde to achieve intermediate **68**, which further reacted with compound **66** and produced triazolyl-chalocones **69**. Cyclization of the triazolyl-chalocones with hydroxylamine followed by deprotection of amino and thio functionalities resulted in the formation of targeted PDST derivatives. The potency of these hybrid molecules as growth and efflux inhibitor (TB-GEI) toward *M. smegmatis* mc (b) and H37Rv strains was determined. It was observed that compounds **73a**, **73b**, **73c**, and **73d** showed promising MIC values of 2, 1, 4, and 2 μg/ml, respectively. Later, the potency of these hybrid molecules to inhibit efflux of ethyl bromide from *Mycobacterium smegmatis* mc (b) cells was tested *via* real-time fluorometry. Compounds **73a** and **73b** were found to be harmless toward human macrophages with IC_{50} values 87.9 and 122.4 μg/ml, respectively. It was found that some of the synthesized compounds were toxic with IC_{50} value as low as 5.5 μg/ml. Moreover, compound **73a** demonstrated good synergistic action with RIF and INH, whereas it failed to exhibit potency in the case of EtBr.

In the same year, Baltas *et al.* synthesized pyrrolidinone and pyrrolidine derivatives as the *Mycobacterium tuberculosis* inhibitor (Matviiuk et al., 2016). As depicted in Scheme 17, the succinimide moiety in compound **6** was reduced *via* BH_3. Me_2S was used to generate compounds pyrrolidinone **74** and pyrrolidine **75** in the ratio of 1:1 mixture, followed by the acylation reaction using benzoyl chloride (Matviiuk et al., 2014b). To determine the potency of all synthesized compounds toward H37Rv strain, inhibition assay tests were performed at 50 μM. The result indicated that compound **77a** has the best inhibition (87%) toward InhA enzyme, which is selected

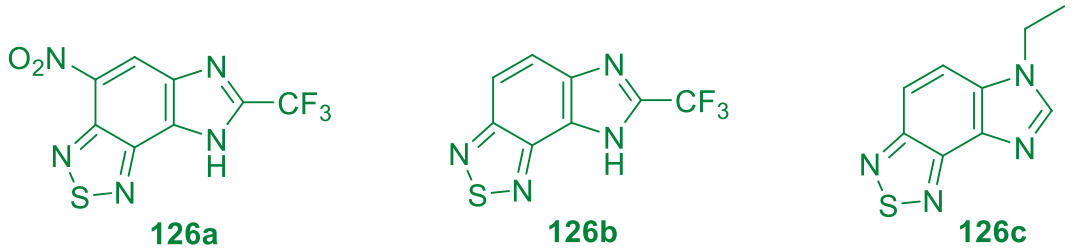

FIGURE 11
Examples of imidazobenzothiazole.

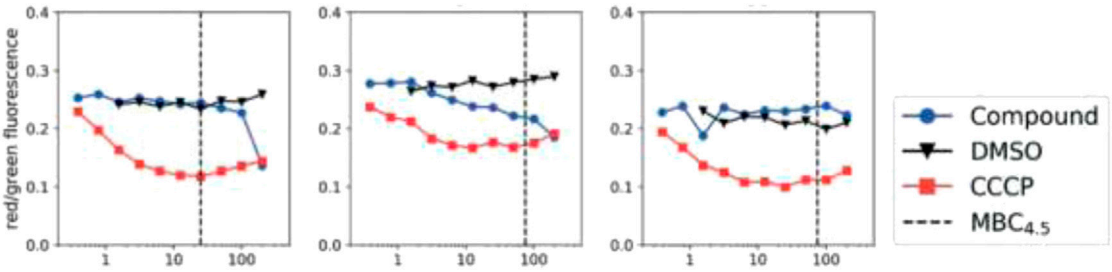

FIGURE 12
M. tb membrane potential disruption at pH 6.8 by benzothiadiazole analogs. Reproduced from Smith et al., 2019, with permission from Royal Society of Chemistry, Copyright 2019.

for docking studies. It is observed from the docking studies that GEQ and compound **77a** (*R* and *S* enantiomers) can adopt a similar conformations and interactions in the active site of InhA (Figure 7) (Chollet et al., 2015). Furthermore, compounds **76a** and **77b** showed medium activities against tuberculosis with MIC values of 10.3 and 21.3 μM, respectively. However, the MIC value of **77c** (1.4 μM) led to further testing against IC2 clinical isolate, which is well resistant toward first- and second-line tuberculosis drugs. According to *in vitro* data, compound **77a** showed less inhibition than GEQ, and the findings from the docking studies also suggest weaker interaction than GEQ.

Dalimba and co-workers in 2016 reported the one-pot synthesis of thiazole–imidazo [2,1-b] [1,3,4]thiadiazole hybrids and investigated their inhibitory action toward tuberculosis (Ramprasad et al., 2016). Compound **79** is the key intermediate, which was synthesized by the reaction of thiosemicarbazone **78** with ketone in the presence of acetyl chloride. In the presence of ethanol, compound **79** was treated with substituted phenacyl bromide at 80–85°C for 24 h to produce compound **80**, which underwent Vilsmeier–Haack formylation to achieve intermediate **81**. In the last step, treatment of intermediate **81** with substituted phenacyl bromide and thiosemicarbazide **78** in the presence of [Bmim]Br–ethanol mixture furnished different analogs of the final product **82** (Scheme 18) (Alegaon et al., 2012; Ramprasad et al., 2015). A plausible mechanism for the synthesis of 1-((6-phenylimidazo [2,1-b][1,3,4]thiadiazol-5-yl)methylene)-2-(4-phenylthiazol-2-yl)hydrazine derivatives **82** is depicted in Scheme 19. The synthesized moieties were screened against H37Rv strain of *M. tb* using the agar dilution process to determine the antimicrobial activity. Among all of the compounds, **82c** is the most active compound with an MIC value of 6.03 μM, which is better than some of the antitubercular drugs such as ethambutol and ciprofloxacin. However, compounds **82a** and **82b** exhibited moderate activity with MIC values 13.94 and 12.72 μM, respectively. It is interesting to note that all trifluoromethyl derivatives have lower MIC values than the corresponding methyl analogs. Furthermore, promising molecules were docked inside (Figure 8) the active site of the InhA enzyme, and the docking score was observed to be −8.89 kcalmol^{-1}, with hydrogen bond interactions along with π–π stacking. The *in vitro* cytotoxicity of the synthesized compounds was examined against NIH/3t3 mouse embryonic fibroblast cell lines using the MTT assay. This study revealed that none of the compounds with significant activity were toxic toward normal cells (Gundersen et al., 2002).

Subsequently, Machado and group reported the activity of 2-(quinolin-4-yloxy) acetamides toward drug-resistant and drug-

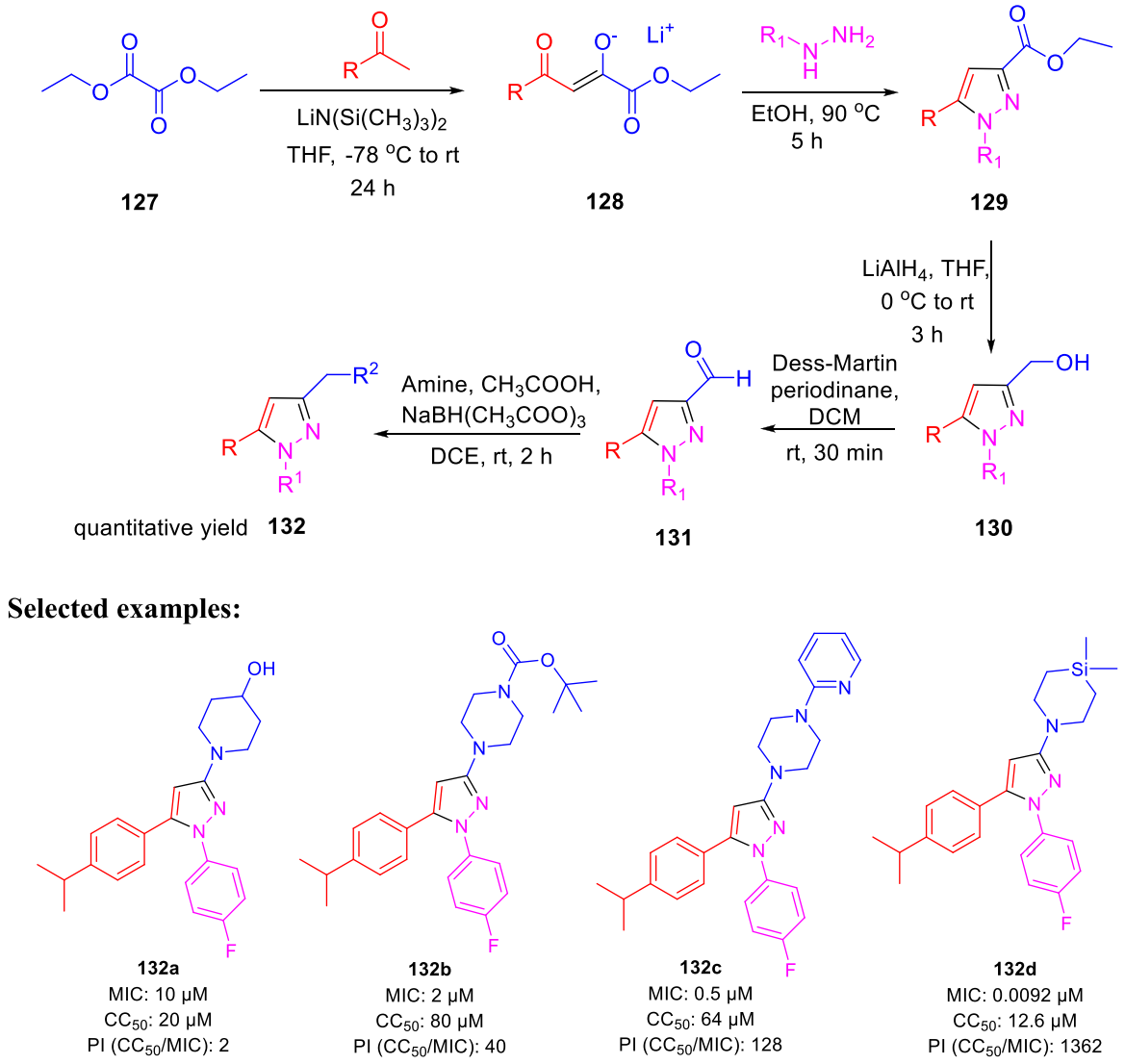

SCHEME 28
Multistep synthesis of pyrazole bearing derivatives.

susceptible strains of *M. tb* (Pissinate et al., 2016). As depicted in Scheme 20, compound **84** was synthesized by the *O*-alkylation reactions of compound **83** with 2-bromo-*N*-arylacetamides using K_2CO_3 as base in DMF solution at 25°C for 16 h. Moreover, *N*-alkylation of compound **85** with bromo acetamides under the same reaction conditions led to the formation of compound **86** with high chemoselectivity. The whole-cell assay test was performed with the synthesized molecules to evaluate the activities toward H37Rv strain of *M. tb* using isoniazid as standard drug. The result showed that compound **84d** has an exceptional activity with the MIC value as low as 0.15 μM, which is better than those of most first-line antitubercular drugs. Similarly, compounds **84a**, **84b**, and **84c** also have significant activity with 0.48, 0.88, and 0.44 μM MIC values, respectively. All of the synthesized acetamide derivatives showed potency toward drug resistant clinical strain with same activity in infected macrophages. The potential compounds were subjected to evaluation of cardiac toxicity in zebrafish (Selderslaghs et al., 2009) and found to be safe at 1 and 5 μM of the embryos.

In the same year, Isloor *et al.* reported the synthesis of 1′-(4-chlorophenyl) pyrazole bearing 3,5-disubstituted pyrazoline analogs and investigated their antitubercular activities (Harikrishna et al., 2016). Compound **87** is a basic pyrazole skeleton, which can be easily achieved by the Vilsmeier–Haack reaction, leading to excellent yields (Harikrishna et al., 2015). As presented in Scheme 21, pyrazole **87** was treated with 5-acetyl-2,3-dihydrobenzofuran using NaOH as base in methanolic solution at room temperature for 3 h to furnish compound **88**, which upon further treatment with hydrazine hydrate for an additional 3 h in

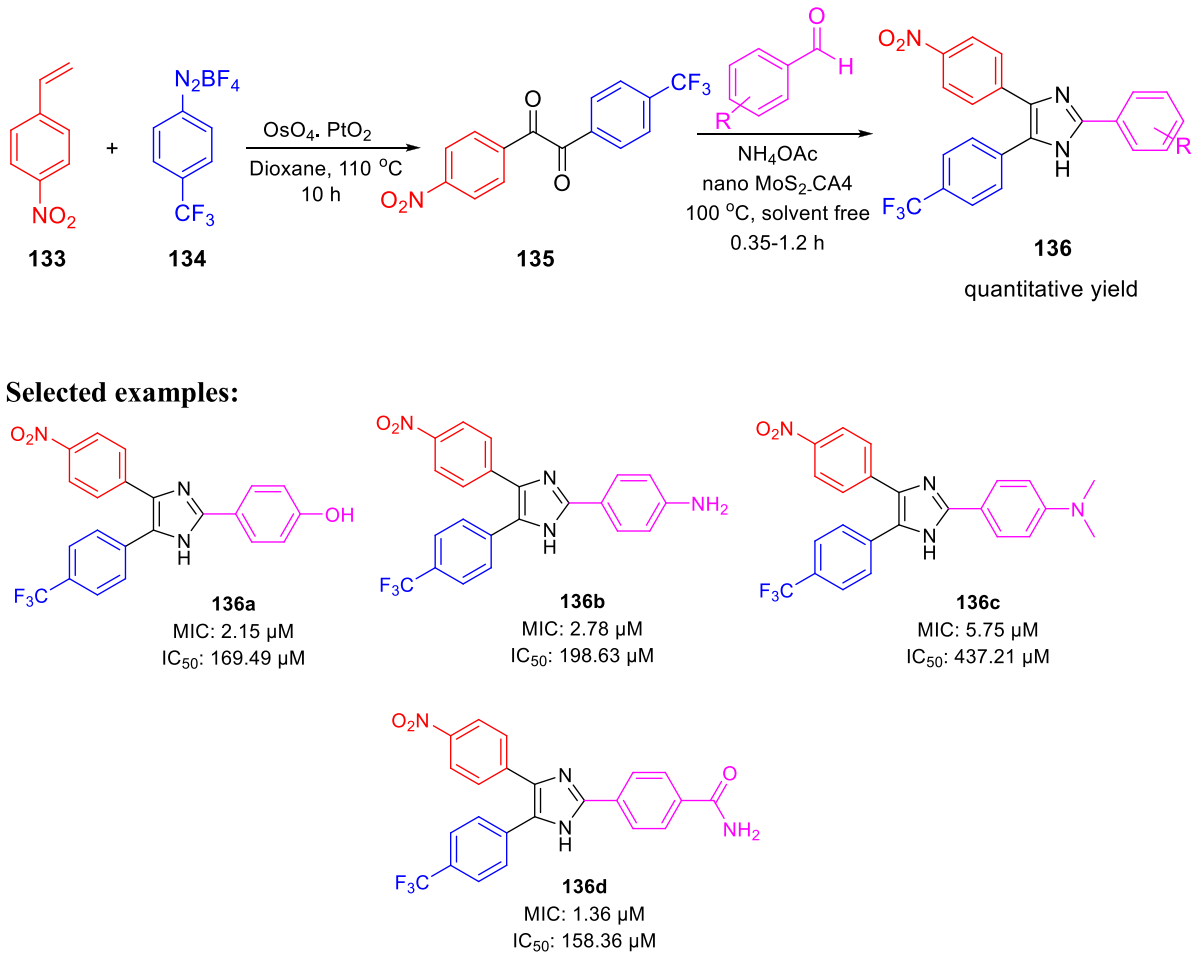

SCHEME 29
One-pot synthesis of 2,4,5-trisubstituted imidazoles.

ethanolic solvent afforded the final product **89**. Similarly, compounds **90** and **92** were formed when pyrazole **87** was treated with 5-acetyl-2-methylfuran and monoacetyl biphenyl, respectively, under the same reaction conditions. The synthesized compounds demonstrated a range of MIC values from 50 to 1.56 μg/ml toward H37Rv strain of *M. tb*. Compound **93a** exhibited an MIC value of 1.56 μg/ml, which is better than that of the first-line antitubercular drug streptomycin, whereas compound **93b** has the same MIC value as that of streptomycin, that is, 6.25 μg/ml. Subsequently, compounds **89a** and **89b** exhibited moderate activity with 12.5 and 25 μg/ml MIC values, respectively. An *in vitro* cytotoxicity study was performed with the potential molecules using HeLa cells. After primary screening of the toxicity studies, compounds **83a** and **93b** appeared to be the best potent molecule with minimum cytotoxicity.

Prashanth *et al.* synthesized imidazo[4,5-c]pyridine derivatives and evaluated their antimicrobial activity (Madaiah et al., 2016). The synthesis of the desired compound involved a series of reactions initiating from the chlorination of 2,6-dichloropyridine **94** in the presence of trifluoroacetic acid, H_2O_2 and $POCl_3$. In the next step, treatment of compound **95** with methylamine resulted in the mixture of isomers **96** and **97**. The nitration of compound **97** was performed to afford compound **98**, which upon reaction with sulfuric acid for 12 h at room temperature formed **99**. In the next step, compound **100** was obtained by the reduction of compound **99** using iron powder and ammonium chloride. The imidazole ring of compound **101** was formed by reacting triethyl orthoformate and compound **100** in refluxing ethanol. Furthermore, Buchwald coupling was carried out to achieve the C–N bond formation leading to the synthesis of intermediate **102**. Finally, the amine group in compound **102** was reacted with $SOCl_2$ in the presence of sodium hydride to afford the final compound **104** (Scheme 22). All derivatives were screened for their antitubercular activity toward H37Rv strain of *M. tb* by the agar dilution method. Compounds **104a**, **104b**, and **104c** with an MIC value of 6.25 μM

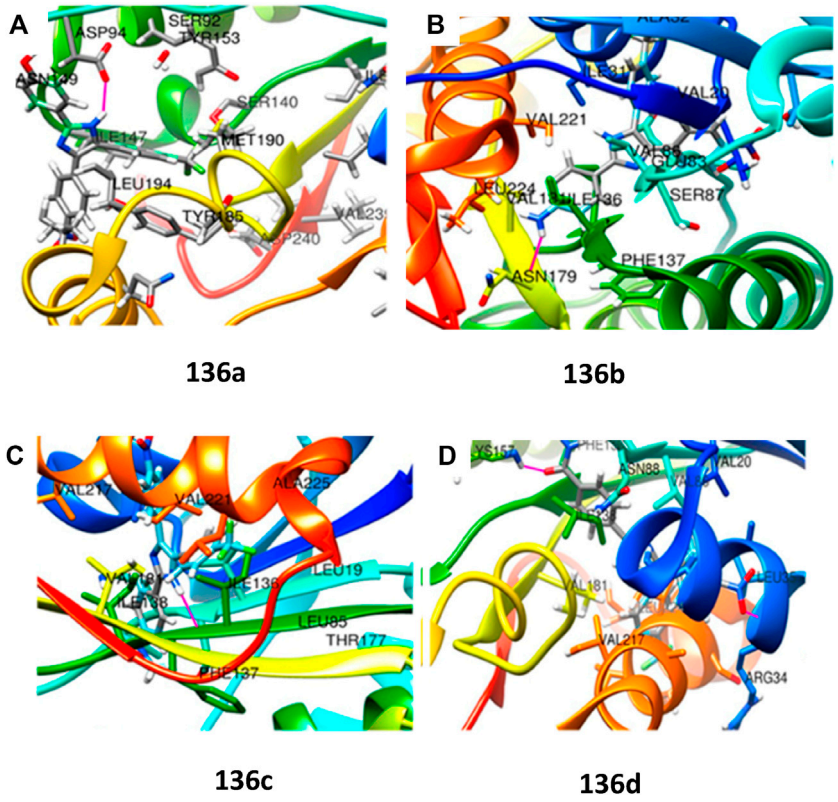

FIGURE 13
(A) Molecular docking of **136a** with MabA protein. **(B)** Molecular docking of **136b** with MabA protein. **(C)** Molecular docking of **136c** with MabA protein. **(D)** Molecular docking of **136d** with MabA protein. Reproduced from Raghu et al., 2020, with permission from American Chemical Society, Copyright 2020.

expressed more potency than popular anti-TB drug ethambutol (MIC: 7.64 μM). However, compound **104d** has an 0.25 μM MIC value, which is more dominant than isoniazid (MIC: 0.36 μM). The findings suggest that imidazopyridine derivatives might be a promising lead contender against tuberculosis that merit further investigation.

In 2017, Parish *et al.* evaluated the *in vitro* activities of unique nitazoxanide (NTZ) derivatives toward *Mycobacterium tuberculosis* with their structure–activity relationship (SAR) (Odingo et al., 2017). In this work, compound **105** was used to regulate the systematic antitubercular SAR study. A total of 56 NTZ (Dubreuil et al., 1996; White, 2004) derivatives were prepared via different pathways using amide bond coupling. As depicted in Scheme 23, treatment of activated acids with aminothiazole **105** afforded compound **106** via amide bond formation. Similarly, reaction of isocyanate with aminothiazole **105** produced compound **107** in the presence of base and THF. On other hand, sulfonyl chloride was used to form sulfonamide derivative **108**. Compound **105** undergoes reductive alkylation reaction in the presence of aldehyde and trifluoroacetic acid to form compound **109**. Minimum inhibitory concentration of compound **106a** was 2.4 μM, whereas compounds **106b** and **106c** have values of around 5.5–5.6 μM toward H37Rv strain of *M. tb*. Toxic concentration (TC_{50}) values of the synthesized molecules suggested no significant toxicity.

Furthermore, the same group accomplished the improved synthesis of phenoxyalkylbenzimidazoles and investigated their potential as the tuberculosis inhibitor to target QcrB (Chandrasekera et al., 2017). Several alkyl derivatives of benzimidazoles were synthesized, as depicted in Scheme 24. Benzimidazole intermediate **112** was formed by the condensation of 1,2- diaminobenzene derivatives **110** with propionic acid **111**. In the next step, the alkylation of intermediate **112** in the presence of dibromoalkane formed *N*-(bromoalkyl)-benzimidazole **113**, which further reacted with anilines, phenols, and thiophenols to form the corresponding benzimidazole alkylamines, alkylethers, and alkylthioethers, respectively. From the SAR study, it was

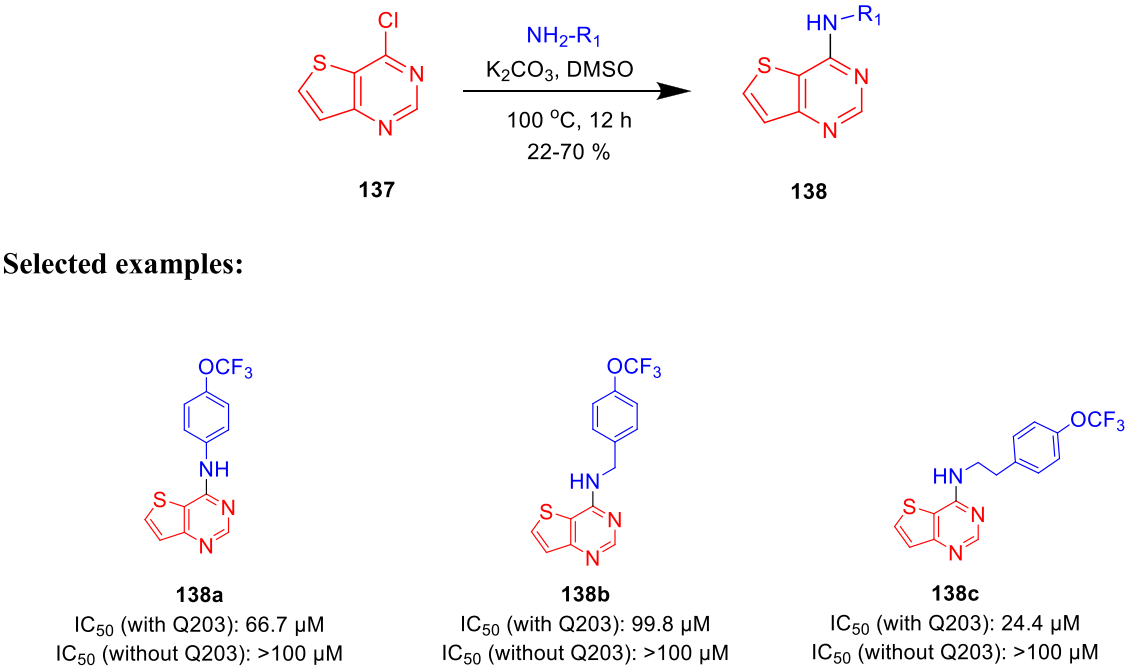

SCHEME 30
One step synthesis of thieno [3,2-*d*]pyrimidin-4-amines.

observed that the substitution with 4-methyl did not affect the activity, whereas the substitution with 4-methoxy reduced the activity by four times. Four derivatives **115a**, **115b**, **115c**, and **115d** have selectivity index greater than 200 with MIC values of 0.061, 0.067, 0.35, and 0.070 μM, respectively, toward H37Rv-LP. The cytotoxicity result against the kidney cell line of African green monkey demonstrated that addition of one methyl group in compound **115b** and two methyl groups in **115d** caused a higher increase in toxicity than **115a**. Several synthesized derivatives have better activity inside macrophages in comparison with liquid culture (Chandrasekera et al., 2015).

Denny *et al.* in the subsequent year synthesized 6-cyano derivatives of bedaquiline as a safe inhibitor of tuberculosis (Tong et al., 2017). The SAR study of almost 200 derivatives was performed to check the significance of four different regions **A**, **B**, **C**, and **D** for antitubercular activity toward the *M. smegmatis* strain (Figure 9) (Guillemont et al., 2011). The IC_{90} of the six-substituted compounds were within a two-fold range in comparison with the lead compound. Most of the compounds were assessed as *RS* and *SR* diastereomers, whereas few molecules were formed as pure *R* and *S* enantiomers.

The major diarylquinoline compounds were synthesized by condensation of the proper A/B and C/D units. The C/D unit was achieved using relevant acetophenones in a one-step Mannich reaction (Scheme 25). Compounds **118a**, **118b**, **118c**, and **118d** demonstrated extraordinary MIC values of 0.09, 0.20, 0.71, 0.94 μg/ml, respectively, determined by MABA assay.

In 2019, Kumar and co-authors synthesized substitutedisoindoline-1,3-dione-4-aminoquinolines and evaluated their antimycobacterial properties along with cytotoxicity (Rani et al., 2019). Stepwise microwave-promoted synthesis was performed under optimized conditions to achieve the derivatives of aminoquinolines. Fluoro-phthalic anhydride **119** was treated with 4-aminoquinoline-diamines **120** in the presence of *N*-methylpyrrolidin-2-one to form compound **121**. The addition of secondary amine to compound **121** under microwave irradiation achieved the targeted moiety **122** (Scheme 26). Subsequently, *N*-(7- chloroquinolin- 4- yl) diamine and compound **123** undergo amide coupling with the help of EDC-HOBt to afford molecule **124** at room temperature. Furthermore, the addition of different amines to compound **124** led to the formation of desired C-5-substituted isoindoline-1,2-dione connected with 4-aminoquinolines **125** through an amide spacer (Scheme 27).

Antimicrobial properties of the synthesized compounds were assayed against mc (b)6230 strain of *M. tb*. To analyze the structure–activity relationship, the isoindoline-1,3-dione secondary amine functionality at C4/C5 location and the

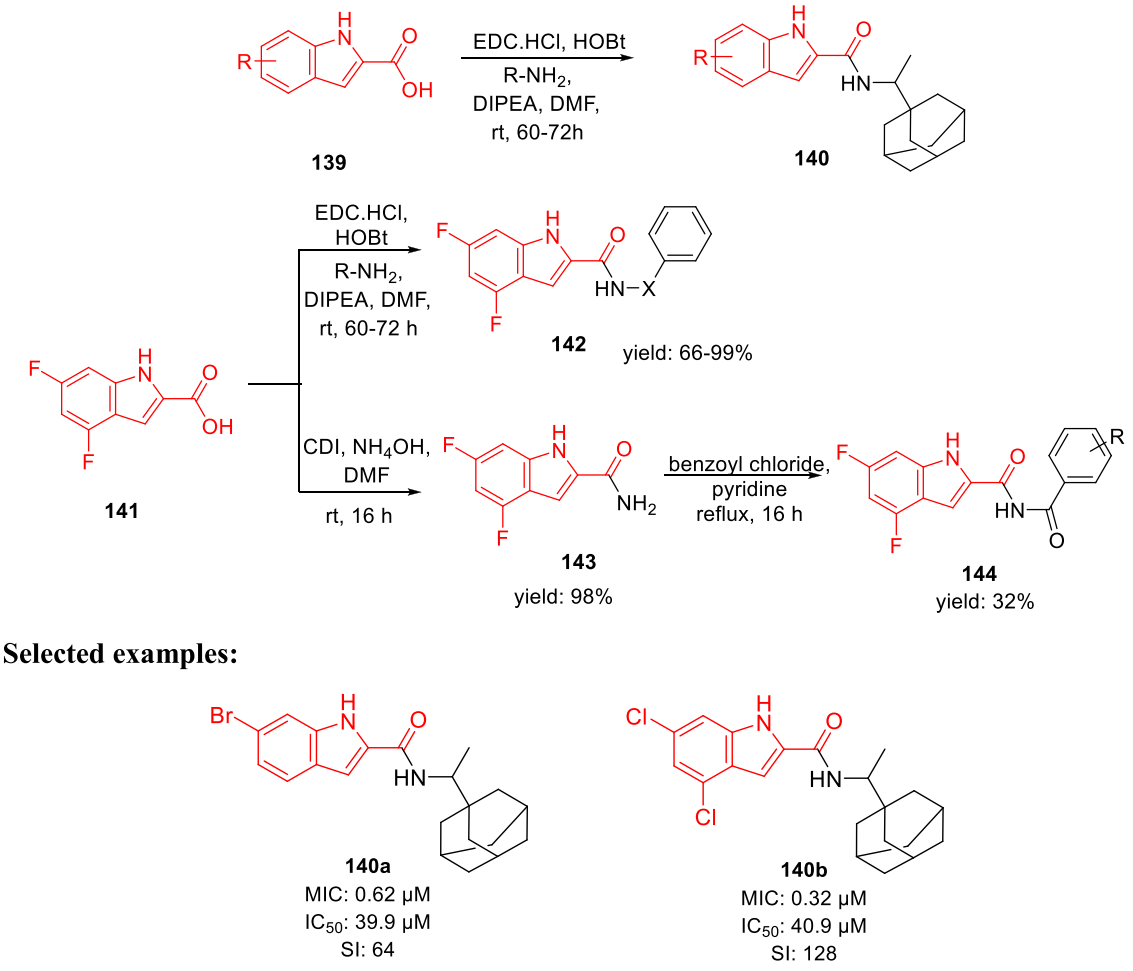

SCHEME 31
Synthesis of indole-2-carboxamides *via* amide coupling.

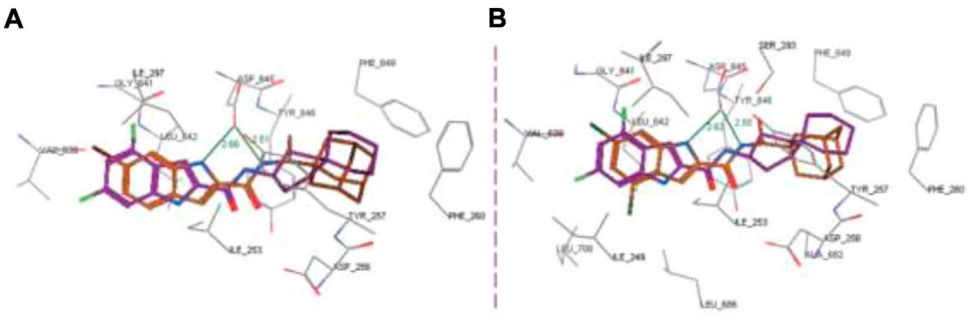

FIGURE 14
Superposition of top-ranked docking pattern of **140(A)** and **140(B)**. Reproduced from Alsayed et al., 2021, with permission from Royal Society of Chemistry, Copyright 2021.

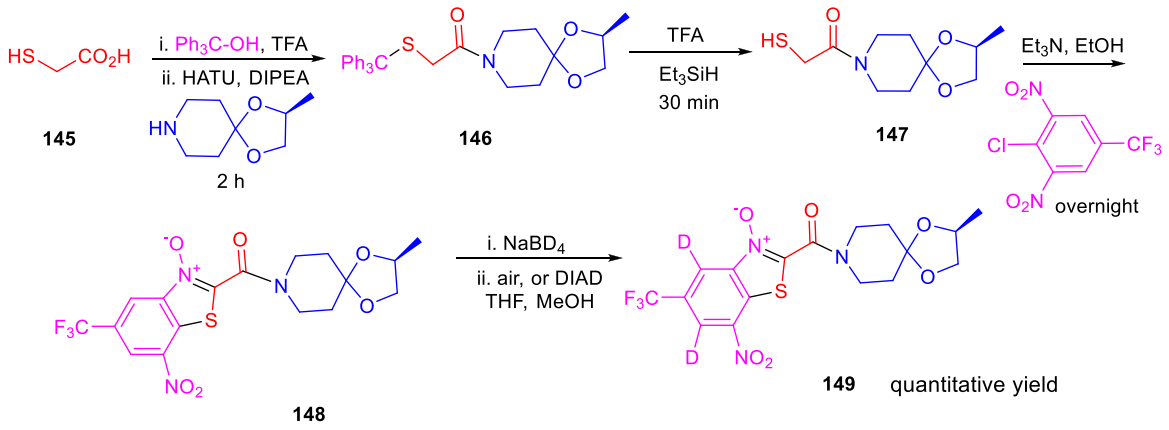

SCHEME 32
Synthesis of BTO with BTZ043 side chain with reduction reoxidation chemistry.

distance between two pharmacophores were carefully changed. It was observed that the activity was dependent on the type of the linker present between two pharmacophores (Figure 10). However, increase in the alkyl chain length (n = 4, n = 6) and the induction of the morpholine ring resulted in the improvement of activity indicating a 6.25 μM MIC value of compounds **122a**, **122b**, and **122c** with lesser cytotoxicity.

Parish and his group in 2019 reported the membrane potential disruption of *M. tb* by imidazobenzathiazole analogs (Figure 11) (Smith et al., 2019). Mensuration of membrane potential toward human liver cells in HepG2 was performed by the conventional method where 50,000 cells were plated per well in 96-well plates. However, minimum bactericidal concentration (MBC) was assessed at different pH values, that is, 4.5, 5.6, and 6.8, by fluorescence at different wavelengths.

M.tb membrane potential disruption was measured at neutral pH by benzothiazole analogs (Figure 12). The results did not suggest any correlation between the HepG2 IC_{50} value and membrane potential disruption (Huang, 2002). A slight increase in activity was noticed at pH 5.6 for the disruption of *M. tb* membrane potential with higher degree of separation. The perspective of benzothiazole analogs appeared favorable, ruling out the membrane potential disruption for both cytotoxicity and antitubercular activity.

In the following year, Poce *et al.* described the effect of pyrazole-containing moieties on *M. tb* by the inhibition of mycobacterium membrane protein large 3, that is, MmpL3 (Poce et al., 2019). The treatment of diethyloxalate **127** with ketones in accordance with lithium bis(trimethylsilyl)-amide formed lithium salt **128**, which further underwent cyclization with relevant hydrazines to produce desired pyrazoles **129**. Pyrazole-3-carbaldehyde **131** was achieved by the conversion of ethyl esters **129** in two steps, as depicted in Scheme 28. Afterward, the reductive amination of **131** with the help of $NaBH(CH_3COO)_3$ in the presence of suitable amine resulted in the formation of pyrazole derivatives **132**. The SAR study was accomplished on a sequence of 1,3,5-trisusbstituted pyrazoles only to find out the significant effect of cyclic amine at the 3-position. Compound **132d**, which has a silicon atom, resulted in an increase of the activity (MIC: 0.00925 μM). Moreover, the genome sequencing results stipulated MmpL3 as a feasible target, confirming the high potential of MmpL3 inhibitors for development in tuberculosis drug discovery (La Rosa et al., 2012).

In 2020, Prasanth and group accomplished the synthesis of 2,4,5- trisubstituted imidazole derivatives by one-pot methodology employing 4-nitrostyrene and 4-(trifluoromethyl) benzene diazonium salt in the presence of PtO_2 and OsO_4 as catalyst (Scheme 29) (Raghu et al., 2020). The pharmacological study indicated significant *in vitro* antitubercular property of compounds **136a**, **136b**, **136c**, and **136d**, revealing MIC values of 2.15, 2.78, 5.75, and 1.36 μM, respectively, toward H37Rv strain of *M. tb*. Very less cytotoxicity was observed with a range of 151.18–437.21 μM IC_{50} values for Vero cells.

Moreover, MabA being the key enzyme in biosynthesis of mycolic acid, which is the substantial cell envelop of *M. tb*'s long-chain fatty acid, was selected as an operating site for the docking study. The anticipated binding free energies in kcal/mol were used to determine the molecular docking scores, as presented in Figure 13. The docking scores of **136a**, **136b**, **136c**, and **136d** with 1UZN were 8.5, 8.4, 8.1, and 8.9 kcal/mol, respectively.

Moraski *et al.* generated the structure-guided thieno[3,2-d] pyrimidine-4-amine and investigated its potency as bd oxidase inhibitors of *M. tb* (Hopfner et al., 2021). Nucleophilic aromatic substitution (S_NAr) reaction was implemented with 4-chlorothieno [3,2-d] pyridine and amines at 100°C in the presence of base, as depicted in Scheme 30 (Neri et al., 2020).

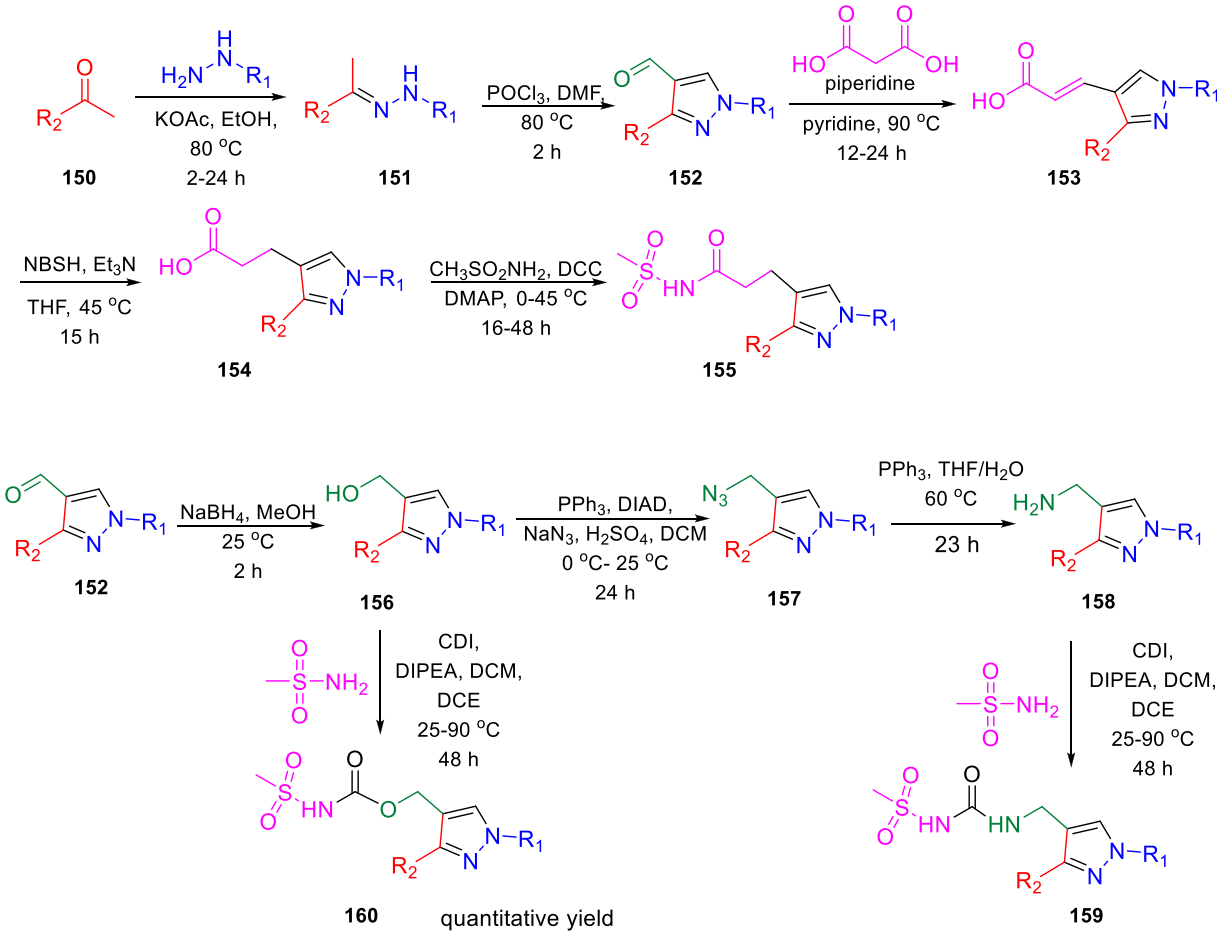

Selected examples:

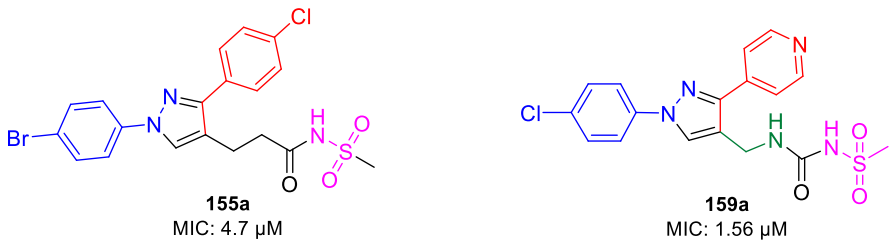

SCHEME 33
Multistep synthesis of 1,3-diarylpyrazolyl-acylsulfonamides.

Thirteen synthesized analogs were screened in a whole-cell ATP cyt-bd assay. The test was performed under replicating circumstances with and without the addition of Q203 in the H37Rv-*M.tb* strain and the clinical isolate N0145-*M.tb*. Subsequently, the BCG strain was utilized for the identification of any common cyt-bd inhibitor. The result shows that H37Rv-*M.tb* strain has overexpressed cyt-bd in comparison with the clinical isolate. Weak potency of the synthesized molecules was increased by functionalizing the para position of the Ph group, making compound **138c** the most potent one. This class of synthetically accessible compounds is one of the rare published examples which can successfully inhibit the cyt-bd in mycobacteria.

Gunosewoyo *et al.* synthesized indole-2-carboxamides as inhibitor of *Mycobacterium tuberculosis* in 2021 (Alsayed et al., 2021). To produce *N*-rimantadine indoleamides **140**,

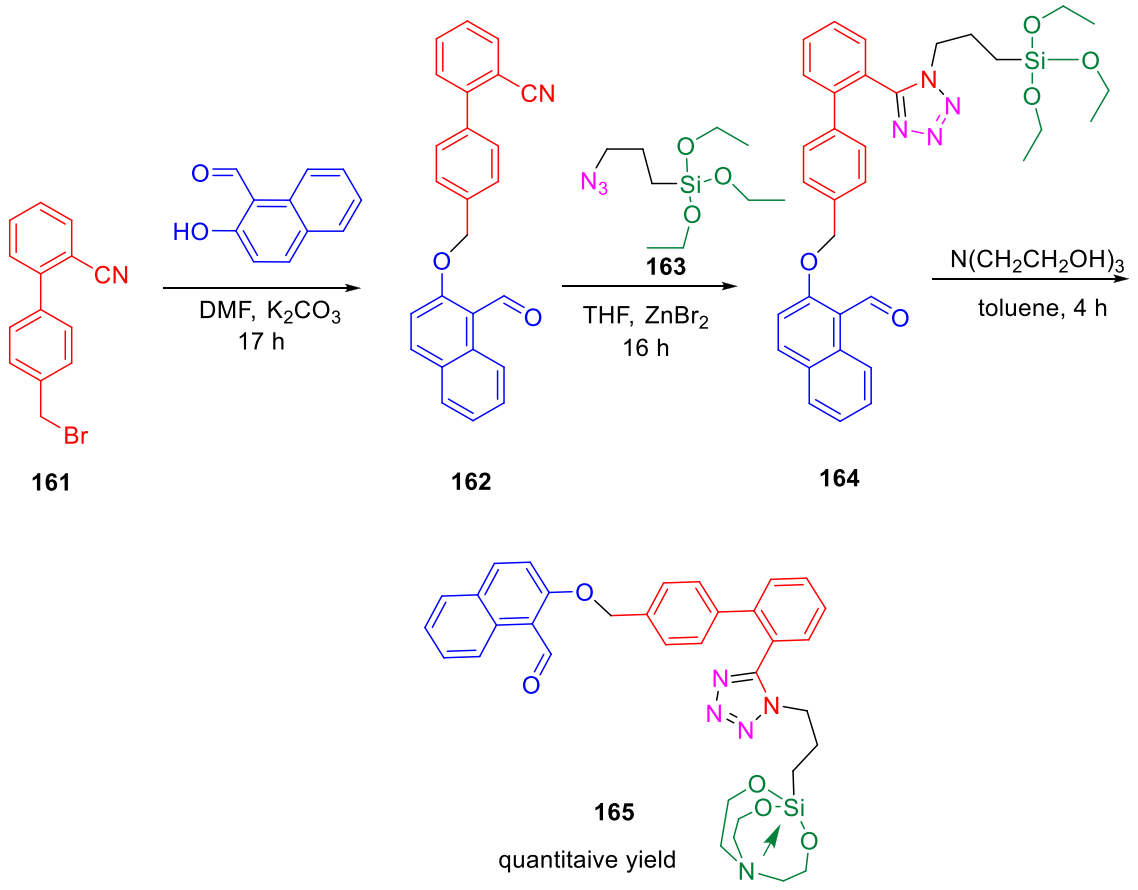

SCHEME 34
Three-step synthetic pathway to tetrazole-appended ether derived organosilane and organosilatrane.

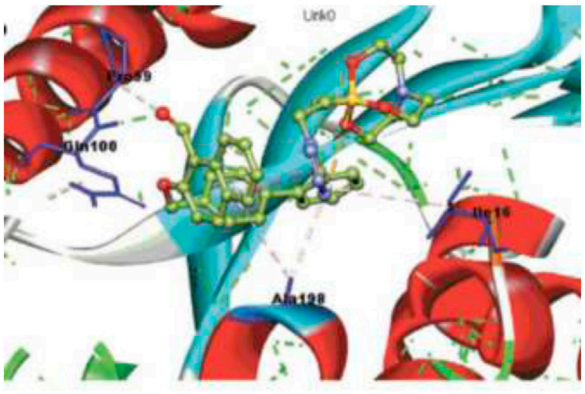

FIGURE 15
Binding pattern of **165** with InhA. Reproduced from Singh et al., 2022, with permission from Royal Society of Chemistry, Copyright 2022.

amide coupling of compound **139** was performed in accordance with DIPEA, EDC HCl, and HOBt. Subsequently, compound **142** was synthesized from 4,6- difluoroindole-2-carboxylic acid **141** *via* amide coupling with appropriate amine. Likewise, the reaction of **141** with 1,1′-carbonyldiimidazole resulted in the formation of *N*-acylimidazole intermediate, which upon *in situ* treatment with ammonium hydroxide achieved the corresponding amide **143** *via* a nucleophilic substitution reaction. Finally, targeted moiety **144** was synthesized by the reaction of benzoyl chloride derivatives with compound **143** in pyridine (Scheme 31). Compounds **140a** and **140b** exhibited the MIC values of 0.62 and 0.32 μM, respectively, for H37Rv strain. An increase in efficacy with high lipophilic groups was noted, whereas 5-methoxy derivatives indicated two times reduced activity compared to 4-methoxy derivatives in the SAR study. The high lipophilic character of the preceding series resulted in diffusion *via* the lipid-rich bilayer of *M. tuberculosis* by their possible interaction with MmpL3 to enhance the anti-TB activity.

In the docking study, as depicted in Figure 14, the S3 hydrophobic site was embedded in the indole moiety, whereas the rimantadine nucleus was inserted in the hydrophobic bulky S5 subsite. On the other hand, the amide

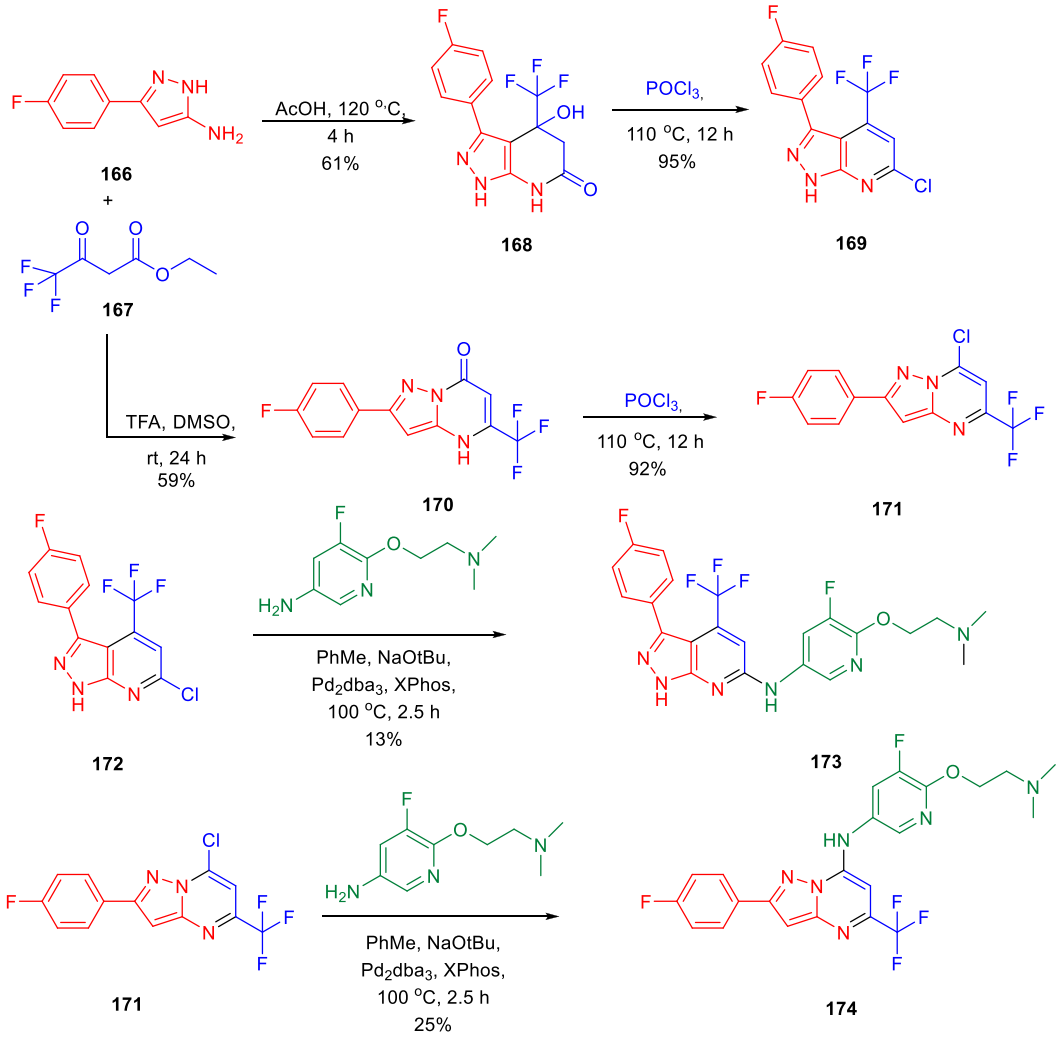

166 + 167 → 168 → 169

169 → 170 → 171

172 + 171 → 173

171 → 174

Selected examples:

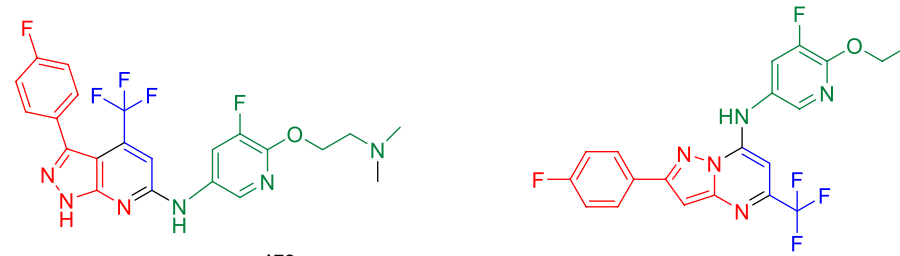

173
MIC (MABA): 7.70 μg/mL
MIC (LORA): 10.95 μg/mL
IC_{50}: 11.43 μg/mL

174
MIC (MABA): 7.9 μg/mL
MIC (LORA): 10.9 μg/mL
IC_{50}: 12.0 μg/mL

SCHEME 35
Synthetic path to pyrazolo[3,4-β]pyrimidine and pyrazolo [1,5-α]pyrimidine.

NH was accommodated in the hydrophilic S4 subsite. The same binding pattern of compounds **140a** and **140b** and the MmpL3 inhibitor **ICA38** stipulated potency through disruption of Asp-Tyr pairs, which is the major player for proton dislocation. These findings suggest that indoleamides can be considered a new class of antitubercular agents.

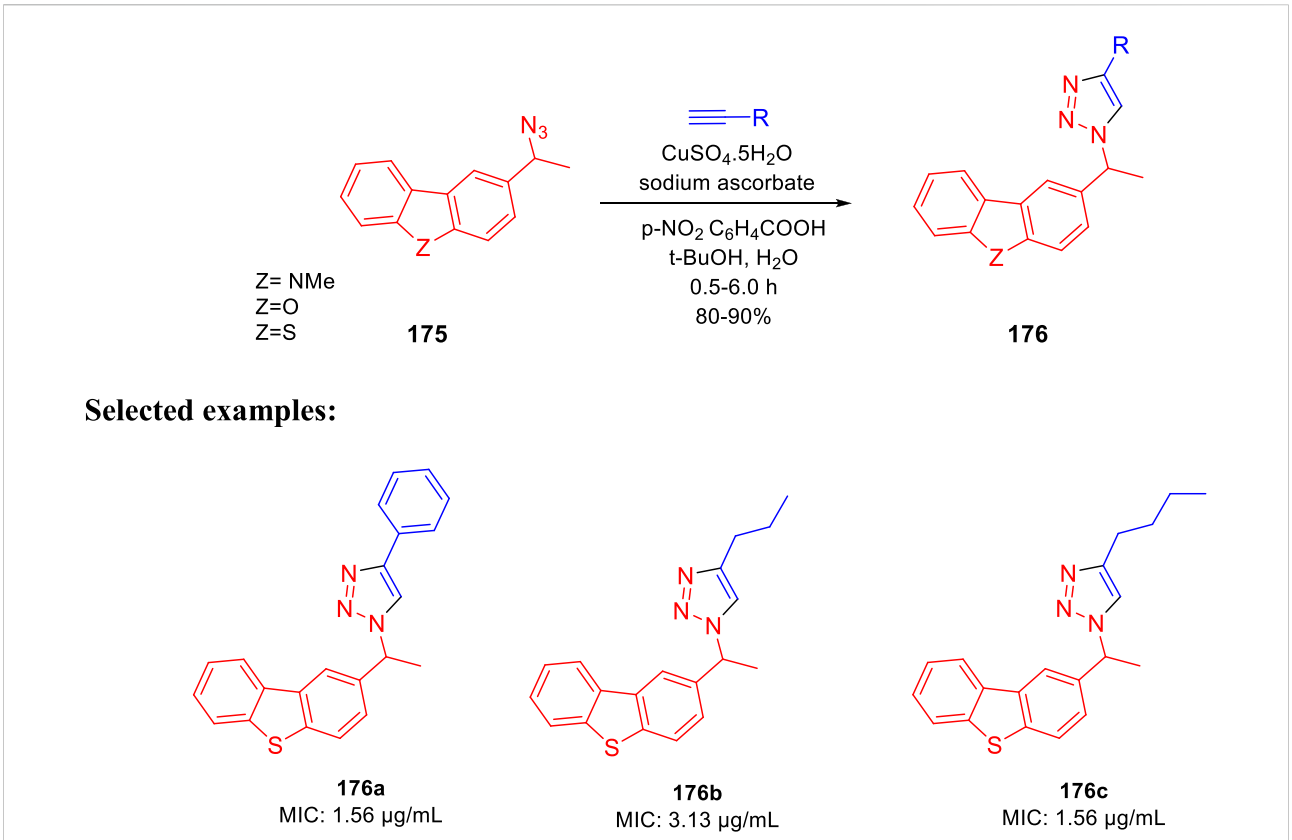

SCHEME 36
Synthesis of azides *via* click reaction.

Miller and his research group reported the formation of hybrid-induced Meisenheimer's complex reflecting the efficacy as an antituberculosis agent in the subsequent year (Liu et al., 2021). BTO analog **148** resembles BTZ043 due to the incorporation of an identical piperidine acetal unit. It was prepared according to previously reported synthetic protocols, which involved the nucleophilic aromatic substitution reaction as a key step followed by cyclization (Kozikowski et al., 2007). Treatment of $NaBD_4$ with compound **148** followed by oxidation generated the deuterium-incorporated starting material (Scheme 32). The intermediates can act as precursors toward the indispensable nitroso moiety, which forms covalent adducts to inhibit DprE1 enzyme. Evaluation of the effects of compounds was assessed by metabolic labeling of H37Rv strain of *M. tb*. The findings suggested the necessity of the incorporation of highly electron deficient substituents to facilitate the molecular recognition by target enzyme (Liu et al., 2019). These compounds have the ability to form the Meisenheimer complex quickly by reacting with hybrids. Interestingly, radiolabeled lipid demonstrated DprE1-related activity during agglomeration of trehalose monomycolates and trehalose dimycolates, and this is due to the scarcity of arabinan chains acting mycolates attachment sites in the mycobacterial cell wall (Landge et al., 2015). The result indicates that further investigation is needed to broaden the scope for the development of potent nitro-substituted antitubercular drugs.

In the same year, Chibale *et al.* reported the ability of 1,3-diarylpyrazolyl-acylsulfonamides to target cell wall biosynthesis of *M. tuberculosis* (Khonde et al., 2021). Several targeted compounds have been synthesized *via* a series of reactions, as depicted in Scheme 33. The mode of action of synthesized derivatives was assessed to check the inhibitory actions toward various strains of tuberculosis. PiniB-LUX bioluminescence assay (Naran et al., 2016) revealed disruption of cell wall biosynthesis by modulating the expression of *ini*BAC operon. This was additionally confirmed by the transcriptional profile study, which indicated the upregulation in the genes that are involved in cell wall biosynthesis. *In vivo* studies indicated the moderate inhibition of intracellular replication of tuberculosis in lungs, whereas the *in vitro* studies specified the adequate stability along with significant plasma protein binding. Compounds **155a** and **159a** showed notable MIC values of 4.7 and 1.56 μM, respectively, with considerable cytotoxicity.

During that year, Singh *et al.* accomplished the tetrazole coalesced organosilane as enoyl ACP reductase inhibitor for *Mycobacterium tuberculosis* (Singh et al., 2022). Tetrazole

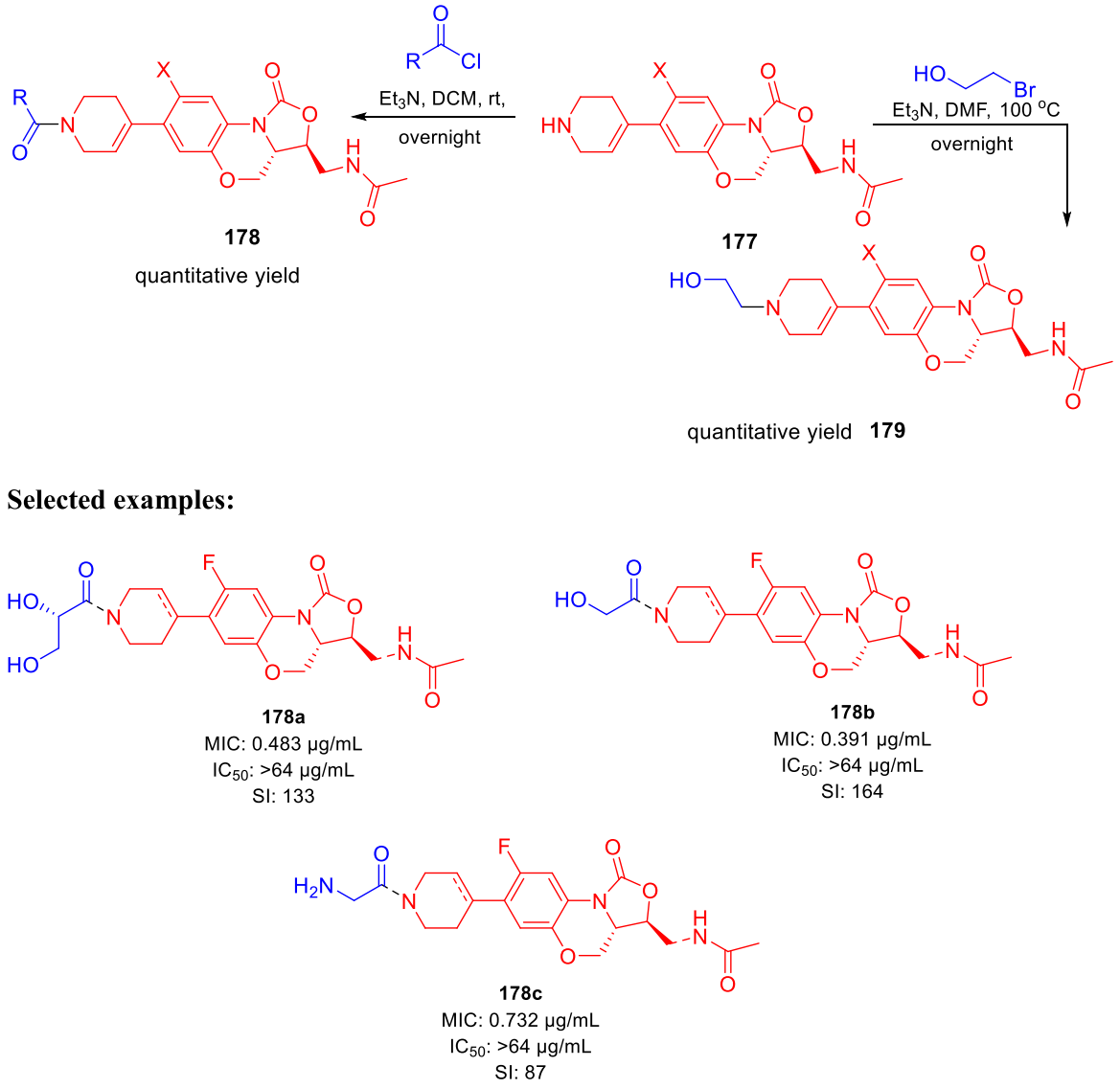

SCHEME 37
Multistep synthesis of fluorine bearing benzoxazinyl-oxazolidinones.

conjoined molecules were synthesized *via* three-step process using 3-azidopropyltriethoxysilane **163** in the presence of catalytic $ZnBr_2$, as shown in Scheme 34.

The docking study of the molecules indicated the successful binding at the active site of the InhA enzyme with hydrogen bond interactions and pi–pi interactions. The various types of interaction lead to binding energy as good as −7.82 kcal mol^{-1} with a 0.00 RMSD value, as depicted in Figure 15.

Choi *et al.* synthesized the pyrazolopyrimidines and assessed its potential as ATP synthesis inhibitors of tuberculosis (Choi et al., 2022). Pyrazolo[3,4-β]-pyrimidinone **168** and pyrazolo [1,5-α]-pyrimidinone **170** were transformed to the relevant chlorides **169** and **171**, respectively, in the presence of phosphorus oxychloride at 110°C. The desired products pyrazolo[3,4-β]-pyrimidine **173** and pyrazolo[1,5-α]-pyrimidine **174** were produced by the Buchwald– Hartwig amination reaction, as depicted in Scheme 35 (Tantry et al., 2016). Pyrazolo[3,4-β]-pyrimidine **173** and pyrazolo [1,5-α]-pyrimidines **174** were tested against both replicating aerobic (MABA) and nonreplicating anerobic (LORA) cultures of *Mycobacterium tuberculosis*. The findings suggest that both the analogs demonstrated medium activity with MIC_{90} values of ~8 μg/ml against MABA and ~11 μg/ml against LORA bacterial cultures. Bedaquiline, which is a well-known inhibitor of ATP synthase to cure multidrug-resistant tuberculosis, was used as a standard inhibitor in this work.

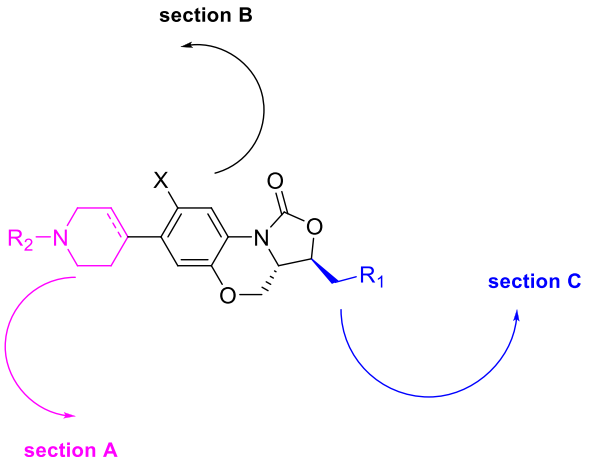

FIGURE 16
SAR study of the target compound.

Further mammalian cell toxicity study in the epithelial kidney cells of green monkey displayed that both compounds **173** and **174** have 11–12 μg/ml IC_{50} values. Moderate activity with low cytotoxicity makes them potential candidates for the ATP synthesis inhibitor of *Mycobacterium tuberculosis*.

Kantevari and co-authors accomplished the synthesis of dibenzo[*b,d*]thiophene, dibenzo[*b,d*]furan, and *N*-methylcarbazole clubbed 1,2,3-triazoles and evaluated their efficacy as the tuberculosis inhibitor (Patpi et al., 2012); 1,3-dipolar cycloaddition reaction between azides **175** and alkynes led to the formation of desired clubbed triazole moieties in the click pathway. Several derivatives of **176** were synthesized by incorporating different heteroatoms as Z groups, that is, S, O, and N-Me, to accomplish the targeted dibenzo[*b,d*]thiophene, dibenzo [*b,d*]furan and *N*-methylcarbazole-clubbed 1,2,3-triazoles (Scheme 36). Both **176a** and **176c** demonstrated significant inhibition with a 1.56 μg/ml MIC value toward H37Rv (ATCC 27294) strain. The cytotoxicity of the dominant compounds was judged using four different cell lines, that is, A549 (adenocarcinomic human lung epithelial cell), DU145 (human prostate cancer), HeLa (human cervical carcinoma epithelial cells), and SK-N-SH (human neuroblastoma) *via* MTT assay to obtain SI values ranging from 55 to 255. Several derivatives had MIC values less than 6.25 μg/ml, which is a value proposed by the global program for the invention of novel antituberculosis drugs as an absolute maximum for evaluating novel *M. tb* therapies.

Huang *et al.* reported the fluorine incorporated benzoxazinyl-oxazolidinone derivatives to treat multidrug-resistant tuberculosis (Zhao et al., 2017). The addition of cyclopropanecarbonyl chloride to compound **177** in the presence of triethylamine formed compound **178** at room temperature. Similarly, compound **179** was formed by the addition of 2-bromoethanol to compound **177** at an elevated temperature of 100°C using triethylamine as base (Scheme 37). A small flexible hydrophilic group appeared to be favorable for antitubercular action from the SAR study. 2-Hydroxyacetyl and 2-hydroxyethyl groups in A section and the acetylamino group in C section were chosen as optimal fragments. They helped investigate the effect of fluorine on the benzene ring and double bond in the tetrahydropyridine ring, as presented in Figure 16. The influence of these three different sections on the cytotoxicity and potency was thoroughly studied in this work.

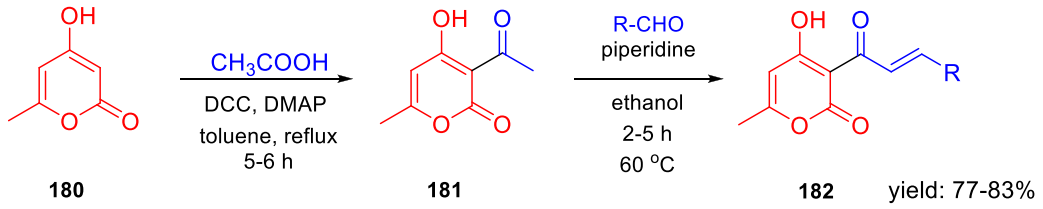

Selected examples:

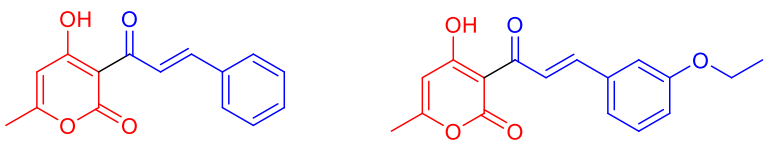

182a
MIC: 4 μg/mL

182b
MIC: 4 μg/mL

SCHEME 38
Piperidine catalyzed synthetic path to 3-cinnamoyl-4-hydroxy-6-methyl-2*H*-pyran-2-one anagrams.

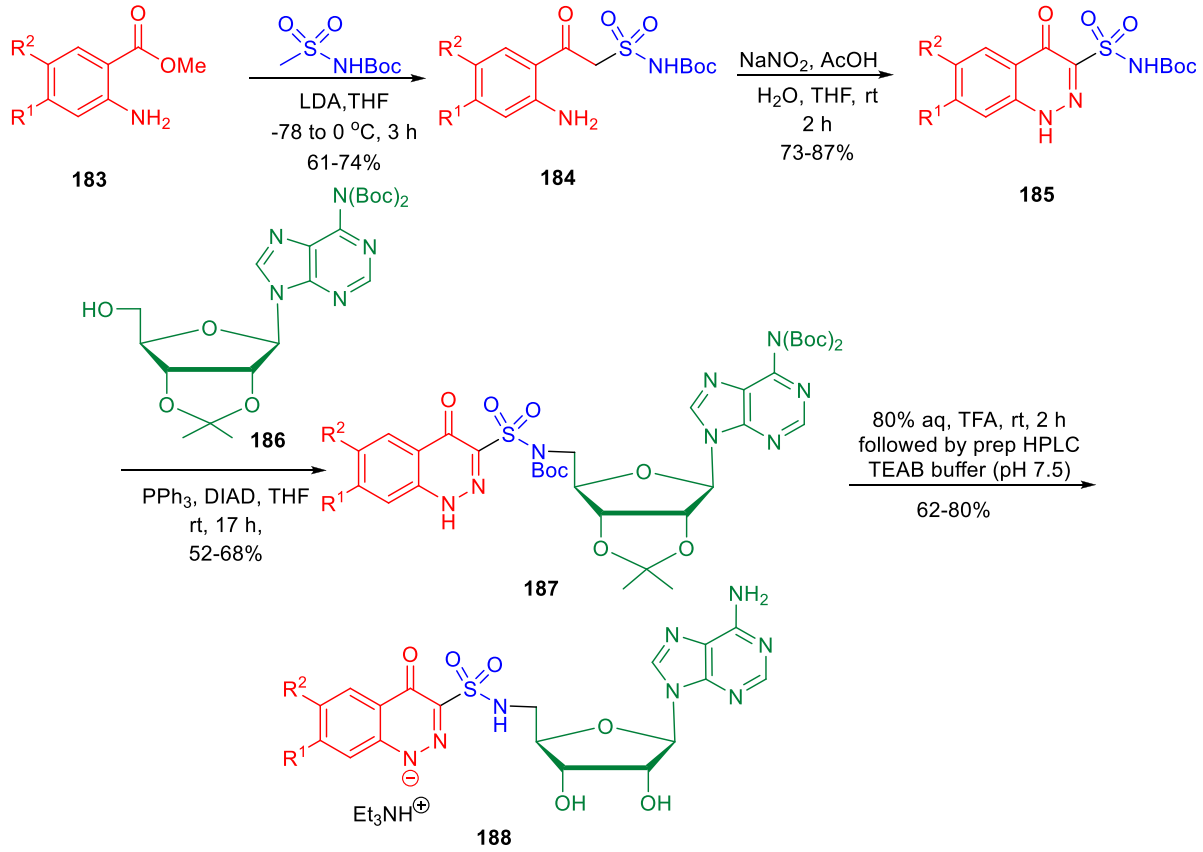

SCHEME 39
Multistep synthetic route to cinnoline nucleoside.

Few compounds were chosen to examine the potential anti-DR-TB activity due to their strong potency toward H37Rv strain and outstanding selectivity index values. *In vitro* potency against the 16892 strain was found to be very satisfying in most of the tested compounds. The compound's effectiveness against the 16802 strain (XDR-TB) was equally encouraging, and it can be now promoted to the next round of clinical trial.

In search of a new antituberculosis agent, Yousuf and his team synthesized and established an *in vitro* assessment of substituted 3-cinnamoyl-4-hydroxy-pyran-2-one (CHP) toward *M. tb* (Bhat et al., 2018). As depicted in Scheme 38, 4-hydroxy-6-methyl-pyran-2-one **180** was refluxed with acetic acid using DCC and DMAP in toluene to achieve the 3-acetyl-4-hydroxy-6-methyl-pyran-2-one **181.** Compound **181** was then further reacted with suitable aldehydes in the presence of piperidine to afford the desired CHP **182**. The MIC value of 4 μg/ml was found in two compounds, that is, **182a** and **182b**, indicating excellent antituberculosis activity against *M. tuberculosis*. These MIC values are close to those found in the standard antitubercular drugs EMB, STR, and LVX, suggesting that these two compounds need further investigation. *M. tuberculosis* cell walls are supposed to contain small polyketide molecules, which can regulate permeability. 2-Pyrone polyketides, a diverse class of secondary metabolites that play critical roles in *M. tuberculosis*, may be responsible for this significant antituberculosis activity (Saxena et al., 2003; Gokulan et al., 2013).

In the subsequent year, conformationally strained cinnoline nucleosides were reported by Aldrich and his group as tuberculosis siderophore biosynthesis inhibitors (Dawadi et al., 2018). Anthranilic acid methyl ester **183** underwent Claisen-like condensation with the dianion of *N*-Boc methyl sulfonamide to achieve β-ketosulfonamide compound **184**, which upon diazotization in a mixture of AcOH-H_2O-THF solvent led to the formation of cinnoline-4-one-3-sulfonamide **185**. In the next step, a regioselective Mitsunobu coupling reaction of compound **185** with bis-Boc adenosine **186** led to the formation of **187**. Deprotection of compound **187** by aqueous TFA afforded the desired cinnoline nucleoside **188** (Scheme 39). A [^{32}P]PP_i-ATP exchange assay with salicylic acid and ATP at physiologically relevant supersaturation concentrations was used to evaluate the inhibition of recombinant MbtA by the synthesized compounds

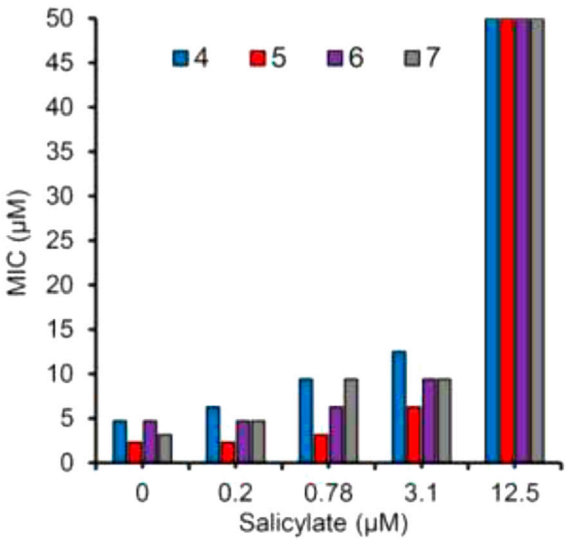

FIGURE 17
Growth sensitivity of *M. tb* in GAST medium supplemented with salicylate at 0, 0.2, 0.78, 3.1, and 12.5 μM. Reproduced from Dawadi et al., 2018, with permission from American Chemical Society, Copyright 2018.

(Somu et al., 2006). According to the Morrison equation, the apparent inhibition constant of tight-binding inhibitors was determined by fitting the concentration–response plot to the Morrison equation (appK_i).

Glycerol–alanine–salt (GAS) medium was used to test the whole-cell activity of H37Rv strain of *M. tuberculosis*. Biochemical data supported the design strategy by showing that the MICs required to inhibit 99.999% of bacterial growth ranged from 2.3to 4.7 μM, as depicted in Figure 17.

Lu *et al.* reported the conformationally strained oxazolidinone for treating multidrug-resistant tuberculosis with improved safety and efficacy profiles (Zhao et al., 2020). Reaction of compound **189** with tosyl chloride resulted in the formation of intermediate **190**, which further underwent nucleophilic substitution in the presence of potassium phthalimide to obtain moiety **191**. In the next step, compound **191** was transformed to intermediate **192** by the addition of methylamine in methanol. Furthermore, acetylation reaction of intermediate **192** led to the formation of **193**, which was transformed into corresponding sulfoxide **194** by the addition of $NaIO_4$ in methanol (Scheme 40). Compound **193** and its sulfoxide metabolite **194** were tested against drug-resistant *M. tuberculosis* strains using sutezolid and linezolid

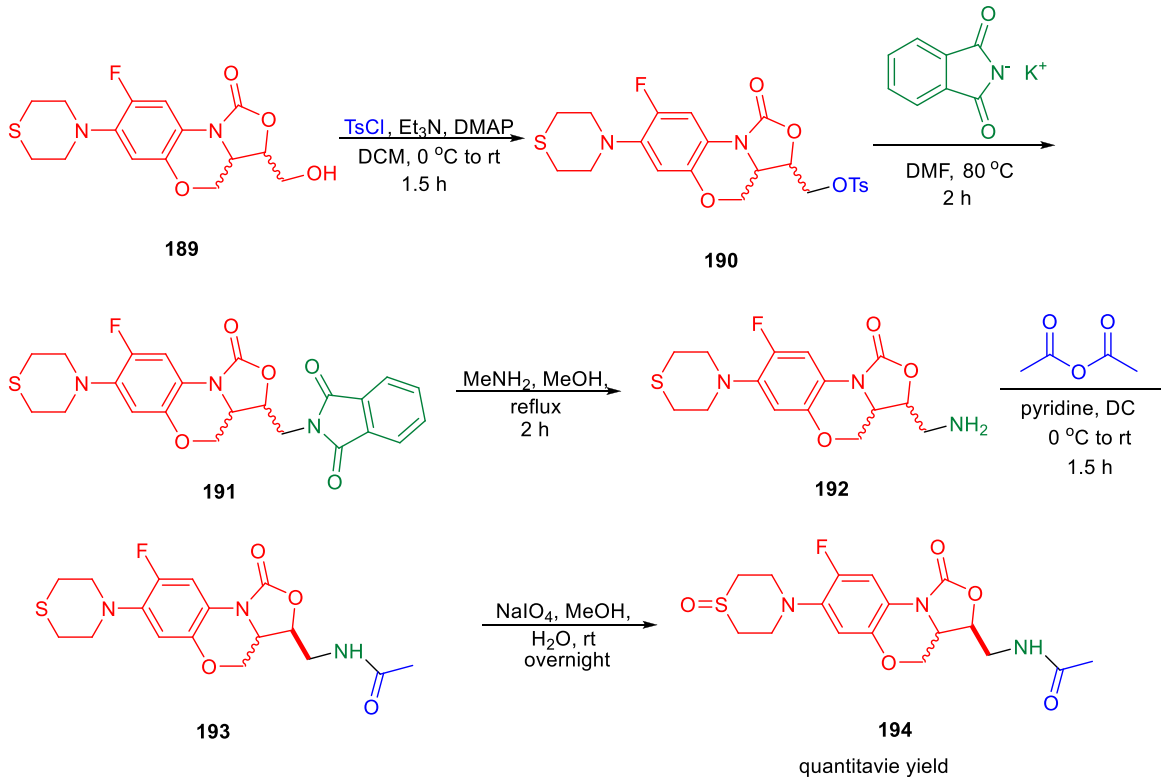

SCHEME 40
Multistep synthesis of constrained oxazolidinones.

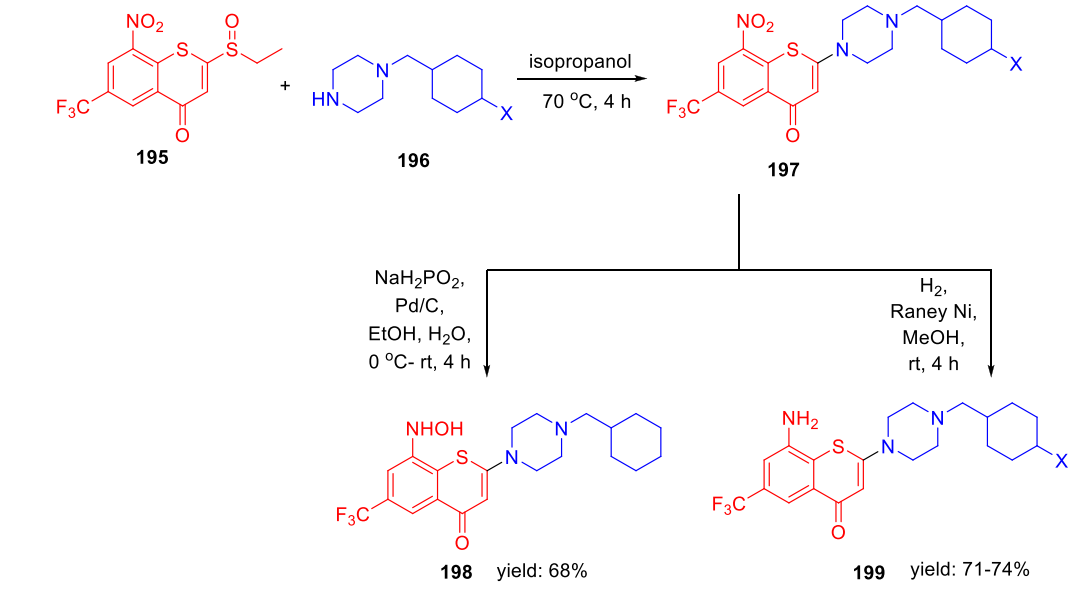

Selected examples:

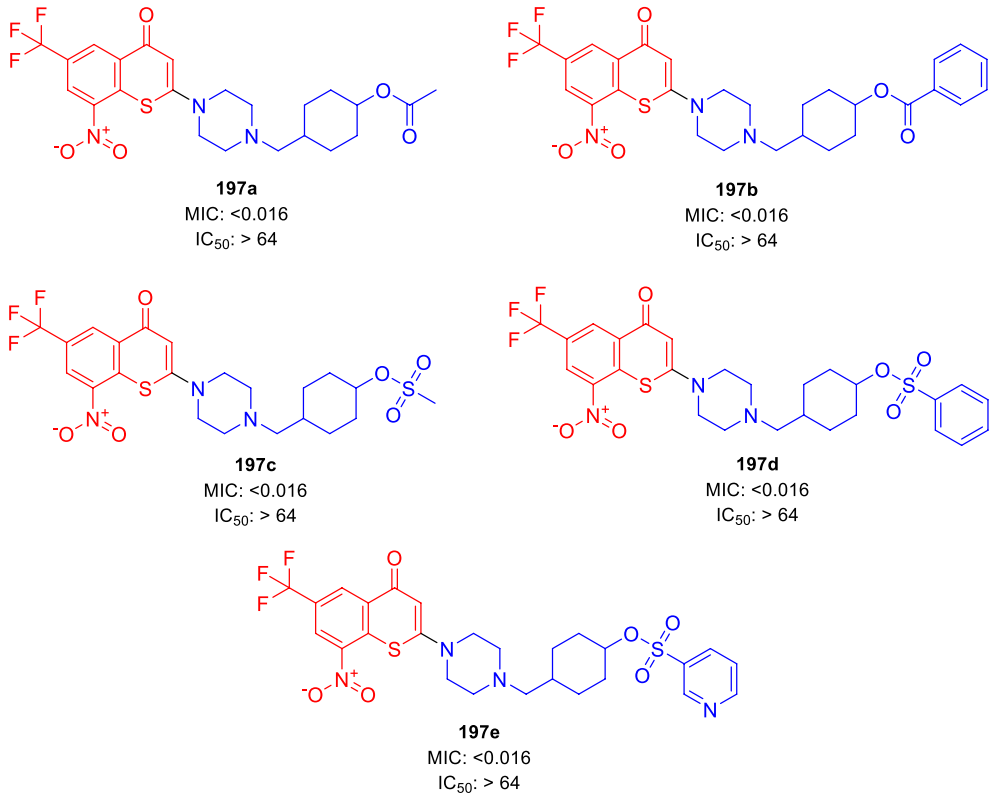

SCHEME 41
Synthesis of target metabolites *via* reduction.

as standard, based on their strong efficacy against H37Rv, modest MPS inhibition, and good microsome stability. The findings indicated that the potency of **193** is much higher than that of **194**, sutezolid, and linezolid. The MIC value of **193** is 4–10-fold higher in the linezolid-resistant, that is, L-R strain than in the H37Rv strain. These findings suggest that compound **193** is likely

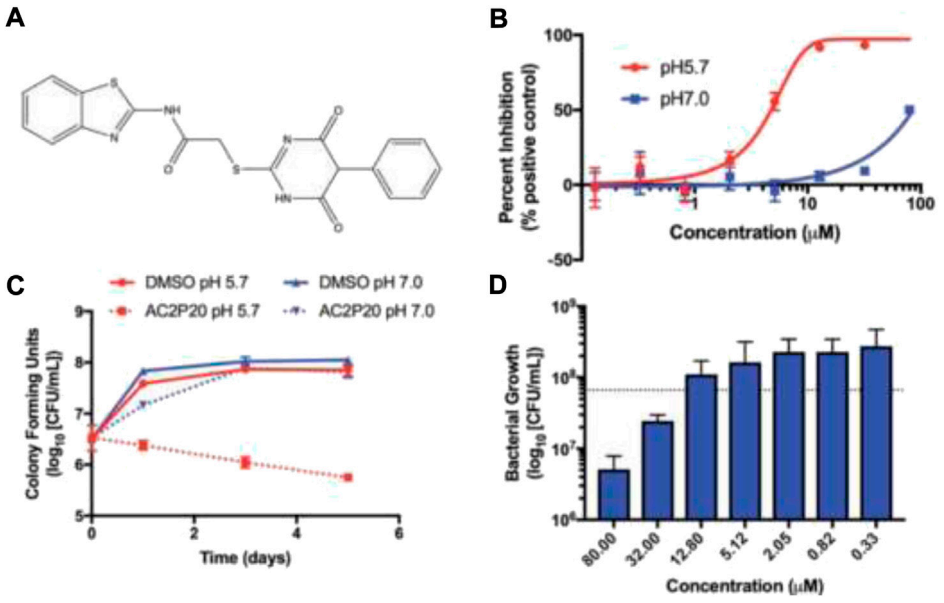

FIGURE 18
(A) Structure of AC2P20, **(B)** dose dependence of *M. tb* growth inhibition with the treatment of AC2P20 at 5.7 and 7.0 pH and exhibition of 4.3 μM EC_{50} after a treatment that lasted for 6 days, **(C)** treatment of 20 μM AC2P20 with *M. tb* for 5 days in a time-dependent way, and **(D)** treatment of AC2P20 with *M. tb* for 7 days at 5.7 pH in a dose-dependent way. Reproduced from Dechow et al., 2021, with permission from Royal Society of Chemistry, Copyright 2021.

to bind to the same location as other oxazolidinones. Several *in vitro* ADME experiments were run on compound **193** to learn more about its drug ability. In hepatocytes from several species, compound **193** demonstrated high metabolic stability. The CYP450 enzymes CYP1A2, CYP2D6, CYP2C9, CYP2C19, and CYP3A4 were also examined with compound **193**. The IC_{50} values against all of these CYP450 isoforms were all greater than 45 μM, which indicates that they have a low risk of drug–drug interactions.

In 2021, Yu Lu and coworkers accomplished the synthesis of benzothiopyranone derivatives, containing amide and ester groups as promising leads toward tuberculosis (Li et al., 2021). Compound **195** was synthesized according to the previously reported synthetic procedures (Li et al., 2019). Treatment of substituted cyclohexylmethylene piperazine **196** with compound **195** in the presence of isopropanol at 70°C to form compound **197** via an y addition elimination strategy. By reducing the nitro group in compound **197** with the help of Pd/C and NaH_2PO_2, hydroxylamine derivative **198** was formed. On the other hand, Raney nickel hydrogenation was performed to transform the nitro group of compound **197** into corresponding amine **199** (Scheme 41). Representative compounds were evaluated against two XDR-TB clinical isolates based on their efficacy against *M. tuberculosis* H37Rv strain. Compounds **197a** and **197b** with an ester motif displayed potent activity against these strains. Furthermore, **197c**, **197d**, and **197e** compounds containing a sulfonate motif showed very significant efficacy against drug-susceptible and drug-resistant tuberculosis. The SAR study indicated that the involvement of small five-membered aromatic heterocycles, that is, furan and thiophene, increased the potency of the molecules.

Abramovitch *et al.* in 2021 established that AC2P20 (N-1,3-benzothiazol-2-yl-2-[(4,6-dioxo-5-phenyl-1,4,5,6-tetrahydropyrimidin-2-yl)thio] is selective in killing *Mycobacterium tuberculosis* at acidic pH through the depletion of free thiols (Dechow et al., 2021). Two *M. tuberculosis* strains, Erdman and CDC1551 and *M. smegmatis* mc (b)155 strains, were employed in all investigations. The lethal mechanisms suggested that AC2P36 and AC2P20 depleted free thiol pools and increased intracellular ROS. Also, it has been found that AC2P20 depletes fewer free thiols than AC2P36, despite the fact that it causes more intracellular ROS to accumulate. While both of them seemed to target *M. tb* free thiols, it is possible that the processes they follow are distinct from one another. Figure 18 demonstrated the no-effect-on-time dependence killing when neutral conditions were employed, whereas at pH 5.7, 100-fold reduction was indicated in comparison with DMSO control as far as viability is concerned. Phenyl-dioxypyrimidine release may also target the secondary undiscovered *M. tb* physiological mechanism, which may explain the larger ROS rise that was reported in comparison to AC2P36.

In light of this recent research, thiol homeostasis as an alternate method to eliminate *M. tb* at acidic pH has been further validated. Auranofin and other chemotypes that work

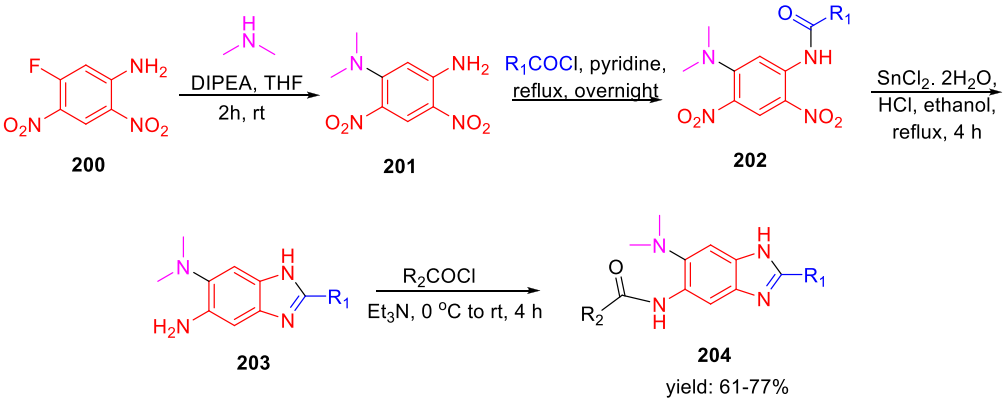

Selected examples:

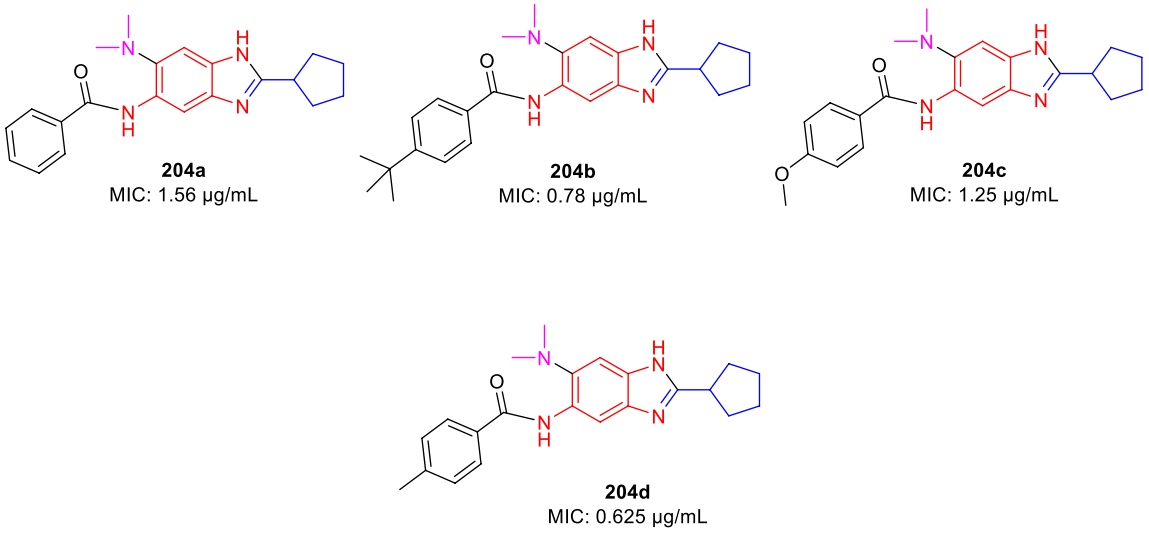

SCHEME 42
Synthetic route to 2,5,6-trisubstituted benzimidazoles *via* amide bond formation.

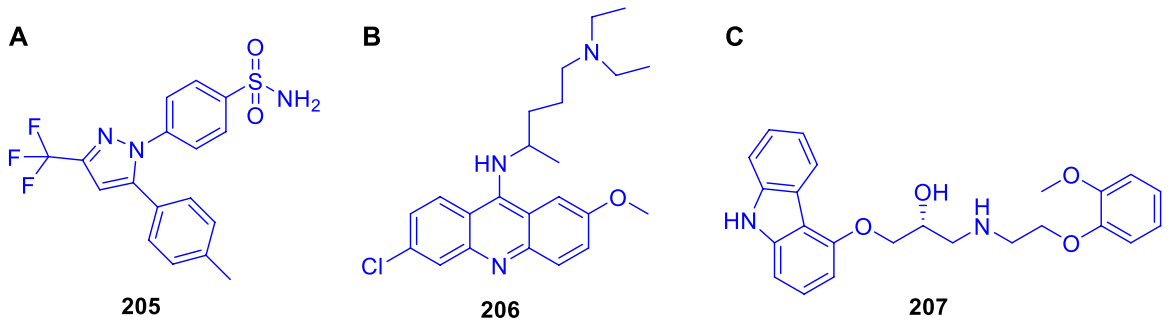

FIGURE 19
(A) Structures of celecoxib **205**, **(B)** Structure of quinacrine **206**, and **(C)** Structure of carvedilol **207**.

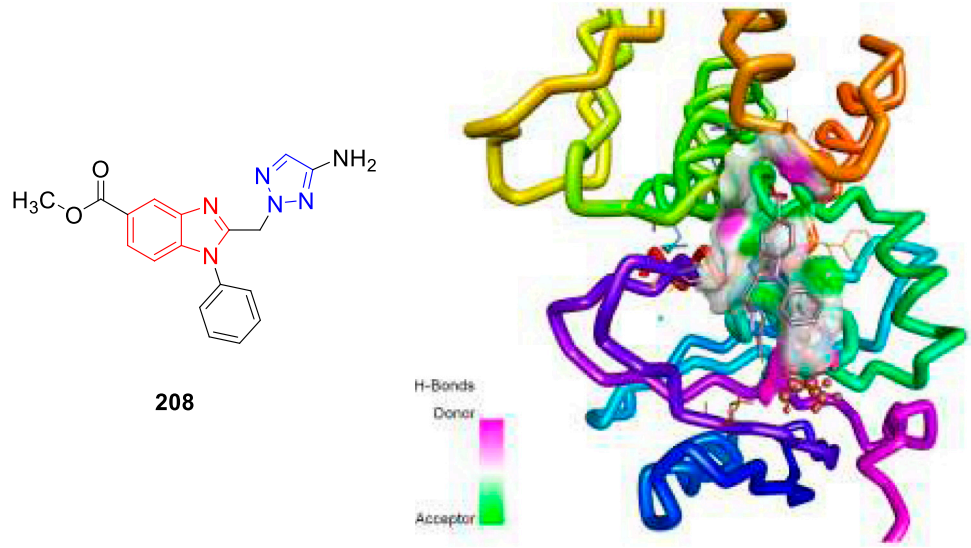

FIGURE 20
Binding pattern of compound **208** with PrpR protein of *Mycobacterium tuberculosis*.

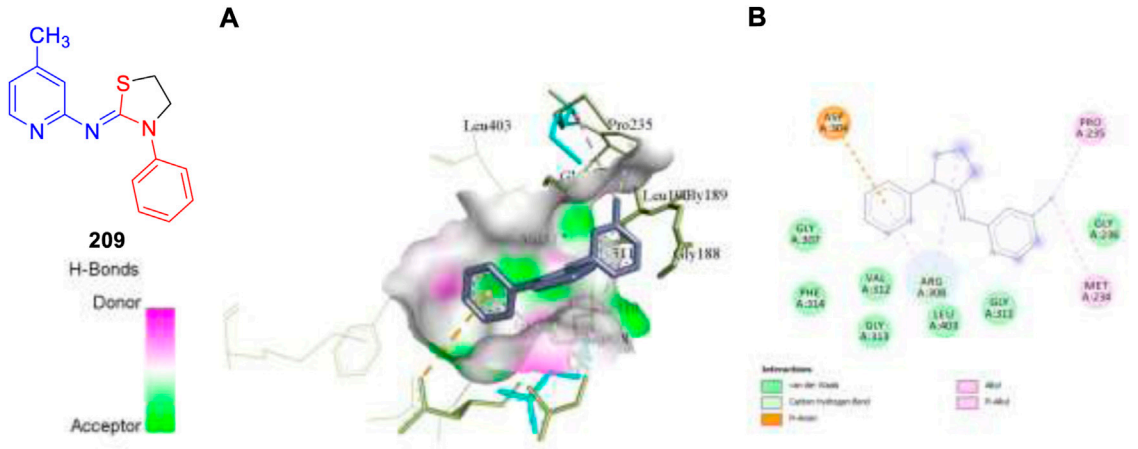

FIGURE 21
Molecular docking visualization and its binding pattern of compound 209. **(A)** Binding of compound **209** at the central cavity. **(B)** 2D depiction and nature of binding interaction involved.

in an indirect manner are usually most promising. Compounds similar to AC2P20 or AC2P36 could, however, be developed into prodrugs that are activated by a *M. tb*-specific enzyme in order to selectively release the thiol-reactive warhead within the bacterial cell. Furthermore, isolating the resistant mutants was not possible for AC2P20 and AC2P36.

Ojima *et al.* accomplished the synthesis of 2,5,6-trisubstituted benzimidazole moieties and assessed their antitubercular activity by targeting *Mtb*-FtsZ (Haranahalli et al., 2021). As depicted in Scheme 42, compound **200** was reacted with secondary amine in the presence of DIPEA to form intermediate **201**. In the next step, acylation of intermediate **201** produced **202**, which further underwent reduction followed by cyclization in the presence of $SnCl_2.H_2O$ to form 2,5,6-trisubstituted benzimidazoles **203** (Kumar et al., 2011; Awasthi et al., 2013). In the last step, acylation of compound **203** achieved the desired moiety **204**. The initial SAR analysis of this library revealed a preference for substituents with cyclopentyl, pent-3-yl, isopropyl, and benzyl groups in their second positions. In the initial screening, none of the compounds with a phenyl or 2-furyl substituent in position 2 had significant activity. When tested

with the resynthesized compound, one compound showed poor inhibition activity of cell growth (MIC >10 μg/ml), despite one hit with a thien-2-yl substituent at position 2. According to these findings, at position 2, a Sp3 hybridized carbon is preferred over a Sp2 carbon. Some of the synthesized compounds exhibited exceptional MIC values toward H37Rv strain such as 0.78 and 0.625 μg/ml for **204b** and **204d**, respectively.

Cheng *et al.* reported the virtual screening of nonbenzofuran inhibitors against *Mycobacterium tuberculosis* Pks13-TE for anti-TB phenotypic discovery based on their structures (Zhao et al., 2021). It seemed that only celecoxib **205** and quinacrine **206** showed inhibitory effects against *M.* tuberculosis strain H37Ra (Figure 19). Pks13-TE soaked with Tam16 is the optimum structure to undertake virtual screening, according to previous studies. Tam16 significantly impairs mycolic acid's ability to bind to the active site and exert its inhibitory effect. This was the first investigation to use Pks13-TE for *in silico* studies based on Glide-SP docking. *In vitro* antimicrobial phenotypic activity tests were also performed to look for novel antitubercular drugs using innovative scaffolds to overcome the restriction of the benzofuran core. Antituberculosis activity with an MIC value of 32 μg/ml was seen in the mild antituberculosis compound carvedilol **207**, whereas the remaining hit compounds had an MIC value of 64 μg/ml. To screen the FDA database for antitubercular medicines, a dependable structure-based digital screening method was developed. Three long-established medications, carvedilol, celecoxib, and quinacrine, were found to have antitubercular action, comparable stability, and binding mechanisms with co-crystal ligand Tam16, which was supported by the simulation data. Excellent druggability and low toxicity of these compounds can be useful for promoting the development of antitubercular agents in future.

In 2021, our group identified a unique class of biheterocyclic molecules to target tuberculosis through a computational study (Rajasekhar et al., 2021). In this regard, we have designed around 20 molecules of substituted benzimidazolyl triazoles to target the *Mycobacterium tuberculosis* protein PrpR, as shown in Figure 20.

It is interesting to observe that in regulating the activity of PrpR protein of *Mycobacterium tuberculosis*, a 4Fe4S cluster binding site and CoA binding site play key roles (Tang et al., 2019). For PrpR to display its role in the methyl citrate cycle (MCC), which involves the elimination of propionyl-CoA a cholesterol degradation product from the system well, there are numerous transcription factors required to be activated. Our understanding is that the designed molecules could inhibit the PrpR protein by ruling out the binding of CoA to its active site, which is further synchronized by the [4Fe4S] clusters binding in the neighboring chain. The mentioned procedure resulted in the several structural deformations that might play an important role in influencing the functions of MCC. We have performed the AutoDock Vina and Glide module for the molecular docking investigation of designed compounds. Based on the Prime-MM/GBSA and the QikProp module, the binding energies and physiochemical properties of the designed molecules were evaluated, respectively. Additionally, a machine learning-based algorithm was used to rank the aforementioned compounds by predicting and evaluating the inhibitory effects of scaffolds. Subsequently, one compound **208** was then subjected to molecular dynamics simulation study to validate the binding characteristics of compounds against PrpR of *Mycobacterium tuberculosis*.

This year also we have designed and computationally evaluated the antitubercular property of substituted thiazolidines, a prominent five-membered N–S heterocycles targeting the PrpR protein of *Mycobacterium tuberculosis* (Rajasekhar et al., 2022).

We have performed the AutoDock Vina and Glide module for the molecular docking investigation of all 17 designed compounds. Based on the Prime-MM/GBSA and the ADMET study, the binding energies and physiochemical properties of the designed molecules were evaluated, and it was found that compound **209** exhibits better binding scores compared to standard drug isoniazid. MD simulation studies of 20 ns validate the structural modifications and dependability of the binding affinities of the top-hit compound **209**.

Conclusion

Pharmaceutical companies have recently faced several roadblocks owing to an enhanced focus on complicated diseases without knowing their biology, followed by a highly competitive landscape from emerging new infectious diseases along with the pricing pressures from patients and buyers. At this juncture, drug discovery scientists along with highly motivated synthetic organic chemists can change the complete scenario by selecting the relevant targets for human diseases and identifying the molecules along with their most feasible synthetic routes. Furthermore, by investing huge resources in synthetic chemistry and chemical technology field, we can advance the area to a position of exploration of chemical moieties in an unimpeded way. Furthermore, it is to be noted that the tremendous progress made in this field of antitubercular drug discovery until now has been possible because of a close coordination between the industry and academia in the last few years. Despite great efforts, only a small number of the hundred powerful compounds found as anti-TB medications were able to enter the clinical stage. There have only been three new medications for tuberculosis in the past 50 years. This may be a result of the difficulties in discovering therapeutic candidates that are both effective and benign, have an appropriate PK profile, and can treat multidrug-resistant TB using innovative mechanisms. The synthetic routes described in this review article for the synthesis

of antitubercular drug candidates will pave the way for inventing new medicines for the betterment of patient lives throughout the world in the future (Figure 21).

Author contributions

UD and KC wrote the manuscript.

Acknowledgments

The authors thank the Chancellor and Vice-Chancellor of Vellore Institute of Technology for providing an opportunity to carry out this study.

Conflict of interest

The authors declare that the research was conducted in the absence of any commercial or financial relationships that could be construed as a potential conflict of interest.

Publisher's note

All claims expressed in this article are solely those of the authors and do not necessarily represent those of their affiliated organizations, or those of the publisher, the editors, and the reviewers. Any product that may be evaluated in this article, or claim that may be made by its manufacturer, is not guaranteed or endorsed by the publisher.

References

Alcaraz, M., Sharma, B., Roquet-Banères, F., Conde, C., Cochard, T., Biet, F., et al. (2022). Designing quinoline-isoniazid hybrids as potent anti-tubercular agents inhibiting mycolic acid biosynthesis. *Eur. J. Med. Chem.* 239, 114531. doi:10.1016/j.ejmech.2022.114531

Alegaon, S. G., Alagawadi, K. R., Sonkusare, P. V., Chaudhary, S. M., Dadwe, D. H., and Shah, A. S. (2012). Novel imidazo[2, 1-b] [1, 3, 4]Thiadiazole carrying rhodanine-3-acetic acid as potential antitubercular agents. *Bioorg. Med. Chem. Lett.* 22 (5), 1917–1921. doi:10.1016/j.bmcl.2012.01.052

Alsayed, S. S. R., Lun, S., Bailey, A. W., Suri, A., Huang, C. C., Mocerino, M., et al. (2021). Design, synthesis and evaluation of novel indole-2-carboxamides for growth inhibition of Mycobacterium tuberculosis and paediatric brain tumour cells. *RSC Adv.* 11 (26), 15497–15511. doi:10.1039/d0ra10728j

Amblard, F., Zhang, H., Zhou, L., Shi, J., Bobeck, D. R., Nettles, J. H., et al. (2013). Synthesis and evaluation of nondimeric HCV NS5A inhibitors. *Bioorg. Med. Chem. Lett.* 23 (7), 2031–2034. doi:10.1016/j.bmcl.2013.02.023

Aono, A., Murase, Y., Chikamatsu, K., Igarashi, Y., Shimomura, Y., Hosoya, M., et al. (2022). *In vitro* activity of tedizolid and linezolid against multidrug-resistant *Mycobacterium tuberculosis*: A comparative study using microdilution broth assay and genomics. *Diagn. Microbiol. Infect. Dis.* 103 (3), 115714. doi:10.1016/j.diagmicrobio.2022.115714

Awasthi, D., Kumar, K., Knudson, S. E., Slayden, R. A., and Ojima, I. (2013). SAR studies on trisubstituted benzimidazoles as inhibitors of Mtb FtsZ for the development of novel antitubercular agents. *J. Med. Chem.* 56 (23), 9756–9770. doi:10.1021/jm401468w

Ballini, R., Bosica, G., Cioci, G., Fiorini, D., and Petrini, M. (2003). Conjugate addition of nitroalkanes to N-substituted maleimides. Synthesis of 3-alkylsuccinimides and pyrrolidines. *Tetrahedron* 59 (20), 3603–3608. doi:10.1016/S0040-4020(03)00508-8

Bartoli, G., Bosco, M., Carlone, A., Cavalli, A., Locatelli, M., Mazzanti, A., et al. (2006). Organocatalytic asymmetric conjugate addition of 1, 3-dicarbonyl compounds to maleimides. *Angew. Chem. Int. Ed. Engl.* 45 (30), 4966–4970. doi:10.1002/anie.200600370

Bergmann, E., and Orchin, M. (1949). Synthesis of fluoranthene and its derivatives. *J. Am. Chem. Soc.* 71, 1917–1918. doi:10.1021/ja01174a005

Bhat, Z. S., Ul Lah, H., Rather, M. A., Maqbool, M., Ara, T., Ahmad, Z., et al. (2018). Synthesis and *in vitro* evaluation of substituted 3-cinnamoyl-4-hydroxy-pyran-2-one (CHP) in pursuit of new potential antituberculosis agents. *MedChemComm* 9 (1), 165–172. doi:10.1039/c7md00366h

Bramhankar, D. M., and Jaiswal, S. B. (1995). *Biopharmaceutics and pharmacokinetics-A treatise*, 111–158.

Cappoen, D., Forge, D., Vercammen, F., Mathys, V., Kiass, M., Roupie, V., et al. (2013). Biological evaluation of bisbenzaldehydes against four Mycobacterium species. *Eur. J. Med. Chem.* 63, 731–738. doi:10.1016/j.ejmech.2013.03.023

Cappoen, D., Claes, P., Jacobs, J., Anthonissen, R., Mathys, V., Verschaeve, L., et al. (2014). 1, 2, 3, 4, 8, 9, 10, 11-octahydrobenzo[j]phenanthridine-7, 12-diones as new leads against *Mycobacterium tuberculosis*. *J. Med. Chem.* 57 (7), 2895–2907. doi:10.1021/jm401735w

Chandrasekera, N. S., Alling, T., Bailey, M. A., Files, M., Early, J. V., Ollinger, J., et al. (2015). Identification of phenoxyalkylbenzimidazoles with antitubercular activity. *J. Med. Chem.* 58 (18), 7273–7285. doi:10.1021/acs.jmedchem.5b00546

Chandrasekera, N. S., Berube, B. J., Shetye, G., Chettiar, S., O'Malley, T., Manning, A., et al. (2017). Improved phenoxyalkylbenzimidazoles with activity against Mycobacterium tuberculosis appear to target QcrB. *ACS Infect. Dis.* 3 (12), 898–916. doi:10.1021/acsinfecdis.7b00112

Chauhan, P. M. S., Sunduru, N., and Sharma, M. (2010). Recent advances in the design and synthesis of heterocycles as anti-tubercular agents. *Future Med. Chem.* 2 (9), 1469–1500. doi:10.4155/fmc.10.227

Cheng, C. F., Lai, Z. C., and Lee, Y. J. (2008). Total synthesis of (±)-Camphorataimides and (±)-Himanimides by $NaBH_4$/$Ni(OAc)_2$ or Zn/AcOH stereoselective reduction. *Tetrahedron* 64 (19), 4347–4353. doi:10.1016/j.tet.2008.02.077

Choi, P. J., Lu, G. L., Sutherland, H. S., Giddens, A. C., Franzblau, S. G., Cooper, C. B., et al. (2022). Synthetic studies towards isomeric pyrazolopyrimidines as potential ATP synthesis inhibitors of Mycobacterium tuberculosis. Structural correction of reported N-(6-(2-(Dimethylamino)Ethoxy)-5-Fluoropyridin-3-Yl)-2-(4-Fluorophenyl)-5-(Trifluoromethyl)Pyrazolo[1, 5-α]Pyrimidin-7-Amine. *Tetrahedron Lett.* 90, 153611. doi:10.1016/j.tetlet.2021.153611

Chollet, A., Mori, G., Menendez, C., Rodriguez, F., Fabing, I., Pasca, M. R., et al. (2015). Design, synthesis and evaluation of new GEQ derivatives as inhibitors of InhA enzyme and Mycobacterium tuberculosis growth. *Eur. J. Med. Chem.* 101, 218–235. doi:10.1016/j.ejmech.2015.06.035

Claes, P., Cappoen, D., Mbala, B. M., Jacobs, J., Mertens, B., Mathys, V., et al. (2013). Synthesis and antimycobacterial activity of analogues of the bioactive natural products sampangine and cleistopholine. *Eur. J. Med. Chem.* 67, 98–110. doi:10.1016/j.ejmech.2013.06.010

Cohn, D. L., Catlin, B. J., Peterson, K. L., Judson, F. N., and Sbarbaro, J. A. (1990). A 62-dose, 6-month therapy for pulmonary and extrapulmonary tuberculosis. A twice-weekly, directly observed, and cost-effective regimen. *Ann. Intern. Med.* 112 (6), 407–415. doi:10.7326/0003-4819-76-3-112-6-407

Conradie, F., Diacon, A. H., Ngubane, N., Howell, P., Everitt, D., Crook, A. M., et al. (2020). Treatment of highly drug-resistant pulmonary tuberculosis. *N. Engl. J. Med.* 382 (10), 893–902. doi:10.1056/NEJMoa1901814

Dawadi, S., Boshoff, H. I. M., Park, S. W., Schnappinger, D., and Aldrich, C. C. (2018). Conformationally constrained cinnolinone nucleoside analogues as siderophore biosynthesis inhibitors for tuberculosis. *ACS Med. Chem. Lett.* 9 (4), 386–391. doi:10.1021/acsmedchemlett.8b00090

Dechow, S. J., Coulson, G. B., Wilson, M. W., Larsen, S. D., and Abramovitch, R. B. (2021). AC2P20 selectively kills Mycobacterium tuberculosisat acidic PH by depleting free thiols. *RSC Adv.* 11 (33), 20089–20100. doi:10.1039/d1ra03181c

Dixit, P. P., Dixit, P. P., and Thore, S. N. (2016). Hybrid triazoles: Design and synthesis as potential dual inhibitor of growth and efflux inhibition in tuberculosis. *Eur. J. Med. Chem.* 107, 38–47. doi:10.1016/j.ejmech.2015.10.054

Dubreuil, L., Houcke, I., Mouton, Y., and Rossignol, J. F. (1996). *In vitro* evaluation of activities of nitazoxanide and tizoxanide against anaerobes and

aerobic organisms. *Antimicrob. Agents Chemother.* 40 (10), 2266–2270. doi:10.1128/aac.40.10.2266

Evans, J. C., and Mizrahi, V. (2018). Priming the tuberculosis drug pipeline: New antimycobacterial targets and agents. *Curr. Opin. Microbiol.* 45, 39–46. doi:10.1016/j.mib.2018.02.006

Fernandes, G. F. S., Thompson, A. M., Castagnolo, D., Denny, W. A., and Dos Santos, J. L. (2022). Tuberculosis drug discovery: Challenges and new horizons. *J. Med. Chem.* 65, 7489–7531. doi:10.1021/acs.jmedchem.2c00227

Forge, D., Cappoen, D., Laurent, J., Stanicki, D., Mayence, A., Huang, T. L., et al. (2012). 1, 4-diarylpiperazines and analogs as anti-tubercular agents: Synthesis and biological evaluation. *Eur. J. Med. Chem.* 49, 95–101. doi:10.1016/j.ejmech.2011.12.035

Fu, H., Lewnard, J. A., Frost, I., Laxminarayan, R., and Arinaminpathy, N. (2021). Modelling the global burden of drug-resistant tuberculosis avertable by a post-exposure vaccine. *Nat. Commun.* 12, 424. doi:10.1038/s41467-020-20731-x

Furin, J., Cox, H., and Pai, M. (2019). Tuberculosis. *Lancet* 393, 1642–1656. doi:10.1016/S0140-6736(19)30308-3

Gandhi, N. R., Nunn, P., Dheda, K., Schaaf, H. S., Zignol, M., van Soolingen, D., et al. (2010). Multidrug-resistant and extensively drug-resistant tuberculosis: A threat to global control of tuberculosis. *Lancet* 375 (9728), 1830–1843. doi:10.1016/S0140-6736(10)60410-2

Gill, C., Jadhav, G., Shaikh, M., Kale, R., Ghawalkar, A., Nagargoje, D., et al. (2008). Clubbed [1, 2, 3] triazoles by fluorine benzimidazole: A novel approach to H37Rv inhibitors as a potential treatment for tuberculosis. *Bioorg. Med. Chem. Lett.* 18 (23), 6244–6247. doi:10.1016/j.bmcl.2008.09.096

Global Preparedness Monitoring Board (2019). *A world at risk. Annual report on global preparedness for health emergencies*. Geneva: World Health Organisation.

Gokulan, K., O'Leary, S. E., Russell, W. K., Russell, D. H., Lalgondar, M., Begley, T. P., et al. (2013). Crystal structure of Mycobacterium tuberculosis polyketide synthase 11 (PKS11) reveals intermediates in the synthesis of methyl-branched alkylpyrones. *J. Biol. Chem.* 288 (23), 16484–16494. doi:10.1074/jbc.M113.468892

Guillemont, J., Meyer, C., Poncelet, A., Bourdrez, X., and Andries, K. (2011). Diarylquinolines, synthesis pathways and quantitative structure-activity relationship studies leading to the discovery of TMC207. *Future Med. Chem.* 3 (11), 1345–1360. doi:10.4155/fmc.11.79

Gundersen, L. L., Nissen-Meyer, J., and Spilsberg, B. (2002). Synthesis and antimycobacterial activity of 6-arylpurines: The requirements for the N-9 substituent in active antimycobacterial purines. *J. Med. Chem.* 45 (6), 1383–1386. doi:10.1021/jm0110284

Guo, H., Courbon, G. M., Bueler, S. A., Mai, J., Liu, J., and Rubinstein, J. L. (2021). Structure of mycobacterial ATP synthase bound to the tuberculosis drug bedaquiline. *Nature* 589, 143–147. doi:10.1038/s41586-020-3004-3

Haranahalli, K., Tong, S., Kim, S., Awwa, M., Chen, L., Knudson, S. E., et al. (2021). Structure-activity relationship studies on 2, 5, 6-trisubstituted benzimidazoles TargetingMtb-FtsZ as antitubercular agents. *RSC Med. Chem.* 12 (1), 78–94. doi:10.1039/d0md00256a

Harikrishna, N., Isloor, A. M., Ananda, K., Obaid, A., and Fun, H. K. (2015). 1, 3, 4-trisubstituted pyrazole bearing a 4-(chromen-2-one) thiazole: Synthesis, characterization and its biological studies. *RSC Adv.* 5 (54), 43648–43659. doi:10.1039/c5ra04995d

Harikrishna, N., Isloor, A. M., Ananda, K., Obaid, A., and Fun, H. K. (2016). Synthesis, and antitubercular and antimicrobial activity of 1′-(4-Chlorophenyl) Pyrazole containing 3, 5-disubstituted pyrazoline derivatives. *New J. Chem.* 40 (1), 73–76. doi:10.1039/c5nj02237a

Holzheimer, M., Buter, J., and Minnaard, A. J. (2021). Chemical synthesis of cell wall constituents of Mycobacterium tuberculosis. *Chem. Rev.* 121 (15), 9554–9643. doi:10.1021/acs.chemrev.1c00043

Hopfner, S. M., Lee, B. S., Kalia, N. P., Miller, M. J., Pethe, K., and Moraski, G. C. (2021). Structure guided generation of thieno[3, 2-d]Pyrimidin-4-AmineMycobacterium tuberculosis bdoxidase inhibitors. *RSC Med. Chem.* 12 (1), 73–77. doi:10.1039/d0md00398k

Huang, S.-G. (2002). Development of a high throughput screening assay for mitochondrial membrane potential in living cells. *J. Biomol. Screen.* 7 (4), 383–389. doi:10.1177/108705710200700411

Igarashi, M., Ishizaki, Y., and Takahashi, Y. (2017). New antituberculous drugs derived from natural products: Current perspectives and issues in antituberculous drug development. *J. Antibiot. (Tokyo)* 71, 15–25. doi:10.1038/ja.2017.126

Jadhav, G. R., Shaikh, M. U., Kale, R. P., Shiradkar, M. R., and Gill, C. H. (2009). SAR study of clubbed [1, 2, 4]-triazolyl with fluorobenzimidazoles as antimicrobial and antituberculosis agents. *Eur. J. Med. Chem.* 44 (7), 2930–2935. doi:10.1016/j.ejmech.2008.12.001

Johansen, M., Salini, S., Sumit, K., Clément, R., Quan, D., Britton, W., et al. (2021). Biological and biochemical evaluation of isatin-isoniazid hybrids as bactericidal candidates against Mycobacterium tuberculosis. *Antimicrob. Agents Chemother.* 65 (8), e0001121–21. doi:10.1128/AAC.00011-21

Kalia, D., Anil Kumar, K. S., Meena, G., Sethi, K. P., Sharma, R., Trivedi, P., et al. (2015). Synthesis and anti-tubercular activity of conformationally-constrained and bisquinoline analogs of TMC207. *MedChemComm* 6 (8), 1554–1563. doi:10.1039/c5md00131e

Karad, S. C., Purohit, V. B., Raval, D. K., Kalaria, P. N., Avalani, J. R., Thakor, P., et al. (2015). Green synthesis and pharmacological screening of polyhydroquinoline derivatives bearing a fluorinated 5-aryloxypyrazole nucleus. *RSC Adv.* 5 (21), 16000–16009. doi:10.1039/c5ra00388a

Keam, S. J. (2019). Pretomanid: First approval. *Drugs* 79, 1797–1803. doi:10.1007/s40265-019-01207-9

Khonde, L. P., Müller, R., Boyle, G. A., Reddy, V., Nchinda, A. T., Eyermann, C. J., et al. (2021). 1, 3-diarylpyrazolyl-acylsulfonamides as potent anti-tuberculosis agents targeting cell wall biosynthesis in Mycobacterium tuberculosis. *J. Med. Chem.* 64 (17), 12790–12807. doi:10.1021/acs.jmedchem.1c00837

Kiran, D., Podell, B. K., Chambers, M., and Basaraba, R. J. (2016). Host-directed therapy targeting the Mycobacterium tuberculosis granuloma: A review. *Semin. Immunopathol.* 38 (2), 167–183. doi:10.1007/s00281-015-0537-x

Kozikowski, A. P., Chen, Y., Gaysin, A., Chen, B., D'Annibale, M. A., Suto, C. M., et al. (2007). Functional differences in epigenetic modulators - superiority of mercaptoacetamide-based histone deacetylase inhibitors relative to hydroxamates in cortical neuron neuroprotection studies. *J. Med. Chem.* 50 (13), 3054–3061. doi:10.1021/jm070178x

Kumagai, N., Matsunaga, S., Kinoshita, T., Harada, S., Okada, S., Sakamoto, S., et al. (2003). Direct catalytic asymmetric aldol reaction of hydroxyketones: Asymmetric Zn catalysis with a Et2Zn/Linked-BINOL complex. *J. Am. Chem. Soc.* 125 (8), 2169–2178. doi:10.1021/ja028926p

Kumar, K., Awasthi, D., Lee, S. Y., Zanardi, I., Ruzsicska, B., Knudson, S., et al. (2011). Novel trisubstituted benzimidazoles, targeting Mtb FtsZ, as a new class of antitubercular agents. *J. Med. Chem.* 54 (1), 374–381. doi:10.1021/jm1012006

La Rosa, V., Poce, G., Canseco, J. O., Buroni, S., Pasca, M. R., Biava, M., et al. (2012). MmpL3 is the cellular target of the antitubercular pyrrole derivative BM212. *Antimicrob. Agents Chemother.* 56 (1), 324–331. doi:10.1128/AAC.05270-11

Landge, S., Mullick, A. B., Nagalapur, K., Neres, J., Subbulakshmi, V., Murugan, K., et al. (2015). Discovery of benzothiazoles as antimycobacterial agents: Synthesis, structure-activity relationships and binding studies with Mycobacterium tuberculosis decaprenylphosphoryl-β-d-ribose 2′-oxidase. *Bioorg. Med. Chem.* 23 (24), 7694–7710. doi:10.1016/j.bmc.2015.11.017

Li, P., Wu, Y., Zhang, T., Ma, C., Lin, Z., Li, G., et al. (2019). An efficient and concise access to 2-amino-4H-Benzothio-Pyran-4-One derivatives. *Beilstein J. Org. Chem.* 15, 703–709. doi:10.3762/bjoc.15.65

Li, P., Wang, B., Fu, L., Guo, K., Ma, C., Wang, B., et al. (2021). Identification of novel benzothiopyranones with ester and amide motifs derived from active metabolite as promising leads against Mycobacterium tuberculosis. *Eur. J. Med. Chem.* 2021, 113603. doi:10.1016/j.ejmech.2021.113603

Libardo, J. M. D., Boshoff, H. I. M., and Barry, C. E. (2018). The present state of the tuberculosis drug development pipeline. *Curr. Opin. Pharmacol.* 42, 81–94. doi:10.1016/j.coph.2018.08.001

Lilienkampf, A., Jialin, M., Baojie, W., Yuehong, W., Franzblau, S. G., and Kozikowski, A. P. (2009). Structure-activity relationships for a series of quinoline-based compounds active against replicating and nonreplicating Mycobacterium tuberculosis. *J. Med. Chem.* 52 (7), 2109–2118. doi:10.1021/jm900003c

Liu, R., Krchnak, V., Brown, S. N., and Miller, M. J. (2019). Deuteration of BTZ043 extends the lifetime of meisenheimer intermediates to the antituberculosis nitroso oxidation state. *ACS Med. Chem. Lett.* 10 (10), 1462–1466. doi:10.1021/acsmedchemlett.9b00308

Liu, R., Markley, L., Miller, P. A., Franzblau, S., Shetye, G., Ma, R., et al. (2021). Hydride-induced meisenheimer complex formation reflects activity of nitro aromatic anti-tuberculosis compounds. *RSC Med. Chem.* 12 (1), 62–72. doi:10.1039/d0md00390e

López-Rodríguez, M. L., Morcillo, M. J., Rovat, T. K., Fernández, E., Vicente, B., Sanz, A. M., et al. (1999). Synthesis and structure-activity relationships of a new model of arylpiperazines. 4. 1-[omega-(4-Arylpiperazin-1-yl)alkyl]-3-(diphenylmethylene) - 2, 5-pyrrolidinediones and -3-(9H-fluoren-9-ylidene)-2, 5-pyrrolidinediones: Study of the steric requirements of the terminal amide fragment on 5-ht1a affinity/selectivity. *J. Med. Chem.* 42 (1), 36–49. doi:10.1021/jm980285e

Lubanyana, H., Arvidsson, P. I., Govender, T., Kruger, H. G., and Naicker, T. (2020). Improved synthesis and isolation of bedaquiline. *ACS Omega* 5 (7), 3607–3611. doi:10.1021/acsomega.9b04037

Madaiah, M., Prashanth, M. K., Revanasiddappa, H. D., and Veeresh, B. (2016). Synthesis and evaluation of novel imidazo[4, 5-: C] pyridine derivatives as antimycobacterial agents against Mycobacterium tuberculosis. *New J. Chem.* 40 (11), 9194–9204. doi:10.1039/c6nj02069k

Mahboobi, S., Eichhorn, E., Winkler, M., Sellmer, A., and Möllmann, U. (2008). Antibacterial activity of a novel series of 3-bromo-4-(1H-3-Indolyl)-2, 5-dihydro-1H-2, 5-pyrroledione derivatives - an extended structure-activity relationship study. *Eur. J. Med. Chem.* 43 (3), 633–656. doi:10.1016/j.ejmech.2007.05.009

Matviiuk, T., Rodriguez, F., Saffon, N., Mallet-Ladeira, S., Gorichko, M., De Jesus Lopes Ribeiro, A. L., et al. (2013). Design, chemical synthesis of 3-(9H-Fluoren-9-Yl)Pyrrolidine-2, 5-dione derivatives and biological activity against enoyl-ACP reductase (InhA) and Mycobacterium tuberculosis. *Eur. J. Med. Chem.* 70, 37–48. doi:10.1016/j.ejmech.2013.09.041

Matviiuk, T., Mori, G., Lherbet, C., Rodriguez, F., Pasca, M. R., Gorichko, M., et al. (2014). Synthesis of 3-heteryl substituted pyrrolidine-2, 5-diones via catalytic Michael reaction and evaluation of their inhibitory activity against InhA and Mycobacterium tuberculosis. *Eur. J. Med. Chem.* 71, 46–52. doi:10.1016/j.ejmech.2013.10.069

Matviiuk, T., Menendez, C., Carayon, C., Saffon, N., Voitenko, Z., Lherbet, C., et al. (2014). LiAlH4-Promoted tandem reduction/oxidation of fluorenyl derivatives under air. *Eur. J. Org. Chem.* 2014 (29), 6538–6546. doi:10.1002/ejoc.201402642

Matviiuk, T., Madacki, J., Mori, G., Orena, B. S., Menendez, C., Kysil, A., et al. (2016). Pyrrolidinone and pyrrolidine derivatives: Evaluation as inhibitors of InhA and Mycobacterium tuberculosis. *Eur. J. Med. Chem.* 123, 462–475. doi:10.1016/j.ejmech.2016.07.028

Menendez, C., Gau, S., Lherbet, C., Rodriguez, F., Inard, C., Pasca, M. R., et al. (2011). Synthesis and biological activities of triazole derivatives as inhibitors of InhA and antituberculosis agents. *Eur. J. Med. Chem.* 46 (11), 5524–5531. doi:10.1016/j.ejmech.2011.09.013

Menendez, C., Gau, S., Ladeira, S., Lherbet, C., and Baltas, M. (2012). Synthesis of α, β-diketotriazoles by aerobic copper-catalyzed oxygenation with triazole as an intramolecular assisting group. *Eur. J. Org. Chem.* 2, 409–416. doi:10.1002/ejoc.201101346

Menendez, C., Rodriguez, F., Ribeiro, A. L. D. J. L., Zara, F., Frongia, C., Lobjois, V., et al. (2013). Synthesis and evaluation of α-ketotriazoles and α, β- diketotriazoles as inhibitors of Mycobacterium tuberculosis. *Eur. J. Med. Chem.* 69, 167–173. doi:10.1016/j.ejmech.2013.06.042

Moraski, G. C., Miller, P. A., Bailey, M. A., Ollinger, J., Parish, T., Boshoff, H. I., et al. (2016). Putting tuberculosis (TB) to rest: Transformation of the sleep aid, ambien, and "anagrams" generated potent antituberculosis agents. *ACS Infect. Dis.* 1 (2), 85–90. doi:10.1021/id500008t

Moyo, S., Ismail, F., Van der Walt, M., Ismail, N., Mkhondo, N., Dlamini, S., et al. (2022). Prevalence of bacteriologically confirmed pulmonary tuberculosis in south Africa, 2017–19: A multistage, cluster-based, cross-sectional survey. *Lancet. Infect. Dis.* 22 (8), 1172–1180. doi:10.1016/S1473-3099(22)00149-9

Naik, M., Ghorpade, S., Jena, L. K., Gorai, G., Narayan, A., Guptha, S., et al. (2014). 2-Phenylindole and arylsulphonamide: Novel scaffolds bactericidal against Mycobacterium tuberculosis. *ACS Med. Chem. Lett.* 5 (9), 1005–1009. doi:10.1021/ml5001933

Naran, K., Moosa, A., Barry, C. E., Boshoff, H. I. M., Mizrahi, V., and Warner, D. F. (2016). Bioluminescent reporters for rapid mechanism of action assessment in tuberculosis drug discovery. *Antimicrob. Agents Chemother.* 60 (11), 6748–6757. doi:10.1128/AAC.01178-16

Neri, J. M., Cavalcanti, L. N., Araújo, R. M., and Menezes, F. G. (2020). 2, 3-dichloroquinoxaline as a versatile building block for heteroaromatic nucleophilic substitution: A review of the last decade. *Arab. J. Chem.* 13 (1), 721–739. doi:10.1016/j.arabjc.2017.07.012

Odingo, J., Bailey, M. A., Files, M., Early, J. V., Alling, T., Dennison, D., et al. (2017). *In vitro* evaluation of novel nitazoxanide derivatives against Mycobacterium tuberculosis. *ACS Omega* 2 (9), 5873–5890. doi:10.1021/acsomega.7b00892

Padmaja, R. D., Balamurali, M. M., and Chanda, K. (2019). One-Pot, Telescopic Approach for the Chemoselective Synthesis of Substituted Benzo[e]Pyrido/Pyrazino/Pyridazino[1, 2-b] [1, 2, 4]Thiadiazine Dioxides and Their Significance in Biological Systems. *J. Org. Chem.* 84 (18), 11382–11390. doi:10.1021/acs.joc.9b00869

Panchangam, R. L., Manickam, V., and Chanda, K. (2019). Assembly of fully substituted 2H-indazoles catalyzed by Cu_2O rhombic dodecahedra and evaluation of anticancer activity. *ChemMedChem* 14 (2), 262–272. doi:10.1002/cmdc.201800707

Panchangam, R. L., Rao, R. N., Balamurali, M. M., Hingamaire, T. B., Shanmugam, D., Manickam, V., et al. (2021). Antitumor effects of Ir(III)-2*H*-indazole complexes for triple negative breast cancer. *Inorg. Chem.* 60 (23), 17593–17607. doi:10.1021/acs.inorgchem.1c02193

Pathak, R., Madapa, S., and Batra, S. (2007). Trifluoroacetic acid: A more effective and efficient reagent for the synthesis of 3-arylmethylene-3, 4-dihydro-1H-Quinolin-2-Ones and 3-arylmethyl-2-amino-quinolines from baylis-hillman derivatives via claisen rearrangement. *Tetrahedron* 63 (2), 451–460. doi:10.1016/j.tet.2006.10.053

Patpi, S. R., Pulipati, L., Yogeeswari, P., Sriram, D., Jain, N., Sridhar, B., et al. (2012). Design, synthesis, and structure-activity correlations of novel dibenzo[b, d furan, dibenzo[b, d]Thiophene, and N-methylcarbazole clubbed 1, 2, 3-triazoles as potent inhibitors of Mycobacterium tuberculosis. *J. Med. Chem.* 55 (8), 3911–3922. doi:10.1021/jm300125e

Pissinate, K., Villela, A. D., Rodrigues, V., Giacobbo, B. C., Grams, E. S., Abbadi, B. L., et al. (2016). 2-(Quinolin-4-Yloxy)Acetamides are active against drug-susceptible and drug-resistant Mycobacterium tuberculosis strains. *ACS Med. Chem. Lett.* 7 (3), 235–239. doi:10.1021/acsmedchemlett.5b00324

Poce, G., Consalvi, S., Venditti, G., Alfonso, S., Desideri, N., Fernandez-Menendez, R., et al. (2019). Novel pyrazole-containing compounds active against Mycobacterium tuberculosis. *ACS Med. Chem. Lett.* 10 (10), 1423–1429. doi:10.1021/acsmedchemlett.9b00204

Raghu, M. S., Pradeep Kumar, C. B., Prasad, K. N. N., Prashanth, M. K., Kumarswamy, Y. K., Chandrasekhar, S., et al. (2020). MoS_2-Calix[4]Arene catalyzed synthesis and molecular docking study of 2, 4, 5-trisubstituted imidazoles as potent inhibitors of Mycobacterium tuberculosis. *ACS Comb. Sci.* 22 (10), 509–518. doi:10.1021/acscombsci.0c00038

Rajasekhar, S., Karuppasamy, R., and Chanda, K. Exploration of potential inhibitors for tuberculosis via structure-based drug design, molecular docking, and molecular dynamics simulation studies. *J. Comput. Chem.* 2021, 42, 1736–1749. doi: doi: doi:10.1002/jcc.26712

Rajasekhar, S., Das, S., Karuppasamy, R., Musuvathi, M. B., and Chanda, K. (2022). Identification of novel inhibitors for prp protein of Mycobacterium tuberculosis by structure-based drug design, and molecular dynamics simulations. *J. Comput. Chem.* 43 (9), 619–630. doi:10.1002/jcc.26823

Ramprasad, J., Nayak, N., Dalimba, U., Yogeeswari, P., Sriram, D., Peethambar, S. K., et al. (2015). Synthesis and biological evaluation of new imidazo[2, 1-b] [1, 3, 4] Thiadiazole-benzimidazole derivatives. *Eur. J. Med. Chem.* 95, 49–63. doi:10.1016/j.ejmech.2015.03.024

Ramprasad, J., Nayak, N., Dalimba, U., Yogeeswari, P., and Sriram, D. (2016). Ionic liquid-promoted one-pot synthesis of thiazole-imidazo[2, 1-b] [1, 3, 4] Thiadiazole hybrids and their antitubercular activity. *MedChemComm* 7 (2), 338–344. doi:10.1039/c5md00346f

Rani, A., Viljoen, A., Johansen, M. D., Kremer, L., and Kumar, V. (2019). Synthesis, anti-mycobacterial and cytotoxic evaluation of substituted isoindoline-1, 3-dione-4-aminoquinolines coupled: Via alkyl/amide linkers. *RSC Adv.* 9 (15), 8515–8528. doi:10.1039/c8ra10532d

Rao, R. N., and Chanda, K. (2022). 2-Aminopyridine – An unsung hero in drug discovery. *Chem. Commun.* 58 (3), 343–382. doi:10.1039/D1CC04602K

Reis, W. J., Bozzi, Í. A. O., Ribeiro, M. F., Halicki, P. C. B., Ferreira, L. A., Almeida da Silva, P. E., et al. (2019). Design of hybrid molecules as antimycobacterial compounds: Synthesis of isoniazid-naphthoquinone derivatives and their activity against susceptible and resistant strains of Mycobacterium tuberculosis. *Bioorg. Med. Chem.* 27 (18), 4143–4150. doi:10.1016/j.bmc.2019.07.045

Ryan, N. J., and Lo, J. H. (2014). Delamanid: First global approval. *Drugs* 74, 1041–1045. doi:10.1007/s40265-014-0241-5

Ryckman, T., Robsky, K., Cilloni, L., Zawedde-Muyanja, S., Ananthakrishnan, R., Kendall, E. A., et al. (2022). Ending tuberculosis in a post-COVID-19 world: A person-centred, equity-oriented approach. *Lancet Infect. Dis.* doi:10.1016/S1473-3099(22)00500-X

Satasia, S. P., Kalaria, P. N., and Raval, D. K. (2013). Acidic ionic liquid immobilized on cellulose: An efficient and recyclable heterogeneous catalyst for the solvent-free synthesis of hydroxylated trisubstituted pyridines. *RSC Adv.* 3 (10), 3184–3188. doi:10.1039/c3ra23052j

Satasia, S. P., Kalaria, P. N., and Raval, D. K. (2014). Catalytic regioselective synthesis of pyrazole based pyrido[2, 3-d] pyrimidine-diones and their biological evaluation. *Org. Biomol. Chem.* 12 (11), 1751–1758. doi:10.1039/c3ob42132e

Saxena, P., Yadav, G., Mohanty, D., and Gokhale, R. S. (2003). A new family of type III polyketide synthases in Mycobacterium tuberculosis. *J. Biol. Chem.* 278 (45), 44780–44790. doi:10.1074/jbc.M306714200

Selderslaghs, I. W. T., Van Rompay, A. R., De Coen, W., and Witters, H. E. (2009). Development of a screening assay to identify teratogenic and embryotoxic chemicals using the zebrafish embryo. *Reprod. Toxicol.* 28 (3), 308–320. doi:10.1016/j.reprotox.2009.05.004

Shiradkar, M. R., Murahari, K. K., Gangadasu, H. R., Suresh, T., Kalyan, C. A., Panchal, D., et al. (2007). Synthesis of new S-derivatives of clubbed triazolyl thiazole as anti-Mycobacterium tuberculosis agents. *Bioorg. Med. Chem.* 15 (12), 3997–4008. doi:10.1016/j.bmc.2007.04.003

Shiradkar, M., Suresh Kumar, G. V., Dasari, V., Tatikonda, S., Akula, K. C., and Shah, R. (2007). Clubbed triazoles: A novel approach to antitubercular drugs. *Eur. J. Med. Chem.* 42 (6), 807–816. doi:10.1016/j.ejmech.2006.12.001

Shrestha, R., Shen, Y., Pollack, K. A., Taylor, J. S. A., and Wooley, K. L. (2012). Dual peptide nucleic acid- and peptide-functionalized shell cross-linked nanoparticles designed to target MRNA toward the diagnosis and treatment of acute lung injury. *Bioconjug. Chem.* 23 (3), 574–585. doi:10.1021/bc200629f

Singh, G., PriyankaSushmaPawanDikshaSuman, et al. (2022). Tetrazole conjoined organosilane and organosilatrane: Via the "click approach": A potent Mycobacterium tuberculosis enoyl ACP reductase inhibitor and a dual sensor for Fe(iii) and Cu(ii) ions. *New J. Chem.* 46 (5), 2094–2104. doi:10.1039/d1nj05126a

Smith, J., Wescott, H., Early, J., Mullen, S., Guzman, J., Odingo, J., et al. (2019). Anthranilic amide and imidazobenzothiadiazole compounds disrupt: Mycobacterium tuberculosis membrane potential. *MedChemComm* 10 (6), 934–945. doi:10.1039/c9md00088g

Somu, R. V., Boshoff, H., Qiao, C., Bennett, E. M., Barry, C. E., and Aldrich, C. C. (2006). Rationally-designed nucleoside antibiotics that inhibit siderophore biosynthesis of Mycobacterium tuberculosis. *J. Med. Chem.* 49 (1), 31–34. doi:10.1021/jm051060o

Tang, S., Hicks, N. D., Cheng, Y. S., Silva, A., Fortune, S. M., and Sacchettini, J. C. (2019). Structural and functional insight into the *Mycobacterium tuberculosis* protein PrpR reveals a novel type of transcription factor. *Nucleic Acids Res.* 47, 9934–9949. doi:10.1093/nar/gkz724

Tantry, S. J., Shinde, V., Balakrishnan, G., Markad, S. D., Gupta, A. K., Bhat, J., et al. (2016). Scaffold morphing leading to evolution of 2, 4-diaminoquinolines and aminopyrazolopyrimidines as inhibitors of the ATP synthesis pathway. *MedChemComm* 7 (5), 1022–1032. doi:10.1039/c5md00589b

Tong, A. S. T., Choi, P. J., Blaser, A., Sutherland, H. S., Tsang, S. K. Y., Guillemont, J., et al. (2017). 6-Cyano analogues of bedaquiline as less lipophilic and potentially safer diarylquinolines for tuberculosis. *ACS Med. Chem. Lett.* 8 (10), 1019–1024. doi:10.1021/acsmedchemlett.7b00196

Torres Ortiz, A., Coronel, J., Vidal, J. R., Bonilla, C., Moore, D. A. J., Gilman, R. H., et al. (2021). Genomic signatures of pre-resistance in Mycobacterium tuberculosis. *Nat. Commun.* 12 (1), 7312. doi:10.1038/s41467-021-27616-7

Tover, C. K., Warrener, P., VanDevanter, D. R., Sherman, D. R., Arain, T. M., Langhorne, M. H., et al. (2000). A small-molecule nitroimidazopyran drug candidate for the treatment of tuberculosis. *Nature* 405 (6789), 962–966. doi:10.1038/35016103

Usmani, S. S., Bhalla, S., and Raghava, G. P. S. (2018). Prediction of antitubercular peptides from sequence information using ensemble classifier and hybrid features. *Front. Pharmacol.* 9, 954. doi:10.3389/fphar.2018.00954

White, A. C., Jr (2004). Nitazoxanide: A new broad spectrum antiparasitic agent. *Expert Rev. anti. Infect. Ther.* 2 (1), 43–49. doi:10.1586/14787210.2.1.43

World Health Organization (2020). *Global tuberculosis report*. Geneva: World Health Organization.

World Health Organization (2021). *Global tuberculosis report 2021*. Available online: https://www.who.int/ ((accessed October 2021).

World Health Organization (2021). *Global tuberculosis report*. Geneva: World Health Organization. Available at: https://www.who.int/publications/i/item/9789240037021.

Yamey, G., Schäferhoff, M., Aars, O. K., Bloom, B., Carroll, D., Chawla, M., et al. (2017). Financing of international collective action for epidemic and pandemic preparedness. *Lancet. Glob. Health* 5 (8), e742–e744. doi:10.1016/S2214-109X(17)30203-6

Yan, M., and Ma, S. (2012). Recent advances in the research of heterocyclic compounds as antitubercular agents. *ChemMedChem* 7 (12), 2063–2075. doi:10.1002/cmdc.201200339

Zhao, H., Lu, Y., Sheng, L., Yuan, Z., Wang, B., Wang, W., et al. (2017). Discovery of fluorine-containing benzoxazinyl-oxazolidinones for the treatment of multidrug resistant tuberculosis. *ACS Med. Chem. Lett.* 8 (5), 533–537. doi:10.1021/acsmedchemlett.7b00068

Zhao, H., Wang, B., Fu, L., Li, G., Lu, H., Liu, Y., et al. (2020). Discovery of a conformationally constrained oxazolidinone with improved safety and efficacy profiles for the treatment of multidrug-resistant tuberculosis. *J. Med. Chem.* 63 (17), 9316–9339. doi:10.1021/acs.jmedchem.0c00500

Zhao, G., Tian, X., Wang, J., Cheng, M., Zhang, T., and Wang, Z. (2021). The structure-based virtual screening of nonbenzofuran inhibitors against M. Tuberculosis pks13-TE for anti-tuberculosis phenotypic discovery. *New J. Chem.* 45 (3), 1286–1300. doi:10.1039/d0nj03828h

Zumla, A., Nahid, P., and Cole, S. T. (2013). Advances in the development of new tuberculosis drugs and treatment regimens. *Nat. Rev. Drug Discov.* 12 (5), 388–404. doi:10.1038/nrd4001

frontiers | Frontiers in Pharmacology

TYPE Review
PUBLISHED 09 December 2022
DOI 10.3389/fphar.2022.1063453

OPEN ACCESS

EDITED BY
Hong Zhou,
Zunyi Medical University, China

REVIEWED BY
Yu Lu,
Capital Medical University, China
Jitendra Narain Singh,
National Institute of Pharmaceutical Education and Research, Mohali, India

*CORRESPONDENCE
Jan-Willem C. Alffenaar,
johannes.alffenaar@sydney.edu.au

†These authors have contributed equally to this work

SPECIALTY SECTION
This article was submitted to Pharmacology of Infectious Diseases, a section of the journal Frontiers in Pharmacology

RECEIVED 07 October 2022
ACCEPTED 22 November 2022
PUBLISHED 09 December 2022

CITATION
Alffenaar J-WC, de Steenwinkel JEM, Diacon AH, Simonsson USH, Srivastava S and Wicha SG (2022), Pharmacokinetics and pharmacodynamics of anti-tuberculosis drugs: An evaluation of *in vitro*, *in vivo* methodologies and human studies.
Front. Pharmacol. 13:1063453.
doi: 10.3389/fphar.2022.1063453

Pharmacokinetics and pharmacodynamics of anti-tuberculosis drugs: An evaluation of *in vitro*, *in vivo* methodologies and human studies

Jan-Willem C. Alffenaar[1,2,3]*, Jurriaan E. M. de Steenwinkel[4†], Andreas H. Diacon[5†], Ulrika S. H. Simonsson[6†], Shashikant Srivastava[7†] and Sebastian G. Wicha[8†]

[1]Sydney Institute for Infectious Diseases, The University of Sydney, Sydney, NSW, Australia, [2]School of Pharmacy, The University of Sydney Faculty of Medicine and Health, Sydney, NSW, Australia, [3]Westmead Hospital, Sydney, NSW, Australia, [4]Department of Medical Microbiology and Infectious Diseases, Erasmus MC, Rotterdam, Netherlands, [5]TASK, Cape Town, South Africa, [6]Department of Pharmaceutical Biosciences, Uppsala University, Uppsala, Sweden, [7]Department of Pulmonary Immunology, University of Texas Health Science Center at Tyler, Tyler, TX, United States, [8]Department of Clinical Pharmacy, Institute of Pharmacy, University of Hamburg, Hamburg, Germany

There has been an increased interest in pharmacokinetics and pharmacodynamics (PKPD) of anti-tuberculosis drugs. A better understanding of the relationship between drug exposure, antimicrobial kill and acquired drug resistance is essential not only to optimize current treatment regimens but also to design appropriately dosed regimens with new anti-tuberculosis drugs. Although the interest in PKPD has resulted in an increased number of studies, the actual bench-to-bedside translation is somewhat limited. One of the reasons could be differences in methodologies and outcome assessments that makes it difficult to compare the studies. In this paper we summarize most relevant *in vitro*, *in vivo*, *in silico* and human PKPD studies performed to optimize the drug dose and regimens for treatment of tuberculosis. The *in vitro* assessment focuses on MIC determination, static time-kill kinetics, and dynamic hollow fibre infection models to investigate acquisition of resistance and killing of Mycobacterium tuberculosis populations in various metabolic states. The *in vivo* assessment focuses on the various animal models, routes of infection, PK at the site of infection, PD read-outs, biomarkers and differences in treatment outcome evaluation (relapse and death). For human PKPD we focus on early bactericidal activity studies and inclusion of PK and therapeutic drug monitoring in clinical trials. Modelling and simulation approaches that are used to evaluate and link the different data types will be discussed. We also describe the concept of different studies, study design, importance of uniform reporting including microbiological and clinical outcome assessments, and modelling approaches. We aim to encourage researchers to consider methods of assessing and reporting PKPD of anti-tuberculosis drugs when designing

studies. This will improve appropriate comparison between studies and accelerate the progress in the field.

KEYWORDS

tuberculosis, pharmacokinetics, pharmacodynamics, modeling and simulation, dose optimization, anti-TB drugs

1 Introduction

After diagnosis, providing each tuberculosis (TB) patient with the right drugs at the right dose for the right duration in the right combination is important to effectively reduce transmission, prevent relapse and control the risk of development of drug resistance (Alffenaar et al., 2022). Following other fields in infectious diseases there has been an increased interest in pharmacokinetics and pharmacodynamics (PKPD) of anti-tuberculosis drugs. A better understanding of the relationship between drug exposure and antimicrobial kill and acquired drug resistance is essential not only to optimize current standard of care regimen but also to design more appropriate dosing regimens for new and repurposed drugs with anti-tuberculosis activity (Peloquin and Davies, 2021). PKPD studies can help to determine which drug exposure indices is best associated with antimicrobial kill as well as suppression of resistance development during the course of therapy. As for any antimicrobial drugs the drug exposure indices associated with the response of *Mycobacterium tuberculosis* to the drug are the area under the unbound drug concentration-time curve over the minimal inhibitory concentration (*f*AUC/MIC), the maximum concentration over the MIC (C_{max}/MIC) and the time the unbound drug concentration exceeds the MIC (%*f*T > MIC). There is a broad range in PKPD studies which are ideally complementary in providing relevant data to optimize the drug dose and regimens for treatment of TB.

In vitro studies are focused on MIC determination, static time-kill kinetics and/or dynamic models that allow to mimic a pharmacokinetic profile *in vitro* such as the hollow fibre infection model (Gumbo and Alffenaar, 2018). These models can include various metabolic populations and strains of *Mycobacterium tuberculosis* (Goossens et al., 2021). Besides assisting in drug development they are able to mimic specific real-life conditions to explore effects on treatment response and acquired drug resistance (Srivastava et al., 2011a). *In vivo* studies able to reflect the pathophysiological conditions of the TB infections study the effect of different drug dosages—exposure on treatment outcome including relapse and drug resistance. Human PKPD is characterized in phase 2a early bactericidal activity (EBA) studies and should be part of Phase 2b-3 studies to further refine the understanding of the exposure-response relationship (Martson et al., 2021). In addition to clinical trials, studies under operational research conditions are relevant to capture drug dosing, exposure, and treatment response under programmatic care (Alffenaar et al., 2020). Modelling and simulation approaches are very helpful to 1) evaluate the population PK of a TB drug in a population of interest, 2) characterize the exposure-response relationship of TB drugs, 3) elucidate exposure-safety profiles, and 4) can link the data from pre-clinical and clinical studies to better understand the drug exposure effect relationship (Märtson et al., 2020).

Although the interest in PKPD has resulted in an increased number of PKPD studies, the actual bench-to-bedside translation is somewhat limited. Firstly, current regimens have by necessity been developed using "trial and error" approaches. This resulted in practically relevant treatment regimens that have stood the test of time but did not create data that would assist in validating today's new preclinical methods that must await further large trials in humans that will determine the value of the predictions made. Secondly, differences in methodologies and outcome assessments make it difficult to compare the studies and link preclinical finding to patient outcomes, which are further complicated by organizational gaps that preclude consequent utilization of pre-clinical data to optimally inform clinical trials. For instance, preclinical combination experiments are carried out with different combination partner drugs than those that are used in clinical trials. Thirdly, costs of phase 3 clinical trials as well as uptake of trials results in guidelines and subsequent implementation in practice challenge the stakeholders' capacity.

To improve the synthesis of PKPD information from preclinical and clinical PKPD studies this review aims to describe the concept of different studies, optimized study design considering drug properties and study aims, importance of uniform reporting including microbiological and clinical outcome assessment, and possible modelling parameters. The information on uniformed methods of assessing and reporting PK/PD parameters of anti-tuberculosis drugs should accelerate the translation to clinical practice.

2 Materials and methods

A non-systematic review of English literature was performed in PubMed and Web of Science. Keywords included *in vivo, in vitro*, early bactericidal activity, pharmacokinetics, pharmacodynamics, tuberculosis, murine model, pharmacometrics, limited sampling. Information retrieved was summarized to describe the concept of different studies and recommendations were provided on optimized study design considering drug properties and study aims, importance of uniform reporting including microbiological and clinical outcome assessment, and possible modelling parameters.

3 *In vitro* pharmacokinetics/pharmacodynamics

Understanding the antimicrobial activity spectrum of the drug is the first key step in preclinical PKPD. Using wide concentration range MIC experiments are performed for which broth micro-dilution is most commonly used and recommended method (Wayne, 2018). By using a broad variety of clinical strains, gathered from around the world, a view on the MIC distribution is obtained. The next step involves the determination of the efficacy and potency of the extent of the drug by performing time-kill kinetic studies, either at static concentrations in the test-tubes or fluctuating concentrations using dynamic models. (de Steenwinkel et al., 2010) In the static time-kill (STK) studies the drug concentration remains fixed over time and the bacterial response are measured in terms change on the optical density (OD_{A600}) and/or colony forming units (CFU). The STK studies are commonly performed using the actively replicating logarithmic phase bacteria in cultures and based on the extent of kill drugs are commonly classified as bactericidal or bacteriostatic (Wald-Dickler et al., 2018).

However, in a lung lesion, *M. tuberculosis* can be present under different metabolic states (Mitchison, 1979), such as actively replicating extracellular bacteria, intracellular bacteria inside the macrophage, slowly replicating bacteria under acidic condition in the caseum, or non-replicating persisters for which the exact location is hard to determine. Since in the STK studies the drug concentrations do not change over time as it is expected *in vivo*, dynamic models had to be developed to allow for drug concentrations to be actively changed over time. One such dynamic model is the hollow fibre model system of tuberculosis (HFS-TB) (Gumbo et al., 2004; Gumbo et al., 2005; Gumbo et al., 2007a; Gumbo et al., 2007b; Srivastava and Gumbo, 2012). The HFS-TB consist of a cartridge housing multiple hollow fiber capillary tubes with pore size such that bacteria cannot cross the membranes. This creates two compartments in the cartridge; an intra-capillary compartment through which drug and nutrients in the media flows across the membrane, and an extra-capillary compartment where the bacteria come into contact with drug containing media. The drug is infused into the central compartment of the HFS-TB *via* programable syringe pump, and the time-to-maximum concentration (T_{max}) can be varied to mimic human-like PK as well as the dosing frequency. Further, the fresh media is continuously infused into the systems using peristaltic pumps and at the same time the media coming out of the cartridge is pumped out using a second set of peristaltic pumps. The dilution rate, using the peristaltic pumps, determines the half-life of the drug in the HFS-TB. Multiple half-lives of the drugs in a combination regimen can be achieved in the HFS-TB, by adjusting the parameters on the programable syringe pumps (Srivastava et al., 2011b; Deshpande et al., 2016). Another dynamic model was developed making use of a central compartment containing a liquid bacteria culture. In the model developed by Vaddady et al. (2010), new medium and/or drug in increasing concentration is added to the central compartment while removing the medium with the drugs is performed *via* a filter leaving the bacteria in place. In both models a sampling port is available to monitor bacterial count and drug concentration over 24 h to validate the concentration-time profile of the drugs in the central compartment, inside the cells (in case of studying intracellular metabolic population), as well as intrabacterial drug concentrations (Vaddady et al., 2010; Deshpande et al., 2019b). Thus, the dynamic models offer an advantage over the STK experiments in terms of precise control of drug concentration-time profiles to which *M. tuberculosis* is exposed as well as longer study duration, this permits to study development of drug resistance during the therapy. However, the dynamic models are limited by relatively low through-put and often unavailable human PK data to set the model parameters correctly.

Given that physical barriers to drug penetration to the anatomical sites (Dheda et al., 2018) and physiological conditions (e.g., pH; attributed to activity of pyrazinamide (McDERMOTT and TOMPSETT, 1954) and recently contradicted (Gumbo et al., 2009; Srivastava et al., 2016b; Lanoix et al., 2016) can affect the efficacy of the drug, the HFS-TB can also be used the PKPD relationship against different *M. tuberculosis* metabolic populations (Gumbo et al., 2009; Srivastava et al., 2011b; Srivastava et al., 2016b; Srivastava et al., 2021b; Ruth et al., 2022). Moreover, it is the non-protein bound (free) drug concentration that exerts the antimicrobial effect. Although highly protein bound drugs may have low unbound concentrations in plasma, accumulation of these drugs at the site of infection as well as intracellularly results in concentrations which are high enough to kill *M. tuberculosis*. (Srivastava et al., 2020) The HFS-TB offers a controlled environment where the hollow fiber membrane material can be changed as per the drugs physicochemical properties and the protein content in the media can be adjusted to minimize the drug binding. Thus, the concentration used in each HFS-TB experiments represent the free drug concentrations. This means that after appropriate adjustments even highly protein bound drugs like bedaquiline can be successfully studied in the HFS-TB.

Finally, to determine the optimal clinical dose to achieve the HFS-TB PK/PD parameter optimized drug exposure and determine the susceptibility breakpoint, *in silico* Monte-Carlo clinical trial simulations are used (D'Argenio and Schumitzky, 1997; D'Argenio et al., 2009). A systemic analysis of the published HFS-TB studies concluded that this dynamic model in combination with *in silico* simulations could predict the clinical outcomes of dose optimization and target attainment in combination regimens fairly accurately (Cavaleri and Manolis, 2015; Chilukuri et al., 2015) and these

TABLE 1 HFS-TB derived drug exposure target and susceptibility breakpoint MIC of drugs with antimycobacterial activity.

Drug	PK/PD target	Susceptibility breakpoint (mg/L)	References
Amikacin	C_{max}/MIC >10.13		Srivastava et al. (2016a)
Cefazolin	%T > MIC = 46.76	1–2	Srivastava et al. (2021c)
Cefdinir	$AUC_{0\text{-}24}$/MIC = 578.86		Srivastava et al. (2021d)
Ceftriaxone	%T > MIC = 68		Srivastava et al. (2020)
Cycloserine	%T > MIC = 30		Deshpande et al. (2018a)
Delamanid	$AUC_{0\text{-}24}$/MIC = 195		Mallikaarjun et al. (2021)
Ertapenem	%T > MIC >40	2	van Rijn et al. (2017)
Ethambutol	C_{max}/MIC >0.51	4	Srivastava et al. (2010)
Ethionamide	$AUC_{0\text{-}24}$/MIC >56.2	2.5	Deshpande et al. (2018c)
Faropenem	%T > MIC >62		Deshpande et al. (2016)
Gatifloxacin	$AUC_{0\text{-}24}$/MIC >184	0.5	Deshpande et al. (2018d)
Isoniazid	$AUC_{0\text{-}24}$/MIC >567	0.0312	Gumbo et al. (2007c)
Levofloxacin	$AUC_{0\text{-}24}$/MIC >146	0.5	Deshpande et al. (2018b)
Linezolid	$AUC_{0\text{-}24}$/MIC >119	2	Srivastava et al. (2017)
Minocycline	$AUC_{0\text{-}24}$/MIC = 71.58	8	Deshpande et al. (2019b)
Moxifloxacin	$AUC_{0\text{-}24}$/MIC >56	1	Gumbo et al. (2004)
Penicillin	%T > MIC >65		Deshpande et al. (2018e)
Pyrazinamide	$AUC_{0\text{-}24}$/MIC >209	50	Gumbo et al. (2009)
Rifampin	$AUC_{0\text{-}24}$/MIC >1,360	0.0625	(Gumbo et al., 2007a; Gumbo, 2010)
Tedizolid	$AUC_{0\text{-}24}$/MIC >200	0.5	Srivastava et al. (2018)
Thioridazine	$AUC_{0\text{-}24}$/MIC = 50.53		Musuka et al. (2013)
Tigecycline	$AUC_{0\text{-}24}$/MIC >42.3		Deshpande et al. (2019a)
Vancomycin	$AUC_{0\text{-}24}$/MIC = 2,954		Srivastava et al. (2021a)

Drugs are arranged in alphabetical order. MIC, minimum inhibitory concentration; Cmax, peak concentration; AUC, area under the concentration-time curve; %T > MIC, percentage of time drug concentration persist above MIC.

findings were also included in the recently published WHO technical report (World Health Organization, 2018) as well as clinical standard for tuberculosis (Alffenaar et al., 2022). In summary (Table 1), dynamic pre-clinical models are useful in the tuberculosis drug development space with the ability to inform future clinical trial design by providing PKPD based proof-of-concept for developing drugs as a single agent or in combination where each drug dose is selected to achieve the pharmacodynamic target (C_{max}/MIC, AUC/MIC, %T > MIC) of the drugs in the regimen. In addition, data from static and dynamic hollow-fibre infection models can be used to develop model-based PKPD relationships linked to human population PK models to support dose selection for first-in-man studies and/or selection of optimized drug combinations. (Wicha et al., 2018)

4 *In vivo* pharmacokinetics/pharmacodynamics

In vivo studies can be performed in sequentially or simultaneously with *in vitro* studies. A reasonable strategy that considers animal welfare, minimizes complexity and saves cost is to move only compounds with good *in vitro* activity further to *in vivo* studies (Nuermberger, 2017). Relapse studies in mice, requiring sacrificing the animals are often performed later while *in vivo* PKPD with biomarkers can be run in parallel with *in vitro* studies (Margaryan et al., 2022). The complexity and costs of *in vivo* studies are the main reason to continue only with the compounds that show good activity in the *in vitro* analysis. The *in vivo* models range from the high-throughput, low-cost zebrafish, *via* the medium-throughput, medium cost mice, to the very low-throughput and expensive non-humane primates (Williams and Orme, 2016). Within this proposal for standardization of methodology, we have chosen only to address the murine models of the TB and the possible role they can play within the PK/PD evaluation. This is done, because the more rudimental *in vivo* models such as the (embryo) zebrafish can provide different steady state exposure results, but the limited duration of the experiments and the completely different PK, makes these models complementary to the mouse TB models (Ali et al., 2011) but not the ideal model for PKPD analysis, which is the focus of this overview.

First of all, it should be clear that mice and man are very different and that PKPD findings in mice should consider the transitional value in the preclinical drug-development. Within murine models of TB, we can study the PKPD relationship and assess the dose- or time dependent nature of the PKPD relationship trough dose fractionation studies. Essential in these studies is that besides dose, the actual drug concentration, preferably at the site of infection, is considered. Measuring the concentration of the (parent drug) compound and the (active) metabolites, *via* a chromatography based bioanalytical methods, the contribution of PKPD parameters can be made.

Preclinical murine TB models come in many different forms. The route of infection (e.g., intravenous, inhalation, or instillation) (de Steenwinkel et al., 2011), the inoculum size (de Steenwinkel et al., 2011), the mycobacterial strain used (Mourik et al., 2017), the pathology of TB in the specific model (Nuermberger, 2017), the treatment-free period before starting therapy and the mouse strain used, are all features that can be changed and tweaked to provide different models. There is no such thing as 'the best murine TB model', all models come with their own advantages and disadvantages. Thus, it seems reasonable to combine a set of preclinical models to inform the design of clinical trials. Broadly speaking there are acute, chronic and latent murine TB models to assess the effect of a treatment regimen. Acute models are informative on EBA and PKPD relationship, whereas the more chronic models assess the efficacy of therapy (prevention of relapse). Models for latent TB fall outside the scope of this paper (Zhang et al., 2011).

Regarding the PD (effect side) of the PKPD relationship, there are different outcome parameters that can be used. Traditionally, the number of colony forming units (CFU) are counted to the determine the mycobacterial load at specific that time-points and used as a biomarker to assess the PD in different organs. PD can also be assessed by time-to-positivity (TTP) measurement, using liquid cultures and automated hourly detection of growth or molecular load determination targeting rRNA, as read-out (de Knegt et al., 2017). Irrespectively of the method used to determine the PD or the type of animal model used, determination of the PK is essential to assess the PK/PD and thus the ability link the different phases of drug-development.

In order to conduct an adequate PKPD analysis using the *in vivo* experimental data, there should be gained insight in the exposure of the parent compound and the different metabolites and subsequently the contribution to the effect of these metabolites should be assessed. Although activity of metabolites has been tested *in vitro* experiments, the *in vivo* studies add additional information as in these studies activity of metabolites is included by nature. Given the different mode of action of the different compounds, the different metabolic states within which the different Mycobacteria are and the different immunological reactions to this infection, the diversity and complexity of these *in vivo* models are one step closer to that of TB patients. Bundling of the information of the different *in vivo* models in a model-based analysis is essential to strengthen the translational value of the different *in vivo* models (Margaryan et al., 2022; Mudde et al., 2022). In addition, the different animal models contribute with different information with respect to bactericidal and sterilizing drug efficacy.

Ideally, the outcomes of PKPD *in vivo* TB studies are informative in the way that human efficacy can be predicted for different drugs and regimens using model-based approaches for PKPD where information from human PK studies is linked to pre-clinical information about PKPD relationships and drug combinations (Wicha et al., 2018; Susanto et al., 2020; Mudde et al., 2022). This phase of the pipeline forms an essential biological bottleneck to increase the success rate of compounds or regimens to be entering the clinical development.

5 In human pharmacokinetics/pharmacodynamics: Early bactericidal activity

Early bactericidal activity (EBA) studies have been conducted since the landmark publication of Jindani et al. (1980), who tested a multitude of then available single agents and combinations over the first 14 days of treatment in small numbers of patients (Jindani et al., 1980). This study established EBA, defined as the fall in colony forming units (CFU) per ml of sputum over time, as a new method to quantify early drug effects. It also provided new insights into the clinical use of agents. Isoniazid (INH), for instance, was clearly the strongest drug in the first 2 days of treatment. Any treatment containing INH reduced the bacterial burden by 95% in 2 days, thereby lowering the risk of transmission (Mitchison, 2000). Its strong 2-day EBA is believed to make INH a good protector of companion drugs from acquisition of resistance because it can quickly eradicate any fast-growing mutants escaping control by other agents in a regimen (Mitchison, 2000).

It is generally accepted that patients with active pulmonary TB harbor a spectrum of bacterial phenotypes ranging from metabolically very active, fast growing, extracellular bacteria expectorated in sputum to more dormant, intracellular bacteria situated within granulomatous lesions. This requires different antibiotics with complementary characteristics to be part of a successful treatment regimen that can kill all these phenotypes (Dartois and Rubin, 2022). In the absence of the preclinical tools that we have available today, it was speculated at the time that strong 2-day activity would predestine a drug for killing mainly active, extracellular bacteria in the early stages of treatment, while other agents with more notable late EBA, such as rifampicin and pyrazinamide, would be sterilizing and contribute to curing patients (Mitchison, 2000).

The role of 14-day EBA studies in the clinical evaluation of novel antibiotics today is to determine whether a drug is active in humans, and to establish relationships between dose, drug exposure and bactericidal activity in small groups of patients (Diacon and Donald, 2014). EBA studies also give an early indication of safety and tolerability of new drugs and allow an indication of the combined effect of drugs given together. Fourteen days of monotherapy has been shown not to cause clinically relevant resistance (Kayigire et al., 2017). Extended EBA studies with strong combinations are limited by the reduced availability of viable bacteria for drug effect quantification. Even though all agents of our current first-line standard treatment regimens have significant 14-day activity it is not clear if and how EBA studies can predict the efficacy of combination regimens, at least not with the current standard biomarkers CFU and TTP.

Quantification of viable bacteria by CFU counting is hazardous, laborious, costly and relatively slow. Besides the recent introduction of TTP in liquid media, which is easier to standardize and more sensitive than CFU (Diacon et al., 2012b), a range of novel, not culture-based biomarkers are currently under investigation to better understand early drug effects (Heyckendorf et al., 2022). Analysis of EBA trials has historically been very diverse and not standardized, which has made it difficult to compare study results. Today, linking dosage, PK and PD data from multiple biomarkers creates an abundance of data and requires innovative analysis techniques.

Accordingly, a novel, model-based analysis methodology for EBA trials has recently been developed. Traditionally EBA was assessed as the observed difference in $\log_{10}$ CFU per ml of sputum between two study days (Jindani et al., 1980). Most commonly reported are 0-2-, 2-14- and 0–14-day intervals (Chan et al., 1992; Jindani et al., 1980; Sirgel et al., 1993). With liquid cultures, EBA is expressed as an increase in TTP over the same intervals (Diacon et al., 2012a). TTP is nowadays the preferred primary variable for EBA, with CFU as the secondary variable. Although CFU and TTP are highly correlated (Diacon et al., 2012b), EBA assessed with TTP can be followed for longer than with CFU. This is due to CFU only quantifying multiplying bacteria whereas TTP is thought to, in addition, capture the metabolism of non-growing bacteria and having a lower limit of detection.

Human studies are costly and thus missing information on an individual level through contamination or drop-out of patients can critically reduce the available information for calculating EBA from groups as small as 12–15 patients. Non-linear mixed effects modeling, in contrast, uses data pooled from all subjects, enabling all observations to contribute to the mathematical model. Missing information can be optimally handled. An innovative, standardized and model-based analysis methodology for analyzing EBA trials, accounting for known co-variates, has recently been developed and was used in the analysis of the EBA trial by De Jager (de Jager et al., 2022). From the model, predicted EBA intervals can be predicted, both on an individual level and population level but this is seen as a *post hoc* step in the approach. Instead, treatment differences for an EBA design with different regimens are evaluated on the model parameter TTP slope which is the parameter that describes the decline in TTP over time. The TTP slope can take on any function where a mono-exponential decline is the simplest. In order to assess the difference between two regimens, the model with no difference in TTP slope is compared for statistical difference to a model where there is a difference in slope between two regimen arms. This can be done for two arms or several arms. In addition to a point estimate in TTP, an imprecision in the EBA difference is obtained. The TTP model approach is therefore also suitable for assessment of efficacy in longer studies, for example seamless and adaptive Phase 2B/C studies where an early and informed decision is needed for potentially dropping arms in a study.

The standardized EBA modeling approach is also suitable for a PKPD approach where a PK summary variable such as AUC or C_{max} is used as a covariate. If there is high between-patient variability in PK, patients might be exposed to the same drug concentration even if they were given different doses or they may be exposed to different drug concentrations while receiving the same dose. Neglecting to collect PK data for such a drug in an EBA study may result in no difference in EBA if only the dose instead of drug exposure is used to evaluate differences in EBA. (Diacon et al., 2011).

Optimization of dosage for a single drug has been done for rifampicin where different monotherapy doses were studied over a 14-day period in order to determine the PK and assess EBA (Boeree et al., 2017; Svensson et al., 2018a; Svensson et al., 2018b). The dose optimization was mainly driven by the lack of PKPD evaluation of rifampicin during the clinical drug development. (van Ingen et al., 2011) However, EBA studies with regimens in addition to monotherapy arms, rather than only monotherapies are warranted in order to speed up clinical trial development as they are able to demonstrate synergistic effect between drugs which would otherwise go unnoticed (Diacon et al., 2012a). As such, the dose optimization and clinical trial prediction using preclinical information should rely on model-informed drug discovery and development (MID3) methods (Marshall et al., 2016).

6 Clinical pharmacokinetics/ pharmacodynamics and therapeutic drug monitoring

In addition to the EBA studies there are several studies where PK/PD is used to answer specific questions related to drug exposure and treatment response. Clinical observations often provide the rationale for these studies and relate to treatment problems like slow response, relapse and acquired resistance. As in the clinical setting the source of these problems can be multifactorial, thus the design of a study needs to accommodate for all the potential sources that may contribute to the problem. When evaluating response to treatment low drug concentrations, drug resistance, non-adherence, and poor clinical condition and co-morbidities of the patient at the start of treatment all can explain the slow response (Alffenaar et al., 2022). Confounding factors can either be listed as exclusion criteria or can

be appropriately quantified and documented to be included in the analysis of the study. Studies can be of observational nature explaining a specific outcome based on PK/PD or can be interventional of nature. In the latter one, dose optimization measures like dose escalation are studied and linked to the treatment outcome. In preparing both types of studies it is important to make use of available PK/PD data in conjunction with relevant clinical and microbiological information to guide a sample size calculation (Martson et al., 2020).

When and how PK should be assessed is guided by the hypothesis of the study or clinical question in routine care. For example, early assessment of PK is important when time to sputum culture conversion is assessed but also when studying acquired resistance. When the bacterial load is high, and bacteria are actively replicating there is a higher chance of development of resistance. In routine care, therapeutic drug monitoring (TDM) is used to assess the drug exposure and adjust the dose in individual patients.

TDM is a strategy that allows for dose individualization based on the measurement of drug concentrations in order to improve the efficacy of the treatment. The procedure includes identification of a patient that potentially benefits from TDM, collection of the appropriate timed samples to estimate the drug exposure, sample analysis, reporting and interpretation of the result, subsequent action which can be dose increase, decrease or decision to maintain the dose the same. Appropriate follow-up TDM needs to be scheduled to evaluate if the dose change has resulted in achieving the predefined target concentration. As the intention of TDM is to intervene where needed, the TDM cycle needs to be completed in a time manner. In TDM, the PK/PD index is compared to an established target where the dose can be increased if the PK/PD index is lower than the target or increased if the PK/PD index is higher than the target. (Alffenaar et al., 2022) From a traditional TDM point of view a sample collected 2 h and 6 h after drug intake are the relevant measures of drug exposure. (Alsultan and Peloquin, 2014) Using a sample collected 2rh after drug intake as surrogate for C_{max} is not sufficient as several studies have demonstrated that the time the C_{max} is achieved has a range of several hours (Sturkenboom et al., 2016). For example, the observed median T_{max} for rifampicin was 2.2 h, ranging from 0.4 h to 5.7 h, underpinning that multiple samples are required to capture the C_{max} (Sturkenboom et al., 2015).

Model-informed precision dosing (MIPD) is an approach where information from a population pharmacokinetic (POPPK) or physiology-based pharmacokinetic (PBPK) model in combination with individually observed plasma drug concentrations is utilized to forecast the dose that leads to the most optimal exposure in an individual patient (Darwich et al., 2017; Wicha et al., 2021) Further, MIPD can incorporate not only PK but also efficacy and safety aspects in the individual dose prediction, i.e. predict the dose given not only a POPPK or PBPK model, but also given PKPD models. When MIPD is used to perform TDM the drug exposure measures like AUC, C_{max} and C_{min} are relevant to calculate AUC/MIC, C_{max}/MIC and %T > MIC. To be able to calculate these appropriate sampling schedules have to be designed. For the assessment of the AUC multiple samples are required. To adequately calculate an AUC using non-compartmental analysis 6-8 samples are required during the dosing interval (Gillespie, 1991; Gabrielsson and Weiner, 2012). Using a MIPD approach, flexible and different sampling schemes can be used and different exposure indicines (AUC, C_{max}, drug concentration). When using population PK models in combination with a limited sampling strategy, 1-3 samples result in adequate accuracy of the AUC calculation (Sturkenboom et al., 2021). It is especially useful for drugs that exhibits large variability in exposure between occasions where it correctly can handle the between-occasion variability in exposure (Svensson et al., 2019a; Keutzer and Simonsson, 2020a). The MIPD approach can also be incorporated into mobile health solutions (Keutzer and Simonsson, 2020b; Keutzer et al., 2020).

The opportunities in routine care to assess the PD are often limited as bacteriological read outs are collected less frequently as in EBA studies. PD include sputum smear and sputum culture. In high incidence setting sputum is performed at start of treatment, after 2 months and close to the end of treatment. If sputum culture is performed, it is often limited to start of treatment and occasionally during treatment when suboptimal treatment is suspected. This limits the opportunity to assess the effect of differences in drug exposure on treatment response. The most frequently used PD endpoints are sputum culture conversion after 2 months of treatment (drug susceptible TB), and 6 months of treatment (drug resistant TB). Time to sputum conversion is relevant as it presents the same data more continuously than the fixed time points. When using the TTP, the bacterial load can be accounted for as well. The end of treatment is used to quantify treatment outcome (cure, failure, relapse, death, lost to follow-up). Subsequently the PK/PD parameter, taking into account drug exposure and pathogen susceptibility, are then correlated with the outcome measures. The simplest analysis includes the analysis of differences in treatment response between the different quartiles of drug exposures. Due to the limited sample size a statistically significant difference between the first and fourth quartile is often considered a proof of principle. More sophisticated regression methods like classification and regression tree analysis (CART) allow for the determination of thresholds associated with better (or worse) treatment outcomes (Zheng et al., 2021, 2022). It is important to account for differences in patient characteristics as earlier work identified a hard-to-treat patient phenotype which showed substantial lower cure rate and which may require longer treatment time compared to the easy to treat patients (Imperial et al., 2018).

Implementing TDM or MIPD poses significant challenges for programmatic care as measurements of drug concentrations need to be made available in a timely manner (Alffenaar et al., 2020). Multi-analyte assays are likely to be the most cost-effective approach when LC-MS/MS is used (Veringa et al., 2016; Kuhlin et al., 2019). However, as LC-MS/MS is not readily available in most high burdened settings alternative assessments can be of value. Dried blood spots are typically more stable and easier to transport to a central laboratory (Vu et al., 2011), but don't solve the long turn-

around time. More recently point-of-care tests using saliva (Alffenaar et al., 2021; Kim et al., 2021) or urine (Szipszky et al., 2021) have been developed to measure the drug exposure. When using targets from HFS-TB it is important that protein binding as well as drug susceptibility testing procedures are taking into account as MIC results may differ based on medium used. (Alffenaar et al., 2022) Likewise, when using saliva or urine are used for TDM targets in these alternative matrices need to be established or they need to reflect the corresponding plasma/serum target using a correction factor. For example, if the concentration in saliva is 80% of the plasma concentration the target concentration is 80% of the plasma target concentration or the saliva concentration needs to be multiplied by 1.25 to reflect the corresponding plasma concentration.

7 Modeling and simulation

Modelling and simulations are frequently used in the preclinical and clinical development, evaluation and optimization of therapeutic regimens and dosing schedules (Marshall et al., 2016; Wilkins et al., 2022).

Firstly, modelling approaches are used to characterize the PK of a TB drug in a population of interest. Thereby, pharmacometric approaches are increasingly used compared to conventional methods (two-stage approach, non-compartmental analysis) as they come with several advantages: pharmacometric models can handle sparse and/or imbalanced data. Thereby even PK data generated in routine TB care can be leveraged (van der Laan et al., 2021; Tietjen et al., 2022). Moreover, pharmacometric models allow to separate PK variability into different sources (e.g., within-patient, between patient, between dosing occasion, *etc.*,). Separation of PK variability, and in particular knowledge about potentialinter-occasion variability is key when the models should be used to calculate personalized doses using model-informed precision dosing, e.g., as shown for rifampicin by Keutzer et al. (Keutzer and Simonsson, 2020a). Likewise, patient covariates can be tested if they explain (parts of) the observed variability in PK. Pharmacometric models including patient covariates can be exploited for simulations. For TB, such approaches have specifically facilitated the evaluation of TB dosing regimens in children, where the impact of body weight and organ maturation is included (Zvada et al., 2014). Also, pharmacometric models have an important role in the evaluation of drug interactions, e.g., with anti-retroviral drugs (van der Laan et al., 2021) in the co-treatment of HIV and TB.

Secondly, modelling approaches are used to characterize the exposure-response relationship of TB drugs (Wilkins et al., 2022). For this purpose, traditionally CFU or TTP are utilised, but biomarkers such as the molecular bacterial load (MBL) are also considered (Honeyborne et al., 2011). Modelling approaches have proven useful to define the links between different biomarkers, e.g. for MBL and TTP in liquid culture (Svensson et al., 2019b). Exposure-response analyses are challenging in TB since TB drugs are only used as monotherapy in dose-ranging EBA studies for a short duration up to 2 weeks (Te Brake et al., 2021). Phase 2b/c trials typically place novel TB drugs into a combination treatment, which makes exposure-response analyses challenging. Moreover, the relationship between relapse and the biomarkers that are detectable only in the early phase of treatment is not conclusively understood. Non-etheless, for example for bedaquiline, using an integrative pharmacometric model that characterized the population PK as well as comprised a time-to-event model to characterize the TTP, Svensson et al. successfully described bedaquilines' exposure-response relationship in data from a phase 2b trial (Svensson and Karlsson, 2017). Modelling of previously acquired clinical data could also help to streamline the design of future phase 2b studies. For example, Gewitz et al. (2021) analysed data from two phase 2b studies on rifapentine. The authors did not only describe the exposure-response of rifapentine in these data, but also performed a sensitivity analysis, which revealed that significant exposure-response and covariate relationships could be detected using truncated TTP data as early as 6 weeks from start of treatment, suggesting alternative phase 2b designs.

In case of safety concerns, pharmacometric models can quantify relationships between a variable that quantifies the side effect and PK. For example, Tanneau et al. (2021) investigated the link between the QTc interval, transaminase levels and bedaquiline exposure in phase 2b clinical data. The concentrations of the bedaquiline M2 concentrations were found to be responsible for the drug-related QTc increase, whereas no exposure-safety relationship was found with transaminase levels despite previous reports of higher levels in patients treated with bedaquiline. In another very illustrative example, Imperial et al. (2022) developed a pharmacometric model based on the Nix-TB trial (NCT02333799) including the toxicodynamics of linezolid. The authors identified links between linezolid exposure and the frequency of thrombocytopenia, neuropathy and anaemia and defined practical markers to guide dose adjustments in the treatment course.

Thirdly, modelling approaches are by no means limited to clinical data and are increasingly used to quantitatively characterize data stemming from pre-clinical TB studies. Indeed, in particular *in vitro* studies using time-kill curve studies, or the hollow-fiber infection model allow for a detailed characterisation of the PK/PD of TB drugs alone and in combination. For example, Clewe et al. (2016) developed the multi-state TB pharmacometric (MTP) model to quantify the effect of rifampicin on fast-, slow- or non-growing mycobacteria. Coupled to PK data and accounting for system-specific variables, the MTP could be used to predict across different preclinical systems up to EBA studies for rifampicin (Wicha et al., 2018), and/or isoniazid (Susanto et al., 2020) in addition to describing semi-mechanistic PKPD relationships in humans (Svensson and Simonsson, 2016; Faraj et al., 2020). Also, the study by Kim et al. (2022) defined the effect of clofazimine in combination with pretomanid, bedaquiline or linezolid against various growth states of TB and profiled their potential for synergistic

TABLE 2 Key aspects of PKPD studies.

Study	Study design	TB	Participants	PK	PD	Application
In vitro	Intracellular Extracellular	H37Ra H37Rv Clinical isolates	cells	Sampling of system (multiple)	CFU	*Define PKPD parameters for optimal kill, prevention of resistance
In vivo	Balb/c C3Heb/Fej		animals	1 sample/animal, different time points different animals	CFU	*Define PKPD parameters for cure, prevention of resistance, relapse
EBA	Selected TB patients with drug susceptible TB	Clinical isolates	patients	Full PK curve	CFU, TTP Daily for 14 days	Confirm activity in humans, confirm PKPD relationship, define dose for phase 2b
Phase 2/3	Selected TB patients with drug susceptible or drug resistant TB	Clinical isolates	patients	Limited samples in all participants, Full PK curve in subset of the patients	Culture conversion, treatment outcome	Define dose for regulatory approval
TDM	Clinical practice	Clinical isolates	patients	Ranging van limited samples to full PK curve	Successful treatment of individual patients	Define subpopulations, situations where standard dose is likely not effective or toxic

TB, tuberculosis; PK, pharmacokinetics; PD, pharmacodynamics; CFU, colony forming units; TTP, time to positivity; TDM, therapeutic drug monitoring; *The MIC of the strain used in the *in vitro/in vivo* study should be determined before each experiment as well as the MIC of the clinical strains to determine if the given clinical dose could achieve the PK/PD exposure target in patients.

interactions. Modelling approaches can also provide quantitative insights into data originating from mouse models (Chen et al., 2017; Wagh et al., 2021). For example, for spectinamide 1810, modelling helped to characterize the PK/PD indices of this new drug candidate and a model accounting for the post-antibiotic effect was developed, which might help to select adequate dosing regimens for future efficacy studies (Wagh et al., 2021). In addition, correlation between treatment length and treatment outcome is an important aspect of *in vivo* studies (Mudde et al., 2022), which is required to efficiently estimate a regimens' treatment-shortening potential. Mourik et al. (2018) developed a new design for *in vivo* relapse studies together with a pharmacometric approach for prediction of probability of cure given different treatment lengths of regimens (Pieterman et al., 2021; Mudde et al., 2022).

In summary, modelling approaches to characterize PK are already highly standardized whereas the model-based characterization of the PK/PD needs to be tailored to the research question and system of interest. Non-etheless, modelling and simulations provides the opportunity to integrate data along the drug development pathway (Bartelink et al., 2017; Wicha et al., 2018; Radtke et al., 2021), which may help to better understand the PK/PD from a quantitative perspective and bridge the translation from pre-clinical to clinical research.

8 Conclusion

In this review we provided an overview of pre-clinical and clinical methods to assess the PKPD of anti-TB drugs (Table 2). By in-depth discussion of design of *in vitro*, *in vivo*, and human studies and subsequent strategies to appropriately integrate the data from these studies using mathematical models, we contribute to debate how to accelerate the translation of findings to clinical practice. *In vitro* static time-kill experiment and dynamic models are to be used for early identification of PKPD relationships and favorable drug regimens. Similarly, simple *in vivo* models (zebra fish) can be used for drug screening studies while rodent models can help to understand PKPD relationships of the drugs in relation to treatment outcome and relapse. Results from adequate *in vitro* and *in vivo* studies can help to guide dose selection for 14-day EBA studies. These studies will determine drug activity and PKPD relationships and safety in humans. Further confirmation of PKPD in large scale phase 3 studies will help to create a better understanding of variability in drug exposure and implications for treatment outcome and hence can contribute to further dose optimization in subpopulations or personalized dosing *via* TDM or MIPD. Modelling and simulations provide the opportunity to integrate data from *in vitro*, *in vivo* and clinical studies, which contributes to a better understanding of the PKPD of a drug and has the opportunity to accelerate the clinical development pathway.

Author contributions

All authors listed have made a substantial, direct, and intellectual contribution to the work and approved it for publication.

Conflict of interest

The authors declare that the research was conducted in the absence of any commercial or financial relationships that could be construed as a potential conflict of interest.

Publisher's note

References

Alffenaar, J. W. C., Akkerman, O. W., Kim, H. Y., Tiberi, S., and Migliori, G. B. (2020a). Precision and personalized medicine and anti-TB treatment: Is TDM feasible for programmatic use? *Int. J. Infect. Dis.* 92S, S5–S9. doi:10.1016/j.ijid.2020.01.041

Alffenaar, J.-W. C., Gumbo, T., Dooley, K. E., Peloquin, C. A., Mcilleron, H., Zagorski, A., et al. (2020b). Integrating pharmacokinetics and pharmacodynamics in operational research to end tuberculosis. *Clin. Infect. Dis.* 70, 1774–1780. doi:10.1093/cid/ciz942

Alffenaar, J. W. C., Jongedijk, E. M., Van Winkel, C. A. J., Sariko, M., Heysell, S. K., Mpagama, S., et al. (2021). A mobile microvolume UV/visible light spectrophotometer for the measurement of levofloxacin in saliva. *J. Antimicrob. Chemother.* 76, 423–429. doi:10.1093/jac/dkaa420

Alffenaar, J. W. C., Stocker, S. L., Forsman, L. D., Garcia-Prats, A., Heysell, S. K., Aarnoutse, R. E., et al. (2022). Clinical standards for the dosing and management of TB drugs. *Int. J. Tuberc. Lung Dis.* 26, 483–499. doi:10.5588/ijtld.22.0188

Ali, S., Champagne, D. L., Spaink, H. P., and Richardson, M. K. (2011). Zebrafish embryos and larvae: A new generation of disease models and drug screens. *Birth Defects Res. C Embryo Today* 93, 115–133. doi:10.1002/bdrc.20206

Alsultan, A., and Peloquin, C. (2014). Therapeutic drug monitoring in the treatment of tuberculosis: an update. *Drugs* 74, 839–854. doi:10.1007/s40265-014-0222-8

Bartelink, I. H., Zhang, N., Keizer, R. J., Strydom, N., Converse, P. J., Dooley, K. E., et al. (2017). New paradigm for translational modeling to predict long-term tuberculosis treatment response. *Clin. Transl. Sci.* 10, 366–379. doi:10.1111/cts.12472

Boeree, M. J., Heinrich, N., Aarnoutse, R., Diacon, A. H., Dawson, R., Rehal, S., et al. (2017). High-dose rifampicin, moxifloxacin, and SQ109 for treating tuberculosis: A multi-arm, multi-stage randomised controlled trial. *Lancet Infect. Dis.* 17 (1), 39–49. doi:10.1016/S1473-3099(16)30274-2

Cavaleri, M., and Manolis, E. (2015). Hollow fiber system model for tuberculosis: The European Medicines Agency experience. *Clin. Infect. Dis.* 61, S1–S4. doi:10.1093/cid/civ484

Chan, S. L., Yew, W. W., Ma, W. K., Girling, D. J., Aber, V. R., Felmingham, D., et al. (1992). The early bactericidal activity of rifabutin measured by sputum viable counts in Hong Kong patients with pulmonary tuberculosis. *Tuber. Lung Dis.* 73 (1), 33–38. doi:10.1016/0962-8479(92)90077-W

Chen, C., Wicha, S. G., De Knegt, G. J., Ortega, F., Alameda, L., Sousa, V., et al. (2017). Assessing pharmacodynamic interactions in mice using the multistate tuberculosis pharmacometric and general pharmacodynamic interaction models. *CPT. Pharmacometrics Syst. Pharmacol.* 6, 787–797. doi:10.1002/psp4.12226

Chilukuri, D., McMaster, O., Bergman, K., Colangelo, P., Snow, K., and Toerner, J. G. (2015). The hollow fiber system model in the nonclinical evaluation of antituberculosis drug regimens. *Clin. Infect. Dis.* 61, S32–S33. doi:10.1093/cid/civ460

Clewe, O., Aulin, L., Hu, Y., Coates, A. R. M., and Simonsson, U. S. H. (2016). A multistate tuberculosis pharmacometric model: A framework for studying anti-tubercular drug effects *in vitro*. *J. Antimicrob. Chemother.* 71, 964–974. doi:10.1093/jac/dkv416

D'Argenio, D., and Schumitzky, A. (1997). *ADAPT II. A program for simulation, identification, and optimal experimental design. User manual.* California: Biomedical Simulations Resource, University of Southern California.

D'Argenio, D., Schumitzky, A., and Wang, X. (2009). *ADAPT 5 user's guide: Pharmacokinetic/pharmacodynamic systems analysis software.* California: Biomedical Simulations Resource, University of Southern California.

Dartois, V. A., and Rubin, E. J. (2022). Anti-tuberculosis treatment strategies and drug development: challenges and priorities. *Nat. Rev. Microbiol.* 20, 685–701. doi:10.1038/s41579-022-00731-y

Darwich, A. S., Ogungbenro, K., Vinks, A. A., Powell, J. R., Reny, J. L., Marsousi, N., et al. (2017). Why has model-informed precision dosing not yet become common clinical reality? lessons from the past and a roadmap for the future. *Clin. Pharmacol. Ther.* 101, 646–656. doi:10.1002/cpt.659

de Jager, V., Gupte, N., Nunes, S., Barnes, G. L., van Wijk, R. C., Mostert, J., et al. (2022). Early bactericidal activity of meropenem plus clavulanate (with or without rifampin) for tuberculosis the COMRADE randomized, phase 2A clinical trial. *Am. J. Respir. Crit. Care Med.* 205, 1228–1235. doi:10.1164/rccm.202108-1976OC

de Knegt, G. J., Dickinson, L., Pertinez, H., Evangelopoulos, D., McHugh, T. D., Bakker-Woudenberg, I. A. J. M., et al. (2017). Assessment of treatment response by colony forming units, time to culture positivity and the molecular bacterial load assay compared in a mouse tuberculosis model. *Tuberculosis* 105, 113–118. doi:10.1016/j.tube.2017.05.002

de Steenwinkel, J. E. M., de Knegt, G. J., ten Kate, M. T., van Belkum, A., Verbrugh, H. A., Kremer, K., et al. (2010). Time-kill kinetics of anti-tuberculosis drugs, and emergence of resistance, in relation to metabolic activity of *Mycobacterium tuberculosis*. *J. Antimicrob. Chemother.* 65, 2582–2589. doi:10.1093/jac/dkq374

de Steenwinkel, J. E. M., ten Kate, M. T., de Knegt, G. J., Verbrugh, H. A., van Belkum, A., Hernandez-Pando, R., et al. (2011). Course of murine tuberculosis and response to first-line therapy depends on route of infection and inoculum size. *Int. J. Tuberc. Lung Dis.* 15, 1478–1484. doi:10.5588/ijtld.11.0012

Deshpande, D., Srivastava, S., Nuermberger, E., Pasipanodya, J. G., Swaminathan, S., and Gumbo, T. (2016). A faropenem, linezolid, and moxifloxacin regimen for both drug-susceptible and multidrug-resistant tuberculosis in children: FLAME path on the milky way. *Clin. Infect. Dis.* 63, S95–S101. doi:10.1093/cid/ciw474

Deshpande, D., Alffenaar, J. W. C., Köser, C. U., Dheda, K., Chapagain, M. L., Simbar, N., et al. (2018a). D-cycloserine pharmacokinetics/pharmacodynamics, susceptibility, and dosing implications in multidrug-resistant tuberculosis: A faustian deal. *Clin. Infect. Dis.* 67, S308–S316. doi:10.1093/cid/ciy624

Deshpande, D., Pasipanodya, J. G., Mpagama, S. G., Bendet, P., Srivastava, S., Koeuth, T., et al. (2018b). Levofloxacin pharmacokinetics/pharmacodynamics, dosing, susceptibility breakpoints, and artificial intelligence in the treatment of multidrug-resistant tuberculosis. *Clin. Infect. Dis.* 67, S293–S302. doi:10.1093/cid/ciy611

Deshpande, D., Pasipanodya, J. G., Mpagama, S. G., Srivastava, S., Bendet, P., Koeuth, T., et al. (2018c). Ethionamide pharmacokinetics/pharmacodynamics-derived dose, the role of MICs in clinical outcome, and the resistance arrow of time in multidrug-resistant tuberculosis. *Clin. Infect. Dis.* 67, S317–S326. doi:10.1093/cid/ciy609

Deshpande, D., Pasipanodya, J. G., Srivastava, S., Bendet, P., Koeuth, K., Bhavnani, S. M., et al. (2018d). Gatifloxacin pharmacokinetics/pharmacodynamics-based optimal dosing for pulmonary and meningeal multidrug-resistant tuberculosis. *Clin. Infect. Dis.* 67, S274–S283. doi:10.1093/cid/ciy618

Deshpande, D., Srivastava, S., Bendet, P., Martin, K. R., Cirrincione, K. N., Lee, P. S., et al. (2018e). Antibacterial and sterilizing effect of benzylpenicillin in tuberculosis. *Antimicrob. Agents Chemother.* 62, 022322-17. doi:10.1128/AAC.02232-17

Deshpande, D., Magombedze, G., Srivastava, S., Bendet, P., Lee, P. S., Cirrincione, K. N., et al. (2019a). Once-a-week tigecycline for the treatment of drug-resistant TB. *J. Antimicrob. Chemother.* 74, 1607–1617. doi:10.1093/jac/dkz061

Deshpande, D., Pasipanodya, J. G., Srivastava, S., Martin, K. R., Athale, S., van Zyl, J., et al. (2019b). Minocycline immunomodulates via sonic hedgehog signaling and apoptosis and has direct potency against drug-resistant tuberculosis. *J. Infect. Dis.* 219, 975–985. doi:10.1093/infdis/jiy587

Dheda, K., Lenders, L., Magombedze, G., Srivastava, S., Raj, P., Arning, E., et al. (2018). Drug-penetration gradients associated with acquired drug resistance in patients with tuberculosis. *Am. J. Respir. Crit. Care Med.* 198, 1208–1219. doi:10.1164/rccm.201711-2333OC

Diacon, A. H., and Donald, P. R. (2014). The early bactericidal activity of antituberculosis drugs. *Expert Rev. anti. Infect. Ther.* 12, 223–237. doi:10.1586/14787210.2014.870884

Diacon, A. H., Dawson, R., Hanekom, M., Narunsky, K., Venter, A., Hittel, N., et al. (2011). Early bactericidal activity of delamanid (OPC-67683) in smear-positive pulmonary tuberculosis patients. *Int. J. Tuberc. Lung Dis.* 15, 949–954. doi:10.5588/ijtld.10.0616

Diacon, A. H., Dawson, R., von Groote-Bidlingmaier, F., Symons, G., Venter, A., Donald, P. R., et al. (2012a). 14-day bactericidal activity of PA-824, bedaquiline, pyrazinamide, and moxifl oxacin combinations: A randomised trial. *Lancet* 380, 986–993. doi:10.1016/S0140-6736(12)61080-0

Diacon, A. H., Maritz, J. S., Venter, A., van Helden, P. D., Dawson, R., and Donald, P. R. (2012b). Time to liquid culture positivity can substitute for colony counting on agar plates in early bactericidal activity studies of antituberculosis agents. *Clin. Microbiol. Infect.* 18, 711–717. doi:10.1111/j.1469-0691.2011.03626.x

Faraj, A., Svensson, R. J., Diacon, A. H., and Simonsson, U. S. H. (2020). Drug effect of clofazimine on persisters explains an unexpected increase in bacterial load in patients. *Antimicrob. Agents Chemother.* 64, e01905-19. doi:10.1128/AAC.01905-19

Gabrielsson, J., and Weiner, D. (2012). Non-compartmental analysis. *Methods Mol. Biol.* 929, 377–389. doi:10.1007/978-1-62703-050-2_16

Gewitz, A. D., Solans, B. P., Mac Kenzie, W. R., Heilig, C., Whitworth, W. C., Johnson, J. L., et al. (2021). Longitudinal model-based biomarker analysis of exposure-response relationships in adults with pulmonary tuberculosis. *Antimicrob. Agents Chemother.* 65, e0179420. doi:10.1128/AAC.01794-20

Gillespie, W. R. (1991). Noncompartmental versus compartmental modelling in clinical pharmacokinetics. *Clin. Pharmacokinet.* 20, 253–262. doi:10.2165/00003088-199120040-00001

Goossens, S. N., Sampson, S. L., and Van Rie, A. (2021). Mechanisms of drug-induced tolerance in mycobacterium tuberculosis. *Clin. Microbiol. Rev.* 34, 001411-20. doi:10.1128/CMR.00141-20

Gumbo, T., and Alffenaar, J. W. C. (2018). Pharmacokinetic/pharmacodynamic background and methods and scientific evidence base for dosing of second-line tuberculosis drugs. *Clin. Infect. Dis.* 67, S267–S273. doi:10.1093/cid/ciy608

Gumbo, T., Louie, A., Deziel, M. R., Parsons, L. M., Salfinger, M., and Drusano, G. L. (2004). Selection of a moxifloxacin dose that suppresses drug resistance in *Mycobacterium tuberculosis*, by use of an *in vitro* pharmacodynamic infection model and mathematical modeling. *J. Infect. Dis.* 190, 1642–1651. doi:10.1086/424849

Gumbo, T., Louie, A., Deziel, M. R., and Drusano, G. L. (2005). Pharmacodynamic evidence that ciprofloxacin failure against tuberculosis is not due to poor microbial kill but to rapid emergence of resistance. *Antimicrob. Agents Chemother.* 49, 3178–3181. doi:10.1128/AAC.49.8.3178-3181.2005

Gumbo, T., Louie, A., Deziel, M. R., Liu, W., Parsons, L. M., Salfinger, M., et al. (2007a). Concentration-dependent *Mycobacterium tuberculosis* killing and prevention of resistance by rifampin. *Antimicrob. Agents Chemother.* 51, 3781–3788. doi:10.1128/AAC.01533-06

Gumbo, T., Louie, A., Liu, W., Ambrose, P. G., Bhavnani, S. M., Brown, D., et al. (2007b). Isoniazid's bactericidal activity ceases because of the emergence of resistance, not depletion of *Mycobacterium tuberculosis* in the log phase of growth. *J. Infect. Dis.* 195, 194–201. doi:10.1086/510247

Gumbo, T., Louie, A., Liu, W., Brown, D., Ambrose, P. G., Bhavnani, S. M., et al. (2007c). Isoniazid bactericidal activity and resistance emergence: integrating pharmacodynamics and pharmacogenomics to predict efficacy in different ethnic populations. *Antimicrob. Agents Chemother.* 51, 2329–2336. doi:10.1128/AAC.00185-07

Gumbo, T., Dona, C. S. W. S., Meek, C., and Leff, R. (2009). Pharmacokinetics-pharmacodynamics of pyrazinamide in a novel *in vitro* model of tuberculosis for sterilizing effect: A paradigm for faster assessment of new antituberculosis drugs. *Antimicrob. Agents Chemother.* 53, 3197–3204. doi:10.1128/AAC.01681-08

Gumbo, T. (2010). New susceptibility breakpoints for first-line antituberculosis drugs based on antimicrobial pharmacokinetic/pharmacodynamic science and population pharmacokinetic variability. *Antimicrob. Agents Chemother.* 54, 1484–1491. doi:10.1128/AAC.01474-09

Heyckendorf, J., Georghiou, S. B., Frahm, N., Heinrich, N., Kontsevaya, I., Reimann, M., et al. (2022). Tuberculosis treatment monitoring and outcome measures: New interest and new strategies. *Clin. Microbiol. Rev.* 0, e0022721–21. doi:10.1128/cmr.00227-21

Honeyborne, I., McHugh, T. D., Phillips, P. P. J., Bannoo, S., Bateson, A., Carroll, N., et al. (2011). Molecular bacterial load assay, a culture-free biomarker for rapid and accurate quantification of sputum *Mycobacterium tuberculosis* bacillary load during treatment. *J. Clin. Microbiol.* 49, 3905–3911. doi:10.1128/JCM.00547-11

Imperial, M. Z., Nahid, P., Phillips, P. P. J., Davies, G. R., Fielding, K., Hanna, D., et al. (2018). A patient-level pooled analysis of treatment-shortening regimens for drug-susceptible pulmonary tuberculosis. *Nat. Med.* 24, 1708–1715. doi:10.1038/s41591-018-0224-2

Imperial, M. Z., Nedelman, J. R., Conradie, F., and Savic, R. M. (2022). Proposed linezolid dosing strategies to minimize adverse events for treatment of extensively drug-resistant tuberculosis. *Clin. Infect. Dis.* 74, 1736–1747. doi:10.1093/cid/ciab699

Jindani, A., Aber, V., Edwards, E., and Mitchison, D. (1980). The early bactericidal activity of drugs in patients with pulmonary tuberculosis. *Am. Rev. Respir. Dis.* 121, 939–949. doi:10.1164/arrd.1980.121.6.939

Kayigire, X. A., Friedrich, S. O., Van Der Merwe, L., and Diacon, A. H. (2017). Acquisition of rifampin resistance in pulmonary tuberculosis. *Antimicrob. Agents Chemother.* 61, 022200-16. doi:10.1128/AAC.02220-16

Keutzer, L., and Simonsson, U. S. H. (2020a). Individualized dosing with high inter-occasion variability is correctly handled with model-informed precision dosing—using rifampicin as an example. *Front. Pharmacol.* 11, 794. doi:10.3389/fphar.2020.00794

Keutzer, L., and Simonsson, U. S. H. (2020b). Medical device apps: an introduction to regulatory affairs for developers. *JMIR Mhealth Uhealth* 8, e17567. doi:10.2196/17567

Keutzer, L., Wicha, S. G., and Simonsson, U. S. H. (2020). Mobile health apps for improvement of tuberculosis treatment: Descriptive review. *JMIR Mhealth Uhealth* 8, e17246. doi:10.2196/17246

Kim, H. Y., Ruiter, E., Jongedijk, E. M., Ak, H. K., Marais, B. J., Pk, B., et al. (2021). Saliva-based linezolid monitoring on a mobile UV spectrophotometer. *J. Antimicrob. Chemother.* 76, 1786–1792. doi:10.1093/jac/dkab075

Kim, S., Louie, A., Drusano, G. L., Almoslem, M., Kim, S., Myrick, J., et al. (2022). Evaluating the effect of clofazimine against *Mycobacterium tuberculosis* given alone or in combination with pretomanid, bedaquiline or linezolid. *Int. J. Antimicrob. Agents* 59, 106509. doi:10.1016/j.ijantimicag.2021.106509

Kuhlin, J., Sturkenboom, M. G. G., Ghimire, S., Margineanu, I., van den Elsen, S. H. J., Simbar, N., et al. (2019). Mass spectrometry for therapeutic drug monitoring of anti-tuberculosis drugs. *Clin. Mass Spectrom.* 14, 34–45. doi:10.1016/j.clinms.2018.10.002

Lanoix, J. P., Betoudji, F., and Nuermberger, E. (2016). Sterilizing activity of pyrazinamide in combination with first-line drugs in a C3HeB/FeJ mouse model of tuberculosis. *Antimicrob. Agents Chemother.* 60, 1091–1096. doi:10.1128/AAC.02637-15

Mallikaarjun, S., Chapagain, M. L., Sasaki, T., Hariguchi, N., Deshpande, D., Srivastava, S., et al. (2021). Cumulative fraction of response for once- and twice-daily delamanid in patients with pulmonary multidrug-resistant tuberculosis. *Antimicrob. Agents Chemother.* 65, e01207-20. doi:10.1128/AAC.01207-20

Margaryan, H., Evangelopoulos, D. D., Wildner, L. M., and McHugh, T. D. (2022). Pre-clinical tools for predicting drug efficacy in treatment of tuberculosis. *Microorganisms* 10, 514. doi:10.3390/microorganisms10030514

Marshall, S. F., Burghaus, R., Cosson, V., Cheung, S., Chenel, M., DellaPasqua, O., et al. (2016). Good practices in model-informed drug discovery and development: Practice, application, and documentation. *CPT. Pharmacometrics Syst. Pharmacol.* 5, 93–122. doi:10.1002/psp4.12049

Märtson, A. G., Sturkenboom, M. G. G., Stojanova, J., Cattaneo, D., Hope, W., Marriott, D., et al. (2020). How to design a study to evaluate therapeutic drug monitoring in infectious diseases? *Clin. Microbiol. Infect.* 26, 1008–1016. doi:10.1016/j.cmi.2020.03.008

Martson, A.-G., Kim, H. Y., Marais, B., and Alffenaar, J.-W. (2021). The importance of pharmacokinetics/pharmacodynamics assessment in Phase IIB/III trials for MDR-TB treatment. *Int. J. Tuberc. Lung Dis.* 25, 336–339. doi:10.5588/ijtld.21.0072

Mcdermott, W., and Tompsett, R. (1954). Activation of pyrazinamide and nicotinamide in acidic environments *in vitro*. *Am. Rev. Tuberc.* 70, 748–754. doi:10.1164/art.1954.70.4.748

Mitchison, D. A. (1979). Basic mechanisms of chemotherapy. *Chest* 76, 771–781. doi:10.1378/chest.76.6_supplement.771

Mitchison, D. A. (2000). Role of individual drugs in the chemotherapy of tuberculosis. *Int. J. Tuberc. Lung Dis.* 4, 796–806.

Mourik, B. C., de Knegt, G. J., Verbon, A., Mouton, J. W., Bax, H. I., and de Steenwinkel, J. E. M. (2017). Assessment of bactericidal drug activity and treatment outcome in a mouse tuberculosis model using a clinical Beijing strain. *Antimicrob. Agents Chemother.* 61, 006966-17. doi:10.1128/AAC.00696-17

Mourik, B. C., Svensson, R. J., de Knegt, G. J., Bax, H. I., Verbon, A., Simonsson, U. S. H., et al. (2018). Improving treatment outcome assessment in a mouse tuberculosis model. *Sci. Rep.* 8, 5714. doi:10.1038/s41598-018-24067-x

Mudde, S. E., Ayoun Alsoud, R., van der Meijden, A., Upton, A. M., Lotlikar, M. U., Simonsson, U. S. H., et al. (2022). Predictive modeling to study the treatment-shortening potential of novel tuberculosis drug regimens, toward bundling of preclinical data. *J. Infect. Dis.* 225, 1876–1885. doi:10.1093/infdis/jiab101

Musuka, S., Srivastava, S., Siyambalapitiyage Dona, C. W., Meek, C., Leff, R., Pasipanodya, J., et al. (2013). Thioridazine pharmacokinetic-pharmacodynamic parameters "wobble" during treatment of tuberculosis: A theoretical basis for shorter-duration curative monotherapy with congeners. *Antimicrob. Agents Chemother.* 57, 5870–5877. doi:10.1128/AAC.00829-13

Nuermberger, E. L. (2017). Preclinical efficacy testing of new drug candidates. *Microbiol. Spectr.* 5. doi:10.1128/microbiolspec.tbtb2-0034-2017

Peloquin, C. A., and Davies, G. R. (2021). The treatment of tuberculosis. *Clin. Pharmacol. Ther.* 110, 1455–1466. doi:10.1002/cpt.2261

Pieterman, E. D., Keutzer, L., van der Meijden, A., van den Berg, S., Wang, H., Zimmerman, M. D., et al. (2021). Superior efficacy of a bedaquiline, delamanid, and linezolid combination regimen in a mouse tuberculosis model. *J. Infect. Dis.* 224, 1039–1047. doi:10.1093/infdis/jiab043

Radtke, K. K., Ernest, J. P., Zhang, N., Ammerman, N. C., Nuermberger, E., Belknap, R., et al. (2021). Comparative efficacy of rifapentine alone and in combination with isoniazid for latent tuberculosis infection: A translational pharmacokinetic-pharmacodynamic modeling study. *Antimicrob. Agents Chemother.* 65, e0170521. doi:10.1128/AAC.01705-21

Ruth, M. M., Raaijmakers, J., van den Hombergh, E., Aarnoutse, R., Svensson, E. M., Susanto, B. O., et al. (2022). Standard therapy of *Mycobacterium avium* complex pulmonary disease shows limited efficacy in an open source hollow fibre system that simulates human plasma and epithelial lining fluid pharmacokinetics. *Clin. Microbiol. Infect.* 28, 448. doi:10.1016/j.cmi.2021.07.015

Sirgel, F. A., Botha, F. J., Parkin, D. P., Van De Wal, B. W., Donald, P. R., Clark, P. K., et al. (1993). The early bactericidal activity of rifabutin in patients with pulmonary tuberculosis measured by sputum viable counts: A new method of drug assessment. *J. Antimicrob. Chemother.* 32 (6), 867–875. doi:10.1093/jac/32.6.867

Srivastava, S., and Gumbo, T. (2012). *In vitro* and *in vivo* modeling of tuberculosis drugs and its impact on optimization of doses and regimens. *Curr. Pharm. Des.* 17, 2881–2888. doi:10.2174/138161211797470192

Srivastava, S., Musuka, S., Sherman, C., Meek, C., Leff, R., and Gumbo, T. (2010). Efflux-pump–derived multiple drug resistance to ethambutol monotherapy in *Mycobacterium tuberculosis* and the pharmacokinetics and pharmacodynamics of ethambutol. *J. Infect. Dis.* 201, 1225–1231. doi:10.1086/651377

Srivastava, S., Pasipanodya, J. G., Meek, C., Leff, R., and Gumbo, T. (2011a). Multidrug-resistant tuberculosis not due to noncompliance but to between-patient pharmacokinetic variability. *J. Infect. Dis.* 204, 1951–1959. doi:10.1093/infdis/jir658

Srivastava, S., Sherman, C., Meek, C., Leff, R., and Gumbo, T. (2011b). Pharmacokinetic mismatch does not lead to emergence of isoniazidor rifampin-resistant *Mycobacterium tuberculosis* but to better antimicrobial effect: A new paradigm for antituberculosis drug scheduling. *Antimicrob. Agents Chemother.* 55, 5085–5089. doi:10.1128/AAC.00269-11

Srivastava, S., Modongo, C., Dona, C. W. S., Pasipanodya, J. G., Deshpande, D., and Gumbo, T. (2016a). Amikacin optimal exposure targets in the hollow-fiber system model of tuberculosis. *Antimicrob. Agents Chemother.* 60, 5922–5927. doi:10.1128/AAC.00961-16

Srivastava, S., Pasipanodya, J. G., Ramachandran, G., Deshpande, D., Shuford, S., Crosswell, H. E., et al. (2016b). A long-term Co-perfused disseminated tuberculosis-3D liver hollow fiber model for both drug efficacy and hepatotoxicity in babies. *EBioMedicine* 6, 126–138. doi:10.1016/j.ebiom.2016.02.040

Srivastava, S., Magombedze, G., Koeuth, T., Sherman, C., Pasipanodya, J. G., Raj, P., et al. (2017). Linezolid dose that maximizes sterilizing effect while minimizing toxicity and resistance emergence for tuberculosis. *Antimicrob. Agents Chemother.* 61, 007511-17. doi:10.1128/aac.00751-17

Srivastava, S., Deshpande, D., Nuermberger, E., Lee, P. S., Cirrincione, K., Dheda, K., et al. (2018). The sterilizing effect of intermittent tedizolid for pulmonary tuberculosis. *Clin. Infect. Dis.* 67, S336–S341. doi:10.1093/cid/ciy626

Srivastava, S., van Zyl, J., Cirrincione, K., Martin, K., Thomas, T., Deshpande, D., et al. (2020). Evaluation of ceftriaxone plus avibactam in an intracellular hollow fiber model of tuberculosis: Implications for the treatment of disseminated and meningeal tuberculosis in children. *Pediatr. Infect. Dis. J.* 39, 1092–1100. doi:10.1097/INF.0000000000002857

Srivastava, S., Chapagain, M., van Zyl, J., Deshpande, D., and Gumbo, T. (2021a). Potency of vancomycin against *Mycobacterium tuberculosis* in the hollow fiber system model. *J. Glob. Antimicrob. Resist.* 24, 403–410. doi:10.1016/j.jgar.2021.01.005

Srivastava, S., Cirrincione, K. N., Deshpande, D., and Gumbo, T. (2021b). Tedizolid, faropenem, and moxifloxacin combination with potential activity against nonreplicating *Mycobacterium tuberculosis*. *Front. Pharmacol.* 11, 616294. doi:10.3389/fphar.2020.616294

Srivastava, S., Gumbo, T., and Thomas, T. (2021c). Repurposing cefazolin-avibactam for the treatment of drug resistant *Mycobacterium tuberculosis*. *Front. Pharmacol.* 12, 776969. doi:10.3389/fphar.2021.776969

Srivastava, S., Thomas, T., Howe, D., Malinga, L., Raj, P., Alffenaar, J.-W., et al. (2021d). Cefdinir and beta-lactamase inhibitor independent efficacy against *Mycobacterium tuberculosis*. *Front. Pharmacol.* 12, 677005. doi:10.3389/fphar.2021.677005

Sturkenboom, M. G. G., Mulder, L. W., de Jager, A., van Altena, R., Aarnoutse, R. E., de Lange, W. C. M., et al. (2015). Pharmacokinetic modeling and optimal sampling strategies for therapeutic drug monitoring of rifampin in patients with tuberculosis. *Antimicrob. Agents Chemother.* 59, 4907–4913. doi:10.1128/AAC.00756-15

Sturkenboom, M. G. G., Bolhuis, M. S., Akkerman, O. W., De Lange, W. C. M., Van Derwerf, T. S., and Alffenaar, J. W. C. (2016). Therapeutic drug monitoring of first-line antituberculosis drugs comprises more than C2h measurements. *Int. J. Tuberc. Lung Dis.* 20, 1695–1696. doi:10.5588/ijtld.16.0550

Sturkenboom, M. G. G., Märtson, A. G., Svensson, E. M., Sloan, D. J., Dooley, K. E., van den Elsen, S. H. J., et al. (2021). Population pharmacokinetics and bayesian dose adjustment to advance TDM of anti-TB drugs. *Clin. Pharmacokinet.* 60, 685–710. doi:10.1007/s40262-021-00997-0

Susanto, B. O., Wicha, S. G., Hu, Y., Coates, A. R. M., and Simonsson, U. S. H. (2020). Translational model-informed approach for selection of tuberculosis drug combination regimens in early clinical development. *Clin. Pharmacol. Ther.* 108, 274–286. doi:10.1002/cpt.1814

Svensson, R. J., Aarnoutse, R. E., Diacon, A. H., Dawson, R., Gillespie, S. H., Boeree, M. J., et al. (2018a). A population pharmacokinetic model incorporating saturable pharmacokinetics and autoinduction for high rifampicin doses. *Clin. Pharmacol. Ther.* 103 (4), 674–683.

Svensson, E. M., and Karlsson, M. O. (2017). Modelling of mycobacterial load reveals bedaquiline's exposure-response relationship in patients with drug-resistant TB. *J. Antimicrob. Chemother.* 72, 3398–3405. doi:10.1093/jac/dkx317

Svensson, R. J., and Simonsson, U. S. H. (2016). Application of the multistate tuberculosis pharmacometric model in patients with rifampicin-treated pulmonary tuberculosis. *CPT. Pharmacometrics Syst. Pharmacol.* 5, 264–273. doi:10.1002/psp4.12079

Svensson, R. J., Niward, K., Davies Forsman, L., Bruchfeld, J., Paues, J., Eliasson, E., et al. (2019a). Individualised dosing algorithm and personalised treatment of high-dose rifampicin for tuberculosis. *Br. J. Clin. Pharmacol.* 85, 2341–2350. doi:10.1111/bcp.14048

Svensson, R. J., Sabiiti, W., Kibiki, G. S., Ntinginya, N. E., Bhatt, N., Davies, G., et al. (2019b). Model-based relationship between the molecular bacterial load assay and time to positivity in liquid culture. *Antimicrob. Agents Chemother.* 63, 006522-19. doi:10.1128/AAC.00652-19

Svensson, R. J., Svensson, E. M., Aarnoutse, R. E., Diacon, A. H., Dawson, R., Gillespie, S. H., et al. (2018b). Greater early bactericidal activity at higher rifampicin doses revealed by modeling and clinical trial simulations. *J. Infect. Dis.* 218 (6), 991–999.

Szipszky, C., Van Aartsen, D., Criddle, S., Rao, P., Zentner, I., Justine, M., et al. (2021). Determination of rifampin concentrations by urine colorimetry and mobile phone readout for personalized dosing in tuberculosis treatment. *J. Pediatr. Infect. Dis. Soc.* 10, 104–111. doi:10.1093/jpids/piaa024

Tanneau, L., Svensson, E. M., Rossenu, S., and Karlsson, M. O. (2021). Exposure–safety analysis of QTc interval and transaminase levels following bedaquiline administration in patients with drug-resistant tuberculosis. *CPT. Pharmacometrics Syst. Pharmacol.* 10, 1538–1549. doi:10.1002/psp4.12722

Te Brake, L. H. M., de Jager, V., Narunsky, K., Vanker, N., Svensson, E. M., Phillips, P. P. J., et al. (2021). Increased bactericidal activity but dose-limiting intolerability at 50 mg·kg−1 rifampicin. *Eur. Respir. J.* 58, 2000955. doi:10.1183/13993003.00955-2020

Tietjen, A. K., Kroemer, N., Cattaneo, D., Baldelli, S., and Wicha, S. G. (2022). Population pharmacokinetics and target attainment analysis of linezolid in multidrug-resistant tuberculosis patients. *Br. J. Clin. Pharmacol.* 88, 1835–1844. doi:10.1111/bcp.15102

Vaddady, P. K., Lee, R. E., and Meibohm, B. (2010). *In vitro* pharmacokinetic/pharmacodynamic models in anti-infective drug development: Focus on TB. *Future Med. Chem.* 2, 1355–1369. doi:10.4155/fmc.10.224

van der Laan, L. E., Garcia-Prats, A. J., Schaaf, H. S., Winckler, J. L., Draper, H., Norman, J., et al. (2021). Pharmacokinetics and drug-drug interactions of abacavir and lamuvudine Co-administered with antituberculosis drugs in HIV-positive children treated for multidrug-resistant tuberculosis. *Front. Pharmacol.* 12, 722204. doi:10.3389/fphar.2021.722204

van Ingen, J., Aarnoutse, R. E., Donald, P. R., Diacon, A. H., Dawson, R., Plemper Van Balen, G., et al. (2011). Why do we use 600 mg of rifampicin in tuberculosis treatment? *Clin. Infect. Dis.* 52, e194–e199. doi:10.1093/cid/cir184

van Rijn, S. P., Srivastava, S., Wessels, M. A., van Soolingen, D., Alffenaar, J.-W. C., and Gumbo, T. (2017). Sterilizing effect of ertapenem-clavulanate in a hollow-fiber model of tuberculosis and implications on clinical dosing. *Antimicrob. Agents Chemother.* 61, 020399-16. doi:10.1128/AAC.02039-16

Veringa, A., Sturkenboom, M. G. G., Dekkers, B. G. J., Koster, R. A., Roberts, J. A., Peloquin, C. A., et al. (2016). LC-MS/MS for therapeutic drug monitoring of anti-infective drugs. *TrAC Trends Anal. Chem.* 84, 34–40. doi:10.1016/j.trac.2015.11.026

Vu, D. H., Alffenaar, J. W. C., Edelbroek, P. M., Brouwers, J. R. B. J., and Uges, D. R. (2011). Dried blood spots: a new tool for tuberculosis treatment optimization. *Curr. Pharm. Des.* 17, 2931–2939. doi:10.2174/138161211797470174

Wagh, S., Rathi, C., Lukka, P. B., Parmar, K., Temrikar, Z., Liu, J., et al. (2021). Model-based exposure-response assessment for spectinamide 1810 in a mouse model of tuberculosis. *Antimicrob. Agents Chemother.* 65, e0174420. doi:10.1128/AAC.01744-20

Wald-Dickler, N., Holtom, P., and Spellberg, B. (2018). Busting the myth of "static vs cidal": A systemic literature review. *Clin. Infect. Dis.* 66, 1470–1474. doi:10.1093/cid/cix1127

Wayne, P. (2018). *Susceptibility testing of mycobacteria, nocardiae, and other aerobic actinomycetes; approved standard. CLSI document M24-A2.* Wayne: CLSI.

Wicha, S. G., Clewe, O., Svensson, R. J., Gillespie, S. H., Hu, Y., Coates, A. R. M., et al. (2018). Forecasting clinical dose–response from preclinical studies in tuberculosis research: Translational predictions with rifampicin. *Clin. Pharmacol. Ther.* 104, 1208–1218. doi:10.1002/cpt.1102

Wicha, S. G., Märtson, A. G., Nielsen, E. I., Koch, B. C. P., Friberg, L. E., Alffenaar, J. W., et al. (2021). From therapeutic drug monitoring to model-informed precision dosing for antibiotics. *Clin. Pharmacol. Ther.* 109, 928–941. doi:10.1002/cpt.2202

Wilkins, J. J., Svensson, E. M., Ernest, J. P., Savic, R. M., Simonsson, U. S. H., and McIlleron, H. (2022). Pharmacometrics in tuberculosis: progress and opportunities. *Int. J. Antimicrob. Agents* 60, 106620. doi:10.1016/j.ijantimicag.2022.106620

Williams, A., and Orme, I. M. (2016). Animal models of tuberculosis: An overview. *Microbiol. Spectr.* 4. doi:10.1128/microbiolspec.tbtb2-0004-2015

World Health Organization (WHO) (2018). *Technical report on the pharmacokinetics and pharmacodynamics (PK/PD) of medicines used in the treatment of drug-resistant tuberculosis*. Geneva: World Health Organization.

Zhang, T., Li, S. Y., Williams, K. N., Andries, K., and Nuermberger, E. L. (2011). Short-course chemotherapy with TMC207 and rifapentine in a murine model of latent tuberculosis infection. *Am. J. Respir. Crit. Care Med.* 184, 732–737. doi:10.1164/rccm.201103-0397OC

Zheng, X., Bao, Z., Forsman, L. D., Hu, Y., Ren, W., Gao, Y., et al. (2021). Drug exposure and minimum inhibitory concentration predict pulmonary tuberculosis treatment response. *Clin. Infect. Dis.* 73, e3520–e3528. doi:10.1093/cid/ciaa1569

Zheng, X., Davies Forsman, L., Bao, Z., Xie, Y., Ning, Z., Schon, T., et al. (2022). Drug exposure and susceptibility of second-line drugs correlate with treatment response in patients with multidrug-resistant tuberculosis: a multicentre prospective cohort study in China. *Eur. Respir. J.* 59, 2101925. doi:10.1183/13993003.01925-2021

Zvada, S. P., Denti, P., Donald, P. R., Schaaf, H. S., Thee, S., Seddon, J. A., et al. (2014). Population pharmacokinetics of rifampicin, pyrazinamide and isoniazid in children with tuberculosis: *In silico* evaluation of currently recommended doses. *J. Antimicrob. Chemother.* 69, 1339–1349. doi:10.1093/jac/dkt524

frontiers | Frontiers in Pharmacology

TYPE Original Research
PUBLISHED 12 December 2022
DOI 10.3389/fphar.2022.1048653

OPEN ACCESS

EDITED BY
Shashikant Srivastava,
University of Texas at Tyler,
United States

REVIEWED BY
Dipti Agarwal,
Dr Ram Manohar Lohia Institute of Medical Sciences, India
Hung-Ling Huang,
Kaohsiung Medical University Hospital, Taiwan

*CORRESPONDENCE
Russell R. Kempker,
rkempke@emory.edu

SPECIALTY SECTION
This article was submitted to Pharmacology of Infectious Diseases, a section of the journal Frontiers in Pharmacology

RECEIVED 19 September 2022
ACCEPTED 01 December 2022
PUBLISHED 12 December 2022

CITATION
Maranchick NF, Alshaer MH, Smith AGC, Avaliani T, Gujabidze M, Bakuradze T, Sabanadze S, Avaliani Z, Kipiani M, Peloquin CA and Kempker RR (2022), Cerebrospinal fluid concentrations of fluoroquinolones and carbapenems in tuberculosis meningitis.
Front. Pharmacol. 13:1048653.
doi: 10.3389/fphar.2022.1048653

Cerebrospinal fluid concentrations of fluoroquinolones and carbapenems in tuberculosis meningitis

Nicole F. Maranchick[1,2], Mohammad H. Alshaer[1,2], Alison G. C. Smith[3], Teona Avaliani[4], Mariam Gujabidze[4], Tinatin Bakuradze[4], Shorena Sabanadze[4], Zaza Avaliani[4], Maia Kipiani[4,5], Charles A. Peloquin[1,2] and Russell R. Kempker[6]*

[1]Infectious Disease Pharmacokinetics Lab, Emerging Pathogens Institute, University of Florida, Gainesville, FL, United States, [2]Department of Pharmacotherapy and Translational Research, College of Pharmacy, University of Florida, Gainesville, FL, United States, [3]Department of Medicine, Division of Internal Medicine, Duke University, Durham, NC, United States, [4]National Center for Tuberculosis and Lung Diseases, Tbilisi, Georgia, [5]David Tvildiani Medical University, Tbilisi, Georgia, [6]Department of Medicine, Division of Infectious Diseases, Emory University, Atlanta, GA, United States

Background: Tuberculosis meningitis (TBM) is the most lethal form of TB. It is difficult to treat in part due to poor or uncertain drug penetration into the central nervous system (CNS). To help fill this knowledge gap, we evaluated the cerebrospinal fluid (CSF) concentrations of fluoroquinolones and carbapenems in patients being treated for TBM.

Methods: Serial serum and CSF samples were collected from hospitalized patients being treated for TBM. CSF was collected from routine lumbar punctures between alternating timepoints of 2 and 6 h after drug administration to capture early and late CSF penetration. Rich serum sampling was collected after drug administration on day 28 for non-compartmental analysis.

Results: Among 22 patients treated for TBM (8 with confirmed disease), there was high use of fluoroquinolones (levofloxacin, 21; moxifloxacin, 10; ofloxacin, 6) and carbapenems (imipenem, 11; meropenem, 6). Median CSF total concentrations of levofloxacin at 2 and 6 h were 1.34 mg/L and 3.36 mg/L with adjusted CSF/serum ratios of 0.41 and 0.63, respectively. For moxifloxacin, the median CSF total concentrations at 2 and 6 h were 0.78 mg/L and 1.02 mg/L with adjusted CSF/serum ratios of 0.44 and 0.62. Serum and CSF concentrations of moxifloxacin were not affected by rifampin use. Among the 76 CSF samples measured for carbapenem concentrations, 79% were undetectable or below the limit of detection.

Conclusion: Fluoroquinolones demonstrated high CSF penetration indicating their potential usefulness for the treatment of TBM. Carbapenems had lower than expected CSF concentrations.

KEYWORDS

tuberculosis meningitis, fluoroquinolones, carbapenems, pharmacokinetics, cerebrospinal fluid, antitubercular agents

Introduction

Tuberculosis (TB) is an infectious disease caused by *Mycobacterium tuberculosis* (Mtb) and remains a major cause of mortality globally. In 2020, approximately 10 million people developed active disease and there were 1.5 million deaths, representing the first annual increase in deaths since 2005 (World Health Organization, 2021). While the lungs are the major site of TB infection, extrapulmonary disease can affect virtually all other body sites. Extrapulmonary TB accounts for approximately 15%–20% of all cases and the most severe manifestation is tuberculosis meningitis (TBM) (Sharma et al., 2021). TBM can be devastating, leading to substantial neurological impairments, paralysis, seizures, and high mortality (Bartzatt, 2011). Mortality rates during treatment for TBM are 20%–69%, with higher rates seen in cohorts of patients with drug resistant TB (Christensen et al., 2011; Dheda et al., 2017).

A major challenge in the treatment of TBM is drug delivery to the site of disease. Central nervous system (CNS) penetration of first-line TB medications including rifampin and ethambutol can be suboptimal at standard dosages, seldom exceeding minimal inhibitory concentrations (MIC) (Donald, 2010). This is especially a concern following resolution of meningeal inflammation (Thwaites et al., 2013; Roos, 2000). Second-line medications including fluoroquinolones appear to have improved penetration across the blood brain barrier, making them appealing antibiotics for the treatment of TBM (Litjens et al., 2020). Fluoroquinolones, such as levofloxacin and moxifloxacin, may be implemented into both short term and long-term regimens (Ghimire et al., 2019). Among the fluoroquinolones, moxifloxacin appears to have the highest *in vitro* activity against Mtb. However, concentrations may be most susceptible to reduction if administered with rifampin, compromising treatment efficacy (Nijland et al., 2007; Ramachandran et al., 2012). While penetration of fluoroquinolones appears to be adequate in bacterial CNS infections, additional data regarding penetration specifically in the treatment of TBM is needed.

Carbapenems are extended-spectrum beta-lactams with broad antimicrobial activity, including activity against Mtb (Jaganath et al., 2016). They are utilized for both multidrug-resistant and extensively drug-resistant TB, even though published data supporting their use is limited. To improve activity against Mtb, carbapenems are often administered with clavulanic acid, which blocks class A beta-lactamases (van Rijn et al., 2019). Data regarding imipenem and meropenem penetration into the CSF suggests adequate exposure to eradicate most pathogens, especially in the presence of CNS inflammation (Zhanel et al., 2007; Craig, 1997). However, data is limited regarding the CNS penetration of carbapenems in TBM (Jaganath et al., 2016).

To further understand the exposure of fluoroquinolones and carbapenems in TBM, our objective was to describe and compare serum and CSF concentrations of fluoroquinolones (levofloxacin, moxifloxacin, and ofloxacin) and carbapenems (imipenem and meropenem) among persons treated for TBM.

Materials and methods

Setting and participants

This prospective study enrolled participants at the National Center for Tuberculosis and Lung Diseases (NCTLD) in Tbilisi, Georgia. The NCTLD includes an inpatient ward for patients with TBM and directly observed therapy clinics for ambulatory care. Study participants were selected from a larger prospective cohort evaluating clinical outcomes among persons treated for TBM (Smith et al., 2021). Written formal consent was obtained from all study participants. The study was approved by the institutional review boards of the NCTLD (IRB# IORG0009467), the University of Florida, Gainesville, FL, United States, and Emory University, Atlanta, GA, United States.

All patients underwent a lumbar puncture and CSF diagnostic testing, including acid-fast bacilli (AFB) staining, molecular testing with Xpert® MTB/RIF assay (Cepheid, United States) and AFB culture on a Lowenstein-Jensen solid and Mycobacterial Growth Indicator Tube liquid media. To identify drug resistance to rifampin and isoniazid, a Genotype® MTBDR*plus* (Hain-Lifescience, Germany) assay was performed on positive cultures. Serial lumbar punctures were performed at 7, 14, 28 days, and then monthly after treatment initiation per standard of care. With regards to treatment and dosing, WHO guidance was followed and treatment regimens were based on the Georgian National TB Program 2015 guidelines, as outlined previously (Smith et al., 2021). Both levofloxacin and moxifloxacin were given by mouth (levofloxacin dose was either 750 mg or 1000mg, moxifloxacin 400 mg or 1000 mg). Ofloxacin was administered as 800 mg intravenously every 12 h. Meropenem and imipenem were administered intravenously as 1000 mg every 12 h. Multiple participants received more than one study drug of interest from the same class, but not concurrently. All participants received multidrug regimens for TBM, although only fluoroquinolones and carbapenems were analyzed in the present study (Smith et al., 2021). For MDR-TBM, regimens were chosen based upon Georgian National TB guidelines, and patients received regimens including carbapenems, injectable agents (such as amikacin),

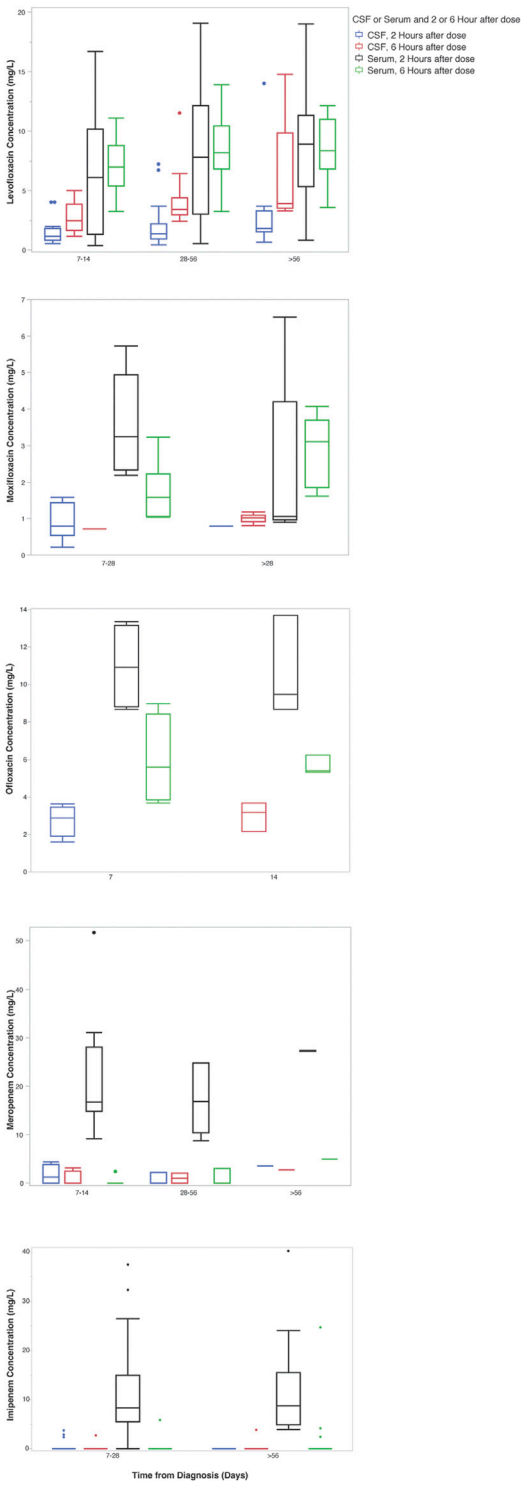

FIGURE 1
Carbapenem and fluoroquinolone CSF and serum concentrations over time from diagnosis. *The x-axis indicates the time in days from the start of any anti-tuberculosis treatment. Boxes indicate the median and interquartile range of the samples.

linezolid, and novel/repurposed anti-TBM agents such as clofazimine, delamanid, and bedaquiline (Smith et al., 2021). Additionally, all participants received adjunctive dexamethasone therapy for 6–8 weeks. Participants were hospitalized for treatment until clinical improvement such that they could be treated in an outpatient setting (Smith et al., 2021; Kempker et al., 2022).

Drug sample collection and quantification

Participants enrolled in the pharmacokinetic (PK) study had both serum and CSF samples collected at baseline and at approximately 7, 14, and 28 days following initiation of treatment. Monthly samples were subsequently collected during hospitalization for up to 112 days. Participants had two- and 6-h samples collected following drug administration from both serum and CSF. The CSF sampling was alternated between two- and 6-h concentrations to assess for early and delayed penetration. Rich serum sampling for non-compartmental analysis (NCA) was performed at 28 days, and the collection timepoints were 0, 2, 4, 8, 12, and 24 h after drug administration with slight variations for persons receiving bedaquiline (0, 2, 6, 12, 24, 48, 72 h) and delamanid (0, 1, 2, 4, 6,8 and 12 h). Following serum and CSF collection, samples were centrifuged then stored at −80°C at the NCTLD until shipping to the Infectious Disease Pharmacokinetic Laboratory (IDPL) at the University of Florida, with the cold chain remaining intact throughout. Total drug concentrations were quantified using validated liquid chromatography tandem mass spectrometry assays. Serum curve was used for the serum samples, while artificial CSF curve was used for CSF samples to match CSF matrix. The plasma and CSF detection ranges for levofloxacin, moxifloxacin, and ofloxacin were 0.2–15 mg/L and 2–100 mg/L for meropenem and imipenem. Intra- and inter-batch precision and accuracy were <10%. Samples below the limit of quantification (BLQ) were assigned a value of "0" for analysis.

Data management

NCA was performed using Phoenix WinNonlin (Certara, v8.3) to determine maximum serum concentration (C_{max}), time to maximum concentration (T_{max}), elimination rate constant (K_e), half-life ($t_{1/2}$) and area under the concentration-time curve over 24 h (AUC_{0-24}). Serum protein binding rates for levofloxacin (31%), moxifloxacin (40%), ofloxacin (32%), imipenem (20%), and meropenem (2%) were obtained from previously published literature and used to estimate free serum drug concentrations (Craig, 1997), (Lamp et al., 1992; Janssen Pharmaceuticals and Inc, 1996; Pickerill et al., 2000; Ortho-McNeil-Janssen Pharmaceuticals and Inc, 2008; Bolon, 2009; Salmon-Rousseau et al., 2020). We assumed there was no

protein binding in the CSF (i.e., 100% free drug) (Bonati et al., 1982; de Lange, 2013). To assess CSF penetration, a ratio of CSF to serum concentrations was calculated for matching time points for participants. Adjusted CSF to serum ratios were calculated to account for serum protein binding. Samples BLQ or zero were excluded in the ratio calculations.

Continuous data were presented as median and interquartile range, and categorical data as count and percentage. Student t-tests were used to assess for differences in drug concentrations at 2 and 6 h, differences in the CSF to serum ratios between 2 and 6 h, and compare CSF concentrations from baseline over the duration of therapy to the final drawn sample for each drug at two and 6-h timepoints. JMP Pro v16.1 (JMP, Cary, NC, United States) was used for statistical analysis.

Results

Twenty-two participants were enrolled in the PK study, all of whom received a fluoroquinolone and/or carbapenem. Over half (55%) of enrolled patients were female and the median (IQR) age was 38 (29.3–47.8) years. Additional information regarding baseline demographics, comorbidities, and relevant clinical measures including CSF composition are included in Tables 1, 2. Of note, CSF white blood cell count declined over the first 28 days of treatment (Table 2). Trends in fluoroquinolone and carbapenem CSF and serum concentrations after diagnosis of TBM can be visualized in (Figure 1).

Fluoroquinolones

A total of 21 participants received levofloxacin during their treatment, resulting in 45 matching CSF and serum samples at 2 h and 38 at 6 h (Table 3). Median (IQR) total serum concentrations for levofloxacin at 2 and 6 h were 7.36 mg/L (2.83–11.21) and 7.68 mg/L (5.75–10.11), while total CSF concentrations at 2 and 6 h were 1.34 mg/L (0.91–1.98) and 3.36 mg/L (2.43–4.03). C_{max} concentrations through NCA were 11.62 mg/L (8.64–13.12), with a T_{max} of 4 h (Table 4). Median CSF to serum ratios adjusted for protein binding were higher at six *versus* 2 h (0.63 vs 0.41, $p = 0.05$). Following TBM diagnosis, levofloxacin CSF concentrations increased significantly from baseline at both 2 h ($p = 0.02$) and 6 h ($p = 0.002$) (Table 5).

Ten participants received moxifloxacin during treatment, 6 (60%) following a change in therapy from levofloxacin. There were 10 and six matching CSF and serum samples at 2 and 6 h, respectively. Median (IQR) total serum concentrations at 2 and 6 h were 2.74 mg/L (1.65–4.84) and 1.91 mg/L (1.56–3.28), while median total CSF concentrations at 2 and 6 h were 0.78 mg/L (0.63–1.40) and 1.02 mg/L (0.78–1.06) (Table 3). C_{max} concentrations through NCA were 4.04 mg/L (2.78–5.34), with a T_{max} of 2 h (Table 4). Median CSF to serum concentrations adjusted for protein binding increased from 2 to 6 h (0.44 vs 0.62, $p = 0.05$). Following TBM diagnosis and treatment initiation, moxifloxacin in CSF trended towards increased concentrations, but this was not statistically significant Among the participants receiving moxifloxacin, seven received concomitant rifampin, yet no difference in moxifloxacin serum $AUC_{0\text{-}24}$ were seen between patients receiving rifampin *versus* those not receiving rifampin (32.86 vs 33.38 Hr*mg/L, $p = 1.00$). Additionally, CSF concentrations were not significantly different between patients receiving rifampin *versus* not receiving rifampin at 2 h (0.78 vs. 0.67 mg/L, $p = 0.78$) or 6 h (1.02 vs 0.72 mg/L, $p = 0.72$).

Five participants received ofloxacin, with four matched CSF to serum samples at 2 h and three at 6 h. Median (IQR) total serum concentrations at 2 and 6 h were 9.47 mg/L (8.67–13.36) and 5.40 mg/L (4.43–6.75), while total CSF concentrations at 2 and 6 h were 2.22 mg/L (0.93–3.11) and 3.20 mg/L (2.17–3.69) (Table 3). Median C_{max} concentrations through NCA were 9.47 mg/L (8.67–13.36), with a T_{max} 2 h (Table 4). Median CSF to serum concentrations adjusted for protein binding were higher at 6 h *versus* 2 h (0.76 vs 0.37, $p = 0.03$) (Table 3). Ofloxacin CSF concentrations at 2 h increased significantly from baseline ($p = 0.04$) whereas concentrations at the 6-h time-point did not ($p = 0.28$) (Table 5).

Carbapenems

There were 11 participants who received imipenem resulting in three matched CSF to serum samples at 2 h and two at 6 h. For meropenem, six participants with six matched CSF to serum samples at 2 h and one matched sample at 6 h were available. With the exception of 2-h serum samples, a substantial number of samples were undetectable or BLQ (<2 mg/L) for both serum and CSF (Table 6). 12/15 (80%) of meropenem total serum concentrations at 6 h were undetectable or BLQ in addition to 6/12 (50%) and 5/9 (56%) meropenem total CSF concentrations at 2 and 6 h 39/43 (91%) imipenem total serum concentrations at 6 h were undetectable or BLQ in addition to 28/32 (88%) and 21/23 (91%) total CSF concentrations at 2 and 6 h, respectively. Meropenem had more detectable levels in the CSF than imipenem.

Discussion

Our findings demonstrate a high CSF penetration of fluoroquinolone antibiotics and provide support for their consideration in the treatment of TBM. In particular, the CSF concentrations of levofloxacin were high and above the Mtb susceptibility cutoff in most samples tested, supporting its ability to achieve effective concentrations in TBM. Our study also provides novel data on the CSF concentrations of antibiotics over time which unexpectedly trended higher with the fluoroquinolones despite decreasing CSF inflammation,

TABLE 1 Participant demographics, clinical characteristics, and clinical outcomes (*n* = 22).

Characteristic	*n* (%), or median (IQR)
Male	10 (45%)
Age, years	38 (29.3–47.8)
BMI, kg/m^2	24.5 (22.2–26.5)
HIV Positive[#]	1 (5%)
Chronic Hepatitis C[¥]	3 (14%)
Prior TB treatment	7 (47%)
IVDU	2 (9%)
Clinical Characteristics	
Baseline GCS	15 (9–15)
TB Meningitis Confirmation	8 (36%)
TB Treatment Category	
Susceptible	16 (72.7%)
MDR-TB defined clinically[§]	3 (13.6%)
MDR-TB confirmed with culture	3 (13.6%)
Clinical Outcomes at End of the Study	
Treatment Completed	21 (95%)
Treatment Failure	1 (5%)
Seizures Reported with Carbapenems	0 (0%)

HIV, human immunodeficiency virus; CSF, cerebral spinal fluid; TB, tuberculosis; IVDU, intravenous drug use; GCS, glascow coma scale; MDR-TB, multidrug resistant TB (resistance to at least both isoniazid and rifampicin).
#One patient received Atripla® (efavirenz, emtricitabine, tenofovir disoproxil) during TBM treatment, with minimal impact on study medications expected.
¥No patients received hepatitis C medications simultaneously with TB treatment.
§Among patients with clinically confirmed MDR-TB, one had a known MDR-TB contact and two previously received TB treatment.

TABLE 2 Cerebrospinal fluid analysis*.

Timepoint (Days)	WBC (cells/μL)	Lymphocyte %	Neutrophil %	Total protein (mg/dl)
0	133 (143)	92 (9.5)	5 (4.8)	99 (66)
7	86.5 (192.5)	90 (13)	4 (5)	66 (33)
14	71 (45)	86 (32)	3 (9)	33 (33)
28	33 (23)	70 (94)	0.5 (2)	33 (27)
56	38 (39)	69.5 (94.3)	0 (11.3)	33 (33)
84	44 (28)	92.5 (20.8)	2.5 (4.5)	49.5 (57.8)
112	32 (20.5)	88 (51)	2 (3)	66 (66)

*Data represented as Median (IQR). WBC, white blood count.

providing data that continued moderate-high CSF concentrations can be obtained during treatment. While current clinical trial data have not shown an ability of fluoroquinolones to improve outcomes among patients treated for drug-susceptible TBM, our study provides key pharmacokinetic data for their continued study in clinical trials and use in drug-resistant TBM (Heemskerk et al., 2016; Huynh et al., 2022). To the contrary, our study revealed that the carbapenems did not achieve adequate concentrations in our patient cohort, questioning their utility for patients with TBM.

All fluoroquinolones in our study had median serum C_{max} values within normal ranges (8–12 mg/L for levofloxacin and

TABLE 3 Fluoroquinolone serum and cerebrospinal fluid concentrations.

Drug	Time from administration to sample collection (hours)	Participants	CSF samples	CSF drug concentration (mg/L) (median, IQR)	Serum samples	Serum drug concentration (mg/L) (median, IQR)	Number of matching samples	Median CSF/serum concentration	Median adjusted CSF/serum concentration
Levofloxacin	2	21	53	1.34 (0.91–1.98)	87	7.36 (2.83–11.21)	45	0.28 (0.13–0.73)	0.41 (0.19–1.06)
	6	21	38	3.36 (2.43–4.03)	68	7.68 (5.75–10.11)	38	0.44 (0.33–0.54)	0.63 (0.47–0.78)
Moxifloxacin	2	10	10	0.78 (0.63–1.40)	17	2.74 (1.65–4.84)	10	0.26 (0.17–0.31)	0.44 (0.28–0.52)
	6	6	6	1.02 (0.78–1.06)	12	1.91 (1.56–3.28)	6	0.37 (0.30–0.50)	0.62 (0.49–0.84)
Ofloxacin	2	5	6	2.22 (0.93–3.11)	7	9.47 (8.67–13.36)	4	0.25 (0.19–0.30)	0.37 (0.29–0.44)
	6	4	3	3.20 (2.17–3.69)	7	5.40 (4.43–6.75)	3	0.51 (0.41–0.68)	0.75 (0.60–1.01)

*CSF, cerebrospinal fluid; IQR, interquartile range.

ofloxacin, 3–5 mg/L for moxifloxacin) indicating typical systemic exposure (Alsultan and Peloquin, 2014). Our finding of increasing CSF concentrations from 2 to 6 h demonstrates delayed penetration which has important implications. In the case of levofloxacin, this delay may have been in part from delayed oral absorption as median serum concentrations increased from 2 to 6 h. These findings suggest clinical sampling of fluoroquinolone serum and CSF concentrations may be optimized by including both early and late samples. Due to their moderate lipophilic and protein bound nature in conjunction with relatively low molecular mass (Nau et al., 2010; Nau et al., 1994), fluoroquinolones enter CSF more completely than other antibiotics, with an estimated CSF concentration of approximately 20–80% of peak serum levels (Andes and Craig, 1999; Wilkinson et al., 2017). Our data support these published estimates, with median levofloxacin CSF concentrations ~41% of total serum concentrations at 2 h and −63% at 6 h, and ofloxacin reaching −37% and −75% of total serum concentrations at 2 and 6 h post dose, respectively. Fluoroquinolone bacterial killing depends on concentration (both C_{max} and AUC), with a proposed C_{max}/MIC ratio target of >8–10 in TB (Turnidge, 1999; Berning, 2001; Levison and Levison, 2009). Although we were unable to calculate CSF C_{max}/MIC or $AUC_{0\text{-}24}$/MIC for this population, fluoroquinolones in our study achieved concentrations within expected ranges, suggesting potential attainment of targets. Assuming susceptible MICs of 1 mg/L for ofloxacin and 0.5 mg/L for levofloxacin and moxifloxacin, levofloxacin may have the best potential to achieve PK/PD targets given our findings (Angeby et al., 2010). In addition, we found that levofloxacin CSF concentrations increased from baseline at both two and 6-h timepoints, supporting previous research that fluoroquinolones may adequately penetrate into the CNS regardless of inflammation (Andes and Craig, 1999; Wilkinson et al., 2017). The increase in CSF concentrations over time may be the result of drug accumulation and changes in the inflammatory state/blood brain barrier. These findings improve confidence that patients receiving fluoroquinolones for TBM can continue to have CSF drug exposure throughout therapy. Interestingly, while coadministration of moxifloxacin with rifampin has been associated with a reduction of moxifloxacin concentrations by approximately 26%–32% due to rifampin's induction of cytochrome P450 enzymes, the present study did not find any statistically significant differences in moxifloxacin exposure (Nijland et al., 2007).

Although carbapenems have shown efficacy in bacterial meningitis and against Mtb in vitro and *in vivo* animal models (Chambers et al., 1995; Hugonnet et al., 2009; Veziris et al., 2011; Kaushik et al., 2015), this study found lower than expected CSF concentrations. While meropenem and imipenem had similar PK profiles to previous literature, median serum Cmax concentrations were below previously reported ranges after a 1-g dose (60–70 mg/L for imipenem and 50–60 mg/L for meropenem) (Zhanel et al., 2007). CSF penetration of

TABLE 4 Pharmacokinetic parameters for fluoroquinolones and carbapenems in participants*.

	Dose (mg)	C_{max} (mg/L)	T_{max} (hr)	K_e (1/Hr)	Half-life (hr)	AUC_{0-24} (Hr*mg/L)
Levofloxacin (n = 20)	750	11.62 (8.64–13.12)	4 (2–5.5)	0.15 (0.12–0.20)	4.79 (3.54–5.97)	94.85 (84.70–127.26)
Moxifloxacin (n = 5)	400	4.04 (2.78–5.34)	2 (1.5–3)	0.14 (0.08–0.16)	4.95 (4.31–8.93)	33.86 (22.21–44.57)
Ofloxacin (n = 7)	800	9.47 (8.67–13.36)	2 (2–2)	0.17 (0.12–0.20)	4.12 (3.52–5.71)	122.4 (101.98–155.68)
Imipenem (n = 11)	1000	20.8 (7.41–37.43)	1.5 (0.5–2)	0.68 (0.50–1.09)	1.02 (0.64–1.40)	65.80 (39.78–144.00)
Meropenem (n = 6)	1000	16.44 (10.00–25.46)	2 (2–2)	0.37 (0.21–0.73)	1.03 (0.95–3.36)	22.91 (0–136.14)

*Data represented as Median (IQR). Some participants had multiple instances of rich sampling, which are included as part of n. C_{max}, maximum concentration of drug; T_{max}, time to achieve maximum drug concentration in serum; K_e, elimination rate constant; AUC_{0-24}, area under the concentration time curve from 0 to 24 h.

TABLE 5 Analysis of increased CSF concentrations and days on treatment for fluoroquinolones.

Drug	CSF concentration	Days on treatment	
		Parameter estimate	*p*-value
Levofloxacin	2-Hour	0.02	0.02*
	6-Hour	0.04	0.002*
Moxifloxacin	2-Hour	−0.0008	0.90
	6-Hour	0.002	0.39
Ofloxacin	2-Hour	0.28	0.04*
	6-Hour	-	-

*Indicates significant value, <0.05. CSF, cerebrospinal fluid. Ofloxacin CSF concentrations at 6 h did not have enough time points to assess concentration over time.

imipenem and meropenem in previously published literature ranged from −16 to 41% of serum for imipenem and −11% for meropenem (Andes and Craig, 1999). In the present study, the majority of imipenem and meropenem CSF concentrations were either undetectable or BLQ. One potential contributor to our unexpected low CSF concentrations is that beta lactams may diffuse from the central nervous compartments to the blood during meningitis due to an increase in CSF pH, facilitating excretion of beta lactams (Nau et al., 2010; Thea and Barza, 1989). However, data suggests that brain tissue concentrations of meropenem may be sufficient, even in non-inflamed brain tissue (Hosmann et al., 2021). Techniques such as cerebral microdialysis or innovative molecular imaging methods are needed for a better understanding of the CNS penetration of carbapenems in the setting of infections such as TBM (Tucker et al., 2018)' (Brunner et al., 2004).

While increased penetration of antimicrobials into the CNS is desired for treatment of TBM, this may be associated with increased risk of CNS-related adverse effects. Previous literature has described adverse CNS effects for fluoroquinolones and carbapenems, potentially due to interferences with gamma-aminobutyric acid receptors (Akahane et al., 1989; Wong et al., 1991; Hikida et al., 1993; Domagala, 1994; Sunagawa et al., 1995; Walton et al., 1997; Kushner et al., 2001; Owens and Ambrose, 2005; Mehlhorn and Brown, 2007; Kalita et al., 2016). Notably, while rate of seizures in patients receiving intravenous imipenem for bacterial meningitis has been reported as high as 33% (Wong et al., 1991), the safety margin is considered to be higher for meropenem (Norrby, 1996). It is promising that in this study, none of the participants experienced seizures.

There are limitations to this study, including a relatively small sample size of 22 patients. Also, due to the descriptive nature of the study, the impact of co-administered medications, renal function, and hepatic function were not controlled for in the analysis. However, expected impact is minimal. While we assumed the CSF samples with undetectable imipenem and meropenem concentrations were due to poor CSF penetration, we could not rule out other causes. The effect of carbapenem instability both before and after sample collection could not be assessed and may have contributed to the low CSF and serum concentrations, even though samples were rapidly stored at −80°C to help minimize degradation. For example, imipenem tested in conjunction with cilastatin only remained 90% stable for 2 h at 37°C or 3 h at 25°C, demonstrating its unstable nature prior to sample freezing (Viaene et al., 2002). With storage at temperatures below −20°C, the data on carbapenem stability is inconclusive (Gravallese et al., 1984; Myers and Blumer, 1984; Garcia-Capdevila et al., 1997). Previous literature suggests that meropenem undergoes

TABLE 6 Carbapenem serum and cerebrospinal fluid concentrations.

Drug	Time from administration to sample collection, h	Participants	CSF samples	CSF drug concentrations BLQ or 0	CSF drug concentration (mcg/ml) (median, IQR)	Serum samples	Serum drug concentrations BLQ or 0	Serum drug concentration (mcg/ml) (median, IQR)	Number of matching samples (excluding BLQ and 0)	Median CSF/serum concentration	Median adjusted CSF/serum concentration
Imipenem	2	11	32	28	0 (0–0)	52	1	8.33 (5.36–15.09)	3	0.47 (0.36–0.48)	0.59 (0.46–0.60)
	6	11	23	21	0 (0–0)	43	39	0 (0–0)	2	1.01 (0.47–1.56)	1.27 (0.59–1.95)
Meropenem	2	6	12	6	0 (0–3.30)	20	0	17.42 (14.82–26.71)	6	0.15 (0.12–0.29)	0.15 (0.13–0.30)
	6	6	9	5	0 (2.54)	15	12	0 (0–0)	4	0 (0–0.42)	0 (0–0.43)

*CSF, cerebrospinal fluid; IQR, interquartile range; BLQ, below limit of quantification.

degradation, even at −20°C, so it is possible unintentional degradation may have occurred during our sample collection, storage, or shipping processes (Gijsen et al., 2021). In addition to these limitations, CSF to serum ratios and PK/PD targets that can improve clinical outcomes in patients with TBM were not ascertained in this study. While these targets are not known, nor their effects on clinical outcomes, it is promising that 21/22 (95%) of participants in our study were able to complete therapy and only 1/22 (5%) had treatment failure. Also, the impact of co-administered medications, renal function, and hepatic function on drug concentrations was not assessed. Finally, the protein content and drug protein binding in CSF are not well established and the assumption of 0% protein binding in the CSF is based on limited data (Bonati et al., 1982; Nau et al., 2010).

In summary, we described fluoroquinolone and carbapenem penetration into the CSF in a cohort of patients treated for TBM. Our study is unique in that serial CSF concentrations were collected at 2 and 6 h over the first few months of TBM treatment, allowing for assessment of delayed penetration. We found that fluoroquinolones showed CSF penetration peaking after serum concentrations, potentially increasing over the duration of treatment. Carbapenems had lower than expected CSF concentrations, with the majority of samples undetectable or BLQ in the CSF while detectable in serum. These findings warrant further exploration with techniques such as cerebral microdialysis to see how carbapenem brain tissue concentrations compare to plasma and CSF concentrations.

Data availability statement

The raw data supporting the conclusions of this article will be made available by the authors, without undue reservation.

Ethics statement

The studies involving human participants were reviewed and approved by National Center for Tuberculosis and Lung Disease, University of Florida, Emory University. The patients/participants provided their written informed consent to participate in this study.

Author contributions

NM performed statistical analysis and led manuscript writing. MA helped with data interpretation and table/figure generation. AS managed/cleaned the dataset prior to analysis. TA and MG participated in data collection and cleaning. TB and SS provided direct care for patients with TB at the National Center for Tuberculosis and Lung Diseases. ZA assisted with study implementation. MK led project implementation and assisted

with data interpretation and logistics. CP oversaw the effort to perform drug concentrations for study patients. RK designed the study, provided input for data collection, and contributed to manuscript writing. All authors reviewed manuscript drafts.

Funding

This work was supported in part by the National Institutes of Health (NIH) including the Fogarty International Center (D43 TW007124) and National Institute of Allergy and Infectious Diseases (R03 AI139871, K23AI103044, TL1TR002382, UL1TR002378, and P30AI168386).

Acknowledgments

The authors are thankful for study participants with tuberculosis meningitis who were willing to participate in the study to contribute meaningful data that may help future patients with the same illness.

Conflict of interest

The authors declare that the research was conducted in the absence of any commercial or financial relationships that could be construed as a potential conflict of interest.

Publisher's note

All claims expressed in this article are solely those of the authors and do not necessarily represent those of their affiliated organizations, or those of the publisher, the editors and the reviewers. Any product that may be evaluated in this article, or claim that may be made by its manufacturer, is not guaranteed or endorsed by the publisher.

References

Akahane, K., Sekiguchi, M., Une, T., and Osada, Y. (1989). Structure-epileptogenicity relationship of quinolones with special reference to their interaction with gamma-aminobutyric acid receptor sites. *Antimicrob. Agents Chemother.* 33 (10), 1704–1708. doi:10.1128/AAC.33.10.1704

Alsultan, A., and Peloquin, C. A. (2014). Therapeutic drug monitoring in the treatment of tuberculosis: An update. *Drugs* 74 (8), 839–854. doi:10.1007/s40265-014-0222-8

Andes, D. R., and Craig, W. A. (1999). Pharmacokinetics and pharmacodynamics of antibiotics in meningitis. *Infect. Dis. Clin. North Am.* 13 (3), 595–618. doi:10.1016/s0891-5520(05)70096-9

Angeby, K. A., Jureen, P., Giske, C. G., Chryssanthou, E., SturEgard, E., NordvallM., et al. (2010). Wild-type MIC distributions of four fluoroquinolones active against *Mycobacterium tuberculosis* in relation to current critical concentrations and available pharmacokinetic and pharmacodynamic data. *J. Antimicrob. Chemother.* 65 (5), 946–952. doi:10.1093/jac/dkq091

Bartzatt, R. (2011). Tuberculosis infections of the central nervous system. *Cent. Nerv. Syst. Agents Med. Chem.* 11 (4), 321–327. doi:10.2174/1871524911106040321

Berning, S. E. (2001). The role of fluoroquinolones in tuberculosis today. *Drugs* 61 (1), 9–18. doi:10.2165/00003495-200161010-00002

Bolon, M. K. (2009). The newer fluoroquinolones. *Infect. Dis. Clin. North Am.* 23 (4), 1027–1051. x. doi:10.1016/j.idc.2009.06.003

Bonati, M., Kanto, J., and Tognoni, G. (1982). Clinical pharmacokinetics of cerebrospinal fluid. *Clin. Pharmacokinet.* 7 (4), 312–335. doi:10.2165/00003088-198207040-00003

Brunner, M., Langer, O., Dobrozemsky, G., Muller, U., Zeitlinger, M., Mitterhauser, M., et al. (2004). [18F]Ciprofloxacin, a new positron emission tomography tracer for noninvasive assessment of the tissue distribution and pharmacokinetics of ciprofloxacin in humans. *Antimicrob. Agents Chemother.* 48 (10), 3850–3857. doi:10.1128/AAC.48.10.3850-3857.2004

Chambers, H. F., Moreau, D., Yajko, D., MiiCk, C., Wagner, C., HaCkbarth, C., et al. (1995). Can penicillins and other beta-lactam antibiotics be used to treat tuberculosis? *Antimicrob. Agents Chemother.* 39 (12), 2620–2624. doi:10.1128/AAC.39.12.2620

Christensen, A. S. H., Roed, C., Omland, L. H., Andersen, P. H., Obel, N., and Andersen, Å. B. (2011). Long-term mortality in patients with tuberculous meningitis: A Danish nationwide cohort study. *PLoS One* 6 (11), e27900. doi:10.1371/journal.pone.0027900

Craig, W. A. (1997). The pharmacology of meropenem, a new carbapenem antibiotic. *Clin. Infect. Dis.* 24, S266–S275. doi:10.1093/clinids/24.supplement_2.s266

de Lange, E. C. M. (2013). Utility of CSF in translational neuroscience. *J. Pharmacokinet. Pharmacodyn.* 40 (3), 315–326. doi:10.1007/s10928-013-9301-9

Dheda, K., Gumbo, T., Maartens, G., Dooley, K. E., McNerney, R., Murray, M., et al. (2017). The epidemiology, pathogenesis, transmission, diagnosis, and management of multidrug-resistant, extensively drug-resistant, and incurable tuberculosis. *Lancet Respir. Med.* 15S2213-2600 (17), 291–360. doi:10.1016/S2213-2600(17)30079-6

Domagala, J. M. (1994). Structure-activity and structure-side-effect relationships for the quinolone antibacterials. *J. Antimicrob. Chemother.* 33 (4), 685–706. doi:10.1093/jac/33.4.685

Donald, P. R. (2010). Cerebrospinal fluid concentrations of antituberculosis agents in adults and children. *Tuberculosis* 90 (5), 279–292. doi:10.1016/j.tube.2010.07.002

Garcia-Capdevila, L., López-Calull, C., Arroyo, C., Moral, M. A., Mangues, M. A., and Bonal, J. (1997). Determination of imipenem in plasma by high-performance liquid chromatography for pharmacokinetic studies in patients. *J. Chromatogr. B Biomed. Sci. Appl.* 692 (1), 127–132. doi:10.1016/s0378-4347(96)00498-7

Ghimire, S., Maharjan, B., Jongedijk, E. M., Kosterink, J. G. W., Ghimire, G. R., Touw, D. J., et al. (2019). Levofloxacin pharmacokinetics, pharmacodynamics and outcome in multidrug-resistant tuberculosis patients. *Eur. Respir. J.* 53 (4), 1802107. doi:10.1183/13993003.02107-2018

Gijsen, M., Filtjens, B., Annaert, P., Armoudjian, Y., Debaveye, Y., Wauters, J., et al. (2021). Meropenem stability in human plasma at -20 °C: Detailed assessment of degradation. *Antibiot. (Basel)* 10 (4), 449. doi:10.3390/antibiotics10040449

Gravallese, D. A., Musson, D. G., Pauliukonis, L. T., and Bayne, W. F. (1984). Determination of imipenem (N-formimidoyl thienamycin) in human plasma and urine by high-performance liquid chromatography, comparison with microbiological methodology and stability. *J. Chromatogr.* 310 (1), 71–84. doi:10.1016/0378-4347(84)80069-9

Heemskerk, A. D., Bang, N. D., Mai, N. T. H., Chau, T. T. H., Phu, N. H., Loc, P. P., et al. (2016). Intensified antituberculosis therapy in adults with tuberculous meningitis. *N. Engl. J. Med.* 374 (2), 124–134. doi:10.1056/NEJMoa1507062

Hikida, M., Masukawa, Y., Nishiki, K., and Inomata, N. (1993). Low neurotoxicity of LJC 10, 627, a novel 1 beta-methyl carbapenem antibiotic: Inhibition of gamma-aminobutyric acidA, benzodiazepine, and glycine receptor binding in relation to lack of central nervous system toxicity in rats. *Antimicrob. Agents Chemother.* 37 (2), 199–202. doi:10.1128/AAC.37.2.199

Hosmann, A., Ritscher, L., Burgmann, H., Al Jalali, V., Wulkersdorfer, B., Wolfl-Duchek, M., et al. (2021). Meropenem concentrations in brain tissue of neurointensive care patients exceed CSF levels. *J. Antimicrob. Chemother.* 76 (11), 2914–2922. doi:10.1093/jac/dkab286

Hugonnet, J. E., Tremblay, L. W., Boshoff, H. I., Barry, C. E., and Blanchard, J. S. (2009). Meropenem-clavulanate is effective against extensively drug-resistant *Mycobacterium tuberculosis*. *Science* 323 (5918), 1215–1218. doi:10.1126/science.1167498

Huynh, J., Donovan, J., Phu, N. H., Nghia, H. D. T., Thuong, N. T. T., and Thwaites, G. E. (2022). Tuberculous meningitis: Progress and remaining questions. *Lancet. Neurol.* 21 (5), 450–464. doi:10.1016/S1474-4422(21)00435-X

Jaganath, D., Lamichhane, G., and Shah, M. (2016). Carbapenems against *Mycobacterium tuberculosis*: A review of the evidence. *Int. J. Tuberc. Lung Dis.* 20 (11), 1436–1447. doi:10.5588/ijtld.16.0498

Janssen Pharmaceuticals, Inc (1996). *Levaquin [package insert]*. Titusville, NJ: Janssen Pharmaceuticals, Inc.

Kalita, J., Bhoi, S. K., Betai, S., and Misra, U. K. (2016). Safety and efficacy of additional levofloxacin in tuberculous meningitis: A randomized controlled pilot study. *Tuberc. (Edinb)* 98, 1–6. doi:10.1016/j.tube.2016.01.004

Kaushik, A., Makkar, N., Pandey, P., Parrish, N., Singh, U., and Lamichhane, G. (2015). Carbapenems and rifampin exhibit synergy against *Mycobacterium tuberculosis* and Mycobacterium abscessus. *Antimicrob. Agents Chemother.* 59 (10), 6561–6567. doi:10.1128/AAC.01158-15

Kempker, R. R., Smith, A. G. C., Avaliani, T., Gujabidze, M., Bakuradze, T., Sabanadze, S., et al. (2022). Cycloserine and linezolid for tuberculosis meningitis: Pharmacokinetic evidence of potential usefulness. *Clin. Infect. Dis.* 29, 682ciab992–689. doi:10.1093/cid/ciab992

Kushner, J. M., Peckman, H. J., and Snyder, C. R. (2001). Seizures associated with fluoroquinolones. *Ann. Pharmacother.* 35 (10), 1194–1198. doi:10.1345/aph.10359

Lamp, K. C., Bailey, E. M., and Rybak, M. J. (1992). Ofloxacin clinical pharmacokinetics. *Clin. Pharmacokinet.* 22 (1), 32–46. doi:10.2165/00003088-199222010-00004

Levison, M. E., and Levison, J. H. (2009). Pharmacokinetics and pharmacodynamics of antibacterial agents. *Infect. Dis. Clin. North Am.* 23 (4), 791–815. vii. doi:10.1016/j.idc.2009.06.008

Litjens, C. H. C., Aarnoutse, R. E., and Te Brake, L. H. M. (2020). Preclinical models to optimize treatment of tuberculous meningitis - a systematic review. *Tuberculosis* 122, 101924. doi:10.1016/j.tube.2020.101924

Mehlhorn, A. J., and Brown, D. A. (2007). Safety concerns with fluoroquinolones. *Ann. Pharmacother.* 41 (11), 1859–1866. doi:10.1345/aph.1K347

Myers, C. M., and Blumer, J. L. (1984). Determination of imipenem and cilastatin in serum by high-pressure liquid chromatography. *Antimicrob. Agents Chemother.* 26 (1), 78–81. doi:10.1128/AAC.26.1.78

Nau, R., Kinzig, M., Dreyhaupt, T., Kolenda, H., Sörgel, F., and Prange, H. W. (1994). Kinetics of ofloxacin and its metabolites in cerebrospinal fluid after a single intravenous infusion of 400 milligrams of ofloxacin. *Antimicrob. Agents Chemother.* 38 (8), 1849–1853. doi:10.1128/AAC.38.8.1849

Nau, R., Sörgel, F., and Eiffert, H. (2010). Penetration of drugs through the blood-cerebrospinal fluid/blood-brain barrier for treatment of central nervous system infections. *Clin. Microbiol. Rev.* 23 (4), 858–883. doi:10.1128/CMR.00007-10

Nijland, H. M. J., Ruslami, R., Suroto, A. J., Burger, D. M., AlisjahBana, B., van Crevel, R., et al. (2007). Rifampicin reduces plasma concentrations of moxifloxacin in patients with tuberculosis. *Clin. Infect. Dis.* 45 (8), 1001–1007. doi:10.1086/521894

Norrby, S. R. (1996). Neurotoxicity of carbapenem antibacterials. *Drug Saf.* 15 (2), 87–90. doi:10.2165/00002018-199615020-00001

Ortho-McNeil-Janssen Pharmaceuticals, Inc (2008). *Ofloxacin [package insert]*. Raritan, NJ: Ortho-McNeil-Janssen Pharmaceuticals, Inc.

Owens, R. C., and Ambrose, P. G. (2005). Antimicrobial safety: Focus on fluoroquinolones. *Clin. Infect. Dis.* 41, S144–S157. doi:10.1086/428055

Pickerill, K. E., Paladino, J. A., and Schentag, J. J. (2000). Comparison of the fluoroquinolones based on pharmacokinetic and pharmacodynamic parameters. *Pharmacotherapy* 20 (4), 417–428. doi:10.1592/phco.20.5.417.35062

Ramachandran, G., Hemanth Kumar, A. K., Srinivasan, R., GeethArAni, A., Sugirda, P., Nandhakumar, B., et al. (2012). Effect of rifampicin & isoniazid on the steady state pharmacokinetics of moxifloxacin. *Indian J. Med. Res.* 136 (6), 979–984.

Roos, K. L. (2000). *Mycobacterium tuberculosis* meningitis and other etiologies of the aseptic meningitis syndrome. *Semin. Neurol.* 20 (3), 329–335. doi:10.1055/s-2000-9428

Salmon-Rousseau, A., Martins, C., Blot, M., Mahy, S., Chavanet, P., Piroth, L., et al. (2020). Comparative review of imipenem/cilastatin versus meropenem. *Med. Mal. Infect.* 50 (4), 316–322. doi:10.1016/j.medmal.2020.01.001

Sharma, S. K., Mohan, A., and Kohli, M. (2021). Extrapulmonary tuberculosis. *Expert Rev. Respir. Med.* 15 (7), 931–948. doi:10.1080/17476348.2021.1927718

Smith, A. G. C., Gujabidze, M., Avaliani, T., Blumberg, H. M., Collins, J. M., Sabanadze, S., et al. (2021). Clinical outcomes among patients with tuberculous meningitis receiving intensified treatment regimens. *Int. J. Tuberc. Lung Dis.* 25 (8), 632–639. doi:10.5588/ijtld.21.0159

Sunagawa, M., Matsumura, H., Sumita, Y., and Nouda, H. (1995). Structural features resulting in convulsive activity of carbapenem compounds: Effect of C-2 side chain. *J. Antibiot.* 48 (5), 408–416. doi:10.7164/antibiotics.48.408

Thea, D., and Barza, M. (1989). Use of antibacterial agents in infections of the central nervous system. *Infect. Dis. Clin. North Am.* 3 (3), 553–570. doi:10.1016/s0891-5520(20)30289-0

Thwaites, G. E., van Toorn, R., and Schoeman, J. (2013). Tuberculous meningitis: More questions, still too few answers. *Lancet. Neurol.* 12 (10), 999–1010. doi:10.1016/S1474-4422(13)70168-6

Tucker, E. W., Guglieri-Lopez, B., Ordonez, A. A., Ritchie, B., Klunk, M. H., Sharma, R., et al. (2018). Noninvasive 11C-rifampin positron emission tomography reveals drug biodistribution in tuberculous meningitis. *Sci. Transl. Med.* 10 (470), eaau0965. doi:10.1126/scitranslmed.aau0965

Turnidge, J. (1999). Pharmacokinetics and pharmacodynamics of fluoroquinolones. *Drugs* 58, 29–36. doi:10.2165/00003495-199958002-00006

van Rijn, S. P., Zuur, M. A., Anthony, R., Wilffert, B., van Altena, R., Akkerman, O. W., et al. (2019). Evaluation of carbapenems for treatment of multi- and extensively drug-resistant *Mycobacterium tuberculosis*. *Antimicrob. Agents Chemother.* 63 (2), E01489-18. doi:10.1128/AAC.01489-18

Veziris, N., Truffot, C., Mainardi, J. L., and Jarlier, V. (2011). Activity of carbapenems combined with clavulanate against murine tuberculosis. *Antimicrob. Agents Chemother.* 55 (6), 2597–2600. doi:10.1128/AAC.01824-10

Viaene, E., Chanteux, H., Servais, H., Mingeot-Leclercq, M. P., and Tulkens, P. M. (2002). Comparative stability studies of antipseudomonal beta-lactams for potential administration through portable elastomeric pumps (home therapy for cystic fibrosis patients) and motor-operated syringes (intensive care units). *Antimicrob. Agents Chemother.* 46 (8), 2327–2332. doi:10.1128/AAC.46.8.2327-2332.2002

Walton, G. D., Hon, J. K., and Mulpur, T. G. (1997). Ofloxacin-induced seizure. *Ann. Pharmacother.* 31 (12), 1475–1477. doi:10.1177/106002809703101206

Wilkinson, R. J., Rohlwink, U., Misra, U. K., van Crevel, R., Mai, N. T. H., Dooley, K. E., et al. (2017). Tuberculous meningitis. *Nat. Rev. Neurol.* 13 (10), 581–598. doi:10.1038/nrneurol.2017.120

Wong, V. K., Wright, H. T., Ross, L. A., Mason, W. H., Inderlied, C. B., and Kim, K. S. (1991). Imipenem/cilastatin treatment of bacterial meningitis in children. *Pediatr. Infect. Dis. J.* 10 (2), 122–125. doi:10.1097/00006454-199102000-00009

World Health Organization (2021). *Global tuberculosis report 2021*. Geneva: World Health Organization. (Accessed June 29, 2022).

Zhanel, G. G., Wiebe, R., Dilay, L., Thomson, K., Rubinstein, E., Hoban, D. J., et al. (2007). Comparative review of the carbapenems. *Drugs* 67 (7), 1027–1052. doi:10.2165/00003495-200767070-00006

frontiers | Frontiers in Pharmacology

TYPE Original Research
PUBLISHED 04 January 2023
DOI 10.3389/fphar.2022.1081123

OPEN ACCESS

EDITED BY
Shashikant Srivastava,
University of Texas at Tyler,
United States

REVIEWED BY
Chiara Resnati,
University of Milan, Italy
Cyprian Onyeji,
University of Nigeria, Nigeria

*CORRESPONDENCE
Tester F. Ashavaid,
dr_tashavaid@hindujahospital.com

†These authors have contributed equally to this work

SPECIALTY SECTION
This article was submitted to Pharmacology of Infectious Diseases, a section of the journal Frontiers in Pharmacology

RECEIVED 26 October 2022
ACCEPTED 12 December 2022
PUBLISHED 04 January 2023

CITATION
Resendiz-Galvan JE, Arora PR, Abdelwahab MT, Udwadia ZF, Rodrigues C, Gupta A, Denti P, Ashavaid TF and Tornheim JA (2023), Pharmacokinetic analysis of linezolid for multidrug resistant tuberculosis at a tertiary care centre in Mumbai, India. *Front. Pharmacol.* 13:1081123. doi: 10.3389/fphar.2022.1081123

Pharmacokinetic analysis of linezolid for multidrug resistant tuberculosis at a tertiary care centre in Mumbai, India

Juan Eduardo Resendiz-Galvan[1†], Prerna R. Arora[2†], Mahmoud Tareq Abdelwahab[1], Zarir F. Udwadia[3], Camilla Rodrigues[2], Amita Gupta[4,5,6], Paolo Denti[1†], Tester F. Ashavaid[2*] and Jeffrey A. Tornheim[4,5,6†]

[1]Division of Clinical Pharmacology, Department of Medicine, University of Cape Town, Cape Town, South Africa, [2]Research Laboratories, P. D. Hinduja National Hospital and Medical Research Centre, Mumbai, India, [3]Division of Respiratory Medicine, P. D. Hinduja National Hospital and Medical Research Centre, Mumbai, India, [4]Center for Infectious Diseases in India, Division of Infectious Diseases, Johns Hopkins University School of Medicine, Baltimore, MD, United States, [5]Center for Tuberculosis Research, Division of Infectious Diseases, Johns Hopkins University School of Medicine, Baltimore, MD, United States, [6]Johns Hopkins Bloomberg School of Public Health, Johns Hopkins University, Baltimore, MD, United States

Linezolid is an oxazolidinone used to treat multidrug-resistant tuberculosis (MDR-TB), including in the recently-endorsed shorter 6-month treatment regimens. Due to its narrow therapeutic index, linezolid is often either dose-adjusted or discontinued due to intolerance or toxicity during treatment, and the optimal balance between linezolid efficacy and toxicity remains unclear. India carries a significant burden of MDR-TB cases in the world, but limited information on the pharmacokinetics of linezolid and minimum inhibitory concentration (MIC) distribution is available from Indian MDR-TB patients. We enrolled participants from a tertiary care centre in Mumbai, India, treated for MDR-TB and receiving linezolid daily doses of 600 or 300 mg. Pharmacokinetic visits were scheduled between 1 and 15 months after treatment initiation to undergo intensive or sparse blood sampling. Linezolid concentration *versus* time data were analysed using non-linear mixed-effects modelling, with simulations to evaluate doses for different scenarios. We enrolled 183 participants (121 females), with a median age of 26 years (interquartile range [IQR] 21–35), weight 55.0 kg (IQR 45.6–65.8), and fat-free mass 38.7 kg (IQR 32.7–46.0). Linezolid pharmacokinetics was best described by a one-compartment model with first-order elimination allometrically scaled by fat-free mass and transit compartment absorption. The typical clearance value was 3.81 L/h. Simulations predicted that treatment with 300 mg daily achieves a high probability of target attainment (PTA) when linezolid MIC was ≤0.25 mg/L (61.5% of participant samples tested), while 600 mg daily would be required if MIC were 0.5 mg/L (29% of samples). While linezolid 300 mg daily is predicted to achieve effective targets for the majority of adults with MDR-TB, it failed to achieve the therapeutic target for 21% participants. A dose of 600 mg had a PTA >90% for all susceptible samples, but with a higher likelihood of exceeding toxicity thresholds (31% vs 9.6%).

These data suggest potential benefit to individualized dosing taking host and microbial characteristics into account to improve the likelihood of treatment efficacy while minimizing risk of toxicity from linezolid for the treatment of MDR-TB. Further prospective evaluation in different clinical settings is urgently needed to inform safety and efficacy of these lower doses.

KEYWORDS

MDR-TB (multidrug resistant-TB), linezolid (LZD), pharmacokinetics, NONMEM modelling, pharmacometrics

Introduction

Multidrug-resistant TB (MDR-TB), defined as tuberculosis caused by *Mycobacterium tuberculosis (Mtb)* isolates resistant to isoniazid and rifampicin, remains a major public health threat. According to the World Health Organization (WHO), India faces one of the highest global burdens of both TB (26%) (World Health Organization, 2020a) and MDR-TB (27%). (World Health Organization, 2020a). Linezolid, an oxazolidinone with demonstrated activity against *Mtb,* is recommended as one of the primary drugs for treatment of MDR-TB in shorter and longer regimens. (Schecter et al., 2010; World Health Organization, 2020b).

Linezolid has a rapid and extensive absorption after oral administration with high bioavailability (~100%). (Qin et al., 2022). Approximately 30% is excreted unchanged through the kidneys, with non-renal clearance accounting for 65% of total clearance, resulting in a terminal half-life of 3.5–7 h. (Macgowan, 2003; Stalker and Jungbluth, 2003). Linezolid works by binding the *Mtb* 23S ribosomal subunit and preventing protein synthesis, (Livermore, 2003), but, unfortunately, it also affects the human mitochondrial 16 S rRNA subunit leading to mitochondrial toxicity, causing dose reductions or interruptions of intended linezolid treatment course. (Wasserman et al., 2016; Conradie et al., 2020). The significant toxicity profile and ongoing uncertainty about optimal linezolid dosing for MDR-TB confounds clinical efforts to balance efficacy, resistance suppression, and adverse events. (Wasserman et al., 2016). Previous studies have proposed a minimum concentration (C_{min}) threshold of 2 mg/L as a marker of adverse effects related to mitochondrial toxicity from linezolid. (Song et al., 2015).

The most widely-used linezolid dose for MDR-TB supported by trial evidence is 600 mg daily, (Conradie et al., 2022), but this frequently is reduced to 300 mg daily because of toxicity, which may fail to achieve the therapeutic target for *Mtb*. (Maartens and Benson, 2015). Previous studies suggest that efficacy is driven by the ratio of the area under the curve of unbound linezolid divided by minimal inhibitory concentration (*f*AUC/MIC), with a target ratio of >100 likely reach an appropriate exposure and minimize toxicity. (Bolhuis et al., 2018). Population-specific pharmacokinetic (PK) models are paramount to ensuring that patients receive the best-possible dosing to achieve the efficacy target. Previous population PK studies of linezolid for MDR-TB have been performed in patients in South Africa, (Garcia-Prats et al., 2019; Abdelwahab et al., 2021; Padmapriyadarsini et al., 2022), Italy, (Tietjen et al., 2022), Brazil, (Alghamdi et al., 2020), United States, (Alghamdi et al., 2020), and China, (Zhou et al., 2022), but despite the global burden, there are limited population PK data from India. Given possible differences in comorbidities, coadministered drugs, diet, and other unmeasured characteristics, we sought to better understand the PK of linezolid in an Indian population. Our study developed a population PK model using linezolid blood levels collected through a cohort study of Indian adolescents and adults with MDR-TB and explored the probability of target attainment (PTA) with daily linezolid treatment at doses of 600 and 300 mg.

Material and methods

Study population

Data were collected through a prospective observational study of adolescents and adults treated for MDR-TB at a tertiary care centre in Mumbai, India that has been described elsewhere. (Udwadia et al., 2019; Tornheim et al., 2020; Tornheim et al., 2022). Briefly, treatment-naïve individuals were enrolled from October 2015-January 2022 at the start of drug susceptibility testing-based personalized 24-month treatment regimens, informed by WHO and national guidelines at a private sector hospital. (World Health Organization, 2020b; Ministry of Health & Family Welfare Government of India, 2021). Participants were followed longitudinally with clinical characteristics, laboratory and imaging results, side effects, and treatment outcomes recorded throughout participation. Adult participants provided written informed consent prior to enrolment and 15–18-year-old participants provided written informed assent with written informed consent for participation provided by their legal guardians. For participants treated with linezolid, an initial dose of 600 mg daily was prescribed, but was reduced to 300 mg daily for those with linezolid-associated toxicity (either peripheral neuropathy, anaemia with haemoglobin <10 g/dl, thrombocytopenia <100,000/μL, or leukopenia with <1,000 neutrophils/μl). Participants at higher

risk of toxicity due to malnutrition, underweight, or neuropathy-associated comorbidities like diabetes and alcohol use were started at lower doses of 300 mg daily. This study was approved by the institutional review boards at the P.D. Hinduja National Hospital and Medical Research Centre ("Hinduja Hospital", IRB00012235) and the Johns Hopkins University School of Medicine (IRB00076738, IRB00012235).

Data collection

Study participants provided blood samples for PK analysis at 1, 2, 6, and 12 months after the treatment initiation, with blood samples collected before and 2 h after observed daily linezolid doses. A random subset of participants provided additional consent for collection of intensive PK sampling at the first or second month time points, with blood collection before and 1, 2, 4, 6, and 8 h after observed daily linezolid doses. Due to the COVID-19 pandemic and associated rescheduling of participant visits, sparse sampling was accepted through the 15th month of MDR-TB treatment and intensive sampling was accepted through the fourth month of MDR-TB treatment.

Isolates collected from participants with culture-positive MDR-TB were submitted for minimum inhibitory concentration (MIC) testing using custom Sensititre plates manufactured by ThermoFisher. Isolates were cultured on Löwenstein–Jensen media and evaluated weekly by laboratory staff until late-log phase growth, at which time they were agitated in saline tween before inoculation into Sensititre plates by a Thermo Scientific AIM autoinoculator. Isolates were tested at linezolid concentrations of 0.12, 0.25, 0.5, 1, 2, 4, and 8 mg/L, which were quality-controlled using two drug-free control wells on each plate and parallel testing of the H37Rv laboratory strain on an identical plate with each batch to confirm expected results. Plates were read using a mirror box on 10-, 14-, 21-, and 28-day following inoculation by two independent readers to ensure concordance, with the final value selected as the first date with adequate growth in both wells. When the two readers reported discordant values, a third independent reader adjudicated the final result.

Linezolid concentrations were measured at the Hinduja Hospital laboratory. Blood samples were collected without anticoagulants and centrifugated at 3,000 rpm for 10 min. Serum was then collected, aliquoted, and stored at -80°C until analysis, depending on laboratory schedule. Quantification employed a commercially available enzyme immunoassay (ARK™ Linezolid Assay) according to manufacturer's instructions with a calibration range of 0.75–30 mg/L, limit of quantification (LOQ) of 0.75 mg/L, limit of detection (LOD) of 0.071 mg/L, and tri-level controls. Samples with concentrations >30 mg/L were assayed by dilution with the corresponding zero calibrator and estimated using the dilution factor.

Model building and analysis

Linezolid serum concentration-versus-time data were analysed using the non-linear mixed-effect model software NONMEM v7.4 (ICON Development Solutions, Hanover, MD, United States) (Beal et al., 2013) and the algorithm first-order conditional estimation with ε-η interaction (FOCE INTER). Graphical diagnostics, managing and organization of the models were handled using Perl-speaks-NONMEM, Xpose4 (Jonsson and Karlsson, 1998) embedded in R, and Pirana (Certara, Princeton, NJ, United States), (Keizer et al., 2013), respectively.

The overall strategy for model development started with only intensively sampled data. Once the model satisfactorily described the intensively sampled data, the sparse sampling data were added for parameter reassessment and additional covariate testing using the complete dataset. One- and two-compartments disposition models, linear and non-linear elimination kinetics, first-order absorption (with and without lag), and transit compartments (Savic et al., 2007) were investigated to determine the best structural model. Random effects were included as between-subject variability (BSV) on all disposition parameters and between-occasion variability (BOV) (Karlsson and Sheiner, 1993) for absorption parameters, assuming a lognormal distribution. Non-observed doses and pre-dose concentrations were considered independent occasions from observed doses (during sample collection) and subsequent concentrations. Residual unexplained variability (RUV) was modelled testing both additive and proportional components, with the additive component bound to ≥20% of the LOQ. All concentration values above the LOD, including those below the LOQ (BLQ), were included in the model as actual values measured, similar to the published "all data" method. (Keizer et al., 2015). Concentrations below the LOD (BLD) were censored by the laboratory, and incorporated in the model by adapting the M6 method. (Beal, 2001). Briefly, BLD concentrations were imputed as LOD/2 (0.0355 mg/L) and the additive component of RUV was inflated by LOD/2 to acknowledge the extra uncertainty and compensate for the effect of imputation. If a series of consecutive BLD concentrations was present, only one value was included in the model, the last one if in the absorption phase and the first one in the elimination phase, while additional BLD concentrations were excluded for parameter estimation and retained for simulation-based diagnostics.

Allometric scaling was evaluated on disposition parameters using total body weight and fat-free mass (FFM). (Anderson and Holford, 2008). Continuous covariates included in model assessments were age, serum creatinine, Cockcroft-Gault creatinine clearance estimates, (Cockcroft and Gault, 1976), and days on linezolid treatment. Categorical covariates assessed included participant sex and

TABLE 1 Characteristics of the study population.

Variable (units)	Intensive sampling n = 48	Sparse sampling n = 182
Age (years)	26 (21–32)	26 (21–35)
Females (n)	32 (66.7)	121 (66.5)
Weight (kg)	56.0 (46.0–66.1)	54.8 (45.4–65.8)
Height (m)	1.58 (1.51–1.66)	1.59 (1.53–1.68)
Fat-free mass (kg)	39.5 (33.1–46.5)	38.5 (32.7–45.8)
Serum creatinine (mg/L)	0.7 (0.6–0.8)	0.70 (0.6–0.8)
HIV positive (n)	2 (4.2)	3 (1.6)

[a]Data presented as median (interquartile range) or number (percent).
No significant differences were identified between the two sampling groups for categorical or continuous covariates evaluated with the Fisher's exact test (Sprent 2011) and the Wilcoxon signed rank test, respectively.

additional drugs prescribed. Differences in covariate distributions between participants with intensive and sparse data were evaluated by the Fisher's exact and Wilcoxon signed rank tests for categorical and continuous variables, respectively, with $p < 0.05$ considered to indicate between-group differences. Covariate relationships were screened and evaluated based on physiological plausibility and improvement in model diagnostics (including goodness of fit plots and visual predictive checks) using a stepwise approach. Forward inclusion of covariates required NONMEM objective function value (ΔOFV) reduction of ≥3.84 for inclusion of one degree of freedom ($p < 0.05$), followed by backward elimination with a ΔOFV≥6.63 ($p < 0.01$) for retention of one degree of freedom. Uncertainty in final model parameter estimates was quantified using the sampling importance resampling method. (Dosne et al., 2017).

Simulations

Monte Carlo simulations were performed using final model parameter estimates to evaluate the PTA defined as the percentage of simulated individuals above the exposure targets. A minimum concentration (C_{min}) > 2 mg/L was employed as the threshold for increased risk of mitochondrial and haematological toxicity. (Song et al., 2015). The pharmacokinetic-pharmacodynamic (PK-PD) index for efficacy to estimate the PTA was $fAUC_{0\text{-}24}/MIC \geq 100$. (Bolhuis et al., 2018). The $fAUC$ was estimated considering an unbound fraction of 70%. (Qin et al., 2022). Exposure was estimated with doses of 300 and 600 mg once daily using an *in silico* population created by repetition of demographic characteristics from participants with drug-susceptible or MDR-TB from previous studies. (Diacon et al., 2007; Wilkins et al., 2008; Pepper et al., 2010; Chigutsa et al., 2011; McIlleron et al., 2012; Smythe, 2016; Chirehwa et al., 2019).

Results

Demographics and clinical profile

Data were available for 183 participants, 121 of whom were female, with median age of 26 years (interquartile range, IQR: 21–35), weight 55 kg (IQR: 45–66), and FFM 39 kg (IQR: 33–46), respectively. Five participants were HIV positive. In addition to linezolid, susceptibility-guided multidrug MDR-TB treatment regimens taken at the time of PK sampling. These included coadministration of moxifloxacin (91% of participants), cycloserine (86%), clofazimine (81%), pyrazinamide (44%), ethambutol (39%), kanamycin (27%), para-aminosalicylic acid (27%), bedaquiline (25%), and ethionamide (23%). Table 1 shows the study population's baseline characteristics, which were not significantly different between participants with intensive and sparse sampling data.

Intensive and sparse blood sampling was performed in 48 participants from 1 to 4 months and from 1 to 15 months after treatment initiation, respectively. Intensive sampling was most frequently performed at 2 months (36 participants, 75%), followed by 1 month (9 participants, 19%) after treatment initiation. This comprised a total of 1,181 linezolid measurements, 288 from intensive and 893 from sparse sampling, and included 74 BLQ and 123 BLD values. Treatment duration and the schedule of the PK visits for each participant is demonstrated in Figure 1. Most participants were initially prescribed 600 mg daily, but a large proportion (75%) were dose-reduced to 300 mg daily due to toxicity by the time of intensive PK (Figure 1). This represents a median time to dose reduction of 69 days (IQR: 63–74). Most PK visits assessed doses of 300 mg (89, 50.3%) or 600 mg daily (86, 48.6%), while a minority (2 visits) assessed linezolid at 300 mg dosed every other day. Of 166 cultured isolates, 11 (6.5%) demonstrated MICs above the critical concentration of 1 mg/L. Among susceptible isolates, we found five to have an MIC of 1 mg/L (3% of all samples), 48 to have an MIC of 0.5 mg/L (29%), 61 to

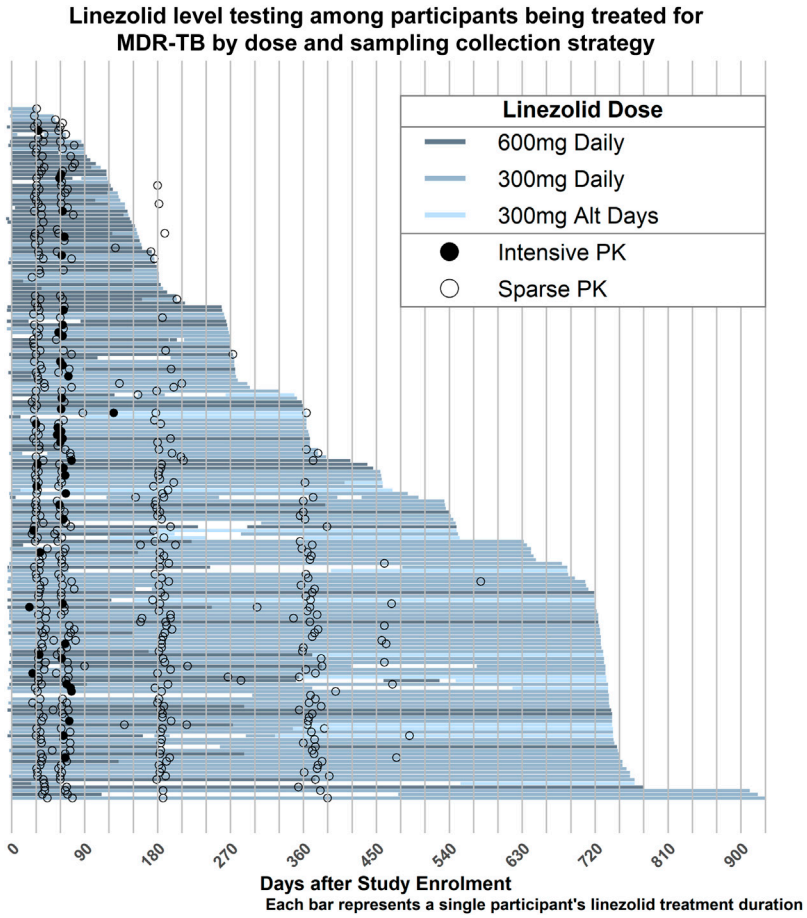

FIGURE 1
Duration of linezolid treatment. Each horizontal line represents a single participant, with the colour coding denoting the dose of linezolid prescribed over that time period. Most participants were treated for 24-month, though dose adjustments frequently occurred due to treatment-associated toxicity. Filled circles indicate intensive sampling visits and open circles indicate sparse sampling visits.

have an MIC of 0.25 mg/L (36.5%), and 41 to have MICs <0.25 mg/L (25%).

Population pharmacokinetic model

Linezolid PK was best described by a one-compartment disposition model with first-order elimination and first-order absorption including a chain of transit compartments. The final PK parameters are presented in Table 2 and a visual predictive check stratified by type of data (intensive and sparse sampling) in Figure 2, showing an adequate interpretation of the observations by the final model. Allometric scaling using FFM best described the effect of body size (ΔOFV 15.6) on the disposition parameters and provided a better fit than using total body weight (ΔOFV 8.57). The model estimated the typical PK parameters for a participant with FFM 39.5 kg; clearance was 3.81 L/h and volume of distribution 31.2 L. Creatinine clearance, serum creatinine, age, and coadministration of linezolid with other TB drugs did not show statistically significant associations with model-derived PK parameters. Pre-dose concentrations were observed to be more variable and more poorly predicted than concentrations measured after observed doses administered at the clinic. To account for this larger variability, we tested the inclusion of a factor increasing the between-occasion variability for all absorption parameters following unobserved doses taken at home. This significantly improved the model fit (ΔOFV = 36.7, 1 degree of freedom, $p < 0.001$).

Probability of target attainment

Considering a target of $fAUC_{0\text{-}24}$/MIC ≥100, the PTA for a linezolid dose of 600 mg once daily was >99% against samples with linezolid MICs ≤0.25 mg/L (61.5% of isolates tested in this study), 97% for MIC = 0.5 mg/L (29% of isolates), 60% when

TABLE 2 Final population pharmacokinetic parameters.

Parameter	Typical value (95% CI[a])	Variability[b] (95% CI[a])
Clearance (L/h)[c]	3.81 (3.41—4.25)	BSV: 31.9 (23.4—42.4)
Volume of distribution (L)[c]	31.2 (29.3—33.4)	
Absorption rate constant (1/h)	2.31 (1.89—4.32)	BOV: 104 (82.0—108)
Mean transit time (h)	0.666 (0.481—0.884)	BOV: 80.5 (62.7—105)
Number of transit compartments (n)	20.5 (12.7—34.9)	
Bioavailability	1 FIXED	BOV: 18.4 (10.1—24.4)
Variability factor for unobserved doses[d] (-fold change)	1.86 (1.44—1.15)	
Proportional error (%)	5.24 (3.54—6.97)	
Additive error (mg/L)	0.362 (0.271—0.473)	

BSV, Between-subject variability; BOV, Between-occasion variability.
[a]Sampling importance resampling (SIR) was used to obtain the 95% Confidence interval (CI).
[b]The unobserved dose factor was considered for the administration of unobserved doses (e.g., doses taken at home on days prior to blood sampling) and consequently the impact on the pre-dose concentration quantified with an extra parameter. This extra variability accounts for absorption rate constant, mean transit time, and bioavailability.
[c]Allometric scaling was used to estimate clearance and volume of distribution for the typical patient with a fat-free mass of 39.5 kg.
[d]BSV, and BOV, were assumed to be log-normally distributed and reported as approximate (%CV).

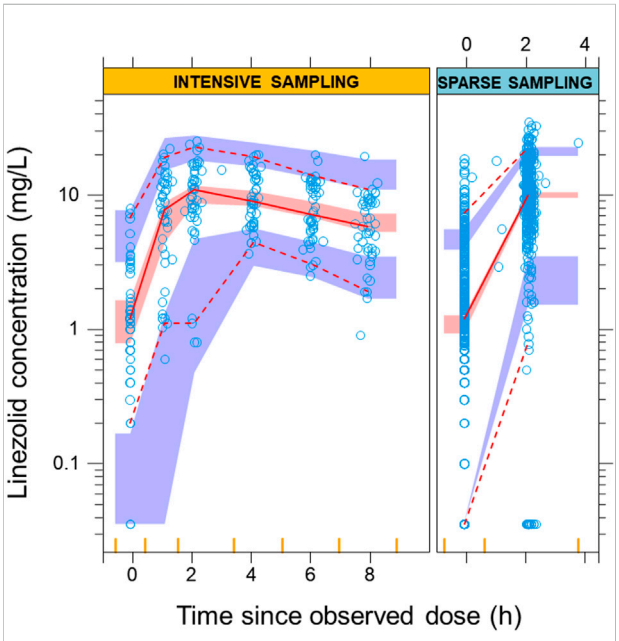

FIGURE 2
Visual predictive check from the final model. The solid and dashed lines correspond to the fifth, 50th, and 95th percentiles from the original observations (blue circles), while the shaded areas represent the 95% confidence intervals for the same percentiles of the model predictions. The left panel shows the intensive data with sampling points from pre-dose up to 8 h post-dose. The right panel shows the predictions for the sparse observations at pre-dose and 2 h post-dose The bins for sampling points are showed as vertical yellow lines on the *x*-axis.

MIC is 1 mg/L (3% of isolates), and <8% when MIC is > 1 mg/L (6.5% of isolates). The PTA for linezolid at a dose of 300 mg once daily was >97% for samples with linezolid MICs ≤0.25 mg/L, but only 60% for samples with MIC of 0.5 mg/L, 8% for samples with MIC of 1 mg/L, and <1% for samples with MIC >1 mg/L (Figure 3). When our model was applied to the total population of study participants with the MIC results for their own isolates, this corresponds to probabilities of 90% and 79% that participants would achieve their expected target at doses of 600 and 300 mg daily, respectively. Regarding the toxicity thresholds, 31% and 9.6% of the simulated patients exceeded a C_{min} of 2 mg/L with 600 and 300 mg, respectively.

Discussion

In this study, we describe the population PK of linezolid in a cohort of Indian adults and adolescents treated for MDR-TB and evaluate dosing strategies to balance treatment efficacy and toxicity. We found that while 300 mg daily is expected to be effective against strains with MICs 0.25 mg/L or lower, 600 mg daily may be more appropriate for MIC levels of 0.5–1 mg/L, albeit with a higher likelihood of treatment-associated toxicity.

Our PK model identified one-compartment disposition with first-order elimination, and first-order absorption with transit compartments. This is consistent with previous studies on linezolid PK, which have primarily employed similar one-compartment models for both drug-susceptible TB and MDR-TB. (Alghamdi et al., 2020; Abdelwahab et al., 2021; Tietjen et al., 2022). Other studies have reported two-compartment disposition with Michaelis-Menten elimination when linezolid is dosed at 1,200 mg daily, (Imperial et al., 2022), or linezolid inhibiting its own clearance with repeated administration. (Plock et al., 2007; Mockeliunas et al., 2022). In our data, testing two-compartments disposition and saturation did not improve model fit, possibly

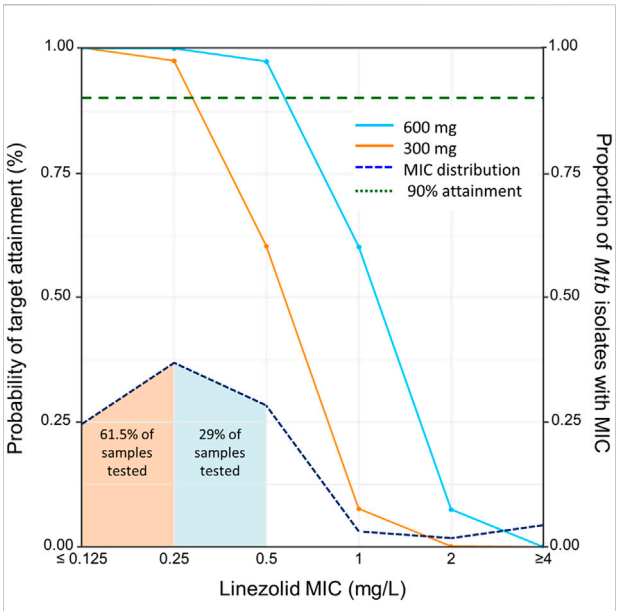

FIGURE 3
Probability of target attainment by dose and minimum inhibitory concentration. Solid lines indicate the probability of target attainment (PTA) on the primary *y*-axis (on left) based on area under the curve of unbound linezolid divided by MIC (*f*AUC/MIC), adjusting for the linezolid minimum inhibitory concentration (MIC) on the *X*-axis. Lines indicate simulated doses of 600 mg once daily (blue solid line) and 300 mg once daily (orange solid line). The horizontal dashed green line indicates the 90% of attainment when *f*AUC/MIC ≥100. The dot-dashed line indicates the distribution of linezolid MIC of *Mycobacterium tuberculosis* isolates cultured from 166 study participants, with the proportion of all tested isolates with each MIC indicated on the secondary *y*-axis (on right). The shaded area under the dot-dashed line indicates the proportion of tested samples with the corresponding MIC (color indicates that of the lowest dose with PTA >90% for that MIC).

due to differences in the sampling schedule and the fact that non-linear kinetics may not be evident at the lower doses prescribed to participants in our study. Due to the limitations of our overall study design, it was not possible to meaningfully evaluate autoinhibition, since that would require PK data from the first days of linezolid administration.

Interestingly, reports for linezolid PK in different populations show different values of clearance. The typical clearance estimated in our population, 3.81 L/h, is similar to the clearance of 3.57 l/h reported in South African patients from two separate clinical trials. (Abdelwahab et al., 2021). Higher clearance has been reported in other publications. For example, clearance was found to be 6.06 l/h in study participants from Brazil and the USA, (Alghamdi et al., 2020), 7.69 l/h in an Italian population, (Tietjen et al., 2022), and 4.59 l/h in a Chinese population. (Zhou et al., 2022). While part of the difference could be ascribed to the larger weight of the participants in the other cohorts, who were slightly heavier than those in our study and in South African studies, the difference persisted despite allometric scaling in our model. Other differences between studies that could have accounted for the variability in the parameters are the linezolid dose ranging from 300 to 600 mg once or twice daily, and the prolonged time on treatment for participants in this study. However, we did not find a significant effect of these covariates in the final model. New evidence has shown that linezolid is mainly metabolized to its inactive metabolites in the liver through oxidation of the morpholine ring by distinct isoforms CYP2J2, CYP4F2, and CYP1B1 of the Cytochrome P450 enzyme family. (Obach, 2022). This could also contribute to differences in linezolid metabolism based on differences in allele distribution frequencies between distinct populations. However, the presence of polymorphisms on these enzymes and their influence on linezolid metabolism needs to be evaluated in future studies. Importantly, we found high between-subject variability for clearance and between-occasion variability for absorption process within the Indian population studied in this cohort, suggesting a potential role for therapeutic drug monitoring to optimize linezolid treatment, though PK laboratory capacity is limited, particularly in high incidence settings.

According to our simulations, 300 mg daily would achieve a *f*AUC/MIC ≥100 in at least 97% of the simulated individuals when the MIC is ≤ 0.25 mg/L, while a dose of 600 mg daily would be more suitable for isolates with higher MICs. This dosing suggestion is similar to the one published for the South African cohort participants, (Abdelwahab et al., 2021), while higher doses have been proposed in studies finding higher clearance values. (Alghamdi et al., 2020; Mockeliunas et al., 2022). It is also important to highlight that the MIC distribution may vary between countries, and indeed we report lower MICs in this study than reported in South Africa. (Abdelwahab et al., 2021). From a toxicity perspective, our simulations suggest that 31% of people receiving 600 mg daily would exceed the literature-derived C_{min} threshold of 2 mg/L, (Song et al., 2015), compared to 9.6% of those receiving 300 mg daily While more data are needed to confirm the predictive value of this threshold for clinical application, particularly as competing toxicity thresholds are considered, (Wasserman et al., 2019a), the high proportion of people affected at either dose and the large between-subject variability we observed offers an argument in support of individualized therapy that considers clinical features such as fat-free mass and the extent of microbiological resistance to better identify the 31% at risk of toxicity as well as to ensure efficacy among those given lower or less frequent doses.

As TB control programs worldwide move to adopt linezolid-based treatments for MDR-TB, (Padmapriyadarsini et al., 2022; World Health Organization, 2022), it will be important to recognize that despite evidence of resistance in high-burden settings, (Tornheim et al., 2020), the majority of such treatment is prescribed in the absence of susceptibility testing for linezolid, let alone MIC testing. While infrequently discussed in the literature and rarely tested in clinical practice, linezolid

resistance is identified with increasing frequency in high-burden settings where testing is performed. Previously considered to be rare, (Bharadwaj, 2021), resistance was noted to affect 1% of isolates tested in Mumbai, India in 2017, (Tornheim et al., 2017), with more recent publications documenting resistance among 6.7%, (Tornheim et al., 2020), similar to rates documented in China (6.9%). (Du et al., 2021). Among South African patients with MDR-TB and treatment failure, linezolid resistance has been reported among 33% of isolates. (Wasserman et al., 2019b). Given the increasing prescription of linezolid in shorter regimens with bedaquiline and pretomanid, with or without moxifloxacin, (World Health Organization, 2022), increased vigilance for emerging linezolid resistance is crucial to secure the success of TB elimination programs. (Bharadwaj, 2021).

Because the efficacy target for linezolid is normalized to MIC, improving local knowledge of drug resistance and MICs can help TB providers determine the MIC distributions to target with different linezolid dosing strategies, with or without assistance from PK models such as this one. Given the WHO-endorsed critical concentration of 1 mg/L, (World Health Organization, 2018), in the absence of local MIC knowledge, a dose of 600 mg would ensure a PTA ≥97% against MICs ≤0.5 mg/L, and which represented 90.5% of isolates in this study. This finding supports the results of the recently published ZeNIX trial demonstrating improved efficacy and toxicity of a 600 mg daily dose compared to other dosing strategies. (Conradie et al., 2022). While the use of higher doses such as 1,200 mg daily in the NIX-TB study may increase drug exposure, (Conradie et al., 2020), the high rates of toxicity-associated linezolid dose reduction or treatment interruption during 6 months of therapy (85%) leaves much room for improvement. Similarly, a dose of 600 mg twice-daily achieves a target attainment of 100% in simulation studies, but with >99% of the simulated individuals exceeding the safety levels. (Millard et al., 2018).

Our study had several limitations. This relatively small, single-site study may not be generalizable to non-Indian populations, populations with different rates of comorbid diseases such as HIV, diabetes, or malnutrition that affect absorption, children, or those with drug-susceptible tuberculosis with different concomitant treatments. Due to the small number of participants coinfected with HIV, we could not assess drug-drug interactions with antiretroviral therapy, which is an important factor that may influence the treatment in people living with HIV. Given that the majority of MDR-TB globally is not associated with HIV, however, our data are relevant to a large proportion of global cases. Additionally, model development was better informed by intensive than sparse PK data, which is easier to obtain in clinical settings, but is simultaneously less-informative because parameters estimation relies on a reduced number of observations within a dosing interval. For this reason, model building and assessment of PK parameters relied in an initial stage only on the intensive data, which was available for only 26% of participants. Additionally, the pre-dose concentrations from both intensive and sparse data were affected by larger variability than post-dose concentrations, likely due to self-reported dosing history. We tried to mitigate the effect of this uncertain information by allowing larger between-occasion variability for absorption parameters and bioavailability in the final model. As shown in the final visual predictive check, the model prioritized intensive data, but still described sparse data adequately. Finally, this non-interventional cohort study assessed the extent to which participants achieved literature-derived efficacy and toxicity targets. Future studies will need to evaluate the impact of model-derived treatment decisions on improved treatment outcomes and frequency of treatment-associated side effects.

Conclusion

To the best of our knowledge, this is the first PK model for linezolid developed in a population of Indian patients with MDR-TB. We report values of clearance similar to those reported in South African patients. These results suggest that while linezolid dosed at 300 mg daily may be effective against isolates with MICs ≤0.25 mg/L, a dose of 600 mg is more likely to achieve the efficacy target for isolates with higher or unknown MICs and improved the PTA from 60% to 97% against such isolates, representing nearly a third of samples tested in this study. The high variability in multiple important PK parameters demonstrates a role for model-based, individualized therapy to optimize linezolid exposure. Additional prospective studies are needed to confirm these findings and evaluate their role in improving both efficacy and toxicity thresholds in clinical settings.

Data availability statement

The raw data supporting the conclusion of this article will be made available by the authors, without undue reservation.

Ethics statement

The studies involving human participants were reviewed and approved by the P. D. Hinduja National Hospital and Medical Research Centre and the Johns Hopkins University School of Medicine. Adult participants provided written informed consent prior to enrolment and 15–18-year-old participants provided written informed assent with written informed consent for participation provided by their legal guardians.

Author contributions

JER-G, MTA, and PD contributed to PK data analysis and manuscript preparation. PRA, ZFU, CR, and TFA supervised study design, data collection, data analysis and interpretation,

and manuscript preparation. AG contributed to study design, data interpretation, and manuscript preparation. JAT contributed to the study design, data analysis and interpretation, and manuscript preparation. All authors contributed to the article and approved the submitted version.

Funding

This publication was made possible by support from the P. D. Hinduja Hospital and Medical Research Centre (PDHNH) (established and managed by National Health and Education Society) and the NIH/DBT RePORT India Consortium with funding in whole or in part from the Government of India's (GOI) Department of Biotechnology (DBT), Department of Science and Technology (DST), the United States National Institutes of Health (NIH), National Institute of Allergy and Infectious Diseases (NIAID), Office of AIDS Research (OAR), and distributed in part by CRDF Global. Participant recruitment and retention for the primary cohort was supported by the National Health and Education Society (P. D. Hinduja Hospital and MRC, Mumbai, India). Sample processing and pharmacokinetic analysis was supported by the DBT India and DST India (BT/PR24492/MED/29/1219/2017 and DST/INT/SOUTH AFRICA/P-24/2017 to TA), a joint DBT-South African Medical Research Council (MRC) Indo-South Africa collaboration. JT and associated MIC work was supported by NIH/NIAID (K23AI135102, R21AI122922, and R01AI134430), and the NIH/Fogarty Global Health Fellows Program Consortium (R25TW009340). MA was supported by the NIH/Fogarty International Center (D43TW010559).

Acknowledgments

The authors would like to thank the study participants for their contributions to this research and Beckman Coulter, BD Diagnostics and Abbott India for providing us partial consumables support. Computational analyses were performed using facilities provided by the University of Cape Town's ICTS High Performance Computing team (http://hpc.uct.ac.za). The MDR-TB MUKT Study Team: Lancelot M. Pinto, Ashok A. Mahashur, Jai B. Mullerpattan, Ayesha Sunavala, Jignesh Patel, Bhamini Keny, Alpa J. Dherai, Ishita Gajjar, Heeral Pandya, and Utkarsha Surve. The Indo-South Africa Study Team: Neil A Martinson, Ebrahim Variava, Firdaus Nabeemeeah.

Conflict of interest

The authors declare that the research was conducted in the absence of any commercial or financial relationships that could be construed as a potential conflict of interest.

Publisher's note

References

Abdelwahab, M. T., Wasserman, S., Brust, J. C. M., et al. (2021). Linezolid population pharmacokinetics in South African adults with drug-resistant tuberculosis. *Antimicrob. Agents Chemother.* 65 (12), e0138121. Published online. doi:10.1128/AAC.01381-21

Alghamdi, W. A., Al-Shaer, M. H., An, G., Alsultan, A., Kipiani, M., Barbakadze, K., et al. (2020). Population pharmacokinetics of linezolid in tuberculosis patients: Dosing regimen simulation and target attainment analysis. *Antimicrob. Agents Chemother.* 64 (10), 011744–e1220. doi:10.1128/AAC.01174-20

Anderson, B. J., and Holford, N. H. G. (2008). Mechanism-based concepts of size and maturity in pharmacokinetics. *Annu. Rev. Pharmacol. Toxicol.* 59 (2), 303–332. doi:10.1146/annurev.pharmtox.48.113006.094708

Beal, S. L., Sheiner, L. B., Boeckmann, A. J., and Bauer, R. J. (2013). *NONMEM users' guides (1989–2013).* Hanover, MD: ICON Development Solutions.

Beal, S. L. (2001). Ways to fit a PK model with some data below the quantification limit. *J. Pharmacokinet. Pharmacodyn.* 28 (5), 481–504. doi:10.1023/A:1012299115260

Bharadwaj, R. (2021). Linezolid-resistant mycobacterium tuberculosis: Will it impact the tuberculosis elimination programme? *Indian J. Med. Res. Suppl.* 154 (1), 16–18. doi:10.4103/IJMR.IJMR_3537_20

Bolhuis, M. S., Akkerman, O. W., Sturkenboom, M. G. G., Ghimire, S., Srivastava, S., Gumbo, T., et al. (2018). Linezolid-based regimens for multidrug-resistant tuberculosis (TB): A systematic review to establish or revise the current recommended dose for TB treatment. *Clin. Infect. Dis.* 67, S327–S335. doi:10.1093/cid/ciy625

Chigutsa, E., Visser, M. E., Swart, E. C., Denti, P., Pushpakom, S., Egan, D., et al. (2011). The SLCO1B1 rs4149032 polymorphism is highly prevalent in South Africans and is associated with reduced rifampin concentrations: Dosing implications. *Antimicrob. Agents Chemother.* 55 (9), 4122–4127. doi:10.1128/AAC.01833-10

Chirehwa, M. T., McIlleron, H., Wiesner, L., Affolabi, D., Bah-Sow, O., Merle, C., et al. (2019). Effect of efavirenz-based antiretroviral therapy and high-dose rifampicin on the pharmacokinetics of isoniazid and acetyl-isoniazid. *J. Antimicrob. Chemother.* 74 (1), 139–148. doi:10.1093/jac/dky378

Cockcroft, D. W., and Gault, M. H. (1976). Prediction of creatinine clearance from serum creatinine. *Nephron* 16 (1), 31–41. doi:10.1159/000180580

Conradie, F., Bagdasaryan, T. R., Borisov, S., Howell, P., Mikiashvili, L., Ngubane, N., et al. (2022). Bedaquiline–pretomanid–linezolid regimens for drug-resistant tuberculosis. *N. Engl. J. Med.* 387 (9), 810–823. doi:10.1056/NEJMoa2119430

Conradie, F., Diacon, A. H., Ngubane, N., Howell, P., Everitt, D., Crook, A. M., et al. (2020). Treatment of highly drug-resistant pulmonary tuberculosis. *N. Engl. J. Med.* 382 (10), 893–902. doi:10.1056/NEJMoa1901814

Diacon, A. H., Patientia, R. F., Venter, A., Smith, P. J., McIlleron, H., et al. (2007). Early bactericidal activity of high-dose rifampin in patients with pulmonary tuberculosis evidenced by positive sputum smears. *Antimicrob. Agents Chemother.* 51 (8), 2994–2996. doi:10.1128/aac.01474-06

Dosne, A. G., Martin, B., and Karlsson, M. O. (2017). An automated sampling importance resampling procedure for estimating parameter uncertainty. *J. Pharmacokinet. Pharmacodyn.* 44, 509–520. doi:10.1007/s10928-017-9542-0

Du, J., Gao, J., Yu, Y., Bai, G., Shu, W., Gao, M., et al. (2021). Low rate of acquired linezolid resistance in multidrug-resistant tuberculosis treated with bedaquiline-linezolid combination. *Front. Microbiol.* 12, 1014. doi:10.3389/fmicb.2021.655653

Garcia-Prats, I. D. A. J., Simon Schaaf, H., Draper, H. R., et al. (2019). Pharmacokinetics, optimal dosing, and safety of linezolid in children with multidrug-resistant tuberculosis: Combined data from two prospective observational studies. *PLoS Med.* 16 (4), e1002789. Published online. doi:10.1371/journal.pmed.1002789

Imperial, M. Z., Nedelman, J. R., Conradie, F., and Savic, R. M. (2022). Proposed linezolid dosing strategies to minimize adverse events for treatment of extensively drug-resistant tuberculosis. *Clin. Infect. Dis.* 74 (10), 1736–1747. doi:10.1093/cid/ciab699

Jonsson, E. N., and Karlsson, M. O. (1998). Xpose - an S-PLUS based population pharmacokinetic/pharmacodynamic model building aid for NONMEM. *Comput. Methods Programs Biomed.* 58 (1), 51–64. doi:10.1016/S0169-2607(98)00067-4

Karlsson, M. O., and Sheiner, L. B. (1993). The importance of modeling interoccasion variability in population pharmacokinetic analyses. *J. Pharmacokinet. Biopharm.* 21 (6), 735–750. doi:10.1007/BF01113502

Keizer, R. J., Jansen, R. S., Rosing, H., Thijssen, B., Beijnen, J. H., Schellens, J. H. M., et al. (2015). Incorporation of concentration data below the limit of quantification in population pharmacokinetic analyses. *Pharmacol. Res. Perspect.* 3 (2), e00131. doi:10.1002/prp2.131

Keizer, R. J., Karlsson, M. O., and Hooker, A. (2013). Modeling and simulation workbench for NONMEM: Tutorial on Pirana, PsN, and Xpose. *CPT Pharmacometrics Syst. Pharmacol.* 2 (6), e50. doi:10.1038/psp.2013.24

Livermore, D. M. (2003). Linezolid *in vitro*: Mechanism and antibacterial spectrum. *J. Antimicrob. Chemother.* 51, 9–16. doi:10.1093/jac/dkg249

Maartens, G., and Benson, C. A. (2015). Linezolid for treating tuberculosis: A delicate balancing act. *EBIOM* 2, 1568–1569. doi:10.1016/j.ebiom.2015.10.014

Macgowan, A. P. (2003). Pharmacokinetic and pharmacodynamic profile of linezolid in healthy volunteers and patients with Gram-positive infections. *J. Antimicrob. Chemother.* 51, 17–25. doi:10.1093/jac/dkg248

McIlleron, H., Rustomjee, R., Vahedi, M., Mthiyane, T., Denti, P., Connolly, C., et al. (2012). Reduced antituberculosis drug concentrations in HIV-infected patients who are men or have low weight: Implications for international dosing guidelines. *Antimicrob. Agents Chemother.* 56 (6), 3232–3238. doi:10.1128/AAC.05526-11

Millard, J., Pertinez, H., Bonnett, L., Hodel, E. M., Dartois, V., Johnson, J. L., et al. (2018). Linezolid pharmacokinetics in MDR-TB: A systematic review, meta-analysis and Monte Carlo simulation. *J. Antimicrob. Chemother.* 73 (7), 1755–1762. doi:10.1093/jac/dky096

Ministry of Health & Family Welfare Government of India (2021). *Guidelines for programmatic management of TB preventive treatment in India 2021 I*. New Delhi: Ministry of Health & Family Welfare Government of India.

Mockeliunas, L., Keutzer, L., Sturkenboom, M. G. G., Bolhuis, M. S., Hulskotte, L. M. G., Akkerman, O. W., et al. (2022). Model-informed precision dosing of linezolid in patients with drug-resistant tuberculosis. *Pharmaceutics* 14 (4), 753. Published online. doi:10.3390/pharmaceutics14040753

Obach, R. S. (2022). Linezolid metabolism is catalyzed by Cytochrome P450 2J2, 4F2, and 1B1. *Drug Metab. Dispos.* 50 (4), 413–421. doi:10.1124/dmd.121.000776

Padmapriyadarsini, C., Vohra, V., Bhatnagar, A., Solanki, R., Sridhar, R., Anande, L., et al. (2022). Bedaquiline, delamanid, linezolid and clofazimine for treatment of pre-extensively drug-resistant tuberculosis. *Clin. Infect. Dis.* 29, ciac528. doi:10.1093/CID/CIAC528

Pepper, D. J., Marais, S., Wilkinson, R. J., Bhaijee, F., Maartens, G., McIlleron, H., et al. (2010). Clinical deterioration during antituberculosis treatment in Africa: Incidence, causes and risk factors. *BMC Infect. Dis.* 10 (1), 83. doi:10.1186/1471-2334-10-83

Plock, N., Buerger, C., Joukhadar, C., Kljucar, S., and Kloft, C. (2007). Does linezolid inhibit its own metabolism?—population pharmacokinetics as a tool to explain the observed nonlinearity in both healthy volunteers and septic patients. *Drug Metab. Dispos.* 35 (10), 1816–1823. doi:10.1124/DMD.106.013755

Qin, Y., Zhang, L. L., Ye, Y. R., Yue-Ting, C., and Jiao, Z. (2022). Parametric population pharmacokinetics of linezolid: A systematic review. *Br. J. Clin. Pharmacol.* 16, 4043–4066. doi:10.1111/BCP.15368

Savic, R. M., Jonker, D. M., Kerbusch, T., and Karlsson, M. O. (2007). Implementation of a transit compartment model for describing drug absorption in pharmacokinetic studies. *J. Pharmacokinet. Pharmacodyn.* 34, 711–726. doi:10.1007/s10928-007-9066-0

Schecter, G. F., Scott, C., True, L., Raftery, A., Flood, J., and Mase, S. (2010). Linezolid in the treatment of multidrug-resistant tuberculosis. *Clin. Infect. Dis.* 50 (1), 49–55. doi:10.1086/648675

Smythe, W. A. (2016). "Characterizing population pharmacokinetic/pharmacodynamic relationships in pulmonary tuberculosis infected adults using nonlinear mixed effects modelling,". Doctoral thesis (Cape Town, 7700, South Africa: University of Cape Town).

Song, T., Lee, M., Jeon, H. S., Park, Y., Dodd, L. E., Dartois, V., et al. (2015). Linezolid Trough concentrations correlate with mitochondrial toxicity-related adverse events in the treatment of chronic extensively drug-resistant tuberculosis. *EBIOM* 2, 1627–1633. doi:10.1016/j.ebiom.2015.09.051

Sprent, P. (2011). "Fisher Exact Test," in *International Encyclopedia of Statistical Science*. Editors M. Lovric (Berlin, Heidelberg: Springer). doi:10.1007/978-3-642-04898-2_253

Stalker, D. J., and Jungbluth, G. L. (2003). Clinical pharmacokinetics of linezolid, a novel oxazolidinone antibacterial. *Clin. Pharmacokinet.* 42 (13), 1129–1140. doi:10.2165/00003088-200342130-00004

Tietjen, A. K., Kroemer, N., Cattaneo, D., Baldelli, S., and Wicha, S. G. (2022). Population pharmacokinetics and target attainment analysis of linezolid in multidrug-resistant tuberculosis patients. *Br. J. Clin. Pharmacol.* 88, 1835–1844. doi:10.1111/bcp.15102

Tornheim, J., Ganatra, S., Deluca, A., Banka, R., Rodrigues, C., Gupta, A., et al. (2017). Linezolid experience among MDR-TB patients in Mumbai. *Eur. Respir. J.* 50 (61), PA3486. doi:10.1183/1393003.CONGRESS-2017.PA3486

Tornheim, J. A., Intini, E., Gupta, A., and Udwadia, Z. F. (2020). Clinical features associated with linezolid resistance among multidrug resistant tuberculosis patients at a tertiary care hospital in Mumbai, India. *Eur. Respir. J.* 56 (64), 477. doi:10.1183/13993003.CONGRESS-2020.477

Tornheim, J. A., Udwadia, Z. F., Arora, P. R., Gajjar, I., Sharma, S., Karane, M., et al. (2022). Increased moxifloxacin dosing among patients with multidrug-resistant tuberculosis with low-level resistance to moxifloxacin did not improve treatment outcomes in a tertiary care center in Mumbai, India. *Open Forum Infect. Dis.* 9 (2), ofab615. doi:10.1093/OFID/OFAB615

Udwadia, Z. F., Tornheim Jeffrey, A., Ganatra, S., DeLuca, A., Rodrigues, C. S., and Gupta, A. (2019). Few eligible for the newly recommended short course MDR-TB regimen at a large Mumbai private clinic. *BMC Infect. Dis.* 19 (94), 94. doi:10.1186/s12879-019-3726-8

Wasserman, S., Denti, P., Brust, J. C. M., Abdelwahab, M., Hlungulu, S., Wiesner, L., et al. (2019). Linezolid pharmacokinetics in South African patients with drug-resistant tuberculosis and a high prevalence of HIV coinfection. *Antimicrob. Agents Chemother.* 63 (3), 021644–e2218. doi:10.1128/AAC.02164-18

Wasserman, S., Louw, G., Ramangoaela, L., Barber, G., Hayes, C., Omar, S. V., et al. (2019). Linezolid resistance in patients with drug-resistant TB and treatment failure in South Africa. *J. Antimicrob. Chemother.* 74 (8), 2377–2384. doi:10.1093/JAC/DKZ206

Wasserman, S., Meintjes, G., and Maartens, G. (2016). Linezolid in the treatment of drug-resistant tuberculosis: The challenge of its narrow therapeutic index linezolid in the treatment of drug-resistant tuberculosis: The challenge of its narrow therapeutic index. *Expert Rev. Anti-infective Ther.* 14 (10), 901–915. doi:10.1080/14787210.2016.1225498

Wilkins, J. J., Savic, R. M., Karlsson, M. O., Langdon, G., McIlleron, H., Pillai, G., et al. (2008). Population pharmacokinetics of rifampin in pulmonary tuberculosis patients, including a semimechanistic model to describe variable absorption. *Antimicrob. Agents Chemother.* 52 (6), 2138–2148. doi:10.1128/AAC.00461-07

World Health Organization 2020 Global tuberculosis report 2020. Accessed June 1, 2022. Available at: https://www.who.int/publications/i/item/9789240013131

World Health Organization (2022). *Rapid communication: Key changes to the treatment of drug-resistant tuberculosis*. Geneva: World Health Organization.

World Health Organization (2018). *Technical report on critical concentrations for drug susceptibility testing of medicines used in the treatment of drug-resistant tuberculosis*. Geneva: World Health Organization.

World Health Organization (2020). *WHO consolidated guidelines on tuberculosis. Module 4, treatment : Drug-resistant tuberculosis treatment*. Geneva, Switzerland: World Health Organization, 98.

Zhou, W., Nie, W., Wang, Q., Shi, W., Yang, Y., Li, Q., et al. (2022). Linezolid pharmacokinetics/pharmacodynamics-based optimal dosing for multidrug-resistant tuberculosis. *Int. J. Antimicrob. Agents* 59 (6), 106589. doi:10.1016/J.IJANTIMICAG.2022.106589

frontiers | Frontiers in Pharmacology

TYPE Original Research
PUBLISHED 09 January 2023
DOI 10.3389/fphar.2022.1032674

OPEN ACCESS

EDITED BY
Karunakaran Kalesh,
Teesside University, United Kingdom

REVIEWED BY
Dario Cattaneo,
Luigi Sacco Hospital, Italy
Anutthaman Parthasarathy,
University of Bradford, United Kingdom

*CORRESPONDENCE
Yi Hu,
yhu@fudan.edu.cn

†These authors have contributed equally to this work and share first authorship

‡These authors have contributed equally to this work and share senior authorship

SPECIALTY SECTION
This article was submitted to Pharmacology of Infectious Diseases, a section of the journal Frontiers in Pharmacology

RECEIVED 31 August 2022
ACCEPTED 15 December 2022
PUBLISHED 09 January 2023

CITATION
Zhang H, He Y, Davies Forsman L, Paues J, Werngren J, Niward K, Schön T, Bruchfeld J, Alffenaar J-W and Hu Y (2023), Population pharmacokinetics and dose evaluations of linezolid in the treatment of multidrug-resistant tuberculosis.
Front. Pharmacol. 13:1032674.
doi: 10.3389/fphar.2022.1032674

Population pharmacokinetics and dose evaluations of linezolid in the treatment of multidrug-resistant tuberculosis

Haoyue Zhang[1†], Yuying He[2†], Lina Davies Forsman[3,4†], Jakob Paues[5,6], Jim Werngren[7], Katarina Niward[5,6], Thomas Schön[5,6,8], Judith Bruchfeld[3,4‡], Jan-Willem Alffenaar[9,10,11‡] and Yi Hu[1*‡]

[1]Department of Epidemiology, School of Public Health and Key Laboratory of Public Health Safety, Fudan University, Shanghai, China, [2]Institute of Tuberculosis Control, Guizhou Provincial Center for Disease Control and Prevention, Guiyang, China, [3]Department of Infectious Diseases, Karolinska University Hospital, Stockholm, Sweden, [4]Department of Medicine, Division of Infectious Diseases, Karolinska Institute, Stockholm, Sweden, [5]Department of Biomedical and Clinical Sciences, Linköping University, Linköping, Sweden, [6]Department of Infectious Diseases, Linköping University Hospital, Linköping, Sweden, [7]Department of Microbiology, The Public Health Agency of Sweden, Stockholm, Sweden, [8]Department of Infectious Diseases, Kalmar County Hospital, Linköping University, Kalmar, Sweden, [9]University of Sydney, Faculty of Medicine and Health, School of Pharmacy, Sydney, NSW, Australia, [10]Westmead Hospital, Sydney, NSW, Australia, [11]Sydney Institute for Infectious Diseases, University of Sydney, Sydney, NSW, Australia

Background: The pharmacokinetic/pharmacodynamics (PK/PD) target derived from the hollow-fiber system model for linezolid for treatment of the multidrug-resistant tuberculosis (MDR-TB) requires clinical validation. Therefore, this study aimed to develop a population PK model for linezolid when administered as part of a standardized treatment regimen, to identify the PK/PD threshold associated with successful treatment outcomes and to evaluate currently recommended linezolid doses.

Method: This prospective multi-center cohort study of participants with laboratory-confirmed MDR-TB was conducted in five TB designated hospitals. The population PK model for linezolid was built using nonlinear mixed-effects modeling using data from 168 participants. Boosted classification and regression tree analyses (CART) were used to identify the ratio of 0- to 24-h area under the concentration-time curve ($AUC_{0\text{-}24h}$) to the minimal inhibitory concentration (MIC) threshold using the BACTEC MGIT 960 method associated with successful treatment outcome and validated in multivariate analysis using data from a different and prospective cohort of 159 participants with MDR-TB. Furthermore, based on the identified thresholds, the recommended doses were evaluated by the probability of target attainment (PTA) analysis.

Result: Linezolid plasma concentrations (1008 samples) from 168 subjects treated with linezolid, were best described by a 2-compartment model with first-order absorption and elimination. An AUC_{0-24h}/MIC > 125 was identified as a threshold for successful treatment outcome. Median time to sputum culture conversion between the group with $AUC_{0\text{-}24h}$/MIC above and below 125 was

2 *versus* 24 months; adjusted hazard ratio (aHR), 21.7; 95% confidence interval (CI), (6.4, 72.8). The boosted CART-derived threshold and its relevance to the final treatment outcome was comparable to the previously suggested target of AUC_{0-24h}/MIC (119) using MGIT MICs in a hollow fiber infection model. Based on the threshold from the present study, at a standard linezolid dose of 600 mg daily, PTA was simulated to achieve 100% at MGIT MICs of ≤ .25 mg which included the majority (81.1%) of isolates in the study.

Conclusion: We validated an AUC_{0-24h}/MIC threshold which may serve as a target for dose adjustment to improve efficacy of linezolid in a bedaquiline-containing treatment. Linezolid exposures with the WHO-recommended dose (600 mg daily) was sufficient for all the *M. tb* isolates with MIC ≤ .25 mg/L.

KEYWORDS

linezolid, pharmacokinetics, dose evaluation, multidrug-resistant tuberculosis, pharmacodynamics

1 Introduction

With the update of World Health Organization (WHO) multidrug-resistant tuberculosis (MDR-TB) treatment guidelines in 2019, linezolid is included as one of the important Group A agent (World Health, 2020). It is expected that this will improve the 6-month sputum culture conversion rate as well as treatment outcome of MDR-TB treatment (Lee et al., 2017; Ahmad et al., 2018; Singh et al., 2019; Padayatchi et al., 2020).

Linezolid is a drug with a narrow therapeutic window which requires close monitoring of participants to prevent toxicity (Wasserman et al., 2016). In the MDR-TB treatment recommendations issued in 2020 (World Health, 2020), the WHO highlighted the urgent need to investigate linezolid dose optimization and treatment duration in order to minimize its toxicity. As linezolid drug concentrations are highly variable (Wasserman et al., 2019), therapeutic drug monitoring (TDM) is recommended to monitor the drug exposure to facilitate dose individualization. Previous studies have consistently shown that higher drug exposure of linezolid in relation to *in vitro* susceptibility of the *Mycobacterium tuberculosis (M. tb)* isolate (Heinrichs et al., 2019) is associated with improved TB treatment outcome (Pasipanodya et al., 2013; Swaminathan et al., 2016; Zheng et al., 2021).

The ratio of 0- to 24-h area under the concentration-time curve (AUC_{0-24h}) to the minimal inhibitory concentration (MIC) is generally used as the thresholds in TDM of TB treatment (Sturkenboom et al., 2021). A study in a hollow fiber infection model of tuberculosis found that optimal microbial kill for linezolid was achieved at an AUC_{0-24h}/MIC ratio of 119 (Srivastava et al., 2017). However, this target was identified *in vitro*, using linezolid in monotherapy and only a single *M. tb* strain H37Rv (ATCC 27294) with MIC identified using the mycobacterial growth indicator tube (MGIT) assay (Becton Dickinson, Franklin Lakes, NJ) (Srivastava et al., 2017). Thus, it is necessary to validate the clinical relevance of previously reported target and to evaluate the sufficiency of the recommended and commonly used doses of linezolid. Therefore, the present study aimed to model the population pharmacokinetics (PK) of linezolid when administered as part of a standardized MDR-TB treatment regimen, identify pharmacokinetic/pharmacodynamics (PK/PD) threshold associated with treatment outcome and to evaluate the current dose of linezolid.

2 Method

2.1 Study design

Participants from two cohorts were included for this analysis. The development cohort derived from a previously reported study (Zheng et al., 2021), targeting the participants with bacteriological diagnosis of MDR-TB from designated hospitals in Jiangsu, Guizhou and Sichuan Province in China between January 2015 and December 2017. The validation cohort enrolled participants from Sichuan, Jiangsu and Henan Province based on the same inclusion criteria. Briefly, eligible participants were ≥ 18 years old and < 70 years old and diagnosed as MDR-TB by GeneXpert MTB/RIF (Cepheid, Sunnyvale, CA) and *M. tb* drug susceptible test. Participants were excluded if critically ill, pregnant, infected with HIV, HBV or HCV, having received treatment for MDR-TB for more than 1 day, or refused to participate.

The development cohort received linezolid-containing regimen including bedaquiline, moxifloxacin or levofloxacin, linezolid as well as the background regimen to complete a full-oral regimen. The validation cohort received a standardized oral regimen of fluoroquinolones, bedaquiline, linezolid, clofazimine and cycloserine for 6 months, followed by fluoroquinolones, linezolid, clofazimine and cycloserine for

18 months (World Health, 2020). All participants were given 600 mg linezolid once daily, as recommended by the WHO (World Health, 2020). The study was approved by the ethics committee of the School of Public Health, Fudan University (IRB#2015-08-0565) and written informed consent was obtained from all subjects.

In both two study cohorts, the participant received the inpatient treatment for the first 2 weeks after treatment initiation, then followed by outpatient treatment. All study participants were routinely examined monthly during the intensive phase (the first 6 months) and once every 2 months during the consolidation phase (the next 18 months). A questionnaire was used to collect demographic data, while medical and laboratory data were extracted from hospital records.

2.2 Blood drug concentration determination

In the development cohort, blood samples for drug concentration analysis were collected prior to dose intake and at 1, 2, 4, 6 and 8 h after dose intake after 2 weeks' inpatient treatment. According to the previously reported study (Kamp et al., 2017), the limited sampling strategy (predose and 2 h after dose intake) proven to have an accurate predication, comparable to intensive sampling (root mean squared error of 6.07%, R^2 of .98). Thus, in the validation cohort, limited sampling strategy were applied at predose, 2 and 6 h after dose intake after 2 weeks' TB treatment. Plasma concentrations were determined using a validated high performance liquid chromatography tandem mass spectrometry (HPLC-MS/MS) method. Linezolid concentrations were measured using linezolid-d3 as the internal standard with m/z of 338.01→296.04. The analytical range for linezolid was .05–30 mg/L, with good linearity of $R^2 \geq 99.53\%$. The inaccuracy was within the range of 87.3%–108% for all concentrations and the imprecision values were less than 11.5% over the entire range of calibration standards.

2.3 Population pharmacokinetic modeling

To build the population PK model, data of 168 study participants from a previously published study were included (Zheng et al., 2021). The population PK model for linezolid was built using the nonlinear mixed-effects method (Phoenix NLME, version 8.0; Certara Inc., Princeto1n, United States). One- and two-compartment models with first-order eliminations were used to fit the data. The residual-error models included additive, proportional, and combined error models were tested. After building the structural model, covariates were added in a stepwise regression with forward inclusion (ΔOFV>3.84, p <.05) and backward elimination (ΔOFV>6.64, p <.01). The final model was evaluated and validated using visual predictive check (VPC) by simulating linezolid concentrations for 1,000 participants from the original data set and the final model. The population PK parameters in the validation cohort were calculated by Bayes Estimation based on the established population PK model.

2.4 Drug susceptibility testing

Sputum samples were collected at each visit and were sent to the prefectural TB reference laboratory for the microbiological examination. The BACTEC MGIT 960 system (Becton Dickinson, Franklin Lakes, NJ, United States) was used for bacterial culture of the *M. tb* isolates, phenotypic drug susceptibility testing and MIC determination for linezolid (Springer et al., 2009). All suspension from the growth in the plain MGIT medium were used within 3 days after found positive in MGIT incubator. The growth control tube containing 1: 100 diluted bacterial suspension, was inoculated in the MGIT 960 instrument as well. The range of concentrations for MIC testing was .06–1 mg/L for linezolid. The MIC was defined as the lowest concentration of a drug that inhibited the bacterial growth. *M. tb* H37Rv (ATCC 27294) was used as the reference strain for the quality control.

2.5 Treatment outcome

The routine follow-up examinations and laboratory tests were performed monthly during the intensive phase, and every second month during the continuation phase of standardized MDR-TB treatment. Cure was defined as completed treatment and at least three consecutive, negative sputum cultures of *M. tb*, with at least 30 days in between sampling. A successful treatment outcome was defined as treatment completion or cure. An unsuccessful treatment outcome included treatment failure, all-cause mortality, and default during treatment or transfer out (World Health, 2013).

2.6 Identification and validation of PK/PD threshold of MDR-TB treatment outcome

The threshold was identified by relating the PK parameters to the treatment outcomes using boosted classification and regression tree analyses (CART). Boosted CART analysis was performed using Salford Predictive Miner System software (San Diego, CA, United States). Boosted CART analysis searched the PK parameters including peak serum concentration (C_{max}), trough concentration (C_{min}), AUC_{0-24h}, AUC_{0-24h}/MIC, C_{max}/AUC_{0-24h} and the possible cutoff values to identify the best predictor for classifying between participants with and without

the studied outcome (i.e., time to sputum culture conversion and successful treatment outcome) using Salford Predictive Miner System software (San Diego, CA, United States). The association between the boosted CART-derived threshold and treatment outcomes was validated by Poisson regression model with robust variance. COX proportional hazard regression model was used for evaluating the relationship between the boosted CART-derived threshold and time to sputum culture conversion. The clinical significance of the identified threshold was also validated by comparing to the previously reported threshold (119) derived from a hollow fiber infection model using the MGIT assay (Becton Dickinson, Franklin Lakes, NJ) (Srivastava et al., 2017).

2.7 Dose regimen evaluation

The Monte Carlo simulation was performed using Phoenix NLME (version 8.0; Certara Inc., Princeton, United States) as well. The characteristic data of a specifically simulated population (n = 1000) needed in the model were duplicated from original validation cohort to ensure its representativeness of the study population. The WHO-recommended dose (600 mg daily) (World Health, 2020), and the other previously proposed doses (300 mg, 900 mg, and 1200 mg daily) were evaluated by an analysis of the probability of target attainment (PTA) in the simulated population (Bolhuis et al., 2018). The PTA was derived by calculating the fraction of subjects who attained the PK/PD target or threshold at different MICs in BACTEC MGIT 960 system. The studied MICs included .06, .12, .25, .5, and 1 mg/L, where 1 mg/L of linezolid was referred to as the critical concentration in MGIT system in the Technical Report on critical concentrations for drug susceptibility testing (World Health, 2018). The dose was defined as sufficient at PTA values of ≥ 90%.

2.8 Statistical analysis

Baseline characteristics were summarized using descriptive statistics expressed as medians with interquartile ranges (IQR) for continuous variables and proportions for categorical variables. Chi-squared test analysis was performed for categorical variables, while one-way analysis of variance or Mann-Whitney U test were used for continuous variables. The main microbiological outcome was time to sputum culture conversion, defined as the time from treatment initiation to sustained sputum culture conversion. The time to sputum conversion was illustrated using the Kaplan-Meier method and difference between comparison groups were assessed using the log-rank test. Poisson regression model with robust variance was used to assess the correlation between the pharmacokinetic parameters and treatment outcomes. The multivariate COX proportional hazard regression model was used to verify the correlation between the CART-derived threshold and time to sputum culture conversion. The start time for the survival analysis was the first date of treatment. The endpoint of the observation was defined as the end of treatment in the survival analysis. As treatment outcome is influenced by multiple factors, we explored weight, BMI, tobacco use, alcohol use, diabetes mellitus type 2 status, albumin, cavity, baseline time to culture positivity and other factors that may be potential confounders based on the previous study (Madzgharashvili et al., 2021; Meregildo-Rodriguez et al., 2022). The association between linezolid drug exposure and treatment outcome were adjusted by the identified covariates based on the univariate analysis. A p-value of <.05 was considered statistically significant. IBM SPSS 20.0 (IBM Corp., Armonk, NY) was used to perform statistical description and COX proportional hazard regression model analysis.

3 Result

3.1 Population characteristics

The study included a total of 327 study participants. Data of 168 participants was used for the development cohort and data of 159 participants for the validation cohort. There was no significant difference between the two cohorts regarding the baseline characteristics (Table 1).

3.2 Drug susceptibility

The median MIGT MICs of the clinical isolates were .25 (range .12–.5) mg/L for linezolid, with MIC ≤ .25 mg/L for the majority (81.1%) of the isolates. The H37Rv (ATCC 27294) as reference had a MIC of .5 mg/L, comparable to that in WHO report (World Health, 2018) (Figure 1). All strains were susceptible to linezolid before initiating the treatment.

3.3 Population pharmacokinetic modeling and parameter calculation

The linezolid concentrations in 1008 plasma samples from 168 subjects were best described by a 2-compartment model with first-order absorption and elimination. An additive error model was used to describe the unexplained residual variability for linezolid. Apart from weight, diabetes type 2 independently influenced linezolid CL and V_d and the inclusion of diabetes type 2 resulted in a reduction of 38.49 points (p <.001) in OFV and explained 3.6% between-subject variability in CL and .6% between-subject variability in V_d (Table 2). The predicted linezolid concentrations reached an acceptable agreement with the observed concentrations, as shown in the goodness of fit and

TABLE 1 Baseline demographic and clinical characteristics of participants in two studied cohorts.

Linezolid	Development cohort (n = 168)	Validation cohort (n = 159)	*P*-value[a]
	Median (IQR) or no. (%)	Median (IQR) or no. (%)	
Age, year	41 (33-45)	40 (29-54)	.47
Bodyweight, kg	53 (47-66)	59 (53-64)	.10
BMI	20 (18-23)	21 (18-22)	.95
Male	125 (74.4)	103 (64.8)	.08
Smoking	43 (25.6)	31 (19.5)	.24
Alcohol consumption	40 (23.8)	28 (17.6)	.12
Diabetes type 2	32 (19.0)	27 (17.0)	.49

Abbreviations: IQR, inter quartile range.
[a]A Chi-square test were used to identify the differences between groups for categorical variables, while one-way analysis of variance or Mann-Whitney *U* test were used for continuous variables. The body mass index (BMI, kg/m^2) was calculated through weight (kg) divided by square of height (m).

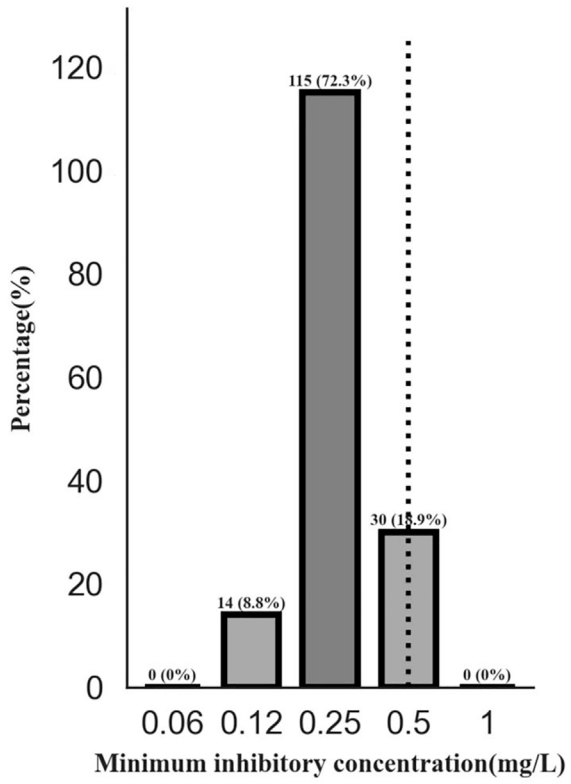

FIGURE 1
The distribution of minimum inhibitory concentration of linezolid for *Mycobacterium tuberculosis* isolates. Note: The BACTEC MGIT 960 system (Becton Dickinson, Franklin Lakes, NJ, United States of America) was used for bacterial culture, phenotype drug susceptibility testing and MIC values. The H37Rv (ATCC 27294) was used for reference to be inoculated with four batches of studied isolates as denoted. The MIC was defined as the lowest concentration of a drug that inhibited the bacterial growth. Abbreviations: MIC, minimum inhibitory concentration.

visual predictive check plots (Figure 2). The VPC for the entire data set demonstrated a good prediction of the model (Figure 3).

Applying the population PK modeling, using the linezolid concentration measured in the samples from the validation cohort, the C_{min} was 2.0 (1.5–2.3) mg/L and the C_{max} was 16.2 (14.8–18.8) mg/L. The AUC_{0-24h} was 108.3 (82.6–119.1) mg h/L after an oral dose of 600 mg daily. The AUC_{0-24h}/MIC values (median and IQR) were 428.3 (301.2–489.8). The C_{max}/MIC values (median and IQR) were 64.0 (45.8–77.1) (Table 3).

3.4 Treatment management in validation cohort

During the treatment, 27 of the study participants experienced linezolid-induced toxicity presenting as cytopenia (14, 8.8%), peripheral neuropathy (11, 6.9%) and optic neuritis (9, 5.7%). Among 18 participants with the linezolid dose reduction or temporary interruption due to severe adverse events, all recovered and 17 participants were back to the standard dosage and one participant continued with a reduced dose of 300 mg daily until end of treatment.

At end of treatment, 149 (93.7%) succeeded in the treatment and median time of sputum conversion was 3 (1, 5) months. Except for sex and CXR-severity, there is no significant difference between the participants with and without successful treatment in terms of sociodemographic characteristic and baseline disease status (Table 4).

3.5 Identification and validation of clinical-significant thresholds

PK parameters including C_{max}, C_{min}, AUC_{0-24h}, AUC_{0-24h}/MIC and C_{max}/AUC_{0-24h} were significantly different between

TABLE 2 Pharmacokinetic parameters of linezolid population pharmacokinetic model in development cohort.

	Linezolid	
	Mean	RSD (%)
Typical value of Population parameters		
Ka (/h)	2.0	11.1
CL (L/h)	5.6	1.6
V_d(L)	35.8	2.0
Q (L/h)	.9	13.7
Vp(L)	58.6	13.2
Tlag(h)	.6	8.4
Variation of parameters between individuals		
CL (L/h)	21.6	14.6
Vd (%CV)	24.4	11.1
Tlag(%CV)	—	—
Covariate		
θ (Bodyweight)-CL	.75	—
θ (Bodyweight)-Vd	1.0	—
θ (Diabetes)-CL	.1	10.5
θ (Diabetes)-Vd	5.0	11.1
θ (Age)-CL	—	—
Additional residual (mg/L)	.5	4.2
Proportion of residual (mg/L)	—	—

Abbreviations: CL, clearance; CV, coefficient of variation; Ka, absorption rate constant; Vc, volume of central compartment distribution; Q, Inter-compartment clearance; Vp, volume of peripheral compartment; Tlag, lag time; V/F, apparent volume of distribution; RSD%, relative standard deviation.

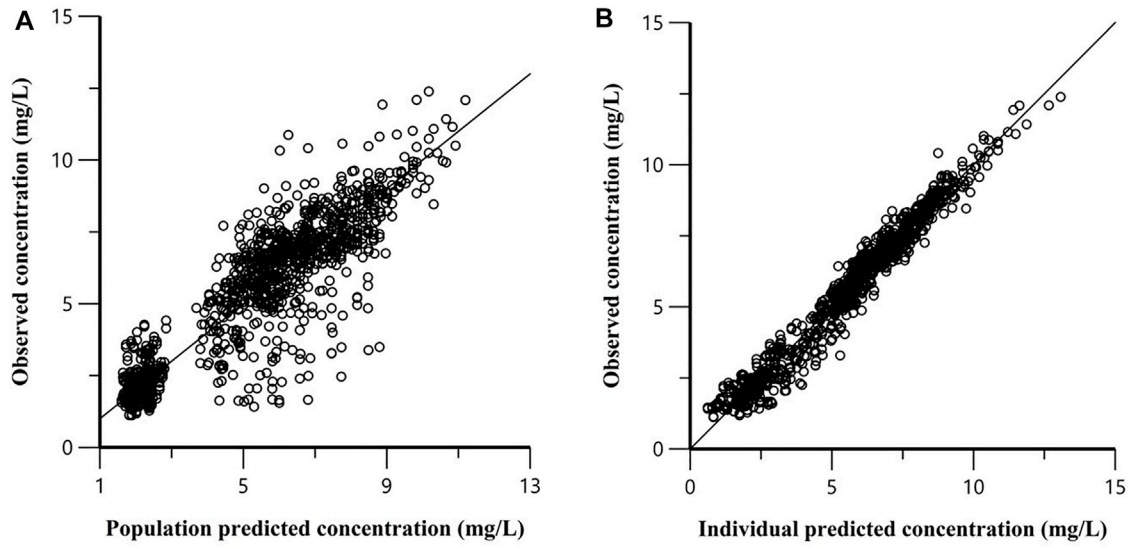

FIGURE 2
Goodness-of-fit plot for the final model. **(A)** Population predicted *versus* population observed concentrations; **(B)** Individual predicted *versus* individual observed concentrations.

groups of successful and unsuccessful treatment (Table 3). By relating PK/PD parameters to treatment outcome and time to sputum culture conversion, the CART-derived threshold of AUC_{0-24h}/MIC (125) was identified (Figure 4). The proportion of study participants above the CART-derived threshold was 91.8% (146/159). The association between the

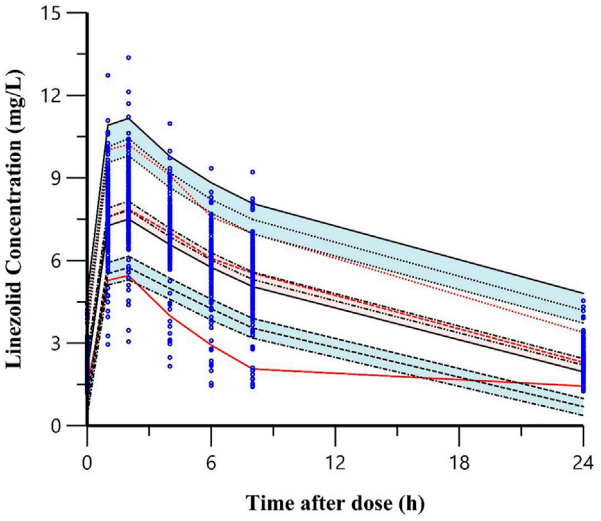

FIGURE 3
Visual predictive check plots of the final model for linezolid in the development cohort. Note: The top, middle, and bottom solid lines were the 95th,50th and 5th percentiles of the observed data, respectively. The shaded areas from top to bottom were the 95% confidence interval for the 95th, 50th, and 5th percentile of the simulated data. The dots were the observed concentrations.

CART-derived threshold and final treatment outcome was validated by Poisson regression model with robust variance (100% vs. 23.1%; adjusted RR, 4.3; 95%CI, 1.6–11.7). Also, the CART-derived threshold was significantly associated with time to sputum conversion (median time to sputum culture conversion between the group with $AUC_{0\text{-}24h}$/MIC above and below 125: 2 vs. 24 months; adjusted HR, 21.7; 95%CI, 6.4–72.8) (Table 5). The association between the CART-derived threshold and final treatment outcome/time to sputum culture conversion was well comparable to the previously reported target of 119 (Srivastava et al., 2017) (Figure 5).

3.6 Dose regimen evaluation

Based on the CART-derived threshold, at a standard linezolid dose of 600 mg daily, PTA was simulated to achieve 100% at MGIT MICs of ≤ .25 mg/L, while at 300 mg daily, commonly used when adverse events happen, PTA attain above 90% at MICs ≤ .125 mg/L and was 74.2% at MIC of .25 mg/L. Comparably, a dose of 900 mg daily had PTA exceeding 90% (100%) at an MIC of .5 mg/L covering all isolates in our study. At the critical concentration of 1 mg/L in MGIT which was not found for any isolate in our study, 1200 mg daily failed to achieve a PTA of ≥ 90% (68.6%) at the $AUC_{0\text{-}24h}$/MIC ratio of 125. Only dose up to 1400 mg had PTA exceeded 90% (93.1%) at MIC of 1 mg/L (Figure 6).

4 Discussion

Our results provide valuable insight into population PK and its association with time to sputum culture conversion and treatment outcome as well as the probability of target attainment with current WHO recommended regimen in participants with MDR-TB in China. A linezolid PK/PD threshold of AUC/MIC > 125, using MGIT MICs, was associated with successful treatment outcome and may be used for TDM.

We found that two-compartment model with an additive error model best fitted the pharmacokinetic profiles of linezolid. Previous studies reported a one-compartment model (Sotgiu et al., 2012; Kamp et al., 2017; Lopez et al., 2019; Alghamdi et al., 2020) to be adequate to describe the pharmacokinetic profile of linezolid while our study found that a two-compartment described data better compared to a one-compartment model as demonstrated by an OFV decrease of 18. This can be explained by smaller sample sizes or collection of fewer blood samples in the elimination phase of the drug. Diabetes type 2 was found to be a major covariate explaining

TABLE 3 Pharmacokinetic parameters between groups with different treatment outcomes in validation cohort.

Pharmacokinetic parameters	Total	Successful treatment	Unsuccessful treatment	*P*-value[a]
	Median (IQR)	Median (IQR)	Median (IQR)	
C_{max} (mg/L)	16.2 (14.8–18.8)	16.4 (15.2–18.9)	13.4 (12.4–15.0)	<.01
C_{min}(mg/L)	2.0 (1.5–2.3)	2.0 (1.6–2.3)	1.2 (.8, 1.3)	<.001
$AUC_{0\text{-}24h}$ (mg h/L)	108.3 (82.6–119.1)	108.8 (87.1–120.6)	50.1 (48.0–56.4)	<.001
$AUC_{0\text{-}24h}$/MIC	428.3 (301.2–489.8)	434.6 (326.1–491.8)	100.1 (96.0–112.8)	<.001
C_{max}/MIC	64.0 (45.8–77.1)	64.7 (49.4–77.5)	26.8 (24.9–30.0)	<.001

Abbreviations: IQR, inter quartile range; 95% CI, 95% confidence interval; peak serum concentration (C_{max}); trough concentration (C_{min}); 0- to 24-h area under the concentration-time curve ($AUC_{0\text{-}24h}$); minimum inhibitory concentrations (MIC).
[a]Comparisons of C_{max}, C_{min}, $AUC_{0\text{-}24h}$, $AUC_{0\text{-}24h}$/MIC, C_{max}/$AUC_{0\text{-}24h}$ between successful treatment outcome group and unsuccessful treatment outcome groups were evaluated using one-way analysis of variance or Mann-Whitney *U* test.

TABLE 4 Socio-demographic features and baseline disease status between groups with different treatment outcomes in validation cohort.

Variables	Successful treatment (n = 149) median (IQR) or no. (%)	Unsuccessful treatment (n = 10) median (IQR) or no. (%)	P Value[a]
Socio-demographic characteristics			
Age, year	40 (29.0, 53.5)	39 (30.3, 57.0)	.80
Height, m	1.70 (1.65, 1.77)	1.65 (1.62, 1.78)	.44
Bodyweight, kg	59 (53, 64)	59.5 (55.5, 69.0)	.24
BMI	20.1 ± 2.99	21.7 ± 3.29	.58
Sex, male	100 (67.1%)	3 (30%)	<.05
Baseline disease status			
Diabetes type 2	26 (17.4)	1 (10.0)	1.00
Albumin, g/L	42 (40.8, 52.0)	42 (40.8, 52.0)	.14
Clinical severity[b]	37 (24.8)	4 (40.0)	.28
CXR severity	22 (14.8)	4 (40.0)	<.05
Cavity	29 (19.5)	4 (40.0)	.22
Baseline time to culture positivity, day	13 (12.5, 15.0)	12 (10.0, 13.0)	.15

[a]Comparisons of continuous variables between successful treatment outcome group and unsuccessful treatment outcome groups were evaluated using one-way analysis of variance or Mann-Whitney *U* test. Categorical variables was performed using the Chi-square or Fisher's exact test.
[b]Clinical severity was defined as the TB score ≥8 (Rudolf et al., 2013).

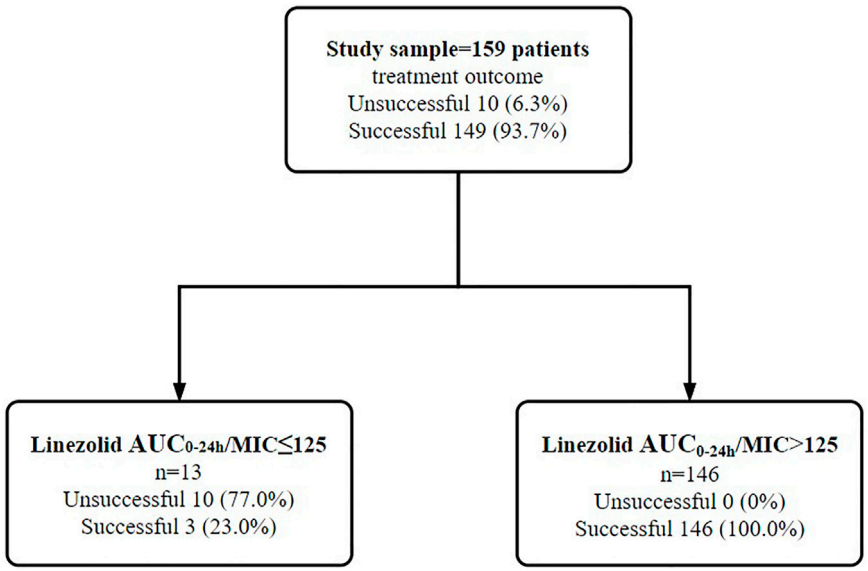

FIGURE 4
Identification of linezolid exposure/susceptibility threshold to differentiate the treatment outcome among 159 study participants in validation cohort. Note: AUC_{0-24h}/MIC of linezolid were examined in the boosted classification and regression tree analyses. Abbreviations: MIC, minimum inhibitory concentration; AUC0-24 h, 0- to 24-h area under drug concentration-time curve.

inter-individual residual variability of clearance and distribution volume for linezolid. Participants with diabetes type 2 commonly take the risk of developing diabetic gastroparesis, thus may affect the absorption of drugs. In previous studies (Singla et al., 2006), TB participants with diabetes type 2 were found to have higher probability of suboptimal drug exposure, which was explained by malabsorption due to diabetic enteropathy or by increased BMI (Chang et al., 2011; Mtabho et al., 2019). The VPC results indicated that the developed model was precise and could be used for simulation purposes. Thus, we established a population PK modeling suitable for TDM of linezolid during the MDR-TB treatment.

We identified an association between linezolid exposure and clinical treatment outcome of MDR-TB. Linezolid is a

TABLE 5 Validation of CART-derived threshold in relation to the final treatment outcome and time to sputum culture conversion in the validation cohort.

Thresholds of $AUC_{0\text{-}24h}$/MIC	Treatment outcome			Time to sputum culture conversion		
	Successful (%)	RR	aRR	Median (IQR) time to culture conversion (month)	HR (95%CI)	Adjusted HR (95%CI)[b]
≤125	3 (23.1)	1	1	24 (24, 24)	1	1
>125	146 (100)	4.3 (1.6, 11.7)	4.3 (1.6, 11.7)	2 (1, 4)	20.4 (6.3, 66.6)	21.7 (6.4, 72.8)
≤119[a]	0 (0)	1	1	24 (24, 24)	1	1
>119[a]	149 (100)	9.9 (1.6, 63.8)	9.9 (1.6, 63.8)	2 (1, 4)	43.5 (6.0, 316.6)	39.8 (5.4, 292.5)

Abbreviations: $AUC_{0\text{-}24h}$: the 0- to 24-h area under drug concentration-time curve; MIC: minimum inhibitory concentration in BACTEC 960 MGIT; RR, relative risk; HR, hazard ratio. CART: classification and regression tree analyses.

[a]The previously reported target of AUC_{0-24h}/MIC 119 (Srivastava et al., 2017) was identified using the MGIT assay (Becton Dickinson, Franklin Lakes, NJ) to identify MIC in hollow fiber infection model as the reference for comparison.

[b]The association between the boosted classification and regression tree analyses (CART)-derived threshold and treatment outcome was validated by Poisson regression model with robust variance. COX proportional hazard regression model was used for evaluating the relationship between the boosted CART-derived threshold and time to sputum culture conversion. Adjusted HR was calculated according to current area, age, sex; CXR severity.

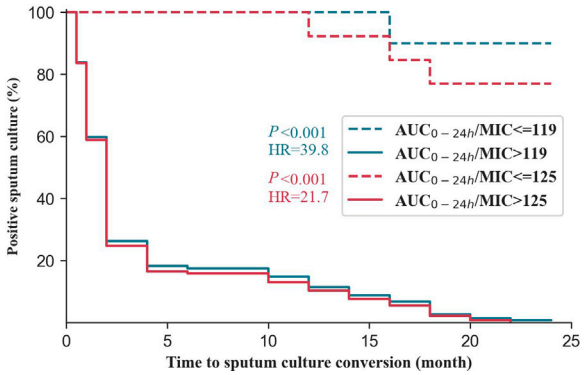

FIGURE 5
Time to culture conversion among the studied participants in validation cohort with multidrug-resistant tuberculosis grouped by the threshold in this study and previously reported target. Note: AUC_{0-24h}/MIC of 125 was derive from boosted classification and regression tree analyses in the study. The previously reported target of AUC_{0-24h}/MIC 119 (Srivastava et al., 2017)was identified using the MGIT assay (Becton Dickinson, Franklin Lakes, NJ) to identify MIC in hollow fiber infection model as the reference for comparison. Abbreviations: AUC0-24 h: 0- to 24-h area under the concentration-time curve; MIC: minimum inhibitory concentrations.

concentration-dependent drug and high drug exposure contributes to treatment efficacy, albeit limited by adverse events (Deshpande et al., 2016). As an oxazolidinone with potent activity against *M. tb*, linezolid suppresses oxidative-phosphorylation protein complexes 1, 3, 4, and 5 and ATP production levels in a clearly exposure-dependent manner for the once-daily (q24 h) regimens (Brown et al., 2015). This present study observed 27 of participants had linezolid-induced toxicity, some of which are thought to be associated with mitochondrial disturbance. However, after dose reduction or interruption, all recovered. Meanwhile, we did not find the impact of mitochondrial toxicity on the treatment outcome, probably due to the healthier participant included in the present study compared to the previously published studies (Brown et al., 2015; Song et al., 2015). In the present study, AUC/MIC was identified to be related to the treatment outcome, which is also demonstrated by previous studies (Alffenaar et al., 2011; Sotgiu et al., 2015).

An AUC_{0-24h}/MIC > 125, applying MGIT MICs was identified by boosted CART as primary node to define the successful treatment outcome of longer regimen in MDR-TB participants among our study population. This threshold was also observed to be strongly associated with the treatment outcome and time to sputum culture conversion, which is supported by the previously reported target for optimal bactericidal activity of an AUC_{0-24h}/MIC >119 (Srivastava et al., 2017). By confirming the clinical significance, this threshold may be applied for dose adjustments in a randomized controlled trial investigating TDM-derived doses of linezolid vs. standard dose of linezolid for MDR-TB treatment before applying it in the routine medical practice.

In the present study, currently recommended dose of linezolid was observed to be effective at MIC ≤ .25 mg/L which covered the majority of the isolates (81.1%). Based on the identified threshold, 600 mg would have a PTA exceeding 90% at MIC ≤ .25 mg/L in MGIT. The clinical efficacy of 600 mg linezolid for susceptible isolates (MIC ≤ .25 mg/L) in Middlebrook 7H10 agar plates is also reported in previous studies (Heinrichs et al., 2019; Alghamdi et al., 2020). In our exploratory analysis, we found PTAs below 90% for 600 mg of linezolid at MICs of .5 and in particular 1 mg/L. Of note, we found no isolate at a MIC of 1 mg/L in our study. Furthermore, it

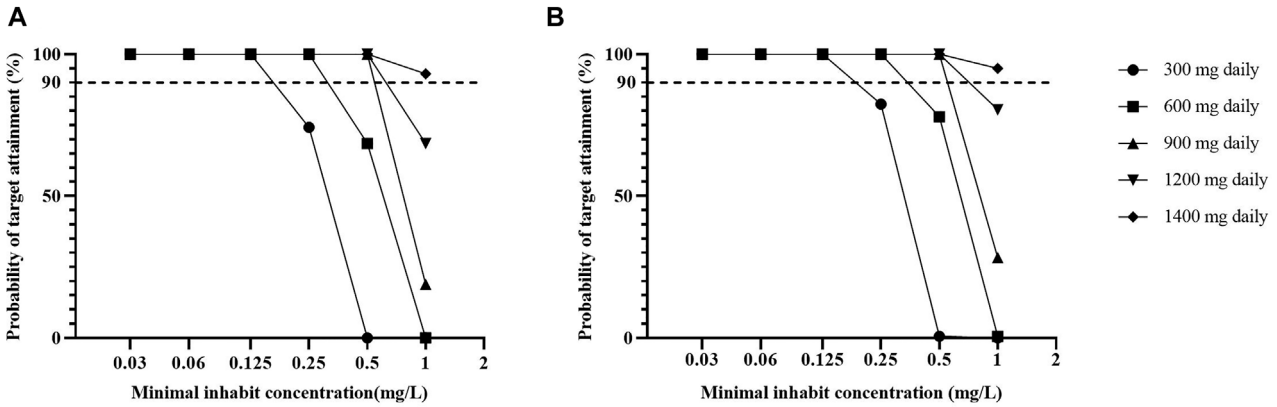

FIGURE 6
The probability of target attainment among the simulating population against varying MGIT minimal inhibitory concentration values for linezolid respectively based on the AUC_{0-24h}/MIC of 125 in this study **(A)** and the 119 previously reported **(B)**. Note: The previously reported target of AUC_{0-24h}/MIC 119 (Srivastava et al., 2017) was identified using the MGIT assay (Becton Dickinson, Franklin Lakes, NJ) to identify MIC in hollow fiber infection model as the reference for comparison. Abbreviations: PTA, probability of target attainment; AUC_{0-24h}: 0- to 24-h area under the concentration-time curve; MIC, minimum inhibitory concentration.

should be noted that if individual TDM is considered at the suggested targets, the technical MIC variability of ± one MIC dilution must be considered since this variability may affect the individual PK/PD value significantly. When considering higher dosing than 600 mg of linezolid daily, it should be noted that the administration of 1200 mg daily in the Nix-TB study was reported to achieve as high as 90% favorable outcome, although with alarming high rates of severe adverse events in the study participants (81% peripheral neuropathy and 48% myelosuppression) (Conradie et al., 2020). Therefore, clinically validated PK/PD thresholds and individual-based dose-guidance by TDM are important tools for dose optimization to avoid adverse events while ensuring treatment efficacy.

The strength of our study is that we developed population PK models for linezolid based on a relatively large number of MDR-TB participants with a standardized MDR-TB treatment regimen in China, where similar studies have not been reported. Additionally, the PK/PD threshold in this study was identified by treatment outcome of a large clinical cohort population, which can provide valuable and clinically-relevant support for the dose adjustment of linezolid using TDM. Another strength is that this study evaluated the validation of current WHO-recommended dose for linezolid using simulations and demonstrated a high target attainment (≥ 90%). Furthermore, the study provided the important example to suggest that, to use the limited sampling for monitoring in daily practice with population pharmacokinetic model, would support AUC guided dosing. Regarding linezolid monitoring in a clinical setting, current recommendations include a trough concentration <2.5 mg/L (Wasserman et al., 2022) or < 2 mg/L (Song et al., 2015) relevant to linezolid-relevant adverse events as well as drug exposure/susceptibility thresholds predictive of favorable treatment outcome (e.g., 125 in present study). Their clinical significances for the dosing adjustment will require the validation from the randomized clinical trials.

This study is subject to some limitations. Firstly, as the study participants required to be healthy enough to receive the whole course of treatment, none die or experienced unmanageable adverse events, which may restrict the representativeness of the study findings to some degree. As repeated DST testing of consecutive *M. tb* cultures was not performed, we were unable to monitor the potential development of linezolid resistance during treatment. However, since a high proportion of participants had sputum cultured converted at 6 months' treatment (77.4%), and that resistance emergence against linezolid is extremely rarely reported in the literature (Lee et al., 2017; Wasserman et al., 2019), we regard the risk for undetected acquired drug resistance to linezolid very low. Meanwhile, during the treatment, we retrieved the data of treatment prognostics from the medical records and we are unable to find the possible impact of treatment-related factors (e.g., acquired resistance to linezolid) on the treatment outcome. Additionally, the treatment outcome may be influenced by baseline disease status, the association between linezolid and treatment outcome has been adjusted for age, sex, area, and CXR severity. The treatment outcome of MDR-TB is the result of the complete treatment regimen. Hence, the observed threshold concentrations associated with successful treatment outcome need to be viewed in context of the provided treatment and setting. Given the comparable results in the development and the validation cohort, we feel confident that results can likely be extrapolated to other settings in China. However, the PK/PD threshold should be used with caution in settings outside China. Additionally, the MIC distribution has substantial influence on the PK/PD analyses and MIC

determinations show technical variability within and between different methods and laboratories. Thus, some our target may need further validation before generalized to other populations and MIC methods.

5 Conclusion

We reported an $AUC_{0\text{-}24h}$/MIC threshold of 125 associated with clinical outcomes in the MDR-TB participant in China, which may serve as a target for dose adjustment of linezolid to improve treatment outcome. Linezolid exposures associated with the WHO-recommended dose (600 mg daily) was sufficient in our setting for the majority of MDR-TB isolates and sufficient for all isolates with MGIT MIC≤.25 mg/L.

Data availability statement

The original contributions presented in the study are included in the article, further inquiries can be directed to the corresponding author.

Ethics statement

The study was approved by the ethics committee of the School of Public Health, Fudan University (IRB#2015-08-0565). The patients/participants provided their written informed consent to participate in this study.

Author contributions

Study design was done by YHu, J-WA, and JB. Participants were recruited and samples were collected under the supervision of YHu, HZ, and YHe. Laboratories were conducted by HZ and YHu. Drafts of the manuscript were prepared by HZ, YHe, and LD. Revisions of the manuscript were carried out by YHu, J-WA, JB, TS, KN, JW, and JP. The corresponding authors had full access to all data in the study and were ultimately responsible for the decision to submit it for publication.

Funding

The research leading to these results has received support from the grants from the National Natural Science Foundation of China (NSFC) (PI, YHu, No. 81874273), the Swedish Heart and Lung Foundation (TS and JB) and the Swedish Research Council (TS, JB, LD, and KN 2019-05 912).

Acknowledgments

We gratefully acknowledge all the support and contributions received from various institutions and individuals.

Conflict of interest

The authors declare that the research was conducted in the absence of any commercial or financial relationships that could be construed as a potential conflict of interest.

Publisher's note

References

Ahmad, N., Ahuja, S. D., Akkerman, O. W., Alffenaar, J. C., Anderson, L. F., Baghaei, P., et al. (2018). Treatment correlates of successful outcomes in pulmonary multidrug-resistant tuberculosis: An individual patient data meta-analysis. *Lancet* 392 (10150), 821–834. doi:10.1016/s0140-6736(18)31644-1

Alffenaar, J. W. C., Van Der Laan, T., Simons, S., Van Der Werf, T. S., Van De Kasteele, P. J., De Neeling, H., et al. (2011). Susceptibility of clinical *Mycobacterium tuberculosis* isolates to a potentially less toxic derivate of linezolid, PNU-100480. *Antimicrob. Agents Chemother.* 55 (3), 1287–1289. doi:10.1128/AAC.01297-10

Alghamdi, W. A., Al-Shaer, M. H., An, G., Alsultan, A., Kipiani, M., Barbakadze, K., et al. (2020). Population pharmacokinetics of linezolid in tuberculosis patients: Dosing regimen simulation and target attainment analysis. *Antimicrob. Agents Chemother.* 64 (10), e01174. doi:10.1128/aac.01174-20

Bolhuis, M. S., Akkerman, O. W., Sturkenboom, M. G. G., Ghimire, S., Srivastava, S., Gumbo, T., et al. (2018). Linezolid-based regimens for multidrug-resistant tuberculosis (tb): A systematic review to establish or revise the current recommended dose for tb treatment. *Clin. Infect. Dis.* 67, S327–s335. doi:10.1093/cid/ciy625

Brown, A. N., Drusano, G. L., Adams, J. R., Rodriquez, J. L., Jambunathan, K., Baluya, D. L., et al. (2015). Preclinical evaluations to identify optimal linezolid regimens for tuberculosis therapy. *mBio* 6 (6), e01741–e01715. doi:10.1128/mBio.01741-15

Chang, J. T., Dou, H. Y., Yen, C. L., Wu, Y. H., Huang, R. M., Lin, H. J., et al. (2011). Effect of type 2 diabetes mellitus on the clinical severity and treatment outcome in patients with pulmonary tuberculosis: A potential role in the emergence of multidrug-resistance. *J. Formos. Med. Assoc.* 110 (6), 372–381. doi:10.1016/s0929-6646(11)60055-7

Conradie, F., Diacon, A. H., Ngubane, N., Howell, P., Everitt, D., Crook, A. M., et al. (2020). Treatment of highly drug-resistant pulmonary tuberculosis. *N. Engl. J. Med.* 382 (10), 893–902. doi:10.1056/NEJMoa1901814

Deshpande, D., Srivastava, S., Nuermberger, E., Pasipanodya, J. G., Swaminathan, S., and Gumbo, T. (2016). Concentration-dependent synergy and antagonism of linezolid and moxifloxacin in the treatment of childhood tuberculosis: The dynamic duo. *Clin. Infect. Dis.* 63, S88–s94. doi:10.1093/cid/ciw473

Heinrichs, M. T., Drusano, G. L., Brown, D. L., Maynard, M. S., Sy, S. K. B., Rand, K. H., et al. (2019). Dose optimization of moxifloxacin and linezolid against tuberculosis using mathematical modeling and simulation. *Int. J. Antimicrob. Agents* 53 (3), 275–283. doi:10.1016/j.ijantimicag.2018.10.012

Kamp, J., Bolhuis, M. S., Tiberi, S., Akkerman, O. W., Centis, R., de Lange, W. C., et al. (2017). Simple strategy to assess linezolid exposure in patients with multi-drug-resistant and extensively-drug-resistant tuberculosis. *Int. J. Antimicrob. Agents* 49 (6), 688–694. doi:10.1016/j.ijantimicag.2017.01.017

Lee, J. Y., Kim, D. K., Lee, J.-K., Yoon, H. I., Jeong, I., Heo, E., et al. (2017). Substitution of ethambutol with linezolid during the intensive phase of treatment of pulmonary tuberculosis: Study protocol for a prospective, multicenter, randomized, open-label, phase II trial. *Trials* 18 (1), 68. doi:10.1186/s13063-017-1811-0

Lopez, B., Siqueira de Oliveira, R., Pinhata, J. M. W., Chimara, E., Pacheco Ascencio, E., Puyén Guerra, Z. M., et al. (2019). Bedaquiline and linezolid MIC distributions and epidemiological cut-off values for *Mycobacterium tuberculosis* in the Latin American region. *J. Antimicrob. Chemother.* 74 (2), 373–379. doi:10.1093/jac/dky414

Madzgharashvili, T., Salindri, A. D., Magee, M. J., Tukvadze, N., Avaliani, Z., Blumberg, H. M., et al. (2021). Treatment outcomes among pediatric patients with highly drug-resistant tuberculosis: The role of new and repurposed second-line tuberculosis drugs. *J. Pediatr. Infect. Dis. Soc.* 10 (4), 457–467. doi:10.1093/jpids/piaa139

Meregildo-Rodriguez, E. D., Asmat-Rubio, M. G., Zavaleta-Alaya, P., and Vásquez-Tirado, G. A. (2022). Effect of oral antidiabetic drugs on tuberculosis risk and treatment outcomes: Systematic review and meta-analysis. *Trop. Med. Infect. Dis.* 7 (11), 343. doi:10.3390/tropicalmed7110343

Mtabho, C. M., Semvua, H. H., van den Boogaard, J., Irongo, C. F., Boeree, M. J., Colbers, A., et al. (2019). Effect of diabetes mellitus on TB drug concentrations in Tanzanian patients. *J. Antimicrob. Chemother.* 74 (12), 3537–3545. doi:10.1093/jac/dkz368

Padayatchi, N., Bionghi, N., Osman, F., Naidu, N., Ndjeka, N., Master, I., et al. (2020). Treatment outcomes in patients with drug-resistant TB-HIV co-infection treated with bedaquiline and linezolid. *Int. J. Tuberc. Lung Dis.* 24 (10), 1024–1031. doi:10.5588/ijtld.20.0048

Pasipanodya, J. G., McIlleron, H., Burger, A., Wash, P. A., Smith, P., and Gumbo, T. (2013). Serum drug concentrations predictive of pulmonary tuberculosis outcomes. *J. Infect. Dis.* 208 (9), 1464–1473. doi:10.1093/infdis/jit352

Rudolf, F., Lemvik, G., Abate, E., Verkuilen, J., Schön, T., Gomes, V. F., et al. (2013). TBscore II: Refining and validating a simple clinical score for treatment monitoring of patients with pulmonary tuberculosis. *Scand. J. Infect. Dis.* 45 (11), 825–836. doi:10.3109/00365548.2013.826876

Singh, B., Cocker, D., Ryan, H., and Sloan, D. J. (2019). Linezolid for drug-resistant pulmonary tuberculosis. *Cochrane Database Syst. Rev.* 3 (3), Cd012836. doi:10.1002/14651858.CD012836.pub2

Singla, R., Khan, N., Al-Sharif, N., Ai-Sayegh, M. O., Shaikh, M. A., and Osman, M. M. (2006). Influence of diabetes on manifestations and treatment outcome of pulmonary TB patients. *Int. J. Tuberc. Lung Dis.* 10 (1), 74–79.

Song, T., Lee, M., Jeon, H. S., Park, Y., Dodd, L. E., Dartois, V., et al. (2015). Linezolid Trough concentrations correlate with mitochondrial toxicity-related adverse events in the treatment of chronic extensively drug-resistant tuberculosis. *EBioMedicine* 2 (11), 1627–1633. doi:10.1016/j.ebiom.2015.09.051

Sotgiu, G., Centis, R., D'Ambrosio, L., Alffenaar, J. W., Anger, H. A., Caminero, J. A., et al. (2012). Efficacy, safety and tolerability of linezolid containing regimens in treating MDR-TB and XDR-TB: Systematic review and meta-analysis. *Eur. Respir. J.* 40 (6), 1430–1442. doi:10.1183/09031936.00022912

Sotgiu, G., Centis, R., D'Ambrosio, L., Castiglia, P., and Migliori, G. B. (2015). Low minimal inhibitory concentrations of linezolid against multidrug-resistant tuberculosis strains. *Eur. Respir. J.* 45 (1), 287–289. doi:10.1183/09031936.00135014

Springer, B., Lucke, K., Calligaris-Maibach, R., Ritter, C., and Böttger, E. C. (2009). Quantitative drug susceptibility testing of *Mycobacterium tuberculosis* by use of MGIT 960 and EpiCenter instrumentation. *J. Clin. Microbiol.* 47 (6), 1773–1780. doi:10.1128/jcm.02501-08

Srivastava, S., Magombedze, G., Koeuth, T., Sherman, C., Pasipanodya, J. G., Raj, P., et al. (2017). Linezolid dose that maximizes sterilizing effect while minimizing toxicity and resistance emergence for tuberculosis. *Antimicrob. Agents Chemother.* 61 (8), e00751. doi:10.1128/aac.00751-17

Sturkenboom, M. G. G., Märtson, A. G., Svensson, E. M., Sloan, D. J., Dooley, K. E., van den Elsen, S. H. J., et al. (2021). Population pharmacokinetics and bayesian dose adjustment to advance TDM of anti-TB drugs. *Clin. Pharmacokinet.* 60 (6), 685–710. doi:10.1007/s40262-021-00997-0

Swaminathan, S., Pasipanodya, J. G., Ramachandran, G., Hemanth Kumar, A. K., Srivastava, S., Deshpande, D., et al. (2016). Drug concentration thresholds predictive of therapy failure and death in children with tuberculosis: Bread crumb trails in random forests. *Clin. Infect. Dis.* 63, S63–s74. doi:10.1093/cid/ciw471

Wasserman, S., Brust, J. C. M., Abdelwahab, M. T., Little, F., Denti, P., Wiesner, L., et al. (2022). Linezolid toxicity in patients with drug-resistant tuberculosis: A prospective cohort study. *J. Antimicrob. Chemother.* 77 (4), 1146–1154. doi:10.1093/jac/dkac019

Wasserman, S., Denti, P., Brust, J. C. M., Abdelwahab, M., Hlungulu, S., Wiesner, L., et al. (2019). Linezolid pharmacokinetics in South African patients with drug-resistant tuberculosis and a high prevalence of HIV coinfection. *Antimicrob. Agents Chemother.* 63 (3), e02164. doi:10.1128/aac.02164-18

Wasserman, S., Meintjes, G., and Maartens, G. (2016). Linezolid in the treatment of drug-resistant tuberculosis: The challenge of its narrow therapeutic index. *Expert Rev. Anti Infect. Ther.* 14 (10), 901–915. doi:10.1080/14787210.2016.1225498

World Health, O. (2013). *Definitions and reporting framework for tuberculosis – 2013 revision: Updated december 2014 and january 2020*. Geneva: World Health Organization.

World Health, O. (2018). *Technical report on critical concentrations for drug susceptibility testing of medicines used in the treatment of drug-resistant tuberculosis*. Geneva: World Health Organization.

World Health, O. (2020). *WHO consolidated guidelines on tuberculosis: Module 4: Treatment - drug-resistant tuberculosis treatment*. Geneva: World Health Organization.

Zheng, X., Davies Forsman, L., Bao, Z., Xie, Y., Ning, Z., Schön, T., et al. (2021). Drug exposure and susceptibility of second-line drugs correlate with treatment response in patients with multidrug-resistant tuberculosis: A multi-centre prospective cohort study in China. *Eur. Respir. J.* 59, 2101925. doi:10.1183/13993003.01925-2021

frontiers | Frontiers in Pharmacology

TYPE Review
PUBLISHED 02 February 2023
DOI 10.3389/fphar.2023.1100488

OPEN ACCESS

EDITED BY
Sebastian G. Wicha,
University of Hamburg, Germany

REVIEWED BY
Michal Letek,
Universidad de León, Spain
Niklas Köhler,
Research Center Borstel (LG), Germany

*CORRESPONDENCE
Jacob A. M. Stadler,
attiestadler@gmail.com

SPECIALTY SECTION
This article was submitted to Pharmacology of Infectious Diseases, a section of the journal Frontiers in Pharmacology

RECEIVED 16 November 2022
ACCEPTED 19 January 2023
PUBLISHED 02 February 2023

CITATION
Stadler JAM, Maartens G, Meintjes G and Wasserman S (2023), Clofazimine for the treatment of tuberculosis.
Front. Pharmacol. 14:1100488.
doi: 10.3389/fphar.2023.1100488

Clofazimine for the treatment of tuberculosis

Jacob A. M. Stadler[1,2]*, Gary Maartens[2,3], Graeme Meintjes[1,2] and Sean Wasserman[2,4]

[1]Department of Medicine, University of Cape Town, Cape Town, South Africa, [2]Wellcome Centre for Infectious Diseases Research in Africa, Institute of Infectious Disease and Molecular Medicine, University of Cape Town, Cape Town, South Africa, [3]Department of Medicine, Division of Clinical Pharmacology, University of Cape Town, Cape Town, South Africa, [4]Division of Infectious Diseases and HIV Medicine, Department of Medicine, University of Cape Town, Cape Town, South Africa

Shorter (6–9 months), fully oral regimens containing new and repurposed drugs are now the first-choice option for the treatment of drug-resistant tuberculosis (DR-TB). Clofazimine, long used in the treatment of leprosy, is one such repurposed drug that has become a cornerstone of DR-TB treatment and ongoing trials are exploring novel, shorter clofazimine-containing regimens for drug-resistant as well as drug-susceptible tuberculosis. Clofazimine's repurposing was informed by evidence of potent activity against DR-TB strains *in vitro* and in mice and a treatment-shortening effect in DR-TB patients as part of a multidrug regimen. Clofazimine entered clinical use in the 1950s without the rigorous safety and pharmacokinetic evaluation which is part of modern drug development and current dosing is not evidence-based. Recent studies have begun to characterize clofazimine's exposure-response relationship for safety and efficacy in populations with TB. Despite being better tolerated than some other second-line TB drugs, the extent and impact of adverse effects including skin discolouration and cardiotoxicity are not well understood and together with emergent resistance, may undermine clofazimine use in DR-TB programmes. Furthermore, clofazimine's precise mechanism of action is not well established, as is the genetic basis of clofazimine resistance. In this narrative review, we present an overview of the evidence base underpinning the use and limitations of clofazimine as an antituberculosis drug and discuss advances in the understanding of clofazimine pharmacokinetics, toxicity, and resistance. The unusual pharmacokinetic properties of clofazimine and how these relate to its putative mechanism of action, antituberculosis activity, dosing considerations and adverse effects are highlighted. Finally, we discuss the development of novel riminophenazine analogues as antituberculosis drugs.

KEYWORDS

clofazimine, riminophenazines, B663, tuberculosis, drug-resistant tuberculosis (DR-TB), multidrug-resistant tuberculosis (MDR-TB)

Introduction

Globally, nearly half a million new cases of multidrug- and rifampicin-resistant tuberculosis (MDR/RR-TB) are estimated to occur each year and this number is likely to increase due to the disruption of tuberculosis control efforts by the coronavirus disease (COVID) pandemic (World Health Organisation, 2021). For many years, treatment options for drug-resistant tuberculosis (DR-TB) were limited and required an extended treatment duration (≥18 months) using drugs with high toxicity and limited efficacy, including daily injections. The past decade has seen major developments in the DR-TB treatment landscape with considerable progress toward shorter, safer and more effective

TABLE 1 Clinical studies reporting efficacy and safety outcomes with regimens containing clofazimine (without* bedaquiline and linezolid) in adult patients with drug-resistant tuberculosis.

Study	Country	Study type	Regimen	Clofazimine dose	Regimen duration	Target population	HIV positive	Sample size	Number receiving clofazimine	Treatment success	Treatment failed	Died	Lost to follow-up	Sputum culture conversion rate	Incidence of skin discolouration
Mitnick, 2008 (Mitnick et al., 2008)	Peru	Retrospective, observational cohort	Individualized background regimen consisting of ≥ 5 of the following drugs: EMB, PZA, AMK, STR, KNM, CPM, CFX, OFX, LFX, SFX, CYS, ETO, PAS, CAC, CLM, CFZ, RFB	200–300 mg/d	Variable - individualized based on sputum culture results (median = 24.9 months)	MDR-TB and XDR-TB	1.4% (9/651)	651	447	MDR-TB: 66.3% (400/603) XDR-TB: 60.4% (29/48)	MDR-TB: 2.1% (13/603) XDR-TB: 10.4% (5/48)	MDR-TB: 20.4 (123/603) XDR-TB: 22.9% (11/48)	MDR-TB: 10.3% (62/603) XDR-TB: 6.2% (3/48)	Median time: MDR-TB: 61 days XDR-TB: 90 days	N/R
Van Deun, 2010 (Van Deun et al., 2010)	Bangladesh	Prospective, observational cohort	Six different standardized regimens used sequentially in consecutive cohorts over the study period. Regimens consisted of different combinations of the following drugs: GFX, OFX, KMC, CFZ, EMB, INH, PTO, PZA. (The most effective regimen consisted of KMC, GFX, CFZ, EMB, INH, PZA, PTO with CFZ + GFX given throughout)	100 mg/d (≥33 kg) 50 mg/d (<33 kg)	9–15 months (Most effective regimen = 9 months)	MDR-TB	Not tested (Reported as "virtually absent" in local population)	427	427 (Intensive phase only: 184; intensive and continuation phase: 243)	Overall: 78.3% (334/427) Most effective regimen: 87.9% (181/206)	Overall: 4.0% (17/427) Most effective regimen: 0.5% (1/206)	Overall: 7.7% (33/427) Most effective regimen: 5.3% (11/206)	Overall: 9.6% (41/427) Most effective regimen: 5.8% (12/206)	N/R	0%
Xu, 2012 (Xu et al., 2012b)	China	Retrospective, observational cohort	Individualized background regimen consisting of ≥ 4 of the following drugs including CFZ: AMK, CAC, AZM, CLM, CPM, EMB, GFX, LFX, MFX, OFX, PNH, PAS, PTO, PZA, INH, RPT, RFB, STR, LZD	100 mg/d	Variable - individualized based on sputum culture results	MDR-TB and XDR-TB	0%	39	39	38% (15/39)	23% (9/39)	0%	10% (4/39)	Median time: 12 weeks Proportion: 56.4% (22/39) *Time frame not specified	79.5% (31/39) 16/31 required CFZ dose adjustment or interrupted due to skin discolouration; 1 patient developed depression reportedly due to skin discolouration
Aung, 2014 (Aung et al., 2014)	Bangladesh	Prospective, observational cohort	Standardized regimen: GFX, CFZ, EMB, PZA, KNM, PTO, INH	100 mg/d (≥33 kg) 50 mg/d (<33 kg)	9–12 months	MDR-TB	Not tested (Reported as "virtually absent" in	515	515	84.5% (435/515)	1.4% (7/515)	5.6% (29/515)	7.8% (40/515)	Proportion: 93% at 2 months	N/R

(Continued on following page)

10.3389/fphar.2023.1100488

TABLE 1 (*Continued*) Clinical studies reporting efficacy and safety outcomes with regimens containing clofazimine (without* bedaquiline and linezolid) in adult patients with drug-resistant tuberculosis.

Study	Country	Study type	Regimen	Clofazimine dose	Regimen duration	Target population	HIV positive	Sample size	Number receiving clofazimine	Treatment success	Treatment failed	Died	Lost to follow-up	Sputum culture conversion rate	Incidence of skin discolouration
							local population)								
Padayatchi, 2014 (Padayatchi et al., 2014)	South Africa	Retrospective, observational cohort	Individualized background regimen consisting of a combination of the following drugs ± CFZ: PZA, CPM, ETO, MFX, OFX, PAS, TRD, EMB, INH, CAC, CLM, RIF	200–300 mg/d	Variable - individualized based on sputum culture results. (Follow-up limited to 12 months after treatment initiation.)	XDR-TB	CFZ group: 88.0% Control group: 82.9%	85	50	N/R	N/R	CFZ group: 36.0 Control group: 54.3	CFZ group: 58% (29/50) Control group: N/R	Median time: CFZ group: 16.4 weeks Control group: 11.9 weeks Culture conversion rate through 6 months favoured CFZ group: adjusted hazard ratio = 2.54, 95% CI: 0.99–6.52 Proportion at 12 months: CFZ group: 40% (20/50) Control group: 28.6% (10/35)	CFZ discontinued in 1 patient due to skin discolouration. 'Skin reaction' reported in 14% of those with adverse event data available (n = 42). Unclear if this refers to discolouration or other skin reactions
Piubello, 2014 (Piubello et al., 2014)	Niger	Prospective, observational cohort	Standardized regimen: GFX, CFZ, EMB, PZA, KNM, PTO, INH	100 mg/d (≥33 kg) 50 mg/d (<33 kg)	12–14 months	MDR-TB	1.7%	65	65	89.2% (58/65)	0%	9.2% (6/65)	1.6% (1/65)	Proportion: 93.8% at 4 months 100% at 6 months	3.1%
Kuaban, 2015 (Kuaban et al., 2015)	Cameroon	Prospective, observational cohort	Standardized regimen: GFX, CFZ, EMB, PZA, KNM, PTO, INH	100 mg/d	12–14 months	MDR-TB	20%	150	150	89.3% (134/150)	0.6% (1/150)	6.67% (10/150)	3.33% (5/150)	Proportion: 99.2% at 3 months	N/R
Tang, 2015 (Tang et al., 2015)	China	Randomized controlled trial	Individualized background regimen consisting of ≥ 5 of the following drugs ± CFZ: PTO, PZA, MFX/LFX/GFX, PAS, CPM/AMK, EMB, CLM	100 mg/d	21 months	MDR-TB	0%	105	53	CFZ arm: 73.6% (39/53) Control arm: 53.8% (28/52)	CFZ arm: 11.3% (6/53) Control arm: 28.8% (15/52)	CFZ arm: 7.5% (4/53) Control arm: 7.7% (4/52)	CFZ arm: 7.5% (4/52) Control arm: 9.6% (5/52)	Point estimates of median time not reported, but Kaplan-Meier analysis favoured CFZ arm (Log-rank p = 0.042)	94.3%
Dalcolmo, 2017 (Dalcolmo et al., 2017)	Brazil	Retrospective, observational cohort	CFZ group (2000–2006): AMK, OFX, TRD, EMB, STR, CFZ Control group (2006-2010): AMK, LFX, TRD, EMB, STR, PZA	100 mg/d (≥45 kg) 50 mg/d (<45 kg)	18 months	MDR-TB, pre-XDR-TB, XDR-TB	CFZ group: 5.5% Control group: 7.0%	2,542	1,446	CFZ arm: 60.9% (880/1,446) Control arm: 64.6% (708/1,096)	CFZ arm: 5.4% (78/1,446) Control arm: 8.7% (95/1,096)	CFZ arm: 23.7% (343/1,446) Control arm: 13.0% (142/1,096)	CFZ arm: 10.0% (144/1,446) Control arm: 13.8% (151/1,096)	N/R	50.2%
Trebucq, 2018 (Trebucq et al., 2018)	Multi-country (West and Central Africa)	Prospective, observational cohort	KNM, MFX, EMB, PZA, PTO, INH, CFZ	N/R	9–11 months	MDR-TB	19.9%	1,006	1,006	81.6% (821/1,006)	5.9% (59/1,006)	7.8% (78/1,006)	4.8% (48/1,006)	N/R	N/R
Wang, 2018 (Wang et al., 2018)	China	Randomized controlled trial	Individualized background regimen consisting of the following drugs ±	100 mg/d	36 months	XDR-TB	0%	49	22	CFZ arm: 36.4% (8/22) Control arm: 44.4% (12/27)	CFZ arm: 31.8% (7/22) Control arm:29.6% (8/27)	CFZ arm: 9.1% (2/22) Control arm: 11.1% (3/27)	CFZ arm: 22.7% (5/22) Control arm: 14.8% (4/27)	Median time: CFZ arm: 19.7 months Control arm: 20.3 months	22.7%

(Continued on following page)

10.3389/fphar.2023.1100488

TABLE 1 (*Continued*) Clinical studies reporting efficacy and safety outcomes with regimens containing clofazimine (without* bedaquiline and linezolid) in adult patients with drug-resistant tuberculosis.

Study	Country	Study type	Regimen	Clofazimine dose	Regimen duration	Target population	HIV positive	Sample size	Number receiving clofazimine	Treatment success	Treatment failed	Died	Lost to follow-up	Sputum culture conversion rate	Incidence of skin discolouration
			CFZ: CPM/AMK, MFX/LFX, PZA, EMB, PAS, PTO												
Duan, 2019 (Duan et al., 2019)	China	Randomized controlled trial	Individualized background regimen consisting of the following drugs ± CFZ: CPM/AMK, LFX, PZA, EMB, PAS, PTO, CAC	100 mg/d	24 months	MDR-TB	0%	140	66	CFZ arm: 65.1% (32/66) Control arm: 47.3% (35/74)	CFZ arm: 13.6% (9/66) Control arm: 32.4% (24/74)	CFZ arm: 6.1% (4/66) Control arm: 2.7% (2/74)	CFZ arm: 15.2% (10/66) Control arm: 15.6% (13/74)	Point estimates median time not reported, but Kaplan-Meier analysis favoured CFZ arm (Log-rank $p = 0.031$)	12.1%
Nunn, 2019 (Nunn et al., 2019)	Multi-country (Africa and Asia)	Randomized controlled trial	Short regimen (experimental): MFX, CFZ, EMB, PZA, KNM, INH, PTO Long regimen (control): Individualised as per local standard of care based on WHO guidelines. CFZ was part of standard of care in South Africa only as an optional drug	100 mg/d (≥33 kg) 50 mg/d (<33 kg)	Experimental arm (short regimen): 9–11 months Control arm (long regimen): 18–20 months	MDR-TB	32.6%	Efficacy mITT population: 369	Short regimen: 245 Long regimen: N/R	Short regimen: 78.8% (193/245) Long regimen: 79.8% (99/124)	Short regimen: 10.6% (26/245) Long regimen: 5.6% (7/124)	Short regimen: 3.7% (9/245) Long regimen: 4.0% (5/124)	Short regimen: 0.4% (1/245) Long regimen: 2.4% (3/124)	Point estimates median time not reported, but survival analysis found no difference between regimens, hazard ratio (95% CI): 1.16 (0.93–1.45)	No reports of skin discolouration. Unclear if this was due to non-occurrence or because it was not viewed as an adverse event
Du, 2020 (Du et al., 2020)	China	Randomized controlled trial	Experimental: CPM, LFX, CFZ, PTO, PZA Control: CPM, EMB, CYS, LFX, PTO, PZA	N/R	Experimental arm: 12 months Control arm: 18 months	MDR-TB	0%	135	67	Experimental arm: 68.7% (46/67) Control arm: 64.7% (44/68)	Experimental arm: 10.4% (7/67) Control arm: 14.7 (10/68)	Experimental arm: 3% (2/67) Control arm: 1.5% (1/68)	Experimental arm: 17.9% (12/67) Control arm: 19.1% (13/68)	Point estimates median time not reported, but Kaplan-Meier analysis did not find a significant difference between arms. Proportion at 3 months: Experimental arm: 68.7% Control arm: 55.9%	10.4%
Misra, 2020 (Misra et al., 2020)	South Africa	Prospective, observational cohort	Unspecified individualized background regimens including CFZ. Some received regimens containing BDQ or LZD.	100–300 mg/d	N/R	MDR-TB, pre-XDR-TB, XDR-TB	77.2%	600	<200 mg/d: 169 ≥ 200 mg/d: 431	Overall: 46.5% (279/600) <200 mg/d: 42.6% (72/169) ≥200 mg/d: 48% (207/431)	N/R	N/R	N/R	N/R	N/R

Abbreviations: AMK, amikacin; AZM, azithromycin; BDQ, bedaquiline; CAC, co-amoxiclav; CPM, capreomycin; CFZ, clofazimine; CLM, clarithromycin; CYS, cycloserine; EMB, ethambutol; ETO, ethionamide; GFX, gatifloxacin; KNM, kanamycin; LFX, levofloxacin; LZD, linezolid; MFX, moxifloxacin; OFX, ofloxacin; PNH, pasiniasid; PAS, p-aminosalicylic acid; PTO, prothionamide; PZA, pyrazinamide; INH, isoniazid; RPT, rifapentine; RFB, rifabutin; STR, streptomycin; TRD, terizidone; HIV, human immunodeficiency virus; mITT, modified intention-to-treat; N/R, not reported; MDR-TB, multidrug-resistant tuberculosis; XDR-TB, extensively drug-resistant tuberculosis; CI, confidence interval; *This is true for the majority of studies, although some patients in the studies by Xu, 2012 and Misra, 2020 received BDQ, and/or LZD.

10.3389/fphar.2023.1100488

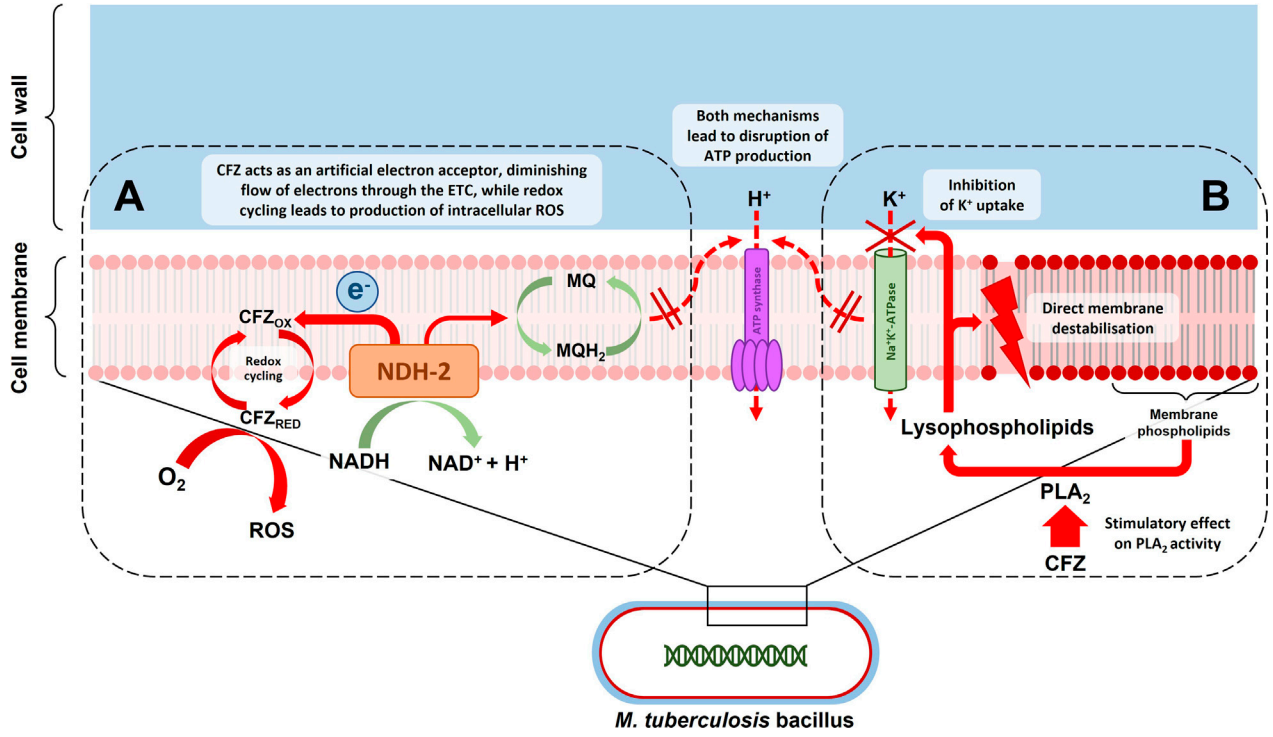

FIGURE 1
Depiction of the putative mechanisms of action of clofazimine (CFZ) acting at the level of the mycobacterial cell membrane: **(A)** CFZ competes with menaquinone (MQ) as a substrate of type 2 NADH dehydrogenase (NDH-2) in the first step of the mycobacterial electron transport chain (ETC). This draws electrons away from the ETC, possibly reducing ATP production. Reduced CFZ produced in the process is spontaneously re-oxidized in the presence of intracellular oxygen (O_2), leading to the formation of intracellular reactive oxygen species (ROS); **(B)** Clofazimine leads to an increase in lysophospholipids in a process mediated by phospholipase A_2 (PLA_2) activity. Lysophospholipids inhibit potassium (K^+) uptake and cause direct membrane destabilisation, thereby also disrupting ATP production.

therapy through the use of new and repurposed drugs. The "BPaL/M" regimen (a combination containing bedaquiline, pretomanid and dose-optimised linezolid with or without moxifloxacin for 6- to 9-month duration) was recently recommended by the World Health Organisation (WHO) as the first-choice option for the treatment of MDR/RR-TB with or without additional resistance to fluoroquinolones (World Health Organisation, 2022a). This fully oral regimen is one of the most important milestones in tuberculosis treatment of the past decade, finally bringing the duration of treatment for DR-TB back down to that of standard therapy for drug-susceptible tuberculosis (DS-TB).

Clofazimine, a repurposed anti-leprosy drug, is recommended as a key drug in shorter as well as longer DR-TB regimens (World Health Organisation, 2020). Though the "BPaL/M" regimen excludes clofazimine, it remains an important drug option for individualised DR-TB therapy and is being evaluated in ongoing trials (summarised in Table 1) as a component of novel, shorter regimens for both DR- and DS-TB. This review presents an overview of the evidence underpinning the use and limitations of clofazimine as an antituberculosis drug. The unusual pharmacokinetic properties of clofazimine and how these relate to its putative mechanism of action, antituberculosis activity, dosing considerations and adverse effects are highlighted. Finally, we discuss the development of novel riminophenazine analogues as antituberculosis drugs.

Search strategy

We performed a PubMed database search using the terms "clofazimine," "B663," "riminophenazine," "tuberculosis" and "drug-resistant tuberculosis" with no restrictions, but only considered English language articles for inclusion in this review. Studies with predominantly paediatric populations (<15 years old) were excluded. Reference lists from included publications were reviewed manually to identify any additional relevant publications and data sources.

History

Clofazimine (formerly B663) was initially described in the mid-1950s as the lead compound in a novel class of antibiotics, the riminophenazines, that showed antituberculosis activity comparable to that of isoniazid in animal studies (Barry et al., 1957). Its discovery was part of a dedicated effort to develop new antituberculosis drugs in the wake of the discovery of streptomycin, para-aminosalicylic acid (PAS) and isoniazid. Clofazimine was derived from a compound called anilinoaposafranine which in turn was synthesized from diploicin, originally extracted from a lichen called *Buellia canescens* (Barry, 1946a; Barry, 1946b; Barry et al., 1956a; Yawalkar and Vischer, 1979). In early studies in mice and hamsters, clofazimine demonstrated impressive activity,

including against isoniazid-resistant strains, without evidence of major toxicity (Barry et al., 1957). More limited activity was observed in subsequent guinea pig and primate models (Barry and Conalty, 1965) and further development of clofazimine for the treatment of tuberculosis was halted. These cross-species discrepancies were later speculated to be due to differences in drug absorption, protein binding or pathological manifestations between species (Barry et al., 1960). By the early 1960s, the efficacy of clofazimine against leprosy was demonstrated in human trials (Browne and Hogerzeil, 1962) and clofazimine became a cornerstone of leprosy treatment and is still recommended by the WHO in standard anti-leprosy multidrug therapy today (World Health Organisation, 2018a). Drug repurposing efforts during the 1990s aimed at addressing the rise in DR-TB cases revived interest in the antituberculosis activity of clofazimine (Mehta et al., 1993; Jagannath et al., 1995; Reddy et al., 1996; Adams et al., 1999). In 2010, an observational study conducted in Bangladesh reported 87% treatment success in MDR/RR-TB patients treated with a 9–11 months regimen containing gatifloxacin, an injectable aminoglycoside and clofazimine, with other drugs (Van Deun et al., 2010). This was a substantial improvement over the 50%–60% success rate seen with conventional longer (≥18 months) injection-containing regimens in programmatic settings at the time (Van Deun et al., 2010). Further clinical studies supported the efficacy of the so-called "Bangladesh regimen" in diverse settings, (Nunn et al., 2019; Schwœbel et al., 2019), while preclinical studies also demonstrated a treatment-shortening effect when clofazimine was added to both first- and second-line combination regimens (Grosset et al., 2013; Tyagi et al., 2015; Lee et al., 2017). This led to the widespread off-label use of clofazimine as part of both shorter (≤12 months) and longer (≥18 months) DR-TB regimens. In 2018, when the WHO revised its grouping of drugs for use in individualised DR-TB regimens, clofazimine was re-classified from a Group 5 agent (drugs with unclear significance) to a Group B agent (drugs with second highest priority for use), solidifying its role as a key drug in DR-TB therapy (World Health Organisation, 2018b). In addition to leprosy and tuberculosis treatment, clofazimine is also used in the treatment of some non-tuberculous mycobacteria (Kim et al., 2021) and as an anti-inflammatory agent in certain autoimmune conditions (Arbiser and Moschella, 1995; Gurfinkel et al., 2009). Clofazimine is also being explored for use against Gram-positive bacteria, (Huygens et al., 2005), as an anti-parasitic, (Tuvshintulga et al., 2016; Zhang et al., 2022a), anti-neoplastic (Ahmed et al., 2019; Xu et al., 2020) and anti-viral agent (Zhang et al., 2022b).

Physicochemical and pharmacokinetic properties

Clofazimine is a cationic, amphiphilic molecule (having both hydrophilic and hydrophobic domains) with extremely high lipophilicity and low aqueous solubility at physiological conditions (Reddy et al., 1999). Its colour varies in a solution depending on the pH, from orange-yellow in alkaline environments to deep red at neutral to mildly acidic pH to violet and eventually colourless in strongly acidic environments (O'Connor et al., 1995). These physicochemical properties contribute to the unusual pharmacokinetics (PK), putative mechanisms of action and adverse effects of clofazimine.

Due to its extremely low aqueous solubility, orally administered clofazimine in coarse crystalline form has low bioavailability with considerable inter-individual variation in absorption kinetics (Barry et al., 1960; Vischer, 1969; Banerjee et al., 1974; Levy, 1974). For this reason, the commercially available preparation (Lamprene®, Novartis Pharmaceuticals Corporation) is provided as a micronized (ultra-fine crystal) suspension in an oil-wax base, which improves absorption to around 70% of the administered dose (Vischer, 1969; Yawalkar and Vischer, 1979). Consistent with its high lipophilicity, intake with fatty food improves absorption (Vischer, 1969; Schaad-Lanyi et al., 1987; Nix et al., 2004). The mechanism by which clofazimine crosses from the gastrointestinal tract into circulation is not established, but a fraction is carried in micelles, reaching the systemic circulation *via* the lymph, although this is not thought to be the primary mode of absorption (Barry et al., 1960; O'Connor et al., 1995).

Once absorbed into the systemic circulation, distribution to peripheral compartments occurs rapidly, followed by slow re-equilibration to the central compartment (Schaad-Lanyi et al., 1987), leading to a slow rise in mean plasma concentration and a low steady-state plateau (Schaad-Lanyi et al., 1987; Abdelwahab et al., 2020). A recently published population PK model derived from DR-TB patients demonstrated an extremely large volume of distribution (10,500 L) and long elimination half-life of approximately 30 days, in contrast to previously reported values of ~10 days (Schaad-Lanyi et al., 1987) and ~70 days (Levy, 1974) based on observed data from older studies in healthy volunteers and leprosy patients. At 100 mg daily, the standard dose for tuberculosis, simulations from the population PK model showed that steady-state plasma concentrations likely exceed clofazimine's minimum inhibitory concentration (MIC) for wild-type *Mycobacterium tuberculosis* of 0.25 μg/mL but remain below the critical concentration of 1 μg/mL for resistant strains (World Health Organistation, 2018). As clofazimine is highly protein bound (Irwin et al., 2014; Swanson et al., 2015), the free (unbound) drug fraction is expected to be well below the MIC. One murine PK study suggested that clofazimine's bactericidal activity is determined by the time plasma concentrations are above MIC (T > MIC) (Swanson et al., 2016), though this *in vivo* exposure-activity relationship has not been confirmed in other studies. In mice receiving clofazimine monotherapy, serum and tissue concentrations were dose- and time-dependent, but bactericidal activity was dose-independent at doses ranging from 6.25 mg/kg to 25 mg/kg (Swanson et al., 2015). In contrast, when clofazimine was added to the standard first-line DS-TB regimen in a mouse model, there was a linear dose-response in terms of bactericidal activity (decline in lung bacterial burden), although there was no difference in the time required to achieve relapse-free cure with the addition of 12.5 mg/kg vs. 25 mg/kg of clofazimine, suggesting the same efficacy can be achieved with the lower of the two doses (Ammerman et al., 2018). Serum concentrations with this dose range in mice are approximately equivalent to that in humans with a 100 mg daily dose, though some inconsistent results in human PK studies mean that uncertainty about dose equivalence remains (Ammerman et al., 2018).

Clofazimine steady-state conditions are reached after several months a consequence of its extended half-life. The use of loading doses shortens time to steady-state, possibly achieving effective concentrations more rapidly, but may increase toxicity related to higher peak exposures. Simulations using the aforementioned

TABLE 2 Ongoing and recently completed clinical trials evaluating clofazimine-containing shorter regimens for drug-susceptible and -resistant tuberculosis.

Trial	Phase	Target population; sample size	Country	Study design and regimens	Primary efficacy outcome
Drug-susceptible tuberculosis					
NCT03474198 (TRUNCATE-TB)	Phase 2/3	DS-TB; 900 (180 per arm)	Multi-country (Asia)	Randomized, open-label, multi-arm, multi-stage trial comparing four experimental 2–3 month regimens (one CFZ-containing) *versus* 6-month standard of care for drug-susceptible tuberculosis	Unfavourable clinical outcome 96 weeks after randomisation
NCT04311502 (CLO-FAST)	Phase 2	DS-TB; 185	Multi-country	Randomized, open-label trial comparing a 3-month RPT/CFZ-containing regimen with CFZ loading dose *versus* 6-month standard of care for drug-susceptible tuberculosis	Time to stable culture conversion in liquid media through 12 weeks
NCT05556746 (PRESCIENT)	Phase 2	DS-TB; 156	South Africa, Haiti	Randomized, open-label trial comparing an 8-week regimen of BDQ, CFZ, PZA, and DLM with standard treatment for drug-susceptible pulmonary tuberculosis	Time to stable culture conversion in liquid media through 8 weeks
Drug-resistant tuberculosis					
NCT04545788	Phase 2	MDR/RR-TB; 200	China	Randomized, open-label, multi-arm trial comparing two fully oral 9–11 month experimental regimens for rifampicin-resistant tuberculosis *versus* standard of care (9–11 months injectable-containing regimen. (All regimens contain CFZ.)	Sputum culture conversion and clinical outcomes (not otherwise specified)
NCT02589782 (TB-PRACTECAL)	Phase 2/3	MDR/RR-TB, pre-XDR-TB; 552	South Africa, Belarus, Uzbekistan	Randomised, open label, multi-arm phase II-III trial evaluating short regimens containing BDQ and PA in combination with existing and re-purposed anti-TB drugs (LZD, MFZ and CFZ) for MDR-TB, irrespective of fluoroquinolone resistance	Percentage of patients with an unfavourable outcome (failure, death, recurrence, loss to follow-up) at week 72 after randomisation
NCT03828201 (DRAMATIC)	Phase 2	MDR/RR-TB; 220	Vietnam, Philippines	Multicentre, randomized, partially blinded, four-arm, phase 2 study examining the efficacy and safety of an all-oral regimen of BDQ, DLM, LFX, LZD, and CFZ for 16, 24, 32 or 40 weeks	Favourable clinical outcome ("treatment success") 76 weeks after randomisation
NCT04062201 (BEAT-TB)	Phase 3	MDR/RR-TB, pre-XDR-TB, XDR-TB; 402	South Africa	Open-label, multi-centre, randomized controlled trial comparing a 6-month regimen of BDQ, DLM, LZD, LFX and CFZ *versus* the local standard of care in South Africa (9 months)	Proportion of participants with a successful outcome at the end of treatment and at week 76
NCT03867136 (TB-TRUST)	Phase 3	MDR-TB; 354	China	Multicentre, open-label, randomized controlled trial comparing a short (24–44 weeks) all-oral regimen consisting of LFX, LZD, CYS and PZA and/or CFZ, guided by PZA susceptibility testing, *versus* the WHO standardized shorter regimen for MDR-TB (36–44 weeks)	Proportion of participants with a successful outcome 84 weeks after randomisation
TB-TRUSTplus (NCT04717908)	Phase 3	pre-XDR; 200	China	Multicentre, open-label trial evaluating a short (24–44 weeks) all-oral regimen consisting of BDQ, LZD, CYS, PZA and/or CFZ, guided by PZA susceptibility testing	Proportion of participants with a successful outcome 84 weeks after randomisation
NCT05278988	Phase 2	MDR-TB; 60	China	Randomized, open-label trial comparing a shorter (6–9 months) all-oral regimen containing BDQ, DLM, PZA and CFZ *versus* the WHO standard of care for MDR-TB (9–11 months)	Clinical outcomes at study end (18 months follow-up), not otherwise specified
NCT02754765 (endTB)	Phase 3	MDR/RR-TB; 754	Multi-country	Randomized, controlled, open-label, non-inferiority, multi-country trial evaluating the efficacy and safety of five new, all-oral, shortened regimens (three CFZ-containing) for multidrug-resistant tuberculosis (MDR-TB)	Proportion of participants with favourable outcome at week 73 after randomisation

(Continued on following page)

TABLE 2 (*Continued*) Ongoing and recently completed clinical trials evaluating clofazimine-containing shorter regimens for drug-susceptible and -resistant tuberculosis.

Trial	Phase	Target population; sample size	Country	Study design and regimens	Primary efficacy outcome
NCT03896685 (endTB-Q)	Phase 3	pre-XDR; 324	Multi-country	Randomized, controlled, open-label, non-inferiority, multi-country trial evaluating the efficacy and safety of two new, all-oral, shortened regimens for multidrug-resistant tuberculosis (MDR-TB) with fluoroquinolone resistance	Proportion of participants with favourable outcome at Week 73 randomisation
NCT05306223 (PROSPECT)	Phase 3	MDR/RR-TB; 212	China	Pragmatic, randomized, controlled trial comparing two oral short regimens (both containing CFZ) for MDR-TB.	Proportion of participants with favourable outcome at the end of treatment (week 40)

Abbreviations: BDQ, bedaquiline; CFZ, clofazimine; CYS, cycloserine; DLM, delamanid; EMB, ethambutol; LFX, levofloxacin; LZD, linezolid; MFX, moxifloxacin; PA, pretomanid; PZA, pyrazinamide; RPT, rifapentine; RFB, rifabutin; MDR-TB, multidrug-resistant tuberculosis; XDR-TB, extensively drug resistant tuberculosis; WHO, world health organisation.

population PK model predicted that a loading dose of 200 mg daily for 2–4 weeks, depending on body fat percentage, can shorten time to steady-state by several weeks without increased risk of cardiotoxicity, based on peak concentrations during the loading period not exceeding those at steady-state, and assuming peak concentration correlates with QT-interval prolongation (Abdelwahab et al., 2020). Using joint PK-pharmacodynamic (PD) modelling, a follow-up study predicted that the risk of significant QT-prolongation with a loading dose of 300 mg daily for 2 weeks was no higher than with the standard dose of 100 mg daily (Abdelwahab et al., 2021). Clinical safety of these clofazimine dosing strategies is currently being evaluated in clinical trials. In two separate studies, body fat percentage (which accounted for the significant sex differences in plasma exposures) was identified as an important determinant of clofazimine PK, suggesting an individualized approach may be required for optimal clofazimine dosing (Abdelwahab et al., 2020; Alghamdi et al., 2020).

In contrast to the low concentrations detected in plasma, massive duration-dependent accumulation of clofazimine occurs in tissues, particularly in adipose tissue and macrophage-rich organs such as the spleen, liver, lungs, gut and lymph nodes (Mansfield, 1974; Baik et al., 2013; Swanson et al., 2015). The mechanisms by which clofazimine crosses cellular membranes and the selective intra-macrophage accumulation are not fully understood, but an active transport mechanism rather than *via* passive diffusion has been hypothesized (O'Connor et al., 1995). PK studies in mice suggest that tissue accumulation of clofazimine occurs in two phases: initially, the highest concentrations are observed in fat, in keeping with passive, concentration-dependent partitioning of a highly lipophilic molecule. Later, drug concentrations in the liver, spleen, lungs and other macrophage-rich organs greatly exceed concentrations in fat (Vischer, 1969; Baik et al., 2013; Keswani et al., 2015). Biopsies of these organs display crystal-like structures of sequestrated clofazimine found exclusively inside macrophages (Baik and Rosania, 2011; Baik et al., 2013). These solid drug aggregates, known as crystal-like drug inclusions (CLDI), contain a hydrochloride salt form of clofazimine and are responsible for the blackish discolouration of macrophage-rich internal organs (Baik and Rosania, 2012; Baik et al., 2013; Murashov et al., 2018a). CLDI formation appears to be an intracellular process related to the lysosomal microenvironment inside macrophages (which have low pH and high chloride concentrations) rather than extracellular precipitation and phagocytosis of drug crystals (Baik and Rosania, 2012; Baik et al., 2013). The tendency of clofazimine to concentrate inside macrophages was recognized early on and was initially viewed as a favourable characteristic, considered to be a form of targeted drug delivery for intracellular pathogens such as *M. tuberculosis and M. leprae* (Conalty et al., 1971). Currently, however, the activity of this large pool of sequestrated drug inside macrophages is less clear. Since this stable, intracellular drug pool in CLDI gets released during *ex vivo* processing, the high concentrations of clofazimine measured in homogenised tissue samples are likely misleading and may have limited value in predicting the exposure-response relationship of clofazimine. Studies of resected lung tissue from DR-TB patients who underwent therapeutic lung resection following clofazimine treatment demonstrated that clofazimine accumulates in the outer cellular layers of granulomas and cavity walls, but penetrates poorly into the acellular, necrotic centre of caseous lesions, further complicating the relationship between tissue concentrations and drug activity (Prideaux et al., 2015; Strydom et al., 2019). Notwithstanding these difficulties with interpreting tissue concentrations, drug accumulation in macrophages and specific tissues likely increases site-of-disease concentrations thereby contributing to the efficacy of clofazimine.

The mechanisms involved in clofazimine in metabolism and excretion are not fully established. The amount of clofazimine excreted unchanged in the urine is negligible (Banerjee et al., 1974; Levy, 1974). Three urinary metabolites of clofazimine, also present in negligible concentrations, has been described (Feng et al., 1981; Feng et al., 1982). In contrast, a relatively large but variable proportion of orally administered clofazimine can be recovered unchanged in the faeces (Banerjee et al., 1974; Levy, 1974). It is unclear if faecal excretion represents incomplete absorption from the gut or biliary excretion, as high levels of clofazimine have been found in the bile and gall bladder in an autopsy study (Mansfield, 1974). Small quantities of clofazimine are also excreted in sweat, sputum, lacrimal fluid, sebum and breastmilk (Vischer, 1969; Venkatesan et al., 1997; Novartis Pharmaceuticals Corporation, 2019). Clofazimine is at least partially metabolised in the liver. An *in vitro* study using human liver microsomes identified eight metabolites of clofazimine as well as the enzymatic pathways involved in their formation, including the

important cytochrome P450 isoenzymes CYP3A4/A5 and CYP1A2 (Howlader et al., 2022). In HepaRG cells, clofazimine was a weak inducer of CYP3A4 at low concentrations, but inhibited CYP3A4 at therapeutic concentrations, suggesting a degree of auto-induction and the potential for clinically significant interactions with drugs metabolized by CYP3A4 (Horita and Doi, 2014; Shimokawa et al., 2015). However, one study among DR-TB patients did not find a significant difference in clearance of bedaquiline (a CYP3A4 substrate) or its M2 metabolite when co-administered with or without clofazimine (Maartens et al., 2018). Clofazimine tissue concentrations are not affected by co-administration with rifampicin, a strong inducer of CYP3A4 (Mamidi et al., 1995), while co-administration with isoniazid produces increased plasma and lung concentration but reduced concentrations in several other tissues (Venkatesan et al., 2007; Lu et al., 2009). In light of the limited evidence, current guidelines do not recommend dose adjustment of clofazimine or specific companion drugs during co-administration. The manufacturer's package insert advises caution when using clofazimine in patients with liver impairment but no need for dose adjustment with mild to moderate renal impairment (Novartis Pharmaceuticals Corporation, 2019), though published literature on use in these scenarios could not be found.

Because of a tendency to accumulate in fatty tissue, clofazimine is likely to equilibrate rapidly into brain tissue and may have therapeutic potential for neurological TB. Clofazimine was undetectable in cerebrospinal fluid (CSF) from patients with tuberculous meningitis (TBM) (Kempker et al., 2022) and brain tissue in autopsy studies from leprosy patients (Mansfield, 1974; Desikan and Balakrishnan, 1976). This is likely a result of extensive protein binding with extremely low concentrations of free drug equilibrating into the central nervous system from plasma; clofazimine concentrations in this compartment may be below the limit of detection of older assays and therefore may not reflect a true absence of drug. Supporting this, time-dependent tissue concentrations and widespread spatial distribution of clofazimine were demonstrated by mass spectrometry imaging throughout the brain in mice at a dose of 100 mg/kg (several-fold the therapeutic dose for tuberculosis) (Baijnath et al., 2015). At the same high dose, monotherapy with clofazimine but not linezolid was able to completely prevent central nervous system dissemination of *M.tb* after aerosol infection of mice (Baijnath et al., 2018). Case reports exist of successful treatment of patients with drug-resistant TBM using clofazimine in combination with other new and repurposed second-line agents (Tucker et al., 2019).

Mechanism of action

Clofazimine's exact mechanism of action against *M. tuberculosis* is not completely understood, but its primary actions are thought to occur at the level of cellular membranes, likely interfering with membrane-associated physiological processes including cellular respiration and ion transport (Cholo et al., 2017). This is depicted in Figure 1. Barry et al. who originally described the antituberculosis activity of clofazimine noted the redox properties of the compound and proposed a mechanism of action whereby redox cycling of clofazimine contributed to growth inhibition and cell death either through the production of intracellular oxygen radicals or partial inhibition of cellular respiration or a combination of these effects (Barry et al., 1956b). A biochemical pathway supporting this hypothesis was later described whereby clofazimine competes with menaquinone as substrate of the respiratory chain enzyme NDH-2, acting as an artificial electron acceptor (Yano et al., 2011; Lechartier and Cole, 2015), thereby shunting electrons away from the respiratory chain and ultimately decreasing adenosine triphosphate (ATP) production. It was also shown that the reduced clofazimine produced through this process is spontaneously re-oxidized in the presence of oxygen, leading to the formation of intracellular reactive oxygen species (Yano et al., 2011). Initially thought to be an NDH-2-dependent process (Yano et al., 2011), it has since been demonstrated that the bactericidal activity of clofazimine in *M. tuberculosis* does not require NDH-2 (Beites et al., 2019). Others have questioned whether this redox mechanism is clofazimine's primary mode of action and have instead produced evidence, based on studies in Gram-positive bacterial organisms, that the bactericidal activity of clofazimine is related to stimulation of phospholipase A_2 activity and production of toxic lysophospholipids which disrupt transmembrane potassium transport (Van Rensburg et al., 1992; Steel et al., 1999). Other proposed mechanisms that may contribute to clofazimine's bactericidal action include i) direct, non-specific membrane disruption (Oliva et al., 2004), ii) direct interference with bacterial potassium uptake (De Bruyn et al., 1996; Steel et al., 1999), iii) selective binding to mycobacterial DNA with blocking of template function (Morrison and Marley, 1976a; Morrison and Marley, 1976b) and iv) reversal of the inhibitory effects of certain mycobacterial proteins on phagocyte activity (Wadee et al., 1988). In summary, clofazimine appears to have multiple mechanisms of antimicrobial activity, possibly with differential importance of specific mechanisms under distinct physiological conditions (Lu et al., 2011; Cholo et al., 2017), which may explain the lack of a single dominant, target-specific genetic marker associated with clofazimine resistance (CRyPTIC Consortium, 2022).

Clofazimine resistance

The selection of clofazimine-resistant *M. tuberculosis* isolates has been demonstrated *in vitro* (Hartkoorn et al., 2014) and reported in clinical isolates (Xu et al., 2017; Nimmo et al., 2020a). The MIC distribution of clofazimine in mycobacterial growth indicator tube (MGIT) culture systems ranges between 0.125 μg/mL-0.5 μg/mL for pan-susceptible and 0.25 μg/mL-1 μg/mL for DR-TB strains (Ismail et al., 2019), with a critical concentration of 1 μg/mL recommended by the WHO (World Health Organistation, 2018). Reliable estimates of the prevalence of clofazimine resistance are not available. In a large multi-national data set of over 12,000 isolates compiled by the CRyPTIC Consortium to study genotype-phenotype associations (55% had resistance to at least one antituberculosis drug), the prevalence of phenotypic clofazimine resistance was 4.4% overall and 41% (59/142) in extensively drug-resistant isolates (XDR; resistance to rifampicin, isoniazid, fluoroquinolones and another WHO Group A drug i.e. bedaquiline or linezolid) (Consortium, 2022). A recent Korean study of 122 MDR- and XDR-TB isolates reported a 4% prevalence of phenotypic clofazimine resistance (Park et al., 2022). Two studies from South Africa examined the presence of resistance-associated variants (RAVs) in the Rv0678 gene (Rv0678 RAVs are associated with phenotypic bedaquiline resistance and cross-resistance to clofazimine) in clinical DR-TB isolates with varying exposure to clofazimine or bedaquiline

(Nimmo et al., 2020a; Nimmo et al., 2020b). Rv0678 RAVs were detected in 1.8% (7/391) and 5.4% (5/92) of pre-treatment isolates, while treatment-emergent Rv0678 RAVs occurred in 2% (8/392) and 5.7% (5/87), respectively. Although these reports give some indication of the frequency of clofazimine resistance observed in relatively large, pooled sets of clinical DR-TB isolates, they do not represent accurate prevalence estimates for the general DR-TB population or specific subgroups due to the heterogenous sampling methodology used. For example, the sampling methodology for the CRyPTIC data set was biased towards collecting resistant isolates with temporally and geographically matched susceptibles wherever possible and differed markedly between contributing sites/countries, while the country-specific reports used pooled samples contributed by multiple primary studies with diverse eligibility criteria conducted at specialized DR-TB treatment centres.

Much uncertainty still exists regarding the genetic basis of clofazimine resistance, though higher clofazimine MICs have been associated with mutations in several genes including Rv0678, Rv 1979c and Rv2535c (*pepQ)* (Zhang et al., 2015a; Almeida et al., 2016). The report by the CRyPTIC Consortium evaluated genotype-phenotype associations using whole genome sequencing and quantitative MIC data for these and other resistance-associated genes (Rv3249c, Rv 1816, mmpL5, mmpS5, mmpL3), but concluded that no single gene or small group of genes fully explains a substantial proportion of clofazimine resistance, indicating that the significance of all these genes needs further evaluation to clarify their potential role as diagnostic markers (Consortium, 2022). The resistance mechanisms involved appear not to be target-based with some genes associated with MIC elevations of more than one drug (Consortium, 2022). In this regard, bedaquiline cross-resistance is of particular concern and appears to be largely due to mutations in Rv0678 (Nimmo et al., 2020a), although Rv 1979c and *pepQ* have also been associated with low-level bedaquiline cross-resistance (Zhang et al., 2015a; Almeida et al., 2016). Rv0678 is a transcriptional repressor of MmpL5 and MmpS5 efflux pumps (Hartkoorn et al., 2014). Loss of function mutations in this gene are associated with a 2- to 4-fold rise in clofazimine MIC (Andries et al., 2014; Zhang et al., 2015a) and confer cross-resistance to bedaquiline and azole antifungal drugs (Hartkoorn et al., 2014), presumably due to over-expression of these multi-substrate efflux pumps leading to decreased intracellular concentrations of these drugs. Although cross-resistance can be selected for by exposure to any of these drugs (Hartkoorn et al., 2014), bedaquiline resistance seems to more strongly predict clofazimine cross-resistance than the converse. In the multinational CRyPTIC data set, 52.4% of bedaquiline-resistant isolates were also resistant to clofazimine, compared to only 10.6% of clofazimine-resistant isolates having cross-resistance to bedaquiline (Consortium, 2022). In another study, 100% (9/9) bedaquiline-resistant isolates were found to also be resistant to clofazimine with almost all of these (8/9) harbouring Rv0678 RAVs, but only 30% (9/30) of clofazimine resistant isolates had bedaquiline cross-resistance (Ismail et al., 2018). While these results may mean that the bulk of clofazimine resistance currently is not due to Rv0678 mutations, the observation that Rv0678-associated bedaquiline resistance strongly predicts clofazimine resistance means this picture may change over time with increasing use of bedaquiline. Adding to this concern is the long emination half-lives of both clofazimine and bedaquiline; treatment lapses with regimens containing either of these drugs may expose remaining viable bacilli to low concentrations without companion drugs for protracted periods, thereby creating a high-risk scenario for selection of resistant and cross-resistant variants. For this reason, given their key role in DR-TB treatment, surveillance capacity for both bedaquiline and clofazimine resistance should be an important pillar of the programmatic use of these drugs. No studies were found that assessed the impact of baseline or treatment-emergent clofazimine resistance on clinical or bacteriological outcomes in the context of bedaquiline-containing multidrug regimens and this warrants further study.

Activity against *M. tuberculosis*

In preclinical studies (*in vitro*, intracellular and different mouse models), clofazimine monotherapy demonstrated bactericidal activity against *M. tuberculosis* similar to that of rifampicin and isoniazid, and importantly, this activity is preserved against strains resistant to these two key first-line antituberculosis drugs (Jagannath et al., 1995; Reddy et al., 1996; Xu et al., 2012a). In mice, monotherapy with doses ranging from 6.25 mg/kg-25 mg/kg does not display early bactericidal activity (EBA; first 7–14 days of treatment) but dose-independent bactericidal activity is evident with longer exposure (Swanson et al., 2015; Ammerman et al., 2017). This lack of EBA has also been demonstrated in a phase 1 trial in patients with tuberculosis (Diacon et al., 2015). Due to the slow elimination of clofazimine, antimicrobial activity is maintained for weeks after treatment cessation, depending on the duration of administration, possibly contributing to the treatment-shortening effect associated with its use (Swanson et al., 2015; Swanson et al., 2016). Clofazimine has potent bactericidal activity against slowly-replicating persister forms of *M. tuberculosis* using diffferent *in vivo* models and a streptomycin-starved *M. tuberculosis* 18b strain infection model in mice (Cho et al., 2007; Zhang et al., 2012a; Khan et al., 2019). The ability to target these drug-tolerant subpopulations is another factor thought to play a role in its treatment-shortening potential. In contrast, clofazimine has been shown to have limited activity in the Kramnik mouse model that exhibits human-like large, caseous granuloma formation in the lungs (Irwin et al., 2014). Clofazimine was also found to be ineffective *in vitro* against biofilm-encased, non-replicating *M. tuberculosis* (Mothiba et al., 2015). It is unclear if this lack of activity is due to a lack of drug penetration to the bacilli in these experimental conditions or the dormant physiological state of the organism under such hypoxic microenvironments. These findings highlight the need for clofazimine to be used as part of combination regimens able to target *M. tuberculosis* in the diverse infection sites and physiological states present in the human host. Clofazimine exhibits additive or synergistic activity with several first- and second-line antituberculosis drugs and has been shown to shorten the time required to achieve relapse-free cure in mice by several weeks when added to both first- and second-line multidrug combinations (Williams et al., 2012; Grosset et al., 2013; Zhang et al., 2015b; Lopez-Gavin et al., 2015; Tyagi et al., 2015; Saini et al., 2019). In particular, the combination of clofazimine, bedaquiline and pyrazinamide has been consistently shown to be a synergistic and highly potent combination in the mouse model (Tasneen et al., 2011; Williams et al., 2012; Silva et al., 2016). A dose-optimized version of this combination, either alone or combined with a fourth companion drug shortens the time required to achieve relapse-free cure in mice by

75%–80%, from 16 weeks to just 3–4 weeks in Kramnik and BALB/c mouse models (Lee et al., 2017; Lee et al., 2018; Clemens et al., 2019). This regimen is currently being advanced into phase II clinical trials to assess its treatment-shortening effect for patients with DS-TB.

In humans, randomized trials evaluating the additive effect of clofazimine for DR-TB treatment are limited to four small-scale trials (49–140 total participants), all conducted in China, that compared clofazimine added to the local standard of care against the standard of care alone (Tang et al., 2015; Wang et al., 2018; Duan et al., 2019; Du et al., 2020). The standard of care regimens in all of these trials consisted of long (≥18 months), injectable-containing regimens that excluded bedaquiline and other new or repurposed drugs. None of these trials included HIV-positive patients, only one trial included patients with XDR-TB and there was no follow-up to assess for relapse or death after treatment completion. In the three trials involving only MDR-TB patients (Tang et al., 2015; Duan et al., 2019; Du et al., 2020), treatment success (the sum of the outcomes "treatment completed" or "cured") in the clofazimine arm ranged between 65.1% and 73.6% and was significantly higher than the control arm in two of the trials. Time to sputum culture conversion was also significantly shorter in the clofazimine arms in these two trials (Tang et al., 2015; Duan et al., 2019), while the other trial showed no difference (Du et al., 2020). The trial in XDR patients did not find a significant difference between arms for either treatment success (36.3% in the clofazimine group vs. 44.4% in the control group) or time to sputum culture conversion (Wang et al., 2018). In a meta-analysis, pooled results of these four trials favoured the clofazimine group with a higher probability of treatment success overall (relative risk (RR): 1.2, 95% confidence interval (CI): 1.0–1.4, $p = 0.020$) and a lower risk of treatment failure (RR: 0.5, 95% CI: 0.5–0.6, $p < 0.001$), but no difference in mortality (Wang et al., 2022). Key characteristics and results of randomized trials and observational studies evaluating the safety and efficacy of clofazimine-containing regimens (without the Group A drugs bedaqualine and linezolid) are summarised in Table 2. Though most observational studies lacked clofazimine-free controls for direct comparison, the treatment success rate in studies of shorter regimens based on the one used by Van Deun et al. in Bangladesh (Van Deun et al., 2010) ranged between 78.8% and 89.3% amongst MDR-TB patients, despite the absence of bedaqualine or linezolid (Aung et al., 2014; Piubello et al., 2014; Kuaban et al., 2015; Trebucq et al., 2018; Nunn et al., 2019). Furthermore, in the original "Bangladesh study" the group receiving clofazimine for the full duration of treatment achieved 87% treatment success compared to 66% in those receiving clofazimine during the intensive phase only (Van Deun et al., 2010). In an individual patient data meta-analysis of observational studies combining records of over 12,000 DR-TB patients from 25 countries, 824 of whom received clofazimine, the use of clofazimine (compared to non-use) was associated with a higher probability of treatment success in pooled analysis (adjusted risk difference (aRD): 0.06, 95% CI: 0.01–0.10) and in the XDR-TB subgroup, its use was associated with reduced mortality (aRD: −0.18, 95% CI: −0.27 to −0.10), but not increased treatment success (Ahmad et al., 2018).

Safety and tolerability

An important factor in the use of clofazimine for DR-TB treatment is its favourable tolerability profile compared with other second-line antituberculosis drugs. Although serious gastrointestinal complications have been reported in leprosy patients after prolonged, high-dose clofazimine treatment (McDougall et al., 1980; Chong and Ti, 1993; Singh et al., 2013), adverse events requiring interruption or cessation of the drug are infrequently reported in the tuberculosis treatment literature. (For leprosy, the WHO currently recommends a dose of 50 mg daily plus 300 mg monthly for 6–12 months (World Health Organisation, 2018c), though much higher doses and longer durations have been used for leprosy in the past and for anti-inflammatory indications e.g. 300 mg–400 mg daily to treat erythema nodosum leprosum and pyoderma gangrenosum.) (Yawalkar and Vischer, 1979; Arbiser and Moschella, 1995) The most concerning and common adverse events attributed to clofazimine are discolouration of the skin, gastrointestinal disturbances and QT interval prolongation.

Reddish-brown or blackish skin discolouration is commonly reported in patients receiving long-term clofazimine therapy for tuberculosis (Xu et al., 2012b; Tang et al., 2015; Dalcolmo et al., 2017). More pronounced skin discolouration in sun-exposed areas is reported, and phototoxicity is listed as a rare adverse effect in the manufacturer's prescribing information (Hastings et al., 1976; Yawalkar and Vischer, 1979; Novartis Pharmaceuticals Corporation, 2019). However, some larger studies reporting on skin discolouration do not seem to confirm this observation (Browne, 1965; Schulz, 1971; Moore, 1983) and a definite link between sun exposure and the severity of clofazimine-induced skin discolouration is unconfirmed. Other skin symptoms frequently reported with clofazimine include ichthyosis and pruritis (Moore, 1983; Xu et al., 2012b). Discolouration of conjunctivae, sclerae, mucosa, urine, faeces and sweat has also been reported in leprosy patients (Browne, 1965; Moore, 1983; Kumar et al., 1987). Incidence of skin discolouration in tuberculosis patients varies widely, ranging between 10% and 94% (Xu et al., 2012b; Tang et al., 2015; Dalcolmo et al., 2017; Wang et al., 2018; Duan et al., 2019; Misra et al., 2019) which may in part be explained by variation in constitutional skin pigmentation between different study populations, differences in treatment dose and duration, and the lack of a standardized definition and objective measurement methodology of skin discoloration. Two distinct discolouration phenomena have been recognized: the first type is an early onset, more subtle and generalized reddish discolouration while the second type occurs later in therapy as dark brown or blackish hyperpigmentation that is more localized and differentially affects the inflammatory lesions found in leprosy patients (Browne, 1965; Levy and Randall, 1970; Job et al., 1990; Bishnoi et al., 2019). Generalized, reddish discolouration also occurs in mice exposed to clofazimine resulting from partitioning of free clofazimine into subcutaneous fat and skin tissue, rather than the hydrochloride salt form found within macrophages containing CLDI (Murashov et al., 2018a). However, skin biopsies from hyperpigmented inflammatory lesions in leprosy patients have confirmed lesional infiltration by foamy macrophages containing both clofazimine CLDI and ceroid lipofuscin pigment aggregates, both of which can contribute to the characteristic darkening of these lesions (Job et al., 1990; Bishnoi et al., 2019). The onset of visible skin discolouration can become noticeable within days to weeks and typically takes several months to resolve after treatment cessation, but detailed time course data are limited (Browne, 1965; Moore, 1983). Subjectively judged severity/intensity of skin and organ discoloration has been reported to correlate with treatment dose and duration in

animal studies (Swanson et al., 2015), but this has not been objectively quantified or related to plasma drug concentrations. One retrospective review of clofazimine toxicity among DR-TB patients in South Africa did not find a statistically significant difference in the occurrence of skin discolouration between different dose-weight categories (Misra et al., 2019). Skin discolouration is not a frequent reason for interruption or cessation of clofazimine therapy by treating clinicians as the condition is largely considered a cosmetic rather than toxicity problem (Moore, 1983; Dalcolmo et al., 2017). However, in one study, patients described skin changes as "stigmatizing" (Ramu and Iyer, 1976) and case reports of depression have been linked to skin discolouration (Tang et al., 2015), illustrating the adverse impact it may have on patients' quality of life. In a recent trial conducted in China evaluating alternative short all-oral regimens that factored in drug affordability and patients' willingness to tolerate skin discolouration, more than 10% of patients opted out of clofazimine treatment when given the option (Fu et al., 2021). These reports suggest that clofazimine-induced skin discoloration may significantly impact on quality of life and psychological wellbeing in some patients or populations and may ultimately affect willingness to adhere to treatment, if ignored.

As with skin, multiple reports exit of brownish discoloration with crystalline deposits affecting the conjunctiva, cornea, and lacrimal fluid of patients (Ohman and Wahlberg, 1975; Wålinder et al., 1976; Nêgrel et al., 1984; Barot et al., 2011). Clofazimine's package insert includes a warning of associated dimness of vision, burning, and itching of eyes (Novartis Pharmaceuticals Corporation, 2019), though in many cases eye discolouration appears to be asymptomatic (Wålinder et al., 1976; Nêgrel et al., 1984). Clofazimine has also been associated with retinal degeneration, though cytomegalovirus could not be excluded as a possible contributing cause in these patients with advanced HIV disease (Craythorn et al., 1986; Cunningham et al., 1990). Ocular complications of clofazimine tend to be associated with higher doses given for anti-inflammatory indications or during very prolonged treatment in patients with leprosy (Wålinder et al., 1976; Nêgrel et al., 1984; Barot et al., 2011), and reports of eye complications is rare in the tuberculosis treatment literature. Like skin discolouration, most eye changes improve over the course of months once clofazimine is stopped (Wålinder et al., 1976; Barot et al., 2011).

Cardiac safety concerns associated with clofazimine are based on several lines of evidence. A case report of *torsade de pointes* in a leprosy patient which occurred after prolonged, high-dose clofazimine treatment identified the drug as the most likely cause of the arrhythmia after the exclusion of other causes (Choudhri et al., 1995). Clofazimine strongly inhibits hERG cardiac potassium channels (Wallis, 2016), which results in QT-prolongation, with potential for ventricular arrhythmias and sudden cardiac death (Chen et al., 1999; Lehmann et al., 2018). Corrected QT-interval (QTc) prolongation ≥ 500 ms has been shown to correlate with an increased risk of *torsade de pointes* (Li and Ramos, 2017). In a 14-day EBA study in DS-TB patients, clofazimine monotherapy produced a duration-dependent increase from baseline in corrected QT-interval (ΔQTc) that was higher than in study arms not including any QT-prolonging drugs (Diacon et al., 2015). Though the QTc increase in this study was modest (range: 16–20 ms), clofazimine exposure was not yet at steady-state due to the short study duration. Using data from the same study, modeling and simulation of the concentration-QTc relationship predicted a mean QTc increase at steady-state of 28.5 ms with a clofazimine dose of 100 mg daily, which is higher than the values reported for the other commonly used QT-prolonging DR-TB drugs moxifloxacin, bedaquiline and delamanid (Abdelwahab et al., 2021). An important concern is a potential for additive cardiotoxicity when clofazimine is co-administered with other QT-prolonging drugs, as is the case in current WHO-recommended DR-TB regimens (World Health Organisation, 2022b). In the EBA trial, an increase from pretreatment baseline (ΔQTc) value ≥ 60 ms was noted in 7% (1/15) of patients receiving clofazimine alone and 27% (4/15) of patients receiving clofazimine, bedaquiline and pretomanid combined (Diacon et al., 2015). A phase 2 bedaquiline trial reported a mean maximum change from baseline in QTc (ΔQTc_{max}) of 12.3 ms in those receiving bedaquiline alone compared to 31.9 ms in those taking bedaquiline plus clofazimine (Pym et al., 2016). In the STREAM-1 trial, the median ΔQTc_{max} was 50 ms (IQR: 36-66) in the intervention arm containing clofazimine plus high-dose moxifloxacin compared to 30 ms (IQR: 22-41) in the control arm containing a fluoroquinolone without clofazimine (Hughes et al., 2022). The rate at which a QTc ≥ 500 ms occurred was also higher in the intervention than the control arm (hazard ratio: 2.3, 95% CI: 1.0–5.3) and the proportion of patients who developed a QTc ≥ 500 ms was numerically higher in those receiving clofazimine, although the difference was not statistically significant (11% vs. 6.4%, $p = 0.14$). Four cases of sudden death were reported in the trial, although only one in each arm was attributed to tuberculosis treatment and not explicitly linked to QT-prolongation. In the same trial, having a QTc of ≥ 400 ms at baseline was predictive for developing a QTc ≥ 500 ms, while the per kilogram dose of clofazimine and moxifloxacin was not (Hughes et al., 2022). Optimised clofazimine dosing strategies, specifically the use of loading doses, should take these cardiac safety concerns into consideration. As discussed earlier, a PK-PD simulation showed that a loading dose of 300 mg daily for 2 weeks may not increase the risk of severe QT prolongation while reducing the time to steady state (Abdelwahab et al., 2021). In this study the predicted proportion with a ΔQTc increase >30 ms from baseline by the end of the loading period was 31%, compared with 33% at steady-state with either the standard 100 mg daily or loading dose regimen and the proportion with an absolute QTc >450 ms was 3.4% at steady state with eitherdosing strategy. In view of these findings, regular electrocardiographic monitoring is recommended with clofazimine-containing regimens, especially when combined with other QT-prolonging drugs.

Gastrointestinal upset (including anorexia, nausea and vomiting, diarrhoea and abdominal pain) is frequently reported as a clofazimine-related adverse event in the leprosy literature and is particularly linked to the use of higher doses for anti-inflammatoryindications (Jopling, 1976). In some cases, abdominal pain was severe enough to warrant laparotomy (Jopling, 1976; Chong and Ti, 1993; Sukpanichnant et al., 2000). The causal role of clofazimine in these symptoms was based on a temporal association between symptom onset and start of treatment, the resolution of symptoms after decreasing or withdrawing the drug and exclusion of other obvious causes for the symptoms (Jopling, 1976). With DR-TB treatment, gastrointestinal intolerance appears to be less of an issue than with leprosy treatment, possibly due to the lower doses used for tuberculosis. Gastrointestinal symptoms have been reported with varying frequency in observational studies of tuberculosis patients treated with clofazimine (Padayatchi et al., 2014; Dalcolmo et al., 2017; Trebucq et al., 2018; Misra et al., 2019), but causal inference is confounded by the co-administration

of several other medications that can cause similar symptoms. The incidence of gastrointestinal symptoms in controlled trials did not differ significantly between those receiving and those not receiving clofazimine (Tang et al., 2015; Duan et al., 2019; Du et al., 2020). Overall, gastrointestinal symptoms appear to be mostly mild, with no reports of clofazimine being stopped due to gastrointestinal intolerance during DR-TB treatment.

Long-term studies in leprosy patients have not found evidence of clinically significant abnormalities in haematological, renal, hepatic or pancreatic blood parameters (Hastings et al., 1976; Costa Queiroz et al., 2002). In the four Chinese randomized trials among DR-TB patients (Tang et al., 2015; Wang et al., 2018; Duan et al., 2019; Du et al., 2020), the rate of haematological abnormalities, renal impairment and hepatic injury did not differ significantly between study arms, except in one trial where liver function test abnormalities were reported in 12% (8/66) of patients in the clofazimine group compared with 3% (2/74) in the standard of care group ($p = 0.046$) (Duan et al., 2019). Taken together, clofazimine does not appear to require routine laboratory investigations other than periodic monitoring of liver function tests.

New developments

Much effort has been dedicated to developing clofazimine derivatives with improved pharmacokinetic and toxicity profiles by targeting less lipophilic compounds, anticipated to cause less tissue accumulation and discolouration as well as improved oral bioavailability (Jagannath et al., 1995; Reddy et al., 1996; van Rensburg et al., 2000; Kamal et al., 2005; Lu et al., 2011; Zhang et al., 2012b; Li et al., 2012; Liu et al., 2012; Zhang et al., 2014; Xu et al., 2019; Bvumbi et al., 2021; Saravanan et al., 2021). An attempt has also been made to alter the intrinsic colour, but this required modifications to the phenazine core, which eliminated antituberculosis activity (Liu et al., 2012). Of the hundreds of analogues synthesized and screened, several have been identified with equivalent or greater *in vitro* and animal model *in vivo* activity against *M. tuberculosis* than clofazimine while reportedly also producing less tissue discolouration and no other overt toxicity (Jagannath et al., 1995; Reddy et al., 1996; van Rensburg et al., 2000; Lu et al., 2011; Zhang et al., 2012b; Liu et al., 2012). One novel riminophenazine, TBI-166 (also called pyrifazimine), has advanced to clinical evaluation (ChiCTR 1800018780, 2018; NCT04670120, 2020). TBI-166 demonstrated activity equivalent to clofazimine in mice and produced less discolouration (Xu et al., 2019). Several TBI-166-containing combination regimens have been evaluated *in vitro* and mice demonstrating synergistic activity with the same companion drugs as clofazimine (Zhang et al., 2019; Ding et al., 2022). The combination of TBI-166 plus bedaquiline and pyrazinamide has been identified as the most potent TBI-166 combination evaluated, showing sterilizing activity comparable to the BPaL regimen in a mouse model (Ding et al., 2022). One study evaluated Rv0678 mutations as a mechanism of TBI-166 resistance and found these caused a lower fold change in MIC for TBI-166 than for both clofazimine and BDQ (Xu et al., 2019). Spontaneous resistance to TBI-166 was reported in *M. tuberculosis* wild-type strains, but the genetic basis for this has not been studied (Xu et al., 2019). Another novel analogue was recently described which maintained activity against a strain resistant to clofazimine, suggesting the possibility of a different mechanism of action (Zhao et al., 2022). In view of the riminophenazines' unique mechanism of action and synergistic activity with the combination of bedaquiline and pyrazinamide, the prospect of a novel riminophenazine analogue producing less skin discolouration that has advanced to the clinical evaluation stage is exciting and ongoing efforts to achieve this goal remain important.

Novel drug delivery strategies are another approach being pursued to overcome some of the limiting properties of clofazimine. Clofazimine can be encapsulated in liposomes, allowing for parenteral administration, which is not possible with the free drug due to its low aqueous solubility (Mehta et al., 1993). In murine models, intravenously administered liposomal clofazimine increased the maximum tolerated dose by 8-fold (Mehta, 1996). Intravenous liposomal clofazimine at a dose of 50 mg/kg showed significantly better *in vivo* therapeutic activity against *M. tuberculosis* than the maximum tolerated dose of the free drug (Mehta, 1996; Adams et al., 1999). Other strategies to improve bioavailability or enable parenteral administration (both intravenous and inhaled) include nanocrystalline suspensions and nanoparticle encapsulation of clofazimine (Peters et al., 2000; Verma et al., 2013; Valetti et al., 2017; Murashov et al., 2018b; Chen et al., 2018). In one study, twice weekly inhaled clofazimine showed some efficacy against *M. tuberculosis* in a mouse model (Verma et al., 2013) and in another study, an intravenously administered formulation appeared to completely circumvent skin discolouration (Murashov et al., 2018b). Nanoparticle-based targeted delivery of clofazimine aimed at improving intra-macrophage activity (Pawde et al., 2020) and central nervous system penetration (de Castro et al., 2021) has also been described. TBM is one of the specific clinical scenarios where these optimised drug delivery strategies may theoretically be of value. However, none of these strategies has advanced beyond the early preclinical stage, likely due to their relative niche, albeit important, applications.

Discussion

Clofazimine entered clinical use without the rigorous pharmacokinetic and safety evaluation which is part of modern drug development. It is hampered by extremely low aqueous solubility, leading to erratic absorption and low plasma concentrations. It has a very long elimination half-life and accumulates extensively in certain tissues leading to skin discolouration and drug crystal deposition in macrophages. However, due to its potent activity against *M. tuberculosis* strains resistant to rifampicin and isoniazid, clofazimine has become widely used in DR-TB treatment over the past decade. Despite its apparent lack of early bactericidal activity, clofazimine contributes synergistic sterilizing activity and treatment-shortening potential to several first- and second-line drug combination regimens. Clofazimine's mechanism of action appears to be multi-modal and is likely related to its interaction with the mycobacterial respiratory chain leading to a combination of intracellular pro-oxidative effects, and disruption of cellular respiration and potassium uptake. Resistance to clofazimine still appears to be relatively uncommon, but is driven to some extent by cross-resistance with bedaquiline and is therefore likely to increase with increasing use of bedaquiline and clofazimine in TB programmes. For this reason, drug susceptibility testing is necessary for patients with prior exposure to these drugs, and population-level

surveillance should be undertaken in high-burden settings where these drugs are used programmatically to monitor the emergence of population-level resistance to these key drugs. Clofazimine-induced skin discolouration is the most frequent adverse effect of the drug, and though it is regarded as a cosmetic rather than a safety concern, it can potentially lead to stigma and may have a profound impact on psychological wellbeing and potentially pose a risk to treatment adherence. The advancement of pyrifazimine, a less lipophilic clofazimine analogue reportedly causing less skin discolouration, into early-phase clinical testing is an encouraging prospect toward improving the tolerability of riminophenazines. The QT prolonging of clofazimine, causing QT prolongation, especially when combined with other QT prolonging drugs such as bedaquiline and fluoroquinolones, areimportant, but infrequently result in clinically significant events (Hewison et al., 2022) and need to be weighed up against the risks associated with alternative drug choices. Electrocardiographic monitoring is indicated when clofazimine is combined with other QT-prolonging drugs. Despite the body of evidence supporting its safety and efficacy for DR-TB treatment and over a decade of used in many national programmes, clofazimine is not yet registered for tuberculosis treatment in several countries, still requiring off-label use and creating a barrier to access in these jurisdictions.

As the incidence of drug-resistant tuberculosis rises and resistance to new and repurposed drugs emerges, the value of each antituberculosis drug class with a distinct mechanism of action cannot be underestimated. For this reason, despite the limitations of clofazimine, the riminophenazines remain important, whether for individualized therapy in people with difficult-to-treat DR-TB or potentially as a first-line agent as part of a novel, shorter DS-TB or DR-TB regimens. In this context, the development of novel riminophenazine analogues with equivalent activity but an improved pharmacokinetic and tolerability profile to eventually replace clofazimine will be highly desirable and efforts toward their discovery and development for clinical use should be a priority.

Author contributions

JS was responsible for drafting and editing the manuscript. SW, GAM and GRM contributed to manuscript revision, and read and approved the submitted version.

Funding

SW was supported by the National Institutes of Health (K43TW011421 and U01AI170426). JS was supported by the National Research Foundation (NRF) of South Africa (Grant No 64787). GRM was supported by the Wellcome Trust (214321/Z/18/Z), and the South African Research Chairs Initiative of the Department of Science and Innovation and National Research Foundation (NRF) of South Africa (Grant No 64787). This work was supported by the Wellcome Trust through core funding from the Wellcome Centre for Infectious Diseases Research in Africa (203135/Z/16/Z).

Conflict of interest

The authors declare that the research was conducted in the absence of any commercial or financial relationships that could be construed as a potential conflict of interest.

Publisher's note

References

Abdelwahab, M. T., Court, R., Everitt, D., Diacon, A. H., Dawson, R., Svensson, E. M., et al. (2021). Effect of clofazimine concentration on QT prolongation in patients treated for tuberculosis. *Antimicrob. Agents Chemother.* 65 (7), e0268720. doi:10.1128/AAC.02687-20

Abdelwahab, M. T., Wasserman, S., Brust, J. C. M., Gandhi, N. R., Meintjes, G., Everitt, D., et al. (2020). Clofazimine pharmacokinetics in patients with TB: Dosing implications. *J. Antimicrob. Chemother.* 75, 3269–3277. doi:10.1093/jac/dkaa310

Adams, L. B., Sinha, I., Franzblau, S. G., Krahenbuhl, J. L., and Mehta, R. T. (1999). Effective treatment of acute and chronic murine tuberculosis with liposome-encapsulated clofazimine. *Antimicrob. Agents Chemother.* 43 (7), 1638–1643. doi:10.1128/AAC.43.7.1638

Ahmad, N., Ahuja, S. D., Akkerman, O. W., Alffenaar, J. C., Anderson, L. F., Baghaei, P., et al. (2018). Treatment correlates of successful outcomes in pulmonary multidrug-resistant tuberculosis: An individual patient data meta-analysis. *Lancet* 392 (10150), 821–834. doi:10.1016/S0140-6736(18)31644-1

Ahmed, K., Koval, A., Xu, J., Bodmer, A., and Katanaev, V. L. (2019). Towards the first targeted therapy for triple-negative breast cancer: Repositioning of clofazimine as a chemotherapy-compatible selective Wnt pathway inhibitor. *Cancer Lett.* 449, 45–55. doi:10.1016/j.canlet.2019.02.018

Alghamdi, W. A., Al-Shaer, M. H., Kipiani, M., Barbakadze, K., Mikiashvili, L., Kempker, R. R., et al. (2020). Pharmacokinetics of bedaquiline, delamanid and clofazimine in patients with multidrug-resistant tuberculosis. *J. Antimicrob. Chemother.*

Almeida, D., Ioerger, T., Tyagi, S., Li, S. Y., Mdluli, K., Andries, K., et al. (2016). Mutations in pepQ confer low-level resistance to bedaquiline and clofazimine in *Mycobacterium tuberculosis*. *Antimicrob. Agents Chemother.* 60 (8), 4590–4599. doi:10.1128/AAC.00753-16

Ammerman, N. C., Swanson, R. V., Bautista, E. M., Almeida, D. V., Saini, V., Omansen, T. F., et al. (2018). Impact of clofazimine dosing on treatment shortening of the first-line regimen in a mouse model of tuberculosis. *Antimicrob. Agents Chemother.* 62 (7), 006366-18. doi:10.1128/AAC.00636-18

Ammerman, N. C., Swanson, R. V., Tapley, A., Moodley, C., Ngcobo, B., Adamson, J., et al. (2017). Clofazimine has delayed antimicrobial activity against *Mycobacterium tuberculosis* both *in vitro* and *in vivo*. *J. Antimicrob. Chemother.* 72 (2), 455–461. doi:10.1093/jac/dkw417

Andries, K., Villellas, C., Coeck, N., Thys, K., Gevers, T., Vranckx, L., et al. (2014). Acquired resistance of *Mycobacterium tuberculosis* to bedaquiline. *PLoS One* 9 (7), e102135. doi:10.1371/journal.pone.0102135

Arbiser, J. L., and Moschella, S. L. (1995). Clofazimine: A review of its medical uses and mechanisms of action. *J. Am. Acad. Dermatol* 32 (2), 241–247. doi:10.1016/0190-9622(95)90134-5

Aung, K. J., Van Deun, A., Declercq, E., Sarker, M. R., Das, P. K., Hossain, M. A., et al. (2014). Successful '9-month Bangladesh regimen' for multidrug-resistant tuberculosis among over 500 consecutive patients. *Int. J. Tuberc. Lung Dis.* 18 (10), 1180–1187. doi:10.5588/ijtld.14.0100

Baijnath, S., Moodley, C., Ngcobo, B., Singh, S. D., Kruger, H. G., Arvidsson, P. I., et al. (2018). Clofazimine protects against *Mycobacterium tuberculosis* dissemination in the central nervous system following aerosol challenge in a murine model. *Int. J. Antimicrob. Agents* 51 (1), 77–81. doi:10.1016/j.ijantimicag.2017.08.020

Baijnath, S., Naiker, S., Shobo, A., Moodley, C., Adamson, J., Ngcobo, B., et al. (2015). Evidence for the presence of clofazimine and its distribution in the healthy mouse brain. *J. Mol. Histol.* 46 (4-5), 439–442. doi:10.1007/s10735-015-9634-3

Baik, J., and Rosania, G. R. (2012). Macrophages sequester clofazimine in an intracellular liquid crystal-like supramolecular organization. *PLoS One* 7 (10), e47494. doi:10.1371/journal.pone.0047494

Baik, J., and Rosania, G. R. (2011). Molecular imaging of intracellular drug-membrane aggregate formation. *Mol. Pharm.* 8 (5), 1742–1749. doi:10.1021/mp200101b

Baik, J., Stringer, K. A., Mane, G., and Rosania, G. R. (2013). Multiscale distribution and bioaccumulation analysis of clofazimine reveals a massive immune system-mediated xenobiotic sequestration response. *Antimicrob. Agents Chemother.* 57 (3), 1218–1230. doi:10.1128/AAC.01731-12

Banerjee, D. K., Ellard, G. A., Gammon, P. T., and Waters, M. F. (1974). Some observations on the pharmacology of clofazimine (B663). *Am. J. Trop. Med. Hyg.* 23 (6), 1110–1115. doi:10.4269/ajtmh.1974.23.1110

Barot, R. K., Viswanath, V., Pattiwar, M. S., and Torsekar, R. G. (2011). Crystalline deposition in the cornea and conjunctiva secondary to long-term clofazimine therapy in a leprosy patient. *Indian J. Ophthalmol.* 59 (4), 328–329. doi:10.4103/0301-4738.82012

Barry, V. C. (1946). Anti-Tubercular compounds. *Nature* 158 (4024), 863–865. doi:10.1038/158863a0

Barry, V. C., Belton, J. G., Conalty, M. L., Denneny, J. M., Edward, D. W., O'Sullivan, J. F., et al. (1957). A new series of phenazines (rimino-compounds) with high antituberculosis activity. *Nature* 179 (4568), 1013–1015. doi:10.1038/1791013a0

Barry, V. C., Belton, J. G., O'Sullivan, J. F., and Twomey, D. (1956). 650. The oxidation of derivatives of o-phenylenediamine. Part IV. A new series of glyoxalinophenazines derived from anilinoaposafranines and their behaviour on hydrogenation. *J. Chem. Soc. (Resumed)* (0), 3347–3350. doi:10.1039/jr9560003347

Barry, V. C., Buggle, K., Byrne, J., Conalty, M. L., and Winder, F. (1960). Absorption, distribution and retention of the riminocompounds in the experimental animal. *Ir. J. Med. Sci.* 416, 345–352. doi:10.1007/BF02945619

Barry, V. C., Conalty, M. L., and Gaffney, E. E. (1956). Antituberculosis activity in the phenazine series; isomeric pigments obtained by oxidation of o-phenylenediamine derivatives. *J. Pharm. Pharmacol.* 8 (12), 1089–1096. doi:10.1111/j.2042-7158.1956.tb12238.x

Barry, V. C., and Conalty, M. L. (1965). The antimycobacterial activity of B 663. *Lepr. Rev.* 36, 3–7. doi:10.5935/0305-7518.19650002

Barry, V. C. (1946). The thyroid and tuberculosis. *Nature* 158 (4004), 131. doi:10.1038/158131d0

Beites, T., O'Brien, K., Tiwari, D., Engelhart, C. A., Walters, S., Andrews, J., et al. (2019). Plasticity of the *Mycobacterium tuberculosis* respiratory chain and its impact on tuberculosis drug development. *Nat. Commun.* 10 (1), 4970. doi:10.1038/s41467-019-12956-2

Bishnoi, A., Chatterjee, D., Narang, T., and Dogra, S. (2019). Image Gallery: Clofazimine-induced hyperpigmentation of leprosy plaques. *Br. J. Dermatol* 181 (4), e88. doi:10.1111/bjd.18171

Browne, S. G., and Hogerzeil, L. M. (1962). "B 663" in the treatment of leprosy. Preliminary report of a pilot trial. *Lepr. Rev.* 33, 6–10. doi:10.5935/0305-7518.19620002

Browne, S. G. (1965). Red and black pigmentation developing during treatment of leprosy with 'B663. *Lepr. Rev.* 36, 17–20. doi:10.5935/0305-7518.19650005

Bvumbi, M. V., van der Westhuyzen, C., Mmutlane, E. M., and Ngwane, A. (2021). Riminophenazine derivatives as potential antituberculosis agents: Synthesis, biological, and electrochemical evaluations. *Molecules* 26 (14), 4200. doi:10.3390/molecules26144200

Chen, J., Zou, A., Splawski, I., Keating, M. T., and Sanguinetti, M. C. (1999). Long QT syndrome-associated mutations in the Per-Arnt-Sim (PAS) domain of HERG potassium channels accelerate channel deactivation. *J. Biol. Chem.* 274 (15), 10113–10118. doi:10.1074/jbc.274.15.10113

Chen, W., Cheng, C. A., Lee, B. Y., Clemens, D. L., Huang, W. Y., Horwitz, M. A., et al. (2018). Facile strategy enabling both high loading and high release amounts of the water-insoluble drug clofazimine using mesoporous silica nanoparticles. *ACS Appl. Mater Interfaces* 10 (38), 31870–31881. doi:10.1021/acsami.8b09069

ChiCTR1800018780 (2018). *The evaluation of pyrifazimine in healthy subjects a single-center, randomized, double-blind, placebo-controlled, multidoses, single-dose, tolerability, pharmacokinetics and pharmacodynamics of phase ia of clinical trial 2018*. available from: http://www.chictr.org.cn/showprojen.aspx?proj=31595.

Cho, S. H., Warit, S., Wan, B., Hwang, C. H., Pauli, G. F., and Franzblau, S. G. (2007). Low-oxygen-recovery assay for high-throughput screening of compounds against nonreplicating *Mycobacterium tuberculosis*. *Antimicrob. Agents Chemother.* 51 (4), 1380–1385. doi:10.1128/AAC.00055-06

Cholo, M. C., Mothiba, M. T., Fourie, B., and Anderson, R. (2017). Mechanisms of action and therapeutic efficacies of the lipophilic antimycobacterial agents clofazimine and bedaquiline. *J. Antimicrob. Chemother.* 72 (2), 338–353. doi:10.1093/jac/dkw426

Chong, P. Y., and Ti, T. K. (1993). Severe abdominal pain in low dosage clofazimine. *Pathology* 25 (1), 24–26. doi:10.3109/00313029309068897

Choudhri, S. H., Harris, L., Butany, J. W., and Keystone, J. S. (1995). Clofazimine induced cardiotoxicity--a case report. *Lepr. Rev.* 66 (1), 63–68. doi:10.5935/0305-7518.19950009

Clemens, D. L., Lee, B. Y., Silva, A., Dillon, B. J., Masleša-Galić, S., Nava, S., et al. (2019). Artificial intelligence enabled parabolic response surface platform identifies ultra-rapid near-universal TB drug treatment regimens comprising approved drugs. *PLoS One* 14 (5), e0215607. doi:10.1371/journal.pone.0215607

Conalty, M. L., Barry, V. C., and Jina, A. (1971). The antileprosy agent B.663 (Clofazimine) and the reticuloendothelial system. *Int. J. Lepr. Other Mycobact. Dis.* 39 (2), 479–492.

Consortium, C. RyP. T. I. C. (2022). A data compendium associating the genomes of 12,289 *Mycobacterium tuberculosis* isolates with quantitative resistance phenotypes to 13 antibiotics. *PLoS Biol.* 20 (8), e3001721. doi:10.1371/journal.pbio.3001721

Costa Queiroz, R. H., de Souza, A. M., Sampaio, S. V., and Melchior, E., Jr (2002). Biochemical and hematological side effects of clofazimine in leprosy patients. *Pharmacol. Res.* 46 (2), 191–194. doi:10.1016/s1043-6618(02)00086-5

Craythorn, J. M., Swartz, M., and Creel, D. J. (1986). Clofazimine-induced bull's-eye retinopathy. *Retina* 6 (1), 50–52. doi:10.1097/00006982-198600610-00003

CRyPTIC Consortium (2022). Genome-wide association studies of global *Mycobacterium tuberculosis* resistance to 13 antimicrobials in 10,228 genomes identify new resistance mechanisms. *PLoS Biol.* 20 (8), e3001755. doi:10.1371/journal.pbio.3001755

Cunningham, C. A., Friedberg, D. N., and Carr, R. E. (1990). Clofazamine-induced generalized retinal degeneration. *Retina* 10 (2), 131–134. doi:10.1097/00006982-199004000-00008

Dalcolmo, M., Gayoso, R., Sotgiu, G., D'Ambrosio, L., Rocha, J. L., Borga, L., et al. (2017). Effectiveness and safety of clofazimine in multidrug-resistant tuberculosis: A nationwide report from Brazil. *Eur. Respir. J.* 49 (3), 1602445. doi:10.1183/13993003.02445-2016

De Bruyn, E. E., Steel, H. C., Van Rensburg, E. J., and Anderson, R. (1996). The riminophenazines, clofazimine and B669, inhibit potassium transport in gram-positive bacteria by a lysophospholipid-dependent mechanism. *J. Antimicrob. Chemother.* 38 (3), 349–362. doi:10.1093/jac/38.3.349

de Castro, R. R., do Carmo, F. A., Martins, C., Simon, A., de Sousa, V. P., Rodrigues, C. R., et al. (2021). Clofazimine functionalized polymeric nanoparticles for brain delivery in the tuberculosis treatment. *Int. J. Pharm.* 602, 120655. doi:10.1016/j.ijpharm.2021.120655

Desikan, K. V., and Balakrishnan, S. (1976). Tissue levels of clofazimine in a case of leprosy. *Lepr. Rev.* 47 (2), 107–113. doi:10.5935/0305-7518.19760020

Diacon, A. H., Dawson, R., von Groote-Bidlingmaier, F., Symons, G., Venter, A., Donald, P. R., et al. (2015). Bactericidal activity of pyrazinamide and clofazimine alone and in combinations with pretomanid and bedaquiline. *Am. J. Respir. Crit. Care Med.* 191 (8), 943–953. doi:10.1164/rccm.201410-1801OC

Ding, Y., Zhu, H., Fu, L., Zhang, W., Wang, B., Guo, S., et al. (2022). Superior efficacy of a TBI-166, bedaquiline, and pyrazinamide combination regimen in a murine model of tuberculosis. *Antimicrob. Agents Chemother.* 66, e0065822. doi:10.1128/aac.00658-22

Du, Y., Qiu, C., Chen, X., Wang, J., Jing, W., Pan, H., et al. (2020). Treatment outcome of a shorter regimen containing clofazimine for multidrug-resistant tuberculosis: A randomized control trial in China. *Clin. Infect. Dis.* 71 (4), 1047–1054. doi:10.1093/cid/ciz915

Duan, H., Chen, X., Li, Z., Pang, Y., Jing, W., Liu, P., et al. (2019). Clofazimine improves clinical outcomes in multidrug-resistant tuberculosis: A randomized controlled trial. *Clin. Microbiol. Infect.* 25 (2), 190–195. doi:10.1016/j.cmi.2018.07.012

Feng, P. C., Fenselau, C. C., and Jacobson, R. R. (1982). A new urinary metabolite of clofazimine in leprosy patients. *Drug Metab. Dispos.* 10 (3), 286–288.

Feng, P. C., Fenselau, C. C., and Jacobson, R. R. (1981). Metabolism of clofazimine in leprosy patients. *Drug Metab. Dispos.* 9 (6), 521–524.

Fu, L., Weng, T., Sun, F., Zhang, P., Li, H., Li, Y., et al. (2021). Insignificant difference in culture conversion between bedaquiline-containing and bedaquiline-free all-oral short regimens for multidrug-resistant tuberculosis. *Int. J. Infect. Dis.* 111, 138–147. doi:10.1016/j.ijid.2021.08.055

Grosset, J. H., Tyagi, S., Almeida, D. V., Converse, P. J., Li, S. Y., Ammerman, N. C., et al. (2013). Assessment of clofazimine activity in a second-line regimen for tuberculosis in mice. *Am. J. Respir. Crit. Care Med.* 188 (5), 608–612. doi:10.1164/rccm.201304-0753OC

Gurfinkel, P., Pina, J. C., and Ramos-e-Silva, M. (2009). Use of clofazimine in dermatology. *J. Drugs Dermatol* 8 (9), 846–851.

Hartkoorn, R. C., Uplekar, S., and Cole, S. T. (2014). Cross-resistance between clofazimine and bedaquiline through upregulation of MmpL5 in *Mycobacterium tuberculosis*. *Antimicrob. Agents Chemother.* 58 (5), 2979–2981. doi:10.1128/AAC.00037-14

Hastings, R. C., Jacobson, R. R., and Trautman, J. R. (1976). Long-term clinical toxicity studies with clofazimine (B663) in leprosy. *Int. J. Lepr. Other Mycobact. Dis.* 44 (3), 287–293.

Hewison, C., Khan, U., Bastard, M., Lachenal, N., Coutisson, S., Osso, E., et al. (2022). Safety of treatment regimens containing bedaquiline and delamanid in the endTB cohort. *Clin. Infect. Dis.* 75 (6), 1006–1013. doi:10.1093/cid/ciac019

Horita, Y., and Doi, N. (2014). Comparative study of the effects of antituberculosis drugs and antiretroviral drugs on cytochrome P450 3A4 and P-glycoprotein. *Antimicrob. Agents Chemother.* 58 (6), 3168–3176. doi:10.1128/AAC.02278-13

Howlader, S., Kim, M. J., Jony, M. R., Long, N. P., Cho, Y. S., Kim, D. H., et al. (2022). Characterization of clofazimine metabolism in human liver microsomal incubation *in vitro*. *Antimicrob. Agents Chemother.* 66 (10), e0056522. doi:10.1128/aac.00565-22

Hughes, G., Bern, H., Chiang, C. Y., Goodall, R. L., Nunn, A. J., Rusen, I. D., et al. (2022). QT prolongation in the STREAM stage 1 trial. *Int. J. Tuberc. Lung Dis.* 26 (4), 334–340. doi:10.5588/ijtld.21.0403

Huygens, F., O'Sullivan, J. F., and van Rensburg, C. E. (2005). Antimicrobial activities of seven novel tetramethylpiperidine-substituted phenazines against multiple-drug-resistant Gram-positive bacteria. *Chemotherapy* 51 (5), 263–267. doi:10.1159/000087454

Irwin, S. M., Gruppo, V., Brooks, E., Gilliland, J., Scherman, M., Reichlen, M. J., et al. (2014). Limited activity of clofazimine as a single drug in a mouse model of tuberculosis exhibiting caseous necrotic granulomas. *Antimicrob. Agents Chemother.* 58 (7), 4026–4034. doi:10.1128/AAC.02565-14

Ismail, N. A., Omar, S. V., Joseph, L., Govender, N., Blows, L., Ismail, F., et al. (2018). Defining bedaquiline susceptibility, resistance, cross-resistance and associated genetic determinants: A retrospective cohort study. *EBioMedicine* 28, 136–142. doi:10.1016/j.ebiom.2018.01.005

Ismail, N. A., Said, H. M., Rodrigues, C., Omar, S. V., Ajbani, K., Sukhadiad, N., et al. (2019). Multicentre study to establish interpretive criteria for clofazimine drug susceptibility testing. *Int. J. Tuberc. Lung Dis.* 23 (5), 594–599. doi:10.5588/ijtld.18.0417

Jagannath, C., Reddy, M. V., Kailasam, S., O'Sullivan, J. F., and Gangadharam, P. R. (1995). Chemotherapeutic activity of clofazimine and its analogues against *Mycobacterium tuberculosis*. *in vitro*, intracellular, and *in vivo* studies. *Am. J. Respir. Crit. Care Med.* 151 (4), 1083–1086. doi:10.1164/ajrccm/151.4.1083

Job, C. K., Yoder, L., Jacobson, R. R., and Hastings, R. C. (1990). Skin pigmentation from clofazimine therapy in leprosy patients: A reappraisal. *J. Am. Acad. Dermatol* 23 (2), 236–241. doi:10.1016/0190-9622(90)70204-u

Jopling, W. H. (1976). Complications of treatment with clofazimine (lamprene: B663). *Lepr. Rev.* 47 (1), 1–3. doi:10.5935/0305-7518.19760001

Kamal, A., Hari Babu, A., Venkata Ramana, A., Sinha, R., Yadav, J. S., and Arora, S. K. (2005). Antitubercular agents. Part 1: Synthesis of phthalimido- and naphthalimido-linked phenazines as new prototype antitubercular agents. *Bioorg Med. Chem. Lett.* 15 (7), 1923–1926. doi:10.1016/j.bmcl.2005.01.085

Kempker, R. R., Smith, A. G. C., Avaliani, T., Gujabidze, M., Bakuradze, T., Sabanadze, S., et al. (2022). Cycloserine and linezolid for tuberculosis meningitis: Pharmacokinetic evidence of potential usefulness. *Clin. Infect. Dis.* 75 (4), 682–689. doi:10.1093/cid/ciab992

Keswani, R. K., Baik, J., Yeomans, L., Hitzman, C., Johnson, A. M., Pawate, A. S., et al. (2015). Chemical analysis of drug biocrystals: A role for counterion transport pathways in intracellular drug disposition. *Mol. Pharm.* 12 (7), 2528–2536. doi:10.1021/acs.molpharmaceut.5b00032

Khan, S. R., Venugopal, U., Chandra, G., Bharti, S., Maurya, R. K., and Krishnan, M. Y. (2019). Effect of various drugs on differentially detectable persisters of *Mycobacterium tuberculosis* generated by long-term lipid diet. *Tuberc. (Edinb).* 115, 89–95. doi:10.1016/j.tube.2019.02.007

Kim, D. H., Kim, B. G., Kim, S. Y., Huh, H. J., Lee, N. Y., Koh, W. J., et al. (2021). *In vitro* activity and clinical outcomes of clofazimine for nontuberculous mycobacteria pulmonary disease. *J. Clin. Med.* 10 (19), 4581. doi:10.3390/jcm10194581

Kuaban, C., Noeske, J., Rieder, H. L., Aït-Khaled, N., Abena Foe, J. L., Trébucq, A., et al. (2015). High effectiveness of a 12-month regimen for MDR-TB patients in Cameroon. *Int. J. Tuberc. Lung Dis.* 19 (5), 517–524. doi:10.5588/ijtld.14.0535

Kumar, B., Kaur, S., Kaur, I., and Gangowar, D. N. (1987). More about clofazimine -3 years experience and review of literature. *Indian J. Lepr.* 59 (1), 63–74.

Lechartier, B., and Cole, S. T. (2015). Mode of action of clofazimine and combination therapy with benzothiazinones against *Mycobacterium tuberculosis*. *Antimicrob. Agents Chemother.* 59 (8), 4457–4463. doi:10.1128/AAC.00395-15

Lee, B. Y., Clemens, D. L., Silva, A., Dillon, B. J., Masleša-Galić, S., Nava, S., et al. (2017). Drug regimens identified and optimized by output-driven platform markedly reduce tuberculosis treatment time. *Nat. Commun.* 8, 14183. doi:10.1038/ncomms14183

Lee, B. Y., Clemens, D. L., Silva, A., Dillon, B. J., Masleša-Galić, S., Nava, S., et al. (2018). Ultra-rapid near universal TB drug regimen identified via parabolic response surface platform cures mice of both conventional and high susceptibility. *PLoS One* 13 (11), e0207469. doi:10.1371/journal.pone.0207469

Lehmann, D. F., Eggleston, W. D., and Wang, D. (2018). Validation and clinical utility of the hERG IC50:C(max) ratio to determine the risk of drug-induced torsades de Pointes: A meta-analysis. *Pharmacotherapy* 38 (3), 341–348. doi:10.1002/phar.2087

Levy, L., and Randall, H. P. (1970). A study of skin pigmentation by clofazimine. *Int. J. Lepr. Other Mycobact. Dis.* 38 (4), 404–416.

Levy, L. (1974). Pharmacologic studies of clofazimine. *Am. J. Trop. Med. Hyg.* 23 (6), 1097–1109. doi:10.4269/ajtmh.1974.23.1097

Li, M., and Ramos, L. G. (2017). Drug-induced QT prolongation and torsades de Pointes. *P t* 42 (7), 473–477.

Li, Y. L., Zhang, C. L., Zhang, D. F., Lu, Y., Wang, B., Zheng, M. Q., et al. (2012). Synthesis and anti-tubercular activity of novel alkyl substituted riminophenazine derivatives. *Yao Xue Xue Bao* 47 (6), 745–754.

Liu, B., Liu, K., Lu, Y., Zhang, D., Yang, T., Li, X., et al. (2012). Systematic evaluation of structure-activity relationships of the riminophenazine class and discovery of a C2 pyridylamino series for the treatment of multidrug-resistant tuberculosis. *Molecules* 17 (4), 4545–4559. doi:10.3390/molecules17044545

Lopez-Gavin, A., Tudo, G., Vergara, A., Hurtado, J. C., and Gonzalez-Martin, J. (2015). *In vitro* activity against *Mycobacterium tuberculosis* of levofloxacin, moxifloxacin and UB-8902 in combination with clofazimine and pretomanid. *Int. J. Antimicrob. Agents* 46 (5), 582–585. doi:10.1016/j.ijantimicag.2015.08.004

Lu, Y., Zheng, M., Wang, B., Fu, L., Zhao, W., Li, P., et al. (2011). Clofazimine analogs with efficacy against experimental tuberculosis and reduced potential for accumulation. *Antimicrob. Agents Chemother.* 55 (11), 5185–5193. doi:10.1128/AAC.00699-11

Lu, Y., Zheng, M. Q., Wang, B., Zhao, W. J., Fu, L., Li, P., et al. (2009). Tissue distribution and deposition of clofazimine in mice following oral administration of isoniazid. *Zhonghua Jie He He Hu Xi Za Zhi* 32 (9), 694–697.

Maartens, G., Brill, M. J. E., Pandie, M., and Svensson, E. M. (2018). Pharmacokinetic interaction between bedaquiline and clofazimine in patients with drug-resistant tuberculosis. *Int. J. Tuberc. Lung Dis.* 22 (1), 26–29. doi:10.5588/ijtld.17.0615

Mamidi, N. V., Rajasekhar, A., Prabhakar, M. C., and Krishna, D. R. (1995). Tissue distribution and deposition of clofazimine in rat following subchronic treatment with or without rifampicin. *Arzneimittelforschung* 45 (9), 1029–1031.

Mansfield, R. E. (1974). Tissue concentrations of clofazimine (B663) in man. *Am. J. Trop. Med. Hyg.* 23 (6), 1116–1119. doi:10.4269/ajtmh.1974.23.1116

McDougall, A. C., Horsfall, W. R., Hede, J. E., and Chaplin, A. J. (1980). Splenic infarction and tissue accumulation of crystals associated with the use of clofazimine (Lamprene; B663) in the treatment of pyoderma gangrenosum. *Br. J. Dermatol* 102 (2), 227–230. doi:10.1111/j.1365-2133.1980.tb05697.x

Mehta, R. T., Keyhani, A., McQueen, T. J., Rosenbaum, B., Rolston, K. V., and Tarrand, J. J. (1993). *In vitro* activities of free and liposomal drugs against Mycobacterium avium-M. intracellulare complex and *M. tuberculosis*. *Antimicrob. Agents Chemother.* 37 (12), 2584–2587. doi:10.1128/aac.37.12.2584

Mehta, R. T. (1996). Liposome encapsulation of clofazimine reduces toxicity *in vitro* and *in vivo* and improves therapeutic efficacy in the beige mouse model of disseminated Mycobacterium avium-M. intracellulare complex infection. *Antimicrob. Agents Chemother.* 40 (8), 1893–1902. doi:10.1128/AAC.40.8.1893

Misra, N., Padayatchi, N., and Naidoo, P. (2019). Dose-related adverse events in South African patients prescribed clofazimine for drug-resistant tuberculosis. *S Afr. Med. J.* 110 (1), 32–37. doi:10.7196/SAMJ.2019.v110i1.13954

Misra, N., Padayatchi, N., and Naidoo, P. (2020). Dose-related treatment outcomes in South African patients prescribed clofazimine for drug-resistant tuberculosis. *S Afr. Med. J.* 111 (1), 61–67. doi:10.7196/SAMJ.2020.v111i1.14605

Mitnick, C. D., Shin, S. S., Seung, K. J., Rich, M. L., Atwood, S. S., Furin, J. J., et al. (2008). Comprehensive treatment of extensively drug-resistant tuberculosis. *N. Engl. J. Med.* 359 (6), 563–574. doi:10.1056/NEJMoa0800106

Moore, V. J. (1983). A review of side-effects experienced by patients taking clofazimine. *Lepr. Rev.* 54 (4), 327–335. doi:10.5935/0305-7518.19830039

Morrison, N. E., and Marley, G. M. (1976). Clofazimine binding studies with deoxyribonucleic acid. *Int. J. Lepr. Other Mycobact. Dis.* 44 (4), 475–481.

Morrison, N. E., and Marley, G. M. (1976). The mode of action of clofazimine: DNA binding studies. *Int. J. Lepr. Other Mycobact. Dis.* 44 (1-2), 133–134.

Mothiba, M. T., Anderson, R., Fourie, B., Germishuizen, W. A., and Cholo, M. C. (2015). Effects of clofazimine on planktonic and biofilm growth of *Mycobacterium tuberculosis* and Mycobacterium smegmatis. *J. Glob. Antimicrob. Resist* 3 (1), 13–18. doi:10.1016/j.jgar.2014.12.001

Murashov, M. D., Diaz-Espinosa, J., LaLone, V., Tan, J. W. Y., Laza, R., Wang, X., et al. (2018). Synthesis and characterization of a biomimetic formulation of clofazimine hydrochloride microcrystals for parenteral administration. *Pharmaceutics* 10 (4), 238. doi:10.3390/pharmaceutics10040238

Murashov, M. D., LaLone, V., Rzeczycki, P. M., Keswani, R. K., Yoon, G. S., Sud, S., et al. (2018). The physicochemical basis of clofazimine-induced skin pigmentation. *J. Invest. Dermatol* 138 (3), 697–703. doi:10.1016/j.jid.2017.09.031

NCT04670120 (2020). *Evaluation of early bactericidal activity and safety in pulmonary tuberculosis with pyrifazimine TBI-166) 2020*. Available from: https://clinicaltrials.gov/ct2/show/NCT04670120?term=TBI-166&draw=2&rank=1.

Nêgrel, A. D., Chovet, M., Baquillon, G., and Lagadec, R. (1984). Clofazimine and the eye: Preliminary communication. *Lepr. Rev.* 55 (4), 349–352. doi:10.5935/0305-7518.19840039

Nimmo, C., Millard, J., Brien, K., Moodley, S., van Dorp, L., Lutchminarain, K., et al. (2020). Bedaquiline resistance in drug-resistant tuberculosis HIV co-infected patients. *Eur. Respir. J.* 55 (6), 1902383. doi:10.1183/13993003.02383-2019

Nimmo, C., Millard, J., van Dorp, L., Brien, K., Moodley, S., Wolf, A., et al. (2020). Population-level emergence of bedaquiline and clofazimine resistance-associated variants among patients with drug-resistant tuberculosis in southern Africa: A phenotypic and phylogenetic analysis. *Lancet Microbe* 1 (4), e165–e174. doi:10.1016/S2666-5247(20)30031-8

Nix, D. E., Adam, R. D., Auclair, B., Krueger, T. S., Godo, P. G., and Peloquin, C. A. (2004). Pharmacokinetics and relative bioavailability of clofazimine in relation to food, orange juice and antacid. *Tuberc. (Edinb).* 84 (6), 365–373. doi:10.1016/j.tube.2004.04.001

Novartis Pharmaceuticals Corporation (2019). *LAMPRENE® (clofazimine) package insert*. Available from: https://www.accessdata.fda.gov/drugsatfda_docs/label/2019/019500s014lbl.pdf.

Nunn, A. J., Phillips, P. P. J., Meredith, S. K., Chiang, C-Y., Conradie, F., Dalai, D., et al. (2019). A trial of a shorter regimen for rifampin-resistant tuberculosis. *N. Engl. J. Med.* 380 (13), 1201–1213. doi:10.1056/NEJMoa1811867

O'Connor, R., O'Sullivan, J. F., and O'Kennedy, R. (1995). The pharmacology, metabolism, and chemistry of clofazimine. *Drug Metab. Rev.* 27 (4), 591–614. doi:10.3109/03602539508994208

Ohman, L., and Wahlberg, I. (1975). Letter: Ocular side-effects of clofazimine. *Lancet* 2 (7941), 933–934. doi:10.1016/s0140-6736(75)92180-7

Oliva, B., O'Neill, A. J., Miller, K., Stubbings, W., and Chopra, I. (2004). Anti-staphylococcal activity and mode of action of clofazimine. *J. Antimicrob. Chemother.* 53 (3), 435–440. doi:10.1093/jac/dkh114

Padayatchi, N., Gopal, M., Naidoo, R., Werner, L., Naidoo, K., Master, I., et al. (2014). Clofazimine in the treatment of extensively drug-resistant tuberculosis with HIV coinfection in South Africa: A retrospective cohort study. *J. Antimicrob. Chemother.* 69 (11), 3103–3107. doi:10.1093/jac/dku235

Park, S., Jung, J., Kim, J., Han, S. B., and Ryoo, S. (2022). Investigation of clofazimine resistance and genetic mutations in drug-resistant *Mycobacterium tuberculosis* isolates. *J. Clin. Med.* 11 (7), 1927. doi:10.3390/jcm11071927

Pawde, D. M., Viswanadh, M. K., Mehata, A. K., Sonkar, R., Narendra, S P., et al. (2020). Mannose receptor targeted bioadhesive chitosan nanoparticles of clofazimine for effective therapy of tuberculosis. *Saudi Pharm. J.* 28 (12), 1616–1625. doi:10.1016/j.jsps.2020.10.008

Peters, K., Leitzke, S., Diederichs, J. E., Borner, K., Hahn, H., Müller, R. H., et al. (2000). Preparation of a clofazimine nanosuspension for intravenous use and evaluation of its therapeutic efficacy in murine *Mycobacterium avium* infection. *J. Antimicrob. Chemother.* 45 (1), 77–83. doi:10.1093/jac/45.1.77

Piubello, A., Harouna, S. H., Souleymane, M. B., Boukary, I., Morou, S., Daouda, M., et al. (2014). High cure rate with standardised short-course multidrug-resistant tuberculosis treatment in Niger: No relapses. *Int. J. Tuberc. Lung Dis.* 18 (10), 1188–1194. doi:10.5588/ijtld.13.0075

Prideaux, B., Via, L. E., Zimmerman, M. D., Eum, S., Sarathy, J., O'Brien, P., et al. (2015). The association between sterilizing activity and drug distribution into tuberculosis lesions. *Nat. Med.* 21 (10), 1223–1227. doi:10.1038/nm.3937

Pym, A. S., Diacon, A. H., Tang, S. J., Conradie, F., Danilovits, M., Chuchottaworn, C., et al. (2016). Bedaquiline in the treatment of multidrug- and extensively drug-resistant tuberculosis. *Eur. Respir. J.* 47 (2), 564–574. doi:10.1183/13993003.00724-2015

Ramu, G., and Iyer, G. G. (1976). Side effects of clofazimine therapy. *Lepr. India* 48 (4), 722–731.

Reddy, V. M., Nadadhur, G., Daneluzzi, D., O'Sullivan, J. F., and Gangadharam, P. R. (1996). Antituberculosis activities of clofazimine and its new analogs B4154 and B4157. *Antimicrob. Agents Chemother.* 40 (3), 633–636. doi:10.1128/AAC.40.3.633

Reddy, V. M., O'Sullivan, J. F., and Gangadharam, P. R. (1999). Antimycobacterial activities of riminophenazines. *J. Antimicrob. Chemother.* 43 (5), 615–623. doi:10.1093/jac/43.5.615

Saini, V., Ammerman, N. C., Chang, Y. S., Tasneen, R., Chaisson, R. E., Jain, S., et al. (2019). Treatment-shortening effect of a novel regimen combining clofazimine and high-dose rifapentine in pathologically distinct mouse models of tuberculosis. *Antimicrob. Agents Chemother.* 63 (6), 003888-19. doi:10.1128/AAC.00388-19

Saravanan, P., Dusthackeer, V. N. A., Rajmani, R. S., Mahizhaveni, B., Nirmal, C. R., Rajadas, S. E., et al. (2021). Discovery of a highly potent novel rifampicin analog by preparing a hybrid of the precursors of the antibiotic drugs rifampicin and clofazimine. *Sci. Rep.* 11 (1), 1029. doi:10.1038/s41598-020-80439-2

Schaad-Lanyi, Z., Dieterle, W., Dubois, J. P., Theobald, W., and Vischer, W. (1987). Pharmacokinetics of clofazimine in healthy volunteers. *Int. J. Lepr. Other Mycobact. Dis.* 55 (1), 9–15.

Schulz, E. J. (1971). Forty-four months' experience in the treatment of leprosy with clofazimine (Lamprene (Geigy)). *Lepr. Rev.* 42 (3), 178–187. doi:10.5935/0305-7518.19710021

Schwœbel, V., Trébucq, A., Kashongwe, Z., Bakayoko, A. S., Kuaban, C., Noeske, J., et al. (2019). Outcomes of a nine-month regimen for rifampicin-resistant tuberculosis up to 24 months after treatment completion in nine African countries. *EClinicalMedicine* 20, 100268. doi:10.1016/j.eclinm.2020.100268

Shimokawa, Y., Yoda, N., Kondo, S., Yamamura, Y., Takiguchi, Y., and Umehara, K. (2015). Inhibitory potential of twenty five anti-tuberculosis drugs on CYP activities in human liver microsomes. *Biol. Pharm. Bull.* 38 (9), 1425–1429. doi:10.1248/bpb.b15-00313

Silva, A., Lee, B. Y., Clemens, D. L., Kee, T., Ding, X., Ho, C. M., et al. (2016). Output-driven feedback system control platform optimizes combinatorial therapy of tuberculosis using a macrophage cell culture model. *Proc. Natl. Acad. Sci. U. S. A.* 113 (15), E2172–E2179. doi:10.1073/pnas.1600812113

Singh, H., Azad, K., and Kaur, K. (2013). Clofazimine-induced enteropathy in a patient of leprosy. *Indian J. Pharmacol.* 45 (2), 197–198. doi:10.4103/0253-7613.108323

Steel, H. C., Matlola, N. M., and Anderson, R. (1999). Inhibition of potassium transport and growth of mycobacteria exposed to clofazimine and B669 is associated with a calcium-independent increase in microbial phospholipase A2 activity. *J. Antimicrob. Chemother.* 44 (2), 209–216. doi:10.1093/jac/44.2.209

Strydom, N., Gupta, S. V., Fox, W. S., Via, L. E., Bang, H., Lee, M., et al. (2019). Tuberculosis drugs' distribution and emergence of resistance in patient's lung lesions: A mechanistic model and tool for regimen and dose optimization. *PLoS Med.* 16 (4), e1002773. doi:10.1371/journal.pmed.1002773

Sukpanichnant, S., Hargrove, N. S., Kachintorn, U., Manatsathit, S., Chanchairujira, T., Siritanaratkul, N., et al. (2000). Clofazimine-induced crystal-storing histiocytosis producing chronic abdominal pain in a leprosy patient. *Am. J. Surg. Pathol.* 24 (1), 129–135. doi:10.1097/00000478-200001000-00016

Swanson, R. V., Adamson, J., Moodley, C., Ngcobo, B., Ammerman, N. C., Dorasamy, A., et al. (2015). Pharmacokinetics and pharmacodynamics of clofazimine in a mouse model of tuberculosis. *Antimicrob. Agents Chemother.* 59 (6), 3042–3051. doi:10.1128/AAC.00260-15

Swanson, R. V., Ammerman, N. C., Ngcobo, B., Adamson, J., Moodley, C., Dorasamy, A., et al. (2016). Clofazimine contributes sustained antimicrobial activity after treatment cessation in a mouse model of tuberculosis chemotherapy. *Antimicrob. Agents Chemother.* 60 (5), 2864–2869. doi:10.1128/AAC.00177-16

Tang, S., Yao, L., Hao, X., Liu, Y., Zeng, L., Liu, G., et al. (2015). Clofazimine for the treatment of multidrug-resistant tuberculosis: Prospective, multicenter, randomized controlled study in China. *Clin. Infect. Dis.* 60 (9), 1361–1367. doi:10.1093/cid/civ027

Tasneen, R., Li, S. Y., Peloquin, C. A., Taylor, D., Williams, K. N., Andries, K., et al. (2011). Sterilizing activity of novel TMC207- and PA-824-containing regimens in a murine model of tuberculosis. *Antimicrob. Agents Chemother.* 55 (12), 5485–5492. doi:10.1128/AAC.05293-11

Trebucq, A., Schwoebel, V., Kashongwe, Z., Bakayoko, A., Kuaban, C., Noeske, J., et al. (2018). Treatment outcome with a short multidrug-resistant tuberculosis regimen in nine African countries. *Int. J. Tuberc. Lung Dis.* 22 (1), 17–25. doi:10.5588/ijtld.17.0498

Tucker, E. W., Pieterse, L., Zimmerman, M. D., Udwadia, Z. F., Peloquin, C. A., Gler, M. T., et al. (2019). Delamanid central nervous system pharmacokinetics in tuberculous meningitis in rabbits and humans. *Antimicrob. Agents Chemother.* 63 (10), e00913-19. doi:10.1128/AAC.00913-19

Tuvshintulga, B., AbouLaila, M., Davaasuren, B., Ishiyama, A., Sivakumar, T., Yokoyama, N., et al. (2016). Clofazimine inhibits the growth of babesia and theileria parasites *in vitro* and *in vivo*. *Antimicrob. Agents Chemother.* 60 (5), 2739–2746. doi:10.1128/AAC.01614-15

Tyagi, S., Ammerman, N. C., Li, S. Y., Adamson, J., Converse, P. J., Swanson, R. V., et al. (2015). Clofazimine shortens the duration of the first-line treatment regimen for experimental chemotherapy of tuberculosis. *Proc. Natl. Acad. Sci. U. S. A.* 112 (3), 869–874. doi:10.1073/pnas.1416951112

Valetti, S., Xia, X., Costa-Gouveia, J., Brodin, P., Bernet-Camard, M. F., Andersson, M., et al. (2017). Clofazimine encapsulation in nanoporous silica particles for the oral treatment of antibiotic-resistant *Mycobacterium tuberculosis* infections. *Nanomedicine (Lond).* 12 (8), 831–844. doi:10.2217/nnm-2016-0364

Van Deun, A., Maug, A. K., Salim, M. A., Das, P. K., Sarker, M. R., Daru, P., et al. (2010). Short, highly effective, and inexpensive standardized treatment of multidrug-resistant tuberculosis. *Am. J. Respir. Crit. Care Med.* 182 (5), 684–692. doi:10.1164/rccm.201001-0077OC

Van Rensburg, C. E., Jooné, G. K., O'Sullivan, J. F., and Anderson, R. (1992). Antimicrobial activities of clofazimine and B669 are mediated by lysophospholipids. *Antimicrob. Agents Chemother.* 36 (12), 2729–2735. doi:10.1128/aac.36.12.2729

van Rensburg, C. E., Jooné, G. K., Sirgel, F. A., Matlola, N. M., and O'Sullivan, J. F. (2000). *In vitro* investigation of the antimicrobial activities of novel tetramethylpiperidine-substituted phenazines against *Mycobacterium tuberculosis*. *Chemotherapy* 46 (1), 43–48. doi:10.1159/000007255

Venkatesan, K., Deo, N., and Gupta, U. D. (2007). Tissue distribution and deposition of clofazimine in mice following oral administration with or without isoniazid. *Arzneimittelforschung* 57 (7), 472–474. doi:10.1055/s-0031-1296634

Venkatesan, K., Mathur, A., Girdhar, A., and Girdhar, B. K. (1997). Excretion of clofazimine in human milk in leprosy patients. *Lepr. Rev.* 68 (3), 242–246. doi:10.5935/0305-7518.19970033

Verma, R. K., Germishuizen, W. A., Motheo, M. P., Agrawal, A. K., Singh, A. K., Mohan, M., et al. (2013). Inhaled microparticles containing clofazimine are efficacious in treatment of experimental tuberculosis in mice. *Antimicrob. Agents Chemother.* 57 (2), 1050–1052. doi:10.1128/AAC.01897-12

Vischer, W. A. (1969). The experimental properties of G 30 320 (B 663)--a new anti-leprotic agent. *Lepr. Rev.* 40 (2), 107–110. doi:10.5935/0305-7518.19690021

Wadee, A. A., Anderson, R., and Rabson, A. R. (1988). Clofazimine reverses the inhibitory effect of *Mycobacterium tuberculosis* derived factors on phagocyte intracellular killing mechanisms. *J. Antimicrob. Chemother.* 21 (1), 65–74. doi:10.1093/jac/21.1.65

Wålinder, P. E., Gip, L., and Stempa, M. (1976). Corneal changes in patients treated with clofazimine. *Br. J. Ophthalmol.* 60 (7), 526–528. doi:10.1136/bjo.60.7.526

Wallis, R. S. (2016). Cardiac safety of extensively drug-resistant tuberculosis regimens including bedaquiline, delamanid and clofazimine. *Eur. Respir. J.* 48 (5), 1526–1527. doi:10.1183/13993003.01207-2016

Wang, M. G., Liu, X. M., Wu, S. Q., and He, J. Q. (2022). Impacts of clofazimine on the treatment outcomes of drug-resistant tuberculosis. *Microbes Infect.* 25, 105020. doi:10.1016/j.micinf.2022.105020

Wang, Q., Pang, Y., Jing, W., Liu, Y., Wang, N., Yin, H., et al. (2018). Clofazimine for treatment of extensively drug-resistant pulmonary tuberculosis in China. *Antimicrob. Agents Chemother.* 62 (4), 021499-17. doi:10.1128/AAC.02149-17

Williams, K., Minkowski, A., Amoabeng, O., Peloquin, C. A., Taylor, D., Andries, K., et al. (2012). Sterilizing activities of novel combinations lacking first- and second-line drugs in a murine model of tuberculosis. *Antimicrob. Agents Chemother.* 56 (6), 3114–3120. doi:10.1128/AAC.00384-12

World Health Organisation (2021). *Global tuberculosis report 2021*.

World Health Organisation (2018). *Guidelines for the diagnosis, treatment and prevention of leprosy*.

World Health Organisation (2018). *Guidelines for the diagnosis, treatment and prevention of leprosy*. available from: https://apps.who.int/iris/bitstream/handle/10665/274127/9789290226383-eng.pdf.

World Health Organisation (2022). *Rapid communication: Key changes to the treatment of drug-resistant tuberculosis*.

World Health Organisation (2020). *WHO consolidated guidelines on tuberculosis, module 4: Drug-resistant tuberculosis treatment*. Available from: https://www.who.int/publications/i/item/9789240007048.

World Health Organisation (2022). *WHO consolidated guidelines on tuberculosis. Module 4: Drug-resistant tuberculosis treatment, 2022 update*. Available from: https://www.who.int/publications/i/item/9789240063129.

World Health Organisation (2018). *WHO rapid communication: MDR-TB*. Available from: https://www.who.int/publications/i/item/WHO-CDS-TB-2018.18.

World Health Organistation (2018). *Technical Report on critical concentrations for drug susceptibility testing of medicines used in the treatment of drug-resistant tuberculosis*.

Xu, H. B., Jiang, R. H., and Xiao, H. P. (2012). Clofazimine in the treatment of multidrug-resistant tuberculosis. *Clin. Microbiol. Infect.* 18 (11), 1104–1110. doi:10.1111/j.1469-0691.2011.03716.x

Xu, J., Koval, A., and Katanaev, V. L. (2020). Beyond TNBC: Repositioning of clofazimine against a broad range of wnt-dependent cancers. *Front. Oncol.* 10, 602817. doi:10.3389/fonc.2020.602817

Xu, J., Lu, Y., Fu, L., Zhu, H., Wang, B., Mdluli, K., et al. (2012). *In vitro* and *in vivo* activity of clofazimine against *Mycobacterium tuberculosis* persisters. *Int. J. Tuberc. Lung Dis.* 16 (8), 1119–1125. doi:10.5588/ijtld.11.0752

Xu, J., Wang, B., Fu, L., Zhu, H., Guo, S., Huang, H., et al. (2019). *In vitro* and *in vivo* activities of the riminophenazine TBI-166 against *Mycobacterium tuberculosis*. *Antimicrob. Agents Chemother.* 63 (5), 021555-18. doi:10.1128/AAC.02155-18

Xu, J., Wang, B., Hu, M., Huo, F., Guo, S., Jing, W., et al. (2017). Primary clofazimine and bedaquiline resistance among isolates from patients with multidrug-resistant tuberculosis. *Antimicrob. Agents Chemother.* 61 (6), 002399-17. doi:10.1128/AAC.00239-17

Yano, T., Kassovska-Bratinova, S., Teh, J. S., Winkler, J., Sullivan, K., Isaacs, A., et al. (2011). Reduction of clofazimine by mycobacterial type 2 NADH:quinone oxidoreductase: A pathway for the generation of bactericidal levels of reactive oxygen species. *J. Biol. Chem.* 286 (12), 10276–10287. doi:10.1074/jbc.M110.200501

Yawalkar, S. J., and Vischer, W. (1979). Lamprene (clofazimine) in leprosy. Basic information. *Basic inf. Lepr. Rev.* 50 (2), 135–144. doi:10.5935/0305-7518.19790020

Zhang, C. X., Love, M. S., McNamara, C. W., Chi, V., Woods, A. K., Joseph, S., et al. (2022). Pharmacokinetics and pharmacodynamics of clofazimine for treatment of cryptosporidiosis. *Antimicrob. Agents Chemother.* 66 (1), e0156021. doi:10.1128/AAC.01560-21

Zhang, D., Liu, Y., Zhang, C., Zhang, H., Wang, B., Xu, J., et al. (2014). Synthesis and biological evaluation of novel 2-methoxypyridylamino-substituted riminophenazine derivatives as antituberculosis agents. *Molecules* 19 (4), 4380–4394. doi:10.3390/molecules19044380

Zhang, D., Lu, Y., Liu, K., Liu, B., Wang, J., Zhang, G., et al. (2012). Identification of less lipophilic riminophenazine derivatives for the treatment of drug-resistant tuberculosis. *J. Med. Chem.* 55 (19), 8409–8417. doi:10.1021/jm300828h

Zhang, M., Sala, C., Hartkoorn, R. C., Dhar, N., Mendoza-Losana, A., and Cole, S. T. (2012). Streptomycin-starved *Mycobacterium tuberculosis* 18b, a drug discovery tool for latent tuberculosis. *Antimicrob. Agents Chemother.* 56 (11), 5782–5789. doi:10.1128/AAC.01125-12

Zhang, S., Chen, J., Cui, P., Shi, W., Zhang, W., and Zhang, Y. (2015). Identification of novel mutations associated with clofazimine resistance in *Mycobacterium tuberculosis*. *J. Antimicrob. Chemother.* 70 (9), 2507–2510. doi:10.1093/jac/dkv150

Zhang, X., Shi, Y., Guo, Z., Zhao, X., Wu, J., Cao, S., et al. (2022). Clofazimine derivatives as potent broad-spectrum antiviral agents with dual-target mechanism. *Eur. J. Med. Chem.* 234, 114209. doi:10.1016/j.ejmech.2022.114209

Zhang, Y., Zhu, H., Fu, L., Wang, B., Guo, S., Chen, X., et al. (2019). Identifying regimens containing TBI-166, a new drug candidate against *Mycobacterium tuberculosis in vitro* and *in vivo*. *Antimicrob. Agents Chemother.* 63 (7), 024966-18. doi:10.1128/AAC.02496-18

Zhang, Z., Li, T., Qu, G., Pang, Y., and Zhao, Y. (2015). *In vitro* synergistic activity of clofazimine and other antituberculous drugs against multidrug-resistant *Mycobacterium tuberculosis* isolates. *Int. J. Antimicrob. Agents* 45 (1), 71–75. doi:10.1016/j.ijantimicag.2014.09.012

Zhao, X., Mei, Y., Guo, Z., Si, S., Ma, X., Li, Y., et al. (2022). Discovery of new riminophenazine analogues as antimycobacterial agents against drug-resistant *Mycobacterium tuberculosis*. *Bioorg Chem.* 128, 105929. doi:10.1016/j.bioorg.2022.105929

frontiers | Frontiers in Pharmacology

TYPE Original Research
PUBLISHED 14 March 2023
DOI 10.3389/fphar.2023.1067295

OPEN ACCESS

EDITED BY
Oscar Della Pasqua,
University College London,
United Kingdom

REVIEWED BY
Andrew Burke,
The University of Queensland, Australia
Gesham Magombedze,
The University of Tennessee,
United States

*CORRESPONDENCE
Ulrika S. H. Simonsson,
ulrika.simonsson@farmbio.uu.se

SPECIALTY SECTION
This article was submitted to Pharmacology of Infectious Diseases, a section of the journal Frontiers in Pharmacology

RECEIVED 11 October 2022
ACCEPTED 27 February 2023
PUBLISHED 14 March 2023

CITATION
Ayoun Alsoud R, Svensson RJ, Svensson EM, Gillespie SH, Boeree MJ, Diacon AH, Dawson R, Aarnoutse RE and Simonsson USH (2023), Combined quantitative tuberculosis biomarker model for time-to-positivity and colony forming unit to support tuberculosis drug development.
Front. Pharmacol. 14:1067295.
doi: 10.3389/fphar.2023.1067295

Combined quantitative tuberculosis biomarker model for time-to-positivity and colony forming unit to support tuberculosis drug development

Rami Ayoun Alsoud[1], Robin J. Svensson[1], Elin M. Svensson[2,3], Stephen H. Gillespie[4], Martin J. Boeree[5], Andreas H. Diacon[6], Rodney Dawson[7,8], Rob E. Aarnoutse[3] and Ulrika S. H. Simonsson[1]* on behalf of the PanACEA consortium

[1]Department of Pharmaceutical Biosciences, Uppsala University, Uppsala, Sweden, [2]Department of Pharmacy, Uppsala University, Uppsala, Sweden, [3]Department of Pharmacy, Radboud Institute for Health Sciences, Radboud University Medical Center, Nijmegen, Netherlands, [4]Division of Infection and Global Health, School of Medicine, University of St Andrews, St Andrews, United Kingdom, [5]Department of Lung Diseases, Radboud University Medical Center, Nijmegen, Netherlands, [6]TASK Applied Science, Cape Town, South Africa, [7]Division of Pulmonology, Department of Medicine, University of Cape Town, Cape Town, South Africa, [8]University of Cape Town Lung Institute, Cape Town, South Africa

Biomarkers are quantifiable characteristics of biological processes. In *Mycobacterium tuberculosis*, common biomarkers used in clinical drug development are colony forming unit (CFU) and time-to-positivity (TTP) from sputum samples. This analysis aimed to develop a combined quantitative tuberculosis biomarker model for CFU and TTP biomarkers for assessing drug efficacy in early bactericidal activity studies. Daily CFU and TTP observations in 83 previously patients with uncomplicated pulmonary tuberculosis after 7 days of different rifampicin monotherapy treatments (10–40 mg/kg) from the HIGHRIF1 study were included in this analysis. The combined quantitative tuberculosis biomarker model employed the Multistate Tuberculosis Pharmacometric model linked to a rifampicin pharmacokinetic model in order to determine drug exposure-response relationships on three bacterial sub-states using both the CFU and TTP data simultaneously. CFU was predicted from the MTP model and TTP was predicted through a time-to-event approach from the TTP model, which was linked to the MTP model through the transfer of all bacterial sub-states in the MTP model to a one bacterial TTP model. The non-linear CFU-TTP relationship over time was well predicted by the final model. The combined quantitative tuberculosis biomarker model provides an efficient approach for assessing drug efficacy informed by both CFU and TTP data in early bactericidal activity studies and to describe the relationship between CFU and TTP over time.

KEYWORDS

rifampicin, TTP, CFU, tuberculosis, biomarker

1 Introduction

Tuberculosis (TB), a bacterial infection caused by *Mycobacterium tuberculosis* (Mtb), is among the top causes of death worldwide and the second leading cause of death due to infection after COVID-19 (Global tuberculosis report 2022). New antibiotics are urgently needed due to resistance development to many existing drugs. In order to develop new antibiotics and regimens, innovative tools are needed in early development together with biomarkers which quantify the biological processes as a response to drug efficacy.

In TB drug development, early bactericidal activity (EBA) in 2-week treatment trials of TB patients are often the first assessment of drug efficacy. Colony forming unit (CFU) and time-to-positivity (TTP) are the two commonly used biomarkers in EBA studies but also in longer Phase 2b trials. Traditionally, EBA has been assessed using each of the two biomarkers where TTP often nowadays is the primary endpoint (Diacon and Donald, 2014). TTP is quantified in liquid media, often in mycobacterial growth indicator tube (MGIT). With time, and as the bacteria grow within the MGIT system, oxygen is depleted and carbon dioxide is produced, resulting in a fluorescence signal where the time to achieve the positive signal is defined as TTP. Whereas CFU only quantifies actively multiplying bacteria on solid media, it has been shown that non-multiplying bacteria can grow in liquid media (Dhillon et al., 2014), and is thought to be the more sensitive of the two (Diacon et al., 2012). The presence of non-multiplying bacteria at the end of treatment is the cause of relapse, as they act as a pool from which multiplying bacteria emerge to cause recurrent disease (Chao and Rubin, 2010). Non-multiplying bacteria most likely exists in different forms in a spectrum from truly non-multiplying to different states of multiplying forms (Tuomanen, 1986; Coates and Hu, 2008).

A study on clinical sputum samples supplemented with resuscitation-promoting factors (rpfs) showed that non-multiplying bacteria constitute the vast majority of the bacterial population pre-treatment and that CFU, as a biomarker of the multiplying bacteria, only quantifies a small proportion of the total bacterial burden in patient samples (Mukamolova et al., 2010). Bowness et al. (2015) studied the relationship between CFU and TTP using data from patients on rifampicin monotherapy through means of linear regression of data per observation day and where the gradient of the regression line and *y*-intercept of the TTP-CFU relationship increased as treatment progressed. This resulted in two samples with identical CFU readings having different TTPs if the samples were collected at different times during treatment which was suggested to be due to that TTP captures an additional sub-population that is not captured in the CFU count.

The different bacterial states can be simplified theoretically and mathematically as fast-, slow- and non-multiplying TB sub-states which have been described by the semi-mechanistic multistate tuberculosis pharmacometric (MTP) model (Clewe et al., 2016). The MTP model was developed using CFU counts from natural growth data of Mtb in an *in vitro* hypoxia system together with the decline in CFU counts in response to treatment in log and stationary phase cultures. The MTP model was since successfully used to describe other *in vitro* systems (Chen et al., 2018; Susanto et al., 2020), and was validated and used in *in vivo* settings (Chen et al., 2017; Clewe et al., 2020), and in clinical settings (Svensson and Simonsson, 2016; Faraj et al., 2020a; Faraj et al., 2020b) to predict the changes in the numbers of bacteria in the different sub-states and subsequently CFU with and without treatment. Likewise, time-to-event approaches for describing drug efficacy using TTP biomarker data in clinical trials have been developed (Chigutsa et al., 2013; Svensson and Karlsson, 2017; Svensson et al., 2018b).

In this work, we aimed to develop a combined quantitative TB biomarker model using CFU and TTP biomarker data for assessing drug efficacy in early bactericidal activity studies and to describe the relationship between CFU and TTP over time.

2 Materials and methods

2.1 Patients and data

Clinical trial data was obtained from the PanACEA HIGHRIF1 trial, an open-label phase 2a trial registered at www.clinicaltrials.gov (NCT01392911) (Boeree et al., 2015). The trial was approved by local Ethical Review Boards and by the Medical Control Council of South Africa and was conducted according to Good Clinical Practice. All patients provided written informed consent before enrollment into the study. Newly diagnosed, pulmonary TB patients, susceptible to isoniazid and rifampicin were randomized to six cohorts assigned to 10 (n = 8, reference arm), 20, 25, 30, 35, or 40 (n = 15/arm) mg/kg daily oral rifampicin monotherapy for the first 7 days. The following seven days, therapy was supplemented with isoniazid, pyrazinamide and ethambutol at standard doses. Sputum samples were collected overnight over a 16-h interval on two consecutive days at baseline and daily for one week. On each day, two replicates from each sample were cultured on agar plates to assess CFU over time, while two other replicates were cultured in liquid media to determine the change in TTP over time. The limit of quantification (LOQ) for log CFU was 1 mL^{-1}, while it was 42 days for TTP samples. CFU samples below LOQ and TTP samples above LOQ were considered negative. One positive replicate was considered enough to include the sample in this analysis regardless of the other replicate as long as the next sample was positive.

In this analysis, data of daily sputum samples from a total of 83 patients on rifampicin monotherapy over the first week were included in the analysis. Contaminated CFU (n = 22) and TTP (n = 14) samples were excluded from the analysis. A total of 40 CFU samples were negative in that period and were removed from the analysis. This is because in all but two individuals, the negative samples were followed by positive CFU samples, and for those two individuals, the negative samples took place on day seven. A total of three negative TTP samples were excluded from the analysis. There were only seven instances in the CFU data and two in the TTP data when only one replicate was positive and the other was negative. Accordingly, 681 and 727 samples of CFU and TTP were included in the analysis, respectively. A description of the data and patient characteristics are summarized in Supplementary Tables S1, S2, respectively, in the Supplementary Materials.

2.2 Modelling strategy

In order to evaluate rifampicin exposure-response relationship using CFU and TTP, a previously developed rifampicin pharmacokinetic (PK) model using the PK data from this study was used (Svensson et al., 2018a). An individual pharmacokinetic parameter (IPP) approach (Zhang et al., 2003) was used where the individual PK model estimates were used as input for the exposure-response analysis for the CFU and TTP data. Initially, the MTP model (Clewe et al., 2016), developed to describe clinical CFU data after rifampicin treatment (Svensson and Simonsson, 2016), was used as a stand-alone model to describe only the CFU data. Thereafter, the combined quantitative TB biomarker model was developed by linking the MTP model to a TTP model. The TTP model was based on a semi-mechanistic time-to-event model previously developed using TTP data from the same clinical trial (Svensson et al., 2018b).

The MTP model had a central role within the combined quantitative TB biomarker model and acted as the link between the CFU and TTP data. While the sum of the fast- and slow-multiplying bacteria in the MTP model was used to predict CFU, the sum of all bacterial sub-states in the MTP model at the end of each sampling day, were transferred to the bacterial population in the TTP model, which thereby initiated the 0–42-day TTP. The TTP model related the mycobacterial growth in the liquid medium to the probability of achieving a positive signal in the MGIT system using a hazard model, treating the TTP observations as time-to-event data (Svensson et al., 2018b). Both CFU and TTP data were simultaneously analyzed to investigate the drug exposure-response relationship on each of the mycobacterial sub-states using the MTP model.

Once developed, the combined quantitative TB biomarker model was applied to predict one biomarker using information from the other. In order to predict the median tendency of TTP from CFU, only the CFU data were used to derive the empirical Bayes estimates (EBEs) of the final model. The opposite was applied when predicting the median tendency of CFU using only TTP data to derive the EBEs of the final model.

2.3 MTP model

The MTP model is a semi-mechanistic pharmacometric model, which describes the different mycobacterial sub-states and allows for the exploration of the exposure-response on those sub-states (Clewe et al., 2016). It consists of three bacterial sub-states: Fast- (F), slow- (S), and non-multiplying (N). The MTP model is represented by Eqs 1–3, in which time was defined as the time since infection.

$$\frac{dF}{dt} = Growth \cdot F \cdot F_G + k_{SF} \cdot S - k_{FS} \cdot F - k_{FN} \cdot F - F_D \cdot F \quad (1)$$

$$\frac{dS}{dt} = k_{FS} \cdot F + k_{NS} \cdot N - k_{SN} \cdot S - k_{SF} \cdot S - S_D \cdot S \quad (2)$$

$$\frac{dN}{dt} = k_{SN} \cdot S + k_{FN} \cdot F - k_{NS} \cdot N - N_D \cdot N \quad (3)$$

where F_G, F_D, S_D, and N_D are the estimated drug effects as inhibition of the fast-multiplying growth and killing of the fast-, slow-, and non-multiplying sub-states, respectively. The transfer rates between the three different sub-states are described by k_{SF}, k_{FS}, k_{FN}, k_{NS}, and k_{SN}.

Only the fast-multiplying sub-state was assumed to grow, with the growth limited by the system carrying capacity parameter (B_{max}). The growth of slow-multiplying sub-state was not included, and the increase of slow-multiplying sub-state took place through the transfer of bacteria from the fast-and non-multiplying state (Clewe et al., 2016). The transfer rates between the three different sub-states were fixed to the *in vitro* estimates (Clewe et al., 2016), as it was not possible to estimate such system-specific parameters separately from drug exposure-response parameters using the current data of rifampicin treatment. In addition, the transfer rate from the non-multiplying bacterial sub-state to the fast-multiplying bacterial sub-state was considered negligible based on the previous publication (Clewe et al., 2016). Furthermore, the transfer rate from the fast-to the slow-multiplying sub-states (k_{FS}) increased linearly with time. A Gompertz growth function was chosen to describe the growth of the fast-multiplying sub-state:

$$Growth = k_G \cdot log\left(\frac{B_{\max}}{F + S + N}\right) \quad (4)$$

where k_G is the growth rate of the fast-multiplying bacterial sub-state in the MTP model and B_{max} is the system carrying capacity, which defines the bacterial at start of treatment.

In this study, patients were assumed to be in the stationary phase of the infection, which is characterized by stable bacterial counts over time in untreated patients (Jindani et al., 1980). Patients were, thus, assumed to start treatment 150 days after the TB infection, a time-point at which the MTP model predicts a negligible change in the bacterial population, and little to no growth is expected. As the data was not sufficient to the estimate the acute bacterial growth phase, the k_G parameter was fixed to the *in vitro* estimate (Clewe et al., 2016). In addition, the initial conditions occurring 150 days before baseline, i.e., at time of infection, were fixed to zero for the non-multiplying stub-state and to 4.10 and 9,770 mL^{-1} for the fast- and slow-multiplying sub-states, respectively, based on the original work and its clinical application (Clewe et al., 2016; Svensson and Simonsson, 2016). On the other hand, the B_{max} parameter was re-estimated, along with its inter-individual variability (IIV), to account for the different individual bacterial baselines without affecting the relative amounts of the bacterial populations.

From the MTP model, the bacterial sub-states were transferred to the TTP model, while CFU was predicted as the sum of only the fast- and slow-multiplying sub-states using Eq 5.

$$log_{10} CFU = log_{10}(F + S) \quad (5)$$

where $\log_{10}$ CFU is the logarithm of CFU at a specific time-point, and F and S are the fast- and slow-multiplying sub-states, respectively, at that same time-point.

2.4 TTP model

The TTP model was based on an earlier published TTP model (Svensson et al., 2018b). The model describes the growth of the bacterial liquid culture from patients' sputum samples. The starting bacterial load in the tube was evaluated in different ways such as a

one subpopulation model and a three-subpopulation model (i.e., MTP model structure). In addition, the use of a correction factor (*CF*) that scaled down the ratio of the non-multiplying bacteria to the total bacteria that is transferred from the MTP model to the tube bacterial compartment was also evaluated ($F + S + N \cdot CF$). The *CF* parameter was both estimated and fixed to 17% (Faraj et al., 2020a). This is because it has been previously shown that the ratio of the non-multiplying sub-state to the total bacteria had to be scaled down to correctly predict the clinical bacterial number using an MTP model developed using *in vitro* data (Faraj et al., 2020a).

In the TTP model, another time scale was used, which was time since inoculation in liquid media. The total bacteria in the bacterial compartment were assumed to give rise to the signal in the MGIT system, as it was expected that, once introduced into the fresh media in the tube, the non-multiplying bacteria will re-initiate protein synthesis (Hu et al., 1998) and contribute to the total bacterial growth. A liquid culture-specific system carrying capacity parameter ($B_{max,lc}$) and a liquid culture-specific growth rate constant ($k_{G,lc}$), both controlling the growth of the bacterial liquid culture, were estimated. This is because the bacterial population is expected to grow differently in the MGIT system, as a growth enhancing substance is added to the MGIT liquid medium to reduce the detection time (Siddiqi and Rüsch-Gerdes, 2006). Different models of growth in the liquid medium were evaluated, including exponential, logistic and Gompertz growth functions.

Sputum samples undergo dilution and centrifugation steps during processing that remove any antibiotics that might have been present in the samples before being placed in the liquid medium. Consequently, the TTP model did not include killing by drug. Taking into consideration that post antibiotic effect (PAE) might take place within the liquid culture, different lag-time models in addition to time-varying growth rate in the liquid culture were evaluated to describe a potential delay or change of bacterial growth after different drug exposures. Furthermore, IIV, reflecting variability in the bacterial metabolic activity, was explored for the different liquid culture parameters.

As the TTP model describes time-to-event data, a hazard model, which described the probability of achieving a positive signal in the MGIT system, was employed, with right censoring occurring on day 42. At any given time-point in the liquid culture (t_{lc}), the hazard, $h(t_{lc})$, was calculated and was equal to the total bacterial load multiplied by a hazard scaler (*HS*) as:

$$h(t_{lc}) = B_{lc}(t_{lc}) \cdot HS \tag{6}$$

where $h(t_{lc})$ is the hazard at one time-point, $B_{lc}(t_{lc})$ is the total bacterial liquid culture at that time-point, and *HS* is a scaling parameter for the hazard.

The hazard at each time point was integrated to calculate a cumulative hazard, $H(t_{lc})$:

$$H(t_{lc}) = \int_0^{t_{lc}} h(t_{lc})\, dt \tag{7}$$

where $H(t_{lc})$ is the cumulative hazard at time in the liquid culture and $h(t_{lc})$ is the hazard at that time-point.

Finally, the survival, which describes the probability of not yet observing a positive signal was:

$$S(t_{lc}) = e^{-H(t_{lc})} \tag{8}$$

where $S(t_{lc})$ is the survival at time in the liquid culture and $H(t_{lc})$ is the cumulative hazard at that time-point.

2.5 Exposure-response relationships

A previously developed rifampicin PK model by Svensson et al. (2018a) was linked to the MTP model. Different exposure-response relationships were evaluated on four different effect sites of the MTP model in four steps using the combined quantitative TB biomarker model and both CFU and TTP data. The different exposure response relationships that were evaluated were on/off, linear, E_{max}, and sigmoidal E_{max} relationships. The four different effect sites that were evaluated were inhibition of the growth of the fast-multiplying sub-state (F_G) and killing of each of the fast- (F_D), slow (S_D), and non-multiplying (N_D) sub-states. The first step was to evaluate all exposure-response relationships on all effect sites in a univariate approach. The models were considered statistically significant at a significance level of 5%, i.e., drop in objective function value (OFV) of at least 3.84, for nested models with one additional parameter. The second step involved evaluating the statistically significant exposure-response models kept from the univariate evaluation of each effect site in combinations of two, three, and then all four effects sites, with at least a linear model on each site. The third step involved re-evaluating the exposure-response relationship at each effect site, and only statistically significant models were kept. The model with the largest OFV drop was selected and evaluated in combination with the model with the second highest significant drop until no significant drop in OFV was observed. The fourth step involved removing one exposure-response relationship from each effect site. In this backward elimination step, a significance level of 1%, i.e. 6.63 OFV drop, was used. After applying the four steps, the model with the final exposure-response relationship was obtained. IIV on the different exposure-response parameters were also evaluated.

2.6 Software and model selection

The CFU and TTP data analyses were performed using NONMEM 7.4.3 (Icon Development Solutions, Elliott City, MD, United States) (Beal et al., 2018) with the Laplacian estimation method. Data management and visualization were done in R statistical software version 4.1.2 (R Foundation for Statistical Computing, Vienna, Austria) (R Development Core Team, 2017). PsN 5.0.0 (Lindbom et al., 2005) was used to run the models and produce visual predictive checks (VPCs) used for model diagnostics (Lindbom et al., 2005). Additional graphical assessments of results were performed in xpose 4.7.2 (Keizer et al., 2013).

Model evaluation was based on parameter uncertainty and scientific plausibility while they were visually assessed using goodness-of-fit plots and VPCs. Nested models were evaluated based on the OFV, using the likelihood ratio test at a 5% significance level. For CFU, conventional VPCs, comparing

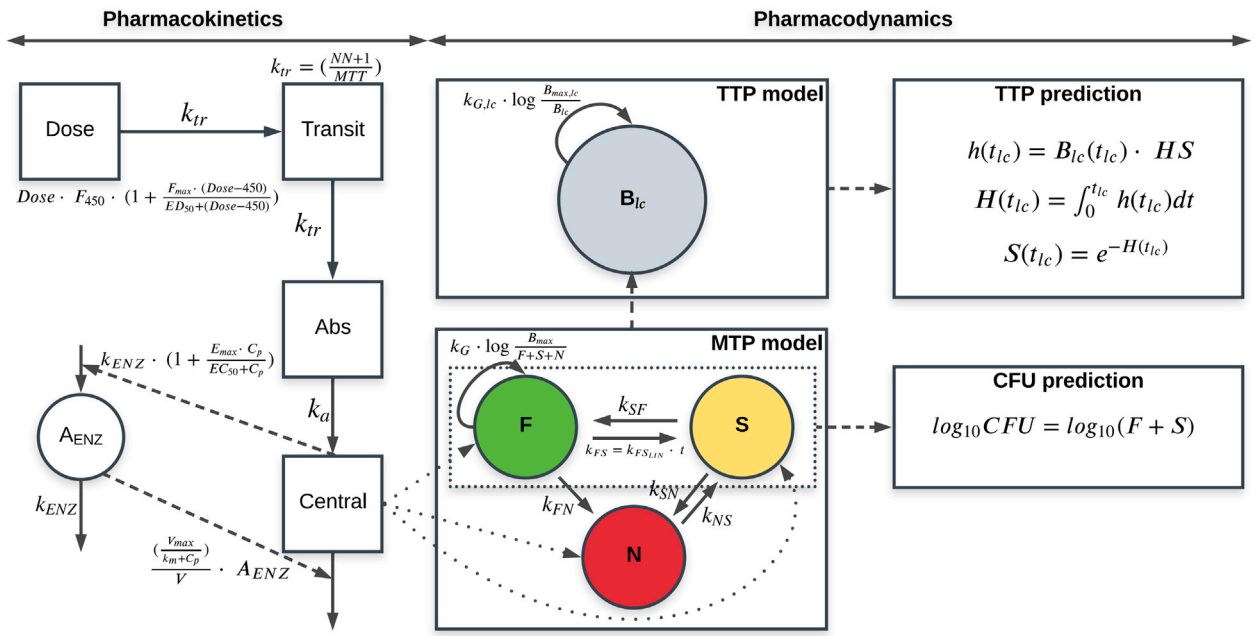

FIGURE 1
Schematic representation of the final quantitative tuberculosis biomarker model, including the pharmacokinetic (PK) model (left), MTP model (lower middle) and time-to-positivity (TTP) model (upper middle) using early bactericidal activity data of rifampicin in monotherapy in tuberculosis patients. CFU and TTP observations are simultaneously informing the MTP and TTP models through the simultaneous fit of the model to the data. The MTP model is represented by different bacterial sub-states; fast- (F), slow (S) and non-multiplying sub-state (N). The PK model is linked to the MTP model through the different killing parameters. CFU is predicted from the MTP model as the sum of the F and S sub-states. The TTP model consists of one bacterial sub-population model (B_{lc}) which is the sum of the F, S, and N sub-states at the starting time in the liquid medium (t_{lc} = 0). The bacterial liquid culture at any given time point in the liquid medium [$B_{lc}(t_{lc})$] was equal to the hazard $h(t_{lc})$ multiplied by a hazard scaler (HS). The probability of a TTP sample without a positive signal at time t_{lc} was given by the survival [$S(t_{lc})$] which was derived from the cumulative hazard [$H(t_{lc})$]. F_{450}, relative bioavailability to 450 mg; F_{max}, maximal increase in relative bioavailability; ED_{50}, dose corresponding to half the F_{max}; NN, number of transit compartments; k_{tr}, transfer rate between transit compartments; MTT, mean transit time; k_a, absorption rate constant; k_{ENZ}, first-order enzyme degradation rate and zero-order enzyme formation rate; E_{max}, maximal increase in enzyme formation rate; EC_{50}, concentration corresponding to 50% of E_{max}; C_p, plasma concentration; V_{max}, the maximal elimination rate; k_m, C_p at half of E_{max}; V, volume of distribution; k_G, growth rate of the fast-multiplying state; B_{max}, system carrying capacity per mL^{-1}; k_{FSLin}, time-dependent linear rate parameter describing transfer from fast-to slow-multiplying states; k_{SF}, first-order transfer rate from slow-to fast-multiplying states; k_{FN}, first-order transfer rate between fast- and non-multiplying states; k_{SN}, first-order transfer rate between slow- and non-multiplying states; k_{NS}, first-order transfer rate between non- and slow-multiplying states; B_{lc}, total bacterial liquid culture; $B_{max,lc}$, system carrying capacity per mL^{-1} in liquid media; $k_{G,lc}$, growth rate of the bacterial liquid culture; HS, hazard scaler; t, time since infection; t_{lc}, time in liquid culture. Solid arrows represent mass transfer, while dashed arrows represent linking between models.

observed and simulated data stratified by dose group, were produced. For TTP, posterior predictive checks (PPC) of the TTP in days versus time since treatment, stratified by each dose group, were used. Sampling importance resampling (SIR) was used to obtain accurate parameter uncertainties (Dosne et al., 2016).

3 Results

The general structure of the final quantitative TB biomarker model consisted of one PK model and two biomarker models: the MTP and TTP models (Figure 1).

All MTP model parameters were fixed to the *in vitro* estimates (Clewe et al., 2016), except for B_{max}, which was estimated. Estimating IIV on B_{max} was necessary to allow for the prediction of the individual bacterial load at baseline. The MTP model previously employed by Svensson and Simonsson (2016) to describe clinical CFU data, was first applied to CFU data as a stand-alone model. The model described the CFU data well, which provided a validation for using the MTP model in this work.

The TTP model comprised a one bacterial population that was initialized as the sum of the fast-, slow-, and non-multiplying sub-states in the MTP model at the sampling occasion. An MTP model structure within the TTP model, representing all three sub-states in the liquid medium with all transfer rates between the sub-states fixed to the *in vitro* estimates, was also evaluated, in which the positive signal in the MGIT system was driven by the sum of the fast-, slow-, and non-multiplying sub-states. However, the TTP data did not support the MTP model structure within the TTP model. Therefore, a one bacterial liquid culture (B_{lc}) was explored and shown to describe the data:

$$\frac{dB_{lc}}{dt_{lc}} = Growth_{lc} \cdot B_{lc} \quad (9)$$

where $Growth_{lc}$ and B_{lc} are the liquid culture-specific growth and total bacterial liquid culture, respectively.

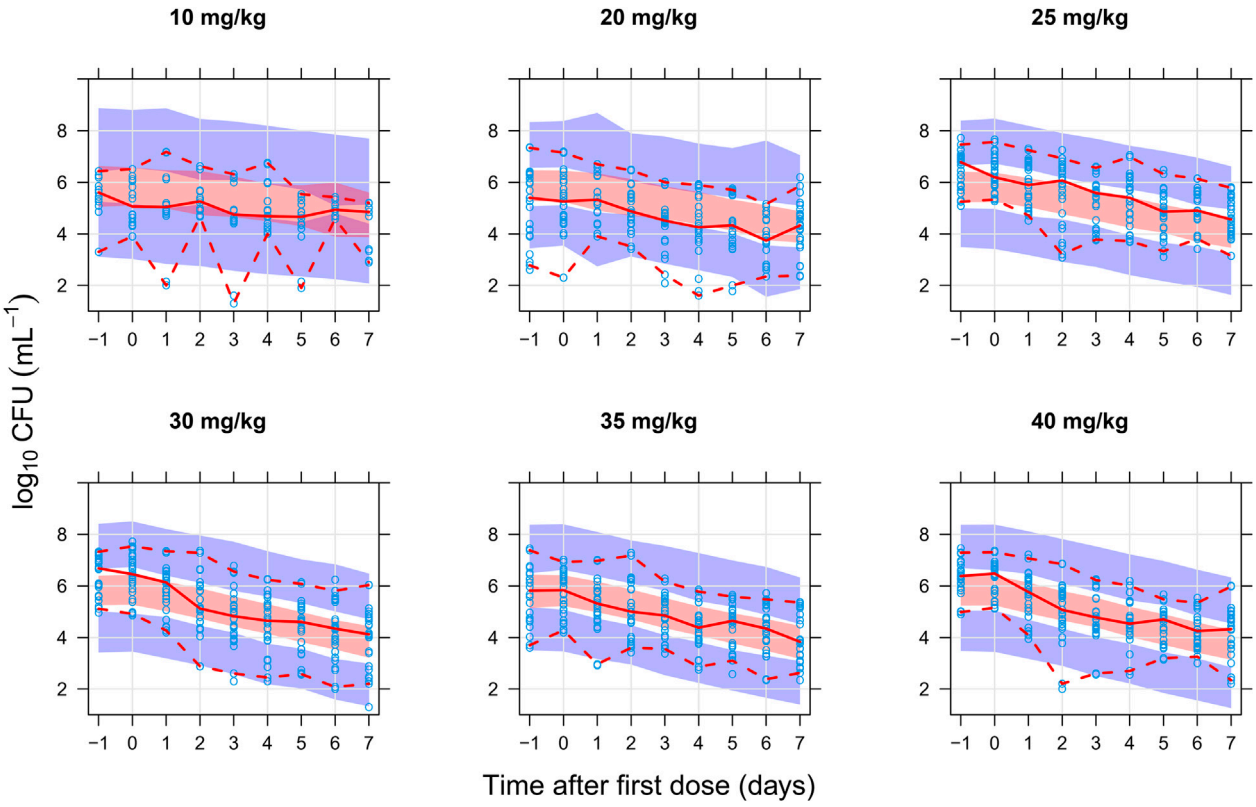

FIGURE 2
Visual predictive check of the final quantitative biomarker model describing colony forming unit (CFU) versus time since first dose and stratified on rifampicin dose group. The solid and dashed lines are the median, 2.5th, and 97.5th percentiles of the observed data, respectively. The shaded areas are the 95% confidence intervals of the 97.5th (blue), median (red), and 2.5th (blue) percentiles of the simulated data based on 1,000 simulations. Open circles are the observations.

Adding a fixed *CF* parameter (*CF* = 17%) to correct for the amount of the non-multiplying sub-state transferred from the MTP model to the TTP compartment resulted in a higher OFV, while estimating it did not improve the model fit to the data, and thus, the *CF* parameter was not used. Instead, the total sum of all bacterial sub-states ($F + S + N$) was transferred from the MTP model to the liquid medium in the TTP model.

The liquid culture-specific growth was described by a Gompertz growth model as it improved model fit compared to logistic and exponential growth models. Estimating a liquid culture-specific bacterial growth rate ($k_{G,lc}$) was necessary and resulted in a 314-point drop in OFV compared to using the fixed *in vitro* k_G parameter. This is in line with the expectation of the different bacterial growth in the MGIT system due to the added growth enhancing substance in the liquid medium (Siddiqi and Rüsch-Gerdes, 2006). Furthermore, a liquid culture-specific $B_{max,lc}$, controlling the growth in the liquid medium, was estimated and provided a significantly better fit to the data with a 629 drop in OFV compared to using the *in vitro* B_{max} parameter. A time-varying mycobacterial growth and a delayed liquid culture growth did not statistically significantly decrease the OFV. Eq.10 shows the Gompertz growth model in the TTP model.

$$Growth_{lc} = k_{G,lc} \cdot log\left(\frac{B_{\max,lc}}{B_{lc}}\right) \quad (10)$$

where $k_{G,lc}$ is the liquid culture growth rate, $B_{\max,lc}$ is system carrying capacity, and B_{lc} is the total bacterial liquid culture.

Using the MTP model approach, a linear effect described the killing of the fast-multiplying sub-state, while an E_{max} effect described the killing of each of the slow- and non-multiplying sub-states. No further significant OFV drop was seen when evaluating more complex models, e.g., E_{max} for the killing of the fast-multiplying sub-state or sigmoidal E_{max} model the killing of either the slow- and non-multiplying sub-states. Additionally, no statistically significant exposure-response relation was found on the inhibition of growth of the fast-multiplying sub-state. IIV was evaluated on all exposure-response parameters but was not supported by the data. The exposure-response relationships identified using both CFU and TTP data were different compared to fitting the CFU stand-alone model to the CFU data. While both models identified an E_{max} relationship on the killing of the slow- and non-multiplying sub-states, using only CFU data identified a simpler on/off model for the inhibition of growth of the fast-multiplying sub-state.

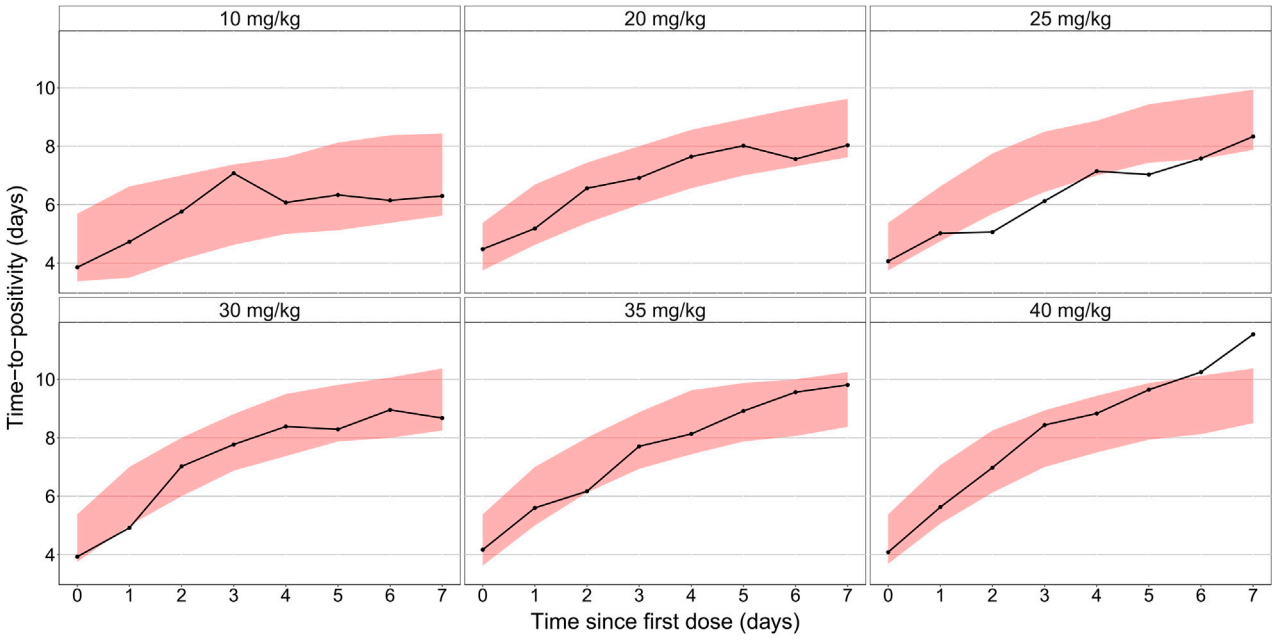

FIGURE 3
Posterior predictive check of the final quantitative biomarker model describing median time-to-positivity (TTP) versus time since first dose and stratified per rifampicin dose group. Solid lines represent the median time to positivity based on the observed data. Shaded areas are the 90% prediction interval based on 1,000 simulations using the model.

The final combined quantitative TB biomarker model provided a good fit to both the CFU and TTP data as seen in the VPC of CFU versus time stratified by dose group (Figure 2) and the PPC of TTP versus time (Figure 3), respectively. A Kaplan-Meier VPC of TTP versus time in the liquid medium for different rifampicin doses and treatment days is included in Supplementary Figure S1. The final parameter estimates from the combined biomarker model is shown in Table 1.

The final quantitative TB biomarker model was also able to describe the median CFU-TTP relationship well (Figure 4). Deriving the EBEs of the final model using data on either biomarker allowed for the prediction of the median tendency of the other biomarker. The final model was able to predict the median tendency of TTP using only CFU data with an R^2 of 0.79 (Figure 5A). However, it was difficult for the model to predict the median tendency of CFU using only TTP data with high precision (R^2 = 0.51; Figure 5B).

4 Discussion

This paper presents the development of a combined quantitative TB biomarker model (Figure 1), consisting of a PK-CFU-TTP model, to identify the relationship between CFU and TTP based on data from patients with pulmonary TB on 10–40 mg/kg rifampicin monotherapy for seven days in an early bactericidal activity (EBA) trial. The MTP model acted as the link between the CFU and TTP data within the combined model where CFU was the sum of the fast- and slow-multiplying sub-states which varied over time due to drug effect, while the total bacterial load predicted from the MTP model at the end of each day was the starting point for the level of bacteria in the TTP model.

This work builds on the MTP concept of three different sub-states; fast-, slow- and non-multiplying bacteria (Clewe et al., 2016). The MTP model has been shown to describe the growth, in the absence of treatment, and decline, in response to treatment, of bacteria in the different sub-states and, subsequently, CFU, using *in vitro* and clinical data (Clewe et al., 2016; Svensson and Simonsson, 2016). Consequently, the MTP model has been successfully applied to describe *in vitro* (Clewe et al., 2016; Susanto et al., 2020), mouse (Chen et al., 2017), and clinical data (Svensson and Simonsson, 2016; Faraj et al., 2020a; Faraj et al., 2020b). In addition, the MTP model has been successfully used to predict observations from early clinical studies using clinical dose-response forecasting from pre-clinical *in vitro* studies of rifampicin (Wicha et al., 2018; Susanto et al., 2020). Furthermore, it has been shown that applying semi-mechanistic modelling approaches, such as the MTP model, can increase the power of phase IIa studies and reduce the number of patients required to characterize drug exposure-response as compared to traditional statistical methods, e.g., *t*-test or ANOVA, and empirical approaches, e.g., mono- or bi-exponential models (Svensson et al., 2017). Applying the MTP model approach for representing bacterial burden presents a number of advantages, as representing drug efficacy on different mycobacterial sub-states is more mechanistically plausible, and it allows the evaluation of the drug exposure-response relationships on each of those populations separately, offering a mechanistic interpretation of rifampicin's effect on different bacterial sub-states.

TABLE 1 Final quantitative tuberculosis biomarker model parameter estimates.

Parameter	Description	Estimate[a]	RSE%[b]
MTP model			
k_G ($days^{-1}$)	Fast-multiplying bacterial growth rate	0.206 FIX	-
k_{FSLin} ($days^{-1}$)	Time-dependent transfer rate from fast- to slow-multiplying state	0.00166 FIX	-
k_{FN} ($days^{-1}$)	Transfer rate from fast- to non-multiplying state	$8.97{\cdot}10^{-7}$ FIX	-
k_{SF} ($days^{-1}$)	Transfer rate from slow- to fast-multiplying state	0.0145 FIX	-
k_{SN} ($days^{-1}$)	Transfer rate from slow- to non-multiplying state	0.186 FIX	-
k_{NS} ($days^{-1}$)	Transfer rate from non- to slow-multiplying state	0.00123 FIX	-
B_{max} (mL^{-1})	System carrying capacity	$4.997{\cdot}10^{4}$	5.27
F_0 (mL^{-1})	Initial bacterial number of fast-multiplying state	4.1 FIX	-
S_0 (mL^{-1})	Initial bacterial number of slow-multiplying state	9770 FIX	-
IIV B_{max} (%)	Inter-individual variability in B_{max}	83.4	12.1
ε (CV%)	Additive residual error on log scale	59.4	4.02
ε_{repl} (CV%)	Additive replicate error on log scale	19.1	24.1
TTP model			
$B_{max\,Jc}$ (mL^{-1})	System carrying capacity per mL in liquid culture	$1.62{\cdot}10^{6}$	7.61
$k_{G,Jc}$ (day^{-1})	Mycobacterial growth rate in liquid culture	0.22	4.34
HS	Hazard scaler	$1.49{\cdot}10^{-6}$	6.99
Exposure-response			
FD_k ($L{\cdot}mg^{-1}{\cdot}days^{-1}$)	Second-order fast-multiplying state death rate	16.5	333
$SD_{E\,max}$ ($days^{-1}$)	Maximum achievable drug-induced slow-multiplying state kill rate	0.30	18.3
SD_{EC50} ($mg{\cdot}L^{-1}$)	Concentration at 50% of $SD_{E\,max}$	24.9	36.5
$ND_{E\,max}$ ($days^{-1}$)	Maximum achievable drug-induced non-multiplying state kill rate	1.93	10.8
ND_{EC50} ($mg{\cdot}L^{-1}$)	Concentration at 50% of $ND_{E\,max}$	4.83	30.5

[a]All fixed parameters in this model were obtained from Clewe et al. (2016), and applied in Svensson and Simonsson (2016).
[b]RSE, relative standard error reported on the approximate standard deviation scale obtained using sampling importance resampling (SIR) (Dosne et al., 2016).

The EBA of rifampicin was evaluated using all available CFU and TTP data simultaneously, which further supported a strong mechanistic approach when developing the work and assessing the drug efficacy. Studies have shown that the combined use of two biomarkers better ranked the efficacy between treatments compared to using only one biomarker, as in the case of the combined use of CFU and RS ratio (Dide-agossou et al., 2022). Liquid media are known to be more sensitive in detecting the Mtb populations than solid media but are more prone to contamination (Cruciani et al., 2004; Diacon et al., 2012). International guidelines, therefore, recommend the use of at least one solid and one liquid medium to quantify the bacterial load accurately (Behr et al., 2022). As such, the simultaneous analysis of both CFU and TTP data in the combined biomarker model provided more information about the drug efficacy than only CFU, although this work only evaluated one drug. The rifampicin PK model used (Svensson et al., 2018a) accounted for the non-linearity in PK by a concentration-dependent apparent clearance and a dose-dependent relative bioavailability. The model also accounted for the decrease in rifampicin exposure with time by employing an enzyme turnover model to incorporate rifampicin's auto-induction. The estimated exposure-response relationships included a linear killing of the fast-multiplying sub-state and a non-linear E_{max} killing for both the slow- and non-multiplying sub-states, with a higher predicted drug potency towards the non-multiplying sub-state (Table 1). In the final combined biomarker model, the precision in the rate of the killing of the fast-multiplying sub-state (FD_k) parameter was low (Table 1). However, omitting the parameter from the model led to an increase in OFV of 174 points, and a simpler on-off model did not provide a good fit of the data. Further, omitting the parameter led to a too low predicted decline in biomarker response at day seven compared to keeping the parameter in the model.

The MTP model applied in this work is in agreement with the conclusions from Bowness et al. (2015) who also used data from the same trial, in that TTP captures an additional bacterial population

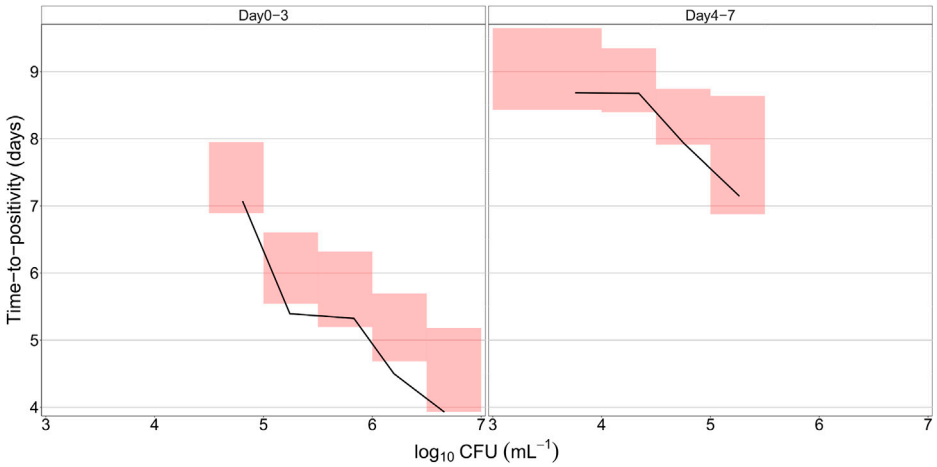

FIGURE 4
Predicted relationship between colony forming unit (CFU) versus time-to-positivity (TTP) using the final quantitative biomarker model. The solid lines represent the median of the observed data, while the shaded areas outline the 95% confidence interval based on 1,000 simulations.

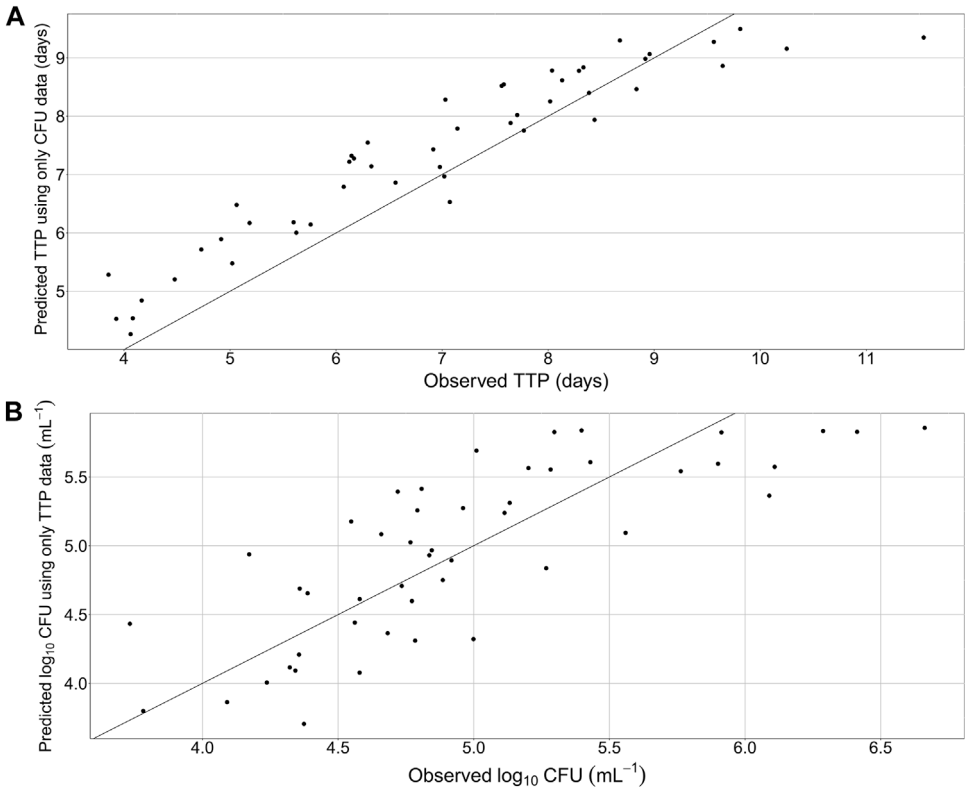

FIGURE 5
Predicted median tendency of the observed time-to-positivity (TTP) versus observed TTP, using only colony forming unit (CFU) data and the final quantitative biomarker model **(A)** and predicted median tendency of the observed CFU versus observed CFU, using only TTP data and the final quantitative biomarker model **(B)**. Solid line is the line of identity.

that is not detected by CFU. In this work, by allowing the transfer of the sum of the bacterial sub-states in the MTP model to the TTP model, we assumed that TTP can capture the non-multiplying sub-state as the extra bacterial population that CFU does not capture, and by doing so the model is able to predict both CFU and TTP adequately well. The relationship between CFU and TTP is non-

linear with respect to time and in this model approach, the non-linear relationship with time is predicted.

Earlier work has shown that the non-multiplying bacteria in sputum is 17% of the *in vitro* levels, suggesting a difference in phenotypic resistance, whereas no difference in multiplying bacteria was found (Faraj et al., 2020a). In this work, we explored the option to only allow for a percentage of the non-multiplying bacteria to be transferred to the TTP bacterial compartment from the MTP model but the data in this work did not support it, and the total bacteria from the MTP model seemed to well represent the bacterial population driving the TTP signal. A semi-mechanistic time-to-event approach was employed to describe the TTP observations in this work. While an implementation of the full MTP model with three bacterial compartments in the liquid medium was not supported by the data, a one-bacterial compartment, representing the total bacterial population in the liquid medium, was sufficient and provided a satisfactory description of the TTP data. Future work should aim at describing the dynamics of the bacterial populations in liquid media.

A stand-alone TTP model has been previously used to assess the exposure-response relationship of rifampicin using TTP data from the same trial (Svensson et al., 2018b). The stand-alone TTP model was not linked to a rifampicin PK model but instead used rifampicin exposure as a covariate on the kill rate parameters. In addition, other models have previously analyzed CFU and TTP simultaneously using EBA data. Gausi et al. (2021) used both biomarkers to describe isoniazid efficacy on a single bacterial population for CFU and TTP in patients with drug-sensitive and drug-resistant TB. Lyons used CFU and TTP to establish pretomanid and bedaquiline exposure-response relationships (Lyons, 2019; Lyons, 2022). This work builds upon the previous work by using both CFU and TTP data simultaneously combined to a rifampicin PK model to evaluate the exposure-response relationship of rifampicin on three bacterial subpopulations using the MTP model, which presents a more mechanistic approach of assessing the exposure-response relationship. Inclusion of a non-multiplying state may provide a deeper link between EBA and predictions of long-term efficacy in TB drug development although this still remains to be further investigated.

While CFU has been the gold standard biomarker in pre-clinical studies and in TB diagnosis, TTP has been suggested as a substitute to CFU in phase IIa EBA studies (Diacon et al., 2012). As such, the combined quantitative TB biomarker model developed in this work (Figure 1) can play a vital role in predicting TTP from trials where only CFU was measured. In addition, the combined quantitative TB biomarker model can be used to predict typical TTP in the case of missing or contaminated samples. In this work, the combined quantitative TB biomarker model was shown to be able to predict the median tendency of the observed TTP using information on CFU with good precision after 7-day rifampicin therapy of drug susceptible TB (Figure 5A). The model was less precise, however, in predicting the median tendency of the observed CFU using only TTP data (Figure 5B). This is because TTP was assumed to correspond to a signal initiated by the growth of the whole bacterial population. Thus, it was difficult for the model to differentiate between the different sub-states using TTP data in order to predict CFU, which was assumed to be the sum of only the fast- and slow-multiplying sub-states.

The combined quantitative TB biomarker model was developed using data from seven-day rifampicin monotherapy of drug susceptible TB (Boeree et al., 2015). As the clinical data did not include information on the acute bacterial growth phase, the growth of the different bacterial sub-states and the transfer rates between them could not be estimated. Using *in vitro* information compensates for this limitation, and thus, the growth and transfer rate parameters were fixed from the *in vitro* setting (Clewe et al., 2016). In this work, the model assumed that the TTP signal is driven by the sum of the fast-, slow-, and non-multiplying population. While several implementations for which population drives the TTP signal have been explored, the whole bacterial population driving the signal provided the best fit. The assumption that TTP can capture all bacterial populations, however, might not be true, and re-evaluation of the population driving the TTP signal might be necessary when applying the model to other data.

It has been reported that the CFU-TTP relationship might differ in certain cases of Mtb mutations (le Roux et al., 2021). As the response to treatment is expected to differ between drug-sensitive and drug-resistant Mtb strains (Bahuguna and Rawat, 2020), the model should be validated using data from treatment of drug-resistant Mtb. Potential differences in CFU-TTP relationship could be accounted for in the model to allow for a mutation specific relationship. Further work should also explore if the identified CFU-TTP relationship is drug-specific, i.e., to apply the model to different EBA clinical trial datasets. It is important to emphasize that the exposure-response relationships always are drug-specific and are better characterized using both biomarkers rather than either. Likewise, further work should also evaluate whether the identified CFU-TTP relationship holds in trials with durations longer than seven days. Therefore, extrapolation to other drugs and outside the dose range, bacterial susceptibly and treatment duration should be done with caution.

The combined rifampicin PK-linked quantitative TB biomarker model was successfully developed using CFU and TTP data from a phase IIa EBA trial. The model used data from both biomarkers to evaluate rifampicin exposure-response relationship in an EBA trial. The final model was able to describe the relationship between CFU and TTP over time.

Data availability statement

The data analyzed in this study is subject to the following licenses/restrictions: Not publicly available. Requests to access these datasets should be directed to PanACEA@radboudumc.nl.

Ethics statement

The studies involving human participants were reviewed and approved by Local Ethical Review Boards and the Medical Control

Council of South Africa. The patients/participants provided their written informed consent to participate in this study.

Author contributions

RAA, RS, and US analyzed the data and conducted the analysis. RAA, RS, ES, SG, MB, AD, RD, RA, and US interpreted the results, wrote the manuscript, revised the manuscript and approved the final version. AD and RD were involved the clinical studies and AD in the laboratory analysis.

Funding

This clinical trial was conducted within PanACEA, which was part of the European and Developing Countries Clinical Trials Partnership (EDCTP) 1 programme [project code IP. 2007.32011.012 (HIGHRIF)] and the EDCTP2 programme supported by the European Union (grant number TRIA 2015-1102-PanACEA).

Acknowledgments

The authors want to thank the patients and site staff participating in the clinical study. The authors gratefully acknowledge all the authors of the original work that generated the data of which this analysis was based on. The computations in this work were enabled by resources in a project [snic 2021-5-541] provided by the Swedish National Infrastructure for Computing (SNIC) at UPPMAX, partially funded by the Swedish Research Council through grant agreement no. 2018-05973.

Conflict of interest

The authors declare that the research was conducted in the absence of any commercial or financial relationships that could be construed as a potential conflict of interest.

Publisher's note

Author disclaimer

The views and opinions of authors expressed herein do not necessarily state or reflect those of EDCTP.

Supplementary material

The Supplementary Material for this article can be found online at: https://www.frontiersin.org/articles/10.3389/fphar.2023.1067295/full#supplementary-material

References

Bahuguna, A., and Rawat, D. S. (2020). An overview of new antitubercular drugs, drug candidates, and their targets. *Med. Res. Rev.* 40, 263–292. doi:10.1002/med.21602

Beal, S. L., Sheiner, L. B., Boeckmann, A. J., and Bauer, R. J. (2018). *NONMEM 7.4.3 users guide*. Gaithersburg, MD. Available at: https://nonmem.iconplc.com/nonmem743/guides.

Behr, M. A., Lapierre, S. G., Kunimoto, D. Y., Lee, R. S., Long, R., Sekirov, I., et al. (2022). Chapter 3: Diagnosis of tuberculosis disease and drug-resistant tuberculosis. *Can. J. Respir. Crit. Care, Sleep. Med.* 6, 33–48. doi:10.1080/24745332.2022.2035638

Boeree, M. J., Diacon, A. H., Dawson, R., Narunsky, K., Du Bois, J., Venter, A., et al. (2015). A dose-ranging trial to optimize the dose of rifampin in the treatment of tuberculosis. *Am. J. Respir. Crit. Care Med.* 191, 1058–1065. doi:10.1164/rccm.201407-1264OC

Bowness, R., Boeree, M. J., Aarnoutse, R., Dawson, R., Diacon, A., Mangu, C., et al. (2015). The relationship between mycobacterium tuberculosis mgit time to positivity and cfu in sputum samples demonstrates changing bacterial phenotypes potentially reflecting the impact of chemotherapy on critical sub-populations. *J. Antimicrob. Chemother.* 70, 448–455. doi:10.1093/jac/dku415

Chao, M. C., and Rubin, E. J. (2010). Letting sleeping dos lie: Does dormancy play a role in tuberculosis? *Annu. Rev. Microbiol.* 64, 293–311. doi:10.1146/annurev.micro.112408.134043

Chen, C., Ortega, F., Rullas, J., Alameda, L., Angulo-Barturen, I., Ferrer, S., et al. (2017). The multistate tuberculosis pharmacometric model: A semi-mechanistic pharmacokinetic-pharmacodynamic model for studying drug effects in an acute tuberculosis mouse model. *J. Pharmacokinet. Pharmacodyn.* 44, 133–141. doi:10.1007/s10928-017-9508-2

Chen, C., Wicha, S. G., Nordgren, R., and Simonsson, U. S. H. (2018). Comparisons of analysis methods for assessment of pharmacodynamic interactions including design recommendations. *AAPS J.* 20, 77. doi:10.1208/s12248-018-0239-0

Chigutsa, E., Patel, K., Denti, P., Visser, M., Maartens, G., Kirkpatrick, C. M. J., et al. (2013). A time-to-event pharmacodynamic model describing treatment response in patients with pulmonary tuberculosis using days to positivity in automated liquid mycobacterial culture. *Antimicrob. Agents Chemother.* 57, 789–795. doi:10.1128/AAC.01876-12

Clewe, O., Aulin, L., Hu, Y., Coates, A. R. M., and Simonsson, U. S. H. (2016). A multistate tuberculosis pharmacometric model: A framework for studying anti-tubercular drug effects *in vitro*. *J. Antimicrob. Chemother.* 71, 964–974. doi:10.1093/jac/dkv416

Clewe, O., Faraj, A., Hu, Y., Coates, A. R. M., and Simonsson, U. S. H. (2020). A model-based analysis identifies differences in phenotypic resistance between *in vitro* and *in vivo*: Implications for translational medicine within tuberculosis. *J. Pharmacokinet. Pharmacodyn.* 47, 421–430. doi:10.1007/s10928-020-09694-0

Coates, A. R. M., and Hu, Y. (2008). Targeting non-multiplying organisms as a way to develop novel antimicrobials. *Trends Pharmacol. Sci.* 29, 143–150. doi:10.1016/j.tips.2007.12.001

Cruciani, M., Scarparo, C., Malena, M., Bosco, O., Serpelloni, G., and Mengoli, C. (2004). Meta-analysis of BACTEC MGIT 960 and BACTEC 460 TB, with or without solid media, for detection of mycobacteria. *J. Clin. Microbiol.* 42, 2321–2325. doi:10.1128/jcm.42.5.2321-2325.2004

Dhillon, J., Fourie, P. B., and Mitchison, D. A. (2014). Persister populations of *Mycobacterium tuberculosis* in sputum that grow in liquid but not on solid culture media. *J. Antimicrob. Chemother.* 69, 437–440. doi:10.1093/jac/dkt357

Diacon, A. H., and Donald, P. R. (2014). The early bactericidal activity of antituberculosis drugs. *Expert Rev. anti. Infect. Ther.* 12, 223–237. doi:10.1586/14787210.2014.870884

Diacon, A. H., Maritz, J. S., Venter, A., Van Helden, P. D., Dawson, R., and Donald, P. R. (2012). Time to liquid culture positivity can substitute for colony counting on agar plates in early bactericidal activity studies of antituberculosis agents. *Clin. Microbiol. Infect.* 18, 711–717. doi:10.1111/j.1469-0691.2011.03626.x

Dide-agossou, C., Bauman, A. A., Ramey, M. E., Rossmassler, K., Al Mubarak, R., Pauly, S., et al. (2022). Combination of *Mycobacterium tuberculosis* RS ratio and CFU

improves the ability of murine efficacy experiments to distinguish between drug treatments. *Antimicrob. Agents Chemother.* 66, e0231021. doi:10.1128/aac.02310-21

Dosne, A. G., Bergstrand, M., Harling, K., and Karlsson, M. O. (2016). Improving the estimation of parameter uncertainty distributions in nonlinear mixed effects models using sampling importance resampling. *J. Pharmacokinet. Pharmacodyn.* 43, 583–596. doi:10.1007/s10928-016-9487-8

Faraj, A., Clewe, O., Svensson, R. J., Mukamolova, G. V., Barer, M. R., and Simonsson, U. S. H. (2020a). Difference in persistent tuberculosis bacteria between *in vitro* and sputum from patients: Implications for translational predictions. *Sci. Rep.* 10, 15537. doi:10.1038/s41598-020-72472-y

Faraj, A., Svensson, R. J., Diacon, A. H., and Simonsson, U. S. H. (2020b). Drug effect of clofazimine on persisters explains an unexpected increase in bacterial load in patients. *Antimicrob. Agents Chemother.* 64, e01905–e01919. doi:10.1128/AAC.01905-19

Gausi, K., Ignatius, E. H., Sun, X., Kim, S., Moran, L., Wiesner, L., et al. (2021). A semimechanistic model of the bactericidal activity of high-dose isoniazid against multidrug-resistant tuberculosis: Results from a randomized clinical trial. *Am. J. Respir. Crit. Care Med.* 204, 1327–1335. doi:10.1164/rccm.202103-0534OC

Global tuberculosis report (2022). Geneva: World Health Organization. Licence: CC BY-NC-SA 3.0 IGO.

Hu, Y. M., Butcher, P. D., Sole, K., Mitchison, D. A., and Coates, A. R. M. (1998). Protein synthesis is shutdown in dormant *Mycobacterium tuberculosis* and is reversed by oxygen or heat shock. *FEMS Microbiol. Lett.* 158, 139–145. doi:10.1111/j.1574-6968.1998.tb12813.x

Jindani, A., Aber, V. R., Edwards, E. A., and Mitchison, D. A. (1980). The early bactericidal activity of drugs in patients with pulmonary tuberculosis. *Am. Rev. Respir. Dis.* 121, 939–949. doi:10.1164/arrd.1980.121.6.939

Keizer, R. J., Karlsson, M. O., and Hooker, A. (2013). Modeling and simulation workbench for NONMEM: Tutorial on pirana, PsN, and xpose. *CPT Pharmacometrics Syst. Pharmacol.* 2, e50. doi:10.1038/psp.2013.24

le Roux, S. P., Upton, C., Vanker, N., Dooley, K. E., Diacon, A. H., Miyahara, S., et al. (2021). Resistance-conferring mycobacterial mutations and quantification of early bactericidal activity. *Am. J. Respir. Crit. Care Med.* 203, 635–637. doi:10.1164/rccm.202007-2740LE

Lindbom, L., Pihlgren, P., and Jonsson, N. (2005). PsN-Toolkit - a collection of computer intensive statistical methods for non-linear mixed effect modeling using NONMEM. *Comput. Methods Programs Biomed.* 79, 241–257. doi:10.1016/j.cmpb.2005.04.005

Lyons, M. A. (2019). Modeling and simulation of pretomanid pharmacodynamics in pulmonary tuberculosis patients. *Antimicrob. Agents Chemother.* 63, e00732–19. doi:10.1128/AAC.00732-19

Lyons, M. A. (2022). Pharmacodynamics and bactericidal activity of bedaquiline in pulmonary tuberculosis. *Antimicrob. Agents Chemother.* 66, e0163621. doi:10.1128/AAC.01636-21

Mukamolova, G. V., Turapov, O., Malkin, J., Woltmann, G., and Barer, M. R. (2010). Resuscitation-promoting factors reveal an occult population of tubercle bacilli in sputum. *Am. J. Respir. Crit. Care Med.* 181, 174–180. doi:10.1164/rccm.200905-0661OC

R Development Core Team (2017). *R: A language and environment for statistical computing*. Vienna, Austria. R Foundation for Statistical Computing, Vienna, Austria. ISBN 3-900051-07-0, Available at: http://www.R-project.org.

Siddiqi, S. H., and Rüsch-Gerdes, S. (2006). MGIT procedure manual: For BACTEC™ MGIT 960™ TB system. Available at: http://www.finddiagnostics.org/export/sites/default/resource-centre/find_documentation/pdfs/mgit_manual_nov_2007.pdf.

Susanto, B. O., Wicha, S. G., Hu, Y., Coates, A. R. M., and Simonsson, U. S. H. (2020). Translational model-informed approach for selection of tuberculosis drug combination regimens in early clinical development. *Clin. Pharmacol. Ther.* 108, 274–286. doi:10.1002/cpt.1814

Svensson, E. M., and Karlsson, M. O. (2017). Modelling of mycobacterial load reveals bedaquiline's exposure-response relationship in patients with drug-resistant TB. *J. Antimicrob. Chemother.* 72, 3398–3405. doi:10.1093/jac/dkx317

Svensson, R. J., Aarnoutse, R. E., Diacon, A. H., Dawson, R., Gillespie, S. H., Boeree, M. J., et al. (2018a). A population pharmacokinetic model incorporating saturable pharmacokinetics and autoinduction for high rifampicin doses. *Clin. Pharmacol. Ther.* 103, 674–683. doi:10.1002/cpt.778

Svensson, R. J., Gillespie, S. H., and Simonsson, U. S. H. (2017). Improved power for TB Phase IIa trials using a model-based pharmacokinetic-pharmacodynamic approach compared with commonly used analysis methods. *J. Antimicrob. Chemother.* 72, 2311–2319. doi:10.1093/jac/dkx129

Svensson, R. J., and Simonsson, U. S. H. (2016). Application of the multistate tuberculosis pharmacometric model in patients with rifampicin-treated pulmonary tuberculosis. *CPT Pharmacometrics Syst. Pharmacol.* 5, 264–273. doi:10.1002/psp4.12079

Svensson, R. J., Svensson, E. M., Aarnoutse, R. E., Diacon, A. H., Dawson, R., Gillespie, S. H., et al. (2018b). Greater early bactericidal activity at higher rifampicin doses revealed by modeling and clinical trial simulations. *J. Infect. Dis.* 218, 991–999. doi:10.1093/infdis/jiy242

Tuomanen, E. (1986). Phenotypic tolerance: The search for β-lactam antibiotics that kill nongrowing bacteria. *Rev. Infect. Dis.* 8, S279–S291. doi:10.1093/clinids/8.supplement_3.s279

Wicha, S. G., Clewe, O., Svensson, R. J., Gillespie, S. H., Hu, Y., Coates, A. R. M., et al. (2018). Forecasting clinical dose-response from preclinical studies in tuberculosis research: Translational predictions with rifampicin. *Clin. Pharmacol. Ther.* 104, 1208–1218. doi:10.1002/cpt.1102

Zhang, L., Beal, S. L., and Sheiner, L. B. (2003). Simultaneous vs. Sequential analysis for population PK/PD data I: Best-case performance. *J. Pharmacokinet. Pharmacodyn.* 30, 387–404. doi:10.1023/b:jopa.0000012998.04442.1f

frontiers | Frontiers in Pharmacology

TYPE Original Research
PUBLISHED 27 March 2023
DOI 10.3389/fphar.2023.1022090

OPEN ACCESS

EDITED BY
Thomas Dorlo,
Uppsala University, Sweden

REVIEWED BY
Elin M. Svensson,
Radboud University Medical Centre, Netherlands
Leen Rigouts,
Institute of Tropical Medicine Antwerp, Belgium

*CORRESPONDENCE
Yi Hu,
yhu@fudan.edu.cn

†These authors contributed equally to this work and share first authorship

‡These authors contributed equally to this work and share senior authorship

SPECIALTY SECTION
This article was submitted to Pharmacology of Infectious Diseases, a section of the journal Frontiers in Pharmacology

RECEIVED 18 August 2022
ACCEPTED 06 March 2023
PUBLISHED 27 March 2023

CITATION
Shao G, Bao Z, Davies Forsman L, Paues J, Werngren J, Niward K, Schön T, Bruchfeld J, Alffenaar J-W and Hu Y (2023), Population pharmacokinetics and model-based dosing evaluation of bedaquiline in multidrug-resistant tuberculosis patients.
Front. Pharmacol. 14:1022090.
doi: 10.3389/fphar.2023.1022090

Population pharmacokinetics and model-based dosing evaluation of bedaquiline in multidrug-resistant tuberculosis patients

Ge Shao[1†], Ziwei Bao[2†], Lina Davies Forsman[3,4†], Jakob Paues[5,6], Jim Werngren[7], Katarina Niward[5,6], Thomas Schön[5,6,8], Judith Bruchfeld[3,4‡], Jan-Willem Alffenaar[9,10,11‡] and Yi Hu[1*‡]

[1]Department of Epidemiology, School of Public Health and Key Laboratory of Public Health Safety, Fudan University, Shanghai, China, [2]The Fifth People's Hospital of Suzhou, Infectious Disease Hospital Affiliated to Soochow University, Suzhou, China, [3]Department of Infectious Diseases, Karolinska University Hospital, Stockholm, Sweden, [4]Department of Medicine, Division of Infectious Diseases, Karolinska Institutet Solna, Stockholm, Sweden, [5]Department of Biomedical and Clinical Sciences, Linköping University, Linköping, Sweden, [6]Department of Infectious Diseases, Region Östergötland, Linköping University Hospital, Linköping, Sweden, [7]Department of Microbiology, Public Health Agency of Sweden, Stockholm, Sweden, [8]Department of Infectious Diseases, Kalmar County Hospital, Kalmar, Linköping University, Linköping, Sweden, [9]University of Sydney, Faculty of Medicine and Health, School of Pharmacy, Sydney, NSW, Australia, [10]Westmead Hospital, Sydney, NSW, Australia, [11]Sydney Institute for Infectious Diseases, University of Sydney, Sydney, NSW, Australia

Aims: Bedaquiline is now recommended to all patients in the treatment of multidrug-resistant tuberculosis (MDR-TB) using standard dosing regimens. As the ability to measure blood drug concentrations is very limited, little is known about drug exposure and treatment outcome. Thus, this study aimed to model the population pharmacokinetics as well as to evaluate the currently recommended dosage.

Methodology: A bedaquiline population pharmacokinetic (PK) model was developed based on samples collected from the development cohort before and 1, 2, 3, 4, 5, 6, 8, 12, 18, and 24 h after drug intake on week 2 and week 4 of treatment. In a prospective validation cohort of patients with MDR-TB, treated with bedaquiline-containing standardized regimen, drug exposure was assessed using the developed population PK model and thresholds were identified by relating to 2-month and 6-month sputum culture conversion and final treatment outcome using classification and regression tree analysis. In an exploratory analysis by the probability of target attainment (PTA) analysis, we evaluated the recommended dosage at different MIC levels by Middlebrook 7H11 agar dilution (7H11).

Results: Bedaquiline pharmacokinetic data from 55 patients with MDR-TB were best described by a three-compartment model with dual zero-order input. Body weight was a covariate of the clearance and the central volume of distribution, albumin was a covariate of the clearance. In the validation cohort, we enrolled 159 patients with MDR-TB. The 7H11 MIC mode (range) of bedaquiline was 0.06 mg (0.008–0.25 mg/L). The study participants with $AUC_{0\text{-}24h}$/MIC above 175.5 had a higher probability of culture conversion after 2-month treatment (adjusted relative risk, aRR:16.4; 95%CI: 5.3–50.4). Similarly, those with $AUC_{0\text{-}24h}$/MIC above 118.2 had a higher probability of culture conversion after 6-month treatment (aRR:20.1; 95%CI: 2.9–139.4), and those with $AUC_{0\text{-}24h}$/MIC above

74.6 had a higher probability of successful treatment outcome (aRR:9.7; 95%CI: 1.5–64.8). Based on the identified thresholds, simulations showed that the WHO recommended dosage (400 mg once daily for 14 days followed by 200 mg thrice weekly) resulted in PTA >90% for the majority of isolates (94%; MICs ≤0.125 mg/L).

Conclusion: We established a population PK model for bedaquiline in patients with MDR-TB in China. Based on the thresholds and MIC distribution derived in a clinical study, the recommended dosage of bedaquiline is sufficient for the treatment of MDR-TB.

KEYWORDS

bedaquiline, multidrug-resistant tuberculosis, population pharmacokinetic modeling, dosage evaluation, target attainment

1 Introduction

Multidrug-resistant tuberculosis (MDR-TB) is defined as tuberculosis (TB) where *Mycobacterium tuberculosis (Mtb)* is at least resistant to isoniazid and rifampicin. China is the world's second-highest TB burden country, with 84,200 new TB cases and 17,528 MDR-TB cases in 2020 (World Health Organization, 2021). The treatment is long and associated with frequent adverse events, with a cure rate of MDR-TB as low as 59% in 2018 (Olaru et al., 2016; World Health Organization, 2021). Hence optimization of treatment is needed to achieve END TB goals.

Bedaquiline is a diarylquinoline drug approved by the U.S. Food and Drug Administration in 2012 and proved to significantly increase the success rate of MDR-TB treatment (Lounis et al., 2006; Diacon et al., 2012; Diacon et al., 2014; Healan et al., 2017; Olayanju et al., 2018; Li et al., 2019). Thus, bedaquiline is now recommended by WHO to all patients with MDR-TB, unless contraindicated (World Health Organization, 2019).

The drug concentrations and pharmacokinetics of anti-TB drugs vary widely among TB patients (Pasipanodya et al., 2013; McLeay et al., 2014). In the case of bedaquiline, drug exposure is related to body weight, albumin, age, race and concomitant use of rifampicin (McLeay et al., 2014; Van Heeswijk et al., 2014; Svensson et al., 2016; Svensson and Karlsson, 2017). The drug concentration of bedaquiline is important as activity has been found to be concentration-dependent, where the high concentrations of bedaquiline were associated with a faster decline in bacterial load in patients within 24 weeks (Tanneau et al., 2020) and sputum culture conversion after 6-month treatment (Zheng et al., 2021). Therefore, an optimal drug exposure of bedaquiline is important to improve the MDR-TB treatment.

Although there have been several studies to model the population pharmacokinetics (PK) of bedaquiline among healthy subjects and patients with drug-susceptible and multidrug-resistant TB (McLeay et al., 2014; Svensson et al., 2016), the threshold for drug exposure associated with optimal treatment outcome remains unknown. Therefore, the present study aimed to build a population PK model of bedaquiline among patients with MDR-TB, identify the threshold to predict the treatment in a prospective cohort of patients with MDR-TB as well as to evaluate the current doses by the probability of target attainment (PTA) analysis.

2 Methods

2.1 Study design and population

A multi-center prospective cohort study of patients with MDR-TB was conducted in Guizhou, Henan, Jiangsu and Sichuan Province in China between June 2016 to June 2019. The patients were aged between 18 and 70 years, diagnosed with MDR-TB by phenotypic drug susceptibility testing (DST), and had received a bedaquiline-containing regimen. Patients with abnormal liver or kidney function, pregnancy, or infected with human immunodeficiency virus, hepatitis B, or C virus were excluded.

From the prospective cohort study, we included subjects with rich sampling into a development cohort for pharmacological modeling, while those with limited sampling and a standardized WHO regimen were included into the validation cohort for identifying the threshold predictive of treatment outcome.

The participants in the development cohort were treated with a standardized bedaquiline-containing regimen for 6 months during the intensive phase, including bedaquiline, moxifloxacin or levofloxacin, linezolid as well as a background regimen to complete a full-oral regimen as we reported previously (Zheng et al., 2021), while those in validation cohorts received a standardized WHO regimen for 6 months containing bedaquiline, moxifloxacin, linezolid, clofazimine, and cycloserine. For both cohorts, the dosage of bedaquiline was 400 mg once daily for the first 2 weeks and 200 mg thrice weekly for the following 22 weeks, and the regimen for the following 18 months during the consolidation phase included at least 3 anti-TB drugs. Non-adherence was defined as discontinued for more than 3 days.

All study participants were routinely examined monthly during the intensive phase (the first 6 months) and once every 2 months during the consolidation phase (the next 18 months). A questionnaire was used to collect demographic data, while medical and laboratory data were extracted from hospital records.

In the development cohort, blood plasma was sampled before and 1, 2, 3, 4, 5, 6, 8, 12, 18, and 24 h after drug intake on week 2 and week 4 of treatment respectively, while in the validation cohort, samples were collected predose and 2, 4 and 6 h after taking the drug on week 4 of treatment as limited sampling strategy indicated that the sparse concentrations performed well enough for simulation (Supplementary Table S1), and the consistency between the measured and predicted value of $AUC_{0\text{-}24h}$ was evaluated by Bland-Altman analysis (Figure 1). After collection, the blood

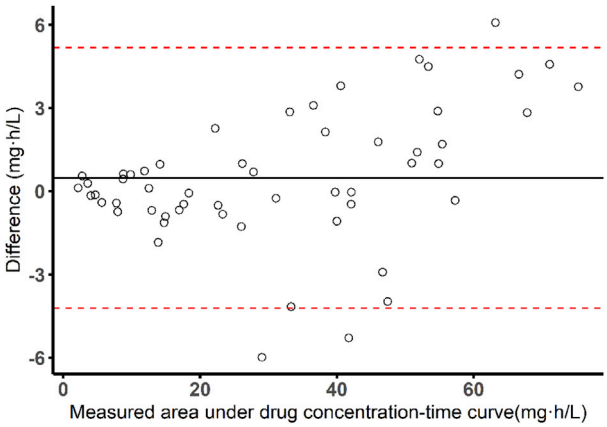

FIGURE 1
Bland-Altman plot of measured AUC *versus* predicted AUC values by Bayesian approach and limited sampling strategy (sampling time: 0, 2, 4, 6 h).

samples were centrifuged at 3,000 rpm for 10 min within 1 h, and the upper plasma was loaded into cryovials and stored at −80°C. Concentrations of bedaquiline were determined using high-performance liquid chromatography (HPLC) with a calibration curve ranging from 0.2 to 20 mg/L. The calibration curve was linear (r^2 = 0.9954) and accuracy and precision were between 91.3%–95.2%. The 5 samples of the development cohort were below the lower limit of quantification (10 ng/mL) and their assay results were ruled out from the analysis as a common way (Beal, 2001).

Sputum samples were collected at each visit and were sent to the prefectural TB reference laboratory for analysis. The bacterial cultures and MIC determination at baseline were performed using the Middlebrook 7H11 agar dilution method at bedaquiline concentration of 0.008–0.05 mg/L using serial two-fold dilution as previously described (Lounis et al., 2016). The Middlebrook 7H11 agar media (Becton Dickinson, Franklin Lakes, NJ, United States) were prepared according to CLSI document M07-A9 (Clinical and Laboratory Institute Standards, 2012). Quality control was performed under conditions equivalent to those of the experiment using *Mtb* strain H37Rv (ATCC 27294).

This study was carried out in accordance with the recommendations of the Declaration of Helsinki (2000). The protocol was approved by the ethics committee of the School of Public Health, Fudan University (IRB#2015-08-0565). Written informed consent was obtained from all participants.

2.2 Population pharmacokinetic modeling

Based on the development cohort, a population PK model was established using the non-linear mixed-effect method in Phoenix NLME (version 8.0; Certara Inc, Princeton, NJ, United States). Since bedaquiline has a unique dual zero-order input, we fixed the absorption rate as 1,000 h^{-1} based on a published population PK model (McLeay et al., 2014), resulting in the dose *via* the input compartment describing an initial zero-order (rather than first-order) input. The duration of infusion into the depot compartment (2.22 h), the duration of infusion into V_c/F (1.48 h) and the fraction of dose into the depot compartment (58.5%) were also fixed from this reference for a better fit.

Inter-subject variability was estimated by exponential model for PK parameters as follows (Eq. 1):

$$\theta_i = \theta_{TV} \times \exp\ (\eta_i)$$

where θ_i is the parameter estimation for the *i*th individual, θ_{TV} is the typical value of the parameter estimation in the population, and η_i is the deviation from the population mean for the *i*th individual under the assumption that η_i are normally distributed with mean 0 and variance ω^2. Furthermore, additive, proportional and combined-error models were explored to estimate the residual error variability.

The structural models were formulated through the objective function value (OFV), Akaike information criterion (AIC), and model goodness-of-fit plot. The models with the lowest values of OFV and AIC were regarded as superior. In the process of model development, weight, age, sex, height, and albumin were included as potential covariates to explain inter-individual pharmacokinetic variations.

The effects of continuous covariates such as weight, age, height and albumin were modeled using a power function after normalization by the population median (Eq. 2):

$$\theta_i = \theta_{TV} \times \left(\frac{cov_i}{cov_{median}}\right)^{\theta_{cov}}$$

Where cov_i is the covariate value for the *i*th individual, cov_{median} is the median value of the covariate. and θ_{cov} is the estimated parameter describing the fixed effect of covariates on the PK parameters.

For categorical covariates, such as sex, the effect was modeled as follow (Eq. 3):

$$\theta_i = \theta_{TV} \times (1 + cov_i \times \theta_{cov})$$

Where cov_i is a dummy variable that took on a value of 1 or 0.

The covariates selection was performed using stepwise regression with forward inclusion (△OFV>3.84, $p < 0.05$) and backward elimination (△OFV>6.64, $p < 0.01$). The covariates were selected or excluded depending on the value changes of OFV. The final model performance was authenticated by a visual predictive check (VPC). In the validation cohort, the pharmacokinetic parameters were calculated by Bayesian approach on the population PK model above.

2.3 Clinical-significant thresholds identification

The developed population PK model was applied for the validation cohort to calculate the pharmacokinetic parameters (C_{max}, C_{min}, $AUC_{0\text{-}24h}$) on week 4 of treatment. Combined with the baseline 7H11 MICs of the clinical *Mtb* isolates, the ratios of bedaquiline drug exposure/susceptibility (C_{max}/MIC, C_{min}/MIC, $AUC_{0\text{-}24h}$/MIC) were obtained. After that, the thresholds were identified by relating the drug exposure and ratio of drug exposure/susceptibility (C_{max}, C_{min}, $AUC_{0\text{-}24h}$, C_{max}/MIC, C_{min}/MIC, $AUC_{0\text{-}24h}$/MIC) to the 2-month sputum culture conversion as a marker of early treatment response, the 6-month culture conversion previously reported to be predictive of treatment outcome, and the successful treatment outcome, using the classification and regression tree (CART) analysis. The "rpart" package in R (version 4.1.2, R Foundation, Vienna, Austria) was used to generate the CART models with the default values specified in "rpart" (Atkinson and Therneau, 2000).

2.4 Dosage evaluation by probability of target attainment analysis

Based on CART-derived thresholds, the probability of target attainment was analyzed to evaluate the WHO recommended regimen (400 mg once daily for 14 days followed by 200 mg thrice weekly) (World Health Organization, 2020) as well as two suggested regimens (200 mg once daily, and 200 mg once daily for 56 days followed by 100 mg once daily) (Salinger et al., 2019) within a distribution of 7H11 MICs of 0.015, 0.03, 0.06, 0.125, 0.25, 0.5, 1 mg/L. Currently, 0.25 mg/L is suggested as a provisionary breakpoint for 7H11 by EUCAST (European Committee for Antimicrobial Susceptibility Testing, 2017). For each regimen, 1,000 patients were simulated based on the characteristics of the studied population. For the WHO recommended regimen and 200 mg once daily, we calculated the $AUC_{0\text{-}24h}$ on week 4 of treatment, while the $AUC_{0\text{-}24h}$ of 200 mg once daily for 56 days followed by 100 mg once daily was calculated on week 10 of treatment.

2.5 Statistical analysis

For demographic data, continuous variables were expressed as the interquartile range (IQR). The differences were compared using a t-test for normally distributed variables and the Mann-Whitney U test for non-normally distributed. Dichotomous variables were expressed as numbers and frequency (%). The differences were compared using the chi-square test. For drug exposure and susceptibility, pharmacokinetic parameters were expressed as median with interquartile range, MIC values were expressed as mode and range, and the Mann-Whitney U test was applied for comparison.

For validation of thresholds and clinical outcomes, a modified Poisson regression with robust standard errors was used to estimate the association between the CART-derived thresholds and the sputum conversion after 2 and 6 months' treatment and successful treatment outcome. The time to sputum culture conversion was illustrated between patients above the CART-derived thresholds and those below using Kaplan–Meier curves and compared using the log rank test. The start point was the treatment initiation. The endpoint was defined as the beginning of consecutive two or more sputum culture conversions in the BACTEC MGIT960 system. The observation time was defined as the duration through start point until the endpoint. Censoring for study participants occurred when there was no sputum conversion observed throughout the whole MDR-TB treatment, death, or loss to follow-up. A Cox proportional hazards model was used to estimate the hazard ratio (HR). The association between thresholds and treatment outcome was adjusted by age, sex, place of residency, weight, adherence, and baseline time to liquid culture positivity as the possible confounders.

Data analyses and plotting were performed using R (version 4.1.2, R Foundation, Vienna, Austria). Levels of significance were set at 5% ($\alpha = 0.05$), and a 95% confidence interval (CI) was calculated.

3 Results

3.1 Demographics and clinical characteristics

Of the 55 study participants in the development cohort, 39 (70.9%) were male, and the median (IQR) age was 44 (34–53) years, while among the 159 patients in the validation cohort, 107 (67.3%) were male, and the median (IQR) age was 44 (29–54) years. The demographic and clinical characteristics of subjects were comparable between the two cohorts, except for weight and BMI (Table 1). The bedaquiline mode MIC (range) of the validation cohort, was 0.06 mg/L (0.008–0.25 mg/L). The majority of the MIC distribution was below 0.125 mg/L (93.7%; Figure 2). The bedaquiline MIC QC range for H37Rv was 0.015–0.06 mg/L, which was within QC range in the WHO report (World Health Organization, 2018).

3.2 Population pharmacokinetic model

In the development cohort, five samples were below the lower limit of quantification (10 ng/mL) and ruled out of the analysis. Of the remained 1,205 bedaquiline concentrations from 55 subjects in the range of 0.04–5.96 mg/L were obtained for population PK modeling. Preliminary analysis of the base model showed the OFVs of the three- and four-compartment model with dual

TABLE 1 Baseline demographic and clinical characteristics of subjects.

Baseline characteristics	Development cohort (n = 55)	Validation cohort (n = 159)
Demographic data		
Age, years (median, IQR)	44 (34,53)	44 (29,54)
Sex (female) (n, %)	16 (29.1)	52 (32.7)
Weight, kg (median, IQR)	67 (59,74)	65 (59,71)
Height, cm (median, IQR)	165 (158,173)	166 (161,172)
BMI, kg/m2 (median, IQR)	23.8 (20.6,26.0)	24.6 (22.0,28.7)
Clinical data		
Albumin, g/L (median, IQR)	37.1 (32.0,40.6)	37.2 (32.4,41.6)
Diabetes Mellitus Type 2 (n, %)	9 (16.4)	27 (17.0)
Smoking (n, %)	6 (10.9)	31 (19.5)
Alcohol consumption (n, %)	5 (9.1)	28 (17.6)
Clinical severity (n, %)	11 (20.0)	41 (25.8)
Chest X-ray severity (n, %)	9 (16.4)	26 (16.4)
Pulmonary cavity (n, %)	9 (16.4)	33 (20.8)
TTP, h (median, IQR)	12 (11,14)	13 (11,14)
Pre -XDR[a] (n, %)	9 (16.4)	13 (8.2)

BMI, body mass index; TTP, time to liquid culture positivity; Pre-XDR, pre-extensive drug resistance.
[a]Pre-XDR-TB, TB, caused by *Mycobacterium tuberculosis* strains that fulfill the definition of multidrug-resistant and rifampicin-resistant TB, with additional resistance to any fluoroquinolone.

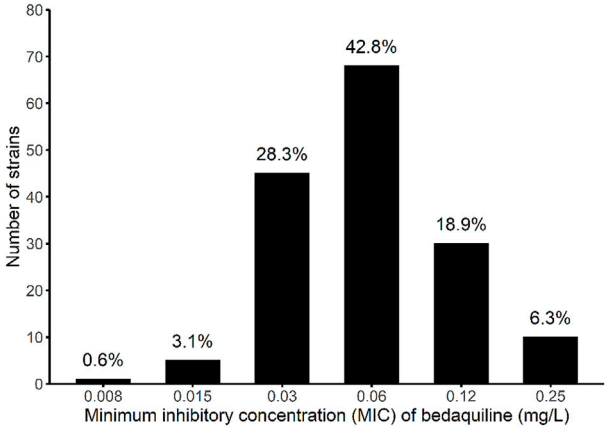

FIGURE 2
Mycobacterium tuberculosis minimum inhibitory concentration distribution of bedaquiline among the participants in the validation cohort.

zero-order input (to capture dual peaks observed during absorption) were 763.6 and 758.0, respectively. Based on OFV, AIC, and diagnostic plots, the plasma concentrations of the development cohort were best described by a three-compartment model with dual zero-order input. A proportional error model was used to evaluate the residual variability. The pharmacokinetic parameters derived from the model included apparent clearance (CL/F) = 3.57 L/h and apparent distribution volume (V_c/F) = 336.97 L (Table 2). Body weight and albumin were included in the final model. The body weight affected the clearance (CL) and the central volume of distribution (Vc), and the covariate effects of body weight on the central volume of distribution and clearance were fixed to 1 and 0.75, respectively, according to the principles of allometric scaling (Anderson and Holford, 2009). The albumin affected the clearance (estimate (CV%) = 3.76 (14.2)) (Table 2) (△OFV = −33.1, $p < 0.01$). Age, sex, and height had no significant effect on population PK parameters. The final model with the two covariates was as follows (Eq. 4, 5):

$$V_c/F\ (L) = 336.97 \times \left(\frac{Weight}{67}\right)^{1} \times \exp\ (\eta_V)$$

$$CL/F\ (L/h) = 3.57 \times \left(\frac{Weight}{67}\right)^{0.75} \times \left(\frac{Albumin}{37.1}\right)^{3.76} \times \exp\ (\eta_{CL})$$

Where 336.97 L and 3.57 L/h were the typical value of V_c/F and CL/F. The median weight was 67 kg. The median albumin was 37.1 g/L, and 3.76 indicates the relationship between CL/F and albumin.

The VPC showed most of the observed values were distributed within the 95% CIs of predicted corresponding quantiles, which indicated the prediction of simulated data matched the observed values (Figure 3).

3.3 Thresholds identification

The validation cohort included 159 MDR-TB cases with 636 person-time concentration observations in the range of 0.16–5.28 mg/L. All of them completed 24 months' MDR-TB treatment without death or loss of follow-up. During the treatment, 13 patients experienced bedaquiline discontinuation or dose reduction due to moderate and serious QT prolongation. As a result, 11 of 13 recovered and 10 resumed the standard dose. With the bedaquiline-containing regimen, 111 (69.8%) achieved sputum culture conversion after 2 months′ treatment, and 123 (77.4%) after 6-month treatment. During the treatment follow-up period, a total of 149 (93.7%) patients had sputum culture conversion with a median time (IQR) to conversion of 2 (1, 4) months. Among the

TABLE 2 Pharmacokinetics parameter estimations of the development cohort.

Parameter	Estimate (RSE%)	95% CI
Typical value parameter of population		
CL/F (L/h)	3.57 (11.9)	2.73–4.40
V_c/F (L)	336.97 (12.6)	253.86–420.08
V_{p1}/F (L)	2839.13 (46.3)	258.19–5420.06
CL_{p1}/F (L/h)	2.97 (41.40)	0.56–5.39
V_{p2}/F (L)	1391.89 (37.41)	370.16–2413.63
CL_{p2}/F (L/h)	9.81 (18.86)	6.18–13.44
FR1 (%)	58.5	—
DUR1 (h)	2.22	—
DUR2 (h)	1.48	—
T_{lag} (h)	1.00 (9.1)	0.82–1.18
$T_{lag,\ add}$ (h)	2.76 (21.0)	1.62–3.90
Covariable effect		
Weight effect on CL	0.75	—
Weight effect on V_c	1	—
Albumin effect on CL	3.76 (14.2)	2.71–4.80
BSV		
ω^2V	0.38 (67.99)	—
ω^2CL	1.33 (166.76)	—
Residual variability		
σ^2_{add}	0.23 (2.75)	0.22–0.24

Abbreviations: RSE%, relative standard error; CI, confidence interval; F, apparent bioavailability; BSV, between subject variability; CL/F, apparent clearance; V_c/F, apparent vol of distribution; V_{p1}/F, apparent vol of distribution for the first peripheral compartment; CL_{p1}/F, Apparent clearance between V_c/F and V_{p1}/F; V_{p2}/F, apparent vol of distribution for the second peripheral compartment; CL_{p2}/F, Apparent clearance between V_c/F and V_{p2}/F; FR1, fraction of dose into the depot compartment; DUR1, duration of infusion into the depot compartment; $T_{lag,\ add}$, Additional lag time prior to administration of the remaining dose into Vc/F; DUR2, Duration of infusion into Vc/F; t_{lag}, Lag time prior to absorption; The reference weight was 59 kg.

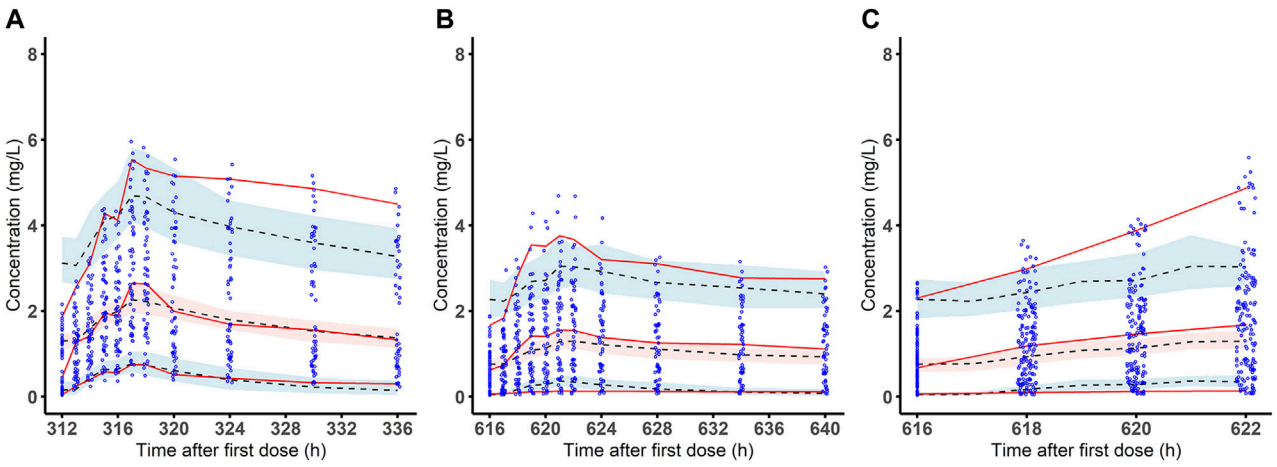

FIGURE 3
Visual predictive check of the final population pharmacokinetic model for bedaquiline. Observed bedaquiline concentration-time data and the visual predictive check (VPC) of the final model on week 2 **(A)** and week 4 **(B)** of treatment in the development cohort and on week 4 **(C)** of treatment in the validation cohort. The blue dots are the observed concentrations. The red solid lines are the 50th, 95th and fifth percentiles of the observed data. The dashed line in the middle and the dashed lines on the upper and lower sides are the 50th, 95th and fifth percentiles of the simulated concentrations, red and blue shaded areas are their model-predicted 95% CIs.

13 discontinued patients, 3 (23.0%) achieved sputum culture conversion after 2 months' and 6 months' treatment, and 8 (61.5%) at the end of treatment.

In the validation cohort, the median (IQR) $AUC_{0\text{-}24h}$ was 31.7 (13.9,48.5) mg·h/L, and the median (IQR) $AUC_{0\text{-}24h}$/MIC was 557.8 (148.5,1059.9). A higher drug exposure on week 4 (C_{max}, C_{min}, $AUC_{0\text{-}24h}$),

10.3389/fphar.2023.1022090

TABLE 3 Distribution of drug exposure and susceptibility among the participants with different treatment outcome in the validation cohort.

	2-month sputum culture			6-month sputum culture			24-month sputum culture		
	Positive(n = 48)	Negative(*n* = 111)	*P*	Positive (n = 36)	Negative (n = 123)	*P*	Positive (*n* = 10)	Negative (n = 149)	*P*
7H11 MIC, mg/L	0.12 (0.03,0.12)	0.06 (0.008,0.06)	<0.001	0.12 (0.03,0.25)	0.06 (0.008,0.06)	<0.001	0.12 (0.12,0.25)	0.06 (0.008,0.06)	<0.001
C_{max}, mg/L	0.7 (0.26,0.87)	2.0 (1.48,2.60)	<0.001	0.5 (0.23,0.68)	2.0 (1.21,2.55)	<0.001	0.1 (0.12,0.48)	1.8 (0.83,2.46)	<0.001
C_{min}, mg/L	0.3 (0.10,0.48)	1.3 (0.84,1.74)	<0.001	0.2 (0.08,0.32)	1.2 (0.61,1.72)	<0.001	0.04 (0.04,0.14)	1.1 (0.41,1.58)	<0.001
$AUC_{0\text{-}24h}$, mg.h/L	11.4 (4.77,16.55)	41.5 (28.64,52.25)	<0.001	8.3 (4.20,12.76)	38.4 (22.52,50.49)	<0.001	2.4 (2.16,7.88)	34.0 (15.89,49.28)	<0.001
C_{max}/MIC	6.2 (4.69,7.88)	41.1 (27.67,67.33)	<0.001	5.9 (4.07,7.03)	40.1 (20.47,66.82)	<0.001	1.1 (0.64,2.76)	32.7 (8.87,62.63)	<0.001
C_{min}/MIC	2.6 (1.80,3.41)	27.9 (15.19,40.79)	<0.001	2.2 (1.45,3.14)	25.6 (12.10,40.23)	<0.001	0.3 (0.19,0.85)	18.1 (4.43,36.39)	<0.001
$AUC_{0\text{-}24h}$/MIC	112.3 (80.72,141.52)	840.5 (527.64,1262.93)	<0.001	103.7 (74.38,137.33)	795.9 (409.49,1235.98)	<0.001	19.6 (11.32,46.46)	613.0 (160.42,1145.16)	<0.001

MIC: minimum inhibitory concentration; C_{max}: maximum drug concentration; C_{min}: minimum drug concentration; $AUC_{0\text{-}24h}$: area under drug concentration-time curve. Pharmacokinetic parameters were expressed as median with interquartile range, MIC, values were expressed as mode and range, and the Mann-Whitney U test was applied for comparison.

especially for $AUC_{0\text{-}24h}$, was observed among the patients with sputum conversion compared to those without, respectively, after 2 months' (median $AUC_{0\text{-}24h}$: 41.5 vs 11.4 mg·h/L), 6 months' treatment (median $AUC_{0\text{-}24h}$: 38.4 vs 8.3 mg·h/L), as well as with successful treatment outcome (median $AUC_{0\text{-}24h}$: 34.0 vs 2.4 mg·h/L). The Middlebrook 7H11 MIC levels were also associated with sputum conversion at the observation time points. The difference was observed to be even more pronounced for $AUC_{0\text{-}24h}$/MIC among patients with sputum conversion compared to those without after 2 months' (median $AUC_{0\text{-}24h}$/MIC: 840.5 vs 112.3) and 6 months' treatment (median $AUC_{0\text{-}24h}$/MIC:795.9 vs 103.7), as well as for successful treatment outcome (median $AUC_{0\text{-}24h}$/MIC:613.0 vs 19.6) (Table 3; Figure 4).

Regarding thresholds predictive of treatment outcome, the $AUC_{0\text{-}24h}$/MIC of 175.5 was derived as the primary node to differentiate sputum culture conversion after 2 months' treatment, with 118.2 for culture conversion after 6 months' treatment and 74.6 for successful treatment outcome (Figure 5). Furthermore, the study participants with $AUC_{0\text{-}24h}$/MIC above 175.5 had a higher probability of culture conversion after 2 months' treatment compared with those below (adjusted relative risk, aRR:16.4; 95% CI: 5.3–50.4). Similarly, those with $AUC_{0\text{-}24h}$/MIC above 118.2 had a higher probability of culture conversion after 6 months of treatment (aRR:20.1; 95%CI: 2.9–139.4), and those with $AUC_{0\text{-}24h}$/MIC above 74.6 had a higher probability of successful treatment outcome (aRR: 9.7; 95%CI: 1.5–64.8). This pattern was also seen for the association between the CART-derived thresholds and time to sputum conversion (Figure 6; Table 4).

3.4 Exploratory analysis of current dosages in relation to Middlebrook 7H11 bedaquiline MICs

Regarding the threshold related to sputum culture conversion after 2 months' and 6 months' treatment and successful treatment outcome, simulations showed that all regimens achieved a PTA of above 90% at MICs ≤0.06 mg/L. At an MIC of 0.125 mg/L, the WHO recommended dosage achieved 70.7% (2 months), 90.6% (6 months) and 98.9% (24 months) attainment based on the CART-thresholds related to different treatment outcomes, while 200 mg once daily was simulated to achieve 79.3% (2 months), 94.8% (6 months) and 99.6% (24 months) attainment. None of the studied regimens reached above 90% at MICs of 0.25 mg/L, 0.5 mg/L and 1 mg/L (Figure 7).

4 Discussion

In this study, we developed a bedaquiline population PK model in patients with MDR-TB and identified the thresholds related to the sputum conversion after 2 months' ($AUC_{0\text{-}24h}$/MIC = 175.5), 6 months' treatment ($AUC_{0\text{-}24h}$/MIC = 118.2) as well as successful treatment outcome ($AUC_{0\text{-}24h}$/MIC = 74.6). Furthermore, these targets were obtained for the majority of the clinical isolates in our study.

Our results showed that the model to best describe the pharmacokinetic data was a three-compartment model with dual zero-order input, which is in agreement with a previously published study (McLeay et al., 2014), indicating that bedaquiline is extensively distributed in tissues and organs. The estimated mean CL value in our

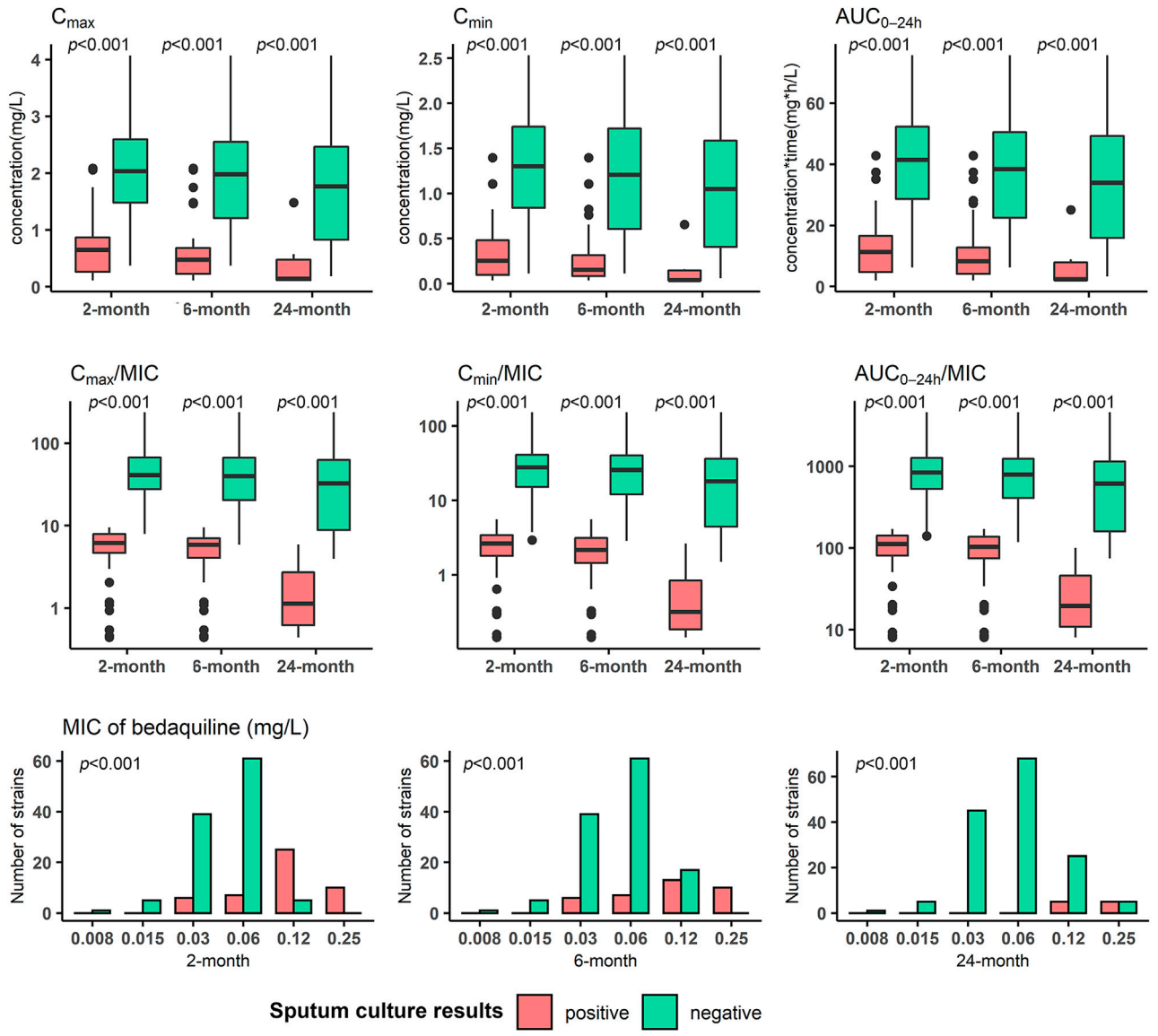

FIGURE 4
Distribution of bedaquiline exposure and susceptibility of *Mycobacterium tuberculosis* isolates respectively in participants with different treatment outcomes in the validation cohort. MIC: minimum inhibitory concentration; C_{max}: maximum drug concentration; C_{min}: minimum drug concentration; $AUC_{0\text{-}24h}$: area under drug concentration-time curve over the last 24 h dosing interval. Mann-Whitney U test was applied for comparison.

study of 3.57 L/h, was similar to the CL value of 2.78 L/h, in the aforementioned study (McLeay et al., 2014), and the V_c/F of 336.97 L in the present study was comparably higher than published studies (McLeay et al., 2014; Svensson et al., 2016; Zhu et al., 2021). This may be due to the higher weight (median: 67 vs. 59 kg) of our subjects and using a standardized WHO regimen. In addition, the dual-zero input model was used to describe absorption, as the estimates of V_c/F can be highly influenced by absorption. The covariates of the final model included body weight (affecting the CL and V_c/F) and albumin (affecting the CL). The effect of albumin on PK disposition may be due to the high protein bounding of bedaquiline in plasma (Van Heeswijk et al., 2014).

We were able to validate the association between bedaquiline drug exposure/susceptibility and treatment outcome. The drug exposure on week 4 ($AUC_{0\text{-}24h}$) was generally higher in subjects with sputum conversion after 2 months' and 6 months' treatment as well as subjects with the successful treatment outcome. The results support that the bactericidal activity of bedaquiline is concentration-dependent, as indicated by studies in a murine model of TB infection (Rouan et al., 2012). This may suggest that drug susceptibility is also a major factor influencing the treatment outcome, as previously reported (Liu et al., 2021). Furthermore, we found the ratio of drug exposure/susceptibility was most significantly associated with sputum culture conversion (Table 4). This confirms that the $AUC_{0\text{-}24h}$/MIC is the main driver of the bactericidal effect (Van Heeswijk et al., 2014), also in well agreement with dose-fractionation experiments (Rouan et al., 2012). Additionally, by relating to the treatment outcome, $AUC_{0\text{-}24h}$/MIC (175.5, 118.2, 74.6) was selected as the primary node to best differentiate the sputum culture conversion after 2 months' and 6 months' treatment as well as the successful treatment outcome. The dose simulation study

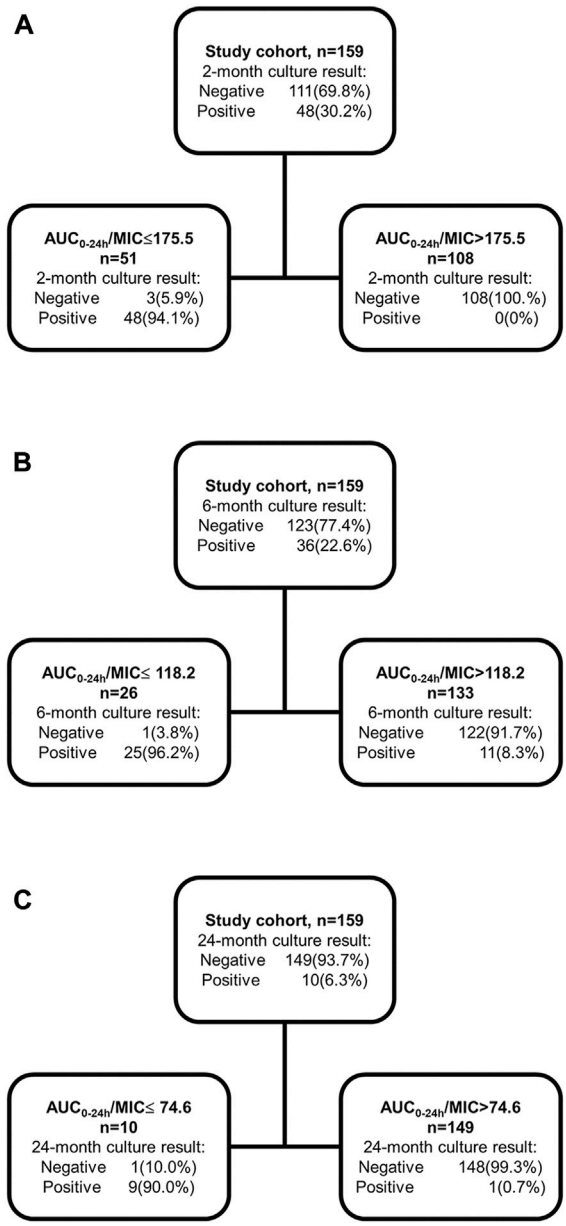

FIGURE 5
Classification and Regression Tree analysis for the thresholds to differentiate the 2-month, 6-month sputum conversion and successful treatment outcome in the validation cohort. Classification and Regression Tree analysis was applied to identify the thresholds predictive of 2-month **(A)**, 6-month **(B)** sputum conversion and successful treatment outcome **(C)**. $AUC_{0\text{-}24h}$: area under drug concentration-time curve over the last 24-h dosing interval; MIC: minimum inhibitory concentration.

of Salinger et al. indicates that the drug exposure remains stable through 4 weeks treatment until the end of treatment (Salinger et al., 2019). The pharmacokinetic data on week 4 is capable enough of estimating the drug exposure during the treatment with bedaquiline and thus the derived thresholds can be used as markers to predicate the short-term and long-term treatments (Kang and Lee, 2009).

In the present study, the current WHO dosage was observed to be effective for most study participants. Based on the identified thresholds predictive of 6 months' sputum culture conversion and the successful treatment outcome, the WHO recommended regimen was able to achieve more than 90% target attainment at MICs ≤0.125 mg/L determined on Middlebrook 7H11 agar media. The vast majority of the *Mtb* isolates included in our study had MICs ≤0.125 mg/L (93.7%), which was similar to previous studies (Kaniga et al., 2016; Peretokina et al., 2020; Kaniga et al., 2022). However, similar to these studies, our MIC distribution was wide indicating poor reproducibility of individual MICs which was also observed in a systematic review by the WHO (World Health Organization, 2018). Additionally, it has been pointed out that it is very difficult if possible to separate technically from biological variability within the wild-type MIC distribution of any drug (Kahlmeter and Turnidge, 2022). Taking these caveats into account, our exploratory analysis showed that an MIC level close to the suggested breakpoint for Middlebrook 7H11 (≥0.25 mg/L), the recommended dosage may need further consideration. As 200 mg once daily has never been tested for longer than 8 weeks and that extensive metabolite accumulation is expected, this is not a current option without further studies. A previous study revealed that 200 mg once daily leads to a higher drug exposure level on week 24 of treatment than the WHO recommended regimen, while the highest metabolite M2 on week 24 of treatment does not exceed 600 ng/mL (Salinger et al., 2019). An open-label 8-week clinical trial found that 200 mg once daily showed efficacy comparable to the recommended regimen in the treatment of drug-susceptible tuberculosis, and there was no significant difference in the incidence of adverse events between the 200 mg once daily (3 out of 60 subjects had a QTc interval increase ≥60 ms) and the WHO recommended dosage (Tweed et al., 2019). In addition, a PK modeling study revealed that higher doses (the M2 concentration ≤1600 ng/mL) are not expected to lead to a substantially higher risk of QT prolongation (Tanneau et al., 2021). These observations highlight that therapeutic drug monitoring for bedaquiline would be beneficial in cases with high levels of MICs; however, a standardized drug susceptibility testing is urgently needed first, since the MIC of bedaquiline varies amply within and between methodologies.

One of the strengths of our study was that the population PK model was built based on a large number of sample points in real patients treated for MDR-TB, and the visual predictive check indicated that the model could be used for simulation purposes. Our study validated the concentration dependence of bedaquiline (Rouan et al., 2012), and further proposed the PK/PD thresholds relating to treatment outcomes after different lengths of treatment. The CART-derived threshold of 175.5 related to sputum conversion after 2-month treatment may be used to reach treatment efficacy for the short-treatment regimen, while the ones of 118.2 and 74.6 related to sputum conversion after 6 months' treatment and successful treatment outcome respectively, may be used for dose adjustment for long-term treatment. In an exploratory analysis, we found that the current dosage was sufficient for most MDR-TB cases, and a dose increase might be required for *Mtb* isolates with resistance mechanisms to bedaquiline such as Rv0678 leading to MIC increases close to the epidemiological cut-off value (e.g., MIC ≥0.25 mg/L).

This study has several limitations. The model is limited by the lack of consideration of dynamic change during treatment in parameters such as albumin and weight, which have been observed to affect the population PK of bedaquiline (Svensson et al., 2016). Additionally, we did not include M2 in the analysis, since it was reported to be more likely to be the main driver for QT prolongation rather than the

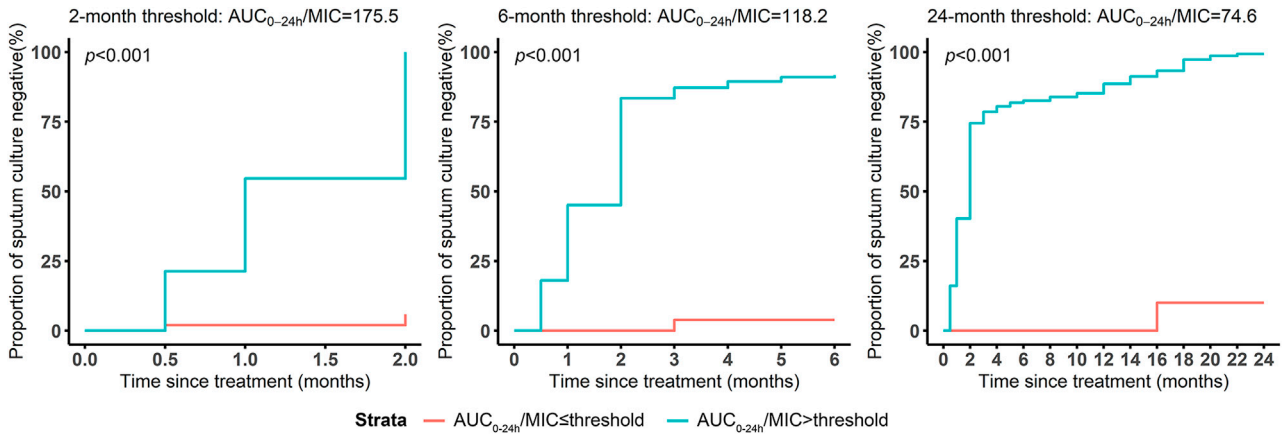

FIGURE 6
Survival analysis of months to sputum culture conversion grouped by the thresholds predictive of different treatment outcomes. The survival curves were illustrated to present the months to sputum conversion and compared using log rank test between the participants above and below the thresholds predictive of 2-/6- months sputum conversion and successful treatment outcome.

TABLE 4 Association between the thresholds and sputum culture conversion among the participants in the validation cohort.

	Robust Poisson regression model			Cox proportional hazards regression model		
	Sputum culture conversion (%)	RR (95%CI)	aRR (95% CI)[a]	Median time (month) to culture conversion (IQR)	HR (95%CI)	aHR (95% CI)[a]
2-month threshold						
AUC_{0-24h}/MIC≤175.5 (n = 51)	5.9	1	1	14 (5,19)	1	1
AUC_{0-24h}/MIC>175.5 (n = 108)	100.0	17 (5.7–51)	16.4 (5.3–50.4)	1 (1,2)	27.3 (8.7–86.3)	29.4 (9.1–95.1)
6-month threshold						
AUC_{0-24h}/MIC≤118.2 (n = 26)	3.8	1	1	18 (14,24)	1	1
AUC_{0-24h}/MIC>118.2 (n = 133)	91.7	23.8 (3.5–163.1)	20.1 (2.9–139.4)	2 (1,2)	47.9 (6.6–344.9)	42.5 (5.9–308.9)
24-month threshold						
AUC_{0-24h}/MIC≤74.6 (n = 10)	10	1	1	24 (24,24)	1	1
AUC_{0-24h}/MIC>74.6 (n = 149)	99.3	9.9 (1.5–63.8)	9.7 (1.5–64.8)	2 (1,3)	36.4 (5–265.8)	31.3 (4.2–232.8)

RR: relative risk; CI: confidence interval; IQR: interquartile range; HR: hazard ratio.
[a]Adjusted according to age, sex, place of residency, weight, adherence and baseline time to liquid culture positivity. Non-adherence was defined as discontinued for more than 3 days.

treatment efficacy (Janssen Pharmaceutical, 2012; Svensson et al., 2016). Due to the lack of sufficiently and clinically-validated targets for bedaquiline, the thresholds for efficacy were based on the principle that the recommended dosing regimen is appropriate from a safety and efficacy perspective. There is a need to further investigate the efficacy in the clinical trials to validate the targets. Additionally, as the study participants were included in the analysis if they were alive and had completed MDR-TB treatment throughout the whole course, this may restrict the representativeness of the study findings to some degree. Meanwhile, given the possible confounding from baseline disease status and adherence, the association between drug exposure and treatment outcome was adjusted for age, sex, area and adherence. Moreover, the PTA of studied regimens is calculated based on the threshold from drug exposure on week 2 or week 10 of treatment, which may not fully characterize the exposure throughout treatment. It also needs to be considered that the variability for MIC testing is substantial and affects target attainment. The results in this study are only valid for Middlebrook 7H11, which is not suitable for clinical routine due to a slow turn over time and complexity. Additionally, we did not account for the interaction from the concomitant use of other TB drugs, which may affect the pharmacokinetics of bedaquiline, like clofazimine (Hartkoorn et al., 2014; Hu et al., 2016; Xu et al., 2017; Liu et al., 2021).

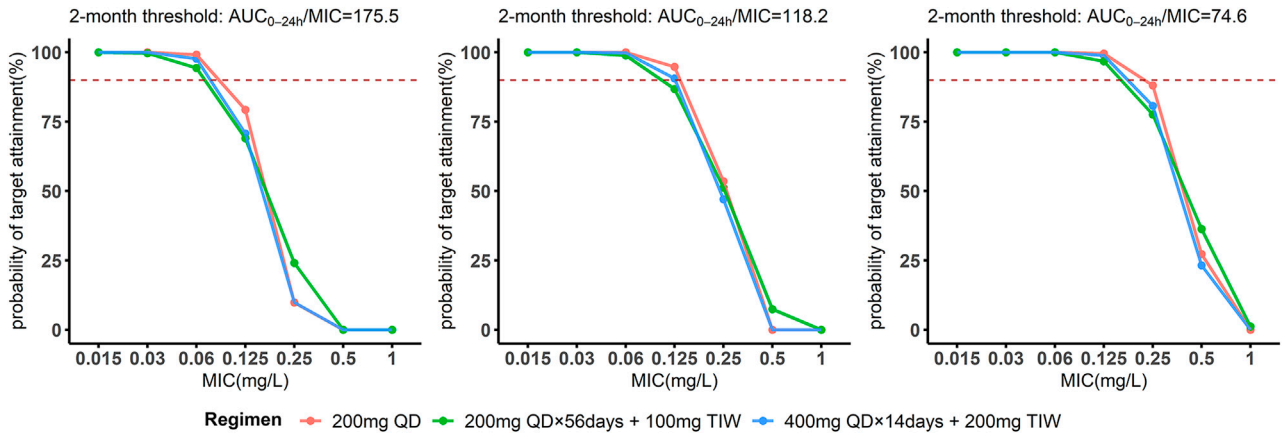

FIGURE 7
The probability of target attainment among the study participant from the validation cohort against varying 7H11 minimal inhibitory concentrations for bedaquiline. Probability of target attainment for bedaquiline taking the thresholds based on the 2-month, 6-month sputum conversion as well as successful treatment outcome as targets. The dashed lines indicate the 90% probability of target attainment.

5 Conclusion

We established a population PK model for bedaquiline in patients with MDR-TB in China. Based on the thresholds derived in a clinical study, the WHO recommended dose (400 mg once daily for 14 days followed by 200 mg thrice weekly) of bedaquiline is sufficient for the treatment of the majority of MDR-TB isolates.

Data availability statement

The original contributions presented in the study are included in the article, further inquiries can be directed to the corresponding author.

Ethics statement

The studies involving human participants were reviewed and approved by the ethics committee of the School of Public Health, Fudan University (IRB#2015-08-0565). The patients/participants provided their written informed consent to participate in this study.

Author contributions

YH and J-WA designed the study; YH and GS supervised patient recruitment and sample collection; GS and ZB did the laboratory work; GS and YH analysed and interpreted the results; GS, ZB and LD drafted the manuscript; YH, J-WA, JB, TS, KN, JW and JP revised the manuscript. The corresponding author had full access to all the data in the study and had final responsibility for the decision to submit the manuscript for publication.

Funding

This work was supported by the National Natural Science Foundation of China (YH, No.81874273), Science and Technology Project of Suzhou City Health Bureau (ZB, No. LCZX201918), Suzhou Key Medical Center (ZB), the Swedish Research Council (TS, LD, KN, 2019-05 912), the Swedish Heart and Lung Foundation (TS), the County of Stockholm (LD) as well as the Research Council of south-eastern Sweden (KN, FORSS-964535).

Conflict of interest

The authors declare that the research was conducted in the absence of any commercial or financial relationships that could be construed as a potential conflict of interest.

The reviewer EMS declared a past co-authorship with one of the authors JA to the handling Editor.

Publisher's note

Supplementary material

The Supplementary Material for this article can be found online at: https://www.frontiersin.org/articles/10.3389/fphar.2023.1022090/full#supplementary-material

References

Anderson, B. J., and Holford, N. H. (2009). Mechanistic basis of using body size and maturation to predict clearance in humans. *Drug Metab. Pharmacokinet.* 24, 25–36. doi:10.2133/dmpk.24.25

Atkinson, E. J., and Therneau, T. M. (2000). *An introduction to recursive partitioning using the RPART routines*. Rochester: Mayo Foundation.

Beal, S. L. (2001). Ways to fit a PK model with some data below the quantification limit. *J. Pharmacokinet. Pharmacodyn.* 28, 481–504. doi:10.1023/a:1012299115260

CLINICAL AND LABORATORY INSTITUTE STANDARDS (2012). *Methods for dilution antimicrobial susceptibility tests for bacteria that grow aerobically; approved standard*. Wayne, PA: Clinical and Laboratory Standards Institute.

Diacon, A. H., Dawson, R., Von Groote-Bidlingmaier, F., Symons, G., Venter, A., Donald, P. R., et al. (2012). 14-day bactericidal activity of PA-824, bedaquiline, pyrazinamide, and moxifloxacin combinations: A randomised trial. *Lancet* 380, 986–993. doi:10.1016/S0140-6736(12)61080-0

Diacon, A. H., Pym, A., Grobusch, M. P., De Los Rios, J. M., Gotuzzo, E., Vasilyeva, I., et al. (2014). Multidrug-resistant tuberculosis and culture conversion with bedaquiline. *New Engl. J. Med.* 371, 723–732. doi:10.1056/NEJMoa1313865

EUROPEAN COMMITTEE FOR ANTIMICROBIAL SUSCEPTIBILITY TESTING (2017). Breakpoint tables for interpretation of MICs and zone diameters. Version 7.1, valid from 2017-03-10. [Online]. Available: http://www.eucast.org/fileadmin/src/media/PDFs/EUCAST_files/Breakpoint_tables/v_7.1_Breakpoint_Tables.xls (Accessed 30 7, 2022).

Hartkoorn, R. C., Uplekar, S., and Cole, S. T. (2014). Cross-resistance between clofazimine and bedaquiline through upregulation of MmpL5 in Mycobacterium tuberculosis. *Antimicrob. agents Chemother.* 58, 2979–2981. doi:10.1128/AAC.00037-14

Healan, A. M., Griffiss, J. M., Proskin, H. M., O'Riordan, M. A., Gray, W. A., Salata, R. A., et al. (2017). Impact of rifabutin or rifampin on bedaquiline safety, tolerability, and pharmacokinetics assessed in a randomized clinical trial with healthy adult volunteers. *Antimicrob. Agents Chemother.* 62, 008555–e917. doi:10.1128/AAC.00855-17

Hu, M., Zheng, C., and Gao, F. (2016). Use of bedaquiline and delamanid in diabetes patients: Clinical and pharmacological considerations. *Drug Des. Dev. Ther.* 10, 3983–3994. doi:10.2147/DDDT.S121630

Janssen Pharmaceutical, C. (2012). *Briefing document, TMC207 (bedaquiline), treatment of patients with MDR-TB, NDA 204–384*. Titusville: Janssen Pharmaceutical Companies.

Kahlmeter, G., and Turnidge, J. (2022). How to: ECOFFs-the why, the how, and the don'ts of EUCAST epidemiological cutoff values. *Clin. Microbiol. Infect.* 28, 952–954. doi:10.1016/j.cmi.2022.02.024

Kang, J. S., and Lee, M. H. (2009). Overview of therapeutic drug monitoring. *Korean J. Intern Med.* 24, 1–10. doi:10.3904/kjim.2009.24.1.1

Kaniga, K., Cirillo, D. M., Hoffner, S., Ismail, N. A., Kaur, D., Lounis, N., et al. (2016). A multilaboratory, multicountry study to determine bedaquiline MIC quality control ranges for phenotypic drug susceptibility testing. *J. Clin. Microbiol.* 54, 2956–2962. doi:10.1128/JCM.01123-16

Kaniga, K., Hasan, R., Jou, R., Vasiliauskienė, E., Chuchottaworn, C., Ismail, N., et al. (2022). Bedaquiline drug resistance Emergence Assessment in multidrug-resistant tuberculosis (MDR-TB): A 5-Year prospective *in vitro* Surveillance study of bedaquiline and other second-line drug susceptibility testing in MDR-TB isolates. *J. Clin. Microbiol.* 60, e0291920. doi:10.1128/JCM.02919-20

Li, Y., Sun, F., and Zhang, W. (2019). Bedaquiline and delamanid in the treatment of multidrug-resistant tuberculosis: Promising but challenging. *Drug Dev. Res.* 80, 98–105. doi:10.1002/ddr.21498

Liu, Y., Gao, M., Du, J., Wang, L., Gao, J., Shu, W., et al. (2021). Reduced susceptibility of Mycobacterium tuberculosis to bedaquiline during antituberculosis treatment and its correlation with clinical outcomes in China. *Clin. Infect. Dis.* 73, e3391–e3397. doi:10.1093/cid/ciaa1002

Lounis, N., Veziris, N., Chauffour, A., Truffot-Pernot, C., Andries, K., and Jarlier, V. (2006). Combinations of R207910 with drugs used to treat multidrug-resistant tuberculosis have the potential to shorten treatment duration. *Antimicrob. agents Chemother.* 50, 3543–3547. doi:10.1128/AAC.00766-06

Lounis, N., Vranckx, L., Gevers, T., Kaniga, K., and Andries, K. (2016). *In vitro* culture conditions affecting minimal inhibitory concentration of bedaquiline against M. tuberculosis. *Med. Maladies Infect.* 46, 220–225. doi:10.1016/j.medmal.2016.04.007

Mcleay, S. C., Vis, P., Van Heeswijk, R. P., and Green, B. (2014). Population pharmacokinetics of bedaquiline (TMC207), a novel antituberculosis drug. *Antimicrob. agents Chemother.* 58, 5315–5324. doi:10.1128/AAC.01418-13

Olaru, I. D., Lange, C., and Heyckendorf, J. (2016). Personalized medicine for patients with MDR-TB. *J. Antimicrob. Chemother.* 71, 852–855. doi:10.1093/jac/dkv354

Olayanju, O., Limberis, J., Esmail, A., Oelofse, S., Gina, P., Pietersen, E., et al. (2018). Long-term bedaquiline-related treatment outcomes in patients with extensively drug-resistant tuberculosis from South Africa. *Eur. Respir. J.* 51, 1800544. doi:10.1183/13993003.00544-2018

Pasipanodya, J. G., Mcilleron, H., Burger, A., Wash, P. A., Smith, P., and Gumbo, T. (2013). Serum drug concentrations predictive of pulmonary tuberculosis outcomes. *J. Infect. Dis.* 208, 1464–1473. doi:10.1093/infdis/jit352

Peretokina, I. V., Krylova, L. Y., Antonova, O. V., Kholina, M. S., Kulagina, E. V., Nosova, E. Y., et al. (2020). Reduced susceptibility and resistance to bedaquiline in clinical M. tuberculosis isolates. *J. Infect.* 80, 527–535. doi:10.1016/j.jinf.2020.01.007

Rouan, M.-C., Lounis, N., Gevers, T., Dillen, L., Gilissen, R., Raoof, A., et al. (2012). Pharmacokinetics and pharmacodynamics of TMC207 and its N-desmethyl metabolite in a murine model of tuberculosis. *Antimicrob. agents Chemother.* 56, 1444–1451. doi:10.1128/AAC.00720-11

Salinger, D. H., Nedelman, J. R., Mendel, C., Spigelman, M., and Hermann, D. J. (2019). Daily dosing for bedaquiline in patients with tuberculosis. *Antimicrob. agents Chemother.* 63, 004633–e519. doi:10.1128/AAC.00463-19

Svensson, E. M., Dosne, A. G., and Karlsson, M. O. (2016). Population pharmacokinetics of bedaquiline and metabolite M2 in patients with drug-resistant tuberculosis: The effect of time-varying weight and albumin. *CPT: pharmacometrics Syst. Pharmacol.* 5, 682–691. doi:10.1002/psp4.12147

Svensson, E. M., and Karlsson, M. O. (2017). Modelling of mycobacterial load reveals bedaquiline's exposure–response relationship in patients with drug-resistant TB. *J. Antimicrob. Chemother.* 72, 3398–3405. doi:10.1093/jac/dkx317

Tanneau, L., Karlsson, M. O., and Svensson, E. M. (2020). Understanding the drug exposure–response relationship of bedaquiline to predict efficacy for novel dosing regimens in the treatment of multidrug-resistant tuberculosis. *Br. J. Clin. Pharmacol.* 86, 913–922. doi:10.1111/bcp.14199

Tanneau, L., Svensson, E. M., Rossenu, S., and Karlsson, M. O. (2021). Exposure-safety analysis of QTc interval and transaminase levels following bedaquiline administration in patients with drug-resistant tuberculosis. *CPT Pharmacometrics Syst. Pharmacol.* 10, 1538–1549. doi:10.1002/psp4.12722

Tweed, C. D., Dawson, R., Burger, D. A., Conradie, A., Crook, A. M., Mendel, C. M., et al. (2019). Bedaquiline, moxifloxacin, pretomanid, and pyrazinamide during the first 8 weeks of treatment of patients with drug-susceptible or drug-resistant pulmonary tuberculosis: A multicentre, open-label, partially randomised, phase 2b trial. *Lancet Respir. Med.* 7, 1048–1058. doi:10.1016/S2213-2600(19)30366-2

Van Heeswijk, R., Dannemann, B., and Hoetelmans, R. (2014). Bedaquiline: A review of human pharmacokinetics and drug–drug interactions. *J. Antimicrob. Chemother.* 69, 2310–2318. doi:10.1093/jac/dku171

WORLD HEALTH ORGANIZATION (2021). *Global tuberculosis report 2021*. Geneva: World Health Organization.

WORLD HEALTH ORGANIZATION (2018). *Technical manual for drug susceptibility testing of medicines used in the treatment of tuberculosis*. Geneva.

WORLD HEALTH ORGANIZATION (2019). *WHO consolidated guidelines on drug-resistant tuberculosis treatment*. Geneva: World Health Organization.

WORLD HEALTH ORGANIZATION (2020). *WHO operational handbook on tuberculosis: Module 4: Treatment Drug-resistant tuberculosis treatment*. Geneva: © World Health Organization.WHO Guidelines approved by the Guidelines review committee

Xu, J., Wang, B., Hu, M., Huo, F., Guo, S., Jing, W., et al. (2017). Primary clofazimine and bedaquiline resistance among isolates from patients with multidrug-resistant tuberculosis. *Antimicrob. agents Chemother.* 61, 002399–e317. doi:10.1128/AAC.00239-17

Zheng, X., Forsman, L. D., Bao, Z., Xie, Y., Ning, Z., SchöN, T., et al. (2021). Drug exposure and susceptibility of second-line drugs correlate with treatment response in patients with multidrug-resistant tuberculosis: A multi-centre prospective cohort study in China. *Eur. Respir. J.* 59, 2101925. doi:10.1183/13993003.01925-2021

Zhu, H., Xie, L., Liu, Z. Q., Wang, B., Gao, M. Q., and Lu, Y. (2021). Population pharmacokinetics of bedaquiline in patients with drug-resistant TB. *Int. J. Tuberc. Lung Dis.* 25, 1006–1012. doi:10.5588/ijtld.21.0158

frontiers | Frontiers in Pharmacology

TYPE Original Research
PUBLISHED 13 April 2023
DOI 10.3389/fphar.2023.1150243

OPEN ACCESS

EDITED BY
Sebastian G. Wicha,
University of Hamburg, Germany

REVIEWED BY
Mike Lyons,
Colorado State University, United States
Charles Peloquin,
University of Florida College of Pharmacy, United States

*CORRESPONDENCE
Ulrika S. H. Simonsson,
ulrika.simonsson@farmbio.uu.se

SPECIALTY SECTION
This article was submitted to Pharmacology of Infectious Diseases, a section of the journal Frontiers in Pharmacology

RECEIVED 23 January 2023
ACCEPTED 31 March 2023
PUBLISHED 13 April 2023

CITATION
Mockeliunas L, Faraj A, van Wijk RC, Upton CM, van den Hoogen G, Diacon AH and Simonsson USH (2023), Standards for model-based early bactericidal activity analysis and sample size determination in tuberculosis drug development.
Front. Pharmacol. 14:1150243.
doi: 10.3389/fphar.2023.1150243

Standards for model-based early bactericidal activity analysis and sample size determination in tuberculosis drug development

Laurynas Mockeliunas[1], Alan Faraj[1], Rob C. van Wijk[1], Caryn M. Upton[2], Gerben van den Hoogen[2], Andreas H. Diacon[2] and Ulrika S. H. Simonsson[1]*

[1]Department of Pharmaceutical Biosciences, Uppsala University, Uppsala, Sweden, [2]TASK, Cape Town, South Africa

Background: A critical step in tuberculosis (TB) drug development is the Phase 2a early bactericidal activity (EBA) study which informs if a new drug or treatment has short-term activity in humans. The aim of this work was to present a standardized pharmacometric model-based early bactericidal activity analysis workflow and determine sample sizes needed to detect early bactericidal activity or a difference between treatment arms.

Methods: Seven different steps were identified and developed for a standardized pharmacometric model-based early bactericidal activity analysis approach. Non-linear mixed effects modeling was applied and different scenarios were explored for the sample size calculations. The sample sizes needed to detect early bactericidal activity given different TTP slopes and associated variability was assessed. In addition, the sample sizes needed to detect effect differences between two treatments given the impact of different TTP slopes, variability in TTP slope and effect differences were evaluated.

Results: The presented early bactericidal activity analysis approach incorporates estimate of early bactericidal activity with uncertainty through the model-based estimate of TTP slope, variability in TTP slope, impact of covariates and pharmacokinetics on drug efficacy. Further it allows for treatment comparison or dose optimization in Phase 2a. To detect early bactericidal activity with 80% power and at a 5% significance level, 13 and 8 participants/arm were required for a treatment with a TTP-$EBA_{0\text{-}14}$ as low as 11 h when accounting for variability in pharmacokinetics and when variability in TTP slope was 104% [coefficient of variation (CV)] and 22%, respectively. Higher sample sizes are required for smaller early bactericidal activity and when pharmacokinetics is not accounted for. Based on sample size determinations to detect a difference between two groups, TTP slope, variability in TTP slope and effect difference between two treatment arms needs to be considered.

Conclusion: In conclusion, a robust standardized pharmacometric model-based EBA analysis approach was established in close collaboration between microbiologists, clinicians and pharmacometricians. The work illustrates the importance of accounting for covariates and drug exposure in EBA analysis in order to increase the power of detecting early bactericidal activity for a single treatment arm as well as differences in EBA between treatments arms in Phase 2a trials of TB drug development.

KEYWORDS

tuberculosis, early bactericidal activity, sample size, pharmacometrics, model-based analysis

1 Introduction

Mycobacterium tuberculosis (Mtb) is the pathogenic bacteria that causes tuberculosis (TB), one of the leading causes of death from an infectious disease (World Health Organization, 2021). While progress in TB treatment shortening has accelerated in recent years, with the success of the Nix-TB trial showing that 6-month treatment is possible for drug-resistant TB (Conradie et al., 2020) and drug-susceptible TB treatment can be shortened to 4-month with rifapentine-moxifloxacin regimen (Dorman et al., 2021), TB remains a global problem. Many novel drugs are in the TB drug development pipeline, promising a potential trove of new medications in the future (Working Group on New TB Drugs, 2022).

One of the critical steps in TB drug development is a Phase 2a early bactericidal activity (EBA) study. An EBA study is an established method to provide clinical proof of concept for antimicrobial drugs under investigation (Jindani et al., 1980; Donald and Diacon, 2008; Food and Drug Administration, 2013; European Medicines Agency, 2017). EBA studies investigate if a drug is active in patients and represents a major milestone that unlocks further investment for clinical development. Most of the drugs active against Mtb show activity in EBA trials with very few exceptions, e.g., clofazimine which has shown no EBA *in vitro*, *in vivo* and patients but is believed to have an activity against persisting bacteria (Ammerman et al., 2017; Faraj et al., 2020). In addition to proof of concept, the EBA trials provide the opportunity to study safety, tolerability and pharmacokinetics (PK) in patients. Depending on the EBA trial design, the relationship between activity and dose can be studied as well as the activity of different treatments can be compared which can guide further clinical development. Usually, EBA studies are conducted in a carefully controlled setting with a small number of patients per group (12–15 participants) for up to 14 days, and include sputum sample collection, PK sampling, and intensive safety assessments.

EBA is quantified by measurement of the viable mycobacterial load in overnight-collected sputum samples over time using colony forming units (CFU) of Mtb (measured in log10 CFU/mL sputum) and/or time-to-positivity (TTP) in liquid culture (measured in hours). The correlation between changes in TTP and CFU varies over time, which is due to that they likely reflect slightly different processes (Diacon et al., 2012; Bowness et al., 2015; Ayoun Alsoud et al., 2022). CFU measures the quantity of viable mycobacteria regardless of the speed of growth, while TTP measures the consumption of critical ingredients in a closed liquid culture system, which is influenced by both the quantity and metabolic activity of the growing mycobacteria (Alffenaar et al., 2022). These assays are inherently variable and should be performed with at least two replicates, where overnight-collected sputum samples from each day are subsequently divided to multiple replicates. In addition to established culture-based biomarkers like CFU and TTP, new biomarkers are currently being developed, which could complement or replace existing ones in the future. With all of the promising progress in the TB drug pipeline, it is critical to have a robust and standardized approach to analyzing EBA trial data.

Approaches present for EBA analysis can be categorized into i) traditional non-model-based EBA analysis, ii) traditional model-based EBA analysis, and iii) pharmacometric model-based EBA analysis. The first paper presenting an EBA trial and analysis was a traditional non-model-based analysis presenting the results of a 14-day duration trial (Jindani et al., 1980). The differences in CFU, expressed as $\log_{10}$ CFU between day 0 and day 2, day 2 and day 14, as well as day 0 and day 14, were derived on the individual level. To compare different treatments, the mean fall in CFU was calculated using ANOVA. Since then, the traditional non-model-based EBA analysis approach was extended to analyze both CFU and TTP biomarkers (Eq. 1), where EBA ($EBA_{t_1-t_2}$) is expressed as a difference between the biomarker observations taken at the second time point (Obs_{t_2}) and the observation taken at first time point t_1 (Obs_{t_1}) divided by the time interval (t_2 minus t_1) (Jindani et al., 1980). This approach provides a model-free estimate of EBA, which can later be used for the comparison of different treatments.

$$EBA_{t_1-t_2} = \frac{Obs_{t_2} - Obs_{t_1}}{t_2 - t_1} \tag{1}$$

Non-model-based EBA approach is frequently substituted by the traditional model-based EBA approach. Here, EBA is estimated using a function, i.e., linear, bi-linear, etc. (Eq. 2), as shown in the paper by Jindani et al. (Jindani et al., 2003):

$$EBA_{t_1-t_2} = \frac{f(t_2) - f(t_1)}{t_2 - t_1} \tag{2}$$

$f(t)$ represents a fitted regression function to the biomarker data, and $f(t_n)$ represents a biomarker value for day n derived using a fitted function.

In the traditional model-based EBA analysis approach, data from all timepoints is used to describe the change in biomarker (CFU and/or TTP) over time using linear, bi-linear or multiple linear regression models. In the case of a linear model, the biomarker gradually changes over time with a constant slope value. In the case of bi-linear regression, two distinct phases of change in load are observable (Diacon et al., 2013).

An extension to the traditional model-based EBA analysis is pharmacometric model-based analysis. A pharmacometric approach is built on non-linear mixed-effects modeling. Usually, these models are composed of structural, stochastic, and covariate sub-models. The structural sub-model defines the underlying change in the biomarker over time and consists of parameters called fixed effects which represent the change in biomarker over time in a "typical patient". The stochastic sub-model includes random effect parameters which describe inter-individual variability (IIV) and residual unexplained variability (RUV). IIV is related to between patient variability, and RUV is due to variation in each observation from the model prediction due to unexplained factors such as imprecision in the biomarker

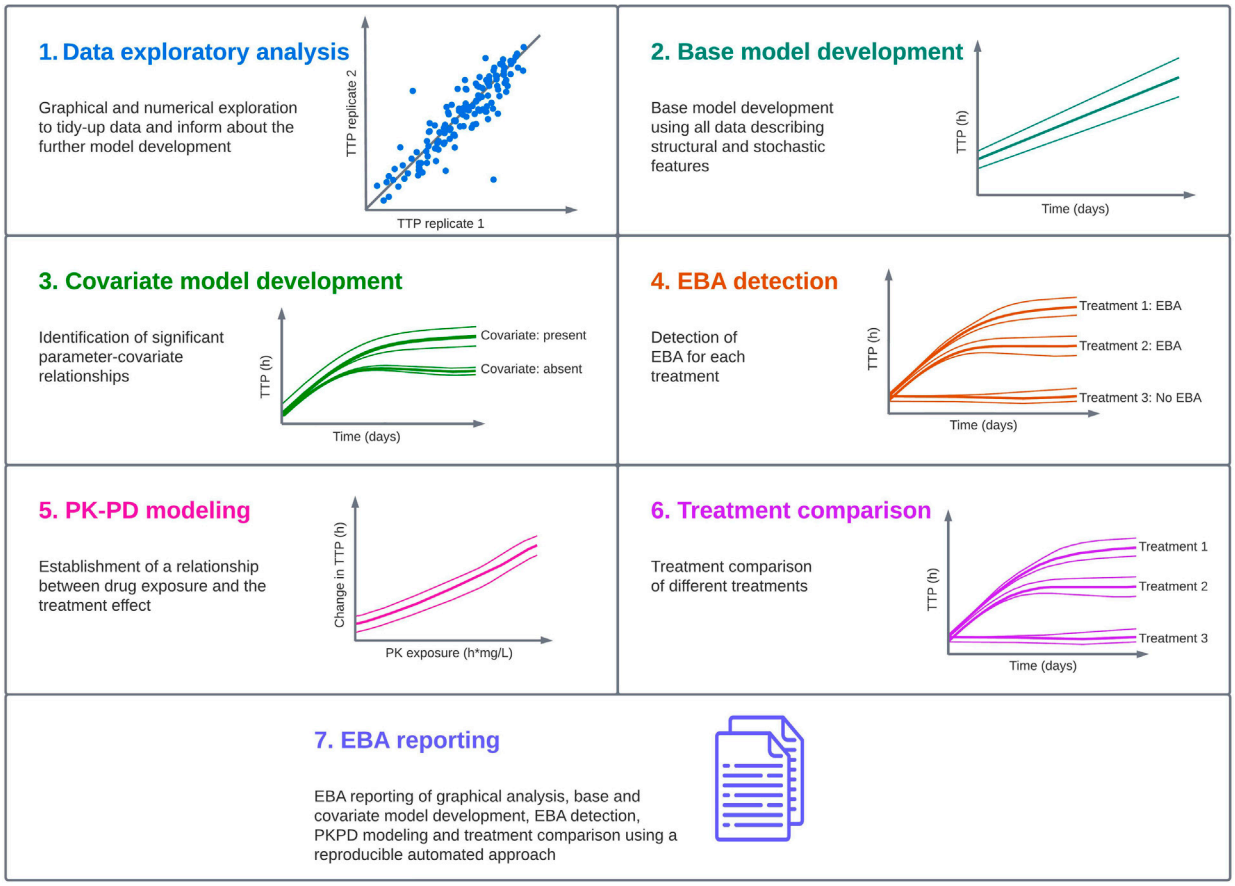

FIGURE 1
Standardized pharmacometric model-based early bactericidal activity (EBA) analysis approach was established in close collaboration between pharmacometricians, clinicians, microbiologists and data managers. In the pharmacometric model-based EBA analysis approach, the first step is to perform data exploratory analysis to familiarize with the data and identify observations that could affect the analysis. In the next step, modeling is started with a base model development, and this model is used in the covariate model building to identify statistically significant parameter-covariate relationships. Afterwards, EBA detection is performed to identify treatments showing EBA. In the next step, if drug exposure information is available, pharmacokinetic-pharmacodynamic (PK-PD) modeling should be performed. This is followed by treatment comparison if multiple treatments are present in the study. In the last step, EBA reporting is done using an automated and reproducible approach to ensure consistency, and the predictions of EBA on typical and individual levels are presented.

assay, sample collection and handling, and model misspecification. The addition of a covariate sub-model containing information about influential factors on variability in data can reduce unexplained variability in the model and can also lead to treatment optimization in sub-populations and improved EBA characterization. In a pharmacometric model-based analysis, drug exposure as a covariate is often considered in the model to explain variability in response, which enables clinical trial simulations using dosing regimens not used in the trial. The pharmacometric model-based approach has been applied to multiple Phase 2a trials in TB, including rifampicin (Svensson and Simonsson, 2016), clofazimine (Faraj et al., 2020) and meropenem-containing treatments (De Jager et al., 2022). In addition, model-based pharmacokinetic-pharmacodynamic (PK-PD) approaches have shown to have higher statistical power compared to other analysis approaches (Svensson et al., 2017).

The aim of this work was to present a standardized pharmacometric model-based EBA analysis approach. In addition, the aim was to perform sample size determinations for detecting EBA or a difference between treatment groups by employing a pharmacometric model-based EBA analysis approach.

2 Materials and methods

2.1 Standardized pharmacometric model-based early bactericidal activity analysis approach

In order to characterize a standardized pharmacometric model-based EBA analysis approach, seven critical steps were identified; exploratory data analysis, base model development, covariate analysis, EBA detection, PK-PD modeling, treatment comparison

and reporting (Figure 1). These steps are in line with the guidelines from the United States Food and Drug Administration (FDA) and the European Medicine Agency (EMA) for conducting and reporting pharmacometric analysis (European Medicines Agency, 2008; Food and Drug Administration, 2022). Close collaboration is required to facilitate an EBA analysis that supports decision making in the clinical development of new TB drugs. This requires efficient, smooth and optimal collaboration between the pharmacometricians performing data analysis and modeling, clinicians responsible for the clinical trial and patients, microbiologists analyzing the samples and quantifying the bacterial burden, and data managers responsible for data handling.

Below, each step of the standardized pharmacometric model-based EBA approach is presented for the analysis of the biomarker TTP. This approach is easily extendable to other EBA biomarkers such as CFU but also to future biomarkers with longitudinal decline or increase over time.

2.1.1 Simulated early bactericidal activity data

In order to visualize every step of the pharmacometric model-based EBA modeling workflow, a 14-day EBA trial was simulated using a simulation model composed of the final parameter estimates from two previous TTP-EBA models based on two meropenem-containing treatments (Supplementary Table S1) from De Jager et al. (De Jager et al., 2022) and unpublished data (ClinicalTrials.gov Identifier: NCT04629378). In total, longitudinal TTP data in 30 participants, divided into two different treatment arms (Arm A and B), were simulated. Four different covariates were simulated; age, sex, cavity extent at baseline and meropenem area under the concentration *versus* time curve from time zero to infinity ($AUC_{0\text{-}inf}$). Cavity extent at baseline had three categories; no cavities, cavities <4 cm, and cavities ≥4 cm. Five participants per each cavity category per treatment were simulated. Meropenem $AUC_{0\text{-}inf}$ at day 14 were sampled from a normal distribution with a mean of 640 h mg/L and a standard deviation of 86 h mg/L (unpublished data, ClinicalTrials.gov Identifier: NCT04629378). No difference in $AUC_{0\text{-}inf}$ between the two treatment groups was assumed. Equal distribution of sex was simulated in the trial (15 males, 15 females). Age distribution was simulated from a normal truncated distribution with a mean of 33 years, a lower boundary of 18 years, an upper boundary of 60 years and a standard deviation of 13 years. The covariate relationships included in the simulations were cavity on TTP baseline and $AUC_{0\text{-}inf}$ on TTP slope (Supplementary Table S1). One of the arms (Arm A) were simulated to receive a meropenem containing regimen consisting of 2 g meropenem, 500 mg amoxicillin and 125 mg clavulanate thrice daily on days 1–14 (De Jager et al., 2022). The second arm (Arm B) was simulated to receive a treatment of 6 g meropenem, 2000 mg amoxicillin, 62.5 mg clavulanate and 400 mg bedaquiline once daily on days 1–14 (unpublished data, ClinicalTrials.gov Identifier: NCT04629378). To resemble a realistic EBA study, a proportion of the simulated observations were randomly assigned to the following status; negative at day 42 (2%), missing (2%), contaminated (2%) and not done (2%).

The simulation model consisted of a mono-exponential model with the following structure:

$$TTP = e^{A_{mono}} \cdot e^{\alpha_{mono} \cdot time} \quad (3)$$

where A is the intercept (TTP baseline), and α is the slope of the *TTP* decline over time. A proportional error model was used with both common and replicate-specific error terms for each replicate (Supplementary Table S1).

2.1.2 Data exploratory analysis

Exploratory analysis of clinical trial data is the first step in model development and it should be performed both graphically and numerically (European Medicines Agency, 2008; Food and Drug Administration, 2022). It should be performed before model development commences and be reviewed by clinicians and microbiologists responsible for the trial conduct and data generated. Discussion around the outcomes of the graphical and numerical exploratory analysis should lead to consensus on exclusion of outlying observations or participants.

Collaborative expertise is vital for a good understanding of the data as well as for adequate quality of the analysis. At this stage, pharmacometricians together with clinicians identify observations in the graphical and numerical analysis, which should be further investigated and potentially excluded from further analysis. Microbiologists investigate observations in question and provide any additional information on the experiments, if available, which could strengthen the grounds for data exclusion.

Graphically, it is important to identify extreme values that could potentially interfere with the analysis, and help familiarize with the data to facilitate model development. Replicate-versus-replicate figures, displaying one replicate on the *x*-axis and the other replicate on the *y*-axis, are expected to show a scatter around the line of identity. Clear outlying datapoints should be reviewed carefully. Biomarker-versus-biomarker plot (showing one biomarker plotted *versus* another biomarker) can be created if multiple biomarkers were used to evaluate the bacterial burden over time, and datapoints outside of the scatter should be reviewed carefully. Biomarker-over-time curves for the population, either as scatter plots or based on summary statistics, will inform on the shape of the bacterial burden over time, and which model functions to evaluate. Individual bacterial burden over time, preferably with adjacent panels for different biomarkers of comparison, can support a review of the outlying datapoints from the replicate-versus-replicate and/or biomarker-versus-biomarker figures. To minimize bias, masking the group allocation and randomization of individuals in graphs should be considered. In addition, baseline bacterial burden can be shown stratified over covariates (boxplots for categorical covariates, scatter plot for continuous covariates), as well as a biomarker-over-time stratified over covariates (categorization of continuous covariates), and this can inform on the covariate relationships to test.

Numerically, the exploratory analysis should help with familiarization with data and numeric comparison between treatment groups. Summary statistics (median, interquartile range, mean, standard deviation) of the bacterial burden will provide initial estimates for baseline population parameters as well as inter-individual and residual variance parameters. Summary statistics on demographics and additional disease biomarkers (e.g., imaging-based markers such as cavity extent) can be used to check randomization processes as these variables

should be similarly distributed across the study arms. These may also suggest covariate relationships to include in the model development strategy. Measures of exposure should also be numerically explored overall and per arm through summary statistics on secondary PK parameters such as area under the curve (AUC), maximum concentration (C_{max}), and minimum concentration (C_{min}). The proportion of missing data, either because of the contaminated sample, no result from the assay, sample not taken/performed, or other reasons, should be assessed for unequal distribution across arms as this otherwise may bias analysis outcomes. The number of censored observations, either 0 $\log_{10}$ CFU/mL sputum for CFU or the negative liquid culture at day 42 for TTP are in general indicative of the presence of EBA and favorable outcome.

2.1.3 Base model development

For the structural model, both mono- and bi-exponential models should be evaluated for each biomarker; TTP (Eqs. 4, 5 and CFU Eqs. 6, 7).

$$TTP_{pred} = e^{A_{mono}} \cdot e^{\alpha_{mono} \cdot time} \tag{4}$$

$$TTP_{pred} = e^{A_{bi}} \cdot e^{\alpha_{bi} \cdot time} + e^{B_{bi}} \cdot e^{\beta_{bi} \cdot time} \tag{5}$$

$$Log_{10}CFU_{pred} = log_{10}\left(e^{A_{mono}} \cdot e^{-\alpha_{mono} \cdot time}\right) \tag{6}$$

$$Log_{10}CFU_{pred} = log_{10}\left(e^{A_{bi}} \cdot e^{-\alpha_{bi} \cdot time} + e^{B_{bi}} \cdot e^{-\beta_{bi} \cdot time}\right) \tag{7}$$

where A_{mono} and A_{bi} are the baseline for mono- and bi-exponential models respectively, B_{bi} is the intercept for the second slope in a bi-exponential model, α_{mono}, α_{bi} and β_{bi} are the slopes of the curve. Log_{10} is the logarithm with base 10, e is the exponential function. CFU_{pred} is the predicted CFU (expressed as $\log_{10}$ CFU/mL sputum), TTP_{pred} is the predicted TTP (expressed as hours). The magnitude of the CFU observations requires the data to be modelled on the log scale where the range of TTP is smaller and therefore indicates that the TTP data can be modelled on the natural logarithm scale.

Generally, these models are sufficient to describe the data, but more advanced non-linear models such as those including time-dependent functions could be considered if model diagnostics for the mono- and bi-exponential models show insufficient model performance (De Jager et al., 2022). For CFU modeling, negative slope(s) should be evaluated, while for TTP modeling positive slope(s) are appropriate.

The stochastic model captures IIV and RUV IIV terms can be evaluated on the population parameters (e.g., intercept, slope) as in Eq. 8, resulting in a lognormal distribution with a lower bound of zero.

$$\text{Parameter}_{individual} = TV_{parameter} \cdot e^{\eta} \tag{8}$$

where TV is the typical value and η is drawn from a normal distribution with a mean of zero and standard deviation ω. Other distributions *via* transformations can be considered if the diagnostics of the η distribution indicate it.

The RUV model should capture the residuals in a homoscedastic manner across time and predictions. For log-transformed data such as CFU, an additive residual error model on the log-transformed scale is appropriate as it approximates a proportional error model on the untransformed scale. For untransformed data, an additive (Eq. 9), proportional (Eq. 10), or combination of additive and proportional error (Eq. 11) model should be evaluated. In the case of multiple replicate measurements from the same sample, a RUV model with combined and separate error terms can be utilized to quantify both the shared part of the residual noise from the single sample as well as the separate part of the residual noise from the assay replicate (Eq. 12), or by quantifying the correlation of the level 2 (L2) random effect in non-linear mixed effects modeling algorithms (Karlsson et al., 1995).

$$Y = IPRED + \varepsilon_a \tag{9}$$

$$Y = IPRED \cdot \left(1 + \varepsilon_p\right) \tag{10}$$

$$Y = IPRED \cdot \left(1 + \varepsilon_p\right) + \varepsilon_a \tag{11}$$

$$\begin{gathered} Y = IPRED + \varepsilon_1 + \varepsilon_2 \\ IF\,(REP.EQ.2)\,Y = IPRED + \varepsilon_1 + \varepsilon_3 \end{gathered} \tag{12}$$

in which Y is the observation, $IPRED$ is the individual prediction, REP is the replicate (here numbered either 1 or 2), ε_a is the additive error term, ε_p is the proportional error term, ε_1 is the shared error term, and ε_2 and ε_3 are the replicate-specific error terms, all of which are randomly drawn from a normal distribution with mean 0 and standard deviation σ.

2.1.4 Covariate model development

An important step in the model-building process is to identify significant parameter-covariate relationships. The overall goal with covariates is to describe and explain observed between patient variability, which in turn will support predicting EBA for relevant subpopulations but most importantly, by explaining between patient variability, the power to detect EBA or differentiate EBA between drugs or treatments, will increase.

In the Phase 2a trial setting, a set of different covariates is collected. A selected list of covariates should be identified based on correlations plots of covariates and individual TTP slope in addition to experience based on historical EBA trials. It is important to pay attention to shrinkage when evaluating plots based on Bayes estimates (Savic and Karlsson, 2009). Covariates which should be evaluated on biomarker baseline (and additional intercepts) are; sex, body mass index (BMI), HIV status, ethnicity and age. Covariates to be evaluated on change in bacterial load over time (TTP and/or CFU slope) are; sex, presence of cavity, grade of cavitation and initial bacterial load. Additional covariates, like drug susceptibility, presence of concomitant diseases/medications and others can be evaluated, if data is available and there are grounds for the covariate to be evaluated. For simplicity in this work, we only illustrate graphical analysis and covariate analysis with sex, age and cavity extent.

Covariate analysis can be performed using different methods. One of the most common methods is stepwise covariate modeling (SCM) (Lindbom et al., 2005). An inclusion criterion for covariates of $p \leq 0.05$ followed by a backwards deletion criteria of $p \leq 0.01$ are suggested to be used. Power functions of relationships between model parameter and covariates are evaluated. Other parametrizations of covariate relationships may be considered if indicated by the data. Categorical covariate-parameter relationships are implemented as a fractional difference to the most common category.

2.1.5 Early bactericidal activity detection

After the covariate model has been established, a formal statistical testing of EBA can be done for each of the different arms in the EBA trial, one by one. An exception could be for control arms which usually have lower sample size than the experimental arms. Typical parameters (excluding baseline bacterial load) will be fixed to 0 and compared to a model estimating the respective parameters, for each treatment one by one in order to confirm EBA. Statistical significance, often at a 5% significance level considering the degrees of freedom, is tested using the likelihood ratio test between the models. Treatment arms for which the TTP (or CFU) slope(s) are statistically significant are considered to have confirmed EBA at the sample size in the trial. Similar, treatment arms for which the TTP (or CFU) slope(s) are statistically not significant are considered to have no EBA at the sample size in the trial. For treatment arms with no identified EBA, the TTP or CFU slope(s) are fixed to zero in the further model development.

2.1.6 Pharmacokinetic-pharmacodynamic modeling

PK-PD modeling allows for accounting for between patient variability in drug exposure which may be a reason for difference in EBA between patients. PK-PD modeling can be done by connecting a population PK model to the EBA model and where predicted concentration over time drives the PK-PD relationship (Zhang et al., 2003). An alternative is to use predicted drug exposure indices (AUC and/or C_{max}) as a covariate on the slope(s) in the EBA model. AUC and C_{max} can be predicted from population PK model or obtained from non-compartmental analysis (NCA) which can be obtained if the PK sampling is rich and well designed. Different PK-PD relationships on the different EBA slope(s) are evaluated such as linear and non-linear relationships. If between-subject variability in EBA slope(s) can be described by PK, this reduce the unexplained between patient variability in EBA which thereby increases the power to detect EBA.

After the PK-PD relationship was established, it can be visualized by performing simulations using the final model, i.e., by using sampling importance resampling (SIR) to derive the uncertainty around the parameters, followed by using the output from SIR in stochastic simulations and estimations to derive the relationship on the typical individual level. In this case, only the typical values are unfixed, and remaining parameters, like IIV and RUV are fixed to zero.

2.1.7 Early bactericidal activity comparison

If multiple treatment arms are included in the EBA trial design, arms that have shown statistically significant EBA, will be taken forward to EBA comparison evaluation to support the comparison of treatment arms. The final covariate EBA model is used to evaluate differences in regimen efficacy. During the evaluation of treatment efficacy, included IIVs, except IIV on baseline bacterial load, will initially be fixed to zero. For treatment arms with no EBA, the TTP slope will be zero. Treatment arms that have shown EBA in the earlier step, are initially defined as having the same TTP (and/or CFU) slope(s). Firstly, univariate analysis is conducted where the slope of each treatment arm is evaluated as different from the common slope of the other EBA confirmed arms. Thereafter, the treatment with the highest significant difference in TTP slope compared to the other arms in the univariate step, will be kept in the model. The second highest statistically significant treatment arm TTP slope will be added thereafter and statistically evaluated at a significance level of 5%. This will be continued for all arms. Arms where no difference in TTP slope can be shown will be grouped together to the same slope and the final model will predict the same EBA for these regimens. In the last step, IIV in the different TTP (and/or CFU) slopes are re-evaluated. It is important to note that EBA trials often are powered to only detected EBA and not to identify differences between arms. There might therefore not be sufficient power to detected small differences between treatments given the commonly used sample size for EBA trials.

2.1.8 Early bactericidal activity reporting

All sections mentioned above should be included in an analysis report (European Medicines Agency, 2008; Food and Drug Administration, 2022). RMarkdown is a powerful tool to reproducibly compile reports on the graphical and numerical exploratory analysis in pdf or word format that are readily sharable with collaborators for review (Allaire et al., 2020; van Wijk et al., 2022). In addition to the sections presented above, reports should also include final parameter estimates from the model and typical and individual model-based predictions. Model-based typical and individual CFU or TTP predictions over time derived using individual Bayes estimates and converted to $EBA_{0\text{-}2}$ (expressed as a difference in biomarker value between day 0 and day 2), $EBA_{0\text{-}7}$, and $EBA_{0\text{-}14}$ together with plots of predictions can be used to compare the activity of the treatments that were shown to have EBA, irrespective of the function applied to describe data.

2.2 Sample size to detect early bactericidal activity

Power is defined as the probability of rejecting the null hypothesis correctly (Eq. 13):

$$Power = 1 - \beta \tag{13}$$

where β is the probability of type II error (i.e., false negative). In EBA trials, the null hypothesis is most often defined as that the treatment or drug has no EBA.

Monte-Carlo Mapped Power (MCMP) method is a model-based approach to derive power curves for scenarios of interest (Vong et al., 2012). MCMP method was used in this work to calculate the power needed to detect EBA given different TTP slopes and variability in TTP slope. MCMP contains two parts; simulation and estimation, followed by power mapping (Vong et al., 2012). In the simulation and estimation step, MCMP simulates initially a large dataset. In this work, 2000 individuals were simulated with a full TTP-EBA model including an EBA efficacy for the two treatments as well as an EBA difference between the two treatments seen as two different TTP slopes and a difference between the slopes (Supplementary Table S2). In liquid culture experiments, the maximum

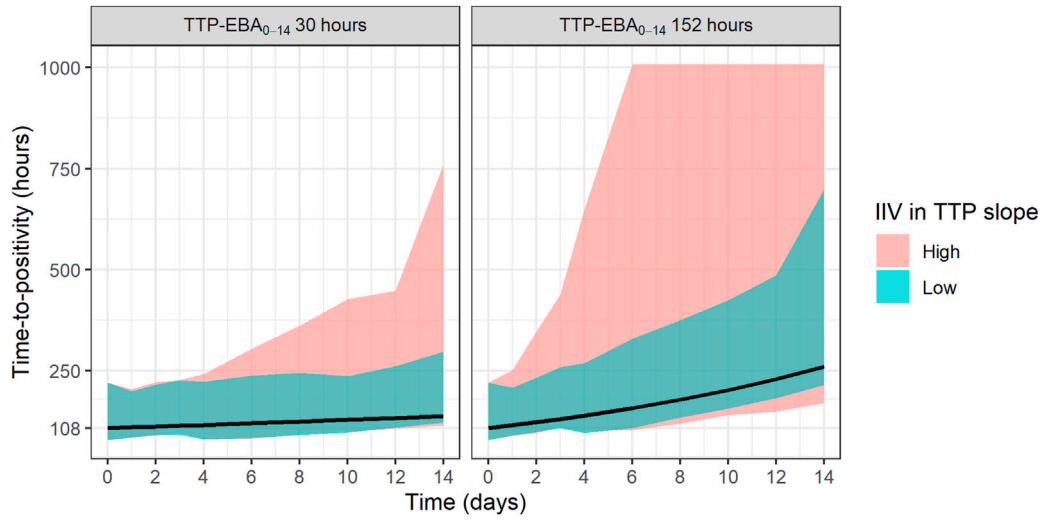

FIGURE 2
Visualization of typical profiles and variability in time-to-positivity (TTP) over time for high [104% coefficient of variation (CV)] and low (22% CV) inter-individual variability (IIV) in EBA. TTP-EBA_{0-14} is early bactericidal activity based on the difference in TTP between 0 and 14 days. Black lines represent the typical individual and shaded areas show the variability in predicted TTP derived from 30 randomly sampled individuals (95% prediction interval). The median baseline TTP was 1,008 h.

incubation period is 42 days, therefore simulated TTP values greater than 42 days were censored at 42 days (1,008 h). This large simulated dataset was re-estimated with the full and reduced models. The reduced model was an TTP-EBA model with a TTP-slope fixed to zero (i.e., no EBA). Individual objective function values (iOFVs) from both the full and reduced models were used to calculate the difference in iOFV for each individual (ΔiOFV). ΔiOFVs were taken to the power mapping step, where Monte Carlo sampling was performed, and the sum of ΔiOFVs was derived multiple times (10,000 times) for each sample size. Power at each sample size was derived based on the number of Monte Carlo sampling instances where the sum of ΔiOFV was greater than the critical χ^2 value (for $p < 0.05$) divided by the total number of Monte Carlo sampling instances performed. Power was presented for up to 30 individuals in the trial scenarios. The goal in every analysis was to reach 80% power at a 5% significance level.

The sample sizes needed to detect EBA in relation to the influence of various TTP slopes and IIV in TTP slope (low and high IIV in TTP slope) was investigated. Explored IIV in TTP slopes were 22% coefficient of variation (CV) for low IIV in TTP slope, and 104% CV for high IIV in TTP slope. This was taken from the earlier quantified IIV in TTP slope from the two trials with meropenem presented in De Jager et al. (De Jager et al., 2022) and unpublished data (ClinicalTrials.gov Identifier: NCT04629378). TTP slope values ranged from 0.0017 h/day to 0.0628 h/day, corresponding to TTP-EBA_{0-14} of 3 h and 152 h, respectively. The different explored scenarios of TTP slope (TTP-EBA_{0-14}) and IIV in TTP slope are presented in Supplementary Table S3. Visualization of typical profiles and variability in TTP over time for high (104%) and low (22%) IIV in TTP slope based on 30 simulated participants are shown in Figure 2.

2.3 Sample size to detect treatment effect difference

To identify the sample sizes needed to detect a difference in EBA between two treatments, the null hypothesis was that there is no difference in EBA between the two treatments. In this work, power for different sample sizes were evaluated for scenarios with different EBA between two treatment groups. In addition, the influence of different IIV in TTP slope on the power for different sample sizes were explored. The MCMP approach described above was used. Effect difference was defined as a percentage increase in TTP slope between two treatments. Combinations of different TTP slopes, IIV in TTP slope and difference in TTP slope (from 25% to 200%) were investigated; TTP slope of 0.0628 h/day (TTP-EBA_{0-14} of 152 h) with low IIV in TTP slope; TTP slope of 0.0628 h/day (TTP-EBA_{0-14} of 152 h) with high IIV in TTP slope; TTP slope of 0.0174 h/day (TTP-EBA_{0-14} of 30 h) with low IIV in TTP slope; and TTP slope of 0.0174 h/day (TTP-EBA_{0-14} of 30 h) with high IIV in TTP slope. High IIV and low IIV in TTP slope were defined as 104% and 22%, respectively based on earlier reported variabilities in De Jager et al. (De Jager et al., 2022) and unpublished data (ClinicalTrials.gov Identifier: NCT04629378). Created scenarios are presented in Supplementary Table S4. Visualization of typical profiles of TTP over time for different effect differences are presented in Figure 3.

To characterize the influence of IIV in TTP slope on the power to detect EBA effect difference, TTP slope of 0.0628 h/day and 0.0174 h/day (TTP-EBA_{0-14} of 152 h and 30 h) were combined with different magnitudes of IIV in TTP slope. The same EBA effect difference of 50% was used in all scenarios and IIV in TTP slope spanned from high IIV (104%) to low IIV (10%). Explored scenarios are presented in Supplementary Table S5.

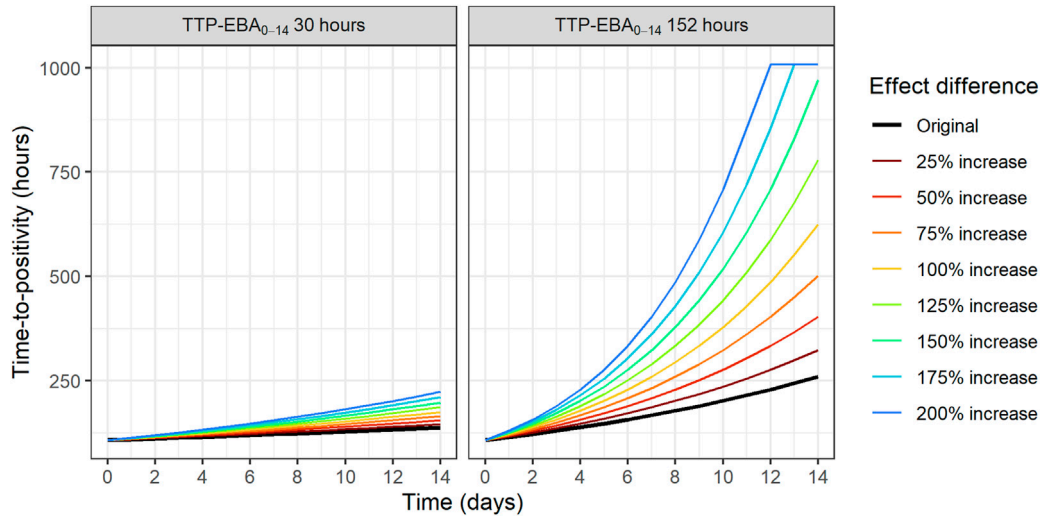

FIGURE 3
Visualization of typical profiles of time-to-positivity (TTP) over time for different effect difference values. Effect difference is expressed as a percentage increase in the TTP slope compared to the original value (red solid line). TTP values were right censored at 1,008 h (42 days).

2.4 Software

Data handling and visualization were performed using R (v.4.0.3, R Foundation for Statistical Computing, Vienna, Austria) (R Core Team, 2020) through the RStudio interface (RStudio Team, 2022). Simulations were performed using non-linear mixed-effects modeling software NONMEM (v.7.5.0, Icon Development Solutions, Ellicott City, MD, United States) (Beal et al., 1989). MCMP were performed using PsN (v.5.3.0) (https://uupharmacometrics.github.io/PsN/).

3 Results

3.1 Standardized pharmacometric model-based early bactericidal activity analysis approach

In order to present each step of the standardized pharmacometric model-based analysis approach for Phase 2a EBA trials (Figure 1), each step was demonstrated using a simulated example based on a model resembling meropenem-containing treatments (Supplementary Table S1). The work is illustrated for TTP but is applicable to CFU as well.

3.1.1 Exploratory data analysis

Before the modeling was started, data exploration to establish an analysis dataset from the raw data should be performed. Firstly, data summary tables were created based on the simulated data. The simulated number of participants and covariate information per treatment group and in total are presented in Supplementary Table S6. Counts of non-positive and censored data at different timepoints are presented in Supplementary Table S7.

Replicate-versus-replicate of the raw data was plotted and any clear deviations from the identity line were further investigated (Figure 4). Additionally, biomarker *versus* time of TTP was plotted to facilitate data comparison between the replicates and over time. An example of an individual plot is shown in Figure 5 (for subject 8 only). Replicates are plotted next to each other to facilitate comparison, while individual plots for all subjects are available in Supplementary Figure S1.

All TTP samples with the status of contaminated, not done, or no result were excluded from the model-based analysis. After discussing the results with clinicians and microbiologists, only samples with scientifically plausible TTP values were kept, and any clear deviations that have potentially arisen due to the experiment errors, unrecorded contamination, or other reasons were removed from the analysis. In Figure 5 for example, the negative sample at time zero is a clear outlier and was removed from the analysis after consensus was reached with clinical, microbiology, and analysis teams. All removed and omitted data points should be summarized in the final report.

After the final analysis dataset was established, additional plots were created showing the relationship between the baseline biomarker and covariates, and biomarker over time and covariates. Supplementary Figure S2 shows the TTP baseline plots *versus* covariates present in the simulated dataset; sex, age and cavity extent. In addition, plots of TTP over time *versus* cavity extent, sex, age, PK drug exposure (AUC), and treatment. These plots should be used to inform the modeling workflow by informing about the potential function describing the change in the biomarker over time as well as about potential parameter-covariate relationships.

3.1.2 Base model building

After the analysis dataset is established, a base model should be developed. In this simulation based EBA example, the mono-exponential function described the data well. IIV was supported on baseline and TTP slope. The proportional error model was used with both common and replicate-specific error terms for each

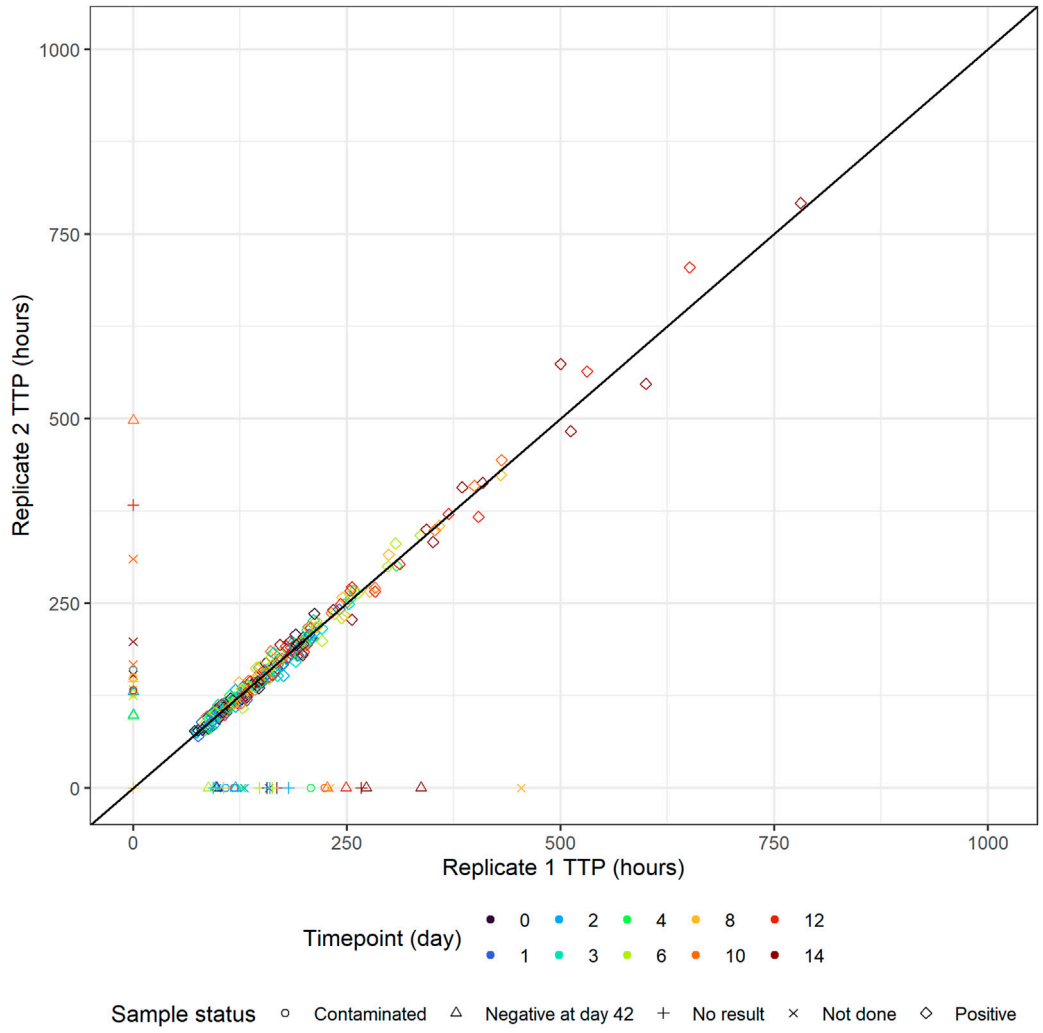

FIGURE 4
Individual time-to-positivity (TTP) replicate 1 *versus* individual TTP replicate 2. Observations are expected to be as close to the identity line as possible, and any clear deviations from the identity line should be investigated. Non-positive values are plotted in the figure axes and their symbol represents the corresponding sample status. For example, if replicate 1 is non-positive, the symbol with the corresponding replicate 2 value is plotted on the *y*-axis and *vice versa*.

replicate. Goodness-of-fit (GOF) plots evaluating the model fit are presented in Supplementary Figures S3A-E. Visual predictive check (VPC) plots stratified per treatment arm are presented in Supplementary Figure S4, column a. Based on GOFs and VPCs stratified on treatment, a satisfactory fit was achieved using a mono-exponential function with IIV on baseline and slope, and the model was carried forward to the covariate modeling.

3.1.3 Covariate model building

In the next step, covariate model building is performed. Age, sex, and cavity extent were tested on both the TTP baseline (intercept) and the TTP slope. Only one covariate was found to be statistically significant after the forward inclusion and backwards deletion step in the SCM. Decrease in TTP baseline values was associated worsening cavity extent states, and a separate TTP baseline was estimated for each category ($p < 0.01$). The highest TTP baseline was predicted when no cavities were present. VPCs stratified on cavity are presented in Supplementary Figure S5.

3.1.4 Early bactericidal activity detection

After the covariate model is built, EBA detection can be performed. Here, in this example, both treatment arms A and B were shown to have EBA at a 5% significance level.

3.1.5 Pharmacokinetic-pharmacodynamic modeling

All treatment arms that were shown to have EBA, were further taken to build the PK-PD model, where a relationship between AUC of meropenem and TTP slope was assessed. Linear, hockey-stick, power and exponential covariate-parameter relationships were evaluated on natural logarithm scale. Out of all assessed parameterizations, the hockey-stick function had the biggest change in objective function value (ΔOFV) (−49.866) but as one

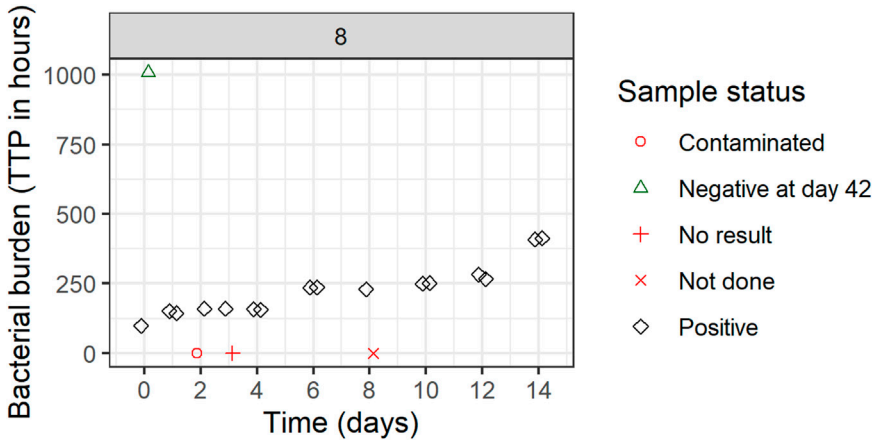

FIGURE 5
Individual biomarker over time plot. Both replicates 1 and 2 are plotted which can seem to overlap because of very comparable values. One participant was selected to visualize the status of each sample. If a replicate value was non-positive, it was plotted in red (missing) or green (negative) on the graph axes with the shape informing on the reason for its non-positive sample status. These symbols are plotted next to each other to facilitate interpretation but belong to the same time point. Plots are based on the simulated data to visualize the standardized pharmacometric model-based EBA analysis approach. Plots of individual biomarker over time for all individuals are available in Supplementary Figure S1.

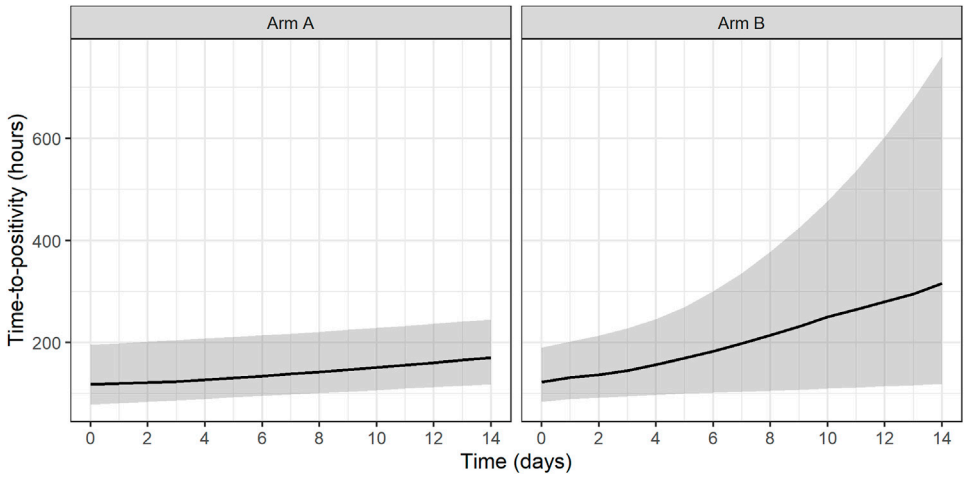

FIGURE 6
Prediction of individual time-to-positivity (TTP) over time based on Bayes estimates of the final model. Lines represent the predicted median with a shaded area corresponding to the 95% prediction interval. Arm A resembling meropenem in 2 g meropenem thrice daily with 500 mg amoxicillin and 125 mg clavulanate thrice daily on days 1–14 (De Jager et al., 2022). Arm B resembling meropenem in 6 g meropenem once daily with 2 × 1000 mg amoxicillin and 62.5 mg clavulanate plus 400 mg bedaquiline once daily on days 1–14 (unpublished data, ClinicalTrials.gov Identifier: NCT04629378).

of the parameters had very high uncertainty, a linear parameterization with second biggest ΔOFV (−45.463) was selected, which resulted in an exponential relationship on normal scale. Additionally, after meropenem AUC was incorporated as a covariate on the TTP slope, IIV in TTP slope decreased from 49.7% to 20.5%, explaining the PK related variability between subjects. VPCs stratified on meropenem AUC are presented in Supplementary Figure S6.

3.1.6 Early bactericidal activity comparison

After PK-PD modeling, a treatment comparison can be performed. In this work, treatment comparison between simulated Arm A and Arm B was performed. Treatments were shown to have statistically significantly different EBAs from each other at a 5% significance level. Arm B was shown to have 3.7 times higher EBA compared to Arm A in this simulated example.

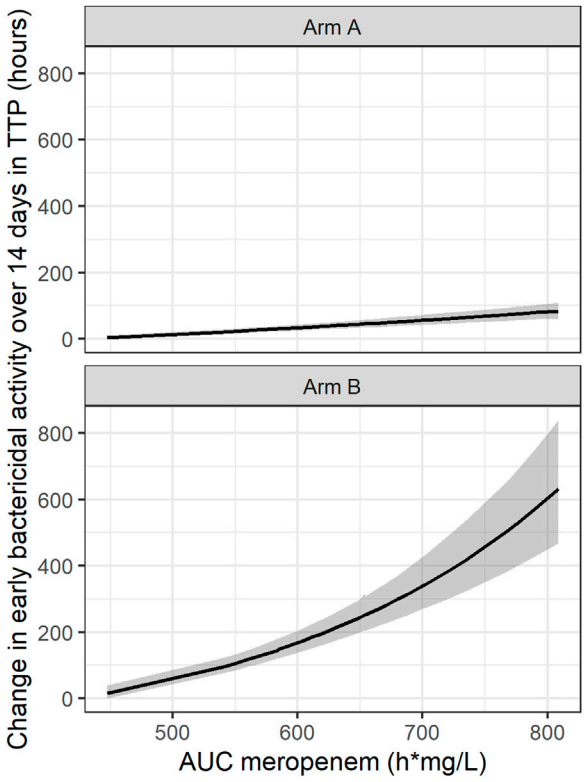

FIGURE 7
Established pharmacokinetic-pharmacodynamic (PK-PD) relationship between area under the curve (AUC) of meropenem and early bactericidal activity (EBA) based on time-to-positivity of 0–14 days (TTP-EBA_{0-14}) for the typical individual with one or several cavities <4 cm. The black line represents the median and the shaded area represents the 95% confidence interval. 95% confidence interval is derived from Sampling Importance Resampling (SIR) method followed by Stochastic Simulation and Estimation (SSE) step of 1,000 samples. Arm A resembling meropenem in 2 g meropenem thrice daily with 500 mg amoxicillin and 125 mg clavulanate thrice daily on days 1–14 (De Jager et al., 2022). Arm B resembling meropenem in 6 g meropenem once daily with 2 × 1000 mg amoxicillin and 62.5 mg clavulanate plus 400 mg bedaquiline once daily on days 1–14 (unpublished data, ClinicalTrials.gov Identifier: NCT04629378).

3.1.7 Early bactericidal activity reporting

The final TTP-EBA model described the data well and the final parameters are shown in Supplementary Table S8. The final TTP-EBA model consisted of a mono-exponential model with IIV in baseline (intercept) and TTP slope. Covariate relationships were cavity extent on TTP baseline and AUC meropenem on TTP slope. A proportional error model with both common and replicate-specific error terms for each replicate was included in the final model. GOF plots are presented in Supplementary Figure S3F-J, stratified VPCs per treatment arm and prediction-corrected VPC are available in Supplementary Figure S7 and Supplementary Figure S4 column b.

Both treatments based on simulated data for Arm A and Arm B were shown to have statistically significant EBA ($p < 0.05$). In addition, simulated Arm B was shown to have statistically significantly higher TTP slope than simulated Arm A (3.7 times higher TTP slope). Predicted typical and individual model-based EBA for 0–2, 0–7, and 0–14 days were derived. Prediction of individual TTP over time using Bayes estimates of the final model is shown in Figure 6. Predicted typical and individual model-based EBA for 0–2, 0–7, and 0–14 days are presented in Supplementary Tables S9, 10.

In addition, an exponential PK-PD relationship between the meropenem AUC and TTP slope and thereby TTP-EBA_{0-14} was established. In this simulated example, TTP increased by 0.44 h per each 1 h mg/L meropenem AUC_{0-inf} on the natural logarithm scale (Figure 7).

3.2 Sample size to detect early bactericidal activity

To investigate the sample size needed to detect EBA, eight different TTP slopes (0.0017 h/day to 0.0628 h/day) corresponding to TTP-EBA_{0-14} values ranging from 3 h to 152 h were combined with low and high IIV in TTP slope (22% and 104%, respectively). In total, 16 scenarios were explored (Supplementary Table S3). Simulated typical profiles and corresponding variability based on 30 individuals (expressed as a 95% prediction interval) are visualized for both low and high variability in TTP slope (22% and 104%) and TTP-EBA_{0-14} values of 30 h (slope 0.0174 h/day) and 152 h (slope 0.0627 h/day) (Figure 2).

Sample sizes per arm needed to detect EBA with 80% power at a 5% significance level are presented in Table 1 and power curves are presented in Figure 8 for the difference scenarios. TTP-EBA_{0-14} had to be equal to or greater than 11 h, irrespective of IIV in TTP slope, to achieve 80% power at a 5% significance level with 13 participants enrolled per treatment arm. An increase in sample size, to 18 participants per arm, resulted in a study having 80% power to detect EBA when TTP-EBA_{0-14} was 7 h and high IIV in TTP slope was present (104%). For a scenario with low IIV in TTP slope (22%) 31 participants/arm were required to reach the same power. If the TTP-EBA_{0-14} was 3 h, 97 and 180 participants/arm for high IIV and low IIV, respectively, were required to achieve 80% power to detect TTP-EBA_{0-14}.

For treatments showing TTP-EBA_{0-14} of 30 h or less (typical prediction), the power to detect the EBA given the same sample size, was higher when IIV was larger. This trend was present for even lower TTP-EBA_{0-14} values (Figure 8). The posthoc step of the Bayes estimates of the IIV showed that the mean of the individual etas was skewed towards large positive values of the TTP slope (Figure 9). Due to this, when low EBA effect (TTP-EBA_{0-14} of 30 h or less) was combined with high IIV in TTP slope, the probability of having a significant EBA was higher compared to a scenario where low EBA was combined with low IIV. Opposite effect was observed with high EBA (TTP-EBA_{0-14} of 152 h), as the distribution of individual TTP-EBA_{0-14} values was narrower (Figure 9) and very few extremely low TTP slope values were present.

3.3 Sample size to detect treatment effect difference

To characterize the sample size needed to detect an effect difference between two treatment groups, several different

TABLE 1 Sample size per group needed to detect early bactericidal activity (EBA) with 80% power at a 5% significance level for various changes in time-to-positivity between days 0 and 14 (TTP-EBA$_{0-14}$) and inter-individual variability (IIV) in TTP slope. Power calculations were performed using a mono-exponential model with various TTP-EBA$_{0-14}$ values for both low and high IIV in TTP slope. For each scenario, power calculations included a minimum of 3 patients.

TTP-EBA$_{0-14}$[a]	N per treatment group	
	Low IIV in TTP slope[b]	High IIV in TTP slope[c]
152 h[d]	3	3
30 h[e]	3	3
25 h	3	3
20 h	5	3
16 h	7	5
11 h	13	8
7 h	31	18
3 h	180	97

[a]TTP-EBA$_{0-14}$: typical change in TTP between day 0 and day 14 (expressed in hours).
[b]Low IIV in TTP slope was 22% coefficient of variation (unpublished data, ClinicalTrials.gov Identifier: NCT04629378).
[c]High IIV in TTP slope was 104% coefficient of variation (De Jager et al., 2022).
[d]TTP-EBA$_{0-14}$ corresponding to treatment composed of 6 g meropenem once daily with 2 × 1,000 mg amoxicillin and 62.5 mg clavulanate plus 400 mg bedaquiline once daily on days 1–14 (unpublished data, ClinicalTrials.gov Identifier: NCT04629378).
[e]TTP-EBA$_{0-14}$ corresponding to treatment composed of 2 g meropenem thrice daily with 500 mg amoxicillin and 125 mg clavulanate thrice daily on days 1–14 (De Jager et al., 2022).
EBA: early bactericidal activity.
IIV: inter-individual variability expressed on coefficient of variation scale.

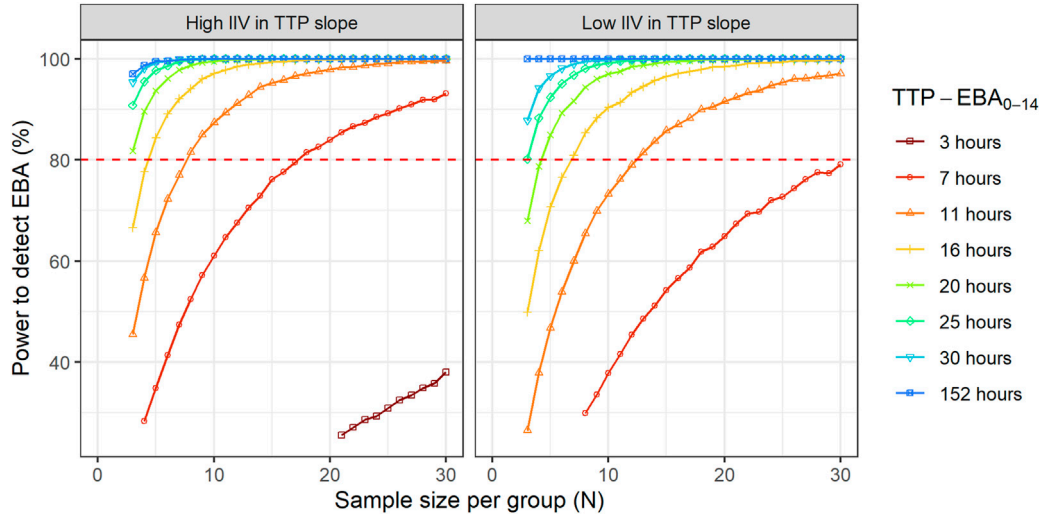

FIGURE 8
The impact of change in time-to-positivity between days 0 and 14 (TTP-EBA$_{0-14}$) on sample size per arm and power to detect early bactericidal activity (EBA). Low and high inter-individual variability (IIV) in TTP slope are represented by 22% and 104% coefficient of variation (CV). The red dashed line represents 80% power.

scenarios with various combinations of different TTP slope (TTP-EBA$_{0-14}$), IIV in TTP slope and effect difference values were explored (Supplementary Table S4). Simulated typical profiles for the different effect differences are presented in Figure 3. Power curves and a summary table presenting the number of participants per group required to achieve 80% power are presented in Figure 10 and Table 2.

For low TTP-EBA$_{0-14}$ (30 h), high IIV in TTP slope and an increased effect difference between the two arms of at least 175%, 15 participants/arm were sufficient to detect a difference between the two treatment groups with 80% power at a 5% significance level (Table 2; Figure 10). At 30 participants/arm, the power was ≥80% to detect an increased effect difference between the two arms of at least 125%. To detect smaller increased effect differences (<100%), more participants were required. For an increased effect difference of 25% at 80% power, more than 125 participants/arm were needed to detect an effect difference between the two arms.

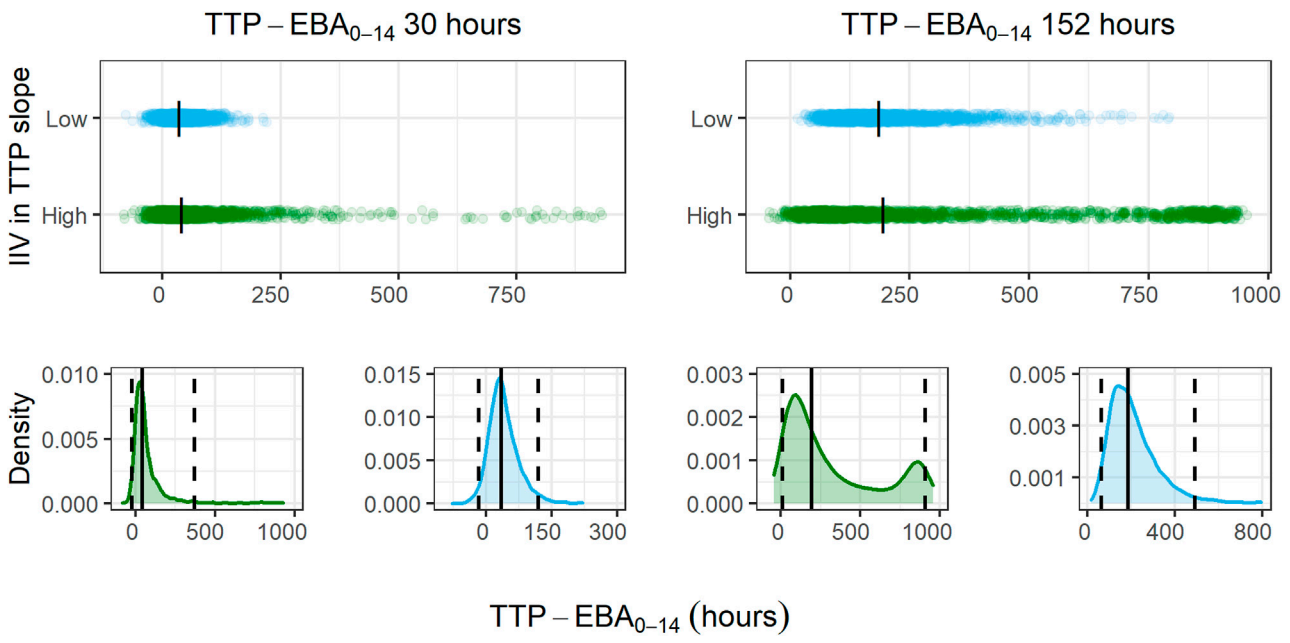

FIGURE 9
Distribution of individual simulated change in time-to-positivity between days 0 and 14 (TTP-EBA_{0-14}) values for two TTP-EBA_{0-14} values; 30 h and 152 h, for different magnitudes of inter-individual variability (IIV) in TTP slope. The blue color is low IIV in EBA (22% coefficient of variation [CV]), and the green color is high IIV in TTP slope (104%). To visualize the spread of values, 2000 individuals per scenario of IIV in TTP slope and TTP-EBA_{0-14} were simulated, and the difference between TTP on day 0 and day 14 was calculated. The top panel of the plot shows the spread of individual TTP-EBA_{0-14} values over the TTP-EBA_{0-14} space. Black dashes represent individual medians. The bottom panels show density plots for the individual TTP-EBA_{0-14} values. A solid black line represents the median, and dashed lines represent the 2.5th and 97.5th percentiles of IIVs. The second peak in TTP-EBA_{0-14} of 152 h and high IIV in TTP slope was related to TTP censoring at 1,008 h.

For high TTP-EBA_{0-14} (152 h) and high IIV in TTP slope, 80% power was only reached when the increased effect difference was at least 150% between the two arms and with 28 participants/arm. None of the explored scenarios reached 80% power with 15 participants/arm or less. To detect 125% increased effect difference, 31 participants/arm were required. For even smaller increased effect differences of 100%, 75%, and 25%, sample sizes of 50, 87 and >125 participants, respectively were required at 80% power and for high TTP-EBA_{0-14} (152 h) and high IIV in TTP slope (Table 2).

At low TTP-EBA_{0-14} (30 h) and low IIV in TTP slope, an increased effect difference of 75% or greater was detected with 15 participants/arm for at least 80% power, while 20 participants/arm were required to detect an increased effect difference of 50%. Similar, 64 participants/arm were required to detect an increased 25% effect difference (Table 2; Figure 10).

For all effect differences, the highest power was seen for scenarios with low IIV in TTP slope and high TTP-EBA_{0-14} (152 h). Less than 15 participants/arm were required for increased effect differences of ≤50%. To detect a 25% increased effect difference between the two arms, 21 participants/arm were sufficient to achieve 80% power at a 5% significance level. For other scenarios, more participants were needed to differentiate between the treatments at this effect difference level (Table 2; Figure 10).

To explore IIV in TTP slope on the power to detect an effect difference between the two arms, a scenario with a 50% increase in effect difference was used. IIV in TTP slope in the simulations ranged from very low to very high IIV in TTP slope, 10% CV to 104% CV (Supplementary Table S5). Power curves and corresponding numbers of participants/arm needed to achieve 80% power are presented in Figure 11 and Table 3.

When TTP-EBA_{0-14} was low (30 h), 90 participants/arm were required to achieve 80% power to detect 50% increase in effect difference between the two treatment groups with IIV in TTP slope of 104%. With a decrease in IIV in TTP slope to 40%, the sample size decreased to 28 participants/arm (Table 3). When IIV in TTP slope was 10% and 50% increase in effect difference, 17 participants/arm were required to reach 80% power for a low TTP-EBA_{0-14} (30 h).

For cases with high TTP-EBA_{0-14} (152 h) and IIV in TTP slope of 104%, 87 participants/arm were required to achieve 80% power to detect an increase of 50% effect difference between the two treatment groups. Decreasing the IIV in TTP slope to 40% resulted in a decreased sample size of 17 participants/arm. Less than seven and three participants/arm were required to achieve a power of 80% when IIV in TTP slope was 22% or 10%, respectively (Table 3; Figure 11).

4 Discussion

This paper presents a standardized pharmacometric model-based EBA analysis approach employing the expertise of microbiologists, clinicians and pharmacometricians. The presented approach is composed of seven pivotal steps, which allows for both model-based pharmacometric EBA detection and treatment comparison in Phase 2a for TB drug development, and is

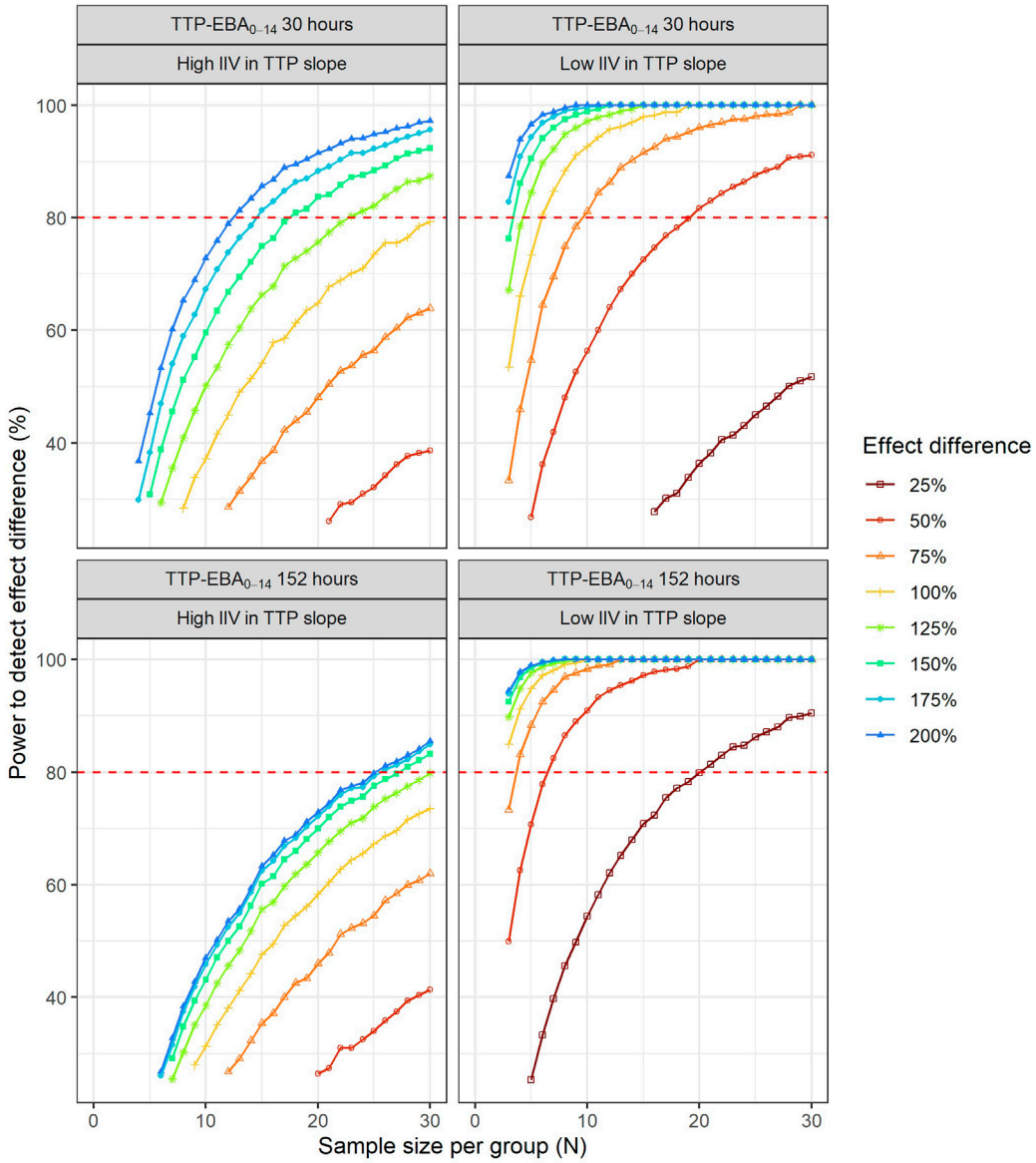

FIGURE 10
The impact of effect difference on the sample size and power to detect a difference between two treatment groups. Low and high inter-individual variability (IIV) in early bactericidal activity (EBA) are represented by 22% and 104% coefficient of variation, respectively. The red dashed line represents 80% power.

identical for evaluation of monotherapies as well as combination regimen. Using the standardized approach, the treatment/drug effect is evaluated through the TTP slope estimation together with uncertainty. It allows for a rational estimation of EBA, as both typical and individual predictions can be derived to perform treatment comparisons, describing the PD response on both the population and individual levels. These model-based predictions can be further used to make the decision for the treatments to be tested in the following phases supporting TB drug development.

The herein presented pharmacometric model-based EBA analysis approach has many advantages over traditional analysis approaches. It provides a robust way to account for covariates that might be influential on TTP slope, and explain variability in EBA. Covariate analysis can be turned into an automated process, where prespecified parameter-covariate relationships are tested, and a higher *p*-value can be set for a backward deletion step of covariates to protect from inflating type 1 error (Lindbom et al., 2005). As IIV reflects the variability on the population level, the application of covariate analysis which can reduce and explain variability in efficacy, i.e., TTP slope is therefore central for detecting treatment arm differences in EBA trial as the power will increase compared to not accounting for IIV. In this example, introducing drug exposure (meropenem AUC) as a covariate on TTP slope decreased the IIV in TTP slope by 29%. Using the standardized approach presented here, all factors contributing to the power to detect EBA and treatment

TABLE 2 Sample size per group in an early bactericidal activity (EBA) clinical trial needed to detect an effect difference between two treatment groups with 80% power at a 5% significance level. Power calculations were performed using a mono-exponential time-to-positivity (TTP) model for different change in TTP between days 0 and 14 (TTP-EBA$_{0\text{-}14}$), inter-individual variability (IIV) in TTP slope, and increased effect difference values. For each scenario, power calculations included a minimum of 3 patients.

Effect difference between two treatments[a]	N per treatment group			
	TTP-EBA0-14 of 30 hours[b]		TTP-EBA0-14 of 152 hours[c]	
	Low IIV in TTP slope[d]	High IIV in TTP slope[e]	Low IIV in TTP slope[d]	High IIV in TTP slope[e]
+25%	64	>125	21	>125
+50%	20	90	7	87
+75%	10	48	3	50
+100%	6	31	3	37
+125%	5	23	3	31
+150%	4	18	3	28
+175%	3	15	3	26
+200%	3	13	3	26

[a]Increase in TTP-EBA$_{0\text{-}14}$ between two drugs.
[b]TTP-EBA$_{0\text{-}14}$ corresponding to treatment composed of 2 g meropenem thrice daily with 500 mg amoxicillin and 125 mg clavulanate thrice daily on days 1–14 (De Jager et al., 2022).
[c]TTP-EBA$_{0\text{-}14}$ corresponding to treatment composed of 6 g meropenem once daily with 2 × 1,000 mg amoxicillin and 62.5 mg clavulanate plus 400 mg bedaquiline once daily on days 1–14 (unpublished data, ClinicalTrials.gov Identifier: NCT04629378).
[d]Low IIV in TTP slope was 22% coefficient of variation (unpublished data, ClinicalTrials.gov Identifier: NCT04629378).
[e]High IIV in TTP slope was 104% coefficient of variation (De Jager et al., 2022).
EBA: early bactericidal activity.
IIV: inter-individual variability expressed on coefficient of variation scale.

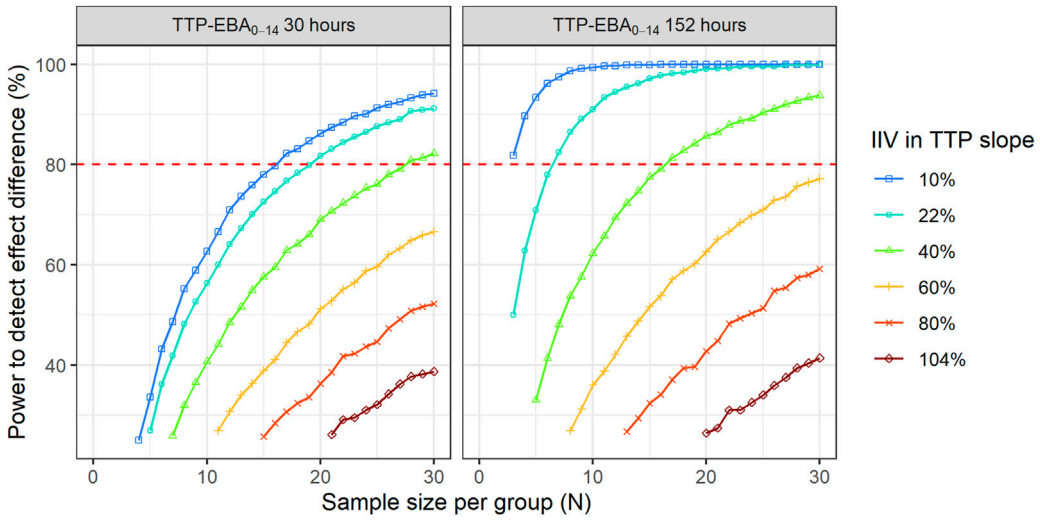

FIGURE 11
The impact of inter-individual variability (IIV) in early bactericidal activity (EBA) on the sample size and power to detect a difference between two treatment groups. The effect difference between the two treatment groups was set to 50%. The red dashed line represents 80% power.

differences between treatment arms can rationally be controlled for. As variability plays a pivotal role in EBA detection and treatment comparison, PK-PD model building is a critical step in the standardized pharmacometric model-based EBA analysis approach, as variability in PK translates into variability in PD, and incorporation of PK information in the model can decrease IIV in efficacy. Population PK models can be used to derive secondary PK parameters such as AUC, C_{max} and C_{min} to drive the PK-PD relationship as an alternative to use a PK-PD model linked to a population PK model. As such, the incorporation of secondary PK parameters into the EBA model may increase the power to detect EBA, and to find a difference between treatment

TABLE 3 Sample size per group in an early bactericidal activity (EBA) clinical trial needed to detect an effect difference between two treatment groups with 80% power at a 5% significance level under different inter-individual variability (IIV) in time-to-positivity (TTP) slope. Power calculations were performed using a mono-exponential model with an effect difference between two treatment groups of 50%, various changes in TTP between days 0 and 14 (TTP-EBA_{0-14}), and inter-individual variability (IIV) in TTP slope. For each scenario, power calculations included a minimum of 3 patients.

IIV in TTP slope (%)	N per treatment group	
	TTP-EBA_{0-14} of 30 h[a]	TTP-EBA_{0-14} of 152 h[b]
10	17	3
22	20	7
40	28	17
60	44	33
80	63	54
104	90	87

[a]TTP-EBA_{0-14} corresponding to treatment composed of 2 g meropenem thrice daily with 500 mg amoxicillin and 125 mg clavulanate thrice daily on days 1–14 (De Jager et al., 2022).
[b]TTP-EBA_{0-14} corresponding to treatment composed of 6 g meropenem once daily with 2 × 1,000 mg amoxicillin and 62.5 mg clavulanate plus 400 mg bedaquiline once daily on days 1–14 (unpublished data, ClinicalTrials.gov Identifier: NCT04629378).
EBA: early bactericidal activity.
CV: coefficient of variation.
IIV: inter-individual variability expressed on coefficient of variation scale.

groups by decreasing the variability in PD. Additionally, information about factors influencing variation in EBA biomarkers could be employed for individualized treatment, if deemed beneficial. Another advantage of PK-PD modeling over traditional EBA analysis is that half maximal effective concentration (EC_{50}) can be estimated with a smaller sample size. In the traditional EBA modeling, dose would be driving the effect if several different dose levels are given, thus, variability in PK will be attributed to variability in EBA and more participants would be required for estimating EBA. Further, in a design with only one dose level, exposure cannot be attributed for in a traditional EBA analysis whereas in the pharmacometric model-based EBA analysis, between patient variability in drug exposure can still be accounted for through a PK summary indice which reduces the IIV in TTP slope and thereby leads to smaller sample sizes compared without accounting for between patient variability in drug exposure.

The presented workflow is built on similar techniques for model development and evaluation as presented in the FDA and EMA guidelines for analysis and reporting (European Medicines Agency, 2008; Food and Drug Administration, 2022). Koele et al. summarize the different historical analysis methods presented in the literature for analyzing EBA trials and concluded that a standardized analysis method, accounting for different levels of variability in the data, could aid the generalization of study results and facilitate comparison between drugs or treatments (Koele et al., 2023).

The presented standardized approach can be easily coupled with other modeling approaches, like the multistate tuberculosis pharmacometric (MTP) model. In the MTP model, data is analyzed using a semi-mechanistic approach describing different bacterial subpopulations (Clewe et al., 2016). This approach determined the contribution of clofazimine to TB treatment and its effect on persisters (Faraj et al., 2020), while it showed no EBA effect when analyzed using a hierarchical Bayesian non-linear mixed effects regression model (Diacon et al., 2015). Incorporation of semi-mechanistic features would help establish EBA when empirical methods are not able to as for the situation for drugs with predominant persister efficacy, and this would further improve drug development.

While the application of the standardized approach was exemplified using TTP, the same approach can be used for CFU as well. In addition, this standardized approach is not limited to CFU or TTP biomarkers and can be easily applied to others. Many novel sputum-based biomarkers have been developed in recent years and are currently in various stages of clinical validation and regulatory approval, and may provide a near real-time quantification of mycobacterial health and/or load, like the molecular bacterial load assay (MBLA) (Sabiiti et al., 2020), RNA synthesis ratio (RS ratio) (Walter et al., 2021), and the lipoarabinomannan enzyme-linked immunosorbent assay (LAM-ELISA) (Jones et al., 2022). Therefore, the approach can be extended to new biomarkers as most of the steps would remain the same, and only the structural model might be different. In addition, novel and more informative biomarkers that better captures efficacy on persistent bacteria will make an empirical model approach more informative.

In addition to providing a structured approach to EBA trial analysis, the models developed using this approach can be further used in other clinical trial simulations and model-based sample size determinations. To exemplify this, models used to visualize the modeling workflow were used in MCMP to characterize the number of participants needed to detect EBA and to detect a difference between two treatment groups with a significance level of 5% and a target power of 80%. Using the presented approach, even extremely low EBA (TTP-EBA_{0-14} of 11 h) 13 and 8 participants was sufficient to reach 80% power for low IIV in TTP slope (22%) and high IIV in TTP slope (104%) scenarios (Figure 8), and less participants were required for treatments with stronger EBA (Table 1).

Sample sizes to identify a treatment difference between two groups were characterized in addition to detecting EBA. Here, it was observed that for drugs with low IIV in TTP slope, irrespective of TTP-EBA_{0-14} value, a sample size of 15 participants/arm were sufficient to detect a difference in EBA with at least 80% power at a 5% significance level when the effect difference is at least 75% for TTP-EBA_{0-14} of 30 h or 50% for

TTP-EBA$_{0\text{-}14}$ of 152 h (Table 2; Figure 10). For scenarios with high IIV in TTP slope, larger sample sizes were required to ensure the same power, as high IIV dilutes the intrinsic difference between the two treatment arms (Table 2; Figure 10). This is seen in the results presented in Figure 11, where the sample size needed to achieve 80% power decreased with decreasing IIV in TTP slope, indicating the importance of decreasing IIV in TTP slope to increase the power where determination of an effect difference is sought after. These results are in accordance with other investigations, where the difference between arms was detected in CFU but not in TTP, as IIV was higher in TTP compared to CFU (104% CV *versus* 48% CV) (De Jager et al., 2022).

In a model-based analysis, preclinical data can be integrated to inform about the expected EBA, which can be used to identify the sample size needed to achieve the desired power. As shown in this study, the standard set-up with 15 participants per arm might not be suitable for all treatments and adjustments might be needed. While a set-up with 15 participants is enough to detect even low TTP-EBA$_{0\text{-}14}$ of 11 h, the trial might be underpowered to detect a difference between two treatment groups. Due to this potential variability should be considered when designing the trial. One way to decrease IIV is to collect PK information in EBA studies and include this in the EBA analysis in order to increase the power and keep the sample sizes on the lower end. If no PK information is included in the EBA analysis, higher sample size should be enrolled into EBA trials.

In this work, an unexpected relationship between IIV in TTP slope and power to detect and/or compare the EBA of treatments was found. The scenario with less spread out individual TTP slope values (low IIV in TTP slope) resulted in a lower probability of overlapping confidence intervals between two arms, compared to high IIV in TTP slope. This subsequently led to a higher power to detect an effect difference when IIV in TTP slope was low, and the TTP slope itself had no impact here. While these results are in accordance with results from EBA detection of TTP-EBA$_{0\text{-}14}$ 152 h (TTP slope 0.0627 h/day), an opposite effect was observed for low TTP slope values (0.0174 h/day and lower). Here, high IIV in TTP slope resulted in smaller sample sizes compared to scenarios with low IIV in TTP slope, as etas of IIV in TTP slope were skewed towards large positive values of the TTP slope.

In conclusion, a robust standardized pharmacometric model-based EBA analysis approach established in close collaboration between microbiologists, clinicians, and pharmacometricians was presented. The work illustrates the importance of accounting for covariates and drug exposure in EBA analysis in order to increase the power of detecting EBA for a single treatment arm as well as differences in EBA between treatments arms in Phase 2a trials of TB drug development.

Data availability statement

The original contributions presented in the study are included in the article/Supplementary Material, further inquiries can be directed to the corresponding author.

Author contributions

LM, AF, RvW, CU, GvH, AD, and US analyzed data, conducted the analysis, interpreted the results, wrote the manuscript, revised the manuscript, and approved the submitted version. This work was carried out within the UNITE4TB consortium.

Funding

This project has received funding from the Innovative Medicines Initiative 2 Joint Undertaking (JU) under grant agreement No 101007873. The JU receives support from the European Union's Horizon 2020 research and innovation programme and EFPIA, Deutsches Zentrum für Infektionsforschung e. V (DZIF), and Ludwig-Maximilians-Universität München (LMU). EFPIA/AP contribute to 50% of funding, whereas the contribution of DZIF and the LMU University Hospital Munich has been granted by the German Federal Ministry of Education and Research.

Acknowledgments

The computations were enabled by resources in projects SNIC 2021/5-541 and SNIC 2021/23-657 provided by the Swedish National Infrastructure for Computing (SNIC) at UPPMAX, partially funded by the Swedish Research Council through grant agreement no. 2018-05973.

Conflict of interest

The authors declare that the research was conducted in the absence of any commercial or financial relationships that could be construed as a potential conflict of interest.

Publisher's note

Supplementary material

The Supplementary Material for this article can be found online at: https://www.frontiersin.org/articles/10.3389/fphar.2023.1150243/full#supplementary-material

References

Alffenaar, J.-W. C., Diacon, A. H., Simonsson, U. S. H., Srivastava, S., and Wicha, S. G. (2022). Pharmacokinetics and pharmacodynamics of anti-tuberculosis drugs: An evaluation of *in vitro*, *in vivo* methodologies and human studies. *Front. Pharmacol.* 13, 1063453. doi:10.3389/fphar.2022.1063453

Allaire, J., Xie, Y., McPherson, J., Lurasch, J., Ushey, K., Atkins, A., et al. (2020). rmarkdown: Dynamic documents for R. Available at: https://rmarkdown.rstudio.com (Accessed December 20, 2022).

Ammerman, N. C., Swanson, R. V., Tapley, A., Moodley, C., Ngcobo, B., Adamson, J., et al. (2017). Clofazimine has delayed antimicrobial activity against *Mycobacterium tuberculosis* both *in vitro* and *in vivo*. *J. Antimicrob. Chemother.* 72, 455–461. doi:10.1093/jac/dkw417

Ayoun Alsoud, R., Svensson, R. J., Svensson, E. M., Gillespie, S. H., Boeree, M. J., Diacon, A. H., et al. (2022). Combined quantitative tuberculosis biomarker model for time-to-positivity and colony forming unit to support tuberculosis drug development. Submitted. *Front. Pharmacol.*

Beal, S., Sheiner, L., Boeckmann, A., and Bauer, R. (1989). *NONMEM 7.4 users guides.*

Bowness, R., Boeree, M. J., Aarnoutse, R., Dawson, R., Diacon, A., Mangu, C., et al. (2015). The relationship between *Mycobacterium tuberculosis* MGIT time to positivity and cfu in sputum samples demonstrates changing bacterial phenotypes potentially reflecting the impact of chemotherapy on critical sub-populations. *J. Antimicrob. Chemother.* 70, 448–455. doi:10.1093/jac/dku415

Clewe, O., Aulin, L., Hu, Y., Coates, A. R. M., and Simonsson, U. S. H. (2016). A multistate tuberculosis pharmacometric model: A framework for studying anti-tubercular drug effects *in vitro*. *vitro. J. Antimicrob. Chemother.* 71, 964–974. doi:10.1093/jac/dkv416

Conradie, F., Diacon, A. H., Ngubane, N., Howell, P., Everitt, D., Crook, A. M., et al. (2020). Treatment of highly drug-resistant pulmonary tuberculosis. *N. Engl. J. Med.* 382, 893–902. doi:10.1056/NEJMoa1901814

De Jager, V., Gupte, N., Nunes, S., Barnes, G. L., van Wijk, R. C., Mostert, J., et al. (2022). Early bactericidal activity of meropenem plus clavulanate (with or without rifampin) for tuberculosis: The COMRADE randomized, phase 2A clinical trial. *Am. J. Respir. Crit. Care Med.* 205, 1228–1235. doi:10.1164/rccm.202108-1976OC

Diacon, A. H., Dawson, R., von Groote-Bidlingmaier, F., Symons, G., Venter, A., Donald, P. R., et al. (2015). Bactericidal activity of pyrazinamide and clofazimine alone and in combinations with pretomanid and bedaquiline. *Am. J. Respir. Crit. Care Med.* 191, 943–953. doi:10.1164/rccm.201410-1801OC

Diacon, A. H., Dawson, R., Von Groote-Bidlingmaier, F., Symons, G., Venter, A., Donald, P. R., et al. (2013). Randomized dose-ranging study of the 14-day early bactericidal activity of bedaquiline (TMC207) in patients with sputum microscopy smear-positive pulmonary tuberculosis. *Antimicrob. Agents Chemother.* 57, 2199–2203. doi:10.1128/AAC.02243-12

Diacon, A. H., Maritz, J. S., Venter, A., van Helden, P. D., Dawson, R., and Donald, P. R. (2012). Time to liquid culture positivity can substitute for colony counting on agar plates in early bactericidal activity studies of antituberculosis agents. *Clin. Microbiol. Infect.* 18, 711–717. doi:10.1111/j.1469-0691.2011.03626.x

Donald, P. R., and Diacon, A. H. (2008). The early bactericidal activity of anti-tuberculosis drugs: A literature review. *Tuberculosis* 88, S75–S83. doi:10.1016/S1472-9792(08)70038-6

Dorman, S. E., Nahid, P., Kurbatova, E. V., Phillips, P. P. J., Bryant, K., Dooley, K. E., et al. (2021). Four-month rifapentine regimens with or without moxifloxacin for tuberculosis. *N. Engl. J. Med.* 384, 1705–1718. doi:10.1056/NEJMoa2033400

European Medicines Agency (2017). Addendum to the guideline on the evaluation of medicinal products indicated for treatment of bacterial infections to address the clinical development of new agents to treat pulmonary disease due to *Mycobacterium tuberculosis*. Available at: https://www.ema.europa.eu/en/documents/scientific-guideline/addendum-guideline-evaluation-medicinal-products-indicated-treatment-bacterial-infections-address_en.pdf (Accessed December 20, 2022).

European Medicines Agency (2008). Guidance on reporting the results of population pharmacokinetic analyses. Available at: https://www.ema.europa.eu/en/documents/scientific-guideline/guideline-reporting-results-population-pharmacokinetic-analyses_en.pdf (Accessed March 24, 2023).

Faraj, A., Svensson, R. J., Diacon, A. H., and Simonsson, U. S. H. (2020). Drug effect of clofazimine on persisters explains an unexpected increase in bacterial load in patients. *Antimicrob. Agents Chemother.* 64, e01905-19–e01919. doi:10.1128/AAC.01905-19

Food and Drug Administration (2022). Population pharmacokinetics guidance for industry. Available at: https://www.fda.gov/media/128793/download (Accessed March 24, 2023).

Food and Drug Administration (2013). Pulmonary tuberculosis: Developing drugs for treatment (guidance for industry). Available at: https://fda.report/media/87194/Pulmonary-Tuberculosis–Developing-Drugs-for-Treatment.pdf (Accessed December 20, 2022).

Jindani, A., Aber, V. R., Edwards, E. A., and Mitchison, D. A. (1980). The early bactericidal activity of drugs in patients with pulmonary tuberculosis. *Am. Rev. Respir. Dis.* 121, 939–949. doi:10.1164/arrd.1980.121.6.939

Jindani, A., Doré, C. J., and Mitchison, D. A. (2003). Bactericidal and sterilizing activities of antituberculosis drugs during the first 14 days. *Am. J. Respir. Crit. Care Med.* 167, 1348–1354. doi:10.1164/rccm.200210-1125OC

Jones, A., Saini, J., Kriel, B., Via, L. E., Cai, Y., Allies, D., et al. (2022). Sputum lipoarabinomannan (LAM) as a biomarker to determine sputum mycobacterial load: Exploratory and model-based analyses of integrated data from four cohorts. *BMC Infect. Dis.* 22, 327. doi:10.1186/s12879-022-07308-3

Karlsson, M. O., Beal, S. L., and Sheiner, L. B. (1995). Three new residual error models for population PK/PD analyses. *J. Pharmacokinet. Biopharm.* 23, 651–672. doi:10.1007/BF02353466

Koele, S. E., Phillips, P. P., Upton, C. M., van Ingen, J., Simonsson, U. S., Diacon, A. H., et al. (2023). Early bactericidal activity studies for pulmonary tuberculosis: A systematic review of methodological aspects. *Int. J. Antimicrob. Agents* 106775, 106775. doi:10.1016/j.ijantimicag.2023.106775

Lindbom, L., Pihlgren, P., and Jonsson, N. (2005). PsN-toolkit—a collection of computer intensive statistical methods for non-linear mixed effect modeling using NONMEM. *Comput. Methods Programs Biomed.* 79, 241–257. doi:10.1016/j.cmpb.2005.04.005

R Core Team (2020). R: A language and environment for statistical computing. Available at: http://www.r-project.org/(Accessed December 20, 2022).

RStudio Team (2022). RStudio: Integrated development environment for R. Available at: http://www.rstudio.com/(Accessed December 20, 2022).

Sabiiti, W., Mtafya, B., Lima, D. A., Dombay, E., Baron, V. O., Azam, K., et al. (2020). A tuberculosis molecular bacterial load assay (TB-MBLA). *J. Vis. Exp.* doi:10.3791/60460

Savic, R. M., and Karlsson, M. O. (2009). Importance of shrinkage in empirical Bayes estimates for diagnostics: Problems and Solutions. *AAPS J.* 11, 558–569. doi:10.1208/s12248-009-9133-0

Svensson, R. J., Gillespie, S. H., and Simonsson, U. S. H. (2017). Improved power for TB Phase IIa trials using a model-based pharmacokinetic–pharmacodynamic approach compared with commonly used analysis methods. *J. Antimicrob. Chemother.* 72, 2311–2319. doi:10.1093/jac/dkx129

Svensson, R. J., and Simonsson, U. (2016). Application of the multistate tuberculosis pharmacometric model in patients with rifampicin-treated pulmonary tuberculosis. *CPT Pharmacometrics Syst. Pharmacol.* 5, 264–273. doi:10.1002/psp4.12079

van Wijk, R. C., Mockeliunas, L., Van den Hoogen, G., Upton, C. M., Diacon, A. H., et al. (2022). *Reproducibility in pharmacometrics applied in a phase III trial of BCG-vaccination for COVID-19.*

Vong, C., Bergstrand, M., Nyberg, J., and Karlsson, M. O. (2012). Rapid sample size calculations for a defined likelihood ratio test-based power in mixed-effects models. *Am. Assoc. Pharm. Sci.* 14, 176–186. doi:10.1208/s12248-012-9327-8

Walter, N. D., Born, S. E. M., Robertson, G. T., Reichlen, M., Dide-Agossou, C., Ektnitphong, V. A., et al. (2021). *Mycobacterium tuberculosis* precursor rRNA as a measure of treatment-shortening activity of drugs and regimens. *Nat. Commun.* 12, 2899. doi:10.1038/s41467-021-22833-6

Working Group on New TB Drugs (2022). Clinical pipeline. Available at: https://www.newtbdrugs.org/pipeline/clinical (Accessed December 20, 2022).

World Health Organization (2021). Tuberculosis. Available at: https://www.who.int/news-room/fact-sheets/detail/tuberculosis#:~:text=Key%20facts,with%20tuberculosis%20(TB)%20worldwide. (Accessed December 20, 2022).

Zhang, L., Beal, S. L., and Sheiner, L. B. (2003). Simultaneous vs. Sequential analysis for population PK/PD data I: Best-case performance. *J. Pharmacokinet. Pharmacodyn.* 30, 387–404. doi:10.1023/b:jopa.0000012998.04442.1fJOPA.0000012998.04442.1f

frontiers | Frontiers in Pharmacology

TYPE Original Research
PUBLISHED 25 April 2023
DOI 10.3389/fphar.2023.1055329

OPEN ACCESS

EDITED BY
Sebastian G. Wicha,
University of Hamburg, Germany

REVIEWED BY
Oscar Della Pasqua,
University College London,
United Kingdom
Hussam Wahab Al-Humadi,
University of Babylon, Iraq

*CORRESPONDENCE
Roeland E. Wasmann,
roeland.wasmann@uct.ac.za

†These authors have contributed equally to this work and share last authorship

SPECIALTY SECTION
This article was submitted to Pharmacology of Infectious Diseases, a section of the journal Frontiers in Pharmacology

RECEIVED 27 September 2022
ACCEPTED 01 March 2023
PUBLISHED 25 April 2023

CITATION
Wasmann RE, Masini T, Viney K, Verkuijl S, Brands A, Hesseling AC, McIlleron H, Denti P and Dooley KE (2023), A model-based approach for a practical dosing strategy for the short, intensive treatment regimen for paediatric tuberculous meningitis.
Front. Pharmacol. 14:1055329.
doi: 10.3389/fphar.2023.1055329

A model-based approach for a practical dosing strategy for the short, intensive treatment regimen for paediatric tuberculous meningitis

Roeland E. Wasmann [1]*, Tiziana Masini [2], Kerri Viney [2], Sabine Verkuijl [2], Annemieke Brands [2], Anneke C. Hesseling [3], Helen McIlleron [1,4], Paolo Denti [1†] and Kelly E. Dooley [5†]

[1]Division of Clinical Pharmacology, Department of Medicine, University of Cape Town, Cape Town, South Africa, [2]World Health Organization, Global Tuberculosis Programme, Geneva, Switzerland, [3]Desmond Tutu TB Centre, Department of Paediatrics and Child Health, Faculty of Medicine and Health Sciences, Stellenbosch University, Cape Town, South Africa, [4]Wellcome Centre for Infectious Diseases Research in Africa (CIDRI-Africa), Institute of Infectious Disease and Molecular Medicine, University of Cape Town, Cape Town, South Africa, [5]Division of Infectious Diseases, Vanderbilt University Medical Center, Nashville, TN, United States

Following infection with *Mycobacterium tuberculosis*, young children are at high risk of developing severe forms of tuberculosis (TB) disease, including TB meningitis (TBM), which is associated with significant morbidity and mortality. In 2022, the World Health Organization (WHO) conditionally recommended that a 6-month treatment regimen composed of higher doses of isoniazid (H) and rifampicin (R), with pyrazinamide (Z) and ethionamide (Eto) (6HRZEto), be used as an alternative to the standard 12-month regimen (2HRZ-Ethambutol/10HR) in children and adolescents with bacteriologically confirmed or clinically diagnosed TBM. This regimen has been used in South Africa since 1985, in a complex dosing scheme across weight bands using fixed-dose combinations (FDC) available locally at the time. This paper describes the methodology used to develop a new dosing strategy to facilitate implementation of the short TBM regimen based on newer globally available drug formulations. Several dosing options were simulated in a virtual representative population of children using population PK modelling. The exposure target was in line with the TBM regimen implemented in South Africa. The results were presented to a WHO convened expert meeting. Given the difficulty to achieve simple dosing using the globally available RH 75/50 mg FDC, the panel expressed the preference to target a slightly higher rifampicin exposure while keeping isoniazid exposures in line with those used in South Africa. This work informed the WHO operational handbook on the management of TB in children and adolescents, in which dosing strategies for children with TBM using the short TBM treatment regimen are provided.

KEYWORDS

WHO, NONMEM, paediatric dosing, rifampicin, rifampin, isoniazid, pyrazinamide, ethionamide

Introduction

Tuberculosis (TB) is a major global health problem with an estimated 9.9 million people falling ill and 1.5 million deaths, in 2020 (World Health Organization, 2021). Following infection with *Mycobacterium tuberculosis*, young children are particularly at risk of developing severe forms of TB, including TB meningitis (TBM), which is associated with significant morbidity and mortality (mortality estimated at 19.3%) and high rates (36.7%) of neurological sequelae among TBM survivors. Up to 15% of children with TB are diagnosed with TBM with an estimated 100000 cases per year. Given the severity of this form of TB, children are often hospitalized for diagnostic evaluation and treatment (Schaaf et al., 2007; Chiang et al., 2014; Wilkinson et al., 2017).

Early treatment with a combination of TB medicines and with doses aimed to optimize efficacy, can be life-saving and can potentially reduce neurological sequelae. However, data from randomized controlled clinical trials to inform optimal treatment regimens for TBM are lacking. Historically, the treatment of TBM in adults and children has used similar medicines as for the treatment of drug-susceptible pulmonary TB with the exception of replacing ethambutol with streptomycin and extending treatment to 12 months (World Health Organization, 2010a). In 2010, the World Health Organization (WHO) released a rapid advice communication recommending a regimen of 12 months duration for the treatment of TBM, consisting of isoniazid (H), rifampicin (R), pyrazinamide (Z), and ethambutol (E) for 2 months, followed by isoniazid and rifampicin for an additional 10 months (2HRZE/10HR); the recommended drug doses were the same as those for the treatment of pulmonary TB (i.e., HRZE 10/15/35/20 mg/kg daily) (World Health Organization, 2010b).

Varying penetration of first-line drugs through the blood-brain and the blood-cerebrospinal fluid (CSF) barriers in and a poor understanding of pharmacokinetics at the site of action (including the effect of protein binding) have historically made it difficult to determine the composition of the ideal regimen and dosing strategy to treat TBM. Indeed, while isoniazid and pyrazinamide show good CSF penetration, this is not true for ethambutol and rifampicin: ethambutol's penetration into the CSF is poor, and rifampicin concentrations observed in the CSF are 5%–10% compared to those in plasma (Donald, 2010a; Donald, 2010b). For people with TBM, concerns about low concentrations of ethambutol and rifampicin at the site of disease have led clinicians to explore alternative options to ethambutol and the use of higher doses of rifampicin and isoniazid to achieve therapeutic concentrations in the brain and CSF (Ruslami et al., 2013). Some small trials have demonstrated benefits when using higher rifampicin dosages in adults and children with TBM (Ruslami et al., 2013; Savic et al., 2015; Svensson et al., 2020; Paradkar et al., 2022); larger, definitive trials are underway.

In South Africa, for several decades, paediatricians have been using a 6-month regimen with higher rifampicin and isoniazid doses (compared to standard WHO recommended dosing for the treatment of drug susceptible pulmonary TB) and replacing ethambutol with ethionamide (Eto) (6HRZEto) to treat TBM (Department of Health - Republic of South Africa, 2021). In observational cohorts, favourable treatment outcomes and no relapses have been observed with this regimen in a subset of patients who were followed up for 2 years after completing treatment (Donald et al., 1998). In one study, 95 children received the 6-month regimen, and although mortality was high (13 children died), the majority of children recovered. 14 In a subsequent study in 184 children, the mortality rate was 3.8% and although 5.6% of the children developed grade 3 or four adverse events related to elevated liver enzymes, all were able to restart the original regimen after liver enzymes normalised (van Toorn et al., 2014). This regimen, included in the South African national tuberculosis guidelines, is administered using daily doses of 20 mg/kg for isoniazid, rifampicin, and ethionamide, and 40 mg/kg for pyrazinamide.

A systematic review and meta-analysis was conducted to compare the effectiveness of the short, intensive regimen used in South Africa *versus* the WHO-recommended 12-month regimen to inform a WHO guideline update (Sulis et al., 2022). The authors report a treatment success (survival with or without sequelae) in 95% (95%CI 74%–99%) of the participants in the 6-month regimen *versus* 75% (95% CI: 69%–81%) in the 12-month regimen. Also in terms of neurological sequelae among survivors the 6-month regimen performed well with 36% (95% CI, 30%–43%) *versus* 66% (95% CI, 55%–75%) in the 12-month regimen (Sulis et al., 2022). Based on this, in March 2022, WHO recommended, that children and adolescents with bacteriologically confirmed or clinically diagnosed TBM (without suspicion or evidence of multi-drug resistant or rifampicin-resistant tuberculosis) could receive the 6-month intensive regimen (6HRZEto) as an alternative option to the 12-month regimen (2HRZE/10HR). (World Health Organization, 2022a).

In South Africa, the 6-month regimen had been administered using a dispersible fixed-dose combination (FDC) of RH 60/60 mg and additional 500-mg pyrazinamide and 250-mg ethionamide tablets as single-drug formulations. The dosing strategy for this regimen in the South African national guideline contains 14 weight bands between 3 and 25 kg, and some weight bands are dosed with quartered or halved tablets (Department of Health - Republic of South Africa, 2021). Moreover, the 1:1 isoniazid and rifampicin FDC used in South Africa is not globally available. Therefore, after the WHO recommendation was made, WHO aimed to develop a simple-to-implement dosing strategy that would achieve exposures in line with the South African 6-month regimen using globally available, child-friendly formulations.

Importantly, the dosing strategy aimed to achieve balanced exposure across weight bands. This acknowledges that administering the same mg/kg dose in all children can be detrimental, as it does not deliver similar exposures across children. It is known that the dose-exposure relationship across different weights and ages is non-linear due to the effects of allometry and maturation (Anderson and Holford, 2008; Denti et al., 2022a). This results in smaller children achieving lower exposures when receiving the same mg/kg dose, unless they are very young, with immature organ function, in which case the exposures may be higher (Denti et al., 2022a). Since TBM is highly fatal and causes significant morbidity in children, it is a condition for which precise dosing is especially critical.

To seek advice on the most suitable dosing strategy for the newly recommended 6-month intensive TBM regimen, WHO convened

an expert consultation involving experts in clinical pharmacology, pharmacokinetics, and pharmacodynamics, as well as TB paediatricians and researchers. First, these experts reviewed the data collected in a meta-analysis to explore if 6HRZEto could be used (Sulis et al., 2022). After the advice that this regimen could indeed be recommended by the WHO, a dosing table needed to be created that took the globally available formulations into account. The process of the expert consultations was reported previously (World Health Organization, 2022b), while in this paper, we describe the methods and processes used to establish the new dosing guidance for the short, intensive TBM regimen, which involved running simulations incorporating established pharmacokinetic models. These simulations informed discussions around the best dosing strategy for the short, intensive TBM regimen, which led to the WHO guidance currently included in the operational handbook.

TABLE 1 Globally available formulations at the time of dosing table development.

Child-friendly formulations	Adult formulations
R/H 75/50 mg dispersible tablet[a]	R/H 150/75 mg film-coated tablet
Pyrazinamide 150 mg dispersible tablet[a]	R/H 300/150 mg film-coated tablet
Ethionamide 125 mg dispersible tablet[a]	Isoniazid 300 mg uncoated tablet
R/H/Z 75/50/150 mg dispersible tablet	Pyrazinamide 400 mg uncoated tablet
Isoniazid 100 mg dispersible tablet	Pyrazinamide 500 mg uncoated tablet
	Ethionamide 250 mg uncoated tablet

[a]The formulations in bold were the preferential formulations for the dosing tables.
Abbreviations: R, rifampicin; H, isoniazid; Z, pyrazinamide.

Methods

Pharmacokinetic models and Monte Carlo simulations

Our goal was to estimate plasma drug exposures that are achieved with different dosing strategies i.e., the original South African regimen with old 1:1 RH formulations and alternatives with currently available 3:2 RH formulations. We used previously published pharmacokinetic models of rifampicin, isoniazid, pyrazinamide, and ethionamide to simulate plasma drug exposures, i.e., steady-state area under the time-concentration curve over a 24-h dose interval ($AUC_{0\text{-}24}$) (Nyberg et al., 2020; Denti et al., 2022b). These models include the effect of body size (either total body weight or fat-free mass) on clearance and volume of distribution (i.e., allometric scaling with fixed exponents of 0.75 and 1 on clearance and volume of distribution, respectively) and the effect of age on clearance (i.e., maturation) (Janmahasatian et al., 2005). The model for rifampicin also included the effect of age on bioavailability—whereby younger children have a lower bioavailability—and saturable hepatic elimination which helps describe the dose-exposure non-linearity seen with higher doses of rifampicin. The isoniazid model also included the effect of age on bioavailability and, additionally, the N-acetyltransferase 2 (NAT2) acetylator status to account for slow acetylating individuals having only half the clearance of fast acetylators (Denti et al., 2022b). Finally, the model of ethionamide included the drug-drug interaction of rifampicin on ethionamide clearance (Nyberg et al., 2020). All simulations were performed using NONMEM (version 7.4.2) and Perl-Speaks-NONMEM (version 4.8.8). R (version 4.1.2) was used for pre- and post-processing of data.

We performed Monte Carlo simulations using a representative virtual paediatric population of 160,000 children with a uniform weight distribution between 3 and 35 kg (5,000 children per 1-kg weight band), 50% female (Wasmann et al., 2021). This provided plausible and coherent values of age, weight, height, and sex that are covariates in the population PK models. The proportions of NAT2 acetylator status in the population, important for isoniazid pharmacokinetics, were set to 44% slow, 42% intermediate, and 14% fast, as reported in a study across eight high-burden countries (Gausi et al., 2021).

Pharmacokinetic target

Currently, there is no evidence of a pharmacokinetic-pharmacodynamic target for paediatric TBM. With a lack of evidence, the $AUC_{0\text{–}24}$ in steady-state conditions is the most robust index to compare exposures between two treatments. To evaluate whether the proposed dosing regimens achieve the desired exposure, we needed to define a target range within which the drug levels were deemed acceptable. As a first step, since no PK data were directly available from children receiving the South African 6-month regimen, we used population PK modelling and the original South African dosing guidelines to estimate the values of expected exposure levels. In addition to the original regimen, we also investigated rifampicin doses up to 30 mg/kg and isoniazid doses between 15 and 20 mg/kg. For each scenario, we translated the mg/kg dose to an exposure ($AUC_{0\text{–}24}$) by using the median of the simulated exposures in the population over the whole weight range (i.e., these were the exposures that are expected in the South African 6-month regimen). These targets were presented to and discussed by an expert panel convened by WHO, who ultimately selected a target range for each drug.

Dose selection

After selection of the target exposure range, we estimated the dose for each 1-kg weight band and each drug with population pharmacokinetic models, using a previously described method (Svensson et al., 2018). We developed an MS Excel dosing tool that would allow us and the expert panel to quickly visualise at a glance the approximate target attainment in each 1-kg weight band for each drug. The tool allows the user to select which formulations will be used, choosing amongst the five available child-friendly formulations and six adult formulations (shown in Table 1), and the number of tablets to administer in each specific weight range. With the tool, one can visualize how closely the selected dosing approaches will reach a dose resulting in an exposure within target exposures for each 1-kg weight band; additionally, there is a

stratification for children under 3 months of age (with immature metabolism). Colour codes in the dosing tool indicate whether the exposure in the 1-kg band is expected to be within the range and, if not, how far (in percent) it is above or below the target. In the context of the advisory meeting, doses could be changed in the tool to explore different dosing strategies. Once final dosing was agreed upon, full simulations with the population pharmacokinetic models were performed to predict exact exposures.

When adjusting the dosing with the tool to select the most suitable regimen, several practical considerations were kept in mind. In general, narrow weight bands, and as such more complexity, are acceptable to attain a more precise dose given the serious nature of the disease. However, we aimed to minimize the number of weight bands to simplify dosing for a global audience. Children below 3 months of age have different pharmacokinetics due to immature organs and were considered as a separate group to improve their dose. To minimize drug manipulation, we aimed at implementing the dosing with whole tablets, whenever acceptable in terms of achieving the exposure target. When the use of half tablets was necessary to deliver the required exposure, this was allowed, especially since some of the formulations used have a functional scoring line or can be administered as aliquots after being dispersed in water. However, quartered tablets (used in the dosing strategy implemented in South Africa) were avoided as they would complicate administration and increase the chance of dosing errors. Wherever possible, we aimed to use FDCs to reduce tablet burden, in line with WHO's recommendation to use FDCs over single-drug formulations for the treatment of people with drug-susceptible TB (World Health Organization, 2022c). However, the proposed dosing strategy is implemented only by using the RH 75/50 mg FDC, and not the RHZ 75/50/150 mg FDC, since the wrong ratio between HR and Z in the latter would have required additional top-ups of isoniazid and rifampicin, thus increasing tablet burden and requiring the availability and stocking of multiple formulations, some of which are not readily available in many settings. For similar reasons, we refrained from using standalone isoniazid formulations as a top-up.

Given the drug formulations that are widely available globally (Table 1), we designed a dosing strategy using child-friendly formulations for all children weighing between 3 and 35 kg. We also prepared two alternative approaches for children above 25 kg using adult formulations and either the 400 mg or the 500 mg pyrazinamide tablet.

Results

The exposures predicted using the population pharmacokinetic models applied to historic South African dosing guidelines (RH in 1:1 formulation, weight bands as per 2011 guidance) are visualized in

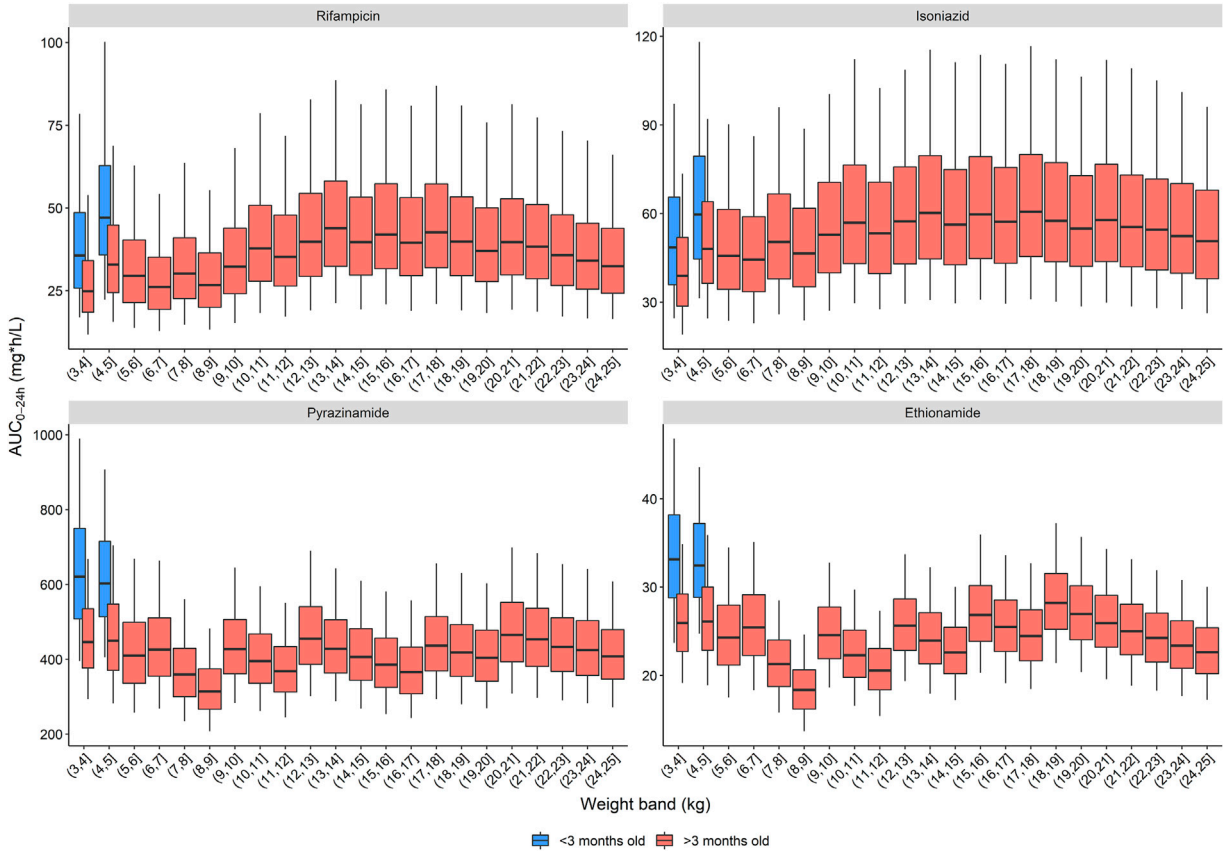

FIGURE 1
Area under the concentration-time curve over a 24-h dose interval (AUC_{0-24h}) after dosing children according to the South African dosing table. The box represents the median and 25th and 75th percentile. The whiskers represent the 5th and 95th percentile.

TABLE 2 Dosing table using child-friendly formulations for children from 3 to 35 kg. The red and white horizontal bands in the formulation's column represent the weight bands receiving the same dose. The colours in the last columns show if exposures are expected to be within (green) or outside the target range where yellow represents the percentage below the lower bound of the target range and purple represents the percentage above the higher bound of the target range. Abbreviations: *p*, child-friendly formulation; R, rifampicin; H, isoniazid; Z, pyrazinamide; Eto, ethionamide.

	Formulations				Simulated exposure				Difference from target range			
Weight band (kg)	pRH 75/50	pZ 150	pETO 125	Tablet burden	Rifampicin (mg·h/L)	Isoniazid (mg·h/L)	Pyrazinamide (mg·h/L)	Ethionamide (mg·h/L)	Rifampicin (%)	Isoniazid (%)	Pyrazinamide (%)	Ethionamide (%)
<3 months old												
3–4	1.5	0.5	0.5	4	89.6	59.9	371	33.1	14.6%	0.8%	−4.6%	9.8%
4–5	1.5	0.5	0.5	4	63.6	50.2	292	26.3	0.0%	0.0%	−24.9%	0.0%
>3 months old												
3–4	1.5	1	0.5	4	59.3	47.9	521	25.7	0.0%	0.0%	0.0%	0.0%
4–5	2	1	0.5	4	68.4	52.8	427	20.8	0.0%	0.0%	0.0%	−5.1%
5–6	2.5	1.5	1	6	69.5	54.6	491	32.2	0.0%	0.0%	0.0%	6.8%
6–7	3	2	1	6	68.7	56.1	506	25.3	0.0%	0.0%	0.0%	0.0%
7–8	3	2	1	6	56.0	50.4	434	21.1	0.0%	0.0%	0.0%	−3.7%
8–9	3.5	2.5	1.5	9	62.7	54.3	475	27.5	0.0%	0.0%	0.0%	0.0%
9–10	3.5	2.5	1.5	9	58.1	51.6	432	24.7	0.0%	0.0%	0.0%	0.0%
10–11	4	3	2	9	65.9	53.5	473	29.8	0.0%	0.0%	0.0%	0.0%
11–12	4	3	2	9	61.8	51.0	442	27.4	0.0%	0.0%	0.0%	0.0%
12–13	4	3	2	9	56.1	47.3	406	25.6	0.0%	−0.6%	0.0%	0.0%
13–14	5	3.5	2	11	73.2	55.3	450	24.1	0.0%	0.0%	0.0%	0.0%
14–15	5	3.5	2	11	66.7	53.0	427	22.6	0.0%	0.0%	0.0%	0.0%
15–16	5	3.5	2	11	60.2	50.1	403	21.4	0.0%	0.0%	0.0%	−2.4%
16–17	6	4	2.5	13	73.4	57.1	438	25.6	0.0%	0.0%	0.0%	0.0%
17–18	6	4	2.5	13	68.9	54.6	419	24.5	0.0%	0.0%	0.0%	0.0%
18–19	6	4	2.5	13	64.2	52.5	401	23.3	0.0%	0.0%	0.0%	0.0%
19–20	6	4	2.5	13	59.2	50.1	386	22.5	0.0%	0.0%	−0.7%	0.0%
20–21	7	5	3	15	70.6	56.3	468	26.0	0.0%	0.0%	0.0%	0.0%
21–22	7	5	3	15	67.5	54.7	448	25.1	0.0%	0.0%	0.0%	0.0%
22–23	7	5	3	15	64.4	52.5	432	24.3	0.0%	0.0%	0.0%	0.0%
23–24	7	5	3	15	60.8	51.6	422	23.4	0.0%	0.0%	0.0%	0.0%
24–25	7	5	3	15	56.6	49.7	409	22.6	0.0%	0.0%	0.0%	0.0%
25–26	9	6	4	19	81.1	61.7	473	29.3	3.7%	3.9%	0.0%	0.0%
26–27	9	6	4	19	76.3	60.3	465	28.6	0.0%	1.5%	0.0%	0.0%
27–28	9	6	4	19	73.3	58.8	453	27.7	0.0%	0.0%	0.0%	0.0%
28–29	9	6	4	19	69.9	57.2	442	27.0	0.0%	0.0%	0.0%	0.0%
29–30	9	6	4	19	66.8	56.0	426	26.2	0.0%	0.0%	0.0%	0.0%
30–31	10	6	4	20	75.8	60.2	419	25.5	0.0%	1.3%	0.0%	0.0%
31–32	10	6	4	20	71.5	58.7	406	25.2	0.0%	0.0%	0.0%	0.0%
32–33	10	6	4	20	69.3	58.2	400	24.4	0.0%	0.0%	0.0%	0.0%
33–34	10	6	4	20	68.0	56.7	390	23.9	0.0%	0.0%	0.0%	0.0%
34–35	10	6	4	20	64.3	55.0	383	23.3	0.0%	0.0%	−1.5%	0.0%
					66.9	54.6	430	25.2	0.0%	0.0%	0.0%	0.0%

10.3389/fphar.2023.1055329

Figure 1 (Department of Health - Republic of South Africa, 2021). Overall, the expected median exposures of all four drugs are balanced over the whole weight range, except for children below 3 months of age. In these youngest children, exposures are higher than for older children of similar weights, and this is especially significant with pyrazinamide and ethionamide. The isoniazid exposure is highly variable due to the impact of NAT2 acetylator status.

Attaining exposures similar to those achieved historically with the RH 60/60 formulation using the newer globally available dispersible RH 75/50 mg FDC would require additional isoniazid top-ups using fractions of a tablet, a dosing strategy judged by the panel to be too complex and undesirable. As a compromise, one could increase the rifampicin target exposure and lower the isoniazid target exposure modestly. Exposures after doses up to 30 mg/kg rifampicin and down to 15 mg/kg isoniazid were simulated and presented to the expert panel. They approved of a compromise aiming at 22.5–30 mg/kg rifampicin dose while keeping the isoniazid dose at 15–20 mg/kg. For pyrazinamide and ethionamide, a target dose of 32–44 mg/kg and 16–22 mg/kg, respectively, were deemed acceptable by the panel.

For each of the recommended dose ranges, we simulated the exposure in children up to 25 kg and calculated the overall median AUC_{0-24h}. The median exposures achieved at the lower and upper end of the dose range were used to define the target exposure range, e.g., from 22.5 to 30 mg/kg and 15 and 20 mg/kg for rifampicin and isoniazid, respectively. Exposure targets of 54.5–78.2, 47.6 to 59.4, 389 to 535, and 21.9–30.1 mg h/L were used for rifampicin, isoniazid, pyrazinamide, and ethionamide, respectively. The estimated doses per 1 kg weight band and per drug to get an exposure within the target range are included in the dosing tool, which has been added to the Supplementary materials.

Three dosing strategies were recommended by the expert panel. The first, using only child-friendly formulations, is shown in Table 2 and Figure 2. We used three child-friendly formulations: the rifampicin/isoniazid 75/50 mg dispersible tablet, the 150 mg pyrazinamide dispersible tablet, and the 125 mg ethionamide dispersible tablet. A total of twelve weight bands were necessary for adequate dosing for the whole age and weight range, six of these for children below 10 kg. Although the median exposure in most 1 kg bands falls within the range, there were specific challenges in achieving exact targets for children below 3 months of age. Overall, the tablet burden using this approach is high, especially in children above 25 kg who will need to take 19 or more tablets daily.

The second and third dosing strategies employed adult formulations. Using adult tablets in children above 25 kg will lower pill burden, but the drug ratio of rifampicin and isoniazid is different (75/50 in child-friendly *versus* 150/75 in adult FDCs). As a result, there is no strategy possible where both rifampicin and isoniazid exposures are within the target range: either rifampicin exposure is above, or isoniazid exposure is below the target range. Since isoniazid dosing for TBM is already on the higher end of the doses commonly recommended to treat drug susceptible TB and given concerns about isoniazid's related hepatotoxicity, the expert panel opted to have isoniazid exposures slightly below the target range. Two strategies using adult formulations are presented here: one using the 400 mg pyrazinamide adult tablet (Table 3) and one with the 500 mg adult tablet, given that both are available to national TB programmes (Table 4). The use of adult tablets in children above 25 kg can reduce the tablet burden to a maximum of 10 tablets per day.

Discussion

In this paper we describe how a practical dosing strategy for the treatment of paediatric TBM with the 6-month regimen using available child-friendly formulations was developed using population pharmacokinetic modelling and simulation. In the recommended dosing strategies, we aimed to find a compromise between close alignment with the target drug exposures *versus* practical considerations necessary for global implementation. Narrow weight bands and split tablets for children below 10 kg were necessary to avoid exposures outside the target range. For children above 10 kg, it was possible to employ a simpler approach and develop a dosing strategy with broader weight bands and, for the majority, use only whole tablets. children below 4 kg and younger than 3 months of age will receive a dose that will likely result in an exposure that is modestly above the selected target range for rifampicin, isoniazid and ethionamide and slightly below that for pyrazinamide. On the other hand, it is expected that these children will quickly grow and gain weight and move into higher weight bands rapidly. Moreover, these children would most likely be hospitalised and monitored for any possible toxicity.

The WHO convened a panel of global experts with expertise in clinical pharmacology, clinical management of paediatric TB, research, policy, community engagement, and programmatic implementation. All simulations were presented to the panel who considered efficacy, safety as well as implementation considerations (such as availability of drug formulations and feasibility of administration) before making their final dosing recommendations to WHO. The panel gave their recommendations in light of current evidence and practices regarding TBM, including the following considerations. i) TBM has high mortality, and post-treatment neurologic sequelae (which occur in about 53% of survivors) (Chiang et al., 2014). ii) The safety of a given drug may be different in ill, hospitalized children than in children receiving outpatient treatment for non-severe forms of TB, but hospitalised children are more closely monitored. iii) There are emerging data on the efficacy and safety of drugs in adult TBM that may be informative for paediatric TBM, especially for rifampicin, even at higher doses than currently recommended (Ruslami et al., 2013; Savic et al., 2015; Svensson et al., 2020). iv) We have good knowledge of the developmental pharmacology of drugs used in RHZEto and can use that information to achieve targets and reduce variability in drug exposures across children of different ages and weights. Final decisions regarding pharmacokinetic targets and dose selection were made by the panel.

In this study, we endeavoured to match the exposures children experienced when receiving the historic 6HRZEto regimen in South Africa. Whether or not those exposures are optimal for the treatment of paediatric TBM is unknown. Practically speaking, the use of the RH 75/50 mg FDC (rather than the RH 60/60 mg FDC) means that a scenario where both drugs are dosed at 20 mg/kg is no longer possible. As a compromise, in the recommended dosing strategies rifampicin exposure is higher while isoniazid is lower,

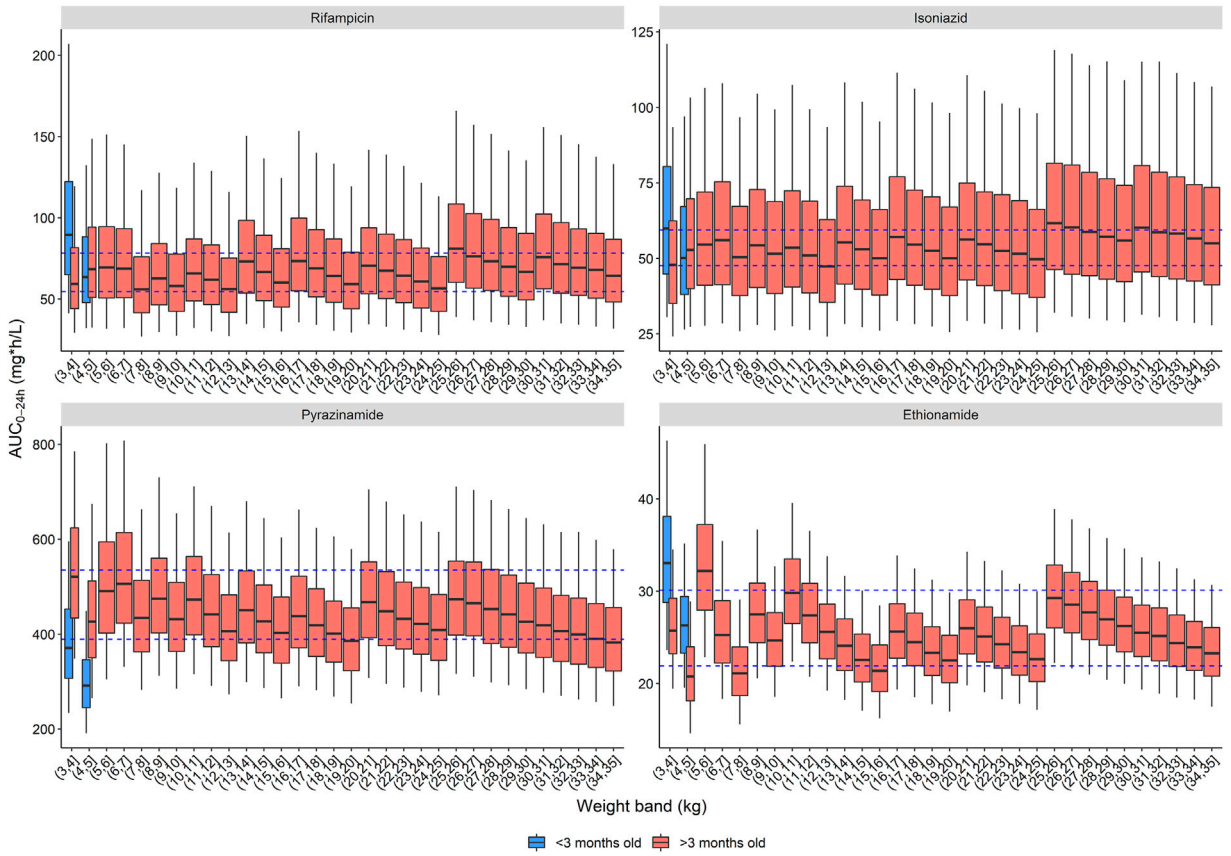

FIGURE 2
Area under the concentration-time curve over a 24-h dose interval (AUC_{0-24h}) after the WHO recommended dose for children with child-friendly formulations. The box represents the median and 25th and 75th percentile. The whiskers represent the 5th and 95th percentile. The dashed blue lines represent the target ranges.

compared to the historic South African dosing strategy. Some adult studies suggest even higher exposures may be beneficial, and a small trial among children suggests that neurocognitive outcomes may be improved with higher rifampicin dosing (Paradkar et al., 2022). A small, randomized trial in adult patients with TBM patients found that mortality decreased from 65% to 35% in patients in which the rifampicin dose was increased from 450 mg delivered orally to 600 mg given intravenously. The higher dose, given intravenously, resulted in a three-fold increase in rifampicin exposure (Ruslami et al., 2013). Furthermore, a model-based study showed that a 30 mg/kg oral rifampicin dose in children would be required for sufficient cerebrospinal fluid exposure and reduction in mortality (Savic et al., 2015). Finally, in a meta-analysis of randomized trials conducted among Indonesian adults with TBM, the exposure of rifampicin was strongly associated with reductions in mortality. Increasing the dose from 10 mg/kg to 30 mg/kg was predicted to increase 6-month survival from 50% to 70% (Svensson et al., 2020). In terms of safety, the data in children on higher dose rifampicin are limited. In adults, doses as high as 35–40 mg/kg appear to be well tolerated and safe (Boeree et al., 2017; Seijger et al., 2019). In children, a dose of 65–70 mg/kg was required to reach a similar exposure seen in adults on 35 mg/kg while a 50 mg/kg dose in these children given for a short time was well tolerated with no grade 3 or higher adverse events (Garcia-Prats et al., 2021). The data from adult trials are also informative when developing dosing strategies for children.

Treatment guidelines often recommend a mg per kg dose to treat people with TB. However, the relative weight range in children is large, for example, from 5 to 25 kg, there is a five-fold difference in body size and the allometric effect of body size on drug clearance significantly deviates from linearity in such a large range (Anderson and Holford, 2008). This means that when only considering body size, a child weighing 5 kg will receive a 5 times lower dose than a child weighing 25 kg, but drug clearance in that child is only 3.3 times lower (Denti et al., 2022a). When using an adult reference, the difference is even larger. As a result, children can be significantly underdosed when mg/kg dosing is used (Chabala et al., 2021; Garcia-Prats et al., 2021; Denti et al., 2022b). Furthermore, dosing children younger than 2 years of age is even more challenging because of the rapid maturation in organ function and fast growth, both of which impact drug clearance and thus exposure. Finally, metabolizing enzymes and drug excreting organs (i.e., kidneys) can mature at different rates and as a result the doses of some drugs need to increase rapidly when a child grows older while other drugs require a more gradual dose increase (Lu and Rosenbaum, 2014). It is therefore important that dose recommendations for children are no longer

TABLE 3 Dosing table using adult formulations for children from 25 to 35 kg and the 400 mg pyrazinamide formulation. The red and white horizontal bands in the formulation's column represent the weight bands receiving the same dose. The colours in the last columns show if exposures are expected to be within (green) or outside the target range where yellow represents the percentage below the lower bound of the target range and purple represents the percentage above the higher bound of the target range. Abbreviations: a, adult formulation; R, rifampicin; H, isoniazid; Z, pyrazinamide; Eto, ethionamide.

	Formulations				Simulated exposure				Difference from target range			
Weight (kg)	aRH 150/75	aZ 400	aETO 250	Tablet burden	Rifampicin (mg·h/L)	Isoniazid (mg·h/L)	Pyrazinamide (mg·h/L)	Ethionamide (mg·h/L)	Rifampicin (%)	Isoniazid (%)	Pyrazinamide (%)	Ethionamide (%)
25–26	4	2	2	8	67.3	41.1	421	29.3	0.0	−13.7%	0.0%	0.0
26–27	4	2	2	8	63.4	40.2	413	28.6	0.0	−15.5%	0.0%	0.0
27–28	4	2	2	8	61.0	39.2	403	27.7	0.0	−17.6%	0.0%	0.0
28–29	4	2	2	8	58.2	38.1	393	27.0	0.0	−20.0%	0.0%	0.0
29–30	4	2	2	8	55.7	37.3	379	26.2	0.0	−21.6%	−2.5%	0.0
30–31	5	2	2	9	75.8	45.2	372	25.5	0.0	−5.0%	−4.3%	0.0
31–32	5	2	2	9	71.5	44.0	361	25.2	0.0	−7.6%	−7.2%	0.0
32–33	5	3	2	10	69.3	43.7	533	24.4	0.0	−8.2%	0.0%	0.0
33–34	5	3	2	10	68.0	42.5	521	23.9	0.0	−10.7%	0.0%	0.0
34–35	5	3	2	10	64.3	41.2	510	23.3	0.0	−13.4%	0.0%	0.0

TABLE 4 Dosing table using adult formulations for children from 25 to 35 kg and the 500 mg pyrazinamide formulation. The red and white horizontal bands in the formulation's column represent the weight bands receiving the same dose. The colours in the last columns show if exposures are expected to be within (green) or outside the target range where yellow represents the percentage below the lower bound of the target range and purple represents the percentage above the higher bound of the target range. Abbreviations: a, adult formulation; R, rifampicin; H, isoniazid; Z, pyrazinamide; Eto, ethionamide.

	Formulations				Simulated exposure				Difference from target range			
Weight (kg)	aRH 150/75	aZ 500	aETO 250	Tablet burden	Rifampicin (mg·h/L)	Isoniazid (mg·h/L)	Pyrazinamide (mg·h/L)	Ethionamide (mg·h/L)	Rifampicin (%)	Isoniazid (%)	Pyrazinamide (%)	Ethionamide (%)
25–26	4	2	2	8	67.3	41.1	526	29.3	0.0	−13.7%	0.0	0.0
26–27	4	2	2	8	63.4	40.2	517	28.6	0.0	−15.5%	0.0	0.0
27–28	4	2	2	8	61.0	39.2	503	27.7	0.0	−17.6%	0.0	0.0
28–29	4	2	2	8	58.2	38.1	491	27.0	0.0	−20.0%	0.0	0.0
29–30	4	2	2	8	55.7	37.3	474	26.2	0.0	−21.6%	0.0	0.0
30–31	5	2	2	9	75.8	45.2	465	25.5	0.0	−5.0%	0.0	0.0
31–32	5	2	2	9	71.5	44.0	452	25.2	0.0	−7.6%	0.0	0.0
32–33	5	2	2	9	69.3	43.7	444	24.4	0.0	−8.2%	0.0	0.0
33–34	5	2	2	9	68.0	42.5	434	23.9	0.0	−10.7%	0.0	0.0
34–35	5	2	2	9	64.3	41.2	425	23.3	0.0	−13.4%	0.0	0.0

10.3389/fphar.2023.1055329

given as a mg per kg dose but include dosing tables and weight bands that are drug-specific.

The available FDCs are designed for the treatment of drug-susceptible TB using the standard doses recommended by WHO. The drug doses for rifampicin and isoniazid in the short TBM regimen are higher than those currently recommended for the treatment of drug-susceptible TB, and as a result there is a high tablet burden. Ideally, this would be solved by a formulation that contains higher doses of rifampicin and isoniazid. In practice, physicians could lower the tablet burden by using the child-friendly RHZ 75/50/150 mg FDC. However, this does make administration more complicated since this would require a "top-up" with the RH 75/50 mg FDC. For example, a 21 kg child could receive five RHZ 75/50/150 mg dispersible tablets, two RH 75/50 dispersible tablets and three 150 mg ethionamide dispersible tablets, reducing the tablet burden from 15 to 10.

An easy-to-use dosing tool was developed in MS Excel that enables users to design their own dosing strategy. The dosing tool bridges the gap between pharmacokinetic models and implementation considerations, to develop a dosing strategy for the short TBM regimen. The tool in the supplementary materials can also be used by physicians to look at alternative dosing strategies in case a recommended formulation is not available or if the tablet burden is high and needs to be lowered. However, it does have some inherent limitations. Because of the non-linear relationships between dose and exposure in young children (i.e., below 2 years of age) and saturable hepatic metabolism of rifampicin, the tool only provides an approximation of target attainment. For a more reliable exposure prediction we therefore simulated the dosing options in population models to confirm the appropriateness of the chosen dosing strategy. A better solution would be to have a browser-based platform (e.g., a Shiny application) that simulates exposures in the background while the user can focus on the formulations and weight bands.

The options from the process described in this paper were presented to a panel who then provided advice on a dosing strategy that enables the implementation of the short, intensive TBM regimen at country level, with globally available formulations.

Conclusion

The development of dosing strategies should be informed by efficacy, safety, and pharmacokinetics data, as well as implementation considerations, such as availability of drug formulations that are appropriate for the specific target population. The combined effects of age and body size on drug exposures makes exposure predictions in children more complex than in adults, and straight mg/kg dosing that does not consider developmental pharmacology can result in toxic or subtherapeutic concentrations, especially for diseases in which precision dosing is essential. Here, we used a modelling approach to identify doses of the four drugs that comprise the newly WHO-recommended 6HRZEto regimen that achieve target exposures in children across the age and weight spectrum, taking into account available formulations, including widely used FDCs. Additionally, we provide a dosing tool that shows practitioners how to use either dispersible tablets or, for older children, adult tablets to achieve treatment goals. Young children are disproportionately at risk for TBM and its attendant high risk of morbidity and mortality. While the optimal doses for children remain to be established, we now have the tools to deliver a highly effective regimen to children globally (Sulis et al., 2022).

Data availability statement

The original contributions presented in the study are included in the article/Supplementary material, further inquiries can be directed to the corresponding author.

Author contributions

RW carried out the simulations, developed the dosing tool, interpreted the results, wrote the first draft, and edited the manuscript; PD and KD developed the dosing tool, interpreted the results, and edited the manuscript; TM co-wrote the first draft and, alongside, KV, SV, and AB, interpreted the results, and edited the manuscript; AH and HM edited the manuscript. All authors contributed to the article and approved the submitted version.

Acknowledgments

Computations were performed using facilities provided by the University of Cape Town's ICTS High Performance Computing team: hpc. uct.ac.za.

Conflict of interest

The authors declare that the research was conducted in the absence of any commercial or financial relationships that could be construed as a potential conflict of interest.

Publisher's note

Author disclaimer

The authors alone are responsible for the views expressed in this article and they do not necessarily represent the views, decisions, or policies of the institutions with which they are affiliated.

Supplementary material

The Supplementary Material for this article can be found online at: https://www.frontiersin.org/articles/10.3389/fphar.2023.1055329/full#supplementary-material

References

Anderson, B. J., and Holford, N. H. G. (2008). Mechanism-based concepts of size and maturity in pharmacokinetics. *Annu Rev. Pharmacol. Toxicol.* 48 (1), 303–332. doi:10.1146/annurev.pharmtox.48.113006.094708

Boeree, M. J., Heinrich, N., Aarnoutse, R., Diacon, A. H., Dawson, R., Rehal, S., et al. (2017). High-dose rifampicin, moxifloxacin, and SQ109 for treating tuberculosis: A multi-arm, multi-stage randomised controlled trial. *Lancet Infect. Dis.* 17 (1), 39–49. doi:10.1016/S1473-3099(16)30274-2

Chabala, C., Turkova, A., Hesseling, A. C., Zimba, K. M., van der Zalm, M., Kapasa, M., et al. (2021). Pharmacokinetics of first-line drugs in children with tuberculosis, using World health organization-recommended weight band doses and formulations. Clin. Infect. Dis. 22, 1767–1775. Published online August. doi:10.1093/cid/ciab725

Chiang, S. S., Khan, F. A., Milstein, M. B., Tolman, A. W., Benedetti, A., Starke, J. R., et al. (2014). Treatment outcomes of childhood tuberculous meningitis: A systematic review and meta-analysis. *Lancet Infect. Dis.* 14 (10), 947–957. doi:10.1016/S1473-3099(14)70852-7

Donald, P. R., Schoeman, J. F., Van Zyl, L. E., De Villiers, J. N., Pretorius, M., and Springer, P. (1998). Intensive short course chemotherapy in the management of tuberculous meningitis. *Int. J. Tuberc. Lung Dis.* 2 (9), 704–711. http://www.ncbi.nlm.nih.gov/pubmed/9755923.

Denti, P., Wasmann, R. E., Francis, J., McIlleron, H., Sugandhi, N., Cressey, T. R., et al. (2022). One dose does not fit all: Revising the WHO paediatric dosing tool to include the non-linear effect of body size and maturation. *Lancet Child. Adolesc. Heal* 6 (1), 9–10. doi:10.1016/S2352-4642(21)00302-3

Denti, P., Wasmann, R. E., van Rie, A., Winckler, J., Bekker, A., Rabie, H., et al. (2022). Optimizing dosing and fixed-dose combinations of rifampicin, isoniazid, and pyrazinamide in pediatric patients with tuberculosis: A prospective population pharmacokinetic study. *Clin. Infect. Dis.* 75 (1), 141–151. doi:10.1093/cid/ciab908

Department of Health - Republic of South Africa (2021). *Circular: Paediatric TB FDC weight-band dosing Tables_24June2021*. Pretoria: Department of Health - Republic of South Africa.

Donald, P. R. (2010). Cerebrospinal fluid concentrations of antituberculosis agents in adults and children. *Tuberculosis* 90 (5), 279–292. doi:10.1016/j.tube.2010.07.002

Donald, P. R. (2010). The chemotherapy of tuberculous meningitis in children and adults. *Tuberculosis* 90 (6), 375–392. doi:10.1016/j.tube.2010.07.003

Garcia-Prats, A. J., Svensson, E. M., Winckler, J., Draper, H. R., Fairlie, L., van der Laan, L. E., et al. (2021). Pharmacokinetics and safety of high-dose rifampicin in children with TB: The opti-rif trial. *J. Antimicrob. Chemother.* 16, 3237–3246. Published online September. doi:10.1093/jac/dkab336

Gausi, K., Wiesner, L., Norman, J., Wallis, C. L., Onyango-Makumbi, C., Chipato, T., et al. (2021). Pharmacokinetics and drug-drug interactions of isoniazid and efavirenz in pregnant women living with HIV in high TB incidence settings: Importance of genotyping. *Clin. Pharmacol. Ther.* 109 (4), 1034–1044. doi:10.1002/cpt.2044

Janmahasatian, S., Duffull, S. B., Ash, S., Ward, L. C., Byrne, N. M., and Green, B. (2005). Quantification of lean bodyweight. *Clin. Pharmacokinet.* 44 (10), 1051–1065. doi:10.2165/00003088-200544100-00004

Lu, H., and Rosenbaum, S. (2014). Developmental pharmacokinetics in pediatric populations. *J. Pediatr. Pharmacol. Ther.* 19 (4), 262–276. doi:10.5863/1551-6776-19.4.262

Nyberg, H. B., Draper, H. R., Garcia-Prats, A. J., Thee, S., Bekker, A., Zar, H. J., et al. (2020). Population pharmacokinetics and dosing of ethionamide in children with tuberculosis. *Antimicrob. Agents Chemother.* 64 (3), 019844-19. doi:10.1128/AAC.01984-19

Paradkar, M. S., Devaleenal, D. B., Mvalo, T., Arenivas, A., Thakur, K. T., Wolf, L., et al. (2022). Randomized clinical trial of high dose rifampicin with or without levofloxacin versus standard of care for paediatric tuberculous meningitis: The TBM-KIDS trial. *Clin. Infect. Dis.* 15, 2022. Published online March. doi:10.1093/cid/ciac208

Ruslami, R., Ganiem, A. R., Dian, S., Apriani, L., Achmad, T. H., van der Ven, A. J., et al. (2013). Intensified regimen containing rifampicin and moxifloxacin for tuberculous meningitis: An open-label, randomised controlled phase 2 trial. *Lancet Infect. Dis.* 13 (1), 27–35. doi:10.1016/S1473-3099(12)70264-5

Savic, R., Ruslami, R., Hibma, J., Hesseling, A., Ramachandran, G., Ganiem, A. R., et al. (2015). Pediatric tuberculous meningitis: Model-based approach to determining optimal doses of the anti-tuberculosis drugs rifampin and levofloxacin for children. *Clin. Pharmacol. Ther.* 98 (6), 622–629. doi:10.1002/cpt.202

Schaaf, H. S., Marais, B. J., Whitelaw, A., Hesseling, A. C., Eley, B., Hussey, G. D., et al. (2007). Culture-confirmed childhood tuberculosis in Cape Town, South Africa: A review of 596 cases. *BMC Infect. Dis.* 7 (1), 140. doi:10.1186/1471-2334-7-140

Seijger, C., Hoefsloot, W., Bergsma-de Guchteneire, I., Te Brake, L., van Ingen, J., Kuipers, S., et al. (2019). High-dose rifampicin in tuberculosis: Experiences from a Dutch tuberculosis centre. *PLoS One* 14 (3), e0213718. doi:10.1371/journal.pone.0213718

Sulis, G., Tavaziva, G., Gore, G., Benedetti, A., Solomons, R., van Toorn, R., et al. (2022). Comparative effectiveness of regimens for drug-susceptible tuberculous meningitis in children and adolescents: A systematic review and aggregate-level data meta-analysis. *Open Forum Infect. Dis.* 9 (6), ofac108–10. doi:10.1093/ofid/ofac108

Svensson, E. M., Dian, S., Te Brake, L., Ganiem, A. R., Yunivita, V., van Laarhoven, A., et al. (2020). Model-based meta-analysis of rifampicin exposure and mortality in Indonesian tuberculous meningitis trials. *Clin. Infect. Dis.* 71 (8), 1817–1823. doi:10.1093/cid/ciz1071

Svensson, E. M., Yngman, G., Denti, P., McIlleron, H., Kjellsson, M. C., and Karlsson, M. O. (2018). Evidence-based design of fixed-dose combinations: Principles and application to pediatric anti-tuberculosis therapy. *Clin. Pharmacokinet.* 57 (5), 591–599. doi:10.1007/s40262-017-0577-6

van Toorn, R., Schaaf, H. S., Laubscher, J. A., van Elsland, S. L., Donald, P. R., and Schoeman, J. F. (2014). Short intensified treatment in children with drug-susceptible tuberculous meningitis. *Pediatr. Infect. Dis. J.* 33 (3), 248–252. doi:10.1097/INF.0000000000000065

Wasmann, R. E., Svensson, E. M., Walker, A. S., Clements, M. N., and Denti, P. (2021). Constructing a representative *in-silico* population for paediatric simulations: Application to HIV-positive African children. *Br. J. Clin. Pharmacol.* 87 (7), 2847–2854. doi:10.1111/bcp.14694

Wilkinson, R. J., Rohlwink, U., Misra, U. K., van Crevel, R., Mai, N. T. H., Dooley, K. E., et al. (2017). Tuberculous meningitis. *Nat. Rev. Neurol.* 13 (10), 581–598. doi:10.1038/nrneurol.2017.120

World Health Organization (2021). Global tuberculosis report. Available at: https://www.who.int/teams/global-tuberculosis-programme/tb-reports.

World Health Organization (2010). *Rapid advice: Treatment of tuberculosis in children*. Geneva, Switzerland: World Health Organization.

World Health Organization (2022). Report of a WHO expert consultation on dosing to enable implementation of treatment recommendations in the WHO consolidated guidelines on the management of TB in children and adolescents. Available at: https://www.who.int/publications/i/item/9789240055193.

World Health Organization (2010). *Treatment of tuberculosis guidelines*. Geneva, Switzerland: World Health Organization.

World Health Organization (2022). WHO consolidated guidelines on tuberculosis - module 5: Management of tuberculosis in children and adolescents. Available at: https://www.who.int/publications/i/item/9789240046764.

World Health Organization (2022). WHO consolidated guidelines on tuberculosis, module 4: Treatment - drug-susceptible tuberculosis treatment. Available at: https://www.who.int/publications/i/item/9789240048126.

frontiers | Frontiers in Pharmacology

TYPE Original Research
PUBLISHED 26 May 2023
DOI 10.3389/fphar.2023.1116226

OPEN ACCESS

EDITED BY
Sebastian G. Wicha,
University of Hamburg, Germany

REVIEWED BY
Ahmed A. Abulfathi,
University of Florida Health, United States
Johannes Alffenaar,
The University of Sydney, Australia

*CORRESPONDENCE
Yong-Soon Cho,
ysncho@gmail.com
Jae-Gook Shin,
phshinjg@gmail.com

RECEIVED 05 December 2022
ACCEPTED 19 April 2023
PUBLISHED 26 May 2023

CITATION
Kim R, Jayanti RP, Lee H, Kim H-K, Kang J, Park I-N, Kim J, Oh JY, Kim HW, Lee H, Ghim J-L, Ahn S, Long NP, Cho Y-S, Shin J-G, On behalf of the cPMTb (2023), Development of a population pharmacokinetic model of pyrazinamide to guide personalized therapy: impacts of geriatric and diabetes mellitus on clearance.
Front. Pharmacol. 14:1116226.
doi: 10.3389/fphar.2023.1116226

Development of a population pharmacokinetic model of pyrazinamide to guide personalized therapy: impacts of geriatric and diabetes mellitus on clearance

Ryunha Kim[1,2], Rannissa Puspita Jayanti[1,2], Hongyeul Lee[3], Hyun-Kuk Kim[4], Jiyeon Kang[5], I-Nae Park[6], Jehun Kim[7], Jee Youn Oh[8], Hyung Woo Kim[9], Heayon Lee[10], Jong-Lyul Ghim[1,2], Sangzin Ahn[1,2], Nguyen Phuoc Long[1,2], Yong-Soon Cho[1,2]*, Jae-Gook Shin[1,2,11]* and On behalf of the cPMTb

[1]Center for Personalized Precision Medicine of Tuberculosis, Inje University College of Medicine, Busan, Republic of Korea, [2]Department of Pharmacology and PharmacoGenomics Research Center, Inje University College of Medicine, Busan, Republic of Korea, [3]Division of Pulmonary, Critical Care Medicine, Department of Internal Medicine, Inje University College of Medicine, Busan Paik Hospital, Busan, Republic of Korea, [4]Division of Pulmonology, Department of Internal Medicine, Inje University Haeundae Paik Hospital, Busan, Republic of Korea, [5]Division of Pulmonary and Critical Care Medicine, Department of Internal Medicine, Inje University Ilsan Paik Hospital, Goyang-si, Republic of Korea, [6]Department of Internal Medicine, Inje University Seoul Paik Hospital, Inje University College of Medicine, Seoul, Republic of Korea, [7]Pulmonary Division, Department of IM, Kosin University Gospel Hospital, Busan, Republic of Korea, [8]Division of Pulmonology, Department of Internal Medicine, Korea University Guro Hospital, Seoul, Republic of Korea, [9]Division of Pulmonary and Critical Care Medicine, Department of Internal Medicine, Incheon St. Mary's Hospital, College of Medicine, The Catholic University of Korea, Incheon, Republic of Korea, [10]Division of Pulmonary, Critical Care and Sleep Medicine, Department of Internal Medicine, Eunpyeong St. Mary's Hospital, College of Medicine, The Catholic University of Korea, Seoul, Republic of Korea, [11]Department of Clinical Pharmacology, Inje University Busan Paik Hospital, Busan, Republic of Korea

Objectives: This study was performed to develop a population pharmacokinetic model of pyrazinamide for Korean tuberculosis (TB) patients and to explore and identify the influence of demographic and clinical factors, especially geriatric diabetes mellitus (DM), on the pharmacokinetics (PK) of pyrazinamide (PZA).

Methods: PZA concentrations at random post-dose points, demographic characteristics, and clinical information were collected in a multicenter prospective TB cohort study from 18 hospitals in Korea. Data obtained from 610 TB patients were divided into training and test datasets at a 4:1 ratio. A population PK model was developed using a nonlinear mixed-effects method.

Results: A one-compartment model with allometric scaling for body size effect adequately described the PK of PZA. Geriatric patients with DM (age >70 years) were identified as a significant covariate, increasing the apparent clearance of PZA by 30% (geriatric patients with DM: 5.73 L/h; others: 4.50 L/h), thereby decreasing the area under the concentration–time curve from 0 to 24 h by a similar degree compared with other patients (geriatric patients with DM: 99.87 μg h/mL; others: 132.3 μg h/mL). Our model was externally evaluated using the test set and

provided better predictive performance compared with the previously published model.

Conclusion: The established population PK model sufficiently described the PK of PZA in Korean TB patients. Our model will be useful in therapeutic drug monitoring to provide dose optimization of PZA, particularly for geriatric patients with DM and TB.

KEYWORDS

pyrazinamide, tuberculosis, geriatric, diabetes mellitus, population pharmacokinetics, therapeutic drug monitoring

Introduction

In the era of the coronavirus disease 19 (COVID-19), tuberculosis (TB) remains a deadly threat globally via single infection and potential coinfection with COVID-19 (Petersen, Al-Abri, Chakaya, Goletti, Parolina, Wejse, et al.). According to the WHO Global TB report in 2021, there were 10 million TB cases worldwide, with an estimated 1.5 million mortalities, representing the first mortality increase in a decade (World Health Organization, 2020). Despite remarkable TB prevention and control policies, Korea has the highest incidence rate of TB among Organisation for Economic Co-operation and Development member countries, with the number of patients imported from overseas continuing to increase (Min et al., 2021). Therefore, for successful treatment of all forms of TB, it is important to optimize the doses of currently used drugs.

The intensive phase of TB treatment uses isoniazid, rifampicin, ethambutol, and pyrazinamide (PZA) as the main components, resulting in rapid improvement of clinical symptoms (Shin and Kwon, 2015). Among the first-line anti-TB drugs, PZA has strong bactericidal activity against *Mycobacterium tuberculosis* during the early stages of treatment (Zhang and Mitchison, 2003). The area under the concentration–time curve from 0 to 24 h ($AUC_{0\text{-}24}$) of PZA is an important predictor of early culture conversion and good bactericidal activity (Pasipanodya et al., 2013). Additionally, maximum concentration (C_{max}) of PZA ranging from 20—60 μg/mL has been linked to the lower risk of treatment failure (Chideya et al., 2009; Pasipanodya et al., 2013). Considering the important role of PZA in TB treatment, it is necessary to maintain the C_{max} of the drug within this efficacy range for obtaining successful treatment of TB.

Currently, the TB treatment guidelines follow body weight-based dosing. In Korea, the recommended daily dose of PZA for treatment of drug-susceptible TB is 20–30 mg/kg, with a maximum dose of 2000 mg (Donald et al., 2012; WHO and Organization, 2017). Nonetheless, similar to other first-line anti-TB drugs, PZA also exhibits wide pharmacokinetic (PK) variability in a population (Wilkins et al., 2006; Zvada et al., 2014; Denti et al., 2015), which is challenging during patient management (Devaleenal Daniel et al., 2017). While overexposure to PZA has been shown to be strongly associated with liver damage (Younossian et al., 2005), hyperuricemia, and arthralgia (Qureshi et al., 2007), underexposure may lead to treatment failure and drug resistance (Srivastava et al., 2011).

Previous studies have shown that the PZA concentration is influenced by many factors, including genetic polymorphisms, age, comorbidities, and body weight (Graham et al., 2006; McIlleron et al., 2006; Chideya et al., 2009). Vinnard et al. (2017) reported that the clearance of PZA was 40% higher in males than in females, while Wilkins et al. (2006) reported a higher volume of distribution in males. Earlier reports also showed that the absorption of PZA was reduced in HIV patients (Gurumurthy et al., 2004; McIlleron et al., 2006; Vinnard et al., 2017). Many PK studies of PZA have been performed, most of which were in children (Thee et al., 2011; Zvada et al., 2014; Chabala et al., 2022). However, our understanding of the characteristics of PK in the elderly population is limited. It is worth noting that new TB patients aged 65 years or older accounted for 65% of the total new cases in Korea in 2020 (Cho, 2018). Elderly individuals generally have a number of physiological changes that may alter the PK of drugs, such as changes in liver and kidney function, which are responsible for the metabolism and excretion of Pyrazinamide (Mangoni and Jackson, 2004; Klotz, 2009). Furthermore, aging is closely associated with an increased risk of comorbidities, particularly type 2 diabetes mellitus (DM) (Lin et al., 2015; Park et al., 2019). DM has been widely reported to hamper successful TB treatment (Baker et al., 2011; Yoon et al., 2017). DM may reduce the exposure of PZA by increasing clearance through enhancing the activity of xanthin oxidase (XO) (Alfarisi et al., 2018), and has been linked to poor treatment outcomes (Alsultan et al., 2017). Therefore, the response should be monitored closely during treatment in geriatric patients, especially those with DM.

Therapeutic drug monitoring (TDM) is useful for optimizing drug therapy by providing a patient-tailored dose according to their PK/pharmacodynamic (PD) results (Alsultan and Peloquin, 2014; Daskapan et al., 2015). The application of TDM in clinical settings has shifted to the concept of model-informed precision dosing (MIPD) (Polasek et al., 2019; Jayanti et al., 2022). MIPD-based TDM involves the use of population PK models and prospective Bayesian forecasting to reduce the variability in treatment responses and to optimize anti-TB drug therapy. Yet, MIPD based TDM is not a common practice in high burden countries (Alffenaar et al., 2020). Several factors such as socioeconomics, healthcare infrastructure, and human resource capacity require further preparation before TDM can be fully integrated into these settings (Ghimire et al., 2016; Alffenaar et al., 2020). Additionally, population PK enables the use of sparse sampling at random post-dose points, thus avoiding the costly and laborious process of conventional TDM (Egelund et al., 2011). However, consideration should be given to the match between the characteristics of the representative population used for model development and the population in which TDM will be performed (Sturkenboom et al., 2021). Recent reports recommended the development of population PK models based on a representative

population to provide appropriate dosing recommendations (Lange et al., 2020; Sturkenboom et al., 2021). Nonetheless, there have been few reports of population PK models of PZA in Asian populations, particularly in Korea. Here, we characterized and identified the influences of demographic and clinical factors on the PK of PZA by developing a population PK model, particularly for the elderly population with DM. This model could be further used to support precision therapy for TB by applying it to MIPD-based TDM.

Materials and methods

Ethical approval

This study was performed in accordance with the tenets of the Declaration of Helsinki and the guidelines of our institution. The current study was part of a multicenter prospective observational cohort study to develop personalized pharmacotherapy for TB patients and was conducted in 18 hospitals in Korea. We provided therapeutic drug monitoring procedure to the enrolled patients; therefore, we have registered our study in clinicaltrial.gov with the clinical trial number NCT05280886. Ethical approval was obtained from the institutional review board of each clinical site involved in the study. All patients provide written informed consent to participate in the study.

Study data and population

Patients aged >18 years diagnosed with drug-susceptible TB and receiving a PZA-based regimen for at least 2 weeks were enrolled in the study. The enrolled patients received an oral daily dose of PZA in the range of 20–30 mg/kg and rounded to the closest tablet size as prescribed by the physician. All patients underwent sputum testing for bacteriologically confirmed diagnosis, which included the use of Xpert MTB/RIF testing capable of detecting *M. tuberculosis* and resistance to rifampin simultaneously, culture test and/or acid-fast bacilli (AFB) staining. The PZA dosing regimen followed the current Korean guidelines for TB treatment. Patients who were nonadherent or not in steady-state were excluded. The demographic characteristics of the enrolled patients, anti-TB drug treatments, comorbidities, TB diagnosis, co-medications, and laboratory testing results were collected.

Sampling strategy of PZA

Blood samples (5 mL) were randomly collected between 0 and 24 h after the last PZA administration and were stored in heparin tubes. Typically, one sample was usually drawn from outpatients, whereas at least two samples among pre-dose and 1, 2, and 5 h after the last dose were drawn from inpatients. A portion of each 3-mL blood sample was centrifuged at 2,000 g at 4°C for 10 min to obtain plasma. The plasma was harvested within 2 h after blood sampling and stored at a temperature below −70°C until used for drug concentration measurements. The remaining 2 mL of each blood sample was stored for genotyping related to the PK of other anti-TB drugs used to treat the patients.

Quantification of plasma PZA

The plasma concentration of PZA was measured using a validated high-performance liquid chromatography–electrospray ionization–tandem mass spectrometry method as described previously by our group (Kim et al., 2015). The previous method was modified and PZA currently used the group 2 method from the published method. Briefly, the plasma samples were prepared by protein precipitation using acetonitrile and were separated by gradient elution on a reverse-phase dC18 column. Detection was performed on the QTRAP 4000 mass spectrometer (Applied Biosystems, Foster City, CA, United States) equipped with a Turbolon-Spray source (Applied Biosystems). The calibration range was 2.0–80.0 μg/mL with a correlation coefficient of 0.9988. The lower limit of quantification (LLOQ) of PZA using this method was 2.0 μg/mL. The coefficient of variation ranges of the validation quality control samples were 5.2%–6.6% and 2.1%–5.44% for the intraday and interday precisions, respectively. The intraday and interday accuracy ranges were 93.3%–109.4% and 93.3%–109.4%, respectively.

Population PK modeling and simulation

Population PK analysis was performed using NONMEM software (version 7.4.1; ICON Development Solutions, Ellicott City, MD, United States), and PK parameters were calculated using first-order conditional estimation via ε-η interaction. R software (version 4.1.0; R Development Core Team, Vienna, Austria) was used to analyze the data and generate graphs. The PZA plasma concentrations below the LLOQ were imputed to half of the LLOQ (1 μg/mL) according to Beal's M5 method (Beal, 2001). Nonadherent patients were excluded based on the low measured concentrations of at least two anti-TB drugs used. The training and test datasets were randomly separated from the total population at a ratio of 4:1. Based on the first order absorption of the drug, the possibility of an absorption delay was examined using several different absorption models, i.e., lag-time model, sequential zero- and first-order absorption models, and transit compartment model. Interindividual variability (IIV) was assumed to follow a log-normal distribution. Additive, proportional, and combined error models were used to describe the residual error. After establishment of the base model, a correlation matrix plot was generated to identify the potential significant covariates. A likelihood ratio test was used for inclusion of covariates. Covariates were applied to the model by evaluating whether the objective function value (OFV) decreased by ≥ 3.84 with use of only one covariate in one PK parameter. Covariates were tested by forward selection and backward elimination. The most statistically significant covariates were entered first, and then other covariates with $p < 0.01$ were added sequentially.

Age, body weight, lean body weight, albumin, and total bilirubin were included as continuous covariates. Meanwhile, sex, fasting or food intake status, DM, liver disease, renal disease, and geriatric (≥60, ≥65, and ≥70 years) DM were investigated as categorical covariates of PK parameters. The effects of continuous covariates were explored using the power function with the following equation:

$$P = \left(\theta_{TV} \times \frac{Cont_{COV\,i}}{Cont_{COV\,median}}\right)^{\theta_p}$$

where θ_{TV} represents the typical value of the PK parameter (P), $Cont_{COV\,i}$ is the value of the continuous variable for the ith patient, $Cont_{COV\,median}$ is the median value for a continuous covariate, and θ_p is the exponent of the power function. On the other hand, the effects of categorical variables were tested using a similar function:

$$P = \theta_i \times (1 + \theta_{i+1} \times Cat\_Cov_{i+1})$$

Following the previous equation, θ_i represents the estimated effect of the ith categorical covariate (when $Cat\_Cov_{i+1} = 0$), and θ_{i+1} is the estimated effect of the i+1st categorical variable relative to θ_i (when $Cat\_Cov_{i+1} = 1$). Allometric scaling of either body weight or lean body mass was applied to apparent clearance (CL/F) and central volume of distribution (Vd/F) using fixed exponents of 0.75 and 1, respectively (Anderson and Holford, 2008).

The base and final models were selected according to the decrease in the OFV generated in the likelihood ratio test, the goodness-of-fit plot, and the physiological plausibility of the estimated parameters. The final model was internally validated through prediction-corrected visual predictive check and robustness of the estimated PK, and parameters were evaluated by nonparametric bootstrap analysis. The final model was considered well validated when the mean values of the estimated parameters fell within the 95% confidence interval (CI). External validation was conducted using a test dataset that was not included in the model development. The predicted concentrations were compared with the observed concentrations using the population or the individual PK parameters estimated using the Bayesian method. The predictive performance of the final model was evaluated by comparing the model prediction errors, such as mean prediction error and absolute prediction error, with those of previously published population PK models. The criteria of previously published population PK model selection as follows: 1) similar model structure, and 2) the model established from different ethnicities compared to the study population. The external validation aims to compare and observe the final model performance with the other published models from different ethnicities when implemented in the same ethnicity with the study population. The equations used to calculate the prediction errors were as follows:

$$MPE = \frac{\sum(C_{Pred} - C_{Obs})}{N}$$

$$APE = \frac{\sum(|C_{Pred} - C_{Obs}|)}{N}$$

Results

Population characteristics

A total of 613 patients were enrolled, and their plasma PZA concentration measurements were used to establish the model. Each patient contributed for one sampling point at random post dose time. The study population had a median age of 54 years (range: 19–96 years), body weight of 60.8 kg (range: 28.8–95.3 kg), and lean body weight of 48.1 kg (range: 23.1–63.79 kg), and the proportion of male patients was approximately 67%. In the total patient population, 55 patients had DM, 15 had liver disease, and 26 had renal disease (estimated glomerular filtration rate: ≤60 mL/min/1.73 m^2). In addition, 110 patients were older than 70 years. The median body weight and lean body weight of this elderly population were 55.5 kg (range: 28.8–81.0 kg) and 44.5 kg (23.14–58.77 kg), respectively. Among the elderly population, 23 patients had DM, 11 had renal disease, and 2 had liver disease. The baseline patient characteristics are presented in Table 1.

Development of a population PK model

A one-compartment model with first-order absorption–elimination with additive residual error adequately described the PK of PZA in our population. IIV was evaluated in terms of the CL/F, Vd/F, and absorption rate constant (Ka). While IIV in both CL/F and Ka were estimated, the IIV in Vd/F was fixed to stabilize the model and obtain minimization successful. The value used to fix the IIV of Vd/F were obtained from the result of model running prior to fixing the IIV value. Allometric scaling was included for both the CL/F and Vd/F using lean body weight as a predictor of body size. The inclusion of allometric scaling with lean body weight into the base model was based on a significant reduction in OFV (ΔOFV: 112.3) in comparison with using total body weight (ΔOFV: 88.5). Several absorption models that were evaluated did not improve model performance and thus were not included in further analysis.

We evaluated the covariates of age, height, sex, feeding status, AST, ALT, albumin, total bilirubin, DM, advanced age (≥60, ≥65, and ≥70 years old), renal disease, and liver disease. However, none of these covariates improved the OFV. Therefore, as most TB patients in Korea are of advanced age, additional evaluation was performed using combinations of age ≥60, ≥65, and ≥70 years with comorbidities, such as DM, renal disease, and liver disease. Among these covariate groups, only age ≥60, ≥65, and ≥70 years combined with DM had a significant effect on the CL/F of PZA, in which the combination of age ≥70 years with DM showed the largest reduction of OFV by 151.3 points (p-value <0.001) and 2.2% decreased in IIV. Given the demographic trend of aging in the Korean population, the incorporation of a covariate representing individuals aged 70 years or older with DM would be more relevant. The CL/F value was estimated as 5.9 L/h for patients aged ≥70 years old with DM and as 4.49 L/h for other patients. The estimated values of Vd/F and Ka were 44.2 L and 1.49 h^{-1}, respectively. The estimated PK parameters of PZA and the NONMEM code of final model are shown in Table 2 and Supplementary File S1.

The basic goodness-of-fit plots showed that the observed and predicted concentrations were evenly distributed around the line of identity without trends, and most of the predicted concentrations were distributed within two standard deviations. The structure and residual error of the model were considered appropriate without any significant bias (Figure 1). The predictive-corrected visual predictive testing also indicated a good predictive capability of the model (Figure 2). Furthermore, all other parameters showed shrinkage below 30%, indicating that the model was not overparameterized. A sparse and limited samples of PZA concentration in the absorption

TABLE 1 Patient demographic characteristics.

Characteristics	Total (n = 613)[a]	Training data (n = 488)	Test data (n = 125)
Sex, n (%)			
Male	415 (67.7)	325 (66.6)	90(72)
Female	198 (32.3)	163 (33.4)	35(28)
Feeding status, n (%)			
Fasted	446 (72.75)	369 (75.6	77(61.6)
Fed	167 (24.25)	119 (24.4)	48 (38.4)
DM, n (%)[b]			
Yes	84 (13.7)	55 (11.27)	29 (23.2)
No	529 (86.3)	433 (88.73)	96 (76.8)
eGFR, n (%)[c]			
Less than 60 mL/min/1.73 m^2	36 (5.87)	19 (3.9)	17 (13.6)
More than 60 mL/min/1.73 m^2	577 (94.13)	469 (96.1)	108 (86.4)
Regimen, n (%)[d]			
RHZE	512 (83.5)	419 (85.8)	93 (74.4)
RHZL	22 (3.6)	14 (2.9)	8 (6.4)
RZEM	21 (3.4)	16 (3.3)	5 (4.0)
RZEL	33 (5.4)	20 (4.1)	13 (10.4)
HZEL	10 (1.6)	8 (1.6)	2 (1.6)
Others	15 (2.4)	11 (2.3)	4 (3.2)
Dose, n (%)			
500 mg	4 (0.7)	3 (0.6)	1 (0.8)
1,000 mg	80 (13.1)	55 (11.3)	25 (20.0)
1,200 mg	30 (4.9)	20 (4.1)	10 (8.0)
1,250 mg	30 (4.9)	20 (4.1)	10 (8.0)
1,500 mg	386 (63.0)	328 (67.2)	58 (46.4)
1,600 mg	69 (11.3)	49 (10.0)	20 (16.0)
2000 mg	8 (1.3)	7 (1.4)	1 (0.8)
Age (y), median (range)	54.9 (19–96)	54.5 (19–96)	56.9 (19–87)
Body weight (kg), median (range)	61.03 (28.8–103.8)	60.8 (28.8–95.3)	58.81 (31.9–103.8)
Lean Body Weight (kg)			
median (range)	48.34 (23.1–69.5)	48.1 (23.1–63.79)	46.5 (27.7–69.5)
Albumin (g/dL),—3.8–5.3 g/dL	4.16 (1.6–14.1)	4.2 (2.0–14.1)	4.04 (1.6–7.6)
AST (U/L),—13–33 U/L[e,d]	29.5 (4.2–576)	27 (4.2–191)	32.6 (4.2–576)
ALT (U/L),—6–27 U/L[f,e]	22.1 (0.8–233)	19 (0.8–233)	25.3 (0.8–192)

[a]Continuous data are given as median (range) and categorical data are given as a number (%).
[b]DM, Diabetes Mellitus.
[c]eGFR, Estimated Glomerular Filtration Rate.
[d]R, rifampicin; H, isoniazid; Z, pyrazinamide; E, ethambutol; L, levofloxacin; M: moxifloxacin.
[e]AST, Aspartate transaminase.
[f]ALT, Alanine transaminase.

TABLE 2 PZA population PK parameter estimates for the final model and bootstrap results.

Parameters[a]	Typical value (%RSE) (% η-shrinkage)[b]	Bootstrap median	Results 95% CI[c]
Fixed-effect parameters[d]			
CL/F; elder patient (≥70 years old) with DM = θ_1 x (1+ θ_2),θ_2	0.32 (47.3)	0.36	0.1–0.9
CL/F (L/h); = θ_1,θ_1	4.49 (2.4)	4.56	4.35–4.8
Vd/F (L) = θ_3,θ_3	44.2 (2.7)	43.15	41.2–45.5
Ka (1/h) = θ_4,θ_4	1.49 (11.1)	1.41	1.14–1.84
Interindividual variability			
ω_2; CL/F (%)	1 (60) (18)	1	0.9–1.5
ω_2; Vd/F (%)	3 (FIX) (28.4)	—	—
ω_2; Ka (%)	100 (1) (32.7)	1	1
Residual variability			
Additive	3.41 (14)	3.5	2.5–4.33

[a]CL/F, apparent clearance; Vd/F, apparent volume of distribution; Ka, absorption rate constant; ω_2, variance of interindividual variability.
[b]% RSE, relative standard error [(SE/mean) x 100%]; % η-shrinkage, η-shrinkage = (1-SD(η)/ω) x 100%, where η are the between individual variation terms and ω is the population model estimate of the standard deviation in η.
[c]CI, confidence interval.
[d]Allometric scaling was applied to the CL/F and Vd/F data, and typical values reported here refer to the typical patient, with lean body weight of 48 kg.

phase might explain the shrinkage values for Ka (>30%). In addition, parameter estimates obtained by bootstrapping analysis fell within the 95% CI and showed concordance with the results of the final model, reflecting the stability and reproducibility of the model.

External validation of the final model

External validation was conducted using the data from 125 patients from the test set. The calculated prediction error and absolute prediction error values are shown in Table 3 and visualized in Figure 3 as a comparison with other published models. Our model showed that both the prediction error and absolute prediction error were closer to zero with narrower CIs compared with the other models. These findings indicated that our model had higher accuracy and precision than those of these previous models.

Bayesian estimation of PZA PK parameters

The estimated $AUC_{0\text{-}24}$ and C_{max}, normalized to a dose of 1,200 mg, according to age group and DM as comorbidities are shown in Figure 4. We divided the patients into four different groups: age <70 years with DM, age <70 years without DM, age ≥70 years with DM, and age ≥70 years without DM, with the sample size for each group was 32 patients, 344 patients, 23 patients and 87 patients, respectively. The sample size and characteristics of subgroup analysis and the concentration at 2 h post-dose among groups are presented in Supplementary Files S2, S3. Using Bayesian forecasting, the median estimated $AUC_{0\text{-}24}$ values were 123.2 μg h/mL (interquartile range [IQR]: 120.5–132.4 μg h/mL), 131.1 μg h/mL (IQR: 122.3–131.1 μg h/mL), 99.87 μg h/mL (IQR: 95.67–116.27 μg h/mL), and 138.4 μg h/mL (IQR: 130.3–159.6 μg h/mL), respectively. The C_{max} values were 21.86 μg/mL (IQR: 20.22–23.94 μg/mL), 23.88 μg/mL (IQR: 21.26–27.11 μg/mL), 21.28 μg/mL (IQR: 19.8–22.37 μg/mL), and 25.92 μg/mL (IQR: 22.62–30.6 μg/mL), respectively. These findings indicated that the exposure to PZA in elderly patients with DM would be significantly decreased due to the higher CL/F. Furthermore, we found that DM increased the CL/F of PZA regardless of age. In addition, in the absence of DM, the CL/F of PZA tended to be decreased in the elderly population compared with younger patients. Taking both covariates into account, advanced age and the presence of DM greatly increased the CL/F of PZA. Therefore, the higher CL/F of PZA may be affected by DM as a comorbidity.

Discussion

To our knowledge, there have been few studies regarding the interaction effect between advanced age and comorbidities in TB. As half of the new cases of TB in Korea were identified in elderly patients, there were concerns about the interaction effect of comorbidities and age that may alter the PK of anti-TB drugs, resulting in a poor treatment outcome or risk of adverse drug reactions. In this study, a PZA population PK model was developed to investigate the effects of age and other crucial clinical characteristics of Korean TB patients. Our one-compartment structural model with first-order absorption–elimination and additive residual error described the PK of PZA well. Our model was consistent with other models reported previously (Alsultan et al., 2017; Vinnard et al., 2017; Gao et al., 2021). Allometric scaling was incorporated into the CL/F and Vd/F with regard to lean body weight and improved the goodness-of-fit of the model. The CL/F of PZA estimated in this study was

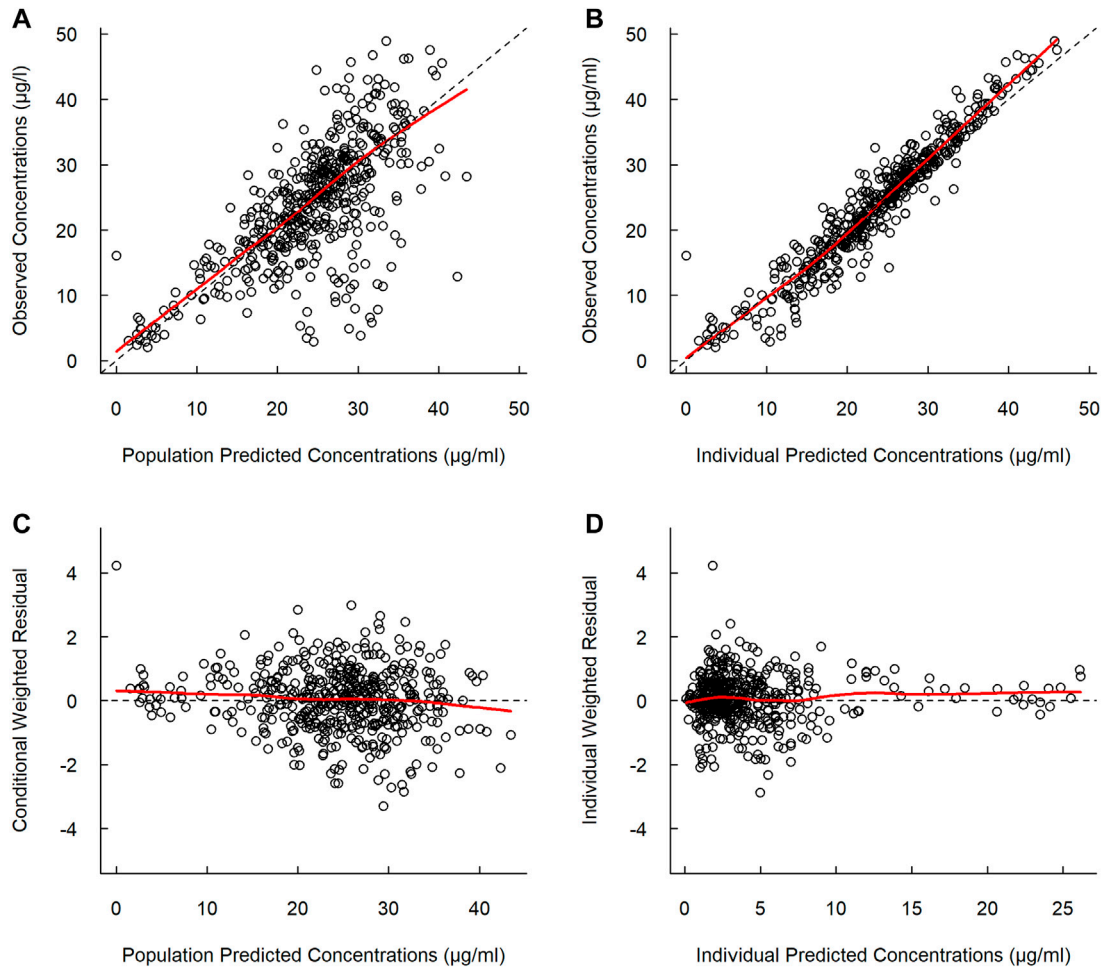

FIGURE 1
Goodness-of-fit plots of the final model. **(A)** Observed versus population predicted concentrations. **(B)** Observed versus individual predicted concentrations. **(C)** Concentration weighted residuals versus population predicted population. **(D)** Individual weighted residuals versus individual predicted concentrations. Open black circles represent the plasma concentrations of PZA, and solid red lines represent locally weighted least-squares regression according to plasma concentration.

consistent with those of previous studies in South African TB patients reported by Rockwood et al. (2016) (CL/F: 4.17 L/h), Mugabo and Mulubwa (2019) (CL/F: 4.28 L/h), and Alsultan et al. (2017) (CL/F: 5.06 L/h).

Although direct comparison between our study and those mentioned studies were not suitable due to different body size descriptors used in the model, the incorporation of allometric scaling marked the similarity of model structure. The median total body weight and lean body weight value of our study were almost similar with Alsultan et al. (2017) and Rockwood et al. (2016), respectively. Additionally, both our study and Mugabo and Mulubwa (2019) study has high density of body weight distribution between 50—70 kg. Thus, it may possibly contribute to the concordance of CL/F estimates. Our model also showed better predictive performance compared with the model of Vinnard et al. (2017), Gao et al. (2021), and Alsultan et al. (2017) in external validation using a dataset from Korean TB patients. Thus, our results suggest that an ethnicity-specific population PK model should be utilized for TDM applications.

In addition to lean body weight, geriatric DM contributed to the IIV in the PZA concentration. We found that age, in terms of elderly patients (≥70 years old), and DM had an explanatory effect on the IIV in the CL/F of PZA in Korean TB patients using a mixed-effects model. This significant effect of advanced age with DM on the CL/F of PZA was distinguished from previous population PK studies (Otalvaro et al., 2021; Sturkenboom et al., 2021). In the subgroup analysis, we found that both younger and older patients with DM tended to have a 32% increase in CL/F compared with those without DM. Even so, the findings were statistically significant only for older patients with DM compared with the other patients. Therefore, our findings suggested an interaction between age and DM that may notably increase the CL/F of PZA. Previous studies also suggested that age may significantly affect the PK of PZA (Hagiwara et al., 2019; Kwon et al., 2020; Rousset et al., 2021). Although the identified

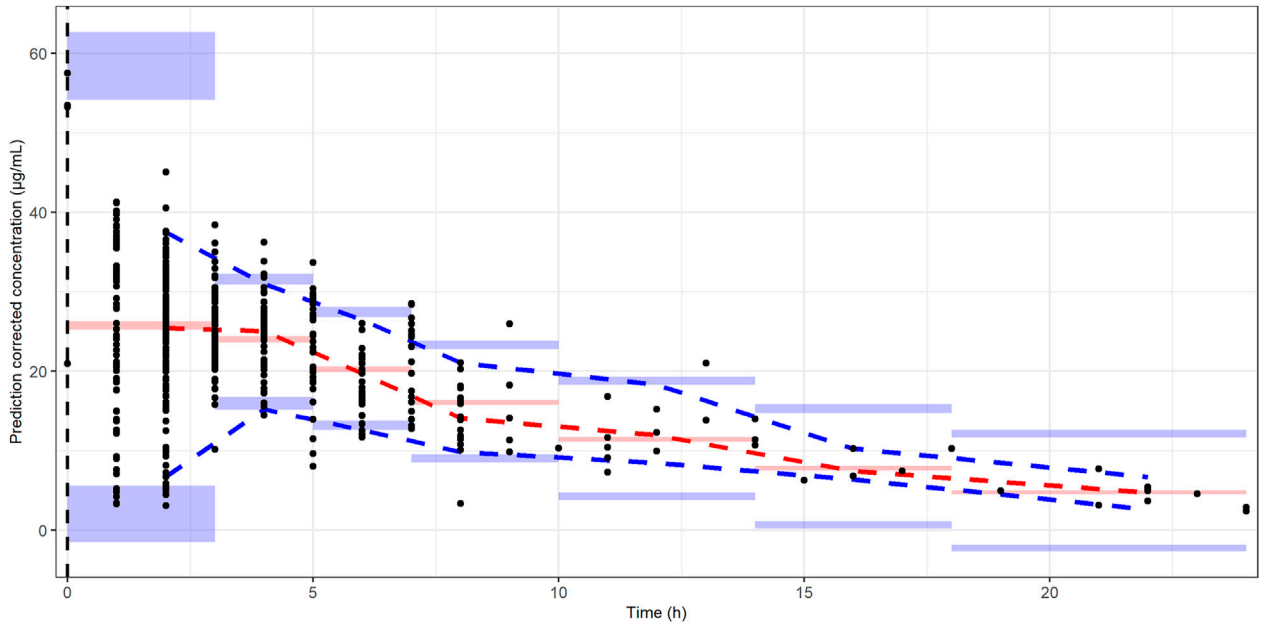

FIGURE 2
Prediction-corrected visual predictive checks. The black dots represent the observed PZA concentrations. The dash blue, red, and blue lines represent the median predicted concentration at 5th, 50th, and 95th percentiles, respectively. The shaded area represents the prediction interval with 95% confidence interval of the simulated PZA concentrations based on the final model.

TABLE 3 Prediction errors calculated by population prediction and individual prediction with external validation.

Model	Population prediction		Individual prediction	
	MPE[a] (95% CI)[b]	APE[c] (95% CI)	MPE (95% CI)	APE (95% CI)
Vinnard et al. (2017)	−17.338 (−44.175-4.87)	17.419 (0.142-44.157)	−11.678 (−33.591-3.623)	11.833 (0.024-33.591)
Gao et al. (2021)	−3.306 (−35.61-1 3.65)	6.429 (0.027-35.61)	−0.853 (−21.389-10.072)	2.978 (0.011-21.389)
Alsultan et al. (2017)	−5.507 (−22.150-14.194)	5.288 (0.011-22.156)	0.175 (−15.082-12.641)	3.845 (0.026-15.08)
Final Model	−0.253 (−26.714-14.894)	4.908 (0.028-26.741)	−0.590 (−21.389-12.641)	2.65 (0.039-15.264)

[a]MPE, Mean Prediction Error.
[b]CI, Confidence Interval.
[c]APE, Absolute Prediction Error.

covariate showed statistically significant, it may not be clinically important due to small decrease of IIV value.

Despite that, several studies have linked DM to a poor TB outcome and an increased risk of TB infection (Kornfeld et al., 2016; Degner et al., 2017; Kumar et al., 2017). It has been speculated that DM may reduce PZA exposure in patients (Kumar et al., 2017; Alfarisi et al., 2018). PZA is a prodrug and is metabolized to 5-hydroxypyrazinoic acid, mainly by XO, in the liver (Lacroix et al., 1989; Hussain et al., 2021). DM results in significantly elevated plasma and liver XO levels in animals with type 1 DM (Matsumoto et al., 2003), and patients with type 2 DM show increased activation of XO (Li et al., 2018; Azenabor et al., 2019). Based on these findings, we speculated that DM-induced elevation of XO may have contributed to a decrease in the PZA concentration (Alfarisi et al., 2018). Additionally, there are some evidence to suggest that DM can affect the absorption of anti-TB drugs (Nijland et al., 2006; Medellin-Garibay et al., 2015). DM may alter the expression and activity of certain transporters in the intestines that are involved in drug absorption (Dash et al., 2015), potentially leading to changes in the absorption phase of anti-TB drugs (Nawa et al., 2011). Most of the studies reported that DM alters the absorption of rifampicin (RIF) through lower gastric acid produced by hyperglycemic condition (Nijland et al., 2006), and alteration of P-glycoprotein expression and activity (Dash et al., 2015). Nonetheless, the alteration of PZA absorption phase due to DM remains uncertain. Different with RIF as the substrate of P-glycoprotein (Huerta-Garcia et al., 2019), it is worth noting that PZA is not recognized as substrates of P-glycoprotein (Alfarisi et al., 2018).

Controlling DM in elderly patients is challenging (Yakaryilmaz and Ozturk, 2017; Leung et al., 2018). The physiological changes in the elderly, characterized by insufficient insulin secretion, changes in

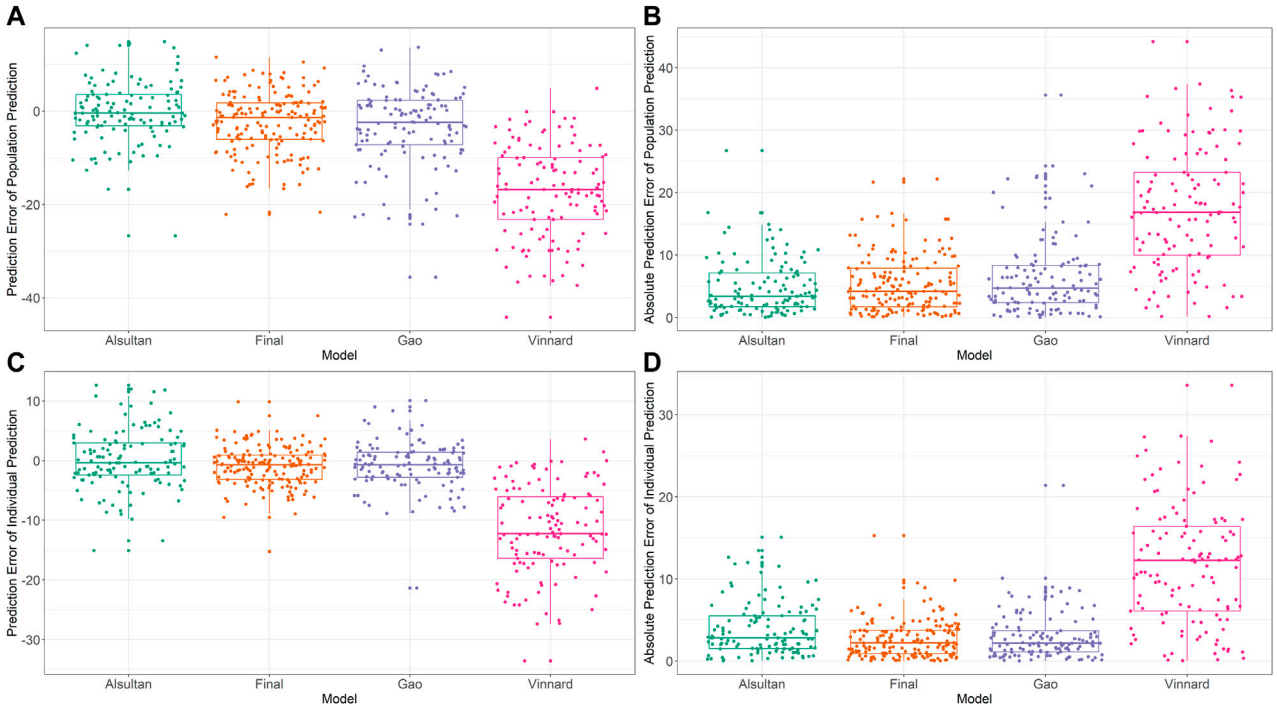

FIGURE 3
External validation and model comparison. Box and whisker plots representing prediction errors and absolute prediction errors calculated by population prediction and individual prediction in external validation. **(A)** Prediction errors computed by population prediction of the tested models. **(B)** Absolute prediction errors computed by population prediction of the tested models. **(C)** Prediction errors computed by the individual prediction of the tested models. **(D)** Absolute prediction errors computed by the individual prediction of the tested models. Different colored closed circles represent the prediction errors or absolute prediction errors for individual patients in the external validation dataset. Horizontal lines represent the medians, with the top and bottom of the boxes representing the first and third quartiles (interquartile range [IQR]), respectively, and whiskers representing extreme data within 1.5× IQR. The tested models were from Alsultan et al., 2017 (Petersen, Al-Abri, Chakaya, Goletti, Parolina, Wejse, et al.), Vinnard et al., 2017 (World Health Organization, 2020), Gao et al., 2021 (Min et al., 2021), and the final model of the present study.

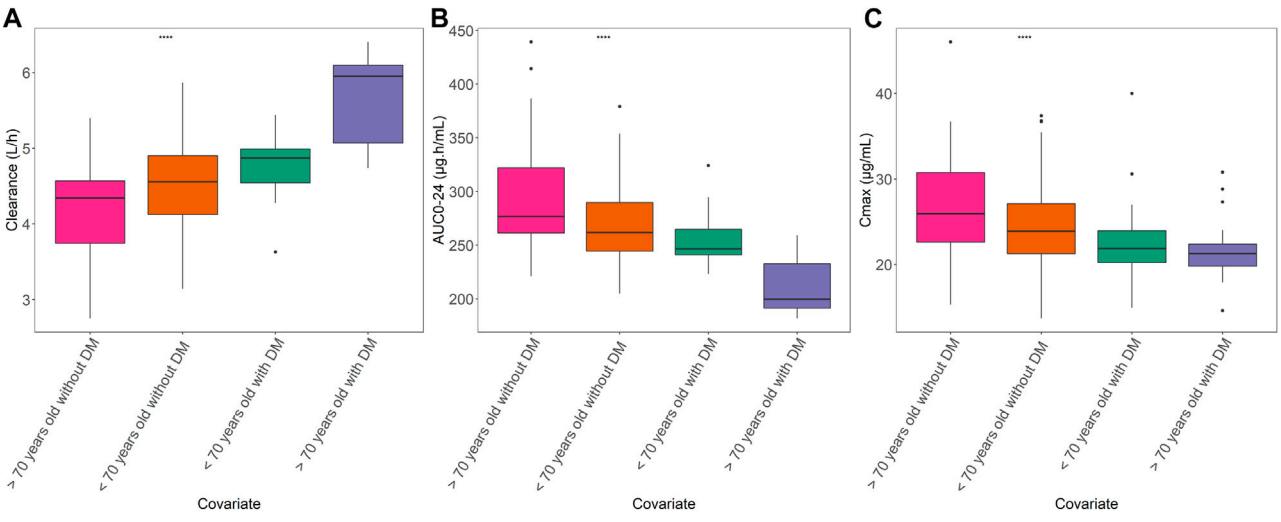

FIGURE 4
Relationships of age and DM with PK parameters. **(A)** Area under the concentration–time curve from 0 to 24 h (AUC_{0-24}). **(B)** Maximum concentration (C_{max}). **(C)** Apparent clearance among age groups with DM or non-DM. Box plot showing the interquartile range of each PK parameter. The groups are represented as follows: blue, >70 years with DM; red, <70 years old with DM; green, <70 years old without DM; and purple, >70 years old without DM. The straight line in the upper part of the box plot represents the ANOVA results. ****$p < 0.001$).

body composition, and increased insulin resistance due to age-related sarcopenia, would increase the blood glucose level (hyperglycemia) (Yakaryilmaz and Ozturk, 2017; Mesinovic et al., 2019). This impaired glucose metabolism exacerbates the effects of DM. Therefore, elderly patients tend to have more severe effects from DM compared with the general population (Gates and Walker, 2014). Hyperglycemia activates endothelial XO, and a previous preliminary clinical study showed that blood XO was activated at high glucose concentrations (Kuppusamy et al., 2005). In fact, the hemoglobin A1c (HbA1c) concentration was reported to be significantly higher in elderly than younger subjects, as a result of the shortened life span of red blood cells due to aging (Masuch et al., 2019). The HbA1c concentration is usually used to diagnose DM in clinical settings and further reflects the blood glucose level in patients (Chehregosha et al., 2019). Earlier reports suggested that a high HbA1c concentration may increase the risk of DM complications (Sherwani et al., 2016; Lee et al., 2021). Therefore, the effects of DM on the PK of PZA may be exacerbated in elderly compared with younger patients with DM.

The effects of DM on the PK of anti-TB drugs are not well understood. Nonetheless, it was reported that the risk of treatment failure is higher in patients with TB and DM (Burhan et al., 2013; Degner et al., 2017). Even though the PK/PD target of PZA efficacy has been reported as AUC/MIC >8.42, the measurement of individual MIC was rarely determined in the clinical practice (Zheng et al., 2021). Furthermore, the extrapolation of this AUC/MIC target to the other region should be cautiously used, since the susceptibility pattern of *M. tuberculosis* may differ from region to region. Thus, the efficacy targets of $AUC_{0\text{-}24} \geq 363$ μg h/mL and/or $C_{max} \geq 30$ μg/mL of PZA were commonly used to adjust the dose due to its association with good treatment outcomes (Alsultan and Peloquin, 2014; Sturkenboom et al., 2021). Taking these criteria into account, none of the patients in our study population achieved the target $AUC_{0\text{-}24}$. However, 14% of the total subjects achieved the target C_{max}. As PZA is widely known for its rapid and excellent sterilizing effect, our results suggested that a higher dose of PZA is needed in DM patients, particularly in those of advanced age. It has long been suggested that a higher dose of PZA is required in TB patients, but studies have been performed mostly in younger adult TB patients (Pasipanodya and Gumbo, 2010; Alsultan et al., 2017; Chirehwa et al., 2017). As the hepatotoxicity and hyperuricemia of PZA would likely be more severe in elderly patients (Kwon et al., 2020), further controlled clinical trials, thorough evaluation of exposure of other anti-TB drugs used in the regimen, and caution with regard to dose adjustment are required to justify our suggestion. Among the few PK data related to PZA in the elderly reported to date, the results of the present study provide additional important insights into the changes in the PK of PZA in elderly patients with DM compared with other groups.

This study had several limitations. First, we collected only one sample from each outpatient in this prospective cohort study, which may have limited the precision of individual PK predictions, such as C_{max} and $AUC_{0\text{-}24}$. However, this was a compromise to reduce the length of hospital stay of the patients. It is recommended to use a dense sampling strategy that includes at least two sampling points in order to obtain more accurate individual PK estimates. Due to our sampling strategy, the C_{max} values presented are calculated and predicted based on the developed model; therefore, have risk of incorrect estimation. Cautious interpretation of the C_{max} values should be carried out when applying it into clinical practice. Second, it was assumed that the patients took their prescription drugs on a regular basis, so the exact timing of repeat dosing was not known prior to the sampling date. Third, the effects of co-administration of other anti-TB drugs were not considered during PK evaluation. However, the interactions among anti-TB drugs remain unclear, and even if there is interaction, it most likely may be clinically unsignificant. Fourth, our population PK model and the PK characteristics described were based on Korean TB data and may vary according to ethnicity and/or patient characteristics.

Conclusion

Using the randomized post-dose point approach, the established model adequately described the PK of PZA in Korean TB patients and showed good performance. In addition to body weight, our model identified geriatric (≥70 years) DM as an important covariate for the CL/F of PZA. We found that the geriatric DM population had a higher CL/F of PZA and lower exposure of PZA compared with other patients. The population PK model that we developed can be further used to optimize TB treatment via MIPD-based TDM implementation.

Data availability statement

The raw data supporting the conclusion of this article will be made available by the authors, without undue reservation.

Ethics statement

The studies involving human participants were reviewed and approved by all the participating hospitals/centers. The patients/participants provided their written informed consent to participate in this study.

Author contributions

RK: conceptualization, data curation, methodology, investigation, formal analysis, validation, visualization, writing–original draft, writing–review and editing. RPJ: data curation, methodology, investigation, formal analysis, validation, visualization, writing–original draft, writing–review and editing. HL: methodology, investigation, writing–original draft, writing–review and editing. H-KK: methodology, investigation, writing–original draft, writing–review and editing. JK: methodology, investigation, writing–original draft, writing–review and editing. I-NP: methodology, investigation, writing–original draft, writing–review and editing. JK: methodology, investigation, writing–original draft, writing–review and editing. JO: methodology, investigation, writing–original draft, writing–review and editing. HK: methodology, investigation, writing–original draft, writing–review and editing. HL: methodology, investigation, writing–original draft, writing–review and editing. J-LG: methodology, investigation, writing–original draft, writing–review and editing. SA: methodology, investigation, writing–original draft, writing–review and editing. NPL: methodology, supervision,

writing–review and editing. Y-SC: conceptualization, methodology, resources, supervision, writing–review and editing. J-GS: conceptualization, methodology, writing–review and editing, resources, supervision, funding acquisition. All authors contributed to the article and approved the submitted version.

Funding

This study was supported by a National Research Foundation of Korea (NRF) grant (No. 2018R1A5A2021242) funded by the Korean government (MSIT).

Acknowledgments

The authors would like to express highest gratitude to Eun-Young Kim, Ji-young Yang, and Ho-Young Lee from Busan Paik Hospital; Sung-Soon Lee, Hyeon-Kyoung Koo, Hyung Koo Kang, Won Bae, Jieun Kang, and So-Hee Park from Ilsan Paik Hospital; Sung Weon Ryoo and Sang-Hee Park from Masan National Tuberculosis Hospital; Hyuk Pyo Lee and Sang Bong Choi from Sanggye Paik Hospital; Hokee Yum and Inae Park from Seoul Paik Hospital; Jeong Ha Mok from Pusan National University Hospital; Jae Hee Lee and Hye Won Seo from Kyungpook National University Hospital; Kyeong Cheol Shin, June Hong Ahn, Eun Young Choi, Hyun Jung Jin, Kwan Ho Lee, and Jin Hong Chung from Yeungnam University Medical Center; Bo Hyong Kang from Dong-A University Hospital; Ho Cheol Kim and Tae Hoon Kim from Gyeongsang National University Changwon Hospital; Ju Sang Kim, Joong Hyun Ahn, Jick Hwan Ha, Ah Young Shin, and Jong Yeol Oh from Incheon St. Mary's Hospital; You Sang Ko, Eun Kyung Mo, Jin Wook Moon, Yong Bum Park, Yong Suk Jo, and Ye Jin Lee from Kangdong Sacred Heart Hospital; Ji Young Kang, Hwa Young Lee, Sung Yeon Cho, and Dong Gun Lee from Seoul St. Mary's Hospital; Jin Soo Min from Daejeon St. Mary's Hospital; Sang Haak Lee, Chang Dong Yeo, Sei Won Kim, and Jung Won Heo from Eunpyeong St. Mary's Hospital; Jin Woo Kim, Hyon Soo Joo, and Kyu Yean Kim from Uijeongbu St. Mary's Hospital; and Sung Kyoung Kim from St. Vincent's Hospital. We are also very grateful to all the staff involved in the cPMTb-001 study.

Conflict of interest

The authors declare that the research was conducted in the absence of any commercial or financial relationships that could be construed as a potential conflict of interest.

Publisher's note

Supplementary material

The Supplementary Material for this article can be found online at: https://www.frontiersin.org/articles/10.3389/fphar.2023.1116226/full#supplementary-material

References

Alfarisi, O., Mave, V., Gaikwad, S., Sahasrabudhe, T., Ramachandran, G., Kumar, H., et al. (2018). Effect of diabetes mellitus on the pharmacokinetics and pharmacodynamics of tuberculosis treatment. *Antimicrob. Agents Chemother.* 62 (11), e01383-18. doi:10.1128/AAC.01383-18

Alffenaar, J. C., Gumbo, T., Dooley, K. E., Peloquin, C. A., McIlleron, H., Zagorski, A., et al. (2020). Integrating pharmacokinetics and pharmacodynamics in operational research to end tuberculosis. *Clin. Infect. Dis.* 70 (8), 1774–1780. doi:10.1093/cid/ciz942

Alsultan, A., and Peloquin, C. A. (2014). Therapeutic drug monitoring in the treatment of tuberculosis: An update. *Drugs* 74 (8), 839–854. doi:10.1007/s40265-014-0222-8

Alsultan, A., Savic, R., Dooley, K. E., Weiner, M., Whitworth, W., Mac Kenzie, W. R., et al. (2017). Population pharmacokinetics of AZD-5847 in adults with pulmonary tuberculosis. *Antimicrob. Agents Chemother.* 61 (6), e01066-17. doi:10.1128/AAC.01066-17

Anderson, B. J., and Holford, N. H. (2008). Mechanism-based concepts of size and maturity in pharmacokinetics. *Annu. Rev. Pharmacol. Toxicol.* 48, 303–332. doi:10.1146/annurev.pharmtox.48.113006.094708

Azenabor, A., Erivona, R., Adejumo, E., Ozuruoke, D., and Azenabor, R. (2019). Xanthine oxidase activity in type 2 diabetic Nigerians. *Diabetes Metab. Syndr.* 13 (3), 2021–2024. doi:10.1016/j.dsx.2019.04.022

Baker, M. A., Harries, A. D., Jeon, C. Y., Hart, J. E., Kapur, A., Lonnroth, K., et al. (2011). The impact of diabetes on tuberculosis treatment outcomes: A systematic review. *BMC Med.* 9, 81. doi:10.1186/1741-7015-9-81

Beal, S. L. (2001). Ways to fit a PK model with some data below the quantification limit. *J. Pharmacokinet. Pharmacodyn.* 28 (5), 481–504. doi:10.1023/a:1012299115260

Burhan, E., Ruesen, C., Ruslami, R., Ginanjar, A., Mangunnegoro, H., Ascobat, P., et al. (2013). Isoniazid, rifampin, and pyrazinamide plasma concentrations in relation to treatment response in Indonesian pulmonary tuberculosis patients. *Antimicrob. Agents Chemother.* 57 (8), 3614–3619. doi:10.1128/AAC.02468-12

Chabala, C., Turkova, A., Hesseling, A. C., Zimba, K. M., van der Zalm, M., Kapasa, M., et al. (2022). Pharmacokinetics of first-line drugs in children with tuberculosis, using world Health organization-recommended weight band doses and formulations. *Clin. Infect. Dis.* 74 (10), 1767–1775. doi:10.1093/cid/ciab725

Chehregosha, H., Khamseh, M. E., Malek, M., Hosseinpanah, F., and Ismail-Beigi, F. (2019). A view beyond HbA1c: Role of continuous glucose monitoring. *Diabetes Ther.* 10 (3), 853–863. doi:10.1007/s13300-019-0619-1

Chideya, S., Winston, C. A., Peloquin, C. A., Bradford, W. Z., Hopewell, P. C., Wells, C. D., et al. (2009). Isoniazid, rifampin, ethambutol, and pyrazinamide pharmacokinetics and treatment outcomes among a predominantly HIV-infected cohort of adults with tuberculosis from Botswana. *Clin. Infect. Dis.* 48 (12), 1685–1694. doi:10.1086/599040

Chirehwa, M. T., McIlleron, H., Rustomjee, R., Mthiyane, T., Onyebujoh, P., Smith, P., et al. (2017). Pharmacokinetics of pyrazinamide and optimal dosing regimens for drug-sensitive and -resistant tuberculosis. *Antimicrob. Agents Chemother.* 61 (8), e00490-17. doi:10.1128/AAC.00490-17

Cho, K. S. (2018). Tuberculosis control in the republic of Korea. *Epidemiol. Health* 40, e2018036. doi:10.4178/epih.e2018036

Dash, R. P., Ellendula, B., Agarwal, M., and Nivsarkar, M. (2015). Increased intestinal P-glycoprotein expression and activity with progression of diabetes and its modulation by epigallocatechin-3-gallate: Evidence from pharmacokinetic studies. *Eur. J. Pharmacol.* 767, 67–76. doi:10.1016/j.ejphar.2015.10.009

Daskapan, A., de Lange, W. C., Akkerman, O. W., Kosterink, J. G., van der Werf, T. S., Stienstra, Y., et al. (2015). The role of therapeutic drug monitoring in individualised drug dosage and exposure measurement in tuberculosis and HIV co-infection. *Eur. Respir. J.* 45 (2), 569–571. doi:10.1183/09031936.00142614

Degner, N. R., Wang, J-Y., Golub, J. E., and Karakousis, P. C. (2017). Metformin use reverses the increased mortality associated with diabetes mellitus during tuberculosis treatment. *Clin. Infect. Dis.* 66 (2), 198–205. doi:10.1093/cid/cix819

Denti, P., Jeremiah, K., Chigutsa, E., Faurholt-Jepsen, D., PrayGod, G., Range, N., et al. (2015). Pharmacokinetics of isoniazid, pyrazinamide, and ethambutol in newly diagnosed pulmonary TB patients in Tanzania. *PLoS One* 10 (10), e0141002. doi:10.1371/journal.pone.0141002

Devaleenal Daniel, B., Ramachandran, G., and Swaminathan, S. (2017). The challenges of pharmacokinetic variability of first-line anti-TB drugs. *Expert Rev. Clin. Pharmacol.* 10 (1), 47–58. doi:10.1080/17512433.2017.1246179

Donald, P. R., Maritz, J. S., and Diacon, A. H. (2012). Pyrazinamide pharmacokinetics and efficacy in adults and children. *Tuberc. (Edinb).* 92 (1), 1–8. doi:10.1016/j.tube.2011.05.006

Egelund, E. F., Barth, A. B., and Peloquin, C. A. (2011). Population pharmacokinetics and its role in anti-tuberculosis drug development and optimization of treatment. *Curr. Pharm. Des.* 17 (27), 2889–2899. doi:10.2174/138161211797470246

Gao, Y., Davies Forsman, L., Ren, W., Zheng, X., Bao, Z., Hu, Y., et al. (2021). Drug exposure of first-line anti-tuberculosis drugs in China: A prospective pharmacological cohort study. *Br. J. Clin. Pharmacol.* 87 (3), 1347–1358. doi:10.1111/bcp.14522

Gates, B. J., and Walker, K. M. (2014). Physiological changes in older adults and their effect on diabetes treatment. *Diabetes Spectr.* 27 (1), 20–28. doi:10.2337/diaspect.27.1.20

Ghimire, S., Bolhuis, M. S., Sturkenboom, M. G., Akkerman, O. W., de Lange, W. C., van der Werf, T. S., et al. (2016). Incorporating therapeutic drug monitoring into the World Health Organization hierarchy of tuberculosis diagnostics. *Eur. Respir. J.* 47 (6), 1867–1869. doi:10.1183/13993003.00040-2016

Graham, S. M., Bell, D. J., Nyirongo, S., Hartkoorn, R., Ward, S. A., and Molyneux, E. M. (2006). Low levels of pyrazinamide and ethambutol in children with tuberculosis and impact of age, nutritional status, and human immunodeficiency virus infection. *Antimicrob. Agents Chemother.* 50 (2), 407–413. doi:10.1128/AAC.50.2.407-413.2006

Gurumurthy, P., Ramachandran, G., Hemanth Kumar, A. K., Rajasekaran, S., Padmapriyadarsini, C., Swaminathan, S., et al. (2004). Decreased bioavailability of rifampin and other antituberculosis drugs in patients with advanced human immunodeficiency virus disease. *Antimicrob. Agents Chemother.* 48 (11), 4473–4475. doi:10.1128/AAC.48.11.4473-4475.2004

Hagiwara, E., Suido, Y., Asaoka, M., Katano, T., Okuda, R., Sekine, A., et al. (2019). Safety of pyrazinamide-including regimen in late elderly patients with pulmonary tuberculosis: A prospective randomized open-label study. *J. Infect. Chemother.* 25 (12), 1026–1030. doi:10.1016/j.jiac.2019.05.030

Huerta-Garcia, A. P., Medellin-Garibay, S. E., Salazar-Gonzalez, R. A., Ortiz-Alvarez, A., Magana-Aquino, M., Rodriguez-Pinal, C. J., et al. (2019). Anthropometric and genetic factors associated with the exposure of rifampicin and isoniazid in Mexican patients with tuberculosis. *Ther. Drug Monit.* 41 (5), 648–656. doi:10.1097/FTD.0000000000000631

Hussain, Z., Zhu, J., and Ma, X. (2021). Metabolism and hepatotoxicity of pyrazinamide, an antituberculosis drug. *Drug Metab. Dispos.* 49 (8), 679–682. doi:10.1124/dmd.121.000389

Jayanti, R. P., Long, N. P., Phat, N. K., Cho, Y. S., and Shin, J. G. (2022). Semi-automated therapeutic drug monitoring as a pillar toward personalized medicine for tuberculosis management. *Pharmaceutics* 14 (5), 990. doi:10.3390/pharmaceutics14050990

Kim, H. J., Seo, K. A., Kim, H. M., Jeong, E. S., Ghim, J. L., Lee, S. H., et al. (2015). Simple and accurate quantitative analysis of 20 anti-tuberculosis drugs in human plasma using liquid chromatography-electrospray ionization-tandem mass spectrometry. *J. Pharm. Biomed. Anal.* 102, 9–16. doi:10.1016/j.jpba.2014.08.026

Klotz, U. (2009). Pharmacokinetics and drug metabolism in the elderly. *Drug Metab. Rev.* 41 (2), 67–76. doi:10.1080/03602530902722679

Kornfeld, H., West, K., Kane, K., Kumpatla, S., Zacharias, R. R., Martinez-Balzano, C., et al. (2016). High prevalence and heterogeneity of diabetes in patients with TB in South India: A report from the effects of diabetes on tuberculosis severity (edots) study. *Chest* 149 (6), 1501–1508. doi:10.1016/j.chest.2016.02.675

Kumar, A. K., Chandrasekaran, V., Kannan, T., Murali, A. L., Lavanya, J., Sudha, V., et al. (2017). Anti-tuberculosis drug concentrations in tuberculosis patients with and without diabetes mellitus. *Eur. J. Clin. Pharmacol.* 73 (1), 65–70. doi:10.1007/s00228-016-2132-z

Kuppusamy, U. R., Indran, M., and Rokiah, P. (2005). Glycaemic control in relation to xanthine oxidase and antioxidant indices in Malaysian Type 2 diabetes patients. *Diabet. Med.* 22 (10), 1343–1346. doi:10.1111/j.1464-5491.2005.01630.x

Kwon, B. S., Kim, Y., Lee, S. H., Lim, S. Y., Lee, Y. J., Park, J. S., et al. (2020). The high incidence of severe adverse events due to pyrazinamide in elderly patients with tuberculosis. *PLoS One* 15 (7), e0236109. doi:10.1371/journal.pone.0236109

Lacroix, C., Hoang, T. P., Nouveau, J., Guyonnaud, C., Laine, G., Duwoos, H., et al. (1989). Pharmacokinetics of pyrazinamide and its metabolites in healthy subjects. *Eur. J. Clin. Pharmacol.* 36 (4), 395–400. doi:10.1007/BF00558302

Lange, C., Aarnoutse, R., Chesov, D., van Crevel, R., Gillespie, S. H., Grobbel, H. P., et al. (2020). Perspective for precision medicine for tuberculosis. *Front. Immunol.* 11, 566608. doi:10.3389/fimmu.2020.566608

Lee, S., Zhou, J., Wong, W. T., Liu, T., Wu, W. K. K., Wong, I. C. K., et al. (2021). Glycemic and lipid variability for predicting complications and mortality in diabetes mellitus using machine learning. *BMC Endocr. Disord.* 21 (1), 94. doi:10.1186/s12902-021-00751-4

Leung, E., Wongrakpanich, S., and Munshi, M. N. (2018). Diabetes management in the elderly. *Diabetes Spectr.* 31 (3), 245–253. doi:10.2337/ds18-0033

Li, X., Meng, X., Gao, X., Pang, X., Wang, Y., Wu, X., et al. (2018). Elevated serum xanthine oxidase activity is associated with the development of type 2 diabetes: A prospective cohort study. *Diabetes Care* 41 (4), 884–890. doi:10.2337/dc17-1434

Lin, Y. H., Chen, C. P., Chen, P. Y., Huang, J. C., Ho, C., Weng, H. H., et al. (2015). Screening for pulmonary tuberculosis in type 2 diabetes elderly: A cross-sectional study in a community hospital. *BMC Public Health* 15, 3. doi:10.1186/1471-2458-15-3

Mangoni, A. A., and Jackson, S. H. (2004). Age-related changes in pharmacokinetics and pharmacodynamics: Basic principles and practical applications. *Br. J. Clin. Pharmacol.* 57 (1), 6–14. doi:10.1046/j.1365-2125.2003.02007.x

Masuch, A., Friedrich, N., Roth, J., Nauck, M., Muller, U. A., and Petersmann, A. (2019). Preventing misdiagnosis of diabetes in the elderly: Age-dependent HbA1c reference intervals derived from two population-based study cohorts. *BMC Endocr. Disord.* 19 (1), 20. doi:10.1186/s12902-019-0338-7

Matsumoto, S., Koshiishi, I., Inoguchi, T., Nawata, H., and Utsumi, H. (2003). Confirmation of superoxide generation via xanthine oxidase in streptozotocin-induced diabetic mice. *Free Radic. Res.* 37 (7), 767–772. doi:10.1080/1071576031000107344

McIlleron, H., Wash, P., Burger, A., Norman, J., Folb, P. I., and Smith, P. (2006). Determinants of rifampin, isoniazid, pyrazinamide, and ethambutol pharmacokinetics in a cohort of tuberculosis patients. *Antimicrob. Agents Chemother.* 50 (4), 1170–1177. doi:10.1128/AAC.50.4.1170-1177.2006

Medellin-Garibay, S. E., Cortez-Espinosa, N., Milan-Segovia, R. C., Magana-Aquino, M., Vargas-Morales, J. M., Gonzalez-Amaro, R., et al. (2015). Clinical pharmacokinetics of rifampin in patients with tuberculosis and type 2 diabetes mellitus: Association with biochemical and immunological parameters. *Antimicrob. Agents Chemother.* 59 (12), 7707–7714. doi:10.1128/AAC.01067-15

Mesinovic, J., Zengin, A., De Courten, B., Ebeling, P. R., and Scott, D. (2019). Sarcopenia and type 2 diabetes mellitus: A bidirectional relationship. *Diabetes Metab. Syndr. Obes.* 12, 1057–1072. doi:10.2147/DMSO.S186600

Min, J., Kim, H. W., and Kim, J. S. (2021). Tuberculosis and Respiratory Diseases. *Tuberc Respir Dis*, 86, 1, 67-69.

Mugabo, P., and Mulubwa, M. (2019). Population pharmacokinetic modelling of pyrazinamide and pyrazinoic acid in patients with multi-drug resistant tuberculosis. *Eur. J. Drug Metab. Pharmacokinet.* 44 (4), 519–530. doi:10.1007/s13318-018-00540-w

Nawa, A., Fujita-Hamabe, W., and Tokuyama, S. (2011). Altered intestinal P-glycoprotein expression levels in a monosodium glutamate-induced obese mouse model. *Life Sci.* 89 (23-24), 834–838. doi:10.1016/j.lfs.2011.08.019

Nijland, H. M. J., Ruslami, R., Stalenhoef, J. E., Nelwan, E. J., Alisjahbana, B., Nelwan, R. H. H., et al. (2006). Exposure to rifampicin is strongly reduced in patients with tuberculosis and type 2 diabetes. *Clin. Infect. Dis.* 43 (7), 848–854. doi:10.1086/507543

Otalvaro, J. D., Hernandez, A. M., Rodriguez, C. A., and Zuluaga, A. F. (2021). Population pharmacokinetic models of antituberculosis drugs in patients: A systematic critical review. *Ther. Drug Monit.* 43 (1), 108–115. doi:10.1097/FTD.0000000000000803

Park, S., Yang, B. R., Song, H. J., Jang, S. H., Kang, D. Y., and Park, B. J. (2019). Metformin and tuberculosis risk in elderly patients with diabetes mellitus. *Int. J. Tuberc. Lung Dis.* 23 (8), 924–930. doi:10.5588/ijtld.18.0687

Pasipanodya, J. G., and Gumbo, T. (2010). Clinical and toxicodynamic evidence that high-dose pyrazinamide is not more hepatotoxic than the low doses currently used. *Antimicrob. Agents Chemother.* 54 (7), 2847–2854. doi:10.1128/AAC.01567-09

Pasipanodya, J. G., McIlleron, H., Burger, A., Wash, P. A., Smith, P., and Gumbo, T. (2013). Serum drug concentrations predictive of pulmonary tuberculosis outcomes. *J. Infect. Dis.* 208 (9), 1464–1473. doi:10.1093/infdis/jit352

Petersen, E., Al-Abri, S., Chakaya, J., Goletti, D., Parolina, L., Wejse, C., et al. (2022). World TB day 2022: Revamping and reshaping global TB control programs by advancing lessons learnt from the COVID-19 pandemic. *Int. J. Infect. Dis.* 124, S1–S3. doi:10.1016/j.ijid.2022.02.057

Polasek, T. M., Rostami-Hodjegan, A., Yim, D. S., Jamei, M., Lee, H., Kimko, H., et al. (2019). What does it take to make model-informed precision dosing common practice? Report from the 1st asian symposium on precision dosing. *AAPS J.* 21 (2), 17. doi:10.1208/s12248-018-0286-6

Qureshi, W., Hassan, G., Kadri, S. M., Khan, G. Q., Samuel, B., and Arshad, A. (2007). Hyperuricemia and arthralgias during pyrazinamide therapy in patients with pulmonary tuberculosis. *Lab. Med.* 38 (8), 495–497. doi:10.1309/7gbyqty62pfehdp1

Rockwood, N., Meintjes, G., Chirehwa, M., Wiesner, L., McIlleron, H., Wilkinson, R. J., et al. (2016). HIV-1 coinfection does not reduce exposure to rifampin, isoniazid, and pyrazinamide in South African tuberculosis outpatients. *Antimicrob. Agents Chemother.* 60 (10), 6050–6059. doi:10.1128/AAC.00480-16

Rousset, S., Lafaurie, M., Guet-Revillet, H., Protin, C., Le Grusse, J., Derumeaux, H., et al. (2021). Safety of pyrazinamide for the treatment of tuberculosis in older patients over 75 Years of age: A retrospective monocentric cohort study. *Drugs Aging* 38 (1), 43–52. doi:10.1007/s40266-020-00811-9

Sherwani, S. I., Khan, H. A., Ekhzaimy, A., Masood, A., and Sakharkar, M. K. (2016). Significance of HbA1c test in diagnosis and prognosis of diabetic patients. *Biomark. Insights* 11, 95–104. doi:10.4137/BMI.S38440

Shin, H. J., and Kwon, Y. S. (2015). Treatment of drug susceptible pulmonary tuberculosis. *Tuberc. Respir. Dis. Seoul.* 78 (3), 161–167. doi:10.4046/trd.2015.78.3.161

Srivastava, S., Pasipanodya, J. G., Meek, C., Leff, R., and Gumbo, T. (2011). Multidrug-resistant tuberculosis not due to noncompliance but to between-patient pharmacokinetic variability. *J. Infect. Dis.* 204 (12), 1951–1959. doi:10.1093/infdis/jir658

Sturkenboom, M. G. G., Martson, A. G., Svensson, E. M., Sloan, D. J., Dooley, K. E., van den Elsen, S. H. J., et al. (2021). Population pharmacokinetics and bayesian dose adjustment to advance TDM of anti-TB drugs. *Clin. Pharmacokinet.* 60 (6), 685–710. doi:10.1007/s40262-021-00997-0

Thee, S., Seddon, J. A., Donald, P. R., Seifart, H. I., Werely, C. J., Hesseling, A. C., et al. (2011). Pharmacokinetics of isoniazid, rifampin, and pyrazinamide in children younger than two years of age with tuberculosis: Evidence for implementation of revised world Health organization recommendations. *Antimicrob. Agents Chemother.* 55 (12), 5560–5567. doi:10.1128/AAC.05429-11

Vinnard, C., Ravimohan, S., Tamuhla, N., Pasipanodya, J., Srivastava, S., Modongo, C., et al. (2017). Pyrazinamide clearance is impaired among HIV/tuberculosis patients with high levels of systemic immune activation. *PLoS One* 12 (11), e0187624. doi:10.1371/journal.pone.0187624

WHO (2017). in *Guidelines for treatment of drug-susceptible tuberculosis and patient care, 2017 update*. Editor W. H. Organization (Geneva, Switzerland: World Health Organization).

Wilkins, J. J., Langdon, G., McIlleron, H., Pillai, G. C., Smith, P. J., and Simonsson, U. S. (2006). Variability in the population pharmacokinetics of pyrazinamide in South African tuberculosis patients. *Eur. J. Clin. Pharmacol.* 62 (9), 727–735. doi:10.1007/s00228-006-0141-z

WHO Expert Committee (2020). *Global tuberculosis report*. Geneva, Switzerland: World Health Organization.

Yakaryilmaz, F. D., and Ozturk, Z. A. (2017). Treatment of type 2 diabetes mellitus in the elderly. *World J. Diabetes* 8 (6), 278–285. doi:10.4239/wjd.v8.i6.278

Yoon, Y. S., Jung, J. W., Jeon, E. J., Seo, H., Ryu, Y. J., Yim, J. J., et al. (2017). The effect of diabetes control status on treatment response in pulmonary tuberculosis: A prospective study. *Thorax* 72 (3), 263–270. doi:10.1136/thoraxjnl-2015-207686

Younossian, A. B., Rochat, T., Ketterer, J. P., Wacker, J., and Janssens, J. P. (2005). High hepatotoxicity of pyrazinamide and ethambutol for treatment of latent tuberculosis. *Eur. Respir. J.* 26 (3), 462–464. doi:10.1183/09031936.05.00006205

Zhang, Y., and Mitchison, D. (2003). The curious characteristics of pyrazinamide: A review. *Int. J. Tuberc. Lung Dis.* 7 (1), 6–21.

Zheng, X., Bao, Z., Forsman, L. D., Hu, Y., Ren, W., Gao, Y., et al. (2021). Drug exposure and minimum inhibitory concentration predict pulmonary tuberculosis treatment response. *Clin. Infect. Dis.* 73 (9), e3520–e3528. doi:10.1093/cid/ciaa1569

Zvada, S. P., Denti, P., Donald, P. R., Schaaf, H. S., Thee, S., Seddon, J. A., et al. (2014). Population pharmacokinetics of rifampicin, pyrazinamide and isoniazid in children with tuberculosis: In silico evaluation of currently recommended doses. *J. Antimicrob. Chemother.* 69 (5), 1339–1349. doi:10.1093/jac/dkt524

Frontiers in Pharmacology

Explores the interactions between chemicals and living beings

The most cited journal in its field, which advances access to pharmacological discoveries to prevent and treat human disease.

Discover the latest Research Topics

See more →

Frontiers

Avenue du Tribunal-Fédéral 34
1005 Lausanne, Switzerland
frontiersin.org

Contact us

+41 (0)21 510 17 00
frontiersin.org/about/contact